University of Alberta

RE-VISITATION OF ACTUAL EVAPORATION THEORIES

by

Dat Tien Quoc Tran

A thesis submitted to the Faculty of Graduate Studies and Research
in partial fulfillment of the requirements for the degree of

Doctor of Philosophy

in

Geotechnical Engineering

Department of Civil and Environmental Engineering

Fall 2013

Edmonton, Alberta

Dedicated to my loving parents,

Tran Tien Dung

Pham Thi Cam

Dearest parents,

This is for you, as promised!

ABSTRACT

Evaporation from a deposit of thickened or cover systems is increasingly becoming a big challenge for geotechnical engineers. Accurate calculation of the actual evaporation from a saturated-unsaturated surface requires accurate specification of vapour pressure or relative humidity at ground surface.

The evaporation of water from a water surface known as potential evaporation is quite well understood. However, the evaporation of water from a saturated-unsaturated surface known as actual evaporation needs to be re-evaluated. Several methods of estimating evaporation from unsaturated soil surfaces can be found in the literature. According to these methods, the actual rate of evaporation has been calculated on basis of the total suction or relative humidity predicted at the soil surfaces. Empirical methods of adjusting total suction or modifying relative humidity at the soil surface have been applied to compute evaporative flux from the soil surface. However, the suitability and accuracy of these methods can be questioned.

The fundamental physics of water transfer from a soil surface are re-considered. At the end, a new soil-atmosphere flux equation is developed for predicting evaporation from a soil surface using the concept of “surface resistance” to vapour water diffusion from the soil surface to atmosphere.

Soil suction and the corresponding water content at which the actual rate of evaporation begins to depart from potential rate of evaporation during drying process are re-assessed using a series of laboratory data collected from the research literature. It is found that the value of suction at evaporation-rate reduction point appears to be approximately 3,000 kPa for the thin soil

sections regardless of the soil texture. However, such suction appears to be in between the air-entry value and residual soil suction for the soil columns. As a result, a formula to determine soil suction at evaporation-rate reduction point is derived for soil columns. Equations are also proposed to calculate the coefficient of surface moisture availability, vapour pressure and soil surface resistance at soil surface.

The effect of pore-water salinity on the evaporation rate from salinized soils was also considered. A function of osmotic suction is derived and verified using data of osmotic suction measured in the laboratory testing program.

Drying tests on thin soil layers as well as thick soil layers were conducted using the selected non-saline and salinized soils. The obtained results were utilized to verify the proposed equations. Good agreement was generally found between the computed and measured rate of evaporation. In addition, these equations were also verified using the evaporative data collected from the research literature. The findings throughout this thesis will help solve the challenge of predicting evaporation from non-saline and salinized soil surfaces with which the geotechnical engineers are facing in many practical problems.

ACKNOWLEDGEMENT

The author would like to express gratitude to Professor Dave H. Chan and Professor Delwyn G. Fredlund for supervising this study.

Professor Chan provided the author opportunities and research materials to accomplish this study. His guidance, patience, generosity, understanding and support throughout this research are greatly appreciated.

Professor Fredlund suggested this topic, granted a generous amount of time and intellectual effort in problem-solving discussions, and offered emotional help and encouragement. Many research articles and technical reports reviewed in this study were delivered and suggested to the author by Professor Fredlund. Throughout the process of completing this study, Professor Fredlund spent many times in visiting University of Alberta and helping the author revise and finalize the thesis. His great advices, constructive criticism, and consistent support have made this work a pleasant and satisfying research experience for the author. Moreover, Professor Fredlund and his wife JoAnne Fredlund treat the author as their family members. Their cares and supports will never be forgotten.

The author would also like to thank the technical and administrative staffs in the Geotechnical Engineering Group at University of Alberta. Special thanks are for Sally Petaske for her support throughout the course of this research.

The author is deeply grateful to his loving wife Nguyen Tran for her patience, understanding, love, and strength. She has sacrificed more to this thesis than could be described on these pages. Her love and support have been and always will be an invaluable part of the author's life.

Finally, the author expresses his special thanks to his family and friends whose support, encouragement and love helped him overcome the most difficult obstacles.

Table of Contents

List of Figures

List of Tables

CHAPTER 1
INTRODUCTION

1.1 PROBLEM BACKGROUND

Accurate prediction of drying rates is desirable to optimize surface deposition of thickened or paste tailings or cover systems which are increasingly becoming a potential solution for environmental concerns (Simms et al., 2007; Fredlund et al., 2012). In the literature, there are several methods which can be used to estimate the rate of evaporation from the surfaces of open water, saline water, bare soil and saline soil. Practically the rate of evaporation depends on climatic conditions such as net radiation, air temperature, air relative humidity, and soil temperature. The rate of evaporation is also dependent upon the soil properties. Unfortunately, not all data from climatic records and soil investigations are measured with sufficient detail to estimate the rate of evaporation from the ground surface.

There are two terms in geotechnical engineering which define the rate of evaporation from water surfaces and soil surfaces. One term is referred to as “potential evaporation” and the other term is “actual evaporation”. Potential evaporation is quite well understood when referring to water surfaces since the relative humidity of the water surface is equal to unity. However, the actual evaporation from a soil surface is related to the relative humidity in the soil at ground surface and may be less than unity. Actual evaporation depends on the temperature and suction or relative humidity at the soil surface. Accurate predictions or measurement of soil temperature and soil suction or relative humidity at ground surface are extremely important in the accurate calculation of actual evaporation. Soil suction not only depends on the character of the soil matrix but also on salt concentration in the pore-water.

In a soil-atmospheric model, the estimation of the soil surface relative humidity and actual vapor pressure at the soil surface is essential to the

calculation of the actual evaporation at soil surface. There have been several proposed formulas of either relative humidity or specific humidity at the soil surface. The first formula, which was established through the thermodynamic relationship between the liquid and vapour water phases, was referred to as Lord Kelvin's formula (Wilson, 1990). This formula is actually describing the relative humidity of the air immediately above the free-water surface in the soil pores. It was later used by many researchers such as McCumber and Pielke (1981), Camillo et al. (1983) and Wilson (1990). However, it was not supposed to represent the air specific humidity at the ground surface and failed to consider the resistance to water transport from the soil pores to the soil-atmosphere interface. It is thought that this theory may be invalid close to the soil surface, especially when the upper layer is dry (Wetzel and Chang, 1987; Avissar and Mahrer, 1988; Kondo et al., 1990; and recently Lee and Pielke, 1992). Three examples can be seen in Figures 1.1, 1.2 and 1.3 for the sand tested by Wilson (1990); Bruch (1993) and Yanful and Choo (1997), respectively where the surface relative humidity is still close to unity even when the Actual Evaporation has dropped far below the Potential Evaporation.

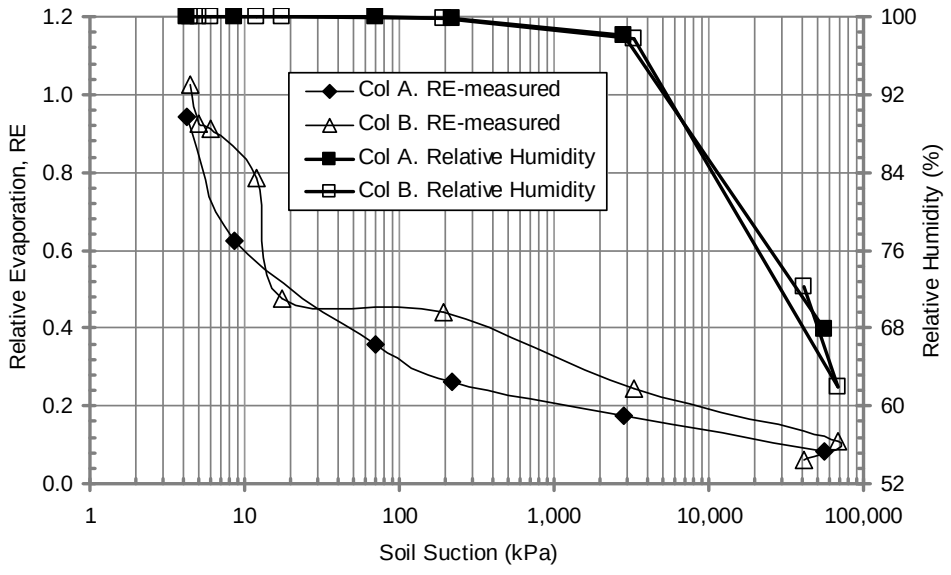

Figure 1.1 Illustration of Measured Relative Evaporation and Relative Humidity computed by Lord Kelvin's formula for Column A and B, Wilson (1990).

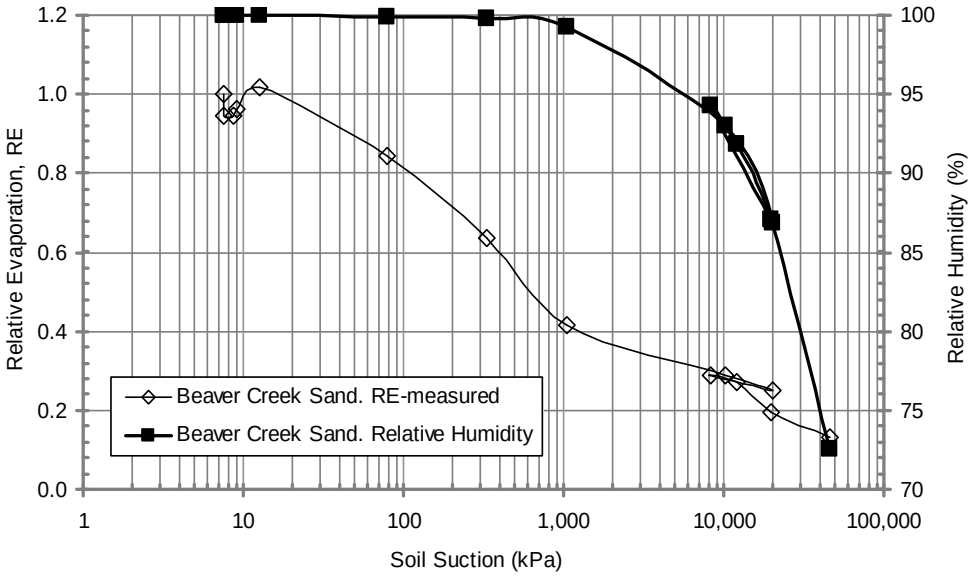

Figure 1.2 Illustration of Measured Relative Evaporation and Relative Humidity computed by Lord Kelvin's formula for Beaver Creek sand Column, Bruch (1993).

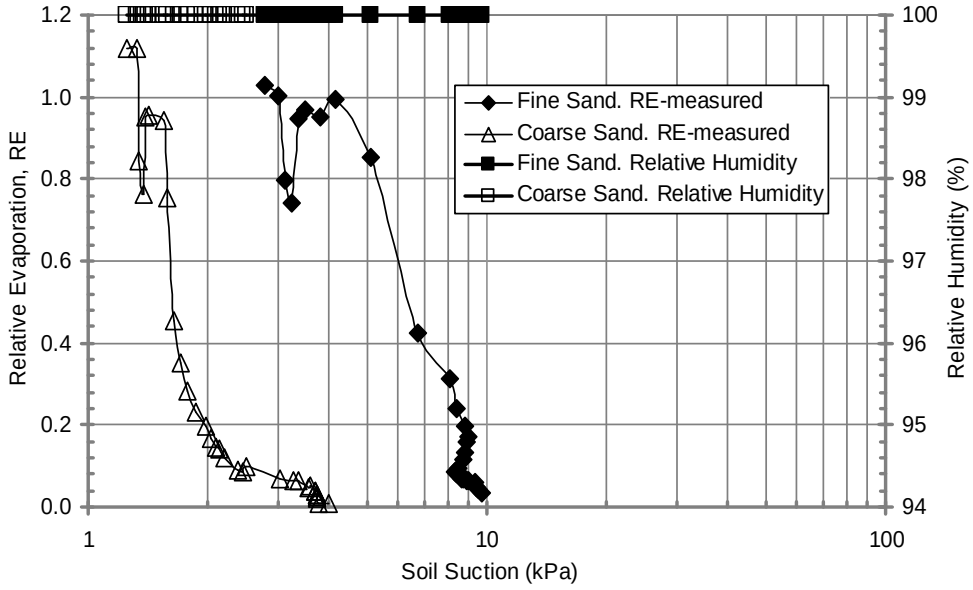

Figure 1.3 Illustration of Measured Relative Evaporation and Relative Humidity computed by Lord Kelvin's formula for Fine Sand and Coarse sand, Yanful and Choo (1997).

In an effort to overcome the deficiency of the Lord Kelvin's formula, it was suggested to introduce an adjustment factor of total suction at the topsoil

surface (Alvenas and Jansson, 1997; recently Fredlund et al., 2011; and Dunmola, 2012). Kondo et al. (1990) empirically developed a second formula by introducing an empirical resistance to the transport of water vapour from the soil pores to the soil-atmosphere interface. Lee and Pielke (1992) proposed another formula which introduced field capacity. The introduction of field capacity as a common reference point practically eliminated the dependence on soil texture (Alvenas and Jansson, 1997). Moreover, in geotechnical engineering, field capacity is not a soil property. Therefore it is difficult to convince geotechnical engineers to use field capacity when dealing with the calculation of relative humidity at the soil surface. Some recent methods of estimation of relative humidity will be reviewed in detail in Chapter 2 prior to further study.

In review of surface-resistance-type models of evaporation from a bare soil, the soil surface resistance was introduced to take into account a resistance to water vapour diffusion through the top of a thin soil layer (0 – 1 cm) to atmosphere. It is a factor to reduce actual evaporation during the drying process. All up-to-date empirical equations of the soil surface resistance were established by application of field capacity as a common reference point where the soil surface relative humidity should begin to reduce from unity. As stated previously, geotechnical engineers have difficulty accepting the term of field capacity. It is essential to introduce a new terminology of water content to account for reduction of evaporation rate.

To date there appears to be two approaches that can be used to estimate the actual evaporation from bare soil bodies (i.e., surfaces without vegetation). One approach is based on the soil suction and soil temperature (i.e., the relative humidity of soil surface; hence the actual vapour pressure) at the soil surface (Wilson, 1990; Yanful and Choo, 1997) while the other approach is based on the soil surface resistance and the actual vapour pressure at the soil surface, namely, a surface-resistance-type model (Mahfouf and Noilhan, 1991; van de Griend and Owe, 1994; Daamen and Simmonds, 1996; Aluwihare and Watanabe, 2003; Fujimaki et al., 2006; Bittelli et al., 2008; and recently Dunmola, 2012). The first approach gave equations of evaporation from the

soil surface without consideration of the soil surface resistance and was recognized to overestimate the evaporation rate due to an overestimation of the relative humidity at the soil surface. Although most estimations of evaporation made by the second approach were derived using energy balance and vapour mass transfer equations, they are not weather-climatic equations and may not be applicable. Recently though their use is becoming increasingly more popular. However there are some existing shortcomings in these equations due to an overestimation of the soil surface resistance.

Observation has shown that the evaporation from fine-grained tailings or paste tailings results in salt accumulations at the ground surface during the drying process. In these instances, a thin salt crust (less than 5 mm) was often seen to develop at the ground surface. Paste tailings from the Bulyanhulu gold mine in Tanzania (Simms et al., 2007) and fine-grained tailings in Western Australia (Newson and Fahey, 2003) are two examples where a thin salt crust can be seen to develop on the surface during the drying process. It has also been observed that once the salt crust develops and the underlying material begins to desaturate, the actual evaporation rate reduces substantially. In this thesis, laboratory experiments on saline soils (sand and silt) were conducted in order to verify such a phenomenon and explain the effect of osmotic suction on actual evaporation due to salt content accumulated on the soil surface.

Therefore, the objective of this thesis is to envisage the existing shortcomings stated in previous paragraphs and re-characterize the soil surface resistance, relative humidity and osmotic suction developed at the soil surface during the drying process. From these observations, a new climatological equation (i.e., related to net radiation, wind speed, air temperature) of evaporation from soil surface will be derived. Figure 1.4 gives an overview on what this thesis focuses.

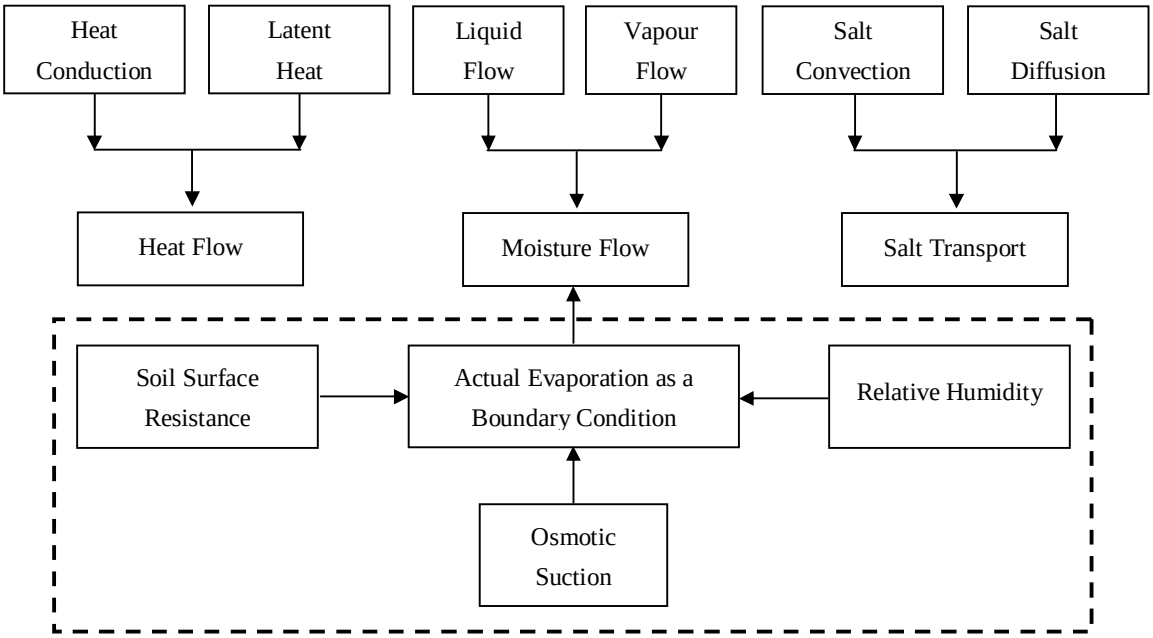

Figure 1.4 Components affecting the transport of water to soil surface.

1.2 RESEARCH OBJECTIVES AND SCOPE

The primary objective of this thesis is to develop a soil-atmospheric equation for the prediction of the actual evaporation from soil surfaces. While equations of moisture and heat flows from/to the soil surfaces of soil columns are available in the research literature, the moisture flux boundary condition is modified by applying the theory of the canopy effect and modification of the relative humidity at the soil surface.

The scope of this thesis is limited to a theoretical study, numerical modeling and a directed laboratory program. This research is intended to propose a new method to give better estimations of actual evaporation from soil surfaces. The research program of this thesis focuses on the evaluation of evaporation from non-vegetated soil surfaces. This approach is not intended to imply that the influence of vegetation is not important, but rather, that the presence of a vegetation cover greatly increases the complexity of the problem of the evaluation of evaporation.

1.3 RESEARCH METHODOLOGY

The research focus of this thesis utilizes the application of canopy-effect concepts for the prediction of the actual evaporation from soil surfaces. A number of methodological steps are established and is considered as a prerequisite for the fulfillment of the primary objective described in the previous section. The methodological steps are as follows:

(i) *Mechanistic soil-atmospheric modeling:* Review of theories associated with the physical processes and variables of the soil-atmospheric model. Further study of the canopy effect at soil surface and development of the current soil-atmospheric model;

(ii) *Data collection and evaporation-rate reduction assessment:* Collection of a database of soils from previous researchers and identifying at what suction and volumetric water content (or gravimetric water content) the actual evaporation rate begins to reduce from the potential evaporation rate. Introduction of new terminologies i.e., suction at evaporation-rate reduction point, volumetric water content or gravimetric water content at evaporation-rate reduction point; as well as modify the methods to predict the relative humidity and the corresponding actual vapour pressure at the soil surface;

(iii) *Laboratory program:* Carry out the laboratory tests to determine the actual evaporation rates from thin soil layers of bare soil surfaces with and without salinity; the actual evaporation fluxes from thick soil layers as well;

(iv) *Analyzing effect of osmotic suction on Actual Evaporation:* Presentation of evidence to account for the effect of osmotic suction on Actual Evaporation and computation of osmotic suction using the database of soils collected from the research literature and measured from the laboratory program;

(v) *Numerical modeling and model verification:* Computation and verification of numerical and analytical models based on the theories developed in the previous section. Suggest a new method to give better solutions on prediction of the actual evaporative flux.

The research methodology established herein was designed in order to envisage shortcomings in the previous methods presented in the literature section. First, the evaporation from a soil surface is based on molecular diffusion in the thin layer at the soil surface and turbulent diffusion in the air. In other words, the aerodynamic function for water vapour is different from that for heat transport; therein the terminology of the soil surface resistance was introduced and implemented.

Secondly, the relative humidity estimated by Lord Kelvin's formula is not representative when the soil is dry (Wetzel and Chang, 1987; Avissar and Mahrer, 1988; Kondo et al., 1990; Lee and Pielke, 1992; and more recently Alvenas and Jansson, 1997). It is suggested that this formula does not represent the air specific humidity at the ground surface and therefore fails to consider the resistance to water transport from the soil pores to the soil-atmosphere interface (Lee and Pielke, 1992).

Thirdly, the effect of osmotic suction on the actual evaporation was taken into account for the case of a saline soil surface boundary condition.

1.4 THESIS OUTLINE

This thesis is organized in seven chapters and six appendices. The present chapter has introduced the problems of predicting the flux boundary condition with respect to water at the surface of tailings or soil-cover surface. The existing issues such as the effects of osmotic suction and soil surface resistance on the evaporation rate from a soil surface, especially a saline-soil surface boundary are also presented. The objectives and scope of the thesis were presented in this chapter. The following paragraphs present a concise description of the contents of the remaining chapters:

Chapter 2 presents a literature review covering the phenomenon of evaporation from various regions around the world. A review of methods of evaporation rate as a boundary condition for the moisture flow is also presented in this chapter. A review of salt accumulation and its effect on evaporation (i.e., osmotic suction and salt crust resistance) from the soil surface during the drying process is presented. Equations to predict the relative humidity and the soil surface resistance at soil surface are reviewed as well. Finally, a review of moisture and heat flow equations currently available in the literature is presented.

Chapter 3 presents a review of the mechanism of mass and heat transfer and then provides the development of the actual evaporation rate as a boundary condition for the moisture flow using the existing soil surface resistance. Finally, this chapter also re-assesses the possibility of evaporation reduction. For example, at what suction or water content does the evaporation rate begin to reduce from the potential evaporation; as a result the equations of relative humidity and soil surface resistance will be modified.

Chapter 4 presents the laboratory testing program on Ottawa sand and Devon silt such as matric suction, total suction and evaporation rate on thin layers. This chapter also describes the laboratory testing procedures developed from the research literature.

Chapter 5 presents the laboratory testing results as well as the interpretation of the results measured in the laboratory program and those collected from the research literature. The explanation of effect of osmotic suction on the decrease in actual evaporation is also presented in this chapter.

Chapter 6 presents information on the verifications of the new proposed equations of the relative humidity and soil surface resistance for thin soil sections and soil columns. Comparisons are made between measured evaporative data and calculated results using the new proposed soil-atmosphere model presented in this chapter. The soil databases used in comparison include data collected from the research literature as well as test results obtained from the laboratory testing program.

Chapter 7 presents a summary of the previous chapters, conclusions and recommendations for future research.

CHAPTER 2
LITERATURE REVIEW

2.1 GENERAL

The inter-boundary exchange of water between the soil and atmosphere above constitutes an important component of hydrologic cycle, as shown in Figure 2.1. This exchange primarily occurs through two processes i.e., infiltration and evaporation (Wilson et al., 1991; Dunmola, 2012). Many researchers, scientists and practitioners in various disciplines may be interested in evaporation for different purposes. For example, while geotechnical engineers may be interested in the development of shear strength of earth structures resulting from evaporation as well as the contribution of evaporation to the stability of natural and engineered slopes, geo-environmental practitioners may be interested in the long-term performance of soil covers deployed over mine waste when such covers are subjected to excessive evaporation (Dunmola, 2012).

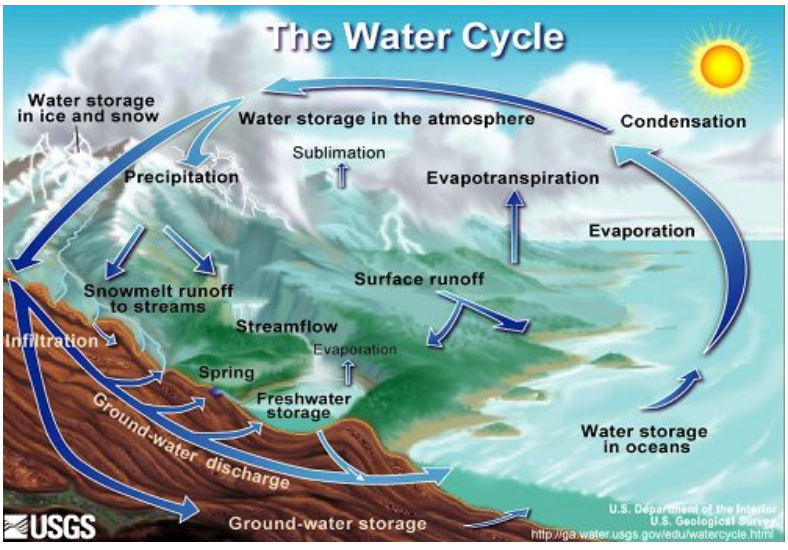

Figure 2.1 Illustration of hydrologic cycle in nature. (http://ga.water.usgs.gov/edu/watercycle.html)

The concepts behind the evaporation of water from the soil surface can be described as follows. Net radiation from the sun heats the ground surface and the air above the ground surface. Wind provides a mixing effect of the air near to the ground surface which results in a removal of water vapour from near ground surface. At the same time when the sun and the wind are removing water vapour from the ground surface, the soil is holding onto and storing water in the pores (i.e., soil suction). It is also hard to deliver water to the ground surface because the permeability of the unsaturated soil can become extremely low. The net result of the competition between the weather-related factors and suction in the soil is a reduction in evaporation from potential evaporation conditions to the net moisture flux or actual evaporation.

Vapour pressure gradients constitute the fundamental driving mechanism for vapour flow (Edlefsen and Anderson, 1943). Weather conditions above the ground surface create a relative humidity (or vapour pressure) condition in the air immediately above the ground surface. The air in the soil at the ground surface also has a relative humidity that is related to the total suction through thermodynamic considerations. The difference in vapour pressure between the soil and the overlying air provides the vapour pressure gradient for actual evaporation. If the vapour pressure in the air above the ground surface and the vapour pressure in the soil at the ground surface are the same, then evaporation from the ground surface will cease since there is no longer a vapour pressure gradient (Fredlund et al., 2011).

The objective of this chapter is to review the evaluation of evaporation from surfaces as well as research contributions relative to earlier work regarding measurement and calculation of evaporation from soil surfaces. Finally, equations describing the flow of water and heat in a soil body are reviewed as well.

2.2 CLIMATOLOGICAL METHODS TO ESTIMATE POTENTIAL EVAPORATION

Evaporation is defined as the rate of liquid water transformation to vapour from open water, bare soil, or vegetation with soil beneath to atmosphere. The mechanism of the evaporative flux has been studied in different ways by many researchers during last several decades. Accordingly, there are three primary and independent factors that influence evaporation from a surface. The energy at the evaporating surface where water can evaporate constitutes the first factor. The second factor is called the aerodynamic function which depends on the vapour pressure gradient between the evaporating surface and the overlying air and the profile of turbulent mixing above the evaporating surface. The third factor that influences evaporation is the availability of water at and below the evaporating surface. The availability of water depends on the water hydraulic conductivity and water storage in the soil (Newson and Fahey, 2003). Recently geotechnical and geo-environmental engineers are frequently called upon to predict evaporation from soil cover as oxygen barriers for acid-generating pyritic mining tailings and from surface-deposited thickened tailings at remote sites.

To date there are many climatological based methods for predicting potential evaporation which are considered to be acceptable for many applications geotechnical engineering. This may be mainly attributed to the fact that these methods require only routine climate data such as net radiation, average temperature, and relative humidity. These methods were developed for either a free water surface or a wet soil surface and hence have limitations in applying to unsaturated soil surfaces. However, the methods developed for the free water surface serves as a reference for estimation of evaporation from soil surfaces. Therefore, it is necessary to review several climatological methods for predicting potential evaporation and methods to predict heat budget using routine climate data herein.

In general, there are three major approaches to estimating evaporation rate and they can be classified as the energy balance method, the aerodynamic method

and a combination of the energy balance and aerodynamic methods. Penman (1948) is the first researcher to combine the energy balance and aerodynamic methods to formulate the equation for *Potential Evaporation*. Several equations for potential evaporation are summarized in Table 2.1 and some of them are reviewed in greater detail in the following section.

Table 2.1 Equations for the indirect calculation of *Potential Evaporation, PE (adapted after Gitirana, 2005).*

Method (1)	Equation (2)	Eq.# (3)	Input parameters (4)
Dalton type equation	$PE = f(u)(p_{vsat} - p_v^{air})$	(2.1)	$f(u)$ = a transmission function which depends on the mean wind speed and turbulent mixing; p_v^{sat} = surface saturation vapour pressure; p_v^{air} = vapour pressure at the near ground surface air.
Water mass conservation	$PE = P - R$	(2.2)	P = precipitation, mm/day; R = runoff, mm/day.
Energy budged (Bowen ratio)	$PE = \frac{Q_n}{\rho_w L_v (1+R)}$	(2.3)	Q_n = net radiation, J/m^2 s; ρ_w = water density, kg/m^3; L_v = latent heat of vaporisation, J/kg; R = Bowen ratio.
Mass transfer Rohwer (1931)	$PE = 0.44(1+0.118u)(p_v - p_v^a)$	(2.4)	u = wind speed, miles/h; p_v = evaporating surface vapour pressure; p_v^a = vapour pressure above the surface;
Aerodynamic Equation Thorntwaite and Holzman (1942)	$PE(x_0, y_0) = Cu_2^{0.76} x_0^{0.88} y_0 (p_v - p_v^a)$	(2.5)	x_0, y_0 = evaporating area, m; C = constant related to the temperature; u_2 = wind speed at 2 m, miles/day; p_v = vapour pressure at the surface; p_v^a = vapour pressure above surface unaffected by evaporation.

Thornthwaite (1948)	$PE = 1.6\left(\frac{L}{12}\right)\left(\frac{N}{30}\right)\left(\frac{10T_a}{30}\right)^a$	(2.6)	L = length of daylight, hours; N = number of days during the month; T_a = mean monthly air temperature, ^oC; a =6.75x10^{-7}I^3–7.71x10^{-5}I^2–1.79x10^{-2}I–0.492 I = Σ12month=1(T_a / 5)1.514.
Combined method Penman (1948)	$PE = \frac{\Gamma Q_n + \eta E_a}{\Gamma + \eta}$	(2.7)	Γ = slope of the saturation vapor pressure; versus temperature curve, mmHg/^{o}F; Q_n = net radiation at the surface, m/s; η = psychrometric const., 0.27 mmHg/^{o}F; E_a = 0.35(1 + 0.15W$_w$)($p_{vsat}^{air} - p_v^{air}$), m/s; W$_w$ = wind speed, km/h; p_v^{air} = near surface air vapour pressure.
Blaney and Criddle (1950)	$PE = (0.457T + 8.13)p$	(2.8)	T = mean daily temperature, ^oC; p = mean annual fraction of day that is in daylight.
Jensen and Haise (1963)	$PE = (0.025T + 0.078)\frac{R_s}{59}$	(2.9)	T = air temperature, ^oC; R_s = incident solar radiation, mm/day.
Penman-Monteith Monteith (1965)	$PE = \frac{1}{\lambda}\left[\frac{\Gamma A + \rho_a c_p D / r_a}{\Gamma + \eta(1 + r_s / r_a)}\right]$	(2.10)	Γ, η = same as in Penman (1948), kPa/^{o}C; $A = R_n - G$, MJ/m^2 day; ρ$_a$ = air vol. heat capacity, MJ/m^3 ^{o}C; c_p = vapour pressure deficit, kPa; D = fraction of day that is in daylight; r_s, r_a = canopy and aerodynamic resistances to vapour transfer, day/m.
Priestley-Taylor (1972)	$PE = \alpha\frac{\Gamma}{\Gamma + \eta}(R_n - G)$	(2.11)	α = empirical constant; Γ, η = same as in Penman (1948); R_n = net radiation, mm/day; G = soil heat flux, mm/day.
Hargreaves (1985)	$PE = 0.0023S_0\sqrt{\delta_T}(T + 17.8)$	(2.12)	S_0 = extraterrestrial radiation, mm/day; δ_T = difference between the mean monthly maximum and minimum temperature, ^oC; T = temperature, ^oC.

2.2.1 The Penman Method

Penman (1948) proposed a method of calculating potential evaporation by using the energy balance and the mass transfer (or aerodynamic) equations simultaneously. The approach is often referred to as the combination method as the formulation is based on the combination of energy budget and the mass transfer equation. The equation presented by Penman (1948) for calculating potential evaporation rates is as follows:

$$PE = \frac{\Gamma Q_n + \eta E_a}{\Gamma + \eta} \tag{2.13}$$

where:

PE = potential evaporation per unit time, mm/day;

$E_a = f(u)(e_{sa} - e_a)$

e_{sa} = saturation vapour pressure of the mean air temperature, usually mm.Hg;

e_a = vapour pressure of the air above the evaporating surface, usually mm.Hg;

$f(u) = 0.35(1 + 0.146U_a)$

U_a = wind speed, usually km/hr;

Q_n = heat budget or all net radiation, mm/day;

Γ = slope of the saturation vapour pressure versus temperature curve at the mean temperature of the air, Pa/ ^oC;

η = psychometric constant, Pa/ ^oC.

The popularity enjoyed by the method is a result of its simplicity and ease of application. The Penman formula requires only the measurement of routine weather parameters such as air temperature, relative humidity and wind speed. The heat budget or all net radiation term may be determined on the basis of the empirical formula given by Penman (1948) is as follows:

$$Q = R_c(1 - r) - \tau T_a^4 (0.56 - 0.092\sqrt{e_a})\left(0.10 + \frac{0.90n}{N}\right) \tag{2.14}$$

where:

R_c = shortwave radiation measured at the site, MJ/m^2;

and

$R_c = 0.95R_a\ (0.18 + 0.55n/N)$

R_a = solar radiation (from charts) for a completely transparent atmosphere, MJ/m^2;

r = reflectance coefficient;

τ = Stefan-Boltzman constant;

T_a = air temperature, Kelvin;

n/N = ratio of actual/possible sunshine hours.

The formula given above by Penman (1948) is most applicable to open water surfaces. However, Penman (1948) extended his formulation to include bare soil and turf (grass) covered surfaces with a plentiful water supply. Monteith (1965) reports that, *"Penman found that the evaporation from well-watered turf was a fraction (f) of open-water evaporation ranging from 0.6 in winter to 0.8 in summer"*.

2.2.2 The Penman-Monteith Method

Studies on the estimation of evaporation originate in the field of hydrology. Penman (1948) was the first researcher to study the evaporation from a free surface pan of water. Later, these results were referred to as potential evaporation. Penman's formula generally over-estimates the actual evapotranspiration when applied to drier regions (Morton, 1969; 1971; 1975; and 1985). Penman found that the evaporation from well-watered turf was a fraction *(f)* of open-water evaporation and ranged from 0.6 in winter and 0.8 in summer. Although he attempted to find a rational explanation for these factors, he was not entirely successful. The simplicity of the Penman (1948) approach attracted many researchers and encouraged attempts to correlate the (*f)* ratio with soil-water content (Monteith, 1965). Doornenbos and Pruitt (1977) developed empirical models which allow crop evaporation to be calculated as a function of stage of growth. Other researchers have defined a quantity similar to the *f* ratio in terms of actual evaporation rate to maximum evaporation rate. It has been demonstrated in restricted circumstances that this

quantity can be predicted from the soil-water content (Ritchie, 1972). Monteith (1965) stated that "*the rate of actual to maximum transpiration for open-water evaporation is a function of mean stomatal resistance, leaf area, windspeed, and crop roughness and therefore cannot be uniquely related to soil-water content or any other simple index of water availability*". Various derivations of the Penman equation included a bulk surface resistance term (Penman, 1953; Covey, 1959; Rijtema, 1965; and Monteith, 1965). The resulting equation is now called the Penman-Monteith equation which represents the evaporating surface as a single "big leaf" (Raupach and Finnigan, 1988) with two parameters; namely, aerodynamic resistance and surface resistance. The Penman-Monteith formula for estimating the evaporation is written as:

$$ET = \frac{\Gamma Q_n + \frac{\rho_a C_p (e_a^* - e_a)}{\lambda \rho_w r_{av}}}{\Gamma + \eta\left(1 + \frac{r_s}{r_{av}}\right)} \qquad (2.15)$$

where:

e^*_a = saturated water vapor pressure at T_a, kPa;

e_a = actual water vapor pressure at T_a, kPa;

Q_n = total net radiation input in mm/day

Γ = slope of the relationship between water vapor pressure and temperature at as specific temperature, Pa/ ^oC;

η = psychromatric constant, 66.8 Pa/ ^oC;

ρ_a = density of air, kg/m^3;

C_p is a specific heat of air (J/kg. ^oK);

r_{av} = the aerodynamic resistances for vapor in s/m;

r_s = the soil surface resistance which results from diffusion across the water-air interface localized in the pores and the water surface to the ground surface through the pores of a dry top layer, unit of s/m;

λ = latent heat of vaporization of air, λ= 2.45e6 J/kg;

ET = transpiration rate from leaf or evaporation rate which is a two step process (mm/day).

The Penman-Monteith method offers some advances in estimating the evaporation from soil surface. Firstly, the Penman-Monteith method can give an estimation of the potential evaporation from a wet soil surface including water diffusion across the water-air interface localized in the pores and the water surface to the ground surface through the pores of a dry layer. Secondly, the Penman-Monteith equation could be modified to estimate approximately the evaporation from a saline water surface by taking the relative humidity at the evaporating surface into account.

2.3 METHODS TO ESTIMATE ACTUAL EVAPORATION FROM THE GROUND SURFACE

The traditional methods for calculating evaporation available in the previous section attempt to predict a maximum or potential rate of evaporation. The fundamental assumption used by the methods above is that water is freely available at the surface for evaporation. In other words, the surface is an open water surface or a saturated soil surface (Wilson et al., 1994). However, evaporation from a soil surface begins to decline as the surface becomes unsaturated and the supply of water to the surface becomes limited (Gray, 1970; Morton, 1975; Brutsaert, 1982; and Wilson et al., 1994). Such evaporation is defined as actual evaporation from soil surface. Declination of the actual evaporation was initially understood that relative humidity at the soil surface decreases due to a reduced availability of liquid water at the soil surface. Later the declination was also accounted for by the development of surface resistance during the drying process. This section focuses on review two approaches to predict actual evaporation from ground surface during last several decades.

The shape of the drying curve shown in Figure 2.2 is well known and has been described by others including Hillel (1980). In general, the drying process undergoes three stages of drying. Stage I of drying process is controlled by climatic conditions and is referred to a constant-rate stage in which the evaporation rate of soil is equal to that from a free water surface at the same

climatic conditions. The evaporation rate in this stage is called *Potential Evaporation* which is a maximum rate of evaporation. Stage II of the drying process begins when the flow of water below cannot supply sufficient groundwater to the surface to maintain potential rate of evaporation. This stage is called a falling-rate stage. During this stage, the evaporation rate continues to decline as the surface continues to desiccate and reaches a low residual value defined as stage III of the drying process which is called a low-rate stage. During Stage III, the soil surface becomes sufficiently desiccated to cause the liquid-water phase to become discontinuous. The flow of liquid water to the surface stops and a few millimetres of the soil surface dry out to air relative humidity; hence water molecules may only migrate to the surface through the process of vapour diffusion (Wilson et al., 1994).

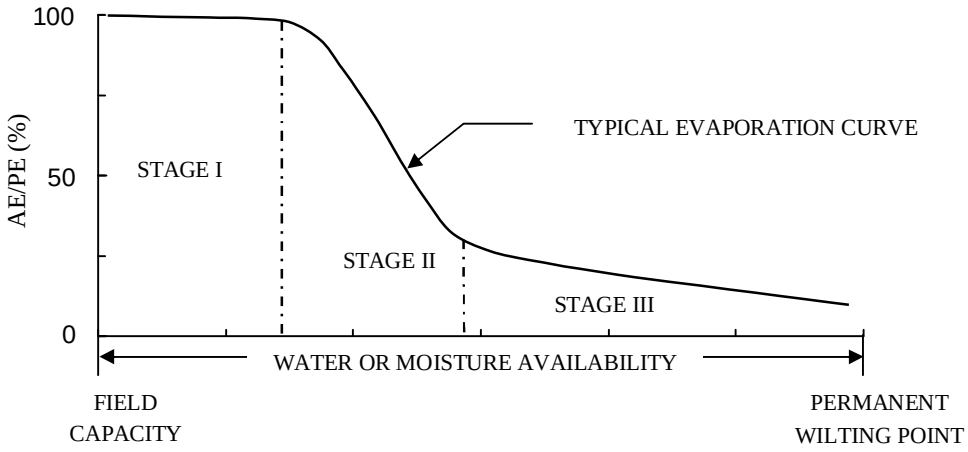

Figure 2.2 The relationship between the rate of actual evaporation and potential evaporation (*AE*/PE) and water availability (after Wilson et al., 1994).

Some equations for *Actual Evaporation* are summarized in Table 2.2 and each equation in the table above has its own advantage and disadvantage. A detailed review of these equations is presented in the following section.

Table 2.2 Equations for the indirect calculation of *Actual Evaporation, AE*

Method (1)	Equation (2)	Eq.# (3)	Input parameters (4)
Modified Penman (Wilson, 1990)	$AE = \frac{\Gamma Q_n + \eta E_a}{\Gamma + \eta A}$	(2.16)	Γ, Q_n, η, W_w, p_v^{air} = as in Penman (1948); AE = actual evaporation; $E_a = 0.35(1 + 0.15W_w)p_v^{air}(B - A)$, m/s; $A = 1/RH$; $B = 1/RH_{air}$; RH = relative humidity at the surface; RH_{air} = relative humidity of the air.
Limiting function (Wilson et al., 1994)	$AE = PE\frac{p_v - p_v^{air}}{p_{vsat} - p_v^{air}} = PE\left[\frac{RH - \left(p_{vsat}^{air} / p_{vsat}\right)RH_{air}}{1 - \left(p_{vsat}^{air} / p_{vsat}\right)RH_{air}}\right]$	(2.17)	AE = actual evaporation; p_v = vapour pressure at the soil surface; p_v^{air} = vapour pressure at the near ground surface air; p_{vsat}^{air} = saturation vapour pressure at the near ground surface air; p_{vsat} = surface saturation vapour pressure; RH, RH_{air} = same as in Wilson (1990).
Empirical Experimental function (Wilson et al., 1997)	$AE / PE = exp\left(\frac{-\psi g \omega_v}{\zeta(1 - RH_{air})\gamma_w R(T + 273.15)}\right)$	(2.18)	AE = actual evaporation; PE = potential evaporation; T = temperature at the soil surface; ψ = total suction at the soil surface; ζ = a dimensional empirical parameter with a suggested value of 0.7 R = universal gas constant g = gravity acceleration; ω_v = molecular weight of water; γ_w = unit weight of water; RH_{air} = same as in Wilson (1990).

2.3.1 Models without Application of Surface Resistance

Although the applications of the methods for potential evaporation have some limitations as described in Sections 2.2.2 and 2.2.3, these methods have been applied to evaluate actual evaporation from ground surface in some cases.

Wilson et al. (1990; 1994; 1997) tried to overcome the limitations of those methods by introducing three equations for the calculation of non-potential evaporation from unsaturated soil surfaces based on climatic conditions and results of laboratory testing evaporation on Beaver Creek sand, Custom silt and Regina clay. These equations have later been used by some researchers including Bruch (1993), Yanful and Choo (1997), Simms et al. (2007) and Dunmola (2012).

A review of development of Wilson's equations is presented in this section prior to further study on evaporation from soil surface.

2.3.1.1 The Wilson-Penman Equation

Wilson (1990) proposed a modification to the well-known Penman (1948) equation for the calculation of the potential evaporation. This modification is also based on the combination of the energy budget and mass transfer at the ground surface. The main assumption to derive Wilson equation (1990) is to assume the functions of a wind speed are the same for the evaporative flux and heat flux equations. Wilson included the relative humidity of soil surface in his equation so that it can estimate evaporation rate from unsaturated surfaces. The equation presented by Wilson (1990) for calculating actual evaporation rates is as follows:

$$AE = \frac{\Gamma Q_n + \eta E_a}{\Gamma + \eta A} \tag{2.16}$$

where:

AE = Evaporation rate from soil surface in mm/day;

Q_n = total net radiation input in mm/day;

Γ = slope of the relationship between water vapor pressure and temperature at as specific temperature, Pa/ ^{o}C;

η = psychrometric constant, 66.8 Pa/ ^{o}C;

E_a = aerodynamic evaporative term, $E_a = f(u)e_a(B - A)$ where $f(u)$ is called as a wind function in mm/day/Pa;

B = inverse of relative humidity at air temperature; and

A = inverse of relative humidity at soil surface temperature.

The primary advantage of Wilson equation (1990) is to be able to reduce to the Conventional Penman equation (1948) for open-water evaporation by taking the relative humidity of soil surface to be unity (i.e., a saturated surface). Furthermore, Wilson (1990) noted that his equation can be reduced to the Priestly-Taylor Model when relative humidity of the air and soil are equal to 100 percent. However, the main disadvantage of the method is that it assumes *f'(u)* in the heat flux equation equal to *f(u)* in the evaporative flux equation using the Principle of Similarity. The validity of this assumption in all applications should be re-evaluated because of the principal similarity of diffusion coefficients. Recently the Wilson-Penman's equation was recognized to over-estimate of the rate of evaporation from a bare soil and saline soil surfaces (Dunmola, 2012).

It is the difficulty in determination of the relative humidity of the soil surface. This will be overcome if the soil temperature and total suction at the soil surface are known. Practically, those data should be measured at the ground surface. However, the measurement during seasons is a challenge. Theoretically, the soil temperature and total suction are resulted from solving partial differential equations of heat flow and moisture flow. The boundary condition of heat flow is estimated using the following equation in which soil surface temperature is a function of the air temperature above the soil surface.

$$T_s = T_a + \frac{Q_n - AE}{C_f \eta f(u)} \tag{2.19}$$

where:

T_s = soil surface temperature, ^{o}C;

T_a = air temperature above the soil surface, ^{o}C; and

C_f = conversion factor, (i.e., 1kPa = 0.00750 mmHg).

2.3.1.2 Limiting Function of Air Pressure Equation

Wilson (1990) conducted soil evaporation tests in the laboratory on three different soil samples of Beaver Creek sand, Custom silt, and Regina clay. The very thin soil sections were saturated and allowed to evaporate to a completely air-dried state. The actual evaporation rate for each soil surface was measured along with the potential evaporation rate for an adjacent water surface (Wilson, 1990). The ratio of actual evaporation to potential evaporation or normalized soil evaporation was then evaluated with respect to drying time, soil-water content, and soil suction. The value of the normalized soil evaporation was found to be approximately equal to unity for all soils until the total suction at the soil surfaces reached approximately 3,000 kPa. The rate of actual soil evaporation was observed to decline when the total suction exceeded 3,000 kPa. A relationship between the actual evaporation rate and total suction which was found to exist for all three soil types appears to be universal and independent of soil texture, drying time, and water content (Wilson et al., 1994).

From results of the thin soil section drying tests, Wilson et al. (1994) proposed a simple equation for calculating actual evaporation from the relative humidity equation for air. The equation takes the form of a "Limiting Function" between zero and potential evaporation depending on the vapour pressure in the soil at ground surface. The actual evaporation is scaled in accordance with Lord Kelvin's equation. The "Limiting Function" equation is written as follows:

$$AE = PE \frac{u_v - u_v^{air}}{u_{v0} - u_v^{air}} \tag{2.17}$$

where:

AE = actual evaporation in mm/day;

PE = potential evaporation in mm/day;

u_v = actual vapour pressure at the soil surface, kPa;

u_{v0} = saturated vapour pressure at the soil surface temperature, kPa;

u_v^{air} = vapour pressure in the air above the soil surface, kPa.

This method by Wilson et al. (1994) gives correlation between actual evaporation and potential evaporation at the same climatic conditions. The inherent weakness of this method is the assumption that the air and soil temperatures are the same. This method was only verified with testing evaporation from very thin layers of sand, silt and clay by Wilson (1990).

2.3.1.3 Empirical Experimental Function of Total Suction Equation

Wilson et al. (1994) presented experimental results that showed a unique relationship between total suction at the soil surface and the ratio of *Actual Evaporation* to *Potential Evaporation, AE/PE*. In 1997, Wilson, Fredlund and Barbour presented an equation that matched the experimental data with reasonable fit. As a consequence, there was another way to empirically relate *Actual Evaporation* and *Potential Evaporation*. Accordingly, the ratio of actual evaporation to potential evaporation, *AE/PE*, can be approximated using the form of the thermodynamic equilibrium relationship between relative humidity and total suction (Edlefsen and Anderson, 1943). The ratio of *AE/PE i*s written as follows:

$$AE / PE = exp\left(\frac{-\psi g \omega_v}{\zeta(1-h_a)\gamma_w R(T_s + 273.15)}\right) \qquad (2.18)$$

where:

ζ = a dimensional empirical parameter with a suggested value of 0.7;

h_a = relative humidity of overlying air;

ψ = total suction (i.e., matric suction plus osmotic suction), kPa;

ω_v = molecular weight of water, 0.018 kg/mol;

γ_w = unit weight of water, 9.807 kN/m^3;

g = gravity acceleration, m/s^2;

R = universal gas constant, 8.314 J/(mol.K); and

T_s = soil surface temperature, ^{o}C.

This equation results from the evaporation rate of Beaver Creek sand, Custom silt and Regina clay with very thin layers. However, its application is limited in that equation (2.18) has not been checked for the thicker layers of soil.

2.3.2 Surface-Resistance-Type Models

The researchers including Camillo and Gurney (1986), Kondo et al. (1990), Lee and Pielke (1992), van de Griend and Owe (1994), Alvenas and Jansson (1997), and Bittelli et al. (2008) suggested that using only the aerodynamic resistance induces overestimation for dry soils because of the assumption of equilibrium in Philip's formula. It was suggested that the Philip's formula is invalid near the surface of a natural soil. It is actually describing the specific humidity of the air immediately above the free-water surface in the soil pores. This formula has also been misused in numerical models since it does not represent the air specific humidity at the ground surface and it fails to consider the resistance of water transport from the soil pore to the soil-atmosphere interface (Wetzel and Chang, 1987; Avissar and Mahrer, 1988; and Kondo et al., 1990). Lee and Pielke (1992) pointed out that the surface relative humidity estimated by Philip's formula is still close to unity even when the volumetric soil-water content has dropped far below the permanent wilting point. Many researchers (Daamen and Simmonds, 1996; Mohamed et al., 1997; Aluwihare and Watanabe, 2003; Bittelli et al., 2008; and Dunmola, 2012) tried to overcome limitations of equations for calculating potential evaporation by introducing a model related to soil surface resistance to propose equations for calculating non-potential evaporation; hence such a model is called a surface-resistance-type model.

The surface-resistance-type model of evaporation from a bare soil surface is supposed to consists of two processes. In the first process, water vapour is transported by molecular diffusion from the water surface in the soil pore to the soil surface. In the second process, water vapour is carried from the soil surface to the atmosphere by laminar or turbulent airflow. Most of these

surface-resistance-type models results from the energy balance of the ground surface (van de Griend and Owe, 1994) as follows:

$$R_{net} + \lambda E + H = G \tag{2.20}$$

where:

R_{net} = the net radiation,

λE and H = the latent and sensible heat fluxes, respectively;

G = the soil heat flux;

All fluxes are expressed in W/m^2.

It is noted that the aerodynamic resistance for water vapour and sensible heat transport from the surface upward to some reference level is assumed to be the same, the latent and sensible heat fluxes can be expresses as,

Latent flux, $$\lambda E = -\frac{\rho c_p}{\gamma}\frac{e_s - e_a}{r_s + r_{av}} \tag{2.21}$$

Sensible flux, $$H = -\rho c_p \frac{T_s - T_a}{r_{ah}} \tag{2.22}$$

where:

e_s = the vapour pressure at the ground surface, kPa;

e_a = the vapour pressure of the air at reference level, kPa;

T_a = the temperature of the air at reference level, ^{o}C;

T_s = the temperature at ground surface, ^{o}C;

r_{av} and r_{ah} = the aerodynamic resistances for vapour and sensible heat, respectively, s/m; and

r_s = the surface resistance, s/m.

Mahfouf and Noilhan (1991) and then Daamen and Simmonds (1996) reviewed surface- resistance-type models of evaporation from bare, most of which are formulated from,

$$E_s = \frac{e_s - e_a}{r_s + r_a} \tag{2.23}$$

where:

e_s = either (1) the saturated absolute humidity at soil surface temperature, (2) the actual absolute humidity at the soil surface, or (3) the absolute humidity at the liquid/vapour interface level at some depth in the soil, depending on which variant of the model is being used, kg/m^3;

e_a = the vapour pressure of the air at reference level, kg/m^3;

r_a = the aerodynamic resistances for vapour, s/m; and

r_s = the surface resistance, s/m.

Aluwihare and Watanabe (2003) proposed two equations of evaporation from land surface depending on availability of water on top soil. These equations incorporated the afore-mentioned two processes and assumed that vapour fluxes are equal during migration from the soil pores to atmosphere. They can be expressed as follows:

For wet top soil,

$$E = \rho \frac{q^*(T_s) - q_a}{r_a + r_s} \tag{2.24}$$

where:

$q^*(T_s)$ = saturated specific humidity of the air adjacent to the soil water, kPa;

q_a = specific humidity of air at the soil surface, kPa;

ρ = density of air, kg/m^3;

r_s = soil surface resistance, s/m;

q_a = specific humidity at a reference level in the atmosphere, kPa; and

r_a = aerodynamic resistance to vapour transfer, s/m.

For dry top soil,

$$E = \rho \frac{q^*(T_e) - h_a q_a^*(T_a)}{r_{sw} + r_d + r_a} \tag{2.25}$$

where:

$q^*(T_e)$ = saturated specific humidity at the evaporative surface temperature T_e in Kelvin;

q_e = specific humidity of pore air at the evaporative surface, kPa;

r_{sw} = resistance imposed on the vapour flux while traveling from the pore of the wet soil layer to the bottom pores of the dry soil layer adjacent to the evaporative surface, s/m;

r_d = resistance imposed on vapour flux in the dry soil layer, s/m;

r_a = aerodynamic resistance to the vapor transfer from the soil to the abovementioned reference height, s/m;

h_a and T_a = relative humidity and temperature of air at a reference height in the atmosphere, respectively; and

$q_a^*(T_a)$ = saturated specific humidity at the air temperature, kPa.

Similarly, Fujimaki et al. (2006) proposed an equation of evaporation from saline soil by adding additional resistance, r_{sc}, (due to a salt crust formed during process of drying) to the denominator of equation (2.24). The additional resistance to vapour diffusion caused by salt crust was evaluated by laboratory tests on drying saline soil columns i.e., Masa loamy sand with Potassium Chloride and Toyoura sand with Sodium Chloride.

Dunmola (2012) carried out a series of laboratory drying tests on non-saline silts of 10 cm soil columns and 2 mm thin soil section. The temperature of the air, the relative humidity of the air and the total suction near the soil surface were continuously measured along with the measurement of the ratio of the rate of actual soil evaporation to the rate of potential evaporation (*AE/PE*). The numerical modeling used Wilson et al. (1997) model (i.e., Eq. 2.16) to predict the ratio of *AE/PE*. As a result, Wilson et al. (1997) model was only validated

for thin soil layers of 2 mm, but not validated for soil columns of 10 cm. Dunmola (2012) inferred that in case of the 10 cm soil columns other water transport process(es) at depths below the soil surface may affect the evaporation rate along with the total suction at the soil surface.

2.4 EFFECT OF OSMOTIC SUCTION AND SOIL SURFACE RESISTANCE DEVELOPED IN SOILS

The objective of this section is to present a review of evaluation the actual evaporation from the ground surface and effects of salt accumulation such as osmotic component and soil surface resistance developed at soil surface. The description of evaporation process from paste tailings and soil cover surfaces shows that the phenomenon of salt accumulation on those surfaces exists. This phenomenon can be seen from field and laboratory experiments. Some examples of certain regions around the world are presented to demonstrate the background problems which are stated in this thesis.

According to the report by Minerals and Energy Research Institute of Western Australia (MERIWA), in the arid regions of Australia, ore processing in the Western Australia gold mining mills have utilized large volume of hyper-saline water with salt concentrations (C = mass of salt/mass of solution) of up to 0.2 (approximately seven times that of sea water). As a consequence, much of the material in tailings storages has extremely high salinities that can approach solution saturation concentration (C=0.26). Fine-grained tailings produced in gold mining operations in this arid region are deposited by thin layers maximize benefits from the evaporation. A phenomenon that a surficial salt crust of about 5 mm thick is formed is often seen in the deposition of hyper-saline tailings. These soluble salts accumulate as evaporation removes water from the tailings. Observations have demonstrated that the evaporation rate reduces during forming thin salt crust. Typical tailings storage in Western Australia is shown in Figure 2.3.

Figure 2.3 Typical saline gold tailings storage in arid region, Western Australia (Newson and Fahey, 2003).

Fahey and Fujiyasu (1994) have carried out tests to determine the rate of evaporation from saline surfaces with various initial salt concentrations thereby demonstrating the effect of salinity of tailings water on the rate of evaporation. A series of laboratory evaporation experiments was conducted using artificial tailings mixed with water with various initial salt (NaCl) contents, ranging from freshwater (zero salt content) to a concentration of 0.23. The experimental results indicate that even a moderate amount of salinity can severely reduce the relative evaporation (ratio of actual evaporation to potential evaporation) from the tailings surface.

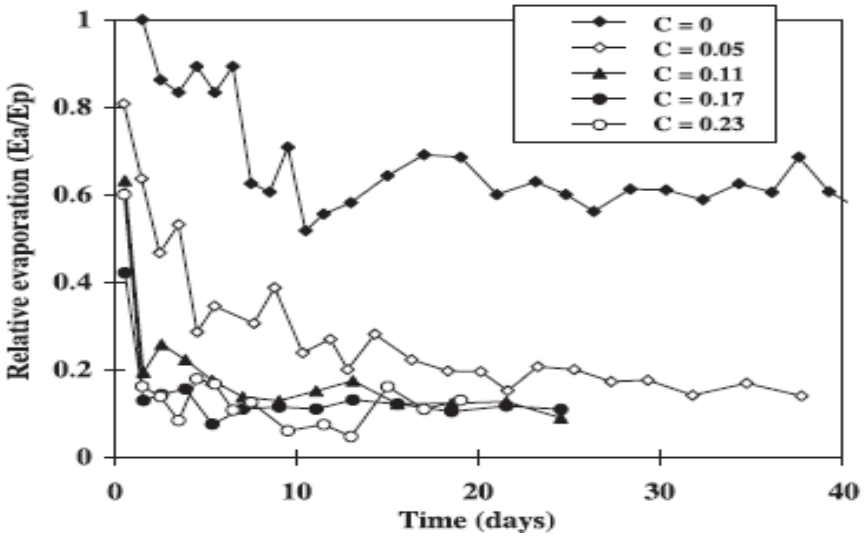

Figure 2.4 Evaporation from saline tailings surfaces with various initial salt contents (Fahey and Fujiyasu, 1994).

Simms et al. (2007) observed the evaporation process of deposition of paste tailings occurring at Bulyanhulu gold mine in Tanzania. They also conducted a series of laboratory and field trials to study evaporation from tailings at the same place. The laboratory tests included two "large-scale" experiments on 10 cm thick layers of tailings 2 m by 1 m in plan, and a smaller column test on a 20 cm thick and 20 cm diameter sample.

It was observed that the formulation of a white precipitates at the surface of the tailings. These precipitates were composed of gypsum and magnesium sulphate salts. It was predicted that the higher rate of evaporation would have increased the total mass of salts brought to the surface, resulting in a more noticeable amount of salt precipitation. This is consistent with the previous reported measurement of evaporation rate from tailings storage by Fahey and Fujiyasu (1994). It was also observed that the salt crust in the field consisted of a desiccated layer less than 5mm thick, below which the tailings remained quite wet.

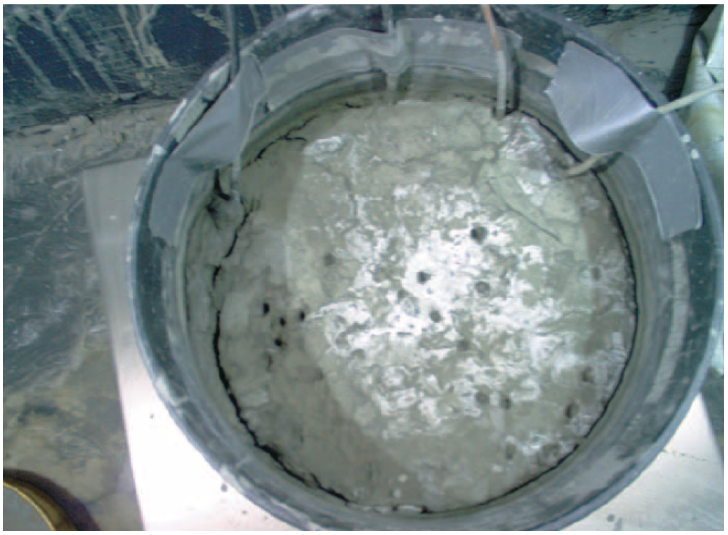

Figure 2.5 Formation of a white precipitate observed during water evaporation from paste tailings obtained in Bulyanhulu gold mine, Tanzania by Simms et al. (2007).

In the arid Australian inland, there are many large playas where the salinities of playas groundwater are high, and often close to Sodium Chloride saturation. Estimates of evaporation from playas and salt-crusted sediment surfaces are substantially lower than those from the freshwater source which have the similar environmental conditions.

Playa surface sediments are often highly moist, lying within the capillary fringe of the water table, and the most characteristic feature is surficial efflorescent salts. Therefore, the reduction in evaporation may be caused by salt accumulation on the surface; and the salt crust is observed being less than 1 cm at Lake Amadeus (Chen, 1992) and Lake Torrens (Schmid, 1985). Table 2.3 below shows estimates of the evaporation rate from salt-encrusted sediment surface in comparison with that from freshwater source in various arid regions in Australia.

Table 2.3 Estimates of the evaporation rate from salt-encrusted sediment surfaces

Site location	Method	Regional pan evaporation (mm/year)	Sediment surface evaporation (mm/year)	Percent of pan evaporation	Author
	Salt accumulation rate			0.4 -1.5	Feth and Brown (1962)
Sabkha, Arabian Gulf	Watertable decline rate; anhydrite depostion	1,240	120 and 60	9.7 and 4.8	Patterson and Kinsman (1981)
Lake Frome, Australia	Deuterium profiles	3,200	170	5.3	Allison and Barnes (1985)
Lake Eyre, Australia	Profiles of Cl and Br	>3,000	9 - 28	0.3 – 0.9	Ulman (1985)
Lake Torrens, Australia	Watertable gradient	3,000	50	1.7	Schmid (1985)
Spring Lake, central Australia	Watertable gradient and decline rate	2,800	50	1.8	Jacobson (1987)

Both field and laboratory experiments were conducted, but especially the laboratory experiment clearly demonstrated the significant reduction of evaporation by a thin salt crust. Accordingly, evaporation was proportional to the vapour pressure difference between the evaporating surface and the overlying atmosphere. The author discussed that for a saline solution, dissolved salts reduced the chemical activity of water, thus reducing the vapour pressure of the solution, resulting in a lower evaporation rate than for fresh water under the same external conditions.

2.4.1 Correlation between Osmotic Suction and Electrical Conductivity

The mechanism associated with the development of osmotic suction in a soil is quite well understood. The osmotic suction is based on the salt concentration in the pore-water. The osmotic suction increases or decreases due to an increase or decrease in the salt content. Therefore, the evaporation from a saline soil is influenced by the accumulation of salt at the top surface. During the drying process, salt accumulates on the surface and a salt crust is formulated which increases the total suction; hence reduces evaporation.

There have been several researchers who gave consideration to osmotic suction by either indirect measurement or direct measurement. In indirect measurement, total suction and matric suction were measured and the difference between them was assumed to be osmotic suction (Sreedeep and Singh, 2006). Their measurement was conducted on the soil collected from the coastal area of Mumbai, India. In conclusion, Sreedeep and Singh (2006) proposed the relationship between osmotic suction and soil water content. Preliminarily, logarithm of osmotic suction linearly changes with change in soil water content.

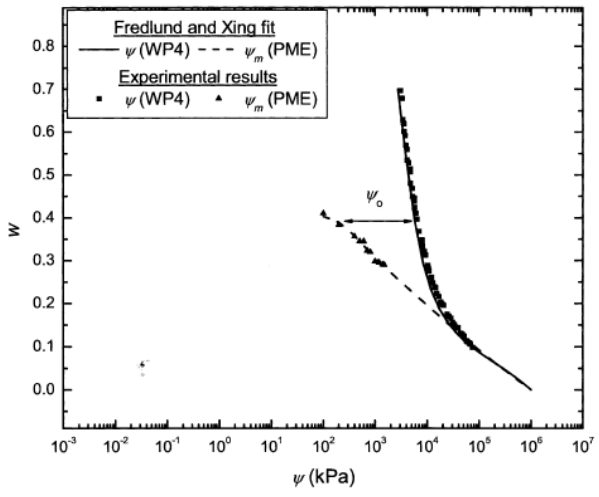

Figure 2.6 Comparison of SWCCs obtained from Dewpoint Potentiameter WP4 for total suction and Pressure Membrane Extractor (PME) for matric suction. The difference between them is referred to as osmotic suction. Measurement was conducted with the soil collected from the coastal area of Mumbai, India (Sreedeep and Singh, 2006).

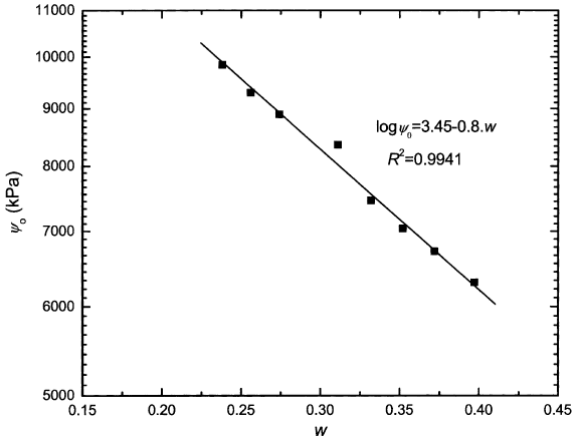

Figure 2.7 Variation of osmotic suction versus gravimetric water content by Sreedeep and Singh (2006).

Later Arifin and Schanz (2009) attempted to measure the osmotic suction of highly plastic clays (i.e., Calcigel and Indian Bentonite) directly using the squeeze technique and very high applied pressures. The osmotic suction was then determined through electrical conductivity of soil pore water squeezed out from a soil sample. The figure below represents the results obtained from the research literature.

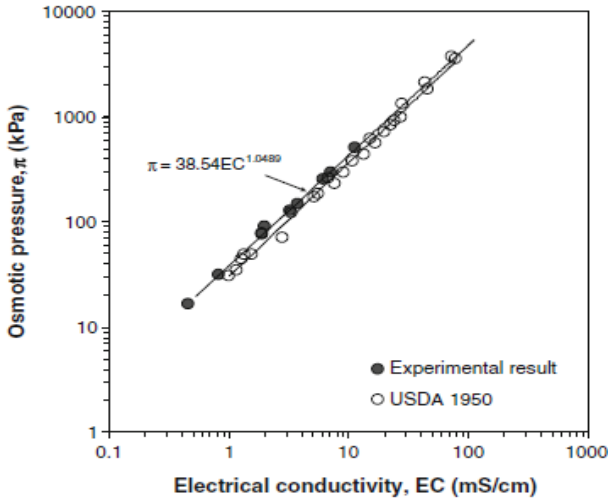

Figure 2.8 Calibration curve for determining osmotic pressure by means of electrical conductivity measurement of soil pore-water by Arifin and Schanz (2009).

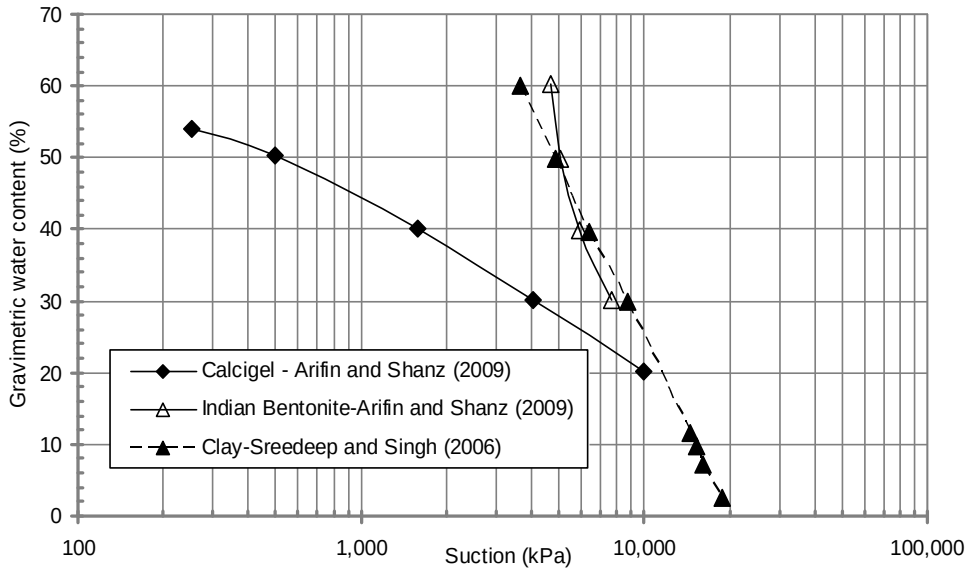

Figure 2.9 Illustration of results of osmotic suction in indirect method by Sreedeep and Singh (2006); in direct method by Arifin and Schanz (2009).

2.4.2 Concepts and Equations of Surface Resistance

The idea of the terminology "surface resistance" has been applied to account for the change in actual evaporation. This idea originated from the surface resistance of a canopy which was derived by Monteith (1965). Later the idea of a soil "surface resistance" was used to derive a formula to estimate the actual evaporation from bare soil bodies (Fen Shu, 1982; Camillo and Gurney, 1986; van de Griend and Owe, 1994; Aluwihare and Watanabe, 2003; Bittelli et al., 2008). The term of soil surface resistance is similar to the stomatal resistance in term of computation of resistances for vegetation (Bittelli et al., 2008). The surface resistance which results from vapour diffusion across the water-air interface localized in the pores and the water surface to the ground surface through the pores of a dry top layer (unit of s/m) (van de Griend and Owe, 1994). The concept of surface resistance has become useful in understanding or representing the resistance of evaporation. Many previous studies (Daamen and Simmonds, 1996; Mohamed et al., 1997) have parametrized the bare soil surface resistance to evaporation, assuming that the evaporation takes place at the soil surface or within soil pores directly adjacent

to the soil surface and that the phenomena is somewhat comparable with the stomatal resistance (Aluwihare and Watanabe, 2003).

Several researchers introduced equations to estimate surface resistance including Fen Shu (1982), Camillo and Gurney (1986), Kondo et al. (1990) and van de Griend and Owe (1994). In both theoretical and practical aspects, the soil surface resistance varies from zero at the wet soil surface to several thousand at the dry soil surface (van de Griend and Owe, 1994). Some methods for determining the bare soil resistance to evaporation are reviewed in the following sections. Recently, the effect of a salt crust on the evaporation from a bare saline soil was investigated by Fujimaki et al. (2006).

Using a data set that included lysimeter measurements of half-hourly averages of evaporation Fen Shu (1982) has proposed that surface resistance, r_s, may be estimated by

$$r_s = 3.5\left(\frac{\theta_{sat}}{\theta}\right)^{2.3} + 33.5 \qquad (2.26)$$

where:

θ = volumetric water content in the 0- 5 mm soil layer;

θ_{sat} = saturated water content of the soil.

It should be noted that the equation was established based on two assumptions; the first being that the aerodynamic resistance was evaluated under a neutral condition of atmosphere, although the data showed that the atmosphere was highly unstable during the day. The second assumption is that the surface vapour pressure was equal to the saturated vapour pressure as estimated from the surface temperature. Practically the surface vapour pressure would be less than the saturated vapour pressure when the soil was nearly fully dry. Therefore, the model was suggested to under-estimate soil surface resistance (Camillo and Gurney, 1986).

Camillo and Gurney (1986) tried to overcome the deficiencies in Fen Shu formula by making the model fit the data and then proposed a linear equation for soil surface resistance which takes into account the actual volumetric water content, θ_{top} and the saturated volumetric water content, θ_s of the first 0-0.5 cm top surface layer:

$$r_s = -885 + 4{,}140 * (\theta_s - \theta_{top}) \tag{2.27}$$

This equation was established by equalizing the modeled and measured equation rates.

Kondo et al. (1990) developed a simple model of evaporation from a bare soil surface based on data collected from an outdoor drying a pan with thickness of 2 cm. This model includes an empirical resistance to the transport of water vapour from the soil pores to the soil-atmosphere interface. The empirical resistance is related to the soil water content of a 2 cm surface layer. The resistance function was found empirically in the same form for three types of soil i.e., loam, sand and fine sand. Accordingly, the resistance function can be repeated in general form as follows:

$$F(\theta) = F_1(\theta_{sat} - \theta)^{F_2} \tag{2.28}$$

The constants for Eq. (2.28) suggested by Kondo et al. (1990) are provided in Table 2.4.

Table 2.4 Constants for Eq. (2.28) suggested by Kondo et al. (1990).

Soil type	F_1 (m)	F_2	θ_{sat}
Loam	2.16×102	10.0	0.490
Sand	8.32×105	16.6	0.392
Fine sand	7.00×103	11.2	0.397

Van de Griend and Owe (1994) developed a method to measure the surface resistance to vapour diffusion in drying topsoil based on Kohsiek's (1981) fast

air chamber. The measurements were made during a process of drying a fine sandy loam. It was realized that surface resistance started to increase at soil volumetric water content of 15 percent in the 0 – 1 cm top layer. It was also concluded that the surface resistance could be modeled as a function of the top 1 cm soil volumetric water content and varied between value close to zero at the wet soil surface and values of several thousand seconds per meter at dry soil surface. With the assumption that topsoil moisture and surface temperature should be known, the relationship between surface resistance and soil topsoil moisture can be described in a typically exponential form as

$$r_s = r_{s1} e^{\alpha(\theta min - \theta)} \qquad \text{for } \theta \le \theta_{min} \tag{2.29}$$

where:

θ = the soil volumetric water content (percentage) in the top 1 cm;

θ_{min} = an empirical minimum value above which the soil is able to deliver vapour at a potential rate.

Figure 2.10 presents an illustration of relationship between surface resistance and soil volumetric water content in the top 1 cm. The resistance to molecular diffusion of water surfaces has been studied intensively with respect to evaporation suppression by monolayers of long-chain alcohols; the value of r_{s1} of 10 s/m was found as a lower reference (La Mer and Healy, 1965). Using this value, the relationship between the surface resistance and soil volumetric water content in the top 1 cm was best described as (van de Griend and Owe, 1994).

$$r_s = 10 e^{0.3563(15 - \theta)} \tag{2.30}$$

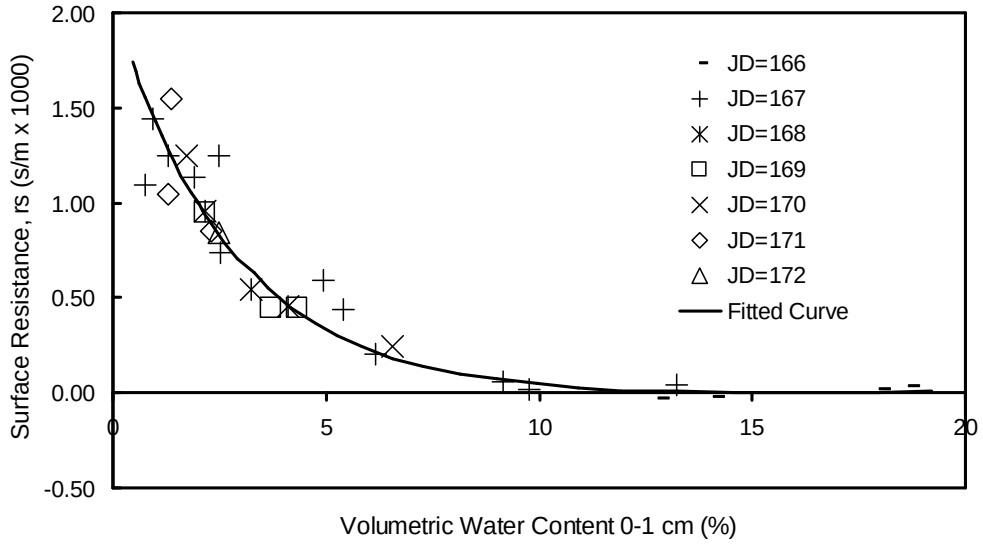

Figure 2.10 Plot of measured surface resistance r_s versus top 0 – 1 cm volumetric water content during the period dry down by van de Griend and Owe (1994).

Daamen and Simmonds (1996) introduced a method for continuous, in situ measurement of hourly evaporation rates from soil using micro-lysimeters and load cells. They found that hourly data are essential for development of realistic models of the actual evaporation. The numerical model of water and heat flow in soils is then used to evaluate the performance of a simple surface resistance model in the estimation of evaporation from bare soil. It was also affirmed that the surface resistance would be a function of soil water content alone and can only provide an adequate description of evaporation from soil under a specific well-defined set of meteorological and soil conditions (Daamen and Simmonds, 1996).

Aluwihare and Watanabe (2003) suggested a new device to measure evaporation from bare soil and then estimate surface resistance. They confirmed the existance of a soil surface resistance which contributes to resist to evaporation through diffusion of water vapor from soil pores. They also tested the results of soil surface resistance for bare soil which somewhat agreed with the conlusions by van de Griend and Owe (1994) and was shown as a power function of soil moisture in the top 0–1 cm of soil in Figure 2.11.

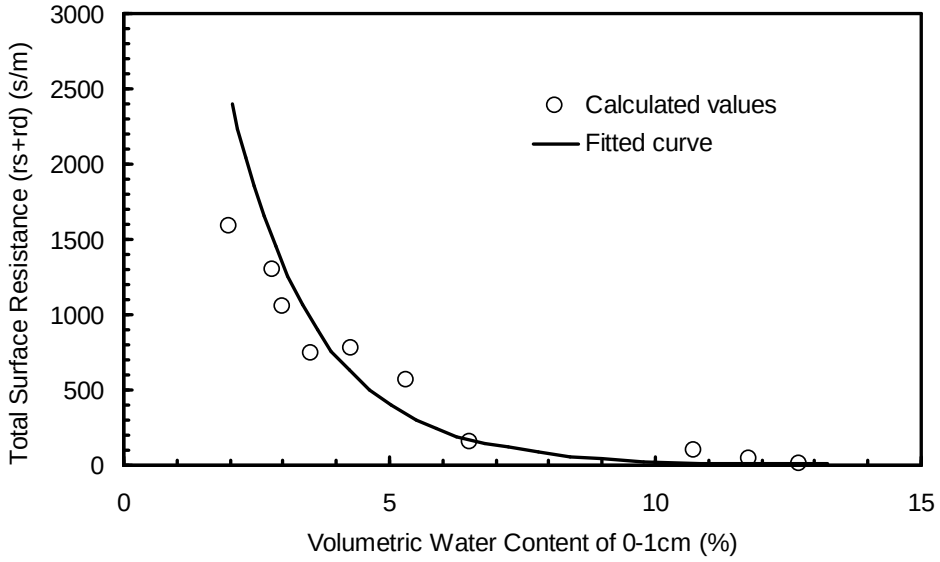

Figure 2.11 Variation of total surface resistance against volumetric water content in top 0 – 1 cm soil layer by Aluwihare and Watanabe (2003).

2.5 REVIEW ON METHODS FOR PREDICTION OF THE RELATIVE HUMIDITY AT SOIL SURFACES

Evaporation is understood to be an exchange of water vapour between the surface and the atmosphere above and calculated as a function of difference between actual vapour pressure at the surface and actual air pressure in the atmosphere. For an open-water surface or a saturated soil surface, water is freely available at the surface for evaporation. At this point, the relative humidity of the pore air at the surface which is defined as a ratio of actual vapour pressure to saturated vapour pressure at the same condition is unity or 100 percent. In other words, the actual vapour pressure at the surface is equal to the saturated vapour pressure. However, geotechnical engineers are traditionally familiar to unsaturated soils where the supply of water becomes limited at the soil surface (Wilson et al., 1994). Accordingly, the relative humidity is less than unity or the actual vapour pressure of the surface is less than the saturated vapour pressure. Therefore, the estimation of soil surface relative humidity is essential to the calculation of the flux boundary condition.

There have been several models to predict the relative humidity of the soil surface. They can be divided into two categories. First the relative humidity is evaluated on the basis of the total suction of the soil through the thermodynamical relationship between the liquid and vapour phases (Wilson, 1990; Alvenas and Jansson, 1997; Bittelli et al., 2008; Fredlund et al., 2011; and recently Dunmola, 2012). The second method is empirically and indirectly based upon parameterization of the surface specific humidity. Such formulas have been examined by several researchers including Kondo et al. (1990), Mahfouf and Noilhan (1991) and Lee and Pielke (1992).

2.5.1 Lord Kelvin's Formula

The free energy state of soil water can be measured in terms of the partial vapour pressure of the soil-water (Edlefsen and Anderson, 1943; Richards, 1965). The thermodynamic relationship between soil suction (or the free water of the soil water) and the partial pressure of the pore-water vapour can be written as follows (Fredlund, 1993):

$$\psi = \frac{-RT\rho_w}{\omega_v} ln\left(\frac{u_v}{u_{v0}}\right) \tag{2.31}$$

where:

ψ = total suction, kPa;

R = universal gas constand, 8.314 J/mol.K;

T = absolute temperature, $T = 273.15 + t^o$, ^{o}K;

t^o = temperature, ^{o}C;

ρ_w = density of water, kg/m^3;

ω_v = molecular mass of water vapour, 18.016 kg/kmol;

u_v = partial pressure of pore-water vapour, kPa;

u_{v0} = saturation pressure of pore-water vapour over a flat surface of pure water at the same temperature, kPa (e.g., Lowe, 1977).

The term, u_v/u_{v0} is called relative humidity, *RH*. At a particular temperature the variables in front of the natural logarithm of *RH* become a constant. Equation

(2.31) can be re-written for the relative humidity of air in equilibrium with the water in the soil pore as:

$$RH = exp\left(\frac{-\psi\omega_v}{RT\rho_w}\right) \tag{2.32}$$

It is noted that Eq. (2.32) is the same as the one proposed by Philip (1957) using thermodynamic laws.

The formula derived by Philip has been used to simulate relative humidity of the air immediately above the free-water surface in the soil pores by several authors including Nappo (1975), McCumber and Pielke (1981); Camillo et al. (1983). However, there have been some evidences to show that the Philip's formula may be invalid close to a soil surface, especially when the upper layer is dry, as suggested by Kondo et al. (1990) and Lee and Pielke (1992). In fact, using the Philip's formula, the air close to the water in the pore will be saturated at very low soil water content and will start to decline until the water content has dropped far below the permanent wilting point (Kondo et al., 1990; Lee and Pielke, 1992). This behaviour led to an overestimation of soil evaporation (Mihalovic et al., 1993). Recently, this behaviour was confirmed by some researchers including Alvenas and Jansson (1997), Fredlund et al. (2011) and Dunmola (2012). In an effort to overcome the deficiency in the Philip's formula, the researchers have proposed their own methods to correct this limitation by introducing either a total suction adjustment factor or an empirical relative humidity. Such methods are reviewed in the following sections.

2.5.2 Kondo et al. (1990) Equation

The evaporation process is usually parameterized by the so-called surface moisture availability. Although there are several ways to express surface moisture availability, it has not been determined which is the most suitable to give a realistic estimate of evaporation (Kondo and Saigusa, 1992). There are

two main forms defining surface moisture availability written as the α–method and the β–method, respectively.

$$E = \rho C_E u(\alpha q^*(T_s) - q) \tag{2.33}$$

$$E = \rho C_E u \beta(q^*(T_s) - q) \tag{2.34}$$

where:

E = the evaporation rate;

ρ = the density of air;

u = the wind speed;

C_E = the bulk coefficient of evaporation;

q = the specific humidity of the air;

$q^*(T_s)$ = the saturation value at the soil surface temperature T_s;

α and β = the coefficients representing the surface moisture availability.

The evaporation rate can be expressed through two main processes (molecular diffusion of water vapour from water surface in the soil pores to the ground surface and either laminar or turbulent diffusion of water vapour from ground surface to the atmosphere) by Kondo et al. (1990).

$$E = \rho C_E u \frac{q^*(T_s) - q}{1 + C_E u F(\theta) / D_{atm}} \tag{2.35}$$

Finally, these authors obtained the formulas for α and β from Eqs. (2.33), (2.34) and (2.35) as follows:

$$\alpha = \frac{q}{q^*(T_s)} + \beta\left(1 - \frac{q}{q^*(T_s)}\right) \tag{2.36}$$

$$\beta = \rho C_E u \frac{q^*(T_s) - q}{1 + C_E u F(\theta) / D_{atm}} \tag{2.37}$$

where:

F(θ) = the resistance function which was empirically determined from experiments performed with a thin layer of loam or sand (with thickness of 2 cm) packed in an evaporation pan. Readers first wish to be clarified the value of *F(θ)*, consult the section 2.4.2.

These formulas show that β depends on θ and *u*, while α depends on θ, *u* and $q/q^*(T_s)$. Thus the parameter β is more useful in a practical sense than the parameter α.

2.5.3 Lee and Pielke (1992) Equation

Lee and Pielke (1992) proposed another model of relative humidity to overcome the deficiency in the Philip's formula (1957). In this model, Lee and Pielke introduced a new terminology as the soil moisture availability, β, which starts to decrease once the soil water content drop below field capacity. With the introduction of the field capacity as a common reference point the soil moisture availability appears to be independent of soil texture (Alvenas and Jansson, 1997). Note that the common practice is to define the field capacity for all soil classes as either a soil-water potential of 33 kPa or a hydraulic conductivity of 0.1 mm/day (Lee and Pielke, 1992). The simple empirical formula of soil moisture availability chosen to fit the data by Kondo et al. (1990) was expressed by Lee and Pielke (1992) in Eq. (2.38). However, engineers have had some difficulty accepting the value of field capacity in the geotechnical engineering since it is not representative for soil texture.

$$\beta = \begin{cases} \frac{1}{4}\left[1 - cos\left(\frac{\theta}{\theta_{fc}}\pi\right)\right]^2 & \theta < \theta_{fc} \\ 1 & \theta \geq \theta_{fc} \end{cases} \qquad (2.38)$$

where:

β = the coefficient representing the surface moisture availability;

θ_{fc} = the field capacity;

θ = the soil volumetric water content of the topsoil layer.

Table 2.5 Field capacity θ_{fc} is associated with a hydraulic conductivity of 0.1 mm/day by Clapp and Hornberger (1978) plus peat (McCumber and Pielke, 1981).

Soil type	Permanent wilting point, θ_{wilt}	Field capacity, θ_{fc}	Saturation volumetric water content, θ_{sat}
Sand	0.068	0.135	0.395
Loamy sand	0.075	0.150	0.410
Sandy loam	0.114	0.195	0.435
Silt loam	0.179	0.255	0.485
Loam	0.155	0.240	0.451
Sandy clay loam	0.175	0.255	0.420
Silty clay loam	0.218	0.322	0.477
Clay loam	0.250	0.325	0.476
Sandy clay	0.219	0.310	0.426
Silty clay	0.283	0.370	0.492
Clay	0.286	0.367	0.482
Peat	0.395	0.535	0.863

2.5.4 Alvenas and Jansson (1997) Method

In an effort to correct the deficiency in the Philip (1957) formula, Alvenas and Jansson (1997) presented a method to adjust total suction in the topsoil layer and a dynamic estimate of the water at the surface. By doing this, non-equilibrium effects caused by rapid moisture fluctuations close to the surface were explained. Alvenas and Jansson proposed an expression for the actual vapour pressure at the surface temperature as

$$e_s = e^*(T_s)e^{\left(\frac{\psi M_w g e_c}{R(T+273.15)}\right)} \tag{2.39}$$

where:

$e^*(T_s)$= the saturated vapour pressure at the surface temperature;

ψ = the mean total suction in the topsoil layer;

g = the gravity constant;

R = the gas constant at the temperature T_s;

e_c = an empirical correction factor which compensates for the difference between the mean total suction in the topsoil layer and the total suction at the surface, defined as (Alvenas and Jansson, 1997):

$$e_c = 10^{\left(-\delta_s \psi_g\right)} \tag{2.40}$$

where:

δ_s = the surface water balance based on the difference between precipitation, *P*, and evaporation and soil vapour flux. δ_s is only allowed to vary between -2 and 1 mm according to:

$$\delta_s(t) = max\left(-2, min\left(1, \delta_c(t-1)\right) + (P - E - q_v)\Delta t\right) \tag{2.41}$$

In association with δ_c, ψ_g in Eq. (2.40) is a parameter the value of which determines the steepness of the total suction gradient from the middle of the top layer to the surface. ψ_g = 0 implies that there is no difference between the total suction at surface and that in the topsoil layer. ψ_g = 1 implies that the water availability at the surface could decrease by up to two orders of magnitude during drying and increase by up to one order of magnitude during wetting (Alvenas and Jansson, 1997).

Fredlund et al. (2011) re-visited the Wilson et al. (1997) model and the sand column drying tested by Wilson (1990). Fredlund et al. (2011) realized that the model over-predicted actual evaporation for the first 5 days of drying. The error was attributed to an over-prediction of the relative humidity at the soil surface. Moreover, this is not the case that the sand should evaporate water at the potential rate of evaporation at a suction value of 3,000 kPa. The sand exceeded residual condition in term of water content at which the matric suction was well below 3,000 kPa. Consequently, Fredlund et al. (2011) suggested an expression of adjustment of total suction at the soil surface to account for surface resistance to evaporation. The purpose was to correct the relative humidity at the soil surface in order to obtain a "match" between the

theoretical formulation solution and experimental results. The Fredlund's expression can be presented as:

$$u_{wa} = u_{w0} \times 10^{-\delta} \qquad (2.42)$$

where:

u_{wa} = adjusted negative pore-water pressure, kPa;

u_{w0} = original negative pore-water pressure computed from differential equation governing moisture and vapour flow, kPa;

δ = empirical adjustment factor, appears to range from 0 to -2. An adjustment factor of -1.8 was proposed for the Beaver Creek sand in their study. It was anticipated that the adjustment factor would vary for different soils with the most negative values applicable for coarse-grained soils.

2.6 PARTIAL DIFFERENTIAL EQUATIONS FOR FLOWS OF WATER, VAPOUR AND HEAT

Computation of the net flux of water across the soil surface implies that the vapour phase of water exists only in the atmosphere above the soil surface. This is correct for the special case where the soil profile is saturated. In unsaturated soils, however, both liquid and vapour phases of water are present at the same time. The flow of water in a body of unsaturated soil occurs in both phases (i.e., liquid and vapour) and across phase boundary (i.e., menisci or contractile skin). Furthermore, when the water molecules transform from the liquid phase to the vapour phase or vice versa heat must be consumed or released, respectively. An appropriate analysis of moisture flow between the atmosphere and soil surface should be provided by the flows of water vapour and heat along with the flow of liquid water for unsaturated soils.

The simultaneous transfer of heat and mass (i.e., liquid and vapour) in unsaturated non-frozen soils has been theoretically developed over time by soil scientists. Probably Bouyoucos (1915) is likely the first researcher to carry out to investigate the transfer of water under the temperature gradients.

However, Bouyoucos didn't realize the importance of water vapour within the system. The presence of water vapour was addressed when Smith (1939) measured the transfer of water under the temperature gradients. Later, other researchers (Wilson, 1990; Gitirana, 2005) have focused on studying the phenomena of heat and moisture flows under non-freezing condition in soils.

Philip and de Vries 1957 (PDV) presented two non-linear partial differential equations describing the simultaneous flow of liquid water, water vapour and heat in porous materials. Some scientists and engineers including Jury (1973); Dempsey et al. (1976); and Couvillion (1981) agreed somewhat with the theory of Philip and de Vries through comparison between the predicted fluxes and measured fluxes of heat and moisture. However, the assumption of flow in response to a volumetric water content gradient makes Philip and de Vries (1957) formulation unacceptable for application to problems in geotechnical engineering. This assumption is fundamentally incorrect, since the flow of liquid water occurs in response to a hydraulic-head gradient (Wilson et al., 1993).

Wilson (1990) tried to overcome the limitations for Philip and de Vries (1957) formulation to develop the partial differential equations (PDEs) of moisture flow, air flow and heat flow which are considered to be applicable to geotechnical engineering. Wilson (1990) derived his rigorous equations using a continuum mechanics approach to describe the flow of air, water vapour, liquid water and heat in soil volume. Fick's law was used to describe the flow of air and water vapour while Darcy's law was used for the flow of liquid water. A conventional heat transfer equation was adopted to compute heat flux. All flow equations for the soil were given in a one-dimension form. Specifically, when soil is saturated, it is considered that there are two phases existing in the elementary soil volume i.e., soil particles and liquid water. In contrast, the elementary soil volume is considered as four distinct phases (i.e., soil particles, liquid water phase, contractile skin or meniscus and air and water vapour phase) when soil is unsaturated. However, Wilson (1990) made several simplifying assumptions to reduce the complexity of solution. As a

result, two coupled PDEs of the transient flow of liquid water, water vapour and heat in soil volume developed by Wilson (1990) are expressed as follows:

For moisture flow,

$$\frac{\partial h_w}{\partial t} = C_w^1 \frac{\partial}{\partial y}\left(k_w \frac{\partial h_w}{\partial y} \right) + C_w^2 \frac{\partial}{\partial y}\left(D_v \frac{\partial P_v}{\partial y} \right) \qquad (2.43)$$

where:

$$C_w^1 = \frac{1}{\rho_w g m_2^w}$$

$$C_w^2 = \frac{(P + P_v)}{P(\rho_w)^2 g m_2^w}$$

g = acceleration due to gravity;

D_v = the diffusion coefficient of the water vapour through the soil;

y = one dimensional elevation;

m^w_2 = *a* coefficient of water storage;

ρ_w = density of water;

P_v = the partial pressure due to water vapour,

$$P_v = P_{vs} \times h_r \qquad (2.44)$$

where:

P_v = the actual vapour pressure within the pore-air;

P_{vs} = the saturation vapour pressure of the soil water at temperature, T;

$h_r = e^{\frac{\psi g W_v}{RT}}$ relative humidity;

ψ = the potential in the liquid water phase (i.e., $(u_a - u_w)$ + osmotic suction);

W_v = molecular weight of air;

R = universal gas constant.

For heat flow,

$$C_v \rho_s \frac{\partial T}{\partial t} = \frac{\partial}{\partial y}\left(\lambda \frac{\partial T}{\partial y}\right) - L_v\left(\frac{P + P_v}{P}\right)\frac{\partial}{\partial y}\left(D_v \frac{\partial P_v}{\partial y}\right) \qquad (2.45)$$

where:

$C_v\rho_s$ = volumetric specific heat;

T = absolute temperature;

λ = the thermal conductivity;

P = total pressure in the bulk air phase (i.e., $u_{atm} + u_a$);

L_v = latent heat of vaporization.

Wilson's PDEs were verified by investigation the simultaneous transfer of water and heat in two soil columns.

Gitirana (2005) presented an overview of flow laws traditionally used for modeling unsaturated flow behaviour summarized in Table 2.6. The flow laws establish relationships between measures of flow and driving potentials. The flow laws presented in Table 2.6 are well established equations that have been experimentally verified.

Pore-water flow and heat flow are the key elements of the investigations. Accordingly, the pore-water flow is once again confirmed in both phases e.g. liquid water described by Darcy's law and water vapour described by Fick's law. Mechanism of heat flow includes conduction, convection and latent heat due to phase change; however, Jame and Norum (1980), Andersland and Anderson (1978), Nixon (1991) pointed out that heat transfer convection is negligible and often 2 to 3 orders of magnitude less than heat transfer due to conduction and latent heat due to phase change.

Table 2.6 Overview of types of flow within an unsaturated soil and the corresponding mechanisms, driving potentials, and flow laws (after Gitirana, 2005).

Type of flow (1)	Flow mechanism (2)	Driving Potential (3)	Flow Law (4)
Flow of water, v^w	Liquid water, v^{wl}	Hydraulic head, h (m)	Darcy's law
	Water vapour diffusion, v^{vd}	Mass concentration of vapour per unit volume of soil, C_v (kg/m^3)	Modified Fick's law
	Water vapour carried by bulk air flow, v^{va}	Mass concentration of air per unit volume of soil, C_a (kg/m^3)	Modified Fick's law
Interphase liquid-vapour flow	Thermodynamic equilibrium	--- (*)	Lord Kelvin's equation
Flow of air, v^a	Free air, v^{af}	Mass concentration of air per unit volume of soil, C_a (kg/m^3)	Modified Fick's law
	Dissolved air diffusion, v^{ad}	Mass concentration of dissolved air per unit volume of soil, C_{ad} (kg/m^3)	Modified Fick's law
	Dissolved air carried by liquid water flow, v^{aa}	Hydraulic head, h (m)	Darcy's law
Flow of heat, q^h	Heat by conduction, q^c	Temperature, T (ºC)	Fourier's law
	Latent heat	--- (*)	Interphase liquid-vapour flow

(*) local thermodynamic equilibrium assumed; function of the rate of vapour flow.

Gitirana (2005) proposed two non-linear PDEs describing the simultaneous flow of liquid water, water vapour and heat in a representative elemental volume of soil. These equations of moisture flow and heat flow are expressed as follows in Eq. (2.46) and Eq. (2.47), respectively.

Equation of moisture flow,

$$\frac{\partial}{\partial x}\left[\left(\frac{k^w + k^v}{\gamma_w}\right)\frac{\partial u_w}{\partial x} - \frac{k^v}{\gamma_w}\left(\frac{u_w}{T+273.15}\right)\frac{\partial T}{\partial x}\right]$$
$$\frac{\partial}{\partial y}\left[\left(\frac{k^w + k^v}{\gamma_w}\right)\frac{\partial u_w}{\partial y} - \frac{k^v}{\gamma_w}\left(\frac{u_w}{T+273.15}\right)\frac{\partial T}{\partial y}\right] = \frac{\partial (nS)}{\partial t} \qquad (2.46)$$

where:

k^w = hydraulic conductivity, $k^w = f(u_a - u_w)$, m/s;

γ_w = unit weight of water, 9.81 kN/m^3;

u_w = pore-water pressure, kPa;

k^v = vapour conductivity;

$$k^v = \frac{\bar{u}_a + p_v}{\bar{u}_a}\frac{gW_v p_v}{R(T+273.15)}\frac{D^{v*}}{\rho_w} \quad , \text{m/s}$$

ρ_w = density of water, kg/m^3;

$\bar{u}_a$ = total pressure in the bulk air phase, $u_a + u_{atm}, kPa$;

u_a = pore-air pressure, kPa;

u_{atm} = atmospheric pressure, 101.325 kPa;

R = universal gas constant, 8.314 kJ/(mol.K);

g = gravity acceleration, 9.81m/s^2;

W_w = molecular weight of water vapour, 0.018016 kg/mol;

p_v = partial vapour pressure of soil water at temperature T, kPa;

$$p_v = p_{vsat} e^{\frac{-\psi g W_v}{\gamma_w R(T+273.15)}}$$

p_{vsat} = saturation vapour pressure of soil water at *T*, kPa;

ψ = total potential of liquid pore-water, m;

T = surface temperature, ^{o}C;

$D^{v*} = (1-S)nD^v W_v / RT$, m^2/s

D^v = molecular diffusivity of vapour in air, $0.229\times10^{-4}(1+T/273.15)^{1.75}$, m^2/s;

S = degree of saturation, $S = V_w/V_v$;

n = porosity, $n = V_v/V_0$.

Equation of heat flow,

$$\frac{\partial}{\partial x}\left[\left(\lambda - L_v k^v \frac{\rho_w}{\gamma_w}\frac{u_w}{T+273.15}\right)\frac{\partial T}{\partial x} + L_v k^v \frac{\rho_w}{\gamma_w}\frac{\partial u_w}{\partial x}\right]$$
$$\frac{\partial}{\partial y}\left[\left(\lambda - L_v k^v \frac{\rho_w}{\gamma_w}\frac{u_w}{T+273.15}\right)\frac{\partial T}{\partial y} + L_v k^v \frac{\rho_w}{\gamma_w}\frac{\partial u_w}{\partial y}\right] = \zeta \frac{\partial T}{\partial t} \quad (2.47)$$

where:

T = temperature, ^oC;

L_v = latent heat of vaporization $4.187\times10^3\times(591 - 0.51T)$, J/kg;

ζ = volumetric specific heat of soil, $\zeta = f(u_a - u_w)$, J/(m^3 ^oC).

In summary, the following flowchart as shown in Figure 2.12 describes two PDE sets and their boundary conditions which are somewhat successful to solve for evaporation of water from a soil domain.

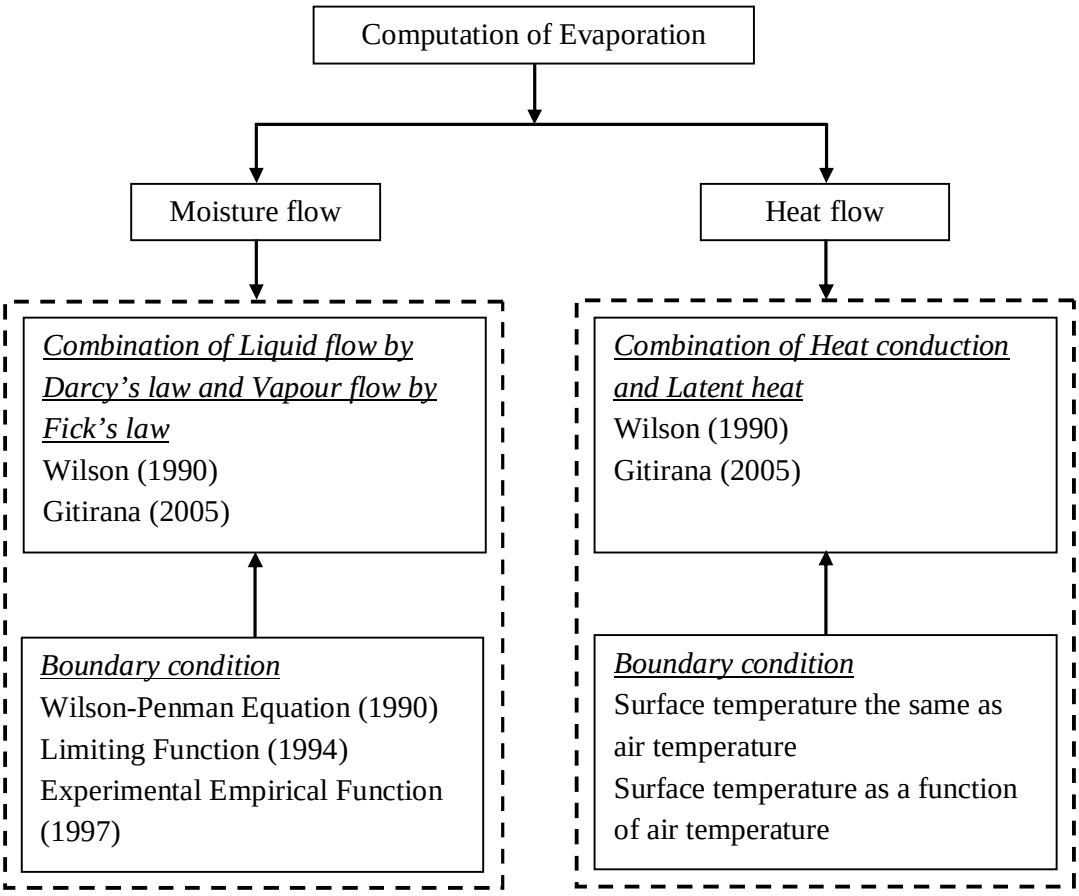

Figure 2.12 Flowchart of equations and their boundary conditions currently implemented in geotechnical engineering.

2.7 SOME RESULTS OF APPLICATION OF SOIL-ATMOSPHERIC MODELS

Wilson (1990) conducted a series of laboratory tests on thin sections of sand, silt and clay as well as two sand column drying tests to verify Wilson's soil-atmosphere model as previously discussed. The results of the thin soil section tests showed that the actual evaporation equals to the potential until suction exceeds approximately 3,000 kPa of total suction. In other words, decrease in relative humidity is not significant until total suction exceeds approximately 3,000 kPa. Wilson found that evaporation to atmosphere would be controlled primarily by the water vapour or total suction in the thin soil sections. As a result, the Wilson et al. (1997) empirical models were established based on

experimentally measured ratios of *Actual Evaporation* to *Potential Evaporation* for these thin sections of sand, silt and clay.

Two sand column drying tests (i.e., column A and column B) were carried out to investigate not only the evaporation rate, but also soil temperature profile and water content profile. Both the soil-atmosphere model and the laboratory test demonstrated the development of the three stages of drying described by Hillel (1980). The high rate of evaporation for saturated or nearly saturated soil during Stage I is approximately equal to potential rate of evaporation for free water. Stage II drying begins when the conductive properties of the soil no longer permit a sufficient flow of water to the surface to maintain the maximum potential rate of evaporation. The rate of evaporation continues to decline during Stage II drying as the surface continues desiccate and reaches a low residual suction value defined as Stages III. Furthermore, numerical simulations of water fluxes in two soil columns were also conducted with a Finite Element Method (FEM) unsaturated flow code which applies the soil-atmospheric model by Wilson (1990). The simulated water content profiles show good agreements between measured data and computed results on some testing days; remarkably, days 5 and 21 for column A and days 14 and 29 for column B. However, there are still some challenges to obtain the good soil temperature profiles.

Yanful et al. (2003) also used the soil-atmosphere model suggested by Wilson (1990) and conventional atmospheric data to estimate evaporation in moisture-retaining soil covers. The modeling results agreed reasonably well with experimental results and indicated that a clayey till would be an effective oxygen barrier in sulphide-bearing mine waste covers. They also found that sands would be effective evaporation and drainage barriers for the till. The results also showed that coarse sand was better than both fine sand and silt as the protective top layer in three-layer cover systems (Yanful et al., 2003). The profile of water content showed that the single-layer coarse sand lost a significant amount of moisture almost throughout its entire depth, while the silt and fine sand lost water only in the upper parts, similar to the clayey till. In

other words, during the drying process, the evaporative front evolves deeper in coarse sand than in silt, fine sand and clayey till (Yanful et al., 2003).

Fujimaki et al. (2006) conducted the experiments of effects of pore-water salinity on evaporation from a bare saline soil under an isothermal condition. They performed the experiments of evaporation with three combinations of soil (i.e., loamy sand and sand soils) and solute (NaCl and KCl). In the experiments, the soil surface was kept wet by keeping the low suction at the bottom, but the evaporation was found to considerably decrease with time. Salinity was observed to cause a reduction in evaporation rates with salt accumulation at the top 1 cm of soil column. Evaporation rates from numerical simulation were significantly higher than the measured rate of evaporation. This discrepancy was attributed to the effect of salt crust, which was not included in the simulation (Fujimaki et al., 2006; and Dunmola, 2012). While salt crust resistance was included, the better numerical solution was obtained. In conclusion, Fujimaki et al. (2006) noted the decrease in evaporation due to pore-water salinity could not be explained by osmotic suction alone, but also by the effect of salt crust.

Simms et al. (2007) conducted small and large-scale drying tests on acid-generating thickened tailings paste collected at Bulyanhulu in Tanzania, conbined with the analysis of field data. Wind and solar radiation were simulated over the three-week drying period, using fan and metal halide lamps, respectively. Data such as albedo of the tailings surface, profiles of matric suction, degree of cracking, volume change, water content, and drying rate were monitored over the drying period. The small-scale drying test was conducted under conditions similar to the large-scale test with wind simulation. Numerical simulations of water fluxes in the large-scale test were also conducted with a FEM unsaturated code implemented the Wilson et al. (1997) model discussed in the previous sections. A slightly elevated albedo was recorded for the test conducted under a higher evaporative demand due to the formation of a white precipitate at the surface of the stack. It was observed during the field investigation, there was an initial correlation between decreasing gravimetric water content (GWC) and increasing albedo, but after

steady-state water content has been reached, the albedo kept increasing. It was believed that salt precipitation is responsible for the continued increase in albedo (Simms et al., 2007; and Dunmola, 2012). The range of albedo measured in the field and observed in the laboratory were similar. Although simulated cumulative evaporation for the small-scale test agreed well with experimental observations, qualitative differences in the suction profiles remained unexplained. The simulated GWC values agreed well with field data up to only three weeks after deposition. Finally, Simms et al. (2007) recommended, " *A more general method of predicting evaporation from paste tailings will likely require further efforts to incorporate the influence cracking and salts into numerical models* ".

Bittelli et al., (2008) implemented a fully coupled numerical model to solve the governing equations for liquid water, water vapour, and heat transport in bare soils. The model used the equation of liquid water transport developed by Richards (1931). They also tested the numerical model with detailed measurements of soil temperature, heat flux, water content, and evaporation from the surface; tested different formulations for the soil surface resistance parameter and their effect on soil evaporation. Simulated soil temperature, heat flux, and water content were in good agreement with the measured data. Comparison between different equations for the soil surface resistance was conducted to help identify the best formulation for the bare soil being studied. The equation of van de Griend and Owe (1994) was recommended to use. In general, the model showed that water vapour transport plays a key role in the soil mass and energy budget and that vapour flux may induce small fluctuations in soil water content near the surface. These results suggest that it is important to consider coupled transport of heat, water vapour and liquid water when computing soil water and energy dynamics in the field, and to obtain a correct quantification of the resistance parameters at the soil-atmosphere interface (Bittelli et al., 2008). Unfortunately, however, a comparison between the predicted and measured profiles of soil moisture was not provided.

Recently, an attempt to re-evaluate the Wilson et al. (1997), Dunmola (2012) conducted a series of laboratory drying tests on non-saline silt, low saline silt, saline silt and high saline silt in columns of 10 cm and 2 mm in thickness. The author found that the work by Wilson et al. (1997) is validated for the non-saline silt columns of 2 mm in thickness, but not valid for the non-saline silt columns of 10 cm in thickness. In fact, the over-prediction of the actual evaporation rate for the 10 cm thick silt columns was attributed to over-estimation of the relative humidity at the surface of the non-saline silt column. In order to overcome this limitation, Dunmola (2012) suggested to raise the total suction "at the soil surface" by introducing the empirical "adjustment factor". Consequently the relative humidity and vapour pressure at soil surface were reduced. It is important to note that this idea was originated from Alvenas and Jansson (1997) and Fredlund et al. (2011). It was concluded that the Wilson et al. (1997) model was only valid for extremely thin layers of soil due to elimination of any flow process(es) at depth below the surface; and should be modified for thick layers through either the total suction adjustment or soil surface resistance to account for the soil resistance to water vapour diffusion from receding evaporation front to the surface (Dunmola, 2012). However, the values of soil surface resistance used by Dunmola (2012) in the numerical modeling were much higher than that found in the literature (i.e., Fen Shu, 1982; Camillo and Gurney, 1986; van de Griend and Owe, 1994 and Aluwihare and Watanabe, 2003).

2.8 RESEARCH CONTRIBUTIONS RELATIVE TO EARLIER WORK

The literature review provided in the previous sections indicates that the available soil-atmospheric models applied in geotechnical engineering need to be re-visited and modified with regards to moisture boundary condition. The specific contributions of this thesis relative to the early work discussed above should be concisely described as follows:

1. To develop an equation describing the evaporation from a soil surface to the atmosphere using surface resistance and coupling with the available equations for the flow of water and heat in soil as a flux boundary condition.

2. To develop a method to determine the suction at which actual evaporation rate begins deviate from the potential evaporation rate. Assess if this suction related to soil properties (i.e., air entry value and residual soil suction); then re-estimate relative humidity at the soil surface for thick layers of soil based on this suction.

3. To conduct laboratory evaporation tests in order to re-evaluate:

   a. The method of estimation of relative humidity at the soil surface during the drying process.

   b. Effect of various salt contents on the evaporation rate.

2.9 CHAPTER SUMMARY

This chapter presented a review of the soil-atmospheric models of evaporation from surfaces as well as partial differential equations of flows of liquid water, water vapour and heat within various media. Some climatological methods to estimate *Potential Evaporation* and their applications were summarized in Section 2.2. In general, the major approaches to estimation of evaporation rate consist of energy balance method, aerodynamic method and combination of energy balance and aerodynamic methods.

Section 2.3 reviewed the models for prediction of actual evaporation from soil surfaces with a limited supply of water at the surface. There are two approaches to derive these models and consist of either models with or without surface resistance and surface-resistance-type models. Accordingly, the models without application of surface resistance by Wilson (1990; 1994; and

1997) were presented; and most of the surface-resistance-type models results from the energy balance of the ground surface.

An overview of effect of various salt contents to reduction of evaporation rate and concepts of surface resistance to evaporation were reviewed in Section 2.4. In the research literature, osmotic suction due to salt content was determined by correlation between osmotic suction and electrical conductivity.

Physically, in order to consider the resistance to water vapour diffusion from soil pores to the soil-atmosphere interface, a surface resistance was introduced. Several equations derived to determine the soil surface resistance were also reviewed. It was noted that soil surface resistance varies from close to zero at a wet surface to several thousand (s/m) at a dry surface.

Section 2.5 presented a review of methods for determination of the relative humidity at the soil surface. The formula to estimate the relative humidity first introduced by Philip (1957) may be valid when the air close to the pore-water surface is in equilibrium with the pore water. However, it may be invalid close to a soil surface, especially when the soil surface is dry. In order to overcome deficiency in Philip's formula, several researchers proposed empirical equations of relative humidity. These equations apparently depend on field capacity which is not generally accepted in the field of geotechnical engineering. Therefore, there is a need to modify one of these equations using soil properties of unsaturated-soil mechanics such as the air entry value and residual soil suction.

Several models for the prediction of heat and water flow in unsaturated soils and soil-atmosphere coupling were reviewed. It was found that the one-dimensional water flow and soil-atmosphere model proposed by Wilson (1990) provides a comprehensive framework that can be used to predict evaporation rate at soil surface.

CHAPTER 3
RE-VISITATION OF RELATIVE HUMIDITY AND THEORY OF SOIL-ATMOSPHERE INTERACTION

3.1 GENERAL

A review of the theoretical approaches for analyzing the evaporation of water from the ground surface and soil-atmosphere models was provided in Chapter 2. The flow of water within a soil volume is coupled with the transfer of water to the atmosphere immediately above the soil surface. This coupling of these processes has been attempted by several researchers including Sophocleous (1978; 1979), Camillo et al. (1983), Passerat de Silans et al., (1989), Wilson et al. (1990; 1994; and 1997), Gitirana (2005), Fujimaki et al. (2006), Bittelli et al. (2008), and recently Dunmola (2012). This chapter reconsiders the fundamental physics of water transfer at a soil surface, focusing on existing shortcomings related to the calculation of relative humidity at the soil surface. The end result is the development of a theoretical model for prediction of evaporation rate from a soil surface. Procedures to develop a new actual evaporative formulation are presented in Figure 3.1.

The proposed model describes the resistance to water vapour diffusion from various depths adjacent to the soil surface to the atmosphere. Surface resistance and relative humidity are re-evaluated to account for these phenomena. A comparison is then made between the proposed methods for calculating relative humidity at the soil surface and other routine methods. The comparison is made for thin soil layers (0.5–1 mm thick) as well as for thick soil layers (greater than 10 cm in thickness). It should be noted that the concept of “surface resistance” to vapour water diffusion originated from the calculation of transpiration from a tree canopy and the stomata of leaves (Monteith, 1965).

A series of laboratory tests collected from the research literature and from the present laboratory program are used to assess the reduction in the evaporation rate caused by free energy (suction). Soil suction can be related to unsaturated soil properties by defining the air-entry value and residual soil suction on a Soil Water Characteristic Curve (SWCC).

This chapter is divided into eight sections. The present section introduces the concepts associated with the prediction of the evaporation rate from a soil surface using surface resistance. Sections 3.2 and 3.3 are a re-visitation of the mechanism of mass and heat transfer and the derivation of the Penman-Monteith equation (1965) of evaporation. The theoretical development of the soil-atmospheric model, including surface resistance is presented in Section 3.4. Section 3.5 presents the assessment of soil suction and the corresponding volumetric water content at evaporation rate reduction during the process of drying. Section 3.6 presents methods for the determination of soil surface resistance and relative humidity at the soil surface. These methods are then utilized in the developed soil-atmospheric model. Section 3.7 presents the effect of pore-water salinity on the evaporation rate from salinized soils. A proposed solution for the soil-atmosphere evaporative flux equation and analyzing evaporation from salinized soils are presented in Section 3.8. Finally, Section 3.9 presents a summary of the chapter.

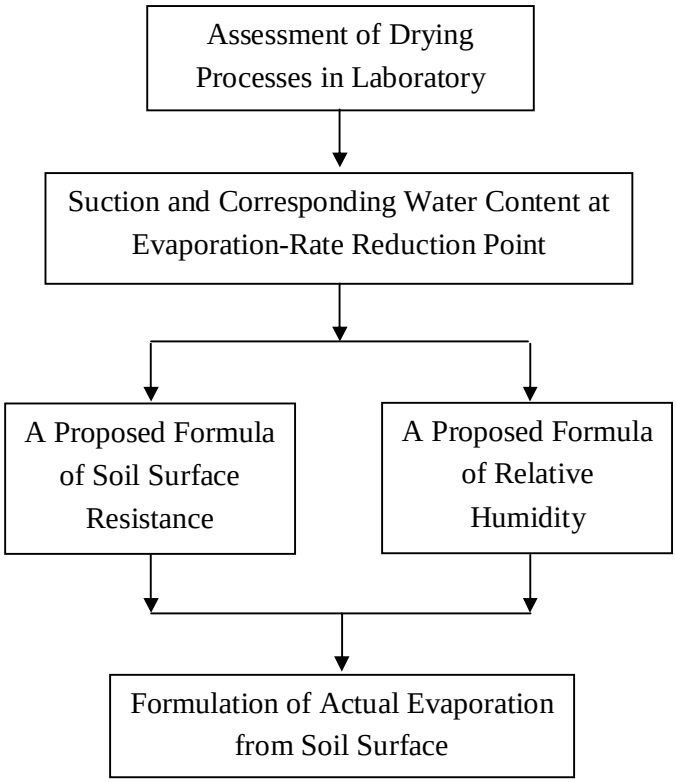

Figure 3.1 Flowchart for the formulation of actual evaporation equation from a soil surface.

3.2 RE-VISITATION OF EVAPORATIVE FLUX AND SENSIBLE HEAT FLUX

The soil-atmosphere system can be divided into a series of boundary layers approximately parallel to the active surface. The boundary can be divided into three layers. The processes associated with water vapour movement in each of the boundary layers influence evaporation from a soil surface. Firstly, the sub-surface layer lies immediately below the soil surface and has a limited thickness in the order 0–1 cm. In this sub-surface layer, water vapour is transported by molecular diffusion from the water surface in the soil pores in the vertical direction towards ground surface.

The water vapour is then subjected to atmospheric demands within the laminar boundary layer which lies immediately above the ground surface (i.e., a few millimetres) (Toth, 1999). The thickness of the laminar sub-layer depends mainly upon the roughness of the ground surface and the external wind speed (Oke, 1993). There is essentially no convection process in this laminar sub-layer and the transfer of moisture is due to the molecular diffusion of water vapour parallel to the ground surface with no cross-stream component. The flux of water vapour through this layer can be expressed using Fick's Law (Oke, 1993). The diffusion coefficients can be assumed to be constant with respect to the elevation above the surface. The diffusion coefficients are also small (i.e., on the order of 10^{-5} m^2/s).

The turbulent ground surface layer is the part of the planetary boundary layer immediately above the surface where small-scale turbulence dominates transfer and vertical variation of the vertical fluxes is less than 10% (Oke, 1993). The turbulent diffusion is considerably more effective than the process due to molecular diffusivity. In addition, the process is very different. There is, however, a similarity between the roles played by eddies in convection and that of molecules in molecular diffusion. Consequently, the flux gradient transfer equations for vapour, heat and momentum can be extended to fluxes in the turbulent zone and the molecular diffusion coefficients are replaced with eddy diffusivities, (i.e., K_W, K_H and K_M with unit of m^2/s). These diffusivities are not constant. They are also larger than molecular diffusion constants and increase with elevation (i.e., 10^{-5} m^2/s to 10^2 m^2/s). Figure 3.2 illustrates the development of the turbulent layer as well as the flux, diffusion coefficients and gradient profiles with elevation.

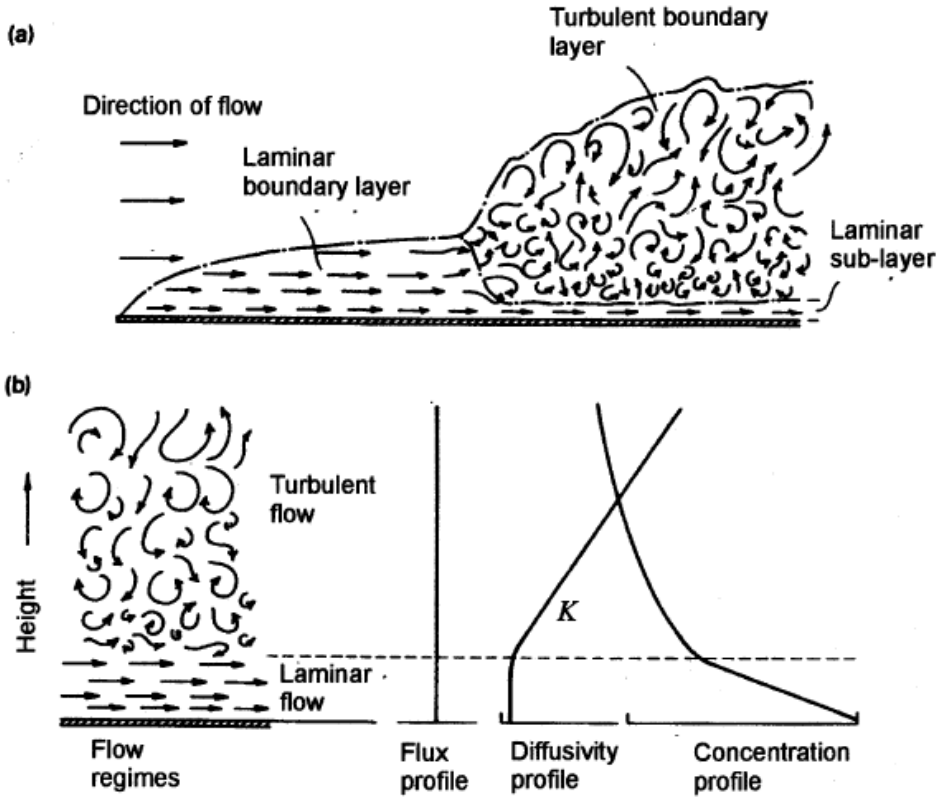

Figure 3.2 The development of (a) laminar boundary layer as well as the transition to turbulent flow, and (b) the vertical variation of the flux of any entity and the associated diffusion coefficients and the concentration of its property (adapted from Oke, 1993).

Solving the transient flow equations for liquid water, water vapour, and heat in a soil profile require a definition of the upper boundary conditions at the soil surface. These boundary equations can be derived using the flux-gradient profiles which were defined as eddy changes that occur with elevation (i.e., specific humidity profile, temperature profile and wind speed profile). The upper boundary condition for heat flow (sensible heat flux) can be derived by combining two flux-gradient profiles such as the temperature profile and the wind speed profile. The upper boundary condition for vapour flow (evaporative flux) needs to be derived from a combination of two flux-gradient profiles such as the specific humidity profile and the wind speed profile (see Figure 3.3).

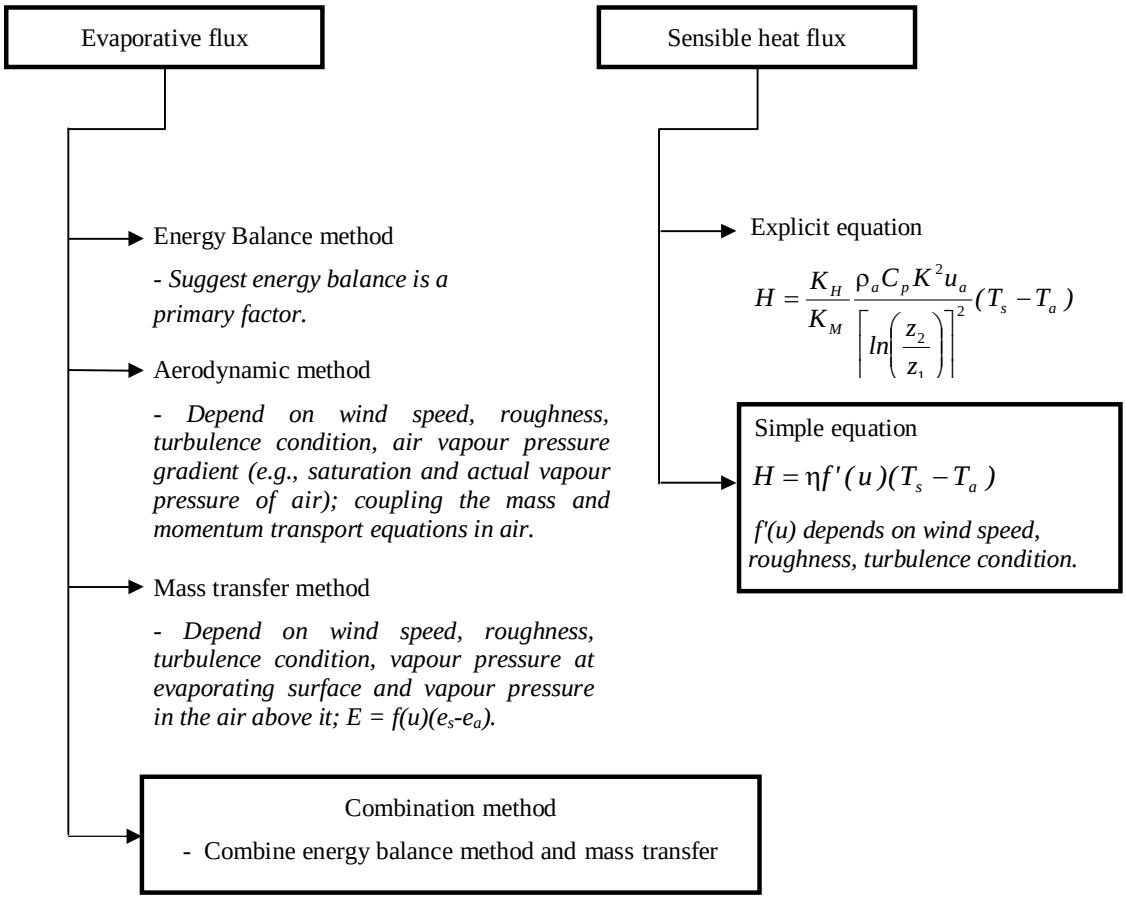

Figure 3.3 Flowchart of evolution of methods for prediction of evaporation.

It is necessary to re-visit the derivation of evaporative flux and sensible heat flux prior to undertaking further study on the evaporation model from a soil surface. It is the evaporation model that is of greatest interest to geotechnical engineers for water balance calculations.

3.2.1 Evaporative Flux - Mass Transfer Method

Wind can be considered as a purely mechanical turbulence. Its role in the removal of water vapour from the turbulent zone means that the wind speed profile must be understood. Unlike temperature and specific humidity profiles, wind speed has a zero boundary condition at ground surface. Consequently, the calculation of the transfer of momentum can be performed if the wind

speed above the surface is known. The transfers of heat and water vapour are then related to the transfer of momentum. The fundamental theory of boundary layer climate has been presented in detail by Oke (1993).

The wind speed profile and the specific humidity profile can be combined to estimate the movement of vapour from an evaporating surface to the atmosphere. Mass and momentum transport occur by the convective process (see Figure 3.4).

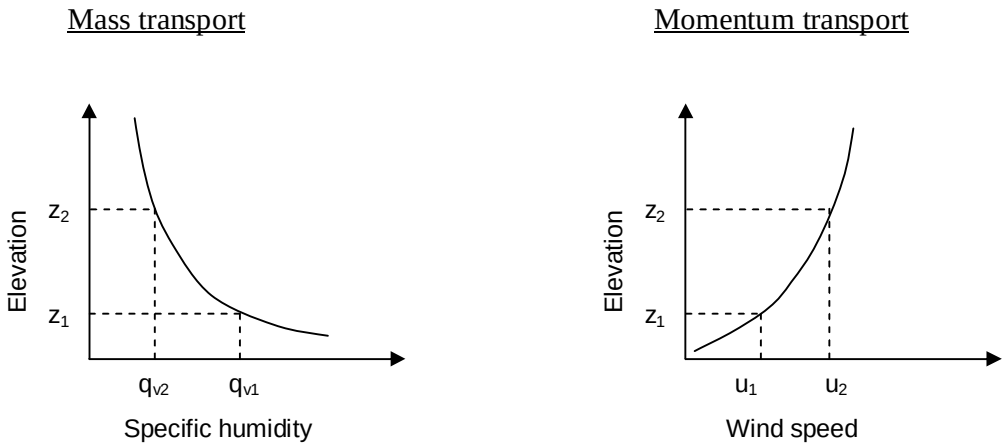

Figure 3.4 Illustration of profiles of specific humidity and wind speed for determination of evaporative flux.

The vertical fluxes of vapour mass (m_v) and momentum (τ) can be written in a mathematical form for the turbulent surface layer. This is an illustration of the way in which the molecular analogy can be extended to turbulent flow. The flux of vapour mass is related to the gradient of specific humidity and the ability of an eddy to transfer mass. The flux of momentum is related to the gradient of horizontal momentum and the ability of an eddy to transfer momentum.

$$m_v = -\rho_a K_W \frac{dq_v}{dz} \tag{3.1}$$

$$\tau = \rho_a K_M \frac{du}{dz} \tag{3.2}$$

where:

K_W = vapour eddy diffusivity (m^2/s);

ρ_a = density of air (kg/m^3);

m_v = change of vapour mass with time ($kg/m^2/s$);

$\frac{dq_v}{dz}$ = change of specific humidity with height (1/m);

K_M = momentum eddy diffusivity (m^2/s);

τ = change of momentum with time ($kg/m/s^2$);

$\frac{du}{dz}$ = change of wind speed with height (1/s).

The change of specific humidity and wind speed from height of z_1 to height of z_2 are determined from profiles of specific humidity and wind speed, as follows (see Figure 3.4):

$$\frac{dq_v}{dz} = \frac{q_{v2} - q_{v1}}{z_2 - z_1} \tag{3.3}$$

$$\frac{du}{dz} = \frac{u_2 - u_1}{z_2 - z_1} \tag{3.4}$$

where:

q_{v1} = specific humidity at height of z_1 (dimensionless);

q_{v2} = specific humidity at height of z_2 (dimensionless);

u_1 = wind speed at height of z_1 (m/s);

u_2 = wind speed at height of z_2 (m/s).

Therefore, the ratio of mass flux to momentum flux can be written as follows:

$$\frac{m_v}{\tau} = -\rho_a K_W \frac{q_{v2} - q_{v1}}{z_2 - z_1} \times \frac{1}{\rho_a K_M} \frac{z_2 - z_1}{u_2 - u_1} \tag{3.5}$$

or

$$\frac{m_v}{\tau} = -\frac{K_W}{K_M} \frac{q_{v2} - q_{v1}}{u_2 - u_1} \tag{3.6}$$

The atmosphere in the turbulent layer can be assumed to be in a neutral condition. Therefore, the wind speed profile can be described using a Natural Logarithmic Law.

$$\frac{u}{u^*} = \frac{1}{K} ln\left(\frac{z}{z_0}\right) \tag{3.7}$$

or $$u = \frac{u^*}{K} ln\left(\frac{z}{z_0}\right) \tag{3.8}$$

where:

K = Von Karman constant, 0.4;

z_0 = roughness height (m);

z = height (m);

u^* = shear velocity or friction velocity, $u^* = \sqrt{\frac{\tau}{\rho_a}}$

Equation (3.8) can be subjected to with different wind speeds between height of z_1 and height of z_2.

$$u_2 - u_1 = \frac{u^*}{K}\left[ln\left(\frac{z_2}{z_0}\right) - ln\left(\frac{z_1}{z_0}\right)\right] \tag{3.9}$$

or $$u^* = \frac{K(u_2 - u_1)}{ln\left(\frac{z_2}{z_1}\right)} \tag{3.10}$$

It follows that;

$$\tau = \rho_a \left[\frac{K(u_2 - u_1)}{ln\left(\frac{z_2}{z_1}\right)}\right]^2 \tag{3.11}$$

Substituting (3.11) into (3.6), gives

$$m_v = -\tau \frac{K_W}{K_M} \frac{q_{v2} - q_{v1}}{u_2 - u_1} = -\frac{K_W}{K_M} \frac{q_{v2} - q_{v1}}{u_2 - u_1} \times \rho_a \left[\frac{K(u_2 - u_1)}{ln\left(\frac{z_2}{z_1}\right)}\right]^2 \tag{3.12}$$

or $$m_v = -\frac{K_W}{K_M}\frac{(q_{v2}-q_{v1})}{ln^2\left(\frac{z_2}{z_1}\right)}\times \rho_a K^2(u_2-u_1) \quad (3.13)$$

Since specific humidity is defined as:

$$q_v = \frac{0.622e}{P} \quad (3.14)$$

where:

P = atmospheric pressure (kPa);

e = vapor pressure at certain height (kPa);

Then the vapour pressure equations can be written in the same form for two elevations $q_{v1} = \frac{0.622e_s}{P}$ and $q_{v2} = \frac{0.622e_a}{P}$ (3.15)

where:

e_s = vapor pressure at the evaporating surface with height of z_1 (kPa);

e_a = vapor pressure in the air above the evaporatin surface with height of z_2 (kPa).

Equation (3.13) therefore becomes:

$$m_v = \frac{K_W}{K_M}\frac{0.622\rho_a K^2(u_2-u_1)(e_s-e_a)}{P\left[ln\left(\frac{z_2}{z_1}\right)\right]^2} \quad (3.16)$$

Let us consider the case of evaporation from the evaporating surface where the wind speed at the evaporating surface is close to zero, $u_1 = 0$ and $u_2 = u_a$; hence

$$m_v = \frac{K_W}{K_M}\frac{0.622\rho_a K^2 u_a(e_s-e_a)}{P\left[ln\left(\frac{z_2}{z_1}\right)\right]^2} \quad (3.17)$$

Dividing equation (3.17) by the density of water, ρ_w, allows the change of water mass with time to be converted into vapour flux with the units of velocity (i.e., m/s),

$$E = \frac{K_W}{K_M} \frac{0.622 \rho_a K^2 u_a (e_s - e_a)}{P \rho_w \left[ln\left(\frac{z_2}{z_1} \right) \right]^2} \tag{3.18}$$

Equation (3.18) can be written in the simple form as follows:

$$E = f(u)(e_s - e_a) \tag{3.19}$$

where:

$$f(u) = \frac{K_W}{K_M} \frac{0.622 \rho_a K^2 u_a}{P \rho_w \left[ln\left(\frac{z_2}{z_1} \right) \right]^2} \tag{3.20}$$

where:

f(u) = the transmission function for water vapour;

E = evaporative flux (m/s).

3.2.2 Sensible Heat Flux - Transfer of Sensible Heat

The wind speed profile and temperature profile can be combined to estimate the ability to transport heat from an evaporating surface to the atmosphere. Heat and momentum transport occur as convective processes (see Figure 3.5).

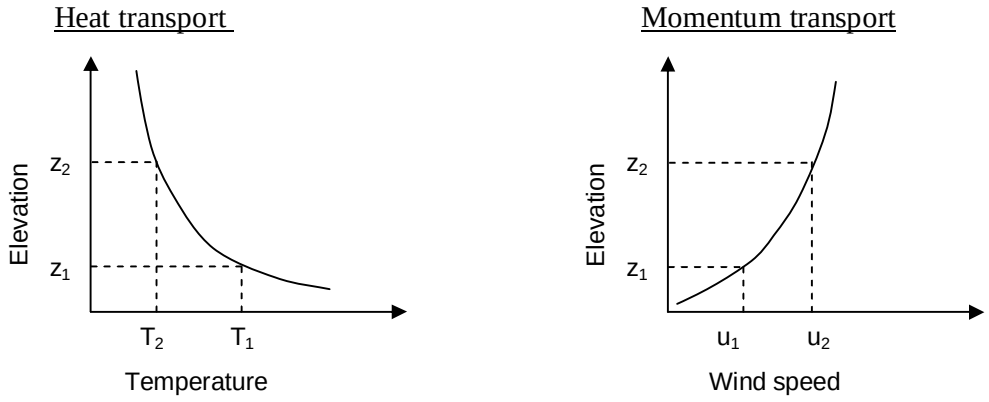

Figure 3.5 llustration of profiles of temperature and wind speed for determination of sensible heat flux.

The vertical fluxes of heat (h) and momentum (τ) can be calculated for the turbulent surface layer as follows:

$$h = -\rho_a C_p K_H \frac{dT}{dz} \tag{3.21}$$

$$\tau = \rho_a K_M \frac{du}{dz} \tag{3.22}$$

where:

K_H = heat eddy diffusivity (m^2/s);

C_p = specific heat capacity of air ($J/kg/^oC$);

$\frac{dT}{dz}$ = change of temperature with height ($^oC/m$);

h = change of heat with time ($J/ m^2/s$).

The profiles of temperature allow the change of temperature from height of z_1 to height of z_2 to be determined as follows (see Figure 3.5):

$$\frac{dT}{dz} = \frac{T_2 - T_1}{z_2 - z_1} \tag{3.23}$$

where:

T_1 = temperature at height of z_1 (^oC);

T_2 = temperature at height of z_2 (^oC);

The ratio of heat flux to momentum flux can be established as follows:

$$\frac{h}{\tau} = -\rho_a C_p K_H \frac{T_2 - T_1}{z_2 - z_1} \times \frac{1}{\rho_a K_M} \frac{z_2 - z_1}{u_2 - u_1} \tag{3.24}$$

or

$$\frac{h}{\tau} = -C_p \frac{K_H}{K_M} \frac{T_2 - T_1}{u_2 - u_1} \tag{3.25}$$

Substituting Eq. (3.11) into Eq. (3.25), gives

$$h = -\tau C_p \frac{K_H}{K_M}\frac{T_2 - T_1}{u_2 - u_1} = -C_p \frac{K_H}{K_M}\frac{T_2 - T_1}{u_2 - u_1} \times \rho_a \left[\frac{K(u_2 - u_1)}{ln\left(\frac{z_2}{z_1}\right)}\right]^2 \tag{3.26}$$

or

$$h = -C_p \frac{K_H}{K_M}\frac{(T_2 - T_1)}{ln^2\left(\frac{z_2}{z_1}\right)} \times \rho_a K^2 (u_2 - u_1) \tag{3.27}$$

Therefore, Equation (3.27) becomes;

$$h = -C_p \frac{K_H}{K_M}\frac{\rho_a K^2 (T_2 - T_1)(u_2 - u_1)}{\left[ln\left(\frac{z_2}{z_1}\right)\right]^2} \tag{3.28}$$

Equation (3.28) deals with heat transport from an evaporating surface where the wind speed and temperature at the evaporating surface are $u_1 = 0$ and $T_1 = T_s$, respectively. The wind speed and temperature in the air above ground surface are $u_2 = u_a$ and $T_2 = T_a$, respectively. Hence,

$$h = \frac{K_H}{K_M}\frac{\rho_a C_p K^2 u_a (T_s - T_a)}{\left[ln\left(\frac{z_2}{z_1}\right)\right]^2} \tag{3.29}$$

Equation (3.29) can be rewritten in a simpler form as follows:

$$H = \eta f'(u)(T_s - T_a) \tag{3.30}$$

where:

$$f'(u) = \frac{K_H}{K_M}\frac{0.622\rho_a K^2 u_a}{P\rho_w\left[ln\left(\frac{z_2}{z_1}\right)\right]^2} \tag{3.31}$$

$f'(u)$ = the transmission function for heat;

$\eta = \frac{C_p P}{0.622\lambda_v}$ and is called the psychrometric constant, 66.8 (Pa/^{o}C);

H = sensible heat flux in m/s.

3.3 RE-VISITATION OF PENMAN-MONTEITH'S EQUATION (1965)

Penman (1948) derived an equation for the estimation of evaporation from an open water pan. The formulation took energy balance into consideration and included net radiation, convective heat exchange between the water and the atmosphere. Heat exchanged with the environment through the pan itself was ignored. Penman (1948) proposed a method of calculating potential evaporation by combining the mass transfer and the transfer of sensible heat from the ground surface to the atmosphere using the ground surface energy balance as follows:

$$Q_n = E + H \tag{3.32}$$

where:

Q_n = net radiant energy available at the surface, mm/day;

E = evaporative flux to the air, mm/day;

H = sensible heat flux to the air, mm/day.

The equation derived by Penman (1948) for calculating evaporation rates is as follows:

$$E_P = \frac{\Gamma Q_n + \eta E_a}{\Gamma + \eta} \tag{3.33}$$

where:

E_p = evaporation rate from an open water pan (mm/day);

E_a = aerodynamic evaporative term, $E_a = f(u)(e_{a0} - e_a)$ (mm/day/Pa);

e_{a0} = saturation vapour pressure of the mean air temperature, kPa;

e_a = vapour pressure of the air above the surface, kPa;

$$f(u) = 3.5(1 + 0.146U_a) \tag{3.34}$$

U_a = wind speed, km/hr;

Q_n = *h*eat budget, (mm/day);

Γ = slope of the saturation vapour pressure versus temperature curve at the mean temperature of the air, (Pa/^{o}C);

η = psychromatric constant, 66.8 (Pa/^{o}C).

Equation (3.33) is based on the assumption that the transfer coefficients for water vapor, momentum and heat are similar on the basis of the "Similarity Theory" developed by Monin-Obhukov (Oke, 1993). Accordingly, the ratios of K_W/K_M and K_H/K_M are approximately 1.0 under stable atmospheric conditions. It then follows that, $f'(u) = f(u)$. Therefore, the Penman (1948) method is only validated for a surface with available free water.

The original Penman (1948) equation included the bulk surface resistance from the soil in the term of the wind function but the surface resistance was not explicitly defined. Consequently, in the aerodynamic forms of the Penman equation, the impact of surface resistance is not incorporated in the E_a term.

Several researchers have included a bulk surface resistance term in the derivation of the Penman's (1948) equation including Penman (1953), Covey (1959), Rijitema (1965), and Monteith (1965). One of revised equations is now referred to as the Penman-Monteith's (1965) equation. The equation was initially used to account for the difference between evaporation from an open water pan and leaf transpiration. The equation was useful for representing the turbulent transport process in terms of atmospheric conductance and the molecular diffusion process to account for leaf transpiration. Later the equation was used to calculate soil-surface evaporation. It should be noted that leaf transpiration involves the movement of water vapor from inside the leaves of plants to the air outside the leaves. This process takes place through aperatures called stomata and it occurs through molecular diffusion. The derivation of the Penman-Monteith's (1965) equation is further re-visited in next section.

Monteith (1965) also used the combination method (i.e., energy balance and mass balance) to derive leaf transpiration.

$$H = \eta f'(u)(T_s - T_a) \times (\lambda_v \rho_w) \tag{3.35}$$

$$E_T = f(u)(e_{s0} - e_a) \tag{3.36}$$

The equation of the energy balance at ground surface can be written as,

$$K + L = H + E_T \times \lambda_v \times \rho_w \tag{3.37}$$

where:

E_T = transpiration rate from a leaf (mm/day);

K = short wave net radiation input (W/m^2);

L = long wave net radiation input (W/m^2);

λ_v = latent heat of vaporization (J/kg);

ρ_w = density of water (kg/m^3);

H = sensible heat flux from a leaf to the atmosphere (W/m^2).

Short and long wave net radiation inputs are measured or estimated in a variety of ways. Therefore, the derivation of the Penman-Monteith (1965) method simply focused on the transfer of sensible heat flux from the leaf to the atmosphere, H. The sensible heat flux was estimated to be a function of the leaf surface temperature, T_s and was presented as follows:

$$H = \eta f'(u)(T_s - T_a) \times (\lambda_v \rho_w) \tag{3.38}$$

where:

T_s = temperature of water surface (^oC);

T_a = temperature of the atmosphere above (^oC);

η = psychrometric constant, 66.8 ($Pa/^oC$);

$f'(u)$ = transmission functions for heat which depends on wind speed, roughness and turbulence condition;

$$f'(u) = 3.5(1 + 0.146U_a) \tag{3.39}$$

U_a = wind speed, km/hr;

$\lambda_v \rho_w$ = a factor to convert unit of m/s into unit of W/m^2.

It is quite rare to have leaf-surface temperature data. However, the difference between the leaf-surface temperature, T_s and air temperature, T_a are related to the difference between the saturated vapor pressures at T_s and T_a. If the

difference between T_s and T_a is small, the following relationship can be written;

$$\Gamma(T_s - T_a) = e_{s0} - e_{a0} \tag{3.40}$$

where:

Γ = slope of the relationship between water vapor pressure and temperature at a specific temperature ;

e_{s0} = saturated vapor pressure at T_s, kPa;

e_{a0} = saturated vapor pressure at T_a, kPa.

One of several proposed procedures can be used as an approximation of the slope of the water vapour pressure versus temperature relationship. Tetens (1930) estimated Γ based on the air temperature as follows:

$$\Gamma = \frac{4098 e_{a0}}{(237.3 + T_a)^2} \tag{3.41}$$

and $$e_{s0} = 0.6108 exp\left(\frac{17.27 T_s}{237.3 + T_s}\right) \tag{3.42}$$

The following equation was obtained from Eq. (3.40).

$$T_s - T_a = \frac{e_{s0} - e_{a0}}{\Gamma} \tag{3.43}$$

Subtitution Eq. (3.43) into Eq. (3.38), gives

$$H = \eta f'(u)(\lambda_v \rho_w)\frac{(e_{s0} - e_{a0})}{\Gamma} \tag{3.44}$$

If the atmospheric water vapor pressure, e_a , are added and subtracted within the brackets of Eq. (3.44), the following equation can be written;

$$H = \eta f'(u)(\lambda_v \rho_w)\frac{(e_{s0} - e_{a0} + e_a - e_a)}{\Gamma} \tag{3.45}$$

$$H = \eta f'(u)(\lambda_v \rho_w)\frac{(e_{s0} - e_a)}{\Gamma} - \eta f'(u)(\lambda_v \rho_w)\frac{(e_{a0} - e_a)}{\Gamma} \tag{3.46}$$

According to the mass transfer approach to evaporation,

$$E_T = f(u)(e_{s0} - e_a)$$

$$E = f(u)(e_s - e_a) \tag{3.19}$$

or $$e_{s0} - e_a = \frac{E_T}{f(u)} \tag{3.47}$$

where:

f(u) = transmission functions for water vapor which depends on wind speed, roughness and turbulence condition;

Substituting Eq. (3.47) into Eq. (3.46), gives

$$H = \frac{\eta f'(u)}{f(u)}(\lambda_v \rho_w)\frac{E_T}{\Gamma} - \eta f'(u)(\lambda_v \rho_w)\frac{(e_{a0} - e_a)}{\Gamma} \tag{3.48}$$

Substituting Eq. (3.48) into Eq. (3.37) and re-arranging, gives

$$E_T = \frac{\Gamma(K + L) + \eta(\lambda_v \rho_w) f'(u)(e_{a0} - e_a)}{\lambda_v \rho_w \left[\Gamma + \eta \frac{f'(u)}{f(u)}\right]} \tag{3.49}$$

or $$E_T = \frac{\Gamma(K + L) + \eta(\lambda_v \rho_w)\frac{f'(u)}{f(u)} f(u)(e_{a0} - e_a)}{\lambda_v \rho_w \left[\Gamma + \eta \frac{f'(u)}{f(u)}\right]} \tag{3.50}$$

Equation (3.50) expresses the Penman-Monteith's (1965) equation in terms of atmospheric conductance and canopy conductance for the evaporation rate from a leaf. Data required to estimate E_T include air temperature, net radiation input, wind speed, vegetation height, relative humidity. Other parameters (e.g., Γ, C_p , ρ_a) can be obtained from air temperature. Equation (3.50) can be used to estimate instantaneous evaporation rate, E_T, if instantaneous measurements of radiation, wind, relative humidity and air temperature are known.

The Penman-Monteith's (1965) equation can be rewritten in the shorter form for leaf transpiration as follows:

$$E_T = \frac{\Gamma Q_n + \eta \frac{f'(u)}{f(u)} E_a}{\Gamma + \eta \frac{f'(u)}{f(u)}} \tag{3.51}$$

where:

E_T = transpiration rate from a leaf which is a two-step process (mm/day);

E_a = aerodynamic evaporative term, $E_a = f(u)(e_{a0} - e_a)$ (mm/day/Pa);

Q_n = *h*eat budget, (mm/day).

Atmospheric conductance can be defined as;

$$C_{at} = \frac{K^2 u_a}{\left[ln\left(\frac{z_2}{z_1} \right) \right]^2} \tag{3.52}$$

Both $f(u)$ and $f'(u)$ can be expressed as functions of atmospheric conductance, C_{at} as follows:

$$f(u) = \frac{K_W}{K_M} \frac{0.622 \rho_a C_{at}}{P \rho_w} \tag{3.53}$$

$$f'(u) = \frac{K_H}{K_M} \frac{0.622 \rho_a C_{at}}{P \rho_w} \tag{3.54}$$

Water vapor movement from a canopy of vegetation can be viewed as a two-step process, as previously discussed. The processes involve canopy conductance, (C_{can}) as well as atmospheric conductance, (C_{at}). Since conductance is the reciprocal of resistance, and the overall resistance to water

vapor transport will be the sum of canopy and atmospheric resistance, the overall conductance, (C_t) can be written as;

$$C_t = \frac{1}{\frac{1}{C_{at}} + \frac{1}{C_{can}}} = \frac{C_{at}}{\left(1 + \frac{C_{at}}{C_{can}}\right)} \tag{3.55}$$

Vapor transport from a vegetative canopy to the atmosphere can be expressed by replacing C_{at} by C_t. The result is the following expression.

$$f(u) = \frac{K_W}{K_M} \frac{0.622 \rho_a C_{at}}{P \rho_w \left(1 + \frac{C_{at}}{C_{can}}\right)} \tag{3.56}$$

If it is assumed that $K_H / K_M = 1$ and $K_W / K_M = 1$ (i.e., Similarity Theory holds true), the aerodynamic function for water vapor, $f(u)$ becomes different from that for heat transport, $f'(u)$.This is primary difference between the Penman (1948) equation and the Penman-Monteith's (1965) equation. The ratio of $f'(u) / f(u)$ can be presented as follows:

$$\frac{f'(u)}{f(u)} = 1 + \frac{C_{at}}{C_{can}} \tag{3.57}$$

or $$\frac{f'(u)}{f(u)} = 1 + \frac{r_{can}}{r_{av}}$$

where:

r_{av} = aerodynamic resistance to turbulent diffusion, (s/m),

$r_{av} = 1/C_{at}$; and

r_{can} = surface resistance to molecular diffusion (s/m), $r_{can} = 1/C_{can}$.

The Monteith (1965) equation is first applied to the estimation of evaporation from a canopy and then to evaporation from a soil surface. The Monteith method takes surface resistance into account and includes the surface resistance embedded in the Penman (1948) equation. Hence the Monteith equation overcomes the main disadvantage of the Penman (1948) equation and provides an estimate of potential evaporation from a wet surface other than a water surface.

3.4 THEORETICAL DEVELOPMENT OF SOIL-ATMOSPHERIC EQUATION FOR ESTIMATION OF ACTUAL SOIL EVAPORATION

Wilson (1990) recognized the main disadvantage of the Penman (1948) equation in that it basically provided an estimation of potential evaporation at a free water surface. The Penman equation gave an over-estimation of evaporation from unsaturated soil surfaces. Wilson (1990) then went on to propose an equation for calculating actual soil evaporation. The Wilson (1990) equation included the relative humidity at the unsaturated soil surface and moved away from the primary disadvantage of the Penman equation. However, Wilson (1990) assumed that the transmission functions of mass and heat were the same (i.e., *f'(u) = f(u)*); Therefore, the Wilson (1990) equation did not account for the existence of soil surface resistance to the diffusion of water vapour from pores at the soil matrix to soil-atmosphere boundary.

The equation presented by Wilson (1990) for calculating evaporation rates from unsaturated soil surfaces was as follows:

$$AE = \frac{\Gamma Q_n + \eta E_a}{\Gamma + \eta A} \tag{3.58}$$

where:

E_a = flux associated with "mixing", $E_a = f(u)e_a(B - A)$;

f(u) = a function depending on wind speed, roughness and turbulence condition; $f(u) = 3.5(1 + 0.146U_a)$

U_a = wind speed, km/hr;

e_a = air pressure in the air above soil surface, (kPa);

Q_n = heat budget, (mm/day);

Γ = slope of the saturation vapour pressure versus temperature curve at the mean temperature of the air, (Pa/^{o}C);

η = psychromatric constant, 66.8 (Pa/^{o}C).

The primary advantage of Eq. (3.58) was the ability to describe evaporation from a soil surface on the basis of net radiation, wind speed and the relative humidities in the air and at the soil surface. Wilson's (1990) equation was convenient in that it reduced to the Penman (1948) equation when A = unity (i.e., relative humidity of 100 percent for a saturated surface).

Over time, it became apparent that the Wilson-Penman's equation over-estimated actual evaporation from unsaturated soil columns. The equation was found to only be valid for thin soil layer, (0.5 – 1 mm thick). Dunmola (2012) modified the Wilson et al. (1997) equation by introducing surface resistance. However, the modified equation did not require routine weather parameters. Moreover, the Dunmola (2012) equation used large values of soil surface resistance to obtain results that agreed with measured data. It is important to have a soil-atmosphere model that uses routine weather parameters and including soil surface resistance to water vapour diffusion from evaporative front of a soil (i.e., the soil-atmosphere boundary).

3.4.1 Proposed Modifications to the Penman-Monteith Equation

The following assumptions are associated with the proposed modifications to the Penman-Monteith equation to describe the upper boundary condition for the flow of water vapor (at soil-atmosphere interface).

1. The atmosphere in the turbulent layer immediately above a soil surface is in a neutral condition, consequently, the profile of wind speed can be expressed as a Natural Logarithmic function;

2. Soil surface resistance exists at the top of the soil surface where water vapor diffusion dominates;

3. The air adjacent to the evaporating front is assumed to lie within 0 – 1 cm and is not in equilibrium with liquid water in soil pores. In other words, thermodynamic laws are invalid in this layer as soil becomes dry.

The evaluation of evaporative flux from a soil surface using Eqs. (3.49) and (3.50) requires detailed information regarding atmospheric stability, surface roughness, wind speed and surface temperature. The energy balance equation at ground surface can be written as follows:

$$Q = H + E_A \text{ or } H = Q - E_A \tag{3.59}$$

where:

$H = \eta f'(u)(T_s - T_a)$ = sensible heat flux (converted to mm/day);

$E_A = f(u)(e_s - e_a)$ = evaporative flux (mm/day);

Q = net radiation (converted to mm/day);

e_s = actual vapor pressure at soil surface, (kPa);

e_a = air pressure in the air above soil surface, (kPa);

T_s = temperature at soil surface, (^{o}C);

T_a = temperature in the air above, (^{o}C);

η = psychrometric constant, 66.8 (Pa/^{o}C); and

f(u) and *f'(u)* = transmission functions for water vapor and heat, respectively which depend on wind speed, roughness and turbulence conditions.

Subsituting $H = \eta f'(u) \times (T_s - T_a)$ into the Eq. (3.59), gives

$$\eta f'(u) \times (T_s - T_a) = Q - E_A \tag{3.60}$$

If the difference between T_s and T_a is small, then

$$\Gamma(T_s - T_a) = e_{s0} - e_{a0} \tag{3.61}$$

and,

$$\eta f'(u) \times \frac{e_{s0} - e_{a0}}{\Gamma} = Q - E_A \tag{3.62}$$

Re-arranging Eq. (3.62), gives

$$f'(u) = \frac{\Gamma(Q - E_A)}{\eta(e_{s0} - e_{a0})} \tag{3.63}$$

Dividing both sides of Eq. (3.63) by *f(u)*, gives

$$\frac{f'(u)}{f(u)} = \frac{\Gamma(Q - E_A)}{\eta f(u)(e_{s0} - e_{a0})} \tag{3.64}$$

Adding and subtracting the term of Ae_a to the denominator of the right side of Eq. (3.64), gives

$$\frac{f'(u)}{f(u)} = \frac{\Gamma(Q - E_A)}{\eta f(u)(e_{s0} - e_{a0} + Ae_a - Ae_a)} \tag{3.65}$$

Noting that, $e_{s0} = Ae_s$ and $e_{a0} = Be_a$, and substituting these terms into Eq. (3.65) and re-arranging, gives

$$\frac{f'(u)}{f(u)} = \frac{\Gamma(Q - E_A)}{\eta f(u)(Ae_s - Ae_a + Ae_a - Be_a)} \tag{3.66}$$

$$\frac{f'(u)}{f(u)} = \frac{\Gamma(Q - E_A)}{\eta A f(u)(e_s - e_a) - \eta f(u) e_a (B - A)} \tag{3.67}$$

Hence, since $E_A = f(u)(e_s - e_a)$ and $E'_a = f(u)e_a(B - A)$

$$\frac{f'(u)}{f(u)} = \frac{\Gamma(Q - E_A)}{\eta A E_A - \eta E'_a} \tag{3.68}$$

where:

A = inverse of soil relative humidity, $A = 1/RH_s$;

B = inverse of the air relative humidity, $B = 1/RH_a$;

RH_s and RH_a = relative humidity at soil surface and the overlying air, respectively;

E'_a = an aerodynamic evaporative term (mm/day/Pa);

T_a = Temperature in the overlying air (^{o}C).

Re-arranging the equation (3.68), gives

$$E_A = \frac{\Gamma Q + \eta \frac{f'(u)}{f(u)} E'_a}{\Gamma + \eta A \frac{f'(u)}{f(u)}} \tag{3.69}$$

Equation (3.69) describes evaporation from a soil surface on the basis of net radiation, wind speed, relative humidity of the air and the soil surface, and soil surface resistance. Details pertaining to soil surface resistance are discussed in the following sections.

Equation (3.69) reduces to conventional Penman (1948) equation when A = unity (i.e., relative humidity of 100 percent for a saturated surface) and surface resistance is assumed to be zero. It is also interesting to note that Eq. (3.69) reduces to the Wilson (1990) equation when $\frac{f'(u)}{f(u)} = 1$ (i.e., the transmission functions for mass and heat are assumed to be the same or the soil surface resistance equals to zero). Equation (3.69) contains not only a component of the relative humidity at a soil surface, but also soil surface resistance. It indicates that the evaporation rate will decrease during the drying process in which the relative humidity of the soil surface decreases and the soil surface resistance increases.

3.4.2 Effect of Soil Surface Resistance on Aerodynamic Functions

Application of the concept that water vapor transport from the canopy involves the movement of water vapor from inside plant leaves to the air through apertures called stomata. The evaporation from a soil surface is based on molecular diffusion through a thin layer at a soil surface and turbulent diffusion in the air. Molecular diffusion appears as part of the soil profile where water vapour dominates (see Section 3.2.1).

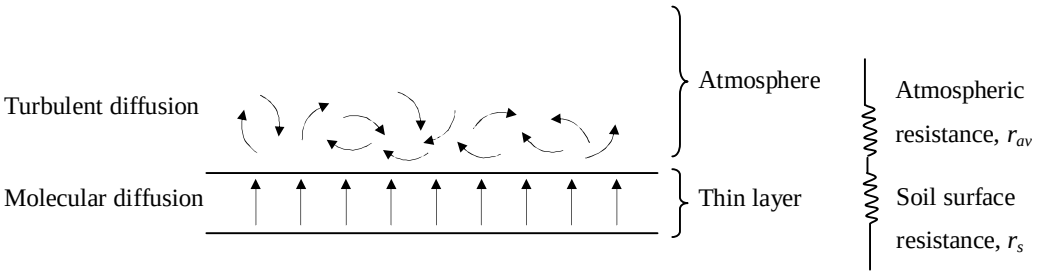

Figure 3.6 Illustration of phenomenon of evaporation from a soil surface.

Evaporation involves the conductance of a thin layer at the soil surface, (C_s) as well as atmospheric conductance (C_{at}). The overall resistance to water vapor transport is the sum of atmospheric resistance, r_{av} and soil surface resistance, r_s.

$$r_t = r_{av} + r_s \tag{3.70}$$

where:

r_t = total resistance to water vapor transport, (s/m), $r_t = 1/C_t$;

r_{av} = atmospheric resistance to water vapor transport, (s/m), $r_{av} = 1/C_{at}$;

r_s = soil surface resistance to water vapor transport, (s/m), $r_s = 1/C_s$;

$C_{at} = \dfrac{K^2 u_a}{\left[ln\left(\dfrac{z_2}{z_1}\right)\right]^2}$ = Atmospheric conductance (m/s).

Replacing resistance by the inverse of conductance, gives

$$\frac{1}{C_t} = \frac{1}{C_{at}} + \frac{1}{C_s} \tag{3.71}$$

or $$C_t = \frac{C_{at}}{1 + \dfrac{C_{at}}{C_s}} \tag{3.72}$$

The transmission function for vapor transport from the soil surface to the atmosphere (e.g., Equation 3.53) can be expressed by replacing C_{at} by C_t. It is assumed that heat transport (e.g., Equation 3.54) doesn't change due to the reasons previously mentioned. The transmission function adheres to the following expression.

$$f(u) = \frac{K_W}{K_M}\frac{0.622\rho_a C_t}{P\rho_w} = \frac{K_w}{K_M}\frac{0.622\rho_a}{P\rho_w}\frac{C_{at}}{1 + \dfrac{C_{at}}{C_s}} \tag{3.73}$$

$$f'(u) = \frac{K_H}{K_M} \frac{0.622 \rho_a C_{at}}{P \rho_w} \tag{3.74}$$

The aerodynamic function for water vapor, $f(u)$ is different from that for heat transport, $f'(u)$ even when assuming K_H/K_M = 1 and K_W/K_M = 1. This is due to the "Similarity Theory". This realization is an important concept arising from the two-step evaporation process (e.g., molecular diffusion and turbulent diffusion). The ratio of $f'(u)/f(u)$ can be presented as follows:

$$\frac{f'(u)}{f(u)} = 1 + \frac{C_{at}}{C_s} = 1 + \frac{r_s}{r_{av}} \tag{3.75}$$

Equation (3.75) can be substituted into Eq. (3.69) for actual evaporation to demonstrate the effect of soil surface resistance on the actual evaporation rate.

3.5 ASSESSMENT OF EVAPORATION-RATE REDUCTION

Field capacity (i.e., volumetric water content at a suction of 33 kPa) can be used to determine not only soil surface resistance, but also specific or relative humidity at the various soil surfaces (Kondo et al., 1990; Lee and Pielke, 1992; van de Griend and Owe, 1994; Aluwihare and Watanabe, 2003; Bittelli et al., 2008). The field capacity has been applied in several disciplines (e.g., hydrology and agricultural engineering). It has not been accepted as a fundamental parameter in geotechnical engineering. Instead, soil suction (or free energy) has been more widely accepted by geotechnical and geo-environmental engineers when dealing with prediction of evaporation rate from soil surfaces. In this section, attempts are made to derive an equation to determine the suction at which the evaporation rate from a soil surface begins to reduce from the potential evaporation rate. The suction at which evaporation reduces should be related to fundamental parameters of an unsaturated soil (e.g., the air-entry value, ψ_{aev} and/or residual soil suction, ψ_{res}).

It is important to take note of how the Soil Water Characteristic Curve (SWCC) is measured and how the key parameters are determined from the SWCC. The air-entry value is defined as the matric suction where the air starts to enter the largest pores of the soil. The residual soil suction is the water content where a large suction change is required to extract additional water from the soil (Fredlund and Xing, 1994). The quantifications of these variables can be determined using the empirical procedure suggested by Fredlund et al. (1994). This procedure is included in the software, SVFlux. The author has made use of this procedure to determine the air-entry and residual soil suction for this thesis.

3.5.1 Assessment of Suction and Corresponding Volumetric Water Content at Evaporation-Rate Reduction Point during Drying Process

It is observed from evaporative tests on various thin soil sections that the volumetric water content at which evaporation starts to reduce, varies from a value of few percent to a value near the saturated soil volumetric water content, θ_{sat}. Kondo et al. (1990) empirically found the relative humidity at the soil surface began to decline at volumetric water contents of 0.392 for sand and 0.490 for loam. Lee and Pielke (1992) suggested the use of soil field capacity as a reference point where the soil surface relative humidity may begin to reduce. This means that when the soil volumetric water content is greater than the field capacity, the soil relative humidity at the soil surface may be close to unity so that the soil may behave as the saturated soil. On the other hand, the relative humidity should begin to drop once the soil volumetric water content is below field capacity. Typical field capacity values have been presented in Table 2.5 of Chapter 2. Van de Griend and Owe (1994) suggested the use of a soil volumetric water content of 15 percent for a fine sandy loam based on their experiments. Suggested values are empirical and are not parameters representative of the SWCC in unsaturated soils engineering.

It is necessary to re-assess drying test experiments based on thin soil sections as well as the results from soil columns that have been published in the research literature. Of key importance is a reliable procedure that can be used to designate the suction and corresponding water content where evaporation begins to reduce from potential evaporation.

3.5.1.1 Re-assessment of Evaporation from Thin Soil Sections

There were nine thin soil section drying tests that were performed on Beaver Creek sand, Custom silt and Regina clay by Wilson (1990). Along with the measurement of the ratio of *AE/PE*, the relative humidity of the air, the soil water content, the temperature of the air, soil and water were continuously measured during drying process. It was found that the "breaking point" gravimetric water contents were 1.7, 4 and 20 percent for the sand, silt and clay, respectively. These values of known water content can be converted to the total suctions from the corresponding SWCCs, of approximately 3,000 kPa (see Figure 3.7). This suction value is larger than the residual suctions of 6.5 kPa, 40 kPa and 925 kPa for the sand, silt and clay, respectively.

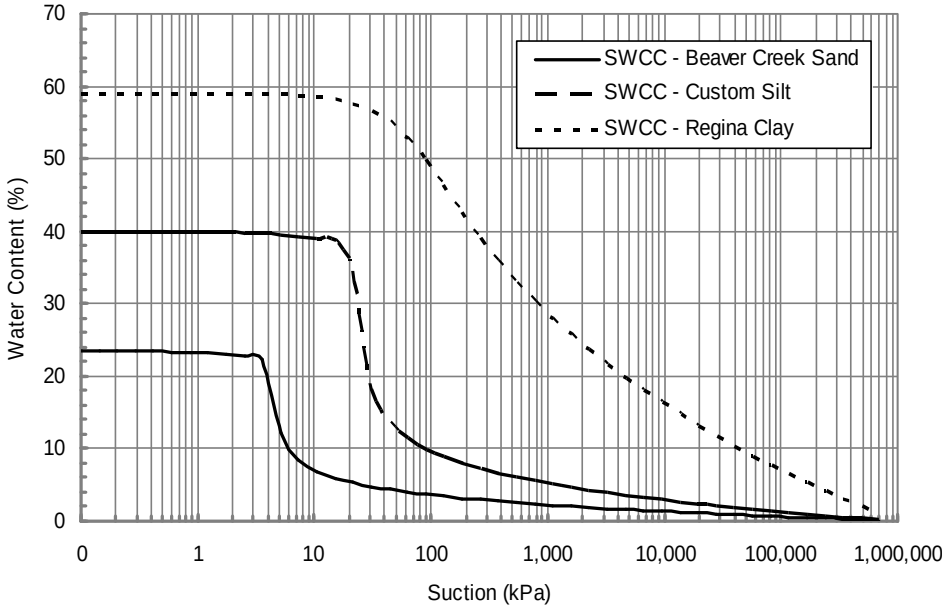

Figure 3.7 Fredlund and Xing (1994) soil-water characteristic curves of the sand, silt and clay (Wilson, 1990).

The above findings agree with the conclusions arrived at by Wilson (1990). It appears that the soil surfaces were kept at or near saturation provided that the total suction was lower than the residual suction of 6.5 kPa for the sand as an example. Evaporation was controlled by laboratory room conditions (i.e., Stage I of the evaporative process). It would appear that the liquid-water interphase at the soil surfaces quickly became discontinuous because there was neither liquid water flow nor water vapour diffusion to the surfaces from below. The soil suctions increased rapidly to the suction of 3,000 kPa with a small change in water content (see Figure 3.8). Water in the thin soil layers was always to be in contact with the atmosphere above. In other words, the air close to the pore-water surface was always in equilibrium with the pore water. Therefore, the Lord Kelvin's formula of the relative humidity is always valid in the thin soil layers during the drying process. Wilson (1990) used the Lord Kelvin's formula to obtain the conclusion that the relative humidity at the soil surface significantly starts to reduce from unity as the surface suction reaches to the value of 3,000 kPa. However, these findings may not be directly applicable to evaporation from soil columns. It is speculated that the “breaking point” water contents (i.e., point at which the rate of evaporation significantly reduces), for soil columns are different from those for thin soil layers of the same soil. It is also speculated that the differences may be attributed to the evaporating surface moving down during the drying process. The low hydraulic conductivity at the soil surface does not permit the sufficient flow of water to reach the soil surface to maintain the maximum or potential rate of evaporation. As a result, water is not in contact with the atmosphere; hence, the Lord Kelvin's formula is no longer valid in drying soil. The laboratory experiments on evaporation from the soil columns by Wilson (1990), Bruch (1993) and Yanful and Choo (1997) may support these findings (see Figures 3.11, 3.12 and 3.13).

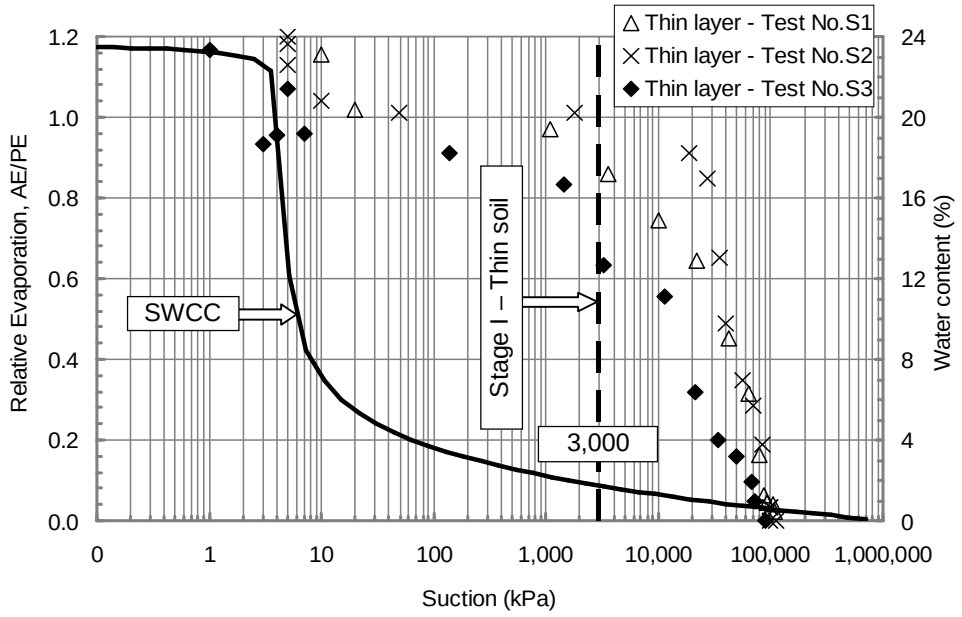

Figure 3.8 Extent of stage I of the evaporative process for thin soil layers of the Beaver Creek sand (Wilson, 1990).

Three other independent drying tests on thin soil layers, (2 mm thick silt), were carried out by Dunmola (2012). The results can be interpreted in a similar manner to that used above on the Wilson (1990) thin soil section tests. The results showed the pattern of having a "breaking point" total suction of 3,000 kPa (see Figure 3.9). It appears that the soil surfaces were kept at or near saturation provided that the total suction was lower than the suction of 3,000 kPa and evaporation was controlled by laboratory room conditions (i.e., Stage I of the evaporative process). Once again it would appear that the evaporating front was near the surface of the soil because the soil samples were relatively thin. The distance for the vapour to travel to the soil-atmosphere interface was negligible. There was little flow of liquid water or water vapour diffusion to the soil surfaces. For these reasons, it can be concluded that the actual rate of evaporation from the thin layers of the silt starts to reduce from the potential rate of evaporation as the total suction exceeds 3,000 kPa.

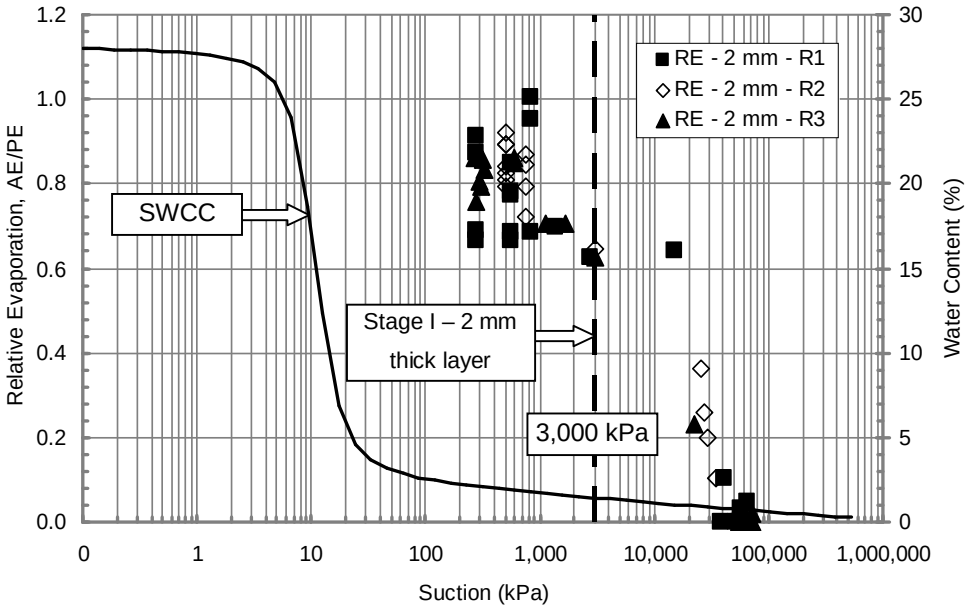

Figure 3.9 Illustration of extent of stage I of the evaporative process for thin soil layers of the non-saline silt (Dunmola, 2012).

3.5.1.2 Re-assessment of Evaporation from Soil Columns

Evaporation from soil surfaces in soil columns can also be observed and re-assessed. A series of test results from laboratory drying tests were collected from the research literature. The soil test columns A and B on Beaver Creek sand by Wilson (1990), the soil columns of Beaver Creek sand, Processed silt and Natural silt by Bruch (1993), and the coarse sand and fine sand columns by Yanful and Choo (1997) have been selected as representative tests for re-assessment. The figures and tables of the other tests which correspond to those presented in this chapter are included in Appendices B, C, D and E.

Figure 3.10 shows the relative evaporation, RE (i.e., ratio of actual to potential soil evaporation) versus soil suction and corresponding water content for Beaver Creek sand columns (i.e., columns A and B) (Wilson, 1990) during the drying tests. It can be seen in Figure 3.10 that the rate of the actual soil evaporation begins to reduce from the potential rate of evaporation at total suction of approximately 5 kPa. This value is well below the total suction of 3,000 kPa. This result would indicate that the soil surface is maintained at or near saturation provided that the total soil suction at the surface is kept lower

than value of 5.0 kPa for the Beaver Creek sand. The corresponding water content generated from the SWCC of the Beaver Creek sand is found to be 11 percent. This value is significantly different from the value of approximately 2 percent measured for the thin soil layers of the same soil, (i.e., Beaver Creek sand).

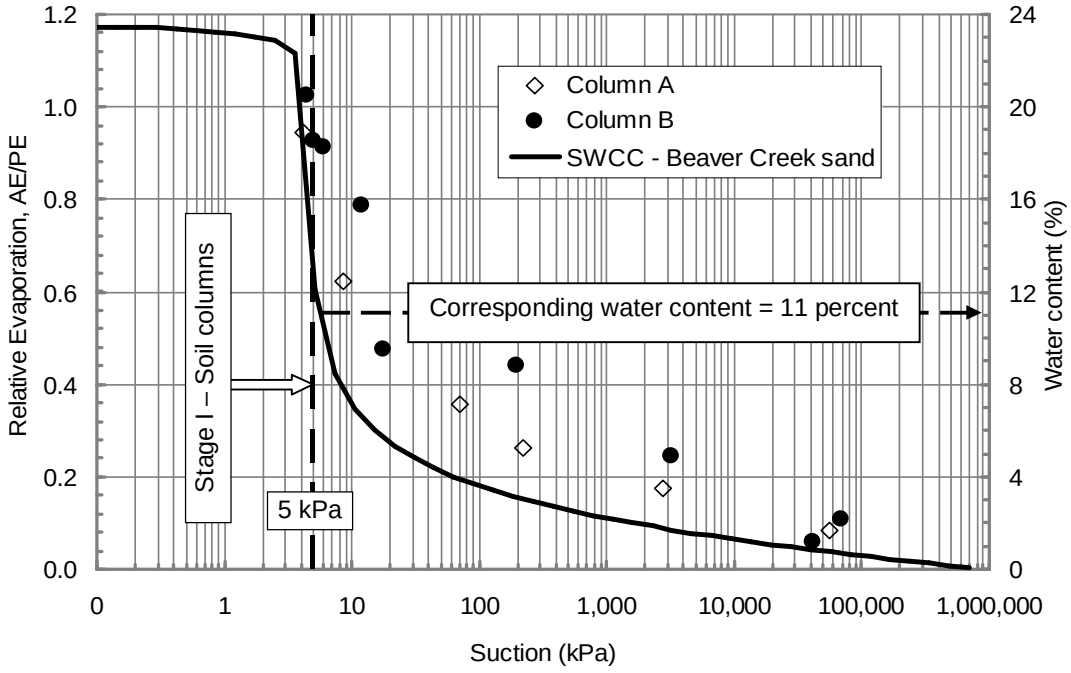

Figure 3.10 Assessment of an evaporation-rate reduction point from the measured data of relative evaporation, *AE/PE* versus soil suction and corresponding water content at the top surface for Beaver Creek sand in soil columns A and B (Wilson, 1990).

Figures 3.11 and 3.12 show the relative evaporation versus soil suction and the corresponding water content for the soil columns of the Beaver Creek sand, Processed silt and Natural silt during the drying tests (Bruch, 1993). The similar findings appear to be consistent with the evaporation tests on the Beaver Creek sand, Processed silt and Natural silt conducted by Bruch (1993). The suction values at evaporation-rate reduction point are found to be 7 kPa, 62 kPa and 116 kPa for Beaver Creek sand, Processed silt and Natural silt, respectively. These values are well below the total suction of 3,000 kPa. These results would indicate that the soil surfaces are maintained at or near saturation provided that the total soil suctions at the surfaces are kept lower than values

of 7 kPa, 62 kPa and 116 kPa for the Beaver Creek sand, Processed silt and Natural silt, respectively. The corresponding water contents at evaporation-rate reduction point which are generated from the SWCCs are 11, 10 and 9 percent for the Beaver Creek sand, Processed silt and Natural silt, respectively.

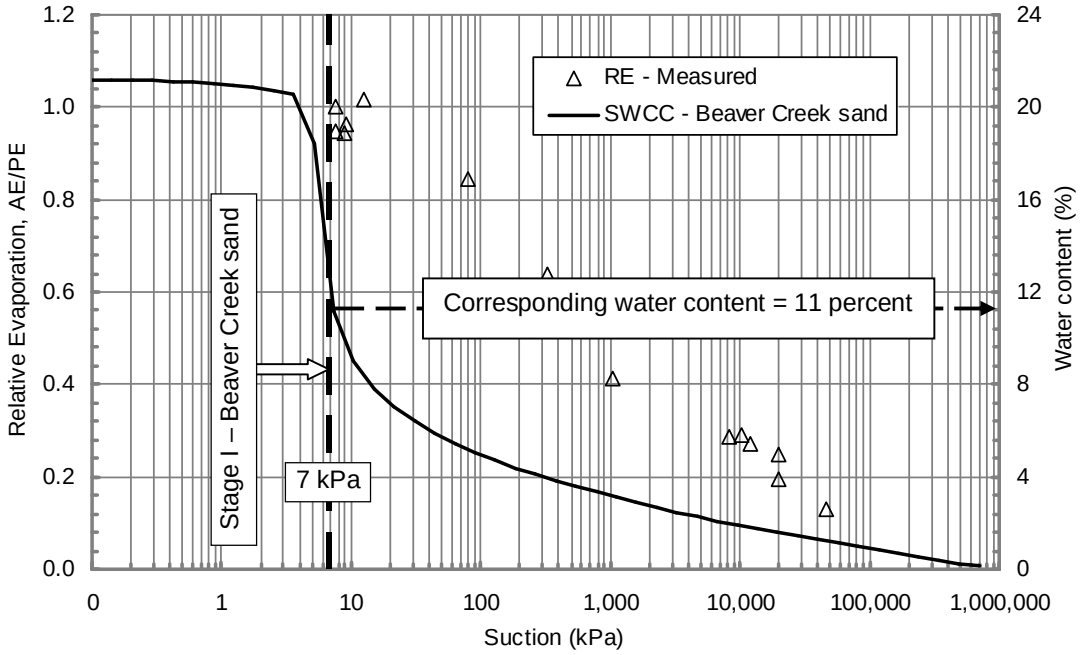

Figure 3.11 Assessment of an evaporation-rate reduction point from the measured data of relative evaporation, *AE/PE* versus soil suction and corresponding water content at the top surface for Beaver Creek sand in soil column (Bruch, 1993).

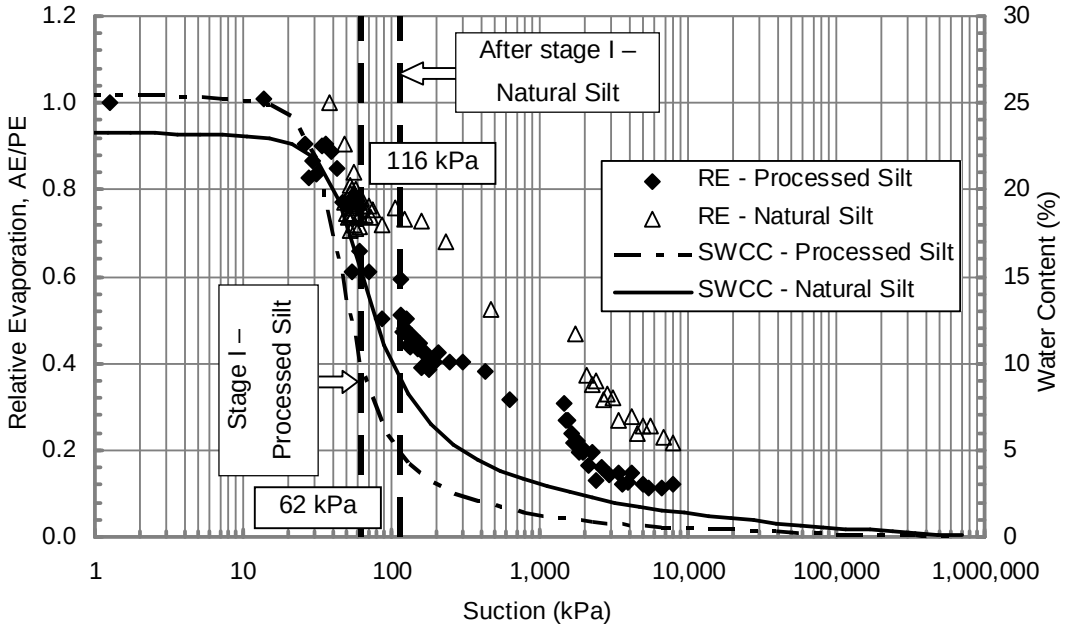

Figure 3.12 Assessment of an evaporation-rate reduction point from the measured data of relative evaporation, *AE/PE* versus soil suction and corresponding water content at the top surface for the Processed silt and Natural silt in soil column (Bruch, 1993).

Figure 3.13 shows the relative evaporation versus soil suction and the corresponding volumetric water content for the soil columns of the coarse sand and fine sand during the drying tests (Yanful and Choo, 1997). The similar findings appear to be consistent with the evaporation tests on the coarse sand and fine sand conducted by Yanful and Choo (1997). The suction values at evaporation-rate reduction point are found to be 1.3 kPa and 3.7 kPa for the coarse sand and fine sand, respectively. These values are well below the total suction of 3,000 kPa. These results would indicate that the soil surfaces are maintained at or near saturation provided that the total soil suctions at the surfaces are kept lower than values of 1.3 kPa and 3.7 kPa for the coarse sand and fine sand, respectively. The corresponding volumetric water contents at evaporation-rate reduction point which are generated from the SWCCs are 15 and 14 percent for the coarse sand and fine sand, respectively.

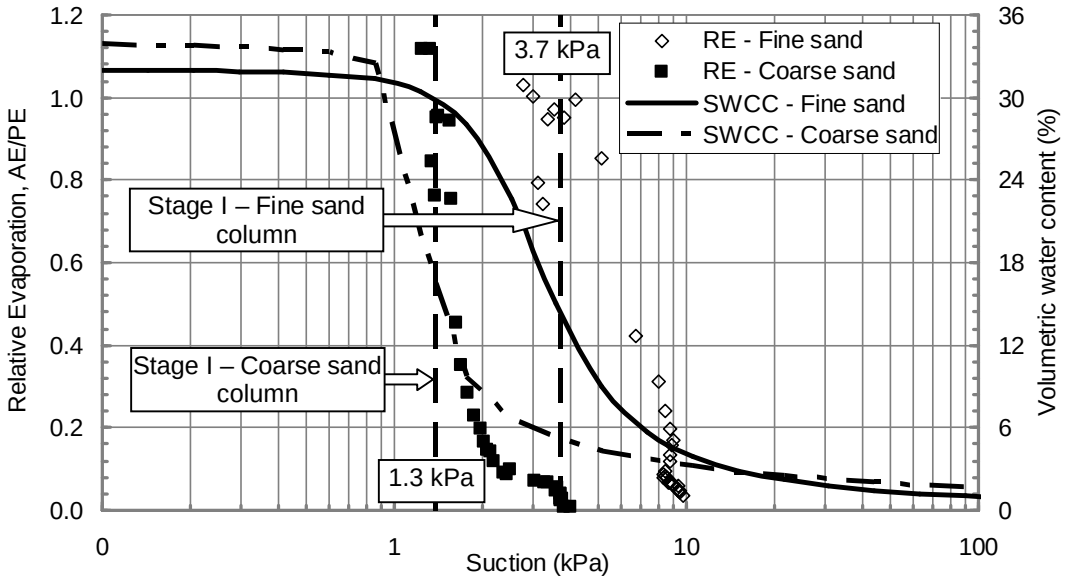

Figure 3.13 Assessment of an evaporation-rate reduction point from the measured data of relative evaporation, *AE/PE* versus soil suction and corresponding volumetric water content at the top surface for the coarse sand and fine sand in soil column (Yanful and Choo, 1997).

Total suction increases at the soil surface during the process of drying. The air entry value is the point where air begins to enter the largest soil pores at the soil surface. Water vapour is present above the soil while the liquid water phase is continuous. Evaporation at this point is still dependent upon liquid water being available to flow upward to the soil surface. Evaporation under these conditions is essentially equal to potential evaporation. Total suction continues to increase and approaches to suction at evaporation-rate reduction point. This suction warrants the designated as a new variable, ψ_R that is of importance to the prediction of actual evaporation. In each case examined, the value of ψ_R is found to be between the air-entry value and residual soil suction value for the observed soils. At this point, the conductive properties of the soil no longer permit the sufficient flow of water to reach the soil surface to maintain the maximum or potential rate of evaporation. The soil surface then becomes sufficiently desiccated to cause the liquid-water phase become discontinuous. These values appear to be sufficiently close to the residual suction for each soil (see Table 3.1).

In summary, the values of water content at the evaporation-rate reduction points for various soils (i.e., Beaver Creek sand, Processed silt, Natural silt, coarse sand and fine sand) were found to be consistent with the findings of the range of volumetric water content in the transition zone from liquid flow to vapour flow in soil columns. The lower limit of this range was found to vary from 5 percent to 10 percent in terms of volumetric water content while the upper limit was found to be between 14 percent and 28 percent (Konukcu et al., 2004).

Water is mostly provided to the soil surface by the diffusion of water vapour once the water phase has become discontinuous. The water molecules migrate to the surface through the soil pores through the process of diffusion. In other words, the addition of water to the surface appears to be dominated by the process of vapour diffusion during this period of time. This phenomenon may occur when the total suction changes between the suction at evaporation-rate reduction point and residual soil suction. Eventually the flow of liquid-water to the surface may cease and the evaporation may take place only under vapour diffusion (i.e., Stage III of evaporative process). At this point, it is anticipated that the total suction exceeds the residual soil suction. The above explanation is consistent with the findings of a lower limit for the water permeability coefficient (Ebrahimi et al., 2004). It was observed that the process of evaporation may occur near the top surface of the soil (i.e., less than 1 cm thick).

Air-entry values, residual suction as well as total suctions at the evaporation-rate reduction point can be determined from the drying tests collected from the research literature. The soil data from the two sand columns A&B (i.e., Beaver Creek sand) by Wilson (1990); Beaver Creek sand column, Processed silt column and Natural silt column by Bruch (1993); coarse sand and fine sand columns by Yanful and Choo (1997). The results from these tests are summarized in Table 3.1.

Table 3.1 Summary of air-entry values, residual soil suctions and total suctions at the points of evaporation-rate reduction from the drying tests collected from the research literature (Wilson, 1990; Bruch, 1993; and Yanful and Choo, 1997).

Soil texture	Data source	Water content at evaporation-rate reduction point (%)	Total suction at evaporation-rate reduction point (kPa)	Air-entry value (kPa)	Residual soil suction (kPa)
Sand	Beaver Creek sand (Wilson, 1990)	11	5.0	3.3	6.5
	Beaver Creek sand (Bruch, 1993)	11	7.0	4.5	8.5
	Coarse sand	(15)	1.3	1.1	1.8
	Fine sand	(14)	3.7	1.8	6.7
Silt	Processed silt	10	61.8	25.3	96.7
	Natural silt	9	116.3	32.1	166.9

Note: The values in brackets are volumetric water content for Coarse sand and Fine sand.

Figures 3.14 and 3.15 show the air-entry value, residual soil suction and total suction at evaporation-rate reduction point, ψ_R for the sand and silt collected in the research literature, respectively. The values of ψ_R appear to occur somewhere between the air-entry value and the residual soil suction. The values tend towards the residual soil suctions as the grain size of the soils become finer. The suction at the point of evaporation-rate reduction depends not only on the thickness of soil section, but also on soil texture. This observed behaviour shows consistency and should be taken into consideration when calculating actual evaporation in geotechnical engineering applications.

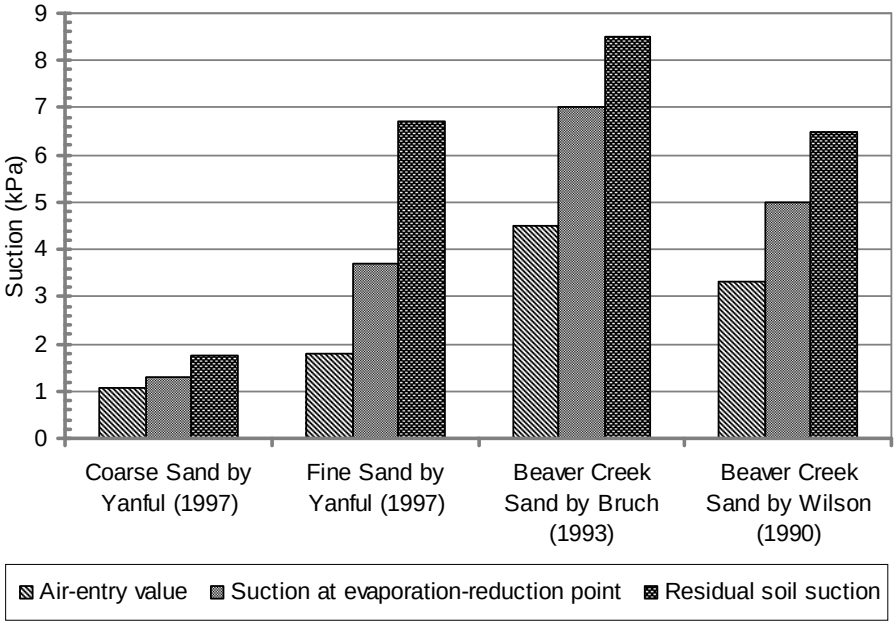

Figure 3.14 Illustration of air-entry value, residual soil suction and suction at the evaporation-rate reduction point (data collected from Beaver Creek sand by Wilson, 1990; Beaver Creek sand by Bruch, 1993; coarse sand and fine sand by Yanful and Choo, 1997).

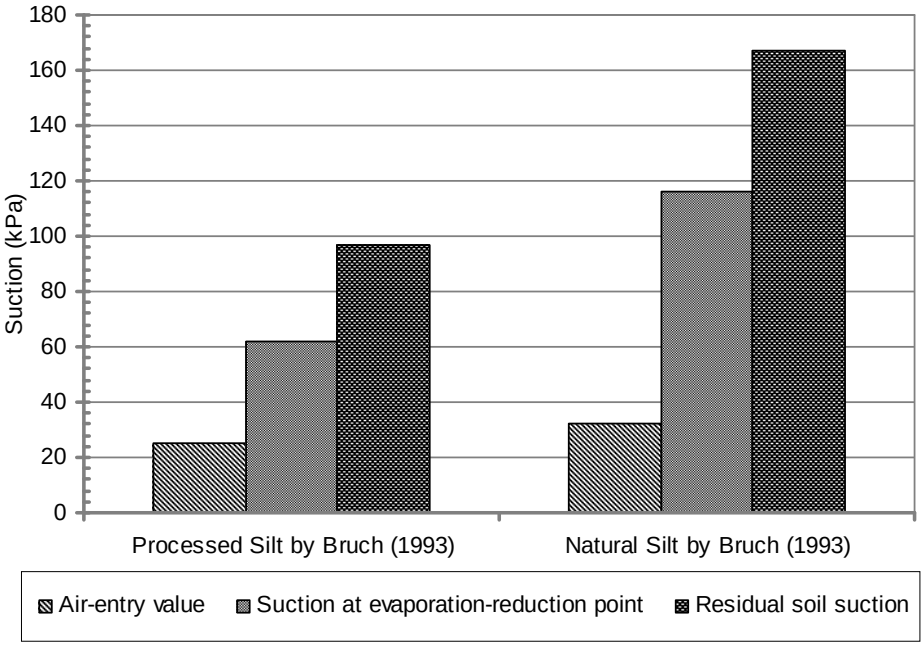

Figure 3.15 Illustration of air-entry value, residual soil suction and suction at the evaporation-rate reduction point (data collected from soil columns of Processed silt and Natural silt by Bruch, 1993).

3.5.1.3 Derivation of an Equation for Determination of Suction at the Evaporation-Rate Reduction Point

The reduction in actual evaporation rate has been observed from the data on a series of soil columns tests collected from the research literature. The suction at the point when the evaporation-rate starts to reduce appears to be between the air-entry value and residual soil suction for the soil. In other words, the suction at the point of evaporation-rate reduction varies between the air-entry value and the residual soil suction. The SWCC for soils vary on a logarithmic scale. It would seem reasonable that the point of evaporation-rate reduction would also vary on a logarithmic scale. The following empirical equation is proposed for the quantification of the evaporation-rate reduction point.

$$log\,\psi_R = log\,\psi_{aev} + a \times \left(log\,\psi_{res} - log\,\psi_{aev}\right) \tag{3.76}$$

Equation (3.76) can be re-arranged and simplied as follows:

$$log\,\psi_R = a \times log\,\psi_{res} + (1-a) \times log\,\psi_{aev} \tag{3.77}$$

$$log\,\psi_R = log\left(\psi_{res}^{a} \times \psi_{aev}^{1-a}\right) \tag{3.78}$$

$$\psi_R = \psi_{res}^{a} \times \psi_{aev}^{1-a} \tag{3.79}$$

where:

ψ_R = suction at evaporation-rate reduction point, kPa;

ψ_{aev} = air-entry value, to be determined from SWCC, kPa;

ψ_{res} = residual soil suction, to be determined from SWCC, kPa;

a = an empirical factor which varies between 0 and 1.

In summary, the total suction at the evaporation-rate reduction point can be formulated as follows:

$$\psi_R = \begin{cases} \psi_{aev} & if\ \ a = 0 \\ \psi_{res} & if\ \ a = 1 \\ \psi_{res}^{a} \times \psi_{aev}^{1-a} & if\ \ 0 < a < 1 \end{cases} \tag{3.80}$$

Equation (3.80) quantifies the values of suction at the point of evaporation-rate reduction for soils. It is a function of the parameters familiar to unsaturated soils engineering such as the air-entry value and residual soil suction. Consequently, the procedure should be accepted to the geotechnical engineering profession.

The values of the power term "*a*" was allowed to vary from zero (i.e., the suction at the evaporation-rate reduction point equals to the air-entry value) to 1.0 (i.e., the suction at the evaporation-reduction point equals to residual soil suction). Equation (3.80) can be used to quantify ψ_R for each soil.

In order to find the best-fitting value of "*a*" for sand and silt, two sets of the suction of evaporation-rate reduction point in Table 3.1 are used for sand and silt material separately. A coefficient of determination, R-squared is a measure of how well the values calculated by Eq. (3.80) fits the data in Table 3.1 with variation of the power "*a*". The following procedures are applied to calculate the value of R-squared for a value of "*a*".

Determine a set of the suction at evaporation-rate reduction point, ψ_R, corresponding to the value of "*a*" by Eq. (3.80);

Apply the formula of coefficient of determination as follows:

$$R^2 = 1 - \frac{\sum \left(y_i - y\right)^2}{\sum \left(y - \bar{y}\right)^2} \tag{3.81}$$

where:

y_i = a set of suction at evaporation-rate reduction point corresponding to a value of "*a*" ;

y = a set of suction at evaporation-rate reduction point in Table 3.1 (i.e., four data points for sand and two for silt);

$\bar{y}$ = *a* mean value of the set of suction, y_i;

R^2 = a coefficient of determination, varying between 0 to 1.

The results of evaporation-rate reduction point calculated by Eq. (3.81) with variation of the value "*a*" are presented in Tables 3.2 and 3.3 for sand and silt, respectively. The shaded rows in the tables show the maximum values of R-squared and the corresponding values of "*a*".

Table 3.2 Values of total suction at evaporation-rate reduction point with variation of the empirical factor, *a*, for Beaver Creek sand, Coarse sand and Fine sand.

Value of "*a*"	Values of total suction at the evaporation-rate reduction point (kPa)				Coefficient of determination, R-squared
	Beaver Creek sand (Wilson, 1990)	Beaver Creek sand (Bruch, 1993)	Coarse sand (Yanful and Choo, 1997)	Fine sand (Yanful and Choo, 1997)	
0	3.30	4.50	1.07	1.80	0.529
0.05	3.41	4.65	1.10	1.92	0.566
0.10	3.53	4.80	1.12	2.05	0.606
0.15	3.65	4.95	1.15	2.19	0.648
0.20	3.78	5.11	1.18	2.34	0.692
0.25	3.91	5.28	1.21	2.50	0.738
0.30	4.04	5.45	1.24	2.67	0.785
0.35	4.18	5.62	1.27	2.85	0.832
0.40	4.33	5.80	1.31	3.05	0.877
0.45	4.48	5.99	1.34	3.25	0.918
0.50	4.63	6.18	1.37	3.48	0.952
0.55	4.79	6.38	1.41	3.71	0.975
0.60	4.96	6.59	1.44	3.96	0.985
0.65	5.13	6.80	1.48	4.23	0.978
0.70	5.30	7.02	1.52	4.52	0.953
0.75	5.49	7.25	1.55	4.83	0.909
0.80	5.68	7.48	1.59	5.16	0.848
0.85	5.87	7.73	1.63	5.51	0.772
0.90	6.07	7.98	1.67	5.88	0.686
0.95	6.28	8.23	1.72	6.28	0.594
1	6.50	8.50	1.76	6.71	0.500

Table 3.3 Values of total suction at evaporation-rate reduction point with the variation of the empirical factor, a, for Processed silt and Natural silt.

Value of "a"	Values of total suction at the evaporation-rate reduction point (kPa)		Coefficient of determination, R-squared
	Processed silt (Bruch, 1993)	Natural silt (Bruch, 1993)	
0	25.30	32.10	0.040
0.05	27.05	34.86	0.048
0.10	28.93	37.85	0.058
0.15	30.94	41.11	0.071
0.20	33.08	44.64	0.086
0.25	35.38	48.47	0.106
0.30	37.83	52.64	0.131
0.35	40.45	57.16	0.163
0.40	43.26	62.07	0.205
0.45	46.25	67.40	0.261
0.50	49.46	73.19	0.334
0.55	52.89	79.48	0.433
0.60	56.56	86.31	0.559
0.65	60.48	93.73	0.711
0.70	64.67	101.78	0.859
0.75	69.16	110.53	0.942
0.80	73.95	120.02	0.900
0.85	79.08	130.34	0.749
0.90	84.57	141.53	0.562
0.95	90.43	153.69	0.395
1	96.70	166.90	0.265

Figure 3.16 presented the variation of total suction at the evaporation-rate reduction point with the value of "a" using Eq. (3.80). As a result, the values of "a" of 0.6 and 0.75 were found for optimization of the suction, ψ_R for sand and silt, respectively. These values are later verified and applied in Chapter 6.

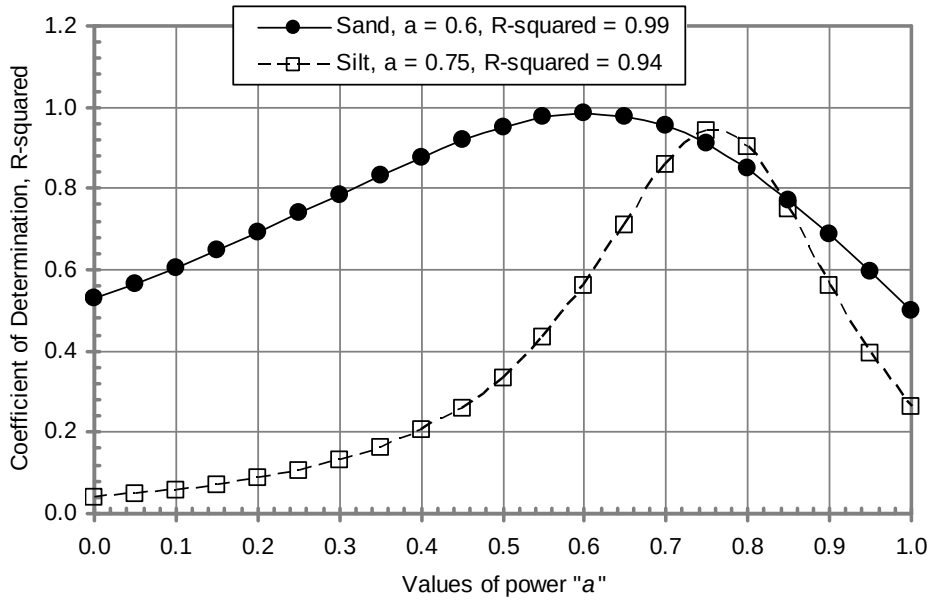

Figure 3.16 Variation of suction at the evaporation-rate reduction point with the value of "*a*".

3.5.1.4 Generation of Volumetric Water Content at Evaporation-Rate Reduction Point

Geotechnical engineers are familiar with the soil-water characteristic curve which is a nonlinear relationship between soil suction and soil-water content. In other words, there is corresponding soil water content for each soil suction. This is true provided the effects of hysteresis are ignored. The soil-water characteristic curve describes a decrease in soil water content with an increase in soil suction along desorption or drying curve. There have been many equations proposed for the soil-water characteristic curves (Fredlund and Xing, 1994), however, the Fredlund and Xing's equation (1994) will be applied using the SVFlux software (SVFlux Users Manual, 2009) throughout this thesis. Practically, suction at evaporation-rate reduction point, ψ_R can be determined using the Eq. (3.80). Then the corresponding volumetric water content, θ_R can be generated using the soil-water characteristic curve.

3.5.2 Estimate of Relative Humidity at Soil Surface Based on Volumetric Water Content at Evaporation-Rate Reduction Point

Chapter 2 presented several methods for the determination of relative or specific humidity at the surface of a soil. The Philip's (1957) formula for predicting the relative humidity at the soil surface was derived from thermodynamic principles. It has been used to simulate surface air humidity by several researchers including Nappo (1975), McCumber and Pielke (1981), Camillo et al. (1983), Wilson (1990), Simms et al. (2007), Bittelli et al. (2008). Recently Kondo et al. (1990), Lee and Pielke (1992), Alvenas and Jansson (1997), Fredlund et al. (2011) and Dunmola (2012) agreed that the Philip's equation may not be valid close to a unsaturated soil surfaces. It was noted that a prerequisite for the validity of the Philip's (1957) equation to be valid, the air close to the pore-water surface must be in equilibrium with the pore-water. However, such a condition is not maintained in a drying soil since vapour pressure of the air adjacent to an evaporating front is not in equilibrium with the liquid water in the soil pores (Alevnas and Jansson, 1997). This finding appears to be confirmed by Figures 1.1, 1.2 and 1.3 as shown in Chapter 1.

There have been numerous soil evaporation models with different parameterization schemes for the evaporation front that have been proposed. There are divergent options as to which methods are the most correct and useful. Kondo et al. (1990), Mahfouf and Noilhan (1991) and Lee and Pielke (1992) proposed a new equation in an attempt to overcome the deficiency of the Philip's equation. The new equation introduced the concept of surface resistance to the transport of water vapour from the soil pores to the soil-atmosphere interface. Alvenas and Jansson (1997), Fredlund et al. (2011) and Dunmola (2012), on the other hand, continued to apply the Philip's equation and suggested adjustment of total suction at the soil surface. Accordingly, empirical correction factors were introduced to compensate for the difference between the mean total suction in the top soil layer and the total suction at the soil surface.

3.5.2.1 Proposed Method for Prediction of Relative Humidity

A method is proposed for the prediction of the relative humidity at the soil surface using the Lee and Pielke's (1992) equation of the soil moisture availability factor, β. It should be noted that one of the main disadvantages associated with the use of the Lee and Pielke's (1992) equation is the introduction of the field capacity as a reference point. Field capacity is not dependent on soil texture and has found little application in geotechnical engineering. Meanwhile, the residual volumetric water content, θ_R would appear to have greater significance in terms of determining the point of the evaporation-rate reduction. Soil texture is taken into consideration through the quantification of the suction at evaporation-rate reduction point, ψ_R . It is therefore suggested that field capacity term in the Lee and Pielke's (1992) equation be replaced by the volumetric water content at the evaporation-rate reduction point. The Lee and Pielke's (1992) equation can be modified accordingly. The modified equation is later studied with respect to the estimation of the relative humidity at the soil surface by considering the results from thin soil sections and soil columns. The results of the analysis are also compared against calculated results found in the research literature. The following equations of soil moisture availability factor, β; and hence relative humidity are recommended by the author of this thesis.

$$\beta = \begin{cases} \frac{1}{4}\left[1 - cos\left(\frac{\theta}{\theta_R}\pi\right)\right]^2 & \theta < \theta_R \\ 1 & \theta \geq \theta_R \end{cases} \qquad (3.82)$$

where:

β = coefficient representing the surface moisture availability;

θ_R = volumetric water content at evaporation-rate reduction point;

θ = soil volumetric water content of the topsoil layer.

The actual water vapour pressure is determined from the soil moisture availability factor, β. The proposed equation has been derived from consideration of the evaporation rate from bare soil (Kondo et al., 1990).

$$p_v = \beta \times p_v^{sat} + (1-\beta) \times p_v^{air} \tag{3.83}$$

where:

p_v = actual vapour pressure at soil surface, kPa;

p_v^{sat} = saturated vapour pressure at soil surface, kPa;

p_v^{air} = actual air pressure immediately above soil surface, kPa.

The relative humidity, in turn, is determined as the definition of the ratio of actual vapor pressure to saturated vapor pressure under the same surface condition (i.e., the same surface temperature).

$$RH = \frac{p_v}{p_v^{sat}} \tag{3.84}$$

3.6 SOIL SURFACE RESISTANCE TO THE ACTUAL EVAPORATION

The terminology of "soil surface resistance", r_s to vapour diffusion from soil pores to soil-atmosphere interface was reviewed in Chapter 2. It was reported that the soil surface resistance varies from close to zero at a wet surface to several thousand seconds per meter at a dry surface (Mahfouf and Noilhan, 1991; van de Griend and Owe, 1994). Collected data on soil surface resistance in the literature was presented from Camillo and Gurney (1986); van de Griend and Owe (1994) and Aluwihare and Watanabe (2003). The equations for soil surface resistance show an increase in soil surface resistance with decreasing soil water content. In a study of the equations to describe soil surface resistance, Bittelli et al. (2008) concluded that the exponential equation by van de Griend and Owe (1994) is the preferred equation to use when computing evaporation. It should also be noted that the van de Griend and Owe's (1994) equation was based on the measurements of soil surface resistance when using a fast-air circulation chamber. The van de Griend and Owe's equation can be written as follows:

$$r_s = 10 \times e^{0.3563(\theta_{min} - \theta_{top})} \tag{3.85}$$

where:

r_s = soil surface resistance at top 0 – 1 cm, s/m;

θ_{top} = volumetric water content of the top 1 cm layer, (%);

θ_{min} = an empirical minimum above which the soil is able to deliver vapour at a potential rate, (%). A value of θ_{min} = 15% was suggested.

The factor of 10 was obtained from studies of molecular diffusion of water surface (La Mer and Healy, 1965).

One disadvantage of this model relates to the use of θ_{min} = 15% as a reference point. Consequently, it is not dependent upon soil texture. Therefore, the suggested value for θ_{min} will be replaced with a volumetric water content value at the evaporation-rate reduction point, θ_R. The θ_R value has been shown to be dependant upon soil texture through the quantification of the suction at the reduction evaporation-rate, ψ_R. The following equation is recommended for the computation of soil surface resistance in this thesis. A comparison between the estimated values of soil surface resistance and data from the literature is made when performing numerical modeling in Chapter 6.

$$r_s = 10 \times e^{0.3563(\theta_R - \theta_{top})} \tag{3.86}$$

where:

r_s = soil surface resistance at top 0 – 1 cm, s/m;

θ_{top} = volumetric water content of the top 1 cm layer, (%);

θ_R = volumetric water content value at the evaporation-rate reduction point, (%), which is generated from the total suction at the evaporation-rate reduction point, ψ_R (e.g., Eq. 3.80).

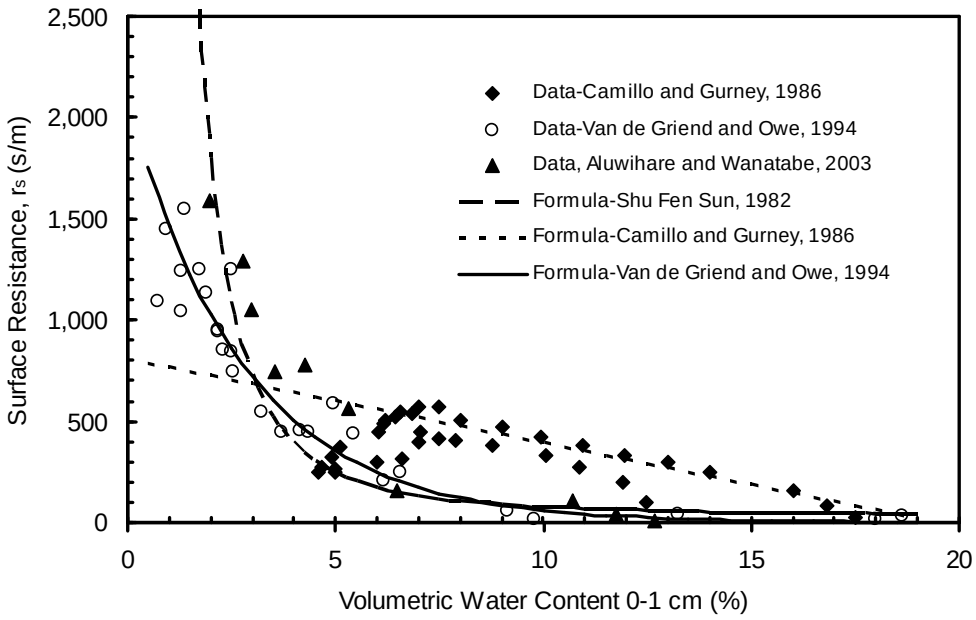

Figure 3.17 Variation of soil surface resistance versus volumetric water content at soil surface collected from the literature.

3.7 EFFECT OF PORE-WATER SALINITY ON EVAPORATION RATE FROM SALINIZED SOIL

The actual evaporation from a soil surface is related to the relative humidity in the soil pores near ground surface. Methods for estimating the relative humidity in the soil were discussed in the previous sections and assessed for bare soil surfaces where the vapour pressure of air adjacent to the evaporating surface is not in equilibrium with the liquid water in the pores during a drying process. In this section, evaporation from salinized soils will be considered, where the relative humidity will be quantified through use of Lord Kelvin's equation (e.g., Eq. 2.19).

The total suction at the soil surface constitutes the primary factor effecting the quantification of relative humidity. Consequently, relative humidity controls the rate of evaporation. Total suction not only depends on the character of the soil matrix (i.e., the matric suction component), but also on salt concentration in the pore-water (i.e., the osmotic suction component). The total suction is the summation of matric suction and osmotic suction.

It is believed that osmotic suction and salt crust formation control the rate of evaporation for salinized soils because salts accumulate at ground surface during the drying process. The increase in osmotic suction and salt crust resistance has been related to the increase in salt concentration (Konukcu et al., 2004; Fujimaki et al., 2006; Gran et al., 2011; and recently Dunmola, 2012). The transport of pore-water solute occurs through the mechanisms of advection, dispersion and diffusion (Shimojima et al., 1996; Dunmola, 2012). In turn, the osmotic suction and salt crust resistance are functions of salt concentration.

3.7.1 Relationship between Salt Content, the Initial Salt Content and Water Content from Soil-Water Characteristic Curve (SWCC)

In order to determine the the salt content in a soil at any time, , the initial salt content and water content from the SWCC, must be known and the following hypothesis must be adhered to:

The slow down in the rate of evaporation is related to the increase in salt concentration (i.e., osmostic suction) as the water content decreases. This could happen in two scenarios: (i) evaporation from a thin salinized soil section, and (ii) evaporation from saturated salt concentration.

There are various ways to define salt content. Salt content can be defined as a ratio of the volume of salts to the volume of water. This appears to be a preferable definition for geotechnical engineering. Under initial conditions, a salinized soil sample is saturated and identified by the term saturated initial volumetric water content, θ_{sat}, and the initial salt content, θ_{salt0}. These terms are expressed as follows:

- Saturated initial water content :

$$\theta_{sat} = \frac{V_{w0}}{V_t} \tag{3.87}$$

$$V_{w0} = \theta_{sat} V_t \tag{3.88}$$

- Initial salt content :

$$\theta_{salt0} = \frac{V_{salt}}{V_{w0}} \tag{3.89}$$

$$V_{salt} = \theta_{salt0} V_{w0} \tag{3.90}$$

Substituting V_{w0} from Eq. (3.88) into Eq. (3.90), yields:

$$V_{salt} = \theta_{salt0} V_{w0} = \theta_{salt0} \theta_{sat} V_t \tag{3.91}$$

where:

V_{w0} = initial volume of water in the soil sample, cm^3;

V_t = total volume of the soil sample, cm^3;

V_{salt} = volume of salt the soil sample which is assumed to remain constant during drying process, cm^3.

During the drying process, the volumetric water content, θ, decreases with time because water, V_w is lost by evaporation from the soil surface. This volumetric water content is related to the soil suction through the SWCC. The volumetric water content can be written as defined as follows:

$$\theta_{SWCC} = \frac{V_w}{V_t} \tag{3.92}$$

or $$V_w = \theta_{SWCC} V_t \tag{3.93}$$

where:

θ_{SWCC} = volumetric water content determined from SWCC.

Salt concentration increases during the drying process due to the reduction in volume of water and constant volume of salt. The volumetric salt content can be written as follows:

$$\theta_{salt} = \frac{V_{salt}}{V_w} \tag{3.94}$$

Substituting V_{salt} and V_{w} from Eqs. (3.91) and (3.93), respectively into Eq. (3.94), yields:

$$\theta_{salt} = \frac{\theta_{salt0}\theta_{sat}V_t}{\theta_{SWCC}V_t} \tag{3.95}$$

or $$\theta_{salt} = \frac{\theta_{salt0}\theta_{sat}}{\theta_{SWCC}} \tag{3.96}$$

Equation (3.96) presents salt content as a function of the volumetric water content of the soil at the surface. Salt content is determined through use of the SWCC when the suction at the soil surface is known. The values of θ_{salt0} and θ_{sat} are the initial salt concentration and saturated initial volumetric water content, respectively, measured at the beginning of the evaporation process.

Equation (3.96) has been studied and verified by comparison of predicted salt concentrations and measured salt concentrations in sandy loam and clay loam. The measured data has been collected from the research literature (Konukcu et al., 2004). Equation (3.96) appears to well-predict the salt concentration at the soil surface as shown in Figure 3.18.

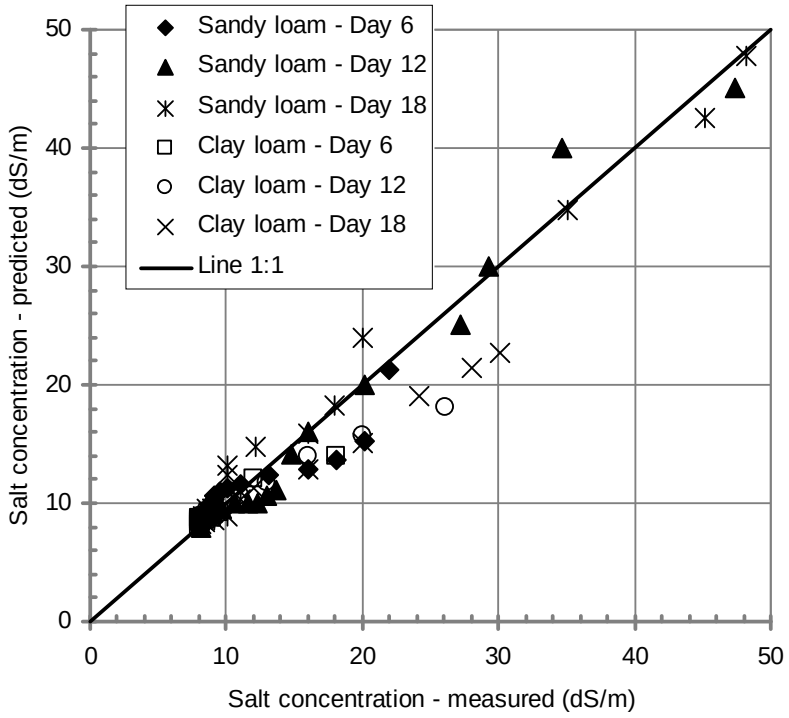

Figure 3.18 Comparison between measured salt concentration (dS/m) and salt concentration (dS/m) predicted by Equation (3.96) (Konukcu et al., 2004).

3.7.2 Osmotic Suction as a Function of Initial Salt Content and Water Content from Soil-Water Characteristic Curve (SWCC)

The osmotic suction can be calculated from thermodynamic principles (Robinson and Stokes, 1968). Van't Hoff proposed the equation to determine osmotic suction as it applies to the transport of salt through a semi-permeable membrane (Campbell, 1985). Osmotic suction is related to salt concentration, C_s, the ideal gas constant, R, and the absolute temperature, T. The magnitude of the osmotic suction written by van't Hoff is as follows (Monteith and Unsworth, 2008; Fredlund et al., 2012):

$$\pi = 2C_s \phi RT \tag{3.97}$$

where:

C_s = summation of molalities of all dissolved ions (mol/cm^3);

R = ideal gas constant, 8.314 J/mol/^{o}K;

T = absolute temperature in Kelvin, ^{o}K;

π = osmotic suction, kPa;

ϕ = osmotic coefficient (unity for an ideal solute).

The value of C_s is determined by mass of salt per unit volume divided by molar mass of salt (e.g., for Sodium Chloride, 58.5 g/mol). It is can be written as:

$$C_s = \frac{M_{salt}}{M_{molar}} \tag{3.98}$$

From Eq. (3.96), the salt concentration can be converted to mol/cm^3 by the following expression:

$$C_s = \frac{\theta_{salt}\rho_s}{M_{molar}} = \frac{\theta_{salt0}\theta_{sat}\rho_s}{\theta_{SWCC}M_{molar}} \tag{3.99}$$

Finally, the function of osmotic suction can be obtained as follows:

$$\pi = 2\times\left(\frac{\theta_{salt0}\times\theta_{sat}\times\rho_s}{\theta_{SWCC}\times M_{molar}}\right)RT \tag{3.100}$$

where:

ρ_s = density of salt, (g/cm^3) (e.g., 2.16 g/cm^3 for Sodium Chloride);

M_{molar} = molar mass of salt, g/mol (e.g., 58.5 g/mol for Sodium Chloride);

Other parameters were previously defined.

3.7.3 Effect of Salt Surface Resistance on Evaporation Rate

Fujimaki et al. (2006) concluded that the decrease in evaporation rate could not be explained through the use of the osmotic suction concept alone. The reduction in evaporation has been verified using osmotic suction and salt crust resistance (unit of s/m) formed during drying process. Fujimaki et al. (2006) also proposed two empirical equations to estimate salt crust resistance as a

function of accumulated salt in the depth of 0.25 cm. The proposed equation for Masa sand with NaCl can be written as follows:

$$r_{sc} = 0.69\, ln(\Gamma_s) - 1.04 \tag{3.101}$$

A similar equation was written for Masa sand with KCl.

$$r_{sc} = 0.62\, ln(\Gamma_s) - 0.62 \tag{3.102}$$

where:

r_{sc} = salt crust resistance (s/m);

Γ_s = mass of salt accumulated at surface (mg/cm^2). It can be obtained from the salt concentration, θ_{salt} (i.e., Eq. 3.96) and the thickness of salt crust layer;

$$\Gamma_s = \theta_{salt} \rho_s t_s \tag{3.103}$$

t_s = thickness of the salt crust layer (assumed to be uniform over soil surface).

Equation (3.101) can be used to verify the effect of salt concentration (i.e., both osmotic suction and salt crust resistance) on evaporation rate from thin salinized soil layers and salinized soil columns or tailings columns.

3.8 PROPOSED SOLUTION FOR THE SOIL-ATMOSPHERE EVAPORATIVE FLUX EQUATION

The governing equations of flow of heat and moisture Eqs. (2.43) and (2.45) can be used in a coupled manner along with Eq. (3.69) to demonstrate the use of the soil-atmosphere approach to calculating evaporative flux.

The governing equations for heat and moisture transfer in the soil are nonlinear. The coefficients of permeability, vapour diffusivity, thermal conductivity, consolidation and volumetric specific heat vary with vertical position due to changes in pressure, temperature and volumetric water content. The finite element method is utilized for simultaneously solving Eqs. (2.43)

and (2.45). It is convenient to use the software Comsol Multiphysics (COMSOL, 2008) to solve these equations.

A brief overview of the solution for the proposed system of equations for heat and mass transfer between the soil and the atmosphere is presented at this point. The coupled heat and mass transfer equations are solved simultaneously in the domain of the soil profile with respect to space and time. Initial values of hydraulic head and temperature in the soil profile must be specified. The partial pressures due to water vapour required for Eqs. (2.43) and (2.45) are obtained from the known pressure heads and Eq. (2.44). However, the partial vapour pressure for the soil-flux atmosphere flux equation is determined using the new set of the proposed equations (3.80), (3.82) and (3.83) associated with the known pressure heads or water content at soil surface.

The flux boundary conditions at the soil surface are defined as follows:

i. The flux of liquid water may be specified on the basis of rainfall data. However, since the focus of this study is evaporation, a zero flux boundary is specified for the liquid phase in all analysis.

ii. The flux of water vapour to the atmosphere is computed using the vapour transfer profile equation (3.69) and the vapour pressure in the soil at the surface (i.e., taken from the previous time step).

iii. The flow of heat to the atmosphere at the soil surface may be computed on the basis of sensible heat flux (e.g., Eq. 3.38) and the temperature of the soil surface taken from the previous time step. The flow of heat to the atmosphere is an optional calculation since the surface temperature may be measured, estimated or calculated using Eq. (2.19).

In summary, the equations of moisture flow and heat flow are solved while marching forward in time from a known initial condition.

3.8.1 Numerical Solution Using Comsol Multiphysics

The solution is limited to solving the equations of moisture flow and heat flow for a 1-D problem, in a coupled manner. The equation of transport of solute through porous media in 1-D was not included. The intent is to recommend a numerical solution for evaporation from bare soil surface.

The governing equations of heat and mass transfer in the soil are of the partial differential equations (PDEs). Solving these PDEs generally take time to set up the equations, material properties, initial conditions, and boundary conditions for a given soil profile. However, proposing a computer code to solve these PDEs is out of the scope of this thesis. Instead, the author utilizes the software, COMSOL Multiphysics, to obtain a solution.

For readers' convenience, some advantages of application modes (i.e., diffusion and heat transfer) included in the software package are concisely presented here. The package consists of predefined templates and user interfaces already set up with equations and variables for specific areas of physics. Material properties are either available or user-defined in the package. In addition, the application mode interfaces consist of customized dialog boxes for the physics in subdomains and on boundaries, edges, and points along with predefined PDEs. A set of application-dependent variables makes it easy to visualize and post-process the important physical quantities using conventional terminology and notation. Adding even more flexibility, the equation system view provides the possibility to examine and modify the underlying PDEs in the case where a predefined application mode does not exactly match the application you want to model. The diffusion and heat transfer modes included in the COMSOL Multiphysics package are presented more detail in Modeling Guide in Version 3.5a.

It should be noted that the coefficients of permeability, vapour diffusivity, thermal conductivity, consolidation and volumetric specific heat must be available for the suggested solution above. For this reason, the uncoupling process may be applied to verify the new soil-atmosphere equation, Eq. (3.69)

in Chapter 6. Accordingly, only moisture flow equation, Eq. (2.43) may be solved for 1-D domain of the soil profile with respect to space and time.

3.8.2 Analyzing Evaporation from Salinized Soils

Evaporative demand induces a net upward flow of pore water. Given an initial uniform profile distribution of pore-solute, the evaporation-induced flow of water to the surface causes co-movement of solute upwards. This leads to the accumulation of solute at or near the surface through an advective process in desiccating soils. Accordingly salt concentration at or near the surface is higher and higher; hence osmotic suction and salt crust resistance increase during evaporation process. Therefore, solute transport should be coupled to evaporation to predict salt concentration at or near the surface. However, this section is not intended to suggest any numerical solution to obtain salt concentration because some parameters for solute transport were not available. Instead, the profile distributions of water content and pore-water solute which were measured along with actual evaporation rate from the surface are used to predict evaporation rate. For instance, the profiles used to quantify the values of osmotic suction and salt crust resistance by Eqs. (3.99) and (3.100), respectively. The rate of evaporation from salinized soils and tailings are analyzed to assess the effect of factors related to salt concentration such as osmotic suction as well as salt crust resistance. A combination of all factors is then considered to get another solution for the salinized soils and tailings in the end. Finally, all predictions of evaporation rate are compared with the measured evaporative data to show the preferred solution.

3.9 CHAPTER SUMMARY

This chapter presented the theoretical development of the soil-atmospheric model of evaporation from soil surface as well as modification of the methods for determination of relative humidity and soil surface resistance at the soil surface. Re-visitation of evaporative flux (e.g. mass transfer method) and sensible heat flux (e.g. sensible transfer flux) was presented in Section 3.2. In

general, the water vapour is transferred in the laminar layer (i.e., from water surface in the soil pores to the soil-atmosphere interface) through the process of molecular diffusion only. The Fick's Law is applied to account for this transfer of water vapour. In the turbulent zone (i.e., a zone immediately above the soil-atmosphere interface) the transfers of water vapour and heat are calculated using the gradient profiles of specific humidity and heat coupling with the gradient profile of wind speed.

Section 3.3 presented the re-visitation of Penman-Monteith's (1965) equation for estimation of evaporation rate from a wet surface. It is the first equation which accounts for effect of surface resistance on estimating evaporation. The idea of surface resistance would be used for theoretical development of the soil-atmosphere model and relative humidity in the subsequent section.

Section 3.4 derived the surface-resistance type equation for prediction of actual evaporation from soil surfaces with the limited supply of water at the surface. Accordingly, the model advanced both the Penman-Monteith's (1965) equation by including the effect of soil surface relative humidity and the Wilson (1990) equation by including effect of soil surface resistance. The newly proposed equation gives reasonable results of evaporation from soil surfaces of soil columns during the drying process.

The assessment of evaporation-rate reduction using the evaporative data collected from the research literature was presented in Section 3.5. Interestingly, the suction at evaporation-rate reduction point was found to be between the air-entry value and residual soil suction. Therein the formula for determination of such suction was established as a function of the air-entry value and the residual soil suction. This formula was also found to be slightly different for sand and silt. Remarkably, the value of such suction has a tendency toward residual soil suction when soil texture is finer. Later the corresponding volumetric water content at evaporation-rate reduction point was generated using Soil-Water Characteristics Curve. Finally, the relative humidity was developed based on this volumetric water content at evaporation-rate reduction point as a reference point.

Section 3.6 presented the equation for determination of soil surface resistance. Empirically, the soil surface resistance was a function of volumetric water content at the top soil surface. It is noted that the equation of soil surface resistance was modified from the original equation proposed by van de Griend and Owe (1994) using volumetric water content at evaporation-rate reduction point.

Section 3.7 presented effects of pore-water salinity on evaporation rate from salinized soils through two factors such as osmotic suction and salt crust resistance. Osmotic suction and salt crust resistance were found as functions of salt concentration accumulated at the soil surface.

Finally, a proposed solution for the soil-atmosphere evaporative flux equation and analyzing evaporation from salinized soil were presented in Section 3.8. A computer code for solving simultaneously the nonlinear equations of heat and water flow in coupling with the newly-derived soil-atmosphere model of evaporation from soil surface was not created. Instead, COMSOL Multiphysics software capable of solving PDEs was introduced to obtain solution. Comparisons of predicted evaporation rate from the salinized soil with the measured evaporative data showed effects of osmotic suction and salt crust resistance separately. A combination of these factors was also considered.

CHAPTER 4
LABORATORY TESTING PROGRAM

4.1 GENERAL

A number of laboratory testing programs related to evaporative fluxes from bare-soil surfaces, as well as from salinized soil surfaces and tailings surfaces have been published in research literature. Each test program has been carried out with specific objectives in mind. The present laboratory testing program has been conducted with two primary objectives in mind: (i) the measurement of evaporative fluxes from bare-soil surfaces and salinized soil surfaces while drying high water content soils under laboratory controlled climatic conditions; and (ii) the evaluation of the effect of osmotic suction on the evaporation rate from a salinized soil.

Other laboratory testing programs available in the research literature are briefly described in this chapter. Datasets were collected that contained measurements of evaporative fluxes from soil surfaces along with measured water contents, relative humidities of ambient air, temperature of the ambient air, and temperature of the soil and evaporative fluxes from freshwater sources.

The testing program presented in this chapter consists of three distinct sections:

1. A pilot drying test along with a description of the material properties for the selected soils and soil specimen preparation,

2. A description of laboratory equipments, and

3. Laboratory testing procedures for the measurement of the Soil-Water Characteristic Curve (SWCC), osmotic suction and the measurement of evaporative fluxes from thin soil surfaces (non-saline and salinized

surfaces) and thick soil layers (non-saline surfaces) that dry under laboratory conditions.

4.2 LABORATORY TESTING PROGRAM

4.2.1 Soil Properties, Pilot Drying Tests and Soil Preparation

The first section of the laboratory testing program contains a description of the properties for the soils tested, the pilot drying tests on thin soil layers and the preparation of the soils for testing and analysis.

4.2.1.1 Soil Properties

Two soils of different textures were used in the testing program; namely, Ottawa sand and Devon silt. Ottawa sand was a washed silica sand with an average grain size of 0.42 mm. The sand was purchased from Fisher Scientific. Devon silt was a naturally-occurring silt composed of quartz, feldspar, and clay minerals. The grain-size distribution of the Devon silt was obtained from the laboratory study undertaken by Arenson et al. (2005) at the Geotechnical Centre of the University of Alberta (see Figure 4.1).

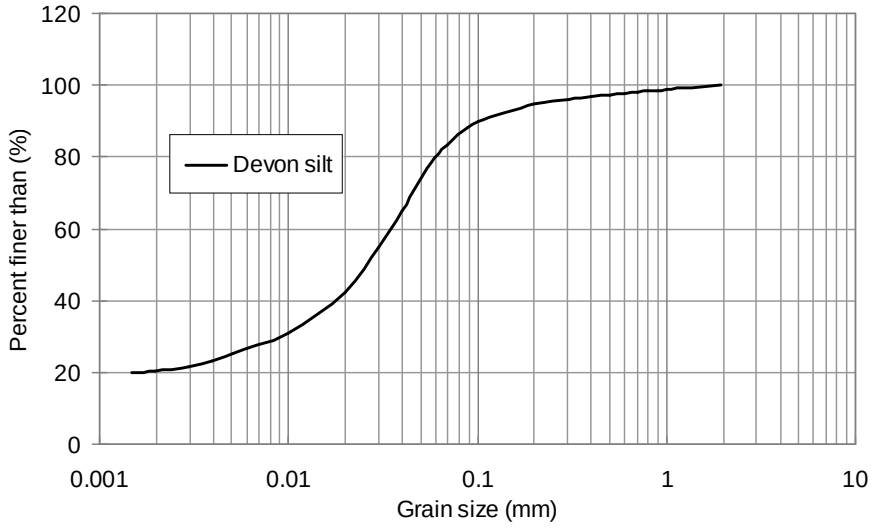

Figure 4.1 Grain size distributions for Devon silt (adapted after Arenson et al., 2005).

The coarse fraction of Devon silt was removed by passing through a No. 40 sieve (0.425 mm). This process eliminated a large of fraction of coarse sand

available in the Natural silt. Figure 4.2 shows the grain-size distribution for the silt material before and after sieving.

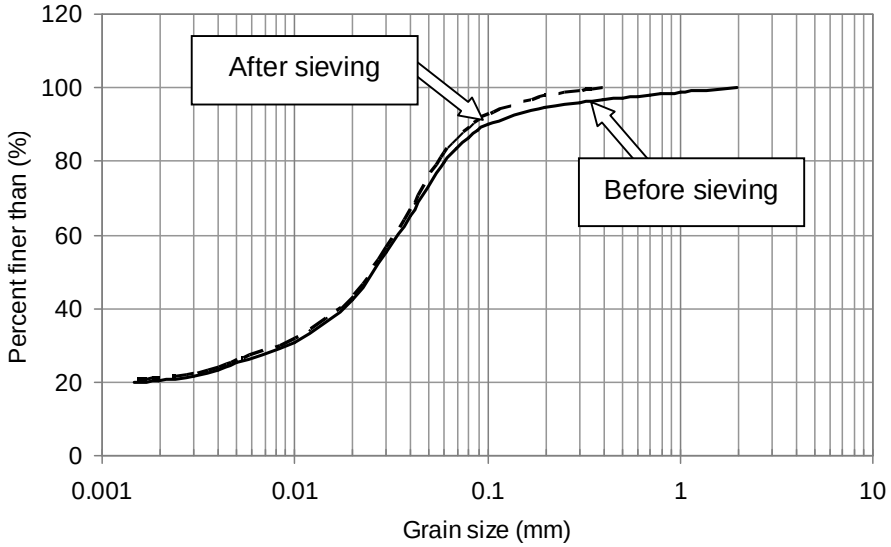

Figure 4.2 Grain size distributions for Devon silt before and after passing through No. 40 sieve.

4.2.1.2 Pilot Drying Test

A pilot drying test was carried out to assess the effect of initial salt contents on laboratory testing programs. The effect of the ambient laboratory conditions was also assessed. The drying tests were conducted at the Graduate Geotechnical Laboratory, NREF L1-120 at the University of Alberta, Edmonton, between December 24, 2011 and January 31, 2012. Two selected soils (Ottawa sand and sieved Devon silt) were mixed with different initial salinities to prepare the salt-soil mixtures for the "pilot experiments" as follows:

1. The sand was mixed with 100 g/l, 200 g/l and 300 g/l of sodium chloride (NaCl).

2. The sieved silt mixed with 100 g/l and 200 g/l NaCl.

Each soil type was placed as saturated slurry in the shallow plastic pans with dimensions of 195 mm x 135 mm x 100 mm to a thickness of about 10 mm.

Two pans of equal dimensions were also filled with distilled water and saline water (e.g., 200 g NaCl dissolved into 1 litre distilled water). These pans of water were placed along side the pans with soil and were used as a reference for potential evaporation.

The samples were allowed to dry in the laboratory at room temperature which varied from 19 ^{o}C to 22 ^{o}C. The relative humidity was quite constant, ranging between 20% and 25%. The rate of evaporation from each pan of soil, the pan of distilled water and the pan of saline water was determined by weighing each pan every 20 minutes. The temperature of each soil sample and the pans of water were not recorded during the evaporation process. Figures 4.3 and 4.4 show the results of the pilot drying tests.

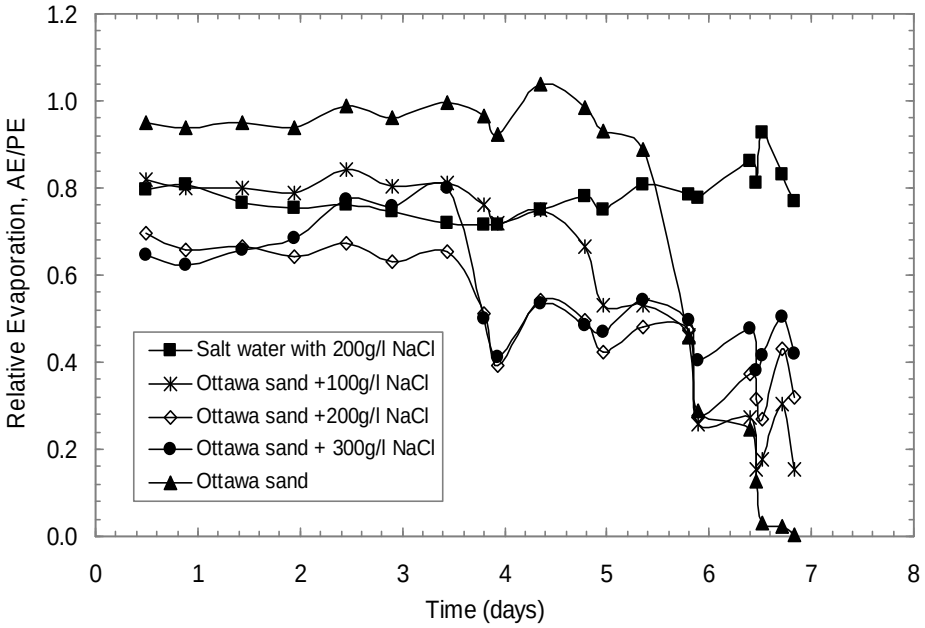

Figure 4.3 Relative Evaporation of Ottawa sand (i.e., ratio of Actual evaporation to Potential evaporation) versus elapsed time for pilot drying test.

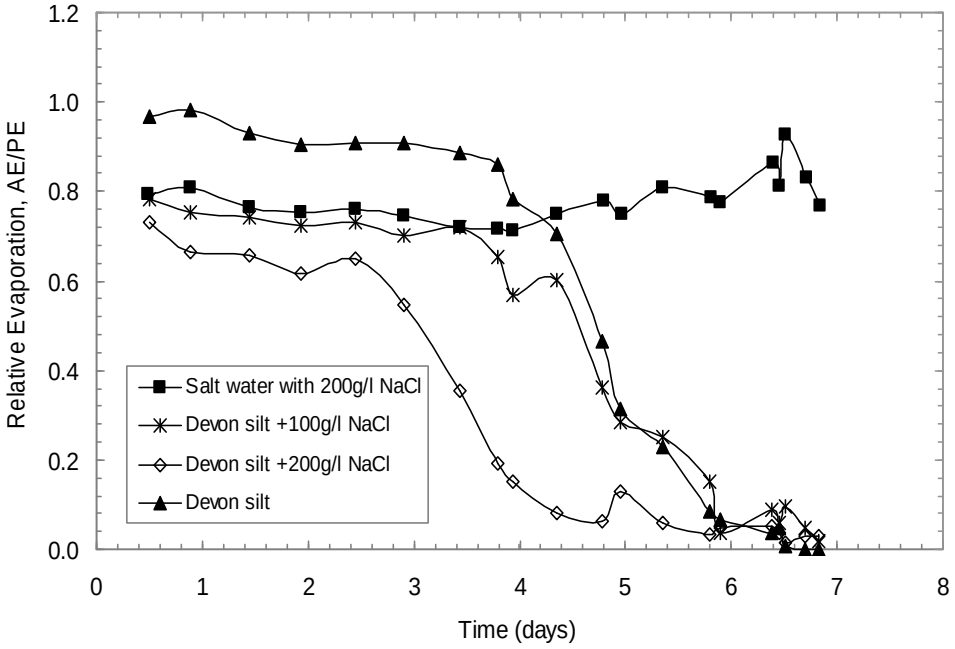

Figure 4.4 Relative Evaporation of Devon silt (i.e., ratio of Actual evaporation to Potential evaporation) versus elapsed time for the pilot drying test.

The results of the pilot experiments showed that soil texture and pore-water salinity have a significant effect on the rate of evaporation. The actual evaporation rate from the clean sand and silt were equal to the potential rate of evaporation for the water during the initial stage of drying. However, the rate of evaporation from saline water and salinized soils (e.g., sand and silt) was significantly depressed. The initial rates of evaporation of saline water were approximately from 20% to 30% below that of the free water surface. The evaporation rates depended upon the initial pore-water salinity. The higher the initial pore-water salinity in the salinized soil, the more depressed the rate of evaporation.

The rate of evaporation from saline water was approximately 20% below that of the free-water surface during 7 days of drying. A salt crust was found at the surfaces of the both salinized sand and silt between days 3 and 4. Figure 4.4 showed that the depressed evaporation rate from the salinized-silt pans was constant after 3 days of evaporation and decreased gradually to zero after 7 days of evaporation. However, Figure 4.3 showed that the depressed

evaporation rate from the salinized-sand pans fluctuated and did not decrease to zero between 4 days and 7 days of evaporation. In fact, it was found that this rate was constant after 3 days of evaporation and then decreased gradually to a low constant residual value after 4 days of evaporation.

Some 10 mm wide cracks appeared on the samples of salinized sand. The cracks may have occurred as a result of bending of the bottom of the plastic pans. It should also be noted that graduate students were often opening the laboratory front doors, thereby disturbing the room conditions. It is speculated that these activities influence the consistency of the condition in the laboratory during drying. The evaporation testing program was subsequently moved to another laboratory room, NREF L2-040 with double front doors that limited the influence from unexpected environmental factors. Metal pans 36 mm in high and 200 mm in diameter were used in place of the plastic pans. Following the initial set of "pilot experiments", another set of more highly controlled experiments were undertaken overnight. Further details pertaining to these experiments are described in Section 4.2.4.

4.2.1.3 Selection of Salt Soil Mixture and Mixture Preparation

Newson and Fahey (2003) found that the salinity of tailings varied from approximately 10 g/l of salt solution for mine tailings or thickened tailings to approximately 250 g/l for hypersaline tailings (i.e., approximately seven times the salinity of seawater of 35 g/l). In the research literature, studies on evaporation have been conducted on the salinized soils with salinities of 5 %, 10 % and 20 % (i.e., mass of salt/mass of solution). These salinities correspond to approximately 50 g/l, 100 g/l and 200 g/l of salt concentration in terms of the volume of salt to volume of water, respectively. The influence of initial pore-water salinity on the soil-water characteristic curve appears to be minimal as shown in Figure 4.5 from Dunmola (2012).

Four mixtures of saline soils with 50 g/l, 100 g/l, 200 g/l and 250 g/l of sodium chloride (NaCl) concentration (i.e., ratio of initial salt mass to initial volume of water) were chosen for studies to test the evaporation from thin soil layers.

However, only non-saline soils and soils mixed with 50 g/l NaCl were chosen for the soil-water characteristic curve program. These mixtures are assumed to reasonably represent the range of salinity commonly occurring in nature.

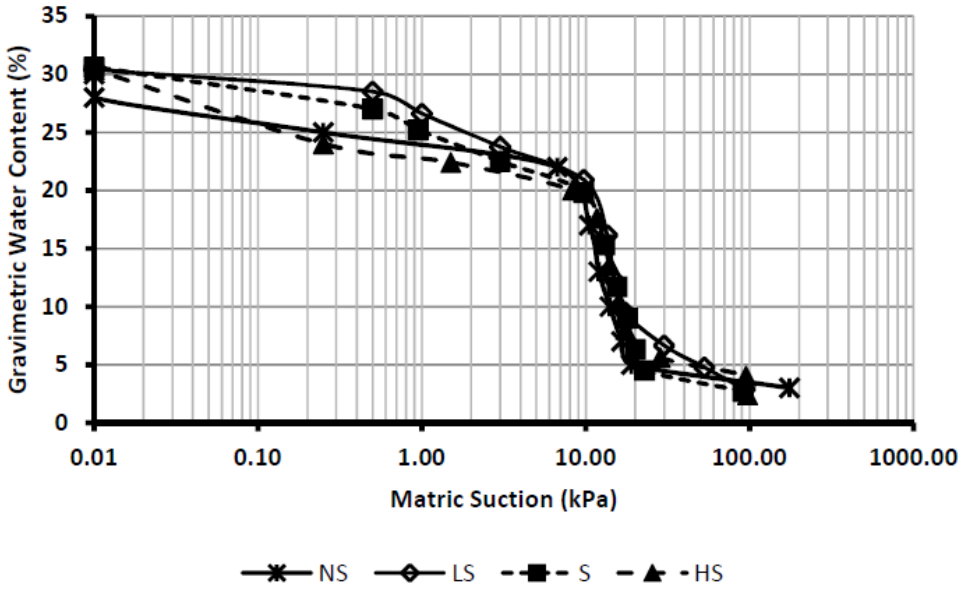

Figure 4.5 Soil-water characteristic curves for the remoulded Low-saline (LS), Saline (S), Hyper-saline (HS) and Non-saline (NS) soils (adapted after Dunmola, 2012).

In order to measure the effect of salt content on the evaporation rate from soil surfaces, three types of experiments were conducted on saline soils in the laboratory (i.e., soil-water characteristic curve test, osmotic suction test and thin-soil layer evaporation test). Figure 4.6 shows the laboratory testing program which consists of equipment, materials and objectives. In order to prepare the salt-saline water mixtures, salt (e.g., NaCl) should be added to distilled water to correspond to the selected salinities. These solutions should be stirred until all salt is completely dissolved into the water. These solutions are then mixed with the selected soils to create the mixtures for testing. Specimen preparation for different tests is described in detail.

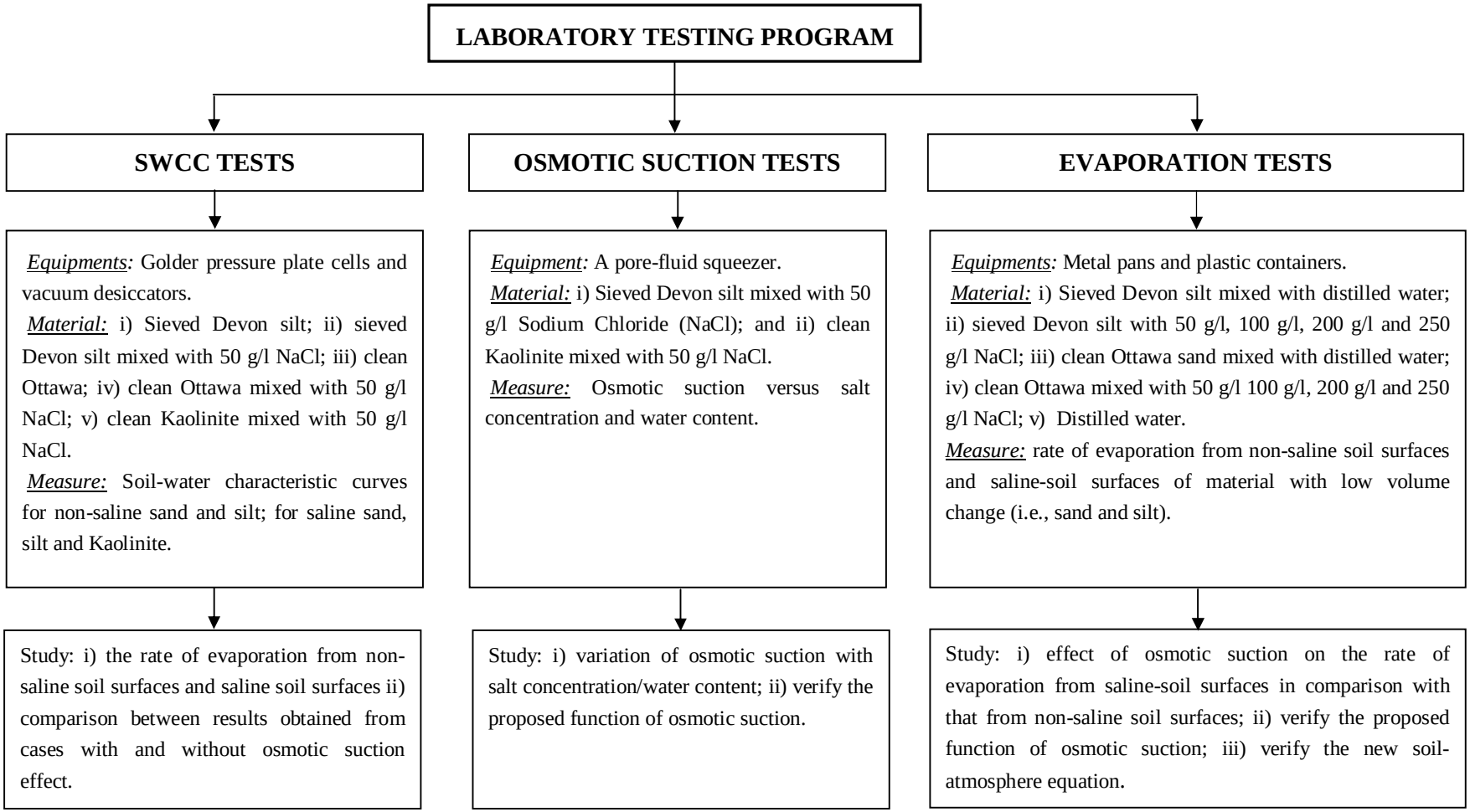

Figure 4.6 Materials, equipments and objectives of the laboratory testing program.

4.2.2 Description of Laboratory Equipments

Three types of equipment were used in the laboratory testing program, namely, a Golder pressure plate apparatus, a pore-fluid squeezer, and vacuum desiccators. Three Golder pressure plate cells which are manufactured by GCTS, Tempe, AZ purchased from the geotechnical company, Golder Associates, Saskatoon, Saskatchewan, Canada. The pore-fluid squeezer was purchased from the Ruhr-University Bochum in Germany. Four vacuum desiccators were purchased from Fisher Scientific.

The functions of each apparatus are concisely presented in this section. The Golder pressure plate apparatuses were used to measure the soil-water characteristic curves at zero and relatively low net mean applied stress. There is no standard testing procedure available although the Golder apparatus has been previously used to measure the SWCC of other soils. Suggested testing procedures for Golder pressure plate cells are presented in next section.

The pore-fluid squeezer was used to extract macro pore-water from salinized-soil samples. Osmotic suctions were indirectly inferred through correlations with the electrical conductivity of the pore-water. The pore-fluid squeezer is described in detail in a subsequent section. The vacuum desiccators were used to equilibrate soil specimens with saturated salt solutions. Total suctions were determined based on thermodynamic principles.

4.2.2.1 Golder Pressure Plate Apparatus

Three Golder pressure plate cells were used in the laboratory testing program. The equipment was manufactured by Geotechnical Consulting and Testing System, Tempe, Arizona, USA (GCTS). The Golder pressure plate cells were designed to work well for applied soil suctions between 3 kPa and 500 kPa (i.e., 5 bar ceramic air entry disk). The Golder pressure plate cells use the axis-transition technique concept to control matric suction in the soil specimen (Hilf, 1956; Fredlund and Rahardjo, 1993).

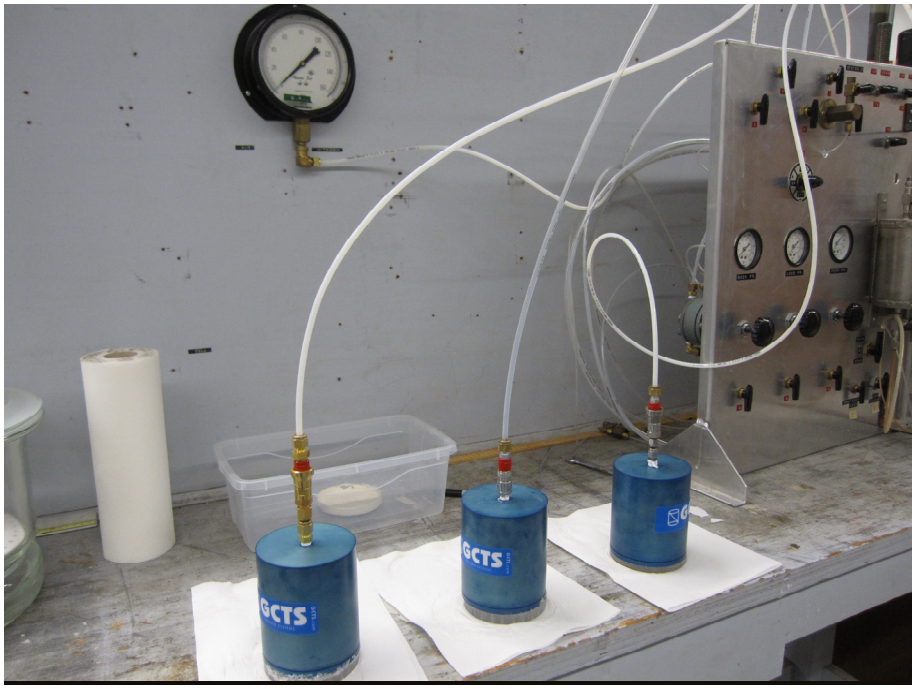

Figure 4.7 Basic Golder pressure plate cells connected to air pressure supply (setup in Graduate Geotechnical Laboratory, NREF L1-120, University of Alberta).

4.2.2.2 Pore-Fluid Squeezer

The research program requires the measurement of osmotic suction over a range of water contents to develop the functional form of osmotic suction with salt concentration (or water content). The squeezing process extracts pore-water from a soil specimen. The pore-fluid squeezing technique has been shown to give reasonable measurement of the osmotic suction of the pore fluid in a soil (Krahn and Fredlund, 1972). The technique consists of squeezing a soil specimen to extract the macro-pore water and measure its electrical conductivity. Osmotic suction is determined using an empirical relationship between osmotic suction and electrical conductivity.

The pore-water squeezer used in this study is shown in Figure 4.8. The squeezer consists of three main parts, (i.e., ram, cylinder, and base). The squeezer is also equipped with accessories such as a Teflon disk, rubber disk, filter holder and rubber washer. From top to bottom, the ram is connected to

cylinder with a Teflon disk with a rubber disk in between. The Teflon disk is used to separate the ram and the rubber disk and to avoid the rubber disk from being damaged or destroyed under high applied pressures. The rubber disk also avoids leakage in the cylinder. The cylinder is connected to the base using a filter holder and a rubber washer. The rubber washer is used to avoid leakage between filter holder and base. The filter holder is used for placing three layers of wire mesh (1 mm in diameter) and filter paper. The filter paper is necessary to retain colloidal clay particles which could alter electrical conductivity readings.

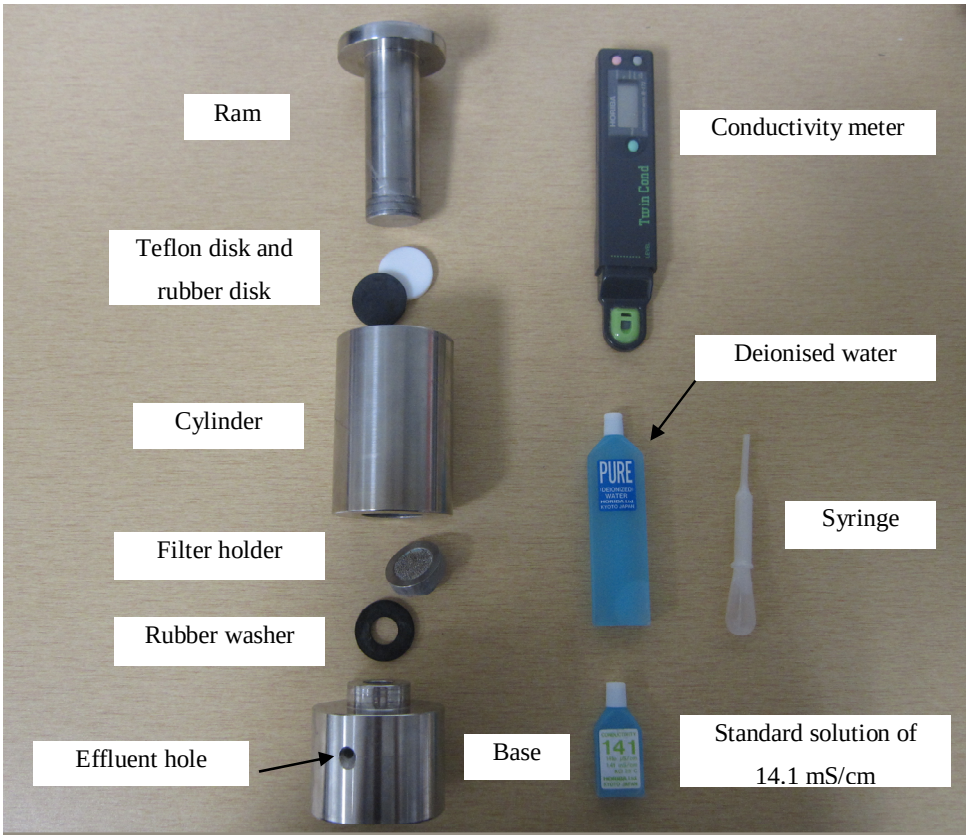

Figure 4.8 A pore-fluid squeezer and conductivity meter used in the squeezing technique.

Figure 4.9 shows the compression testing machine, Forney FX 700, used to apply loads on the pore-fluid squeezer. The machine has a maximum capacity of approximately 3,114 kN (or 700,000 lbs) and the minimum capacity of approximately 31 kN (7,000 lbs) with the loading rate of 250 kPa/s. Pressure was applied one-dimensionally until drop of pore-water expelled.

Figure 4.9 The compression testing machine at the University of Alberta used for loading the squeezer.

4.2.2.3 Vacuum Desiccators and Vapour Pressure Equilibrium Technique

This section describes the determination of high soil suctions (total suction) corresponding to low water contents in the soil. The vapor pressure equilibrium technique requires establishing a constant relative humidity environment in the laboratory and then allowing soil specimens to equalize to a water content corresponding to the selected relative humidity environment. Desiccators with various saturated salt solutions can be used to establish such an environment. The use of saturated salt solutions to control relative humidity is both a convenient and inexpensive method. Saturated salt solutions are

preferable to salts of various concentrations because they can liberate and adsorb large quantities of water without changing the equilibrium humidity. Total suction can be determined using the thermodynamic relationship between total suction and the partial pressure of the pore-water (Edlefsen and Anderson, 1943; Richards, 1965).

Some of the salt solutions that are most commonly used to create a range of relative humidity environments can be found in the ASTM Designation E 104-02. Four salt solutions were selected to give a suitable range of controlled humidities. A summary of the relative humidity for the selected saturated salt solutions at temperature of 20 degrees Celcius is shown in Table 4.1.

Table 4.1 Approximate Equilibrium Relative Humidities for Selected Saturated Salt Solutions at 20 degrees Celcius.

Salt Solution	Average Relative Humidity **(%)**
Lithium chloride	12
Sodium chloride	75
Potassium chloride	85
Potassium sulfate	98

The generated relative humidity values created are also a function of temperature. The temperature in the laboratory room was found to vary between 19.5 ^{o}C to 22 ^{o}C. Consequently, the information in Table 4.1 is suitable for the determination of high suctions.

Typical laboratory results obtained using desiccators and the vapour equilibrium technique for Regina clay, are shown in Figure 4.10 (Fredlund, 1964). A second dataset is also shown with results obtained by Ebrahimi-Birang et al. (2007). The two datasets show similar results even though the tests were performed several years apart.

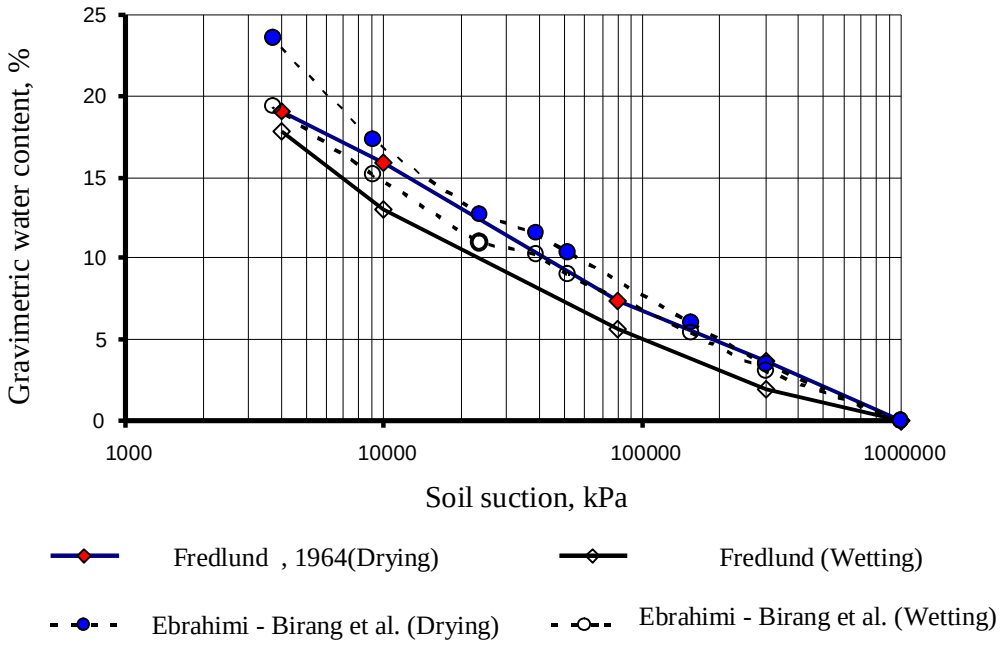

Figure 4.10 Drying and wetting SWCCs for Regina clay measured in 1964 and 2007.

4.2.3 Soil-Water Characteristic Curve and Osmotic Suction

The next step in the laboratory testing program was to determine the soil-water characteristic curves for the selected soils along with the osmotic suction from saline soils at various initial salt contents.

4.2.3.1 Objectives of Measurement

The soil-water characteristic curves (SWCC) of the selected soil types (i.e., sieved Devon silt and clean Ottawa sand) were required for subsequent studies. The calculation of the evaporative flux from a soil surface requires that the actual vapour pressure at the soil surface be known. The vapour pressure at the soil surface can be calculated using Eq. (2.19) after Edlefsen and Anderson (1943) which provides a relationship between absolute vapour pressure and total suction of the pore-water at the soil surface. Total suction can range from zero to 1,000,000 kPa and is compromised of a capillary (or matric) component and an osmotic component. For example, total suction is

related to soil water content through the soil-water characteristic curve of the soil as shown in Figure 3.7 in Chapter 3.

As reviewed, evaporation is affected by the pore-water salinity. It should be noted that osmotic suction depends on the pore-water salinity. Higher pore-salinity results in higher osmotic suction. Evaporation eventually depends on not only matric suction but also osmotic suction.

4.2.3.2 Laboratory Testing Procedures

The low suction portion of the soil-water characteristic curves was determined for the clean Ottawa sand, the clean Ottawa sand mixed with 50 g/l NaCl, the sieved Devon silt, the sieved Devon silt mixed with 50 g/l NaCl, and clean Kaolinite mixed with 50 g/l NaCl using Golder pressure plate cells. In addition, the high suction portion of the SWCC was determined for the sieved Devon silt, the sieved Devon silt mixed with 50 g/l NaCl and clean Kaolinite mixed with 50 g/l NaCl. The clean Ottawa sand was found to desaturate quickly and abruptly at low values of matric suction. Air-dried samples of each soil type were slurried with distilled water and NaCl solution. The sand, silt and clay were prepared at water contents of 35%, 44% and 74%, respectively. The following procedures were applied to each type of mixture (i.e., non-saline mixtures and saline mixtures):

1. It was important that Kaolin paste be plastered as a thin layer on the surface of the high air entry value disk of Golder pressure plate cells (HAEV disk) to ensure good contact between the ceramic and the soil specimen. This procedure assisted in the efficient water movement to/from the soil specimen;

2. Each slurried sample was prepared in a metal ring placed on HAEV disk. The volume of the soil sample and mass of (soil + ring + HAEV disk) were recorded prior to testing;

3. The high entry value disk was allowed to soaked for one day for sand, silt; and two days for clay;

4. Assembly the HAEV disk into the Golder pressure plate cell and weigh the entire apparatus (soil + ring + cell) for later water content determination;

5. Increasing pressures of 7, 15, 30, 60, 125, 250 and 480 kPa were applied to the air phase with the cells. The reading of the gauge pressure was recorded;

6. The mass of the entire apparatus was continually monitored during the drainage phase of each air-pressure increment until mass equilibrium was obtained. There was no need to dismantle the apparatus after equilibrium at each air-pressure increment;

7. At the end of the test, the air-pressure was reduced to zero; the volume of the soil sample and mass of the entire apparatus were recorded.

Each sample was removed from the Golder pressure plate cells after the testing was completed. Four smaller samples weighing between 1 and 5 grams were immediately trimmed from each sample after being tested in the Golder pressure plate cells. The specimens were weighed to the nearest 0.01 gram and placed on a standard glass desiccator. The saturated salt solutions shown in Table 4.1 were created by mixing salt with distilled water until free salt appears in the bottom of the glass desiccators in an undissolved state. The saturated salt solutions were prepared at room temperature or slightly higher than room temperature, in order to clearly observe when the solutions are saturated. The specimens were allowed to reach equilibrium at each humidity controlled desiccators for a period of 2 to 3 weeks. The change in mass of each specimen was continually monitored to ensure equilibrium water content. It was found that equilibrium was achieved more rapidly under low relative humidity conditions than under high relative humidity conditions. The

gravimetric water content of samples removed from the Golder pressure plate cells and the desiccating chambers were determined by oven-drying samples at 105^0C.

For saline-soil samples, osmotic suction was measured using the squeezing technique. These saline-soil samples were made from mixing silt and clay with the selected salt contents (i.e., 50 g/l NaCl). Each sample was placed inside the pore-fluid squeezer. Every part of the squeezer was washed and rinsed three times with distilled water or deionised water in order to reduce contamination of the pore-liquid as much as possible.

Pressures of 500, 1,000, 2,000, 5,000, 10,000, 15,000, 20,000, 25,000 kPa or more were vertically applied using the compression testing machine and held for 5 minutes to 10 minutes until obtaining the first drop of pore-water for each pressure. The squeezed-out soil pore-water was collected using a syringe and placed in a sterile container. The electrical conductivity of the soil pore-water was measured using an electrical conductivity meter. The electrical conductivity meter was calibrated using a standard solution with an electrical conductivity of 14.1 mS/cm provided by the manufacturer of the pore-fluid squeezer. At least 2 ml of soil pore-water was required for the measurement of electrical conductivity. The change in mass of each sample was continually monitored before and after each pressure increment. The gravimetric water content of samples removed from the pore-fluid squeezer was determined by oven-drying the soil specimen at 105 ^{o}C.

4.2.4 Thin Soil Layer Drying Testing

In this section, the desiccating tests on the thin soil layers are described. The thin soil layers of non-saline soils and saline soils with various initial salt contents are investigated.

4.2.4.1 Testing Criteria and Objectives

The vapour pressure gradient between a soil surface and the atmosphere above the surface were assumed to be a fundamental driving force that causes the evaporative flux from the soil surface. The vapour pressure gradient appeared to have been accepted in disciplines such as hydrological, agricultural and geotechnical engineering. Wilson (1990) has demonstrated the validity of the vapour pressure gradient through a series of thin soil section drying tests on bare soils (i.e., Beaver Creek sand, Custom silt and Regina clay of 0.5 – 1 mm thick). Recently, Dunmola (2012) monitored the evaporative flux from three replicates of thin non-saline silt layers that were 2 mm thick. It was concluded that the Wilson (1997) equation based on this assumption was valid for thin layers. However, these investigators did not investigate the effect of salt concentrations on the evaporative flux from thin soil section drying.

Other researchers, including Konucku et al. (2004), Fujimaki et al. (2006) and Gran et al. (2011) investigated on the rate of evaporation and salt transport from saline-soil columns. The conclusion of their results was not consistent. Some stated that osmotic suction and temperature gradients play an important role in the reduction of the evaporation rate from a soil surface while other did not; rather a salt crust was formed. The details of the mechanisms involved with soil salinization appear to be poorly understood.

The objectives of the thin soil section drying tests were to directly measure the evaporative flux from a saline-soil surface as it dried from a saturated state to a completely air-dried state. These thin soil section drying tests in the laboratory program are somewhat different from those conducted by Wilson (1990) and Dunmola (2012). The evaporative fluxes were measured relative to time and soil water content. The evaporative fluxes from the soil surface and water surface were measured as reference points along with the measurement of the evaporative fluxes from the saline-soil surface. The thin saline-soil surfaces and soil surfaces were artificially formed in the laboratory. The saline-soil surfaces and soil surfaces were made as thin as physically possible so as to minimize the effects of moisture gradients and flow in the soil beneath

the surface. Tests were conducted using each of the two previously selected soils (Ottawa sand and Devon silt). The measured results were used to re-evaluate effect of each factor (osmotic suction and salt crust) on the evaporation rate from the saline-soil. This re-evaluation of the evaporation rates appears to be necessary prior to any further studies being conducted on salt transport inside the saline-soil columns.

4.2.4.2 Laboratory Testing Procedures

Figure 4.11 shows a photo of the pans used to conduct the thin soil layer evaporation tests. The tests were conducted using six identical 200 mm diameter evaporation pans. The pan labels with filled materials are presented in Table 4.2. While Pan 6 was filled with distilled water (and functioned as the reference pan for potential evaporation), Pan 1 contained the evaporating soil surface for measuring actual evaporation as the reference pan for evaporation from saline-soil surfaces. The change in mass of all pans was monitored manually using a Mettler TOLEDO balance with the accuracy of 0.05 grams. One pan was weighed after another in sequence. Soil surface temperature and water surface temperature were not monitored in the laboratory program. A digital Relative Humidity/Temperature Meter (Traceable) was placed 300 mm above the pans to record air temperature and the relative humidity on a continual basis.

All thin soil layer tests were conducted at the University of Alberta in the Geotechnical laboratory NREF L2-040 between February 20 and February 24, 2012. The tests were conducted at a room temperature of approximately 20 ^{o}C. Control of the relative humidity in the room was not provided. However, the fluctuation in the laboratory during the period of any test was noted to be relatively minor.

All samples were permitted to dry in the absence of any direct radiative forcing such as heat lamps or infrared bulbs. These were avoided to ensure a uniform energy budget over the entire surface of each evaporating soil. The

overhead fluorescent room lights (Phillip F32T8/TL841 PLUS, 32 watts) were turned on for the duration of all tests.

Table 4.2 Pan No. and label with filled materials for each set used in the laboratory program.

Pan No.	Material	Pan label
Pan 1	Soil	S1
Pan 2	Soil + 50 g/l NaCl	S1-50
Pan 3	Soil + 100 g/l NaCl	S1-100
Pan 4	Soil + 200 g/l NaCl	S1-200
Pan 5	Soil + 250 g/l NaCl	S1-250
Pan 6	Distilled water	W1

Two sets of thin soil layer were conducted for each of the selected soils. The thin soil layers were prepared by gently dusting a layer of dry soil onto a metal pan of 200 mm diameter. The dusting procedure was carried out using a hand held sieve filled with soil. A No. 40 sieve was used for the Devon silt and Ottawa sand. Soil was placed uniformly over the pans by gently shaking the soil filled sieve in circular motion of the surface area of the pans. The application of soil would cease when the soil layer as sufficiently thick to mask the underlying pans. The final layer thicknesses for the Devon silt and Ottawa sand varied between 0.5 – 1 mm.

Each dry soil layer was subsequently saturated with distilled water or saline water. The distilled water or saline water was applied to the soil using a fine mist. The mist applicator was held approximately 1.0 meter above the soil surface and move in a circular motion around the soil during the application. The misting procedure continued until each soil surface appeared uniformly saturated. Each saturated layer of soil was kept in a sealed Ziploc plastic bag until all five pans of soil were prepared. All soil layers were permitted to evaporate at the same time.

The change in mass due to evaporation from the soil surfaces were manually recorded at regular intervals. A 15 minute interval was used for the tests with

Ottawa sand. A 20 minute interval was used throughout the tests on Devon silt. Shorter time intervals were used for the sand as this soil desiccated more quickly than the silt. The change in mass of the water surfaces were manually recorded at the same regular time intervals. The temperatures of the evaporating soil and water surfaces were not recorded. The air temperatures and the relative humidity of air were also recorded at the same time interval as the pans of soil.

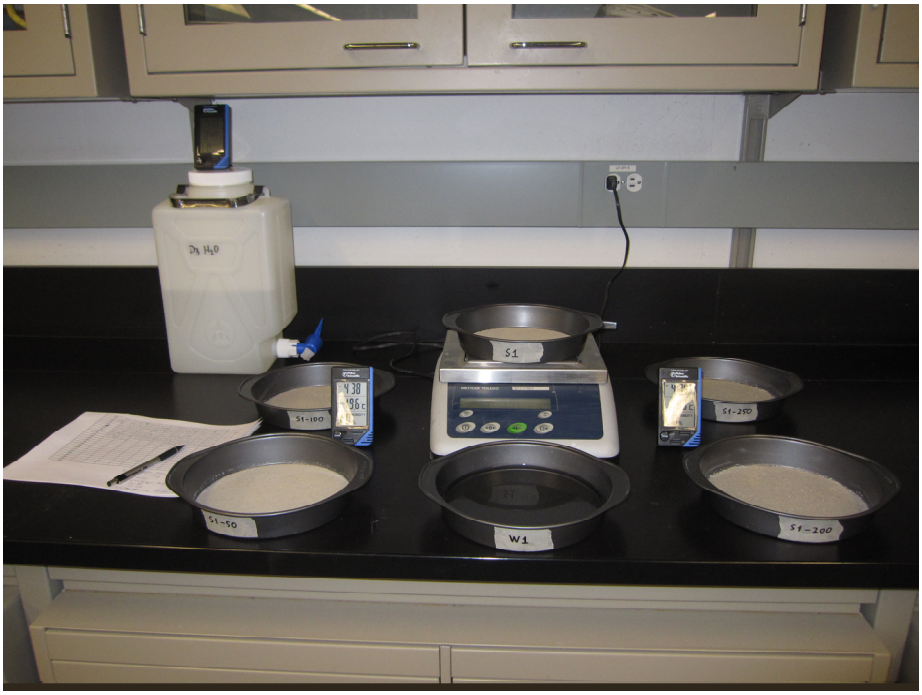

Figure 4.11 Illustration of evaporating tests for thin soil layers.

4.2.5 Thick Soil Layer Drying Testing

In this section, the desiccating tests on the thick soil layers are described. Evaporative data obtained from the thick soil layers of non-saline sand and silt are used to verify the new soil-atmosphere equation as well as the new set of proposed equation of relative humidity and soil surface resistance.

4.2.5.1 Testing Criteria and Objectives

The soil layers were made extremely thin in order to minimize the effects of transfer mechanisms within the soil matrix. In this way, the soil surface was not supplied water from the underlying wetter soil. The objective of this section is to measure evaporation fluxes from the soil layers sufficient thickness such that the influence of soil matrix and flow mechanism within soil on the evaporation rate from the soil surface could be re-evaluated.
Ottawa sand and sieved Devon silt were selected materials for the laboratory thick soil layer drying test. The drying tests were carried out in such a way that effect of volume change is minimized. Isolation of the volume change effects will permit clearer observations of the primary process of evaporation from a desiccating soil profile. Profiles of soil moisture content need to be monitored during the drying process. The measured evaporative data as well as soil moisture content profiles provides information on the verification of the new set of the proposed equations of vapour pressure (i.e., Eqs. 3.80, 3.82 and 3.83) and the new soil-atmosphere equation (i.e., Eq. 3.69).

The use of a radiative flux is avoided in the drying tests with the thick soil layers for the same reasons as those given for the thin soil layer drying tests.

4.2.5.2 Laboratory Testing Procedures

The soil filled evaporation containers for Ottawa sand were constructed using 105 mm diameter ID Concrete Test Cylinders with a wall thickness of 1.5 mm. Such containers for Devon silt were constructed using 75 ID mica tubes with a wall thickness of 6 mm. All soil filled evaporation containers measured 50 mm in height. Ottawa sand, Devon silt and distilled water were filled up to the thickness of 30 mm. Waxed paper was placed around and the bottoms of Devon silt specimens so the coefficient of friction were reduced on the edges and bottoms; and hence Devon silt specimens might not crack (see Figure 4.12). The soil filled containers were gently tapped around so that the soil surfaces had a flat surface. All soil filled containers were open for 24 hours before recording their mass in consecutive hours.

Total of eleven replicates of the sand containers were prepared for the drying experiment of Ottawa sand such that one replicate was destructively sampled at specific time intervals to obtain the profile of soil moisture content. Total of eight replicates of the silt containers were for the drying experiment of Devon silt. The change in mass due to evaporation from the replicates was manually recorded regular intervals using a Mettler TOLEDO balance with the accuracy of 0.05 grams. A six hour interval and a twelve hour interval were used for the tests with Ottawa sand and Devon silt, respectively. The change in mass of the water surfaces, water surface temperature and soil surface temperature were manually recorded at the same regular time intervals. A digital Relative Humidity/Temperature Meter (Traceable) was placed 300 mm above the soil filled containers to record air temperature and the relative humidity on continual basis.

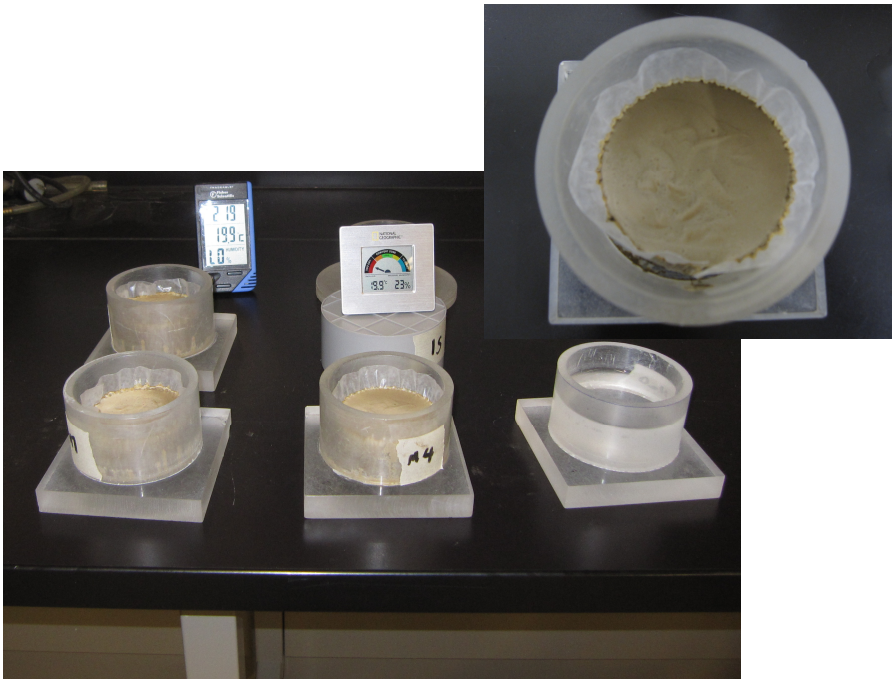

Figure 4.12 Illustration of the soil filled evaporation containers for Devon silt.

Destructive sampling entailed sectioning the soils into 1 mm thick slices using a small spatula which is used for the Atterberg Limits. The slices were obtained at the depths of 1 mm, 10 mm, 20 mm and 30 mm for determining profiles of soil moisture content. These slices were placed on aluminum tares

and kept in sealed plastic Ziploc bags to minimize water lost due to additional evaporation. The parameters of the profile sample would present the average for the corresponding depth of 1 mm.

4.3 OTHER LABORATORY TESTING PROGRAMS COLLECTED FROM THE RESEARCH LITERATURE

In addition to measurement of the evaporative fluxes from thick soil layers carried out in the laboratory testing program, dataset of soil columns were collected from the research literature. The dataset for various soil textures (i.e., sand and silt) were collected from the soil columns of Beaver Creek sand (Wilson, 1990), the soil columns of sand and silt (Bruch, 1993), the soil columns of coarse sand and fine sand (Yanful and Choo, 1997), and the soil columns of non-saline silt and saline silt (Dunmola, 2012). The subsequent sections present the equipment, soil preparation and the laboratory testing procedures used by the other researchers to obtain the dataset. Further details on these testing procedures can be found in the following references by Wilson (1990), Bruch (1993), Yanful and Choo (1997) and Dunmola (2012).

4.3.1 Soil Columns of Beaver Creek Sand (Wilson, 1990)

Beaver Creek sand datasets were selected for collection since this material offered several advantages. Beaver Creek sand has the low porosity and therefore was desaturated quickly under a specific evaporative flux. Beaver Creek sand also has a low air-entry value and a steep soil-water characteristic curve. Therefore, the distinct drying front develops as evaporation progresses. The drying front provides the opportunity to observe the transfer of moisture to soil surface through both liquid flow and vapour diffusion (Wilson, 1990). In addition, the change in water content at the soil surface was recorded along with the measurement of evaporation rate from the soil surface. This measurement provides the opportunity to evaluate at what water content and corresponding total suction the actual evaporation rate starts to reduce from the potential evaporation rate. Finally, Beaver Creek sand was selected to

minimize the effect of volume change as desiccation occurs. The influence of volume change on the evaporative process is outside the scope of this thesis. The soil properties and schemes of drying experiment in Wilson (1990) are provided in Appendix B.

The effect of the energy budget on the evaporative process was deliberately set aside so that the fundamental process of soil evaporation could be observed.

The column drying test was conducted within a Model 3478-1 Bally Refrigeration Environmental Chamber in the Environmental Engineering Laboratory at the University of Saskatchewan (Wilson, 1990). The temperature of the chamber was maintained at 38.0 ^{o} ± 1.0 ^{o}C to accelerate evaporative fluxes. The relative humidity of the chamber was maintained between 11 and 23 percent with a mean of 15 percent.

The evaporation fluxes were measured on two soil columns of PVC (i.e., column A and column B) with 300 mm in height, 169 mm in outer diameter and 7.7 mm thick. Four and eight series of vertical sampling ports 10 mm in diameter were drilled 20 mm on centre down the length at 90^{o} and 45^{o} intervals around the perimeter of column A and column B, respectively for collection of water content samples. Soft AA stoppers were pressed into each sample port as seal before and after sample collection.

Six Premium grade HFD-30-TT thermocouples were positioned at the surface and at depths of 10 mm, 25 mm, 50 mm, 100 mm and 250 mm below the surface. The Mettler PJ3000 and P10 electronic scales were used to record change in mass for column A and column B during evaporation process at 900 second intervals, respectively. The water filled pan was recorded manually three times per day using a Mettler P1200 scale. Relative humidity readings were also taken manually three times per day. Temperatures were recorded automatically at 900 second intervals using twelve thermocouple leads from the two soil columns; and the thermocouple leads from the water surface and the air space above evaporation columns. All thermocouples were connected to the microcomputer.

Both column A and column B were filled with Beaver Creek sand mixed with distilled water at a water content slight below 24 percent. Each column was prepared using 50 mm lifts of sand. The lifts were liquified by tapping the columns along the sides to ensure the removal of voids and obtain a uniform density. The sand surface of each column was trimmed level with the top of the PVC casing and sealed with aluminum foil until the start of the test.

The evaporative fluxes (the change in mass for the columns) from both column A and column B were continually recorded in daily basis for the period of 42 days immediately after removing the aluminum foil from the sand columns. Water content profiles were taken from column A after 5, 9, 12, 21 and 35 days of evaporation and from column B after 1, 2, 3, 6, 7, 14, 29 and 42 days of evaporation.

The evaporative flux from the water filled pan required constant replenishment with water to maintain a full pan. Approximately 130 ml of distilled water was added daily. The temperature of the distilled water added for replenishment was carefully adjusted to ensure its temperature matched the water in the water filled pan.

4.3.2 Soil Columns of sand and silt (Bruch, 1993)

The column evaporation tests carried out by Bruch (1993) were designed to be similar to those performed by Wilson (1990) in term of the equipment and the laboratory testing procedures. The soil properties and schemes of drying experiment by Bruch (1993) are provided in Appendix C. The following sections present some distinguishing features of the tests such as the environmental conditions, tested materials and boundary conditions.

The temperature of the environmental chamber was maintained at $36.0^{o} \pm 0.5\ ^{o}C$ to accelerate evaporative fluxes. A piece of polyethylene sheet was suspended below the ceiling fans in the chamber to reduce air currents

around the evaporative surfaces of the columns. The relative humidity of the chamber varied between 7.6 to 14 percent with a mean of 11 percent.

The evaporation columns were constructed using PVC casing with 600 mm in height, 127 mm in inner diameter and 6.7 mm in thickness.

Aeolian sand (locally Beaver Creek sand) and glacial lacustrine silt (Revelstoke Redi-Mix Pit in Saskatoon, Saskatchewan) were selected for the column evaporation tests which were carried out for both homogeneous samples and layered samples.

Geotechnical and hydraulic properties of the sand and silt are shown in Appendix C. Six soil columns prepared for the tests consisted of three homogeneous columns (i.e., Beaver Creek sand, Processed silt and Natural silt) and three layered columns (i.e., sand over silt, silt over sand, and sand/silt in multi layers). However, this thesis does not intend to deal with layered columns. The layered columns will not be included in the subsequent sections. In other words, only three soil columns of homogeneous sand, Natural silt and Processed silt were collected for the subsequent theoretical studies.

The column evaporation tests were carried out in two phases. The first phase was referred to as the constant head boundary condition (CHBC). In this phase, a water reservoir was connected to the outlet port to simulate the presence of a water table at an elevation 5 mm above the base of the soil columns. The evaporative fluxes (the change in mass for the columns) from the soil columns were continually recorded in daily basis for the period of 31 days. The air temperature and relative humidity were measured along with the measurement of the evaporation fluxes at the same intervals.

After approximately 31 days of evaporation under the CHBC, the second phase was referred to a zero flux boundary condition (ZFBC). In this phase, the water reservoir at the base of the soil column was removed and the outlet port was sealed to change the base of the soil column. The evaporative fluxes

along with the air temperature and relative humidity were continually recorded in daily basis for another 31 days.

Water content profiles, soil temperature profiles and soil suction profiles were measured for two phases at the intervals shown in Table 4.3.

Table 4.3 Summary of water content, soil temperature and soil suction profile measurements during the column evaporation tests (adapted after Bruch, 1993).

Column description	Elapsed times for water content, soil temperature and soil suction profile measurements	
	Constant Head Boundary Condition	Zero Flux Boundary Condition
Homogeneous sand	0, 1, 3, 5, 7, 10, 14, 21, 31	32, 34, 38, 45 and 60
Homogeneous Natural silt	0, 1, 3, 5, 7, 10, 13, 22, 31	32, 34, 38, 45 and 61
Homogeneous Processed silt	0, 1, 3, 5, 7, 10, 14, 21, 31	32, 34, 38, 45 and 60

Potential evaporation was determined by measuring the evaporation fluxes from the water filled pans. A water filled pan was placed adjacent to each soil filled column with the water surface at approximately the same elevation as the soil surface. The water pans were frequently replenished to keep the water surface at the same elevation.

4.3.3 Soil Columns of Coarse Sand and Fine Sand (Yanful and Choo, 1997)

Yanful and Choo (1997) measured actual evaporation rates from candidate soils used in the construction of covers for mitigating acid drainage from reactive sulphide-bearing mine waste. Water content and soil temperature profiles were also measured. The four types of soil in Yanful and Choo's evaporation tests were varved clay, a fine sand, a coarse sand and a topsoil. For the study described in this thesis, only data from fine sand and coarse sand

were collected because the objective was the prediction of evaporation flux from soil with low volume change.

The sand samples used in this study were obtained from the vicinity of the Waite Amulet tailings site and are similar to those used in the construction of the multi-layered soil covers described by Yanful and St-Arnaud (1991). Eighty percent of the fine sand consisted of particles finer than 0.2 mm; there were no gravel-sized particles. The coarse sand consisted of 8% particles finer than 0.2 mm and about 20% gravel-sized particles. Geotechnical and hydraulic properties of the sands have been measured by Machibroda et al. (1993) and are shown in Appendix D.

A specially designed cylindrical column was fabricated from a 6.4 mm thick, ABS (acrylontrile-butadiene-styrene) pipe with an internal diameter of 101.6 mm and a height of 209.6 mm. A circular plexiglas base plate with a diameter of 133 mm and a thickness of 9.5 mm was glued to the bottom of the column. The column was drilled with 12 holes of diameter 1.61 mm to install probes to measure water content and and six holes of diameter 2.38 mm to install thermocouples to measure temperature. The center line of each thermocouple hole was 90^0 from the center line of a probe hole. The soil column tests were similar to those performed by Wilson (1990) and Bruch (1993).

The soil column was prepared in lifts to install probes and thermocouples. A volumetric water content profile was measured along the soil column using a Tektronix Model 1502B time-domain reflectometry (TDR). The TDR probes were calibrated using the relationship between volumetric water content and the relative dielectric permittivity before applying them to the column evaporation tests. Six thermocouples and 12 TDR probes were installed in the soil columns for the duration of the tests. The thermocouples and TDR probes were silicone-sealed in place on the exterior of the soil column once they were inserted into the column. The soil column was filled up to 203 mm in height. A column filled up to the same height with distilled water was placed in the environmental chamber beside the other soil columns.

Soil columns equipped with TDR probes and thermocouples were placed at a designated location on a 46 cm diameter plywood turntable. The turntable was then placed in an environmental chamber to maintain control of the temperature, humidity and air circulation. Air temperature and humidity in the chamber were measured with a thermohygrometer. A compact fan (Caframo Model 707) was set up in the chamber to maintain a uniform distribution of air, moisture, and heat. A 20 W fluorescent light inside the chamber and ceiling fluorescent lights in the laboratory were considered radiative sources for the duration of the test. During the test, the average air temperature was 24.2 ^{o}C in the environmental chamber. A small trolley was used to facilitate the transport of all soil columns from/into the chamber, and into/from the laboratory for the measurements of mass, soil temperature, and water content.

Mass, soil temperature, and water content were measured outside the environmental chamber in the open laboratory. Columns were covered for one day after filling completed and placed in the chamber. The initial mass of soil and water in the columns were recorded before evaporation permitted. The change in mass of water in the columns due to evaporation was measured daily for 42 days using a Sartorius Model BP8100 electronic balance with an accuracy of ± 0.1 g. The air temperature and relative humidity in the chamber were also recorded at the same intervals. Soil temperature and water content profiles were taken from the soil columns after 0, 1, 2, 3, 4, 7, 10, 19, 31 and 41 days of evaporation. Only one device with an LCD display was used to connect to thermocouples for measurement of soil temperature and then to TDR probes for measurement of water content. The measurement took 10 minutes. The laboratory temperature and relative humidity were monitored during the experiments with a Cole Parmer Model 3309-50 thermohygrometer. The average air temperature in the laboratory was 22.7 ^{o}C.

4.3.4 Soil Columns of non-saline silt and saline silt (Dunmola, 2012)

A series of evaporative tests on non-saline silt and saline silt conducted by Dunmola (2012) was collected for theoretical studies on effect of pore-water

salinity on the evaporative rate from a saline-soil surface. The tested soil was silt-sized spherical glass micro-beads (Potter Industries Inc. LaPrairie, Quebec, Canada) with geotechnical properties as shown in Table 4.4. The grain-size distribution determined by a hydrometer is presented in Figure 4.13. The soil-water characteristic curve of this silt was shown in Figure 4.14. The detailed schemes of drying experiment by Dunmola (2012) are provided in Appendix E.

Table 4.4 Geotechnical properties of silt and thickened mine tailings used for soil columns (adapted after Dunmola, 2012).

Parameter	Mine Tailings	Silt
Specific Gravity	2.9	2.48
D_{10}, D_{50}, D_{60} (microns)	2, 35, 55	1, 31, 41
Cu (D_{60}/D_{10})	27.5	41
Liquid limit (%)	20	19
Plastic limit (%)	19	13
Saturated hydraulic conductivity (m/s)*	2.0E-7	1.7E-6

*Saturated hydraulic conductivity values were determined by falling head tests at void ratio of 0.8 as per Fisseha et al. (2007) and Fisseha et al. (2010).

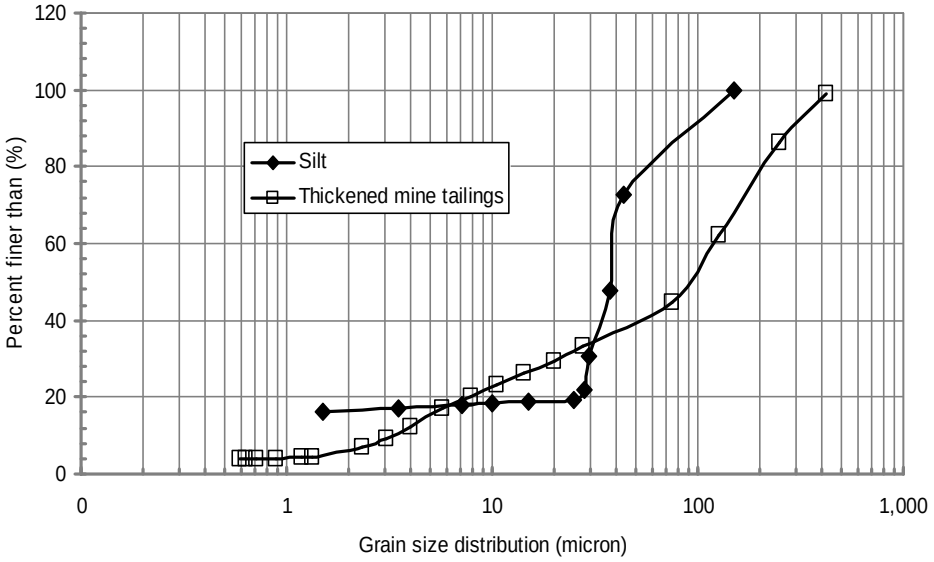

Figure 4.13 Grain size distribution of tested silt and thickened mine tailings determined by hydrometer (adapted after Dunmola, 2012).

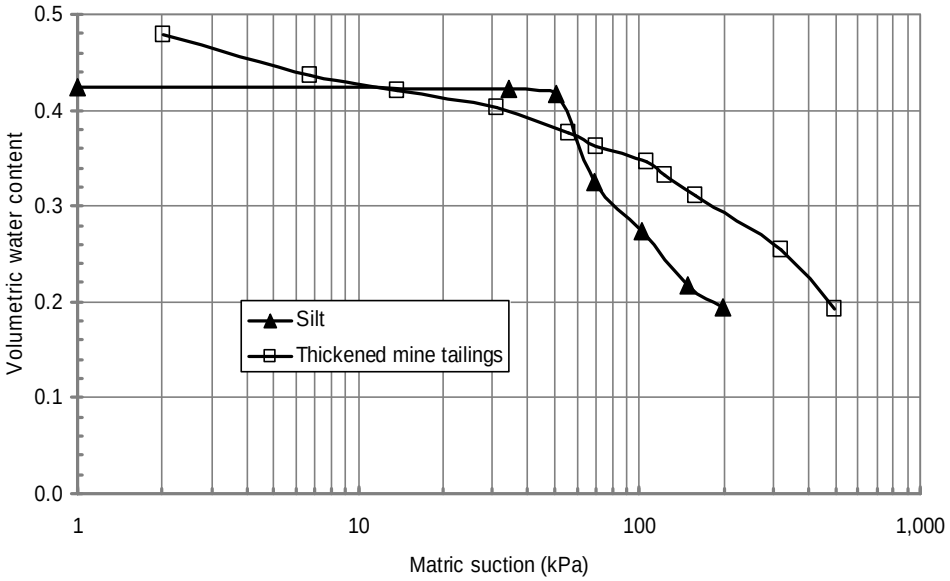

Figure 4.14 Soil-water characteristic curves for tested silt and thickened mine tailings obtained using the axis-translation technique in a pressure plate apparatus (adapted after Dunmola, 2012).

Three initial solutions pore-water salinities of 5, 10 and 20% (mass of salt/mass of solution) associated with deionised water were used to prepare soil columns with a homogeneous pore-water salt concentration and non-saline soil column. Hereafter they are referred to as non-saline (NS), low saline (LS),

saline (S) and hyper-saline treatments, respectively. Several replicates were prepared for each treatment such that these replicates were destructively sampled on 2, 3, 4, 5, 7, 9, 11 and 14 days of evaporation to obtain profiles of NaCl concentration, total suction and gravimetric water content. Solutions of reagent-grade Sodium Chloride (Lot # 8J9286, purity greater than 99%, BioShop Canada Inc. Burlington, ON) were used in the tests. Initial gravimetric water content prepared for the LS, S and HS treatments was 28.5, 29.7 and 24%, respectively. The saline soils were prepared thoroughly homogenized using a mechanical mixer. Each soil column was gently tapped three times immediately after pouring the soil slurry into the wax column which was made by the petroleum jelly wax-column technique of Khasawneh and Solileau (1969). According to this technique, a molten mixture of petroleum jelly (1 part by mass) and paraffin wax (2.5 parts) was poured and solidified to form a mould with a cylindrical cavity that could be used to pack, dry and destructively sample soil. The cavity was created by placing a cylindrical aluminum can inside an empty milk carton, pouring the molten petroleum jelly-wax mixture inside the milk carton and allowing the pour to set for 24 hours.

The soil columns were permitted to dry under ambient laboratory conditions and simulated wind (so-called AW and SW) after their mass and volume were recorded. The replicate of each treatment (LS, S and HS) was destructively sampled by sectioning into 1 cm thin slices using a hacksaw and mitre box. The soil from each slice was kept inside a sealed Ziploc plastic bag and thoroughly homogenized by hand before conducting different soil analyses on subsamples. As a result, the soil parameters determined and recorded for each profile sample was the average value for the respective 1 cm thick profile depth of the soil. The subsamples obtained from the column slices were analyzed for electrical conductivity (EC), NaCl concentration, gravimetric water content and total suction.

The evaporative tests on the columns of thickened mine tailings were conducted in the same manner as those applied to the saline-soil treatments. The geotechnical properties of the thickened mine tailings were presented in

Table 4.3. Grain-size distribution and the soil-water characteristic curve of the thickened mine tailings were presented in Figures 4.13 and 4.14, respectively.

4.4 CHAPTER SUMMARY

This chapter presented the current laboratory testing program and other laboratory test program data collected from the research literature. The current laboratory testing on the Soil-Water Characteristic Curve, osmotic suction and measurement of evaporative fluxes from thin soil layers of non-saline soils and saline soils were presented in Section 4.2. Soil properties of the selected soils (Ottawa sand and Devon silt) were presented in Subsection 4.2.1.1. The pilot drying tests were conducted to assess preliminarily the effect of initial salt contents on the laboratory testing program in Subsection 4.2.1.2. The effect of the ambient laboratory conditions was also assessed in this Subsection. Selection and preparation of salt soil mixtures were described in Subsection 4.2.1.3.

Subsection 4.2.2 presented the description of three types of equipments used in the laboratory testing program. The Golder pressure plate cells were used to measure the soil-water characteristic curves at zero and the stress of 500 kPa. The pore-fluid squeezer was used to extract macro pore-water from salinized-soil samples. Osmotic suction was indirectly measured through its correlation with the electrical conductivity of the pore-water. The vacuum desiccators were used to equilibrate soil specimens to saturated salt solution, and then total suction was determined using theory of thermodynamic principles.

Subsection 4.2.3 presented the laboratory testing procedures to obtain the SWCC on the selected soils (i.e., Devon silt and Ottawa sand). The influence of the initial pore-water salinity on the SWCC appears to be minimal, only the selected soils mixed with 50 g/l NaCl were chosen for the SWCC program. Osmotic suction was conducted on the selected silt and Kaolinite mixed with 50 g/l NaCl.

The thin soil layer tests of non-saline soils and saline soil were presented in Subsection 4.2.4. Devon silt and Ottawa sand mixed with 50 g/l, 100 g/l, 200 g/l and 250 g/l NaCl were conducted for evaporative fluxes from the thin layer. The measurement of the evaporative fluxes from those surfaces was conducted along with measurement of distilled water as a reference rate.

Section 4.3 reviewed concisely the collection of the laboratory testing programs on the evaporative fluxes from soil columns from the research literature. The collection of the equipment, soil preparation and laboratory testing procedures were obtained from research by Wilson (1990), Bruch (1993), Yanful and Choo (1997) and Dunmola (2012). Only the evaporation fluxes from silt and sand surfaces were collected since the objective of this thesis focuses on prediction of the evaporation flux from soil with low volume change. The datasets from these laboratory testing programs will be presented in the following chapters for subsequent comparison with theoretical considerations.

CHAPTER 5
PRESENTATION AND INTERPRETATION OF TEST RESULTS

5.1 GENERAL

The laboratory testing procedures have been described in Chapter 4. This chapter presents the experimental results of the current laboratory testing program. Datasets collected from the research literature interpreted in this chapter are included in Appendices B, C, D and E. The data presented included the results of:

1. Tests for the soil-water characteristic curves on the Ottawa sand, sieved Devon silt and Kaolinite;

2. Tests for osmotic suction for the sieved Devon silt mixed with 50 g/l NaCl and Kaolinite mixed with 50 g/l NaCl;

3. The thin soil layer evaporation tests for Ottawa sand mixed with 50 g/l, 100 g/l, 200 g/l and 250 g/l NaCl; and the sieved Devon silt mixed with 50 g/l, 100 g/l, 200 g/l and 250 g/l NaCl.

4. The thick soil layer evaporation tests for Ottawa sand and Devon silt.

The test results are interpreted along with the presentation of the test results.

5.2 TEST RESULTS OF THE LABORATORY TESTING PROGRAM

5.2.1 Test Results of Soil-Water Characteristic Curve

The soil-water characteristic curves for the Ottawa sand, sieved Devon silt and Kaolinite were measured using Golder pressure plate cells (manufactured by GCTS , Tempe, AZ) and vacuum desiccators.

5.2.1.1 Test Results from Golder Pressure Plate Cells

The soil-water characteristic curves for saline-soil mixtures were determined using the methods described in Section 4.2.3.2. Tests were conducted on three sets of the Ottawa sand, Ottawa sand mixed with 50 g/l NaCl; two sets of the sieved Devon silt mixed with 50 g/l NaCl and one set of Kaolinite mixed with 50 g/l NaCl. Three Golder pressure plate cells were placed on three hole-punched mica plates for ease of water flow under the applied pressure. These cells were operated at the same time. It was found that salt moved through the ceramic entry disk and accumulated at the bottom of the Golder pressure plate cells during the tests. Water and salt at the bottom of the cells were cleaned by tissue paper before measuring the mass of the cells.

Table 5.1 presents a summary of the Golder pressure plate cell test results. The gravimetric water contents were calculated based on oven-dried samples taken at the end of each test. The water contents at the lower suctions of 7, 15, 30, 60, 125, 250 and 480 kPa were back-calculated based on the amount of water expelled after each pressure increment and the total mass of dry sample in each cell. Only one set of matric suction results of the Ottawa sand and Ottawa sand mixed with 50 g/l NaCl is presented since they were found to be close.

Table 5.1 Summary of Golder pressure plate cell results between December 11, 2010 and February 4, 2011.

Matric suction (kPa)	Gravimetric water content (%)			
	Ottawa sand	Ottawa sand + 50 g/l NaCl	Sieved Devon silt + 50 g/l NaCl	Kaolinite + 50 g/l NaCl
7	33.17	3.56	44.11	73.68
15	3.04	2.25	43.62	72.62
30	2.68	1.77	42.83	70.63
60	2.09	1.77	41.49	68.06
125	1.62	1.17	39.67	63.51
250	1.50	1.06	37.36	60.38
480	0.79	0.70	34.45	59.53

The results of the detailed Golder pressure plate cell tests conducted between December 11, 2010 and February 4, 2011 are included in Table 5.1. Figures 5.1, 5.2 and 5.3 present the soil-water characteristic curves for sand, silt and clay, respectively.

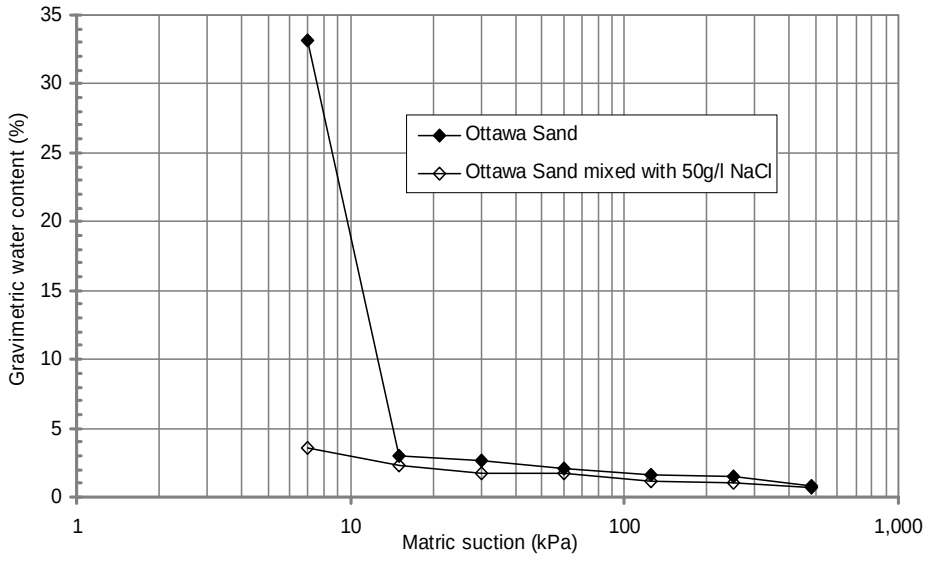

Figure 5.1 Test results of matric suction for the Ottawa sand and Ottawa sand mixed with 50 g/l NaCl.

Figure 5.1 shows that the initial pore-water salinity on the soil-water characteristic curve is minimal. Similar behaviour on the soil-water characteristic curve was also observed by Dunmola (2012). However, there was a discrepancy that appeared at an applied air-pressure of 7 kPa. The variation was attributed to the fact that part of the salt diffused through the ceramic disk for the Ottawa sand mixed with 50 g/l NaCl. The test results of matric suction for both the Ottawa sand and Ottawa sand mixed 50 g/l NaCl also showed that water content was small at the completion of Golder pressure plate cell tests. Vapour equilibrium testing was not conducted for these sand samples. The following section provides the test results from vacuum desiccator tests for the sieved Devon silt mixed with 50 g/l NaCl and Kaolinite mixed with 50 g/l NaCl.

5.2.1.2 Test Results from Vacuum Desiccators

The description of vapour equilibrium testing was presented in Section 4.2.3.2. Testing was conducted for sieved Devon silt mixed with 50 g/l NaCl and Kaolinite mixed with 50 g/l NaCl. The soil specimens placed in the glass desiccators were recovered from the Golder pressure plate cells after the specimens had come to equilibrium at the matric suction of 480 kPa. The temperature of the environment inside desiccators was monitored using a Thermometer Model Traceble purchased from Fisher Scientific. The temperature was found to be approximately 21.6 ^{o}C.

The vapour equilibrium testing began on February 4, 2011. Each sample taken from the Golder pressure plate cells varied between 3 and 5 grams. Each specimen was placed in a 10 cm diameter glass plate and weighed by Mettler TOLEDO scale with the accuracy of 0.05 gram. Four glass plates were prepared for each soil and placed in the desiccators containing different saturated salt solutions. Glass lids and plastic tape were used to seal the desiccators. The mass of all soil specimens was monitored daily during the desiccation process until no change in mass occurred. Then the samples were removed from the desiccators and oven-dried at 105 ^{o}C for determination of

water content. Table 5.2 presents the results of the vapour equilibrium testing for sieved Devon silt mixed with 50 g/l NaCl and Kaolinite mixed with 50 g/l NaCl. Finally, soil-water characteristic curves for the salinized silt and Kaolinite are plotted in Figures 5.2 and 5.3, respectively, as combination of matric suction from the pressure plate cells and total suction from vacuum desiccators.

Table 5.2 Summary of vacuum desiccator results for the sieved Devon silt and Kaolinite mixed with 50 g/l NaCl between February 4, 2011 and March 13, 2011.

Salt solution	Relative humidity (%)	Temperature (^{o}C)	Total suction (kPa)	Gravimetric water content (%)	
				Sieved Devon Silt + 50 g/l NaCl	Kaolinite + 50 g/l NaCl
LiCl	12	21.4	288,460	2.13	2.38
K_2CO_3	43	21.0	114,665	2.17	3.85
NaCl	75	21.1	39,099	3.92	5.26
K_2SO_4	98	21.6	2,750	22.97	35.71

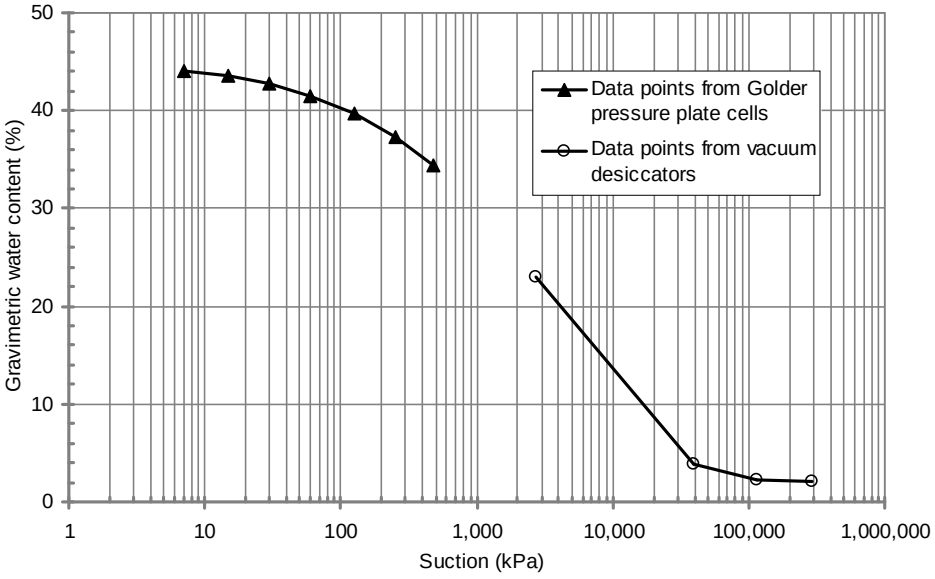

Figure 5.2 Soil-water characteristic curve for the Devon Silt mixed with 50 g/l NaCl.

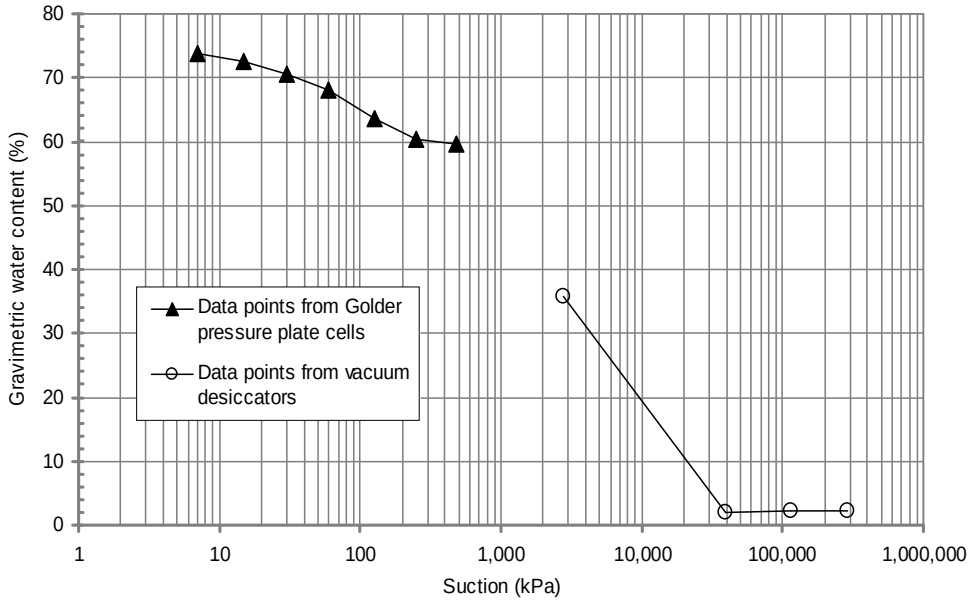

Figure 5.3 Soil-water characteristic curve for Kaonite mixed with 50 g/l NaCl.

5.2.2 Test Results of Osmotic Suction

Two laboratory tests for osmotic suction were conducted on the sieved Devon silt mixed with 50 g/l Sodium Chloride (NaCl) and Kaolinite mixed with 50 g/l NaCl on February 7, 2011 and February 9, 2011, respectively. The laboratory testing procedures for osmotic suction were described in Chapter 4. This section presents results of osmotic suction obtained using combination of the pore-fluid squeezer and the conductivity meter.

The Devon silt was mixed with 50 g/l NaCl using a spatula. The mixture was placed in the pore-fluid squeezer. Load was applied one-dimensionally using the compression testing machine until the first drop of pore-water expelled. The loads of 0.53 KN, 1.45 kN, 4.21 kN and 11.2 kN were applied for a duration of 10 minutes for each load. Squeezed pore-water was collected using a syringe and subsequently transferred to the conductivity meter to measure its electrical conductivity. The silt pore-water of about 2 ml was carefully placed on the sensor surface of the conductivity meter. In about 5 s, after placement, the value of the electrical conductivity in mS/cm was shown the digital display

of the equipment. The load was subsequently increased until the next drops of water were obtained. The obtained values for osmotic suction are presented in Table 5.3. It should be noted that additional soil pore-water could be not collected with loadings higher than 11.2 kN because the soil started to leak from the pore-fluid squeezer. Results of matric suction, osmotic suction and total suction for the sieved Devon Silt mixed with 50 g/l NaCl are plotted in Figure 5.4.

The theoretical magnitude for osmotic suction was also calculated through use of the relationship between the electrical conductivity and osmotic suction proposed by Rao and Shivananda (2005):

$$\pi = 38.54 \times EC^{1.0489} \tag{5.1}$$

where:

π = osmotic suction in kPa;

EC = electrical conductivity in mS/cm.

Table 5.3 Summary of pore-fluid squeezer results measured for the sieved Devon Silt mixed with 50 g/l Sodium Chloride on February 7, 2011.

Squeezing load (kN)	Gravimetric water content (%)	Electrical conductivity (mS/cm)	Osmotic suction (kPa) (Eq. 5.1)
0.53	43	58	2,726
1.45	35	85	4,071
4.21	33	92	4,423
11.2	31	93	4,473

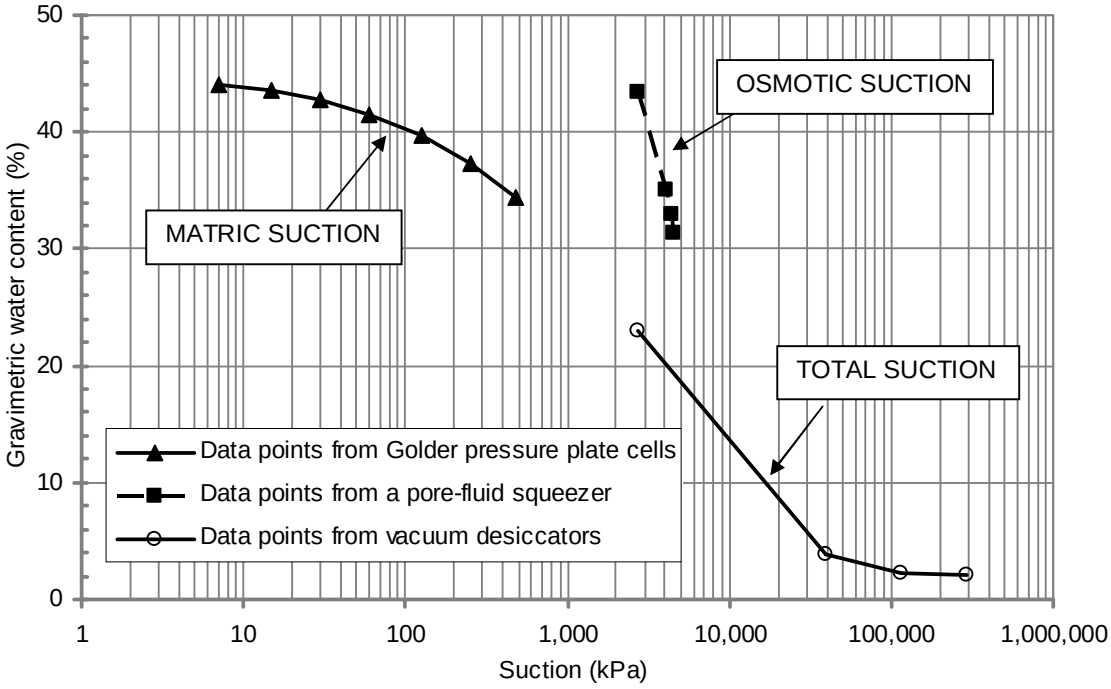

Figure 5.4 Test results of osmotic suction plotted along with soil-water characteristic curve for the sieved Devon Silt mixed with 50 g/l NaCl.

Similarly, Kaolinite was mixed with 50 g/l NaCl using a spatula. The mixture was squeezed at the load of 0.26 KN, 0.6 kN, 1.0 kN and 2.1 kN with duration of 8 minutes for each load. It should be noted that soil pore-water could be not collected when loadings higher than 2.1 kN were applied because the soil started to leak from the squeezer. The obtained values of osmotic suction were presented in Table 5.4. Results of matric suction, osmotic suction and total suction for Kaolinite mixed with 50 g/l NaCl are plotted in Figure 5.5.

Table 5.4 Summary of pore-fluid squeezer results measured for Kaolinite mixed with 50 g/l Sodium Chloride on February 9, 2011.

Squeezing load (kN)	Gravimetric water content (%)	Electrical conductivity (mS/cm)	Osmotic suction (kPa) (Eq. 5.1)
0.26	55	62	2,924
0.60	50	69	3,271
1.00	45	71	3,371
2.10	38	69	3,271

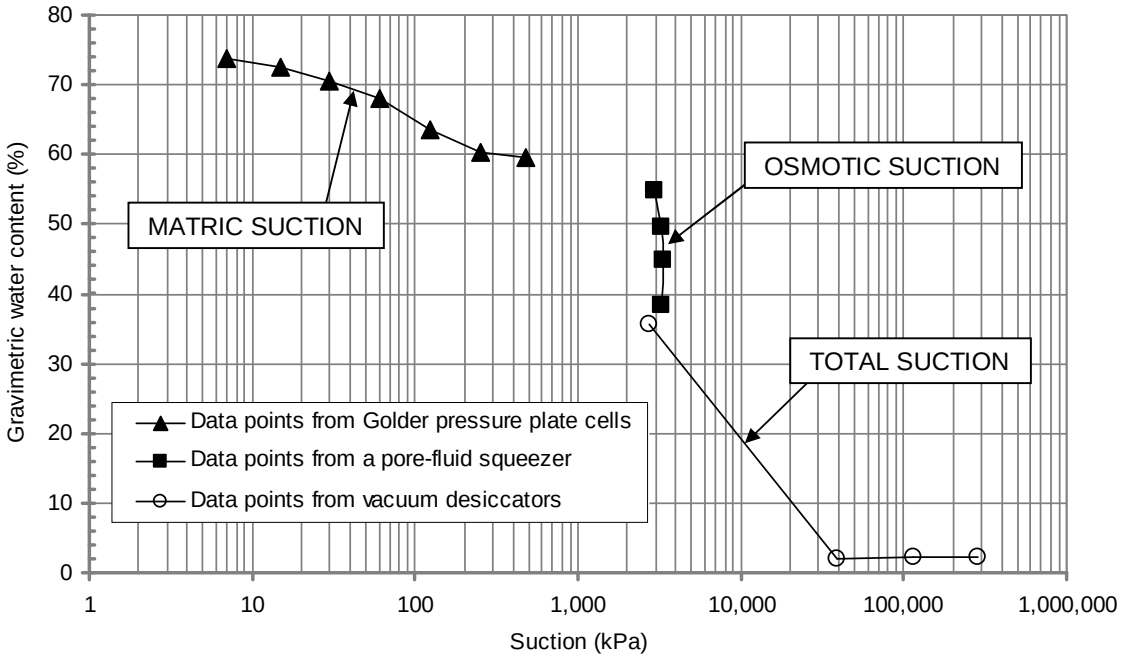

Figure 5.5 Test results of osmotic suction plotted along with soil-water characteristic curve for Kaolinite mixed with 50 g/l NaCl.

5.2.3 Thin Soil Layer Drying Test

Thin soil layer evaporating tests were conducted in the Soil Preparation Laboratory, NREF L2-040, University of Alberta. Two independent sets of the evaporation tests were carried out. The first set was conducted on February 21 and 22, 2012. The second set was conducted on December 1 and 3, 2012. The air temperature and relative humidity in the laboratory room were recorded to be approximately 19.5 ^{o}C and 20 percent, respectively. A summary of evaporation tests conducted is presented in Table 5.5. A total of twenty thin soil layer drying tests were completed. Typical plots of the test results for the Ottawa sand and the mixtures of the Ottawa sand with salinized water in Set 1 are presented in Figures 5.6 through 5.15 and Tables 5.6 through 5.8.

Figure 5.6 shows a plot of the actual evaporation rates from Ottawa sand and Ottawa sand mixed with 50 g/l NaCl versus drying time for comparison. The relative evaporation (*AE/PE*) versus the gravimetric water content of the sand is shown in Figure 5.7. Figures from 5.16 to 5.25 show the corresponding plots

for the sieved Devon Silt in Set 1. The figures and tables for the other drying tests listed in Table 5.5 are included in Appendix A.

Table 5.5 Summary of thin soil layer evaporation testing on February 21, 22 and December 1 and 3, 2012.

Tested materials	Testing day		Initial water content (%)		Duration (min)	
	Set 1	Set 2	Set 1	Set 2	Set 1	Set 2
Ottawa sand	February 21	December 1	29.6	27.2	339	420
Ottawa sand mixed with 50 g/l NaCl	February 22	December 1	27.4	25.7	360	420
Ottawa sand mixed with 100 g/l NaCl	February 21	December 1	30.6	25.6	380	420
Ottawa sand mixed with 200 g/l NaCl	February 21	December 1	26.3	20.4	380	420
Ottawa sand mixed with 250 g/l NaCl	February 21	December 1	25.9	21.0	402	420
Devon silt	February 21	December 3	62.0	58.3	318	320
Devon silt mixed with 50 g/l NaCl	February 22	December 3	69.6	53.2	360	320
Devon silt mixed with 100 g/l NaCl	February 21	December 3	59.3	58.7	402	320
Devon silt mixed with 200 g/l NaCl	February 21	December 3	54.0	53.2	402	320
Devon silt mixed with 250 g/l NaCl	February 21	December 3	53.4	50.2	402	320

Table 5.6 Summary of measured evaporation and gravimetric water contents for the Ottawa sand in Set 1 on February 21, 2012.

Time (min)	PE (mm/day)	Actual Evaporation (mm/day)				Gravimetric water content (%)			
		S1	S1+100	S1+200	S1+250	S1	S1+100	S1+200	S1+250
21.5	2.89	2.88	2.77	2.21	2.20	29.6	30.6	26.3	25.9
43.3	2.54	2.42	2.33	2.02	1.92	27.1	28.0	24.2	23.9
62.4	2.38	2.16	2.03	1.55	2.03	25.2	26.0	22.7	22.0
82.1	2.34	2.22	1.99	1.64	1.64	23.1	24.0	21.2	20.4
108.0	2.30	2.12	1.86	1.50	1.68	20.6	21.5	19.3	18.3
130.8	2.42	2.31	1.92	1.51	1.82	18.1	19.2	17.6	16.3
152.0	2.36	2.38	1.94	1.52	1.73	15.7	17.0	16.1	14.5
174.8	2.51	2.31	1.80	1.60	1.80	13.2	14.9	14.3	12.5
200.0	2.65	2.64	1.91	1.82	1.73	10.1	12.4	12.1	10.4
219.9	2.53	2.65	1.73	1.73	1.73	7.6	10.6	10.4	8.7
241.3	2.57	2.58	1.71	1.72	1.72	5.1	8.7	8.6	6.9
268.9	2.66	2.33	1.66	1.65	1.65	2.0	6.3	6.4	4.7
295.4	2.59	1.47	1.73	1.74	0.87	0.2	3.9	4.2	2.8
316.1	2.78	0.11	1.21	1.54	0.55	0.1	2.1	2.7	2.0
338.8	2.62	0.00	0.51	0.51	0.31	0.1	1.1	1.6	1.8
359.6	2.65	0.00	0.22	0.22	0.11	0.1	0.8	1.2	1.8
379.7	2.74	0.00	0.00	0.00	0.00	0.1	0.8	1.2	1.8
401.7	2.61	0.00	0.00	0.00	0.00	0.1	0.8	1.2	1.8

Table 5.7 Summary of measured evaporation and gravimetric water contents for the sieved Devon silt in Set 1 February 21, 2012.

Time (min)	PE (mm/day)	Actual Evaporation (mm/day)				Gravimetric water content (%)			
		M1	M1+100	M1+200	M1+250	M1	M1+100	M1+200	M1+250
22.9	2.89	2.53	2.31	1.98	2.08	62.0	59.3	54.0	53.4
44.5	2.54	2.23	2.02	1.71	1.92	56.3	54.5	50.3	49.2
63.7	2.38	2.14	1.91	1.79	1.66	51.5	50.5	46.9	45.9
83.3	2.34	2.10	1.75	1.52	1.51	46.6	46.7	44.0	42.9
109.2	2.30	1.95	1.77	1.50	1.50	40.7	41.7	40.1	38.9
131.9	2.42	2.22	1.81	1.62	1.72	34.8	37.2	36.5	34.9
153.1	2.36	2.06	1.73	1.51	1.63	29.6	33.2	33.3	31.4
176.1	2.51	2.30	1.70	1.51	1.60	23.5	28.9	29.9	27.6
201.3	2.65	2.27	1.82	1.63	1.82	16.7	23.9	25.9	23.0
221.2	2.53	2.19	1.50	1.50	1.61	11.6	20.6	22.9	19.7
242.5	2.57	1.93	1.71	1.39	1.40	6.7	16.6	20.0	16.6
270.3	2.66	1.16	1.57	1.08	0.99	3.0	11.8	17.0	13.8
296.6	2.59	0.35	1.47	0.61	0.78	1.9	7.5	15.4	11.7
317.5	2.78	0.00	1.10	0.55	0.55	1.9	5.0	14.3	10.5
340.0	2.62	-	0.71	0.51	0.61	1.9	3.3	13.2	9.1
360.9	2.65	-	0.22	0.44	0.44	1.9	2.8	12.2	8.2
380.9	2.74	-	0.11	0.45	0.45	1.9	2.5	11.3	7.3
402.6	2.61	-	0.00	0.32	0.32	1.9	2.5	10.7	6.6

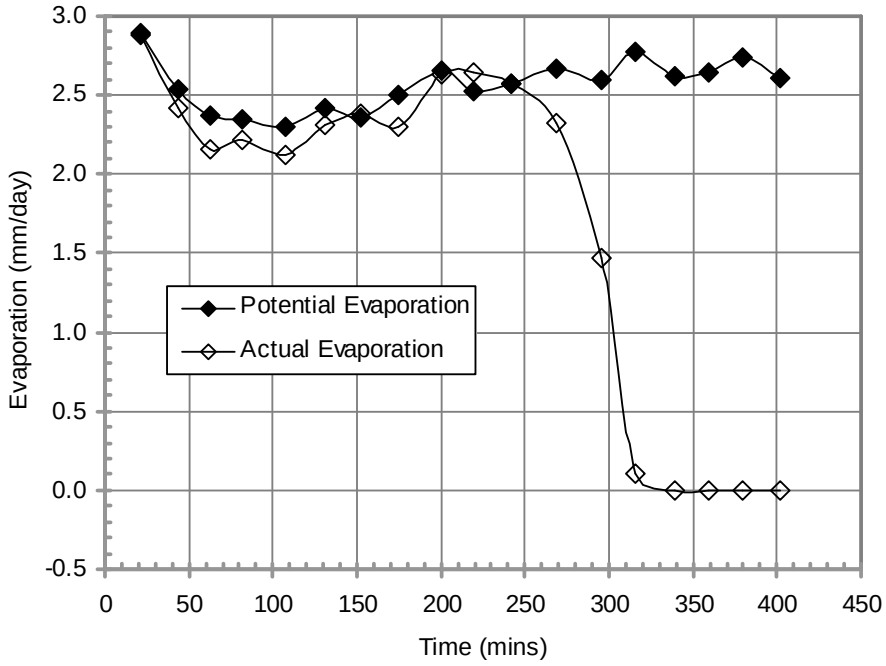

Figure 5.6 Typical Actual and Potential Evaporation rates versus drying time for Ottawa sand in Set 1.

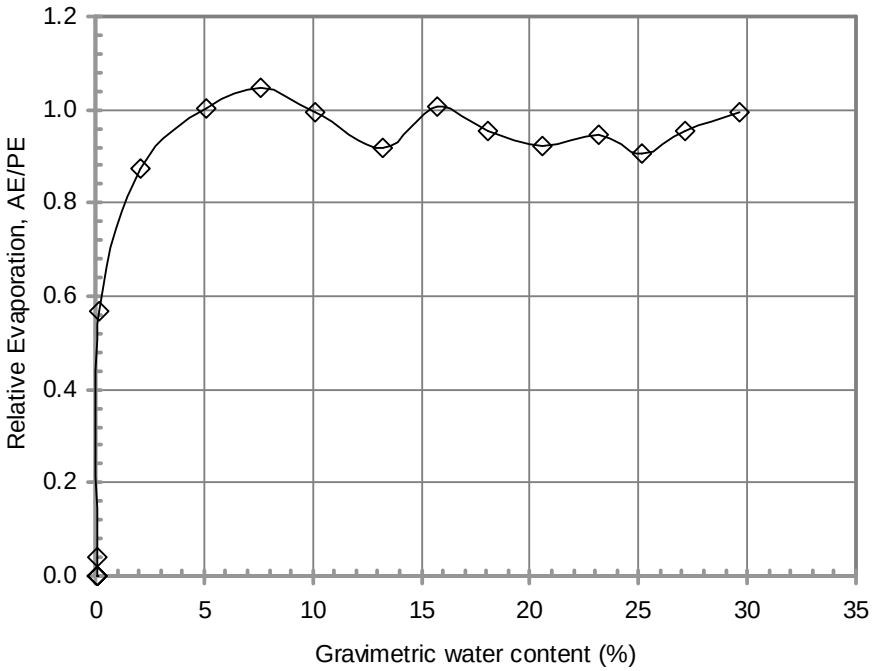

Figure 5.7 Typical plot of Relative Evaporation (*AE/PE*) versus gravimetric water content for Ottawa sand in Set 1.

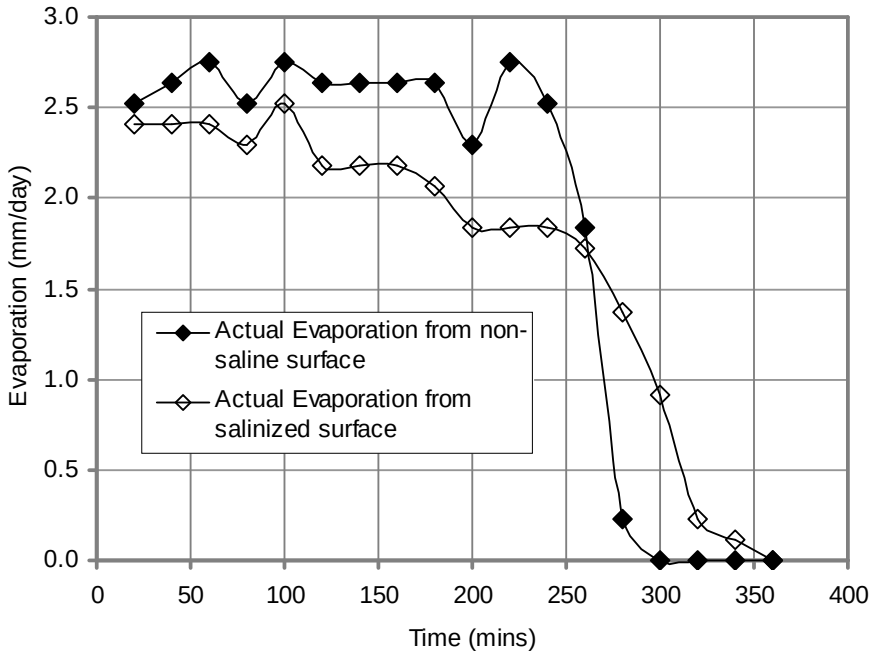

Figure 5.8 Typical Actual Evaporation rates versus drying time for the Ottawa sand and Ottawa sand mixed with 50 g/l NaCl in Set 1.

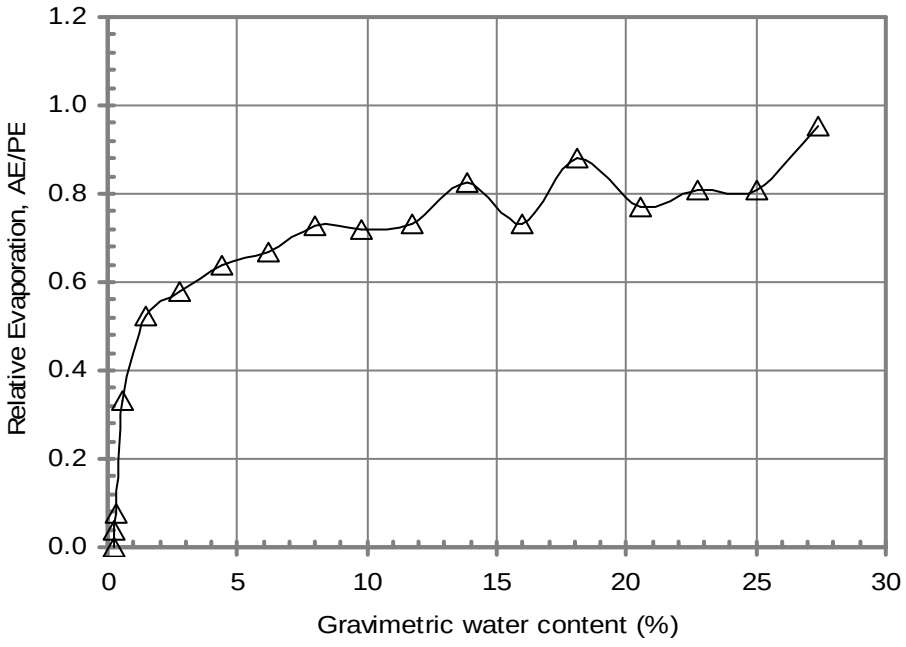

Figure 5.9 Typical plot of Relative Evaporation (*AE/PE*) versus gravimetric water content for Ottawa sand mixed with 50 g/l NaCl in Set 1.

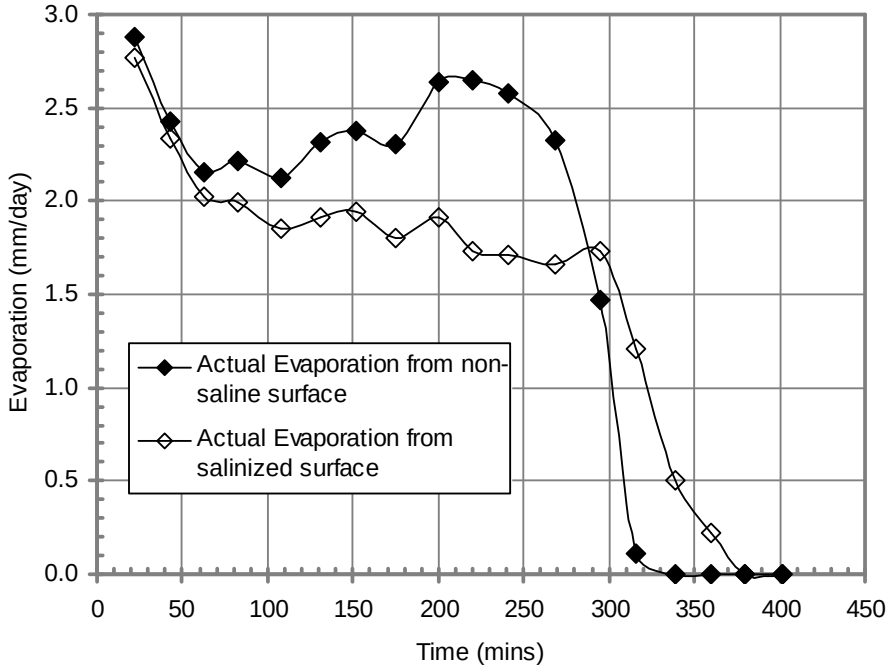

Figure 5.10 Typical Actual Evaporation rates versus drying time for Ottawa sand and Ottawa sand mixed with 100 g/l NaCl in Set 1.

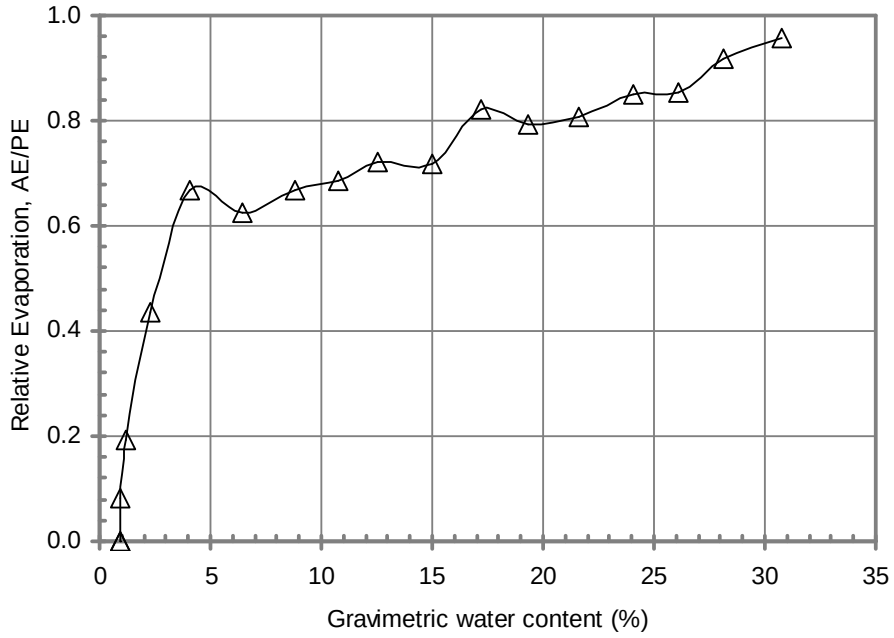

Figure 5.11 Typical plot of Relative Evaporation (*AE/PE*) versus gravimetric water content for Ottawa sand mixed with 100 g/l NaCl in Set 1.

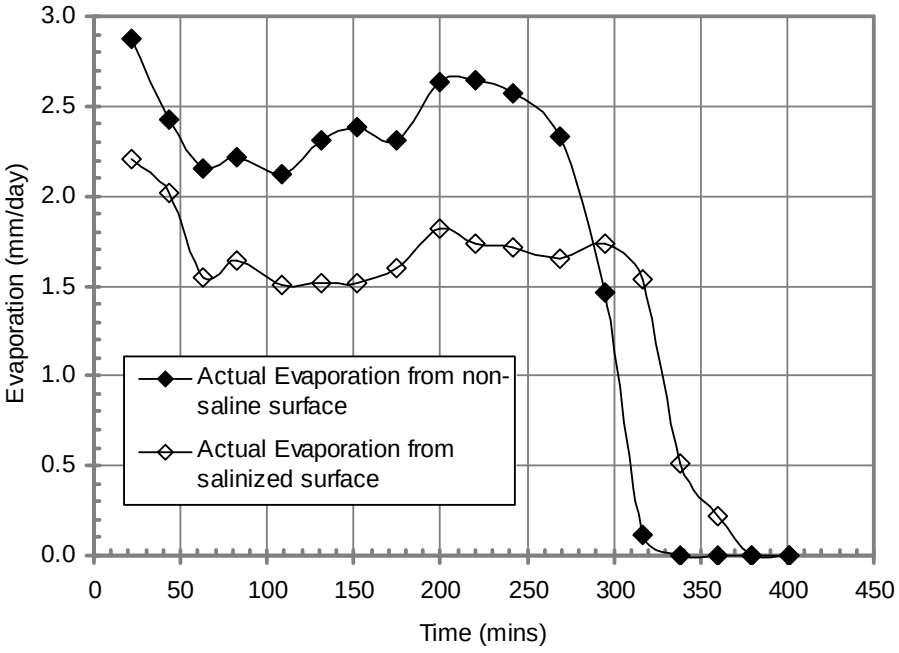

Figure 5.12 Typical Actual Evaporation rates versus drying time for Ottawa sand and Ottawa sand mixed with 200 g/l NaCl in Set 1.

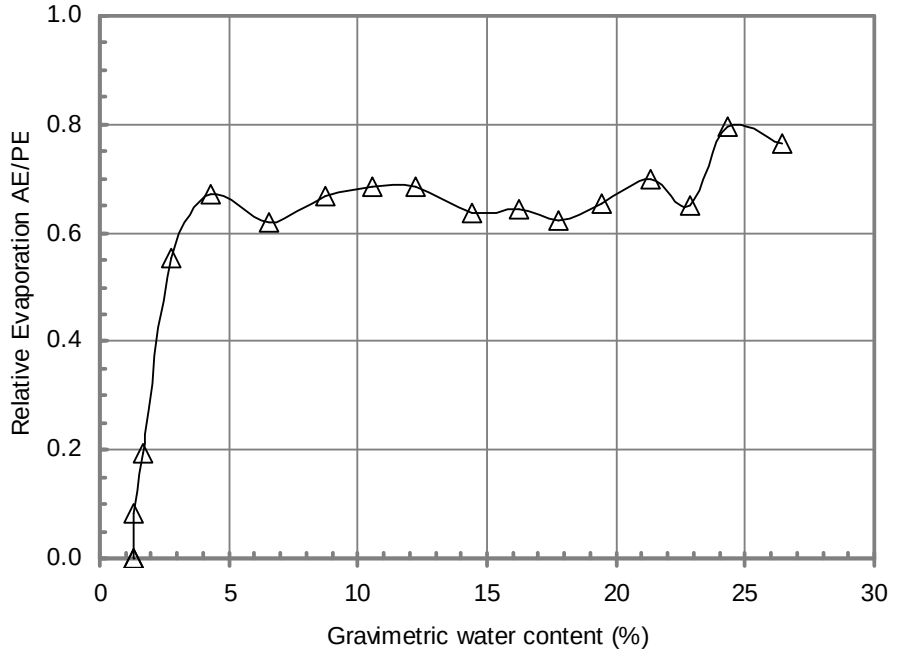

Figure 5.13 Typical plot of Relative Evaporation (*AE/PE*) versus gravimetric water content for Ottawa sand mixed with 200 g/l NaCl in Set 1.

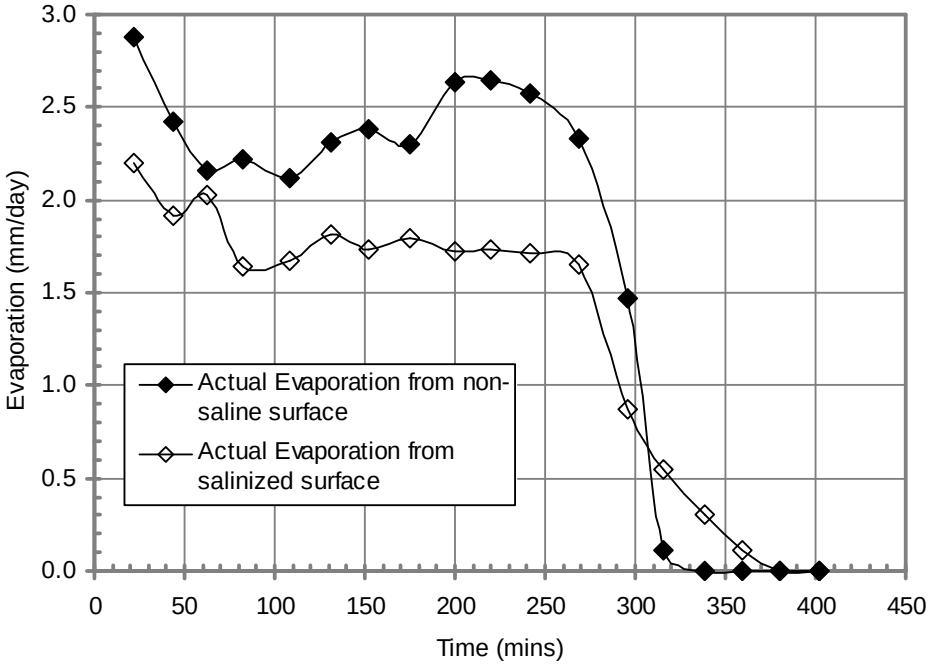

Figure 5.14 Typical Actual Evaporation rates versus drying time for Ottawa sand and Ottawa sand mixed with 250 g/l NaCl in Set 1.

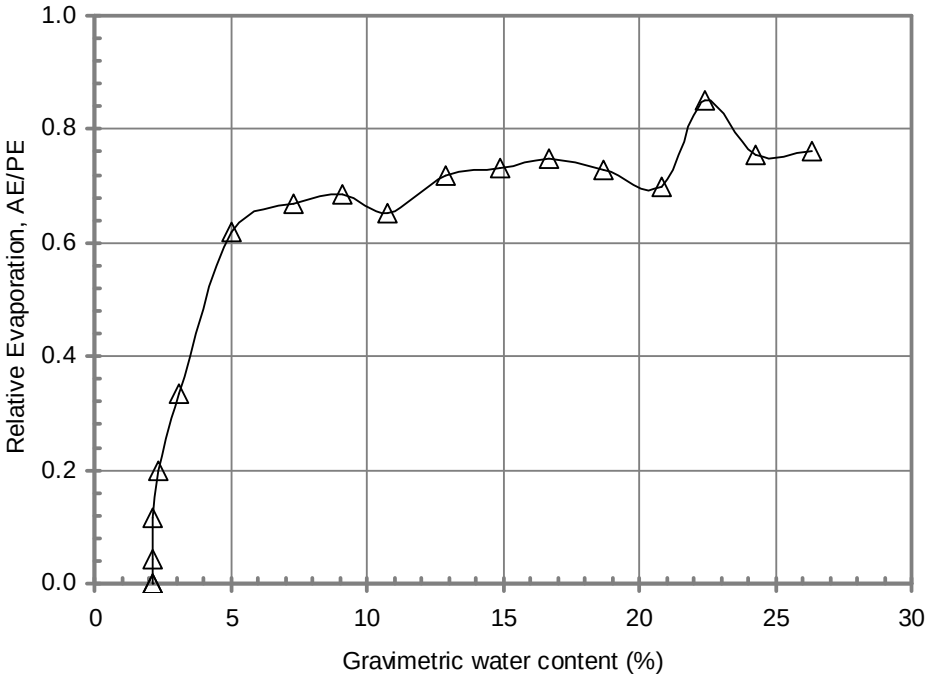

Figure 5.15 Typical plot of Relative Evaporation (*AE/PE*) versus gravimetric water content for Ottawa sand mixed with 250 g/l NaCl in Set 1.

Table 5.8 Summary of measured evaporation and gravimetric water contents for the Ottawa sand and sieved Devon silt in Set 1 on February 22, 2012.

Time (min)	PE (mm/day)	Actual Evaporation (mm/day)				Gravimetric water content (%)			
		S1	S1+50	M1	M1+50	S1	S1+50	M1	M1+50
20	2.52	2.52	2.41	2.64	2.18	31.0	27.4	70.9	69.6
40	2.98	2.64	2.41	2.64	2.29	28.4	25.1	60.8	60.8
60	2.98	2.75	2.41	2.52	2.41	25.6	22.7	51.1	51.5
80	2.98	2.52	2.29	2.64	2.29	23.1	20.5	41.0	42.7
100	2.86	2.75	2.52	2.52	2.29	20.3	18.1	31.3	33.9
120	2.98	2.64	2.18	2.52	2.29	17.7	16.0	21.6	25.1
140	2.64	2.64	2.18	2.52	1.83	15.1	13.9	11.9	18.1
160	2.98	2.64	2.18	1.83	1.83	12.4	11.8	4.8	11.0
180	2.86	2.64	2.06	0.57	1.15	9.8	9.8	2.6	6.6
200	2.52	2.29	1.83	0.11	0.69	7.5	8.0	2.2	4.0
220	2.75	2.75	1.83	0.00	0.34	4.7	6.2	2.2	2.6
240	2.86	2.52	1.83	-	0.11	2.2	4.4	-	2.2
260	2.98	1.83	1.72	-	0.00	0.3	2.8	-	2.2
280	2.64	0.23	1.38	-	-	0.1	1.4	-	-
300	2.75	0.00	0.92	-	-	0.1	0.6	-	-
320	2.98	-	0.23	-	-	-	0.3	-	-
340	3.09	-	0.11	-	-	-	0.2	-	-
360	2.75	-	0.00	-	-	-	0.2	-	-

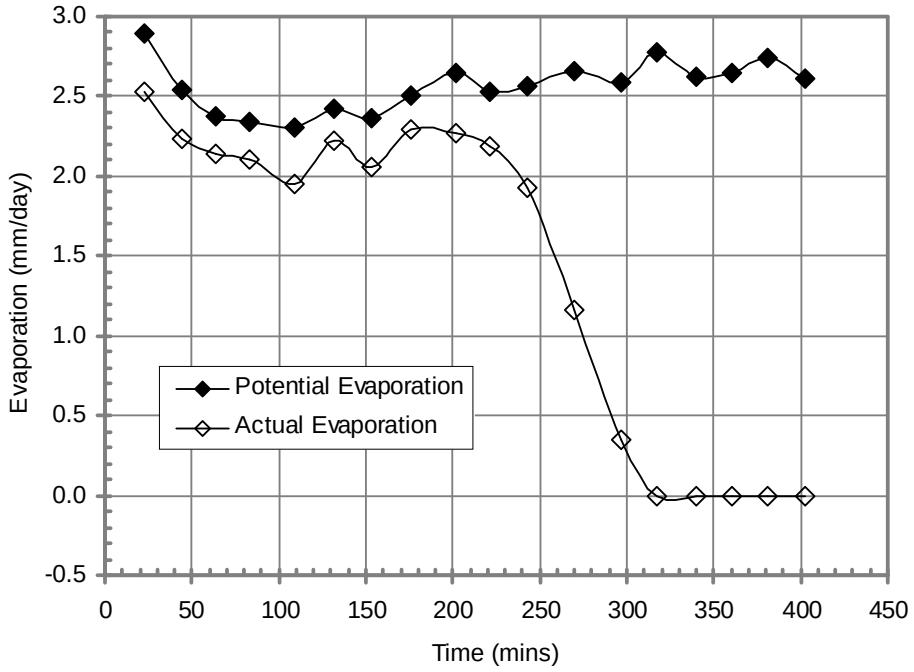

Figure 5.16 Typical Actual and Potential Evaporation rates versus drying time for the sieved Devon silt in Set 1.

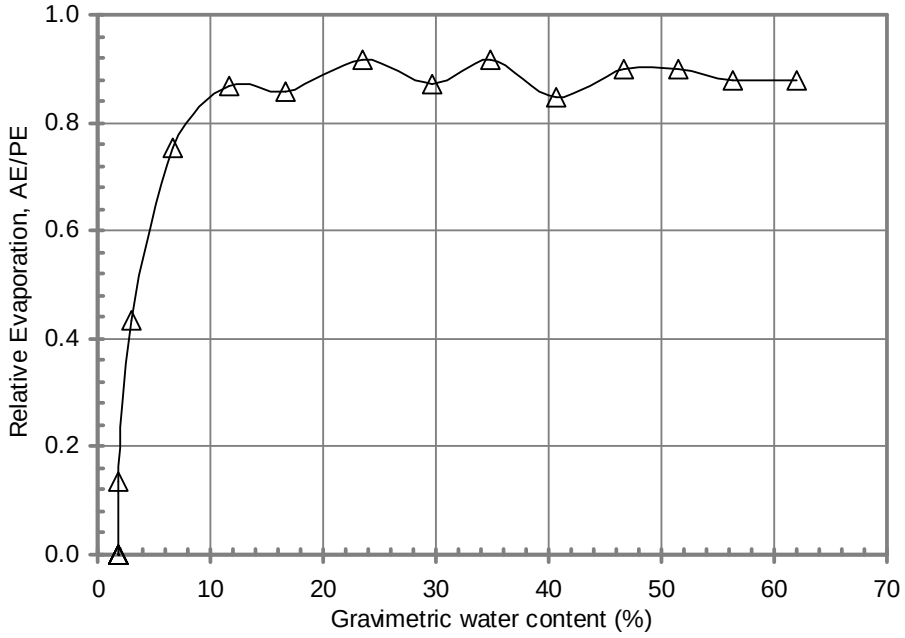

Figure 5.17 Typical plot of Relative Evaporation (*AE/PE*) versus gravimetric water content for the sieved Devon silt in Set 1.

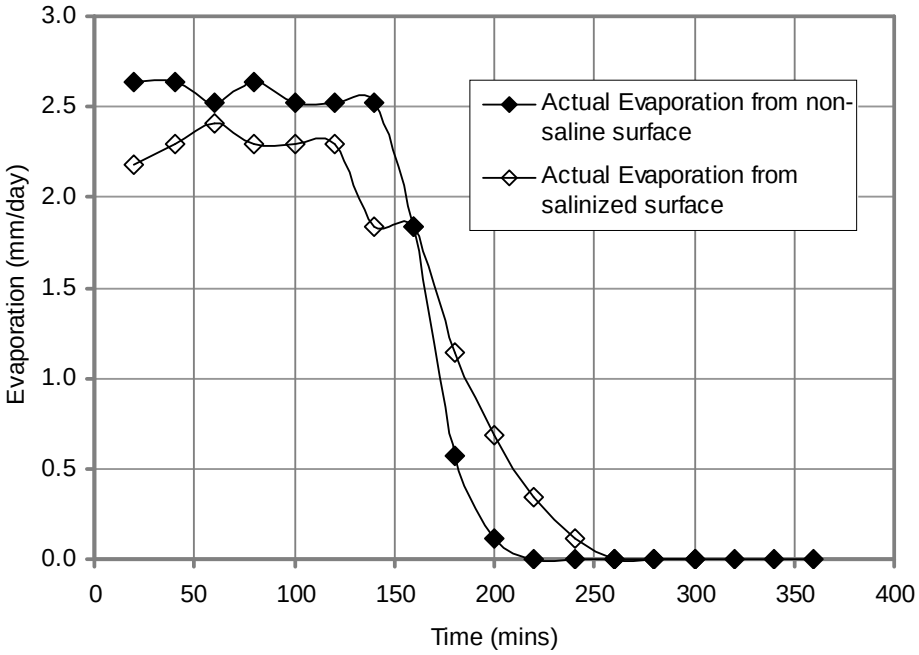

Figure 5.18 Typical Actual Evaporation rates versus drying time for the sieved Devon silt and the sieved Devon silt mixed with 50 g/l NaCl in Set 1.

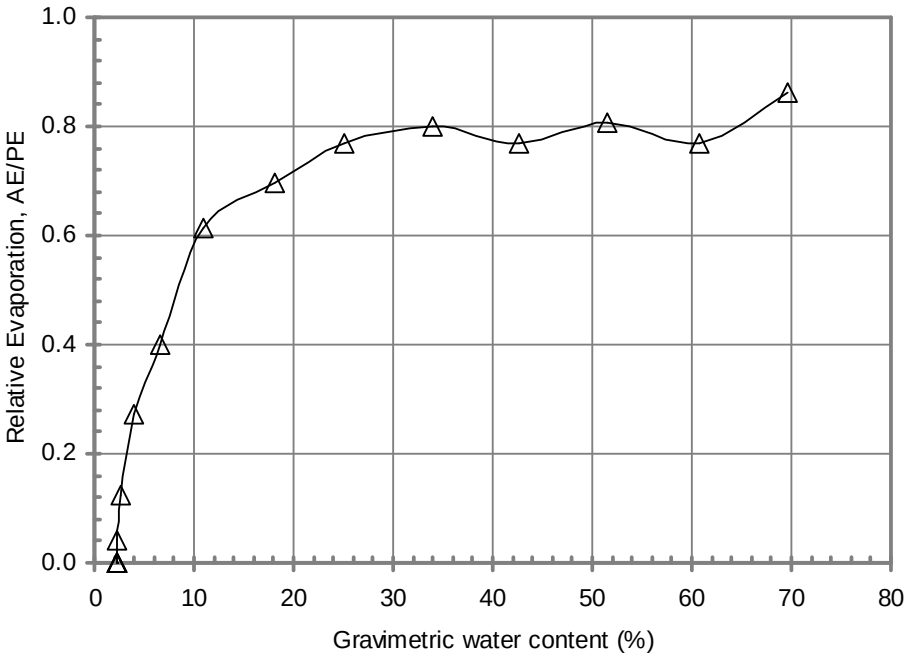

Figure 5.19 Typical plot of Relative Evaporation (*AE/PE*) versus gravimetric water content for the sieved Devon silt mixed with 50 g/l NaCl in Set 1.

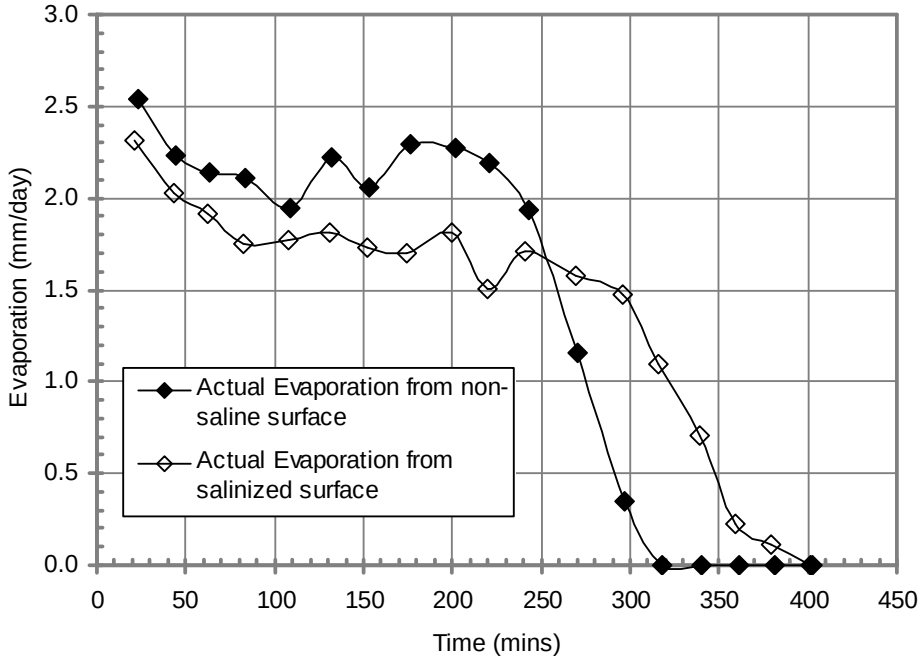

Figure 5.20 Typical Actual Evaporation rates versus drying time for the sieved Devon silt and the sieved Devon silt mixed with 100 g/l NaCl in Set 1.

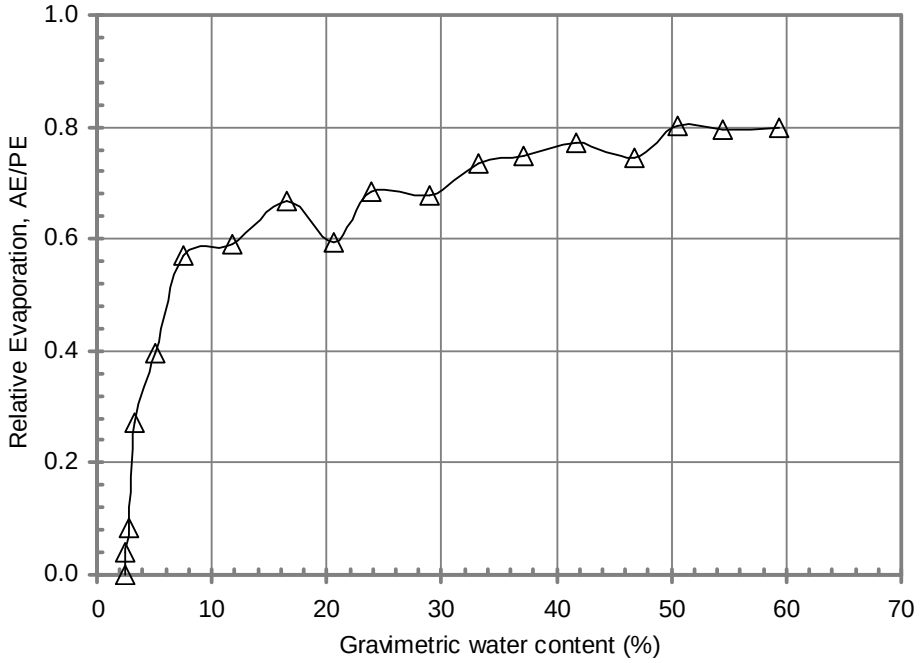

Figure 5.21 Typical plot of Relative Evaporation (*AE/PE*) versus gravimetric water content for the sieved Devon silt mixed with 100 g/l NaCl in Set 1.

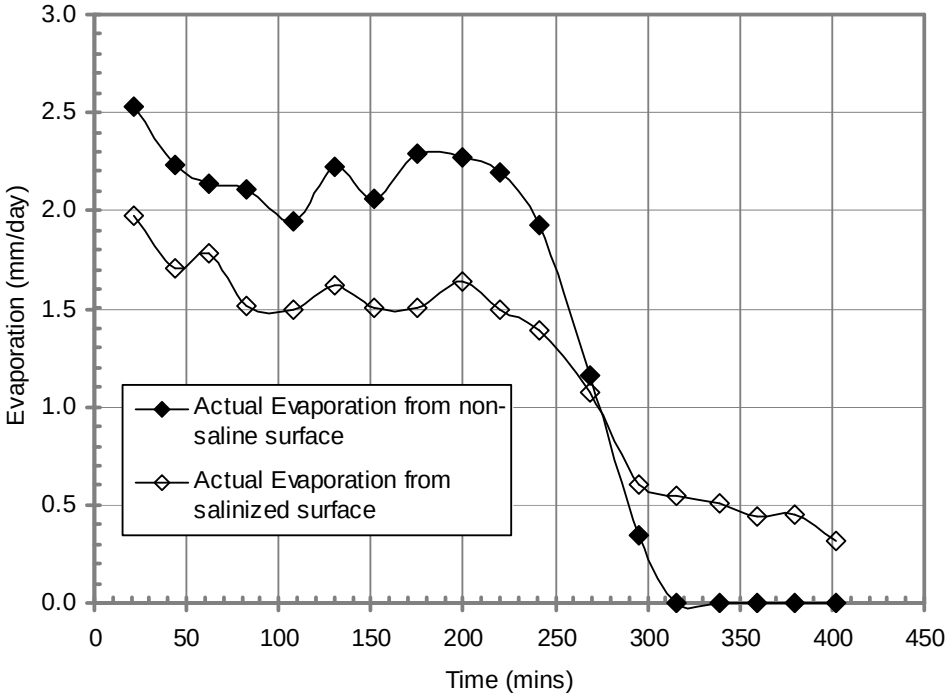

Figure 5.22 Typical Actual Evaporation rates versus drying time for the sieved Devon silt and the sieved Devon silt mixed with 200 g/l NaCl in Set 1.

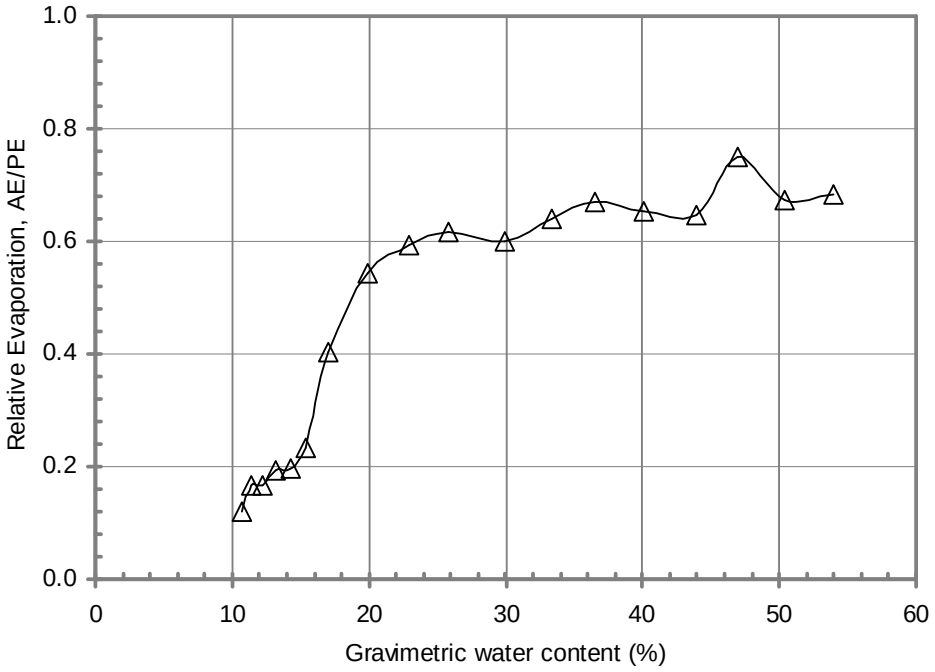

Figure 5.23 Typical plot of Relative Evaporation (*AE/PE*) versus gravimetric water content for the sieved Devon silt mixed with 200 g/l NaCl in Set 1.

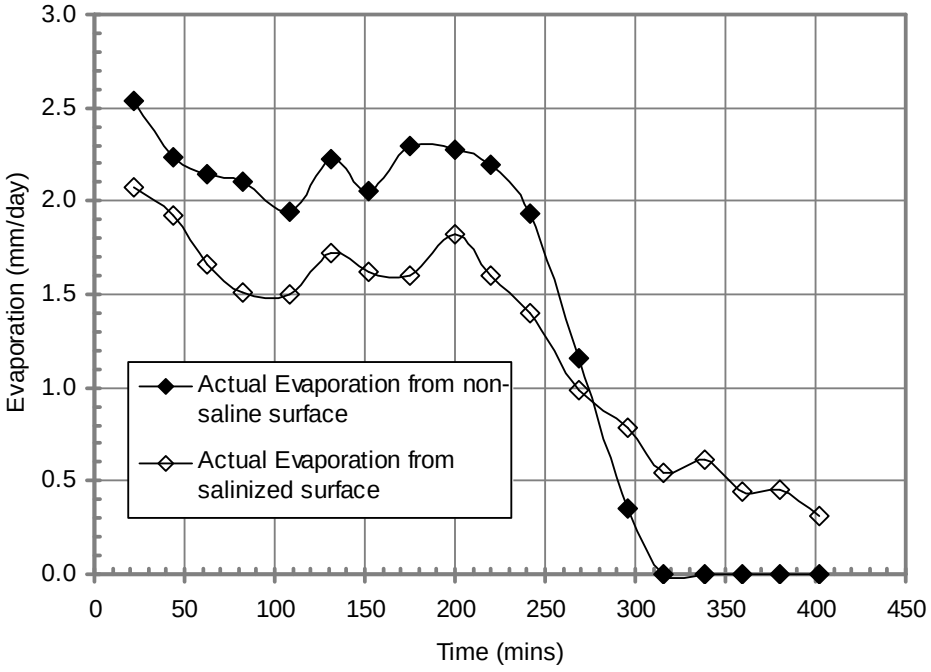

Figure 5.24 Typical Actual Evaporation rates versus drying time for the sieved Devon silt and the sieved Devon silt mixed with 250 g/l NaCl in Set 1.

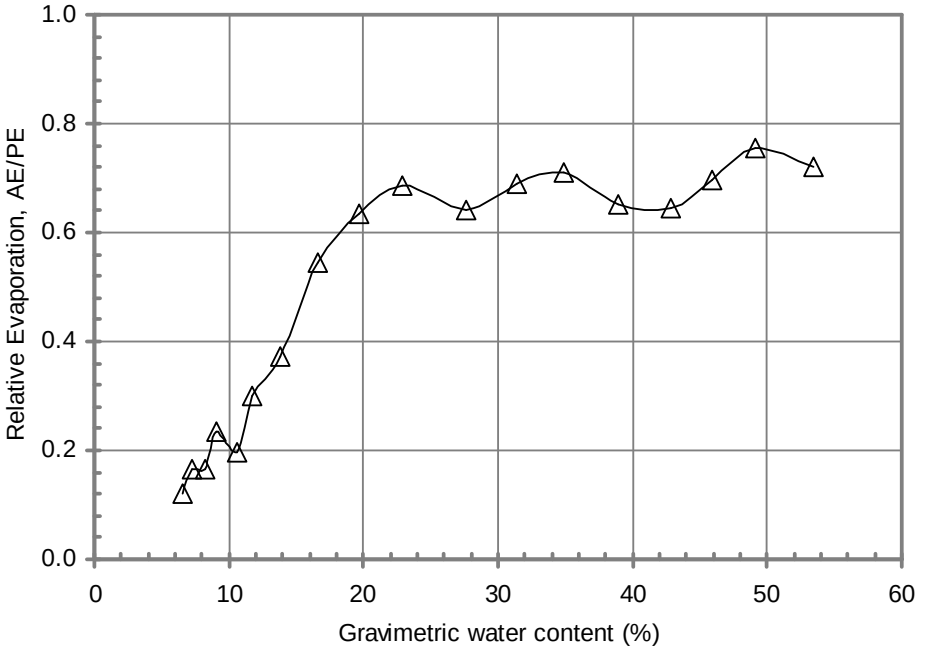

Figure 5.25 Typical plot of Relative Evaporation (*AE/PE*) versus gravimetric water content for the sieved Devon silt mixed with 250 g/l NaCl in Set 1.

The slurry method was tried to prepare some test specimens for thin soil layer evaporation tests. The soil samples were prepared as a slurry and poured into the evaporation pans. The soil-water slurry was then distributed over the entire surface of the pan using a trowel. This slurry method was attempted for the Ottawa sand and sieved Devon silt. The Ottawa sand was too clean to slurry and trowelling the wet sand over the surface of evaporation pan was difficult. The Devon silt was found to be too difficult to trowel in a thin and uniform layer pattern. This disadvantage led to the development of the dry sieve-mist saturation procedure described in Section 4.2.4.

All test specimens for thin soil layer evaporation tests were prepared using the method developed in Section 4.2.4. Numerous trials were attempted for both Ottawa sand and sieved Devon silt. There were some difficulties encountered during preparation. It appears to be difficult to control an equal mass of wet soil filled in all evaporation pans along with preparation of a uniform layer. For example, two evaporation pans needed to be filled with the equal mass of wet soil. These evaporation pans had to be weighed at first. A uniform dry soil layer was sieved over the first pan and its mass was determined. The mass of a uniform dry soil layer for the second pan would be controlled to be equal to that of the first one. A pan would be discarded and prepared again if either non-uniformity or different mass on the pan occurred. Distilled water or saline water added to two uniform dry soil filled pans using a fine mist sprayer would be also controlled to be equal. In order to obtain that each soil filled pan was weighed continuously immediately after some sprayings. Water on the wall of the pans was continually cleaned to avoid the soil on outer edges wetter than that at the central area.

The second difficulty occurred was associated with preparation for saline soil surfaces. The fine mist sprayer was often stuck while spraying. Consequently, there was some saline water that visually stagnated on the soil surfaces. It was attributed to salt accumulated at the spray nozzle. It was difficult for saline water to be added uniformly over saline-soil surfaces. For this reason, more trials were attempted for saline-soil surfaces rather than non-saline soil

surfaces. More difficulties occurred during the preparation for the four saline-soil pans for each soil.

Despite of the above difficulties, the mass of wet soil pans were finally measured to be approximately 241.25 grams and 215.45 grams for the sand and silt, respectively. Correspondingly, the thicknesses of the sand and silt layers were obtained to be approximately 1.0 and 0.5 mm, respectively.

5.2.4 Interpretation of Test Results from Thin Soil Layer Drying Tests

For non-saline soil, test No. S1 (non-saline Ottawa sand in set 1) has been selected as a representative test for interpretation. The actual rate of soil evaporation was close to potential evaporation rate from the water-filled pan during the first 250 minutes of drying at which point it suddenly begins to decline. The evaporation rate declined rapidly to zero at approximately 320 minutes of drying as shown in Figure 5.6. The actual and potential evaporation rates can be expressed as relative evaporation, *AE/PE*, for which a value of unity indicates equality. Figure 5.7 shows the relative evaporation versus water content for the Ottawa sand. The gravimetric water content at the breaking point in evaporation was found to be approximately 1 percent for Ottawa sand. The breaking point water contents were different for each tested material. For example, it was found to be approximately 9 percent for the Devon silt (i.e., Figure 5.17). This finding agrees with the observation made by Wilson (1990) for the Beaver Creek sand, Custom silt and Regina clay.

Data on the evaporation rate from the salinized soil surfaces were measured along with those from the non-saline surfaces. Over several hours of drying, the magnitude of difference in actual evaporation rates between the non-saline soil surfaces and salinized soil surfaces depended on the initial pore-water salinity. This pattern of depression was found to be the same in both the sand and silt surfaces and similar to observations for mine tailings by Fujiyasu and Fahey (2000) and for the columns of the salinized silt by Dunmola (2012). The evaporation rates from salinized surfaces were depressed and lower than that

from non-saline surface during the first period of drying. The depression in evaporation rate appeared to be dependant on the initial pore-water salinity of these surfaces. The more initial pore-water salinity had a surface, the more depression occurred in actual evaporation rate from the surface. For example, the relative evaporation was 0.8, 0.75, 0.65 and 0.63 for the Ottawa sand mixed with 50 g/l, 100 g/l, 200 g/l and 250 g/l NaCl, respectively (i.e., Figures 5.9, 5.11, 5.13 and 5.15). This pattern is similar to the sieved Devon silt (i.e., Figures 5.19, 5.21, 5.23 and 5.25). It was attributed to the effect of osmotic suction due to availability of pore-water salinity. It should be noted that osmotic suction depends on pore-water salinity. Higher pore-water salinity results in higher osmotic suctions.

The osmotic suction affects the total suction and hence reduces the relative humidity at the soil-salinized surface. The reduced evaporation rate from the soil-salinized surface is due to a reduction in the vapour pressure gradient between the soil surface and the atmosphere above. Over the time of drying, water was lost in evaporation process and the salt concentration (i.e. ratio of volume of salt to volume of water) was increased. Hence, the osmotic suction increased and lowered the evaporative demand for higher initial pore-water salinity surface. This phenomenon also explains why evaporation from the salinized-soil surface occurred longer than that from the non-saline soil surface. For example, with the same amount of water added at beginning, evaporation from the Ottawa sand ceased at 320 minutes of drying earlier than that from Ottawa sand mixed with Sodium Chrolide at 380 minutes of drying.

Figure 5.16 shows that evaporation from the sieved Devon silt also ceased at 320 minutes of drying while evaporation from the sieved Devon silt mixed 100 g/l NaCl ceased at 400 minutes of drying (i.e., Figure 5.20). However, the evaporation rates from the sieved Devon silt mixed with 200 g/l and 250 g/l NaCl were still approximately 0.3 mm/day at 400 minutes of drying (i.e., Figures 5.22 and 5.24). Figure 5.18 shows that evaporation from the sieved Devon silt and the sieved Devon silt mixed with 50 g/l NaCl ceased at 220 minutes and 260 minutes of drying, respectively. It was attributed to less water added in these soil-filled pans.

The pattern of the evaporating process in Set 2 is included in Appendix A and was essentially the same as that observed for Set 1.

5.2.5 Test Results from Thick Soil Layer Drying Tests

The thick soil layer evaporating tests were also conducted in the Soil Preparation Laboratory, NREF L2-040, University of Alberta between December 19 and 25, 2012 for Ottawa sand and between January 5 and 14, 2013 for Devon silt. Each 105 mm-diameter container was filled with the equal mass of the soil and distilled water up to the thickness of 30 mm. The soil filled evaporation containers were tapped around so that the soil surface had a flat surface. All soil filled containers were open for 24 hours before recording their mass in consecutive hours. The initial water content was recorded to be approximately 30 percent and 51 percent for Ottawa sand specimen and Devon silt specimen, respectively. The drying experiment of Ottawa sand consisted of eleven sand filled containers along with one container filled with distilled water (see Figure 5.26). Eight of silt filled containers along with one container filled with distilled water were prepared for the drying experiment of Devon silt. After recording mass of the soil filled containers, a container was destructively sampled to determine water content at 1 mm, 10 mm, 20 mm and 30 mm deep.

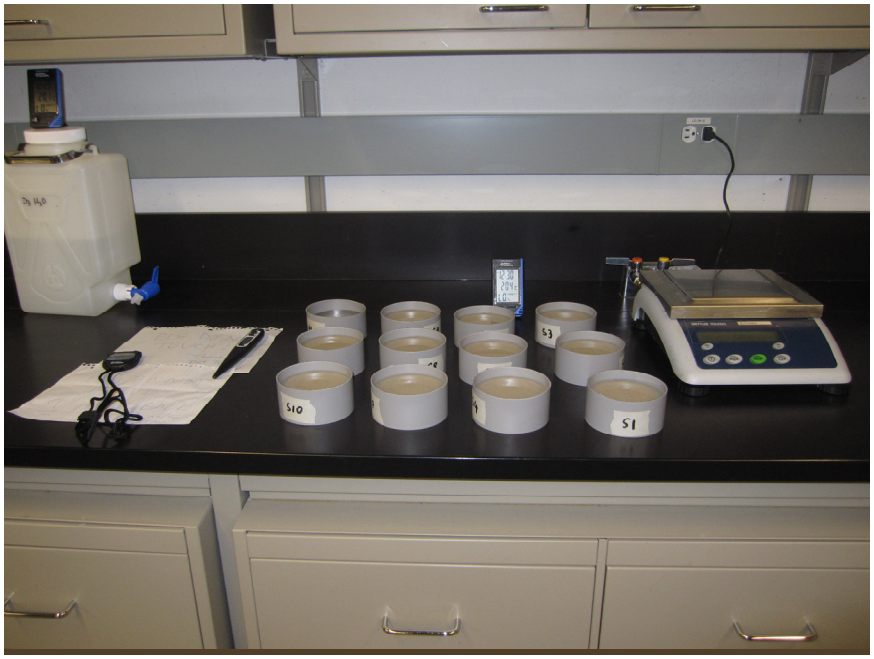

Figure 5.26 Typical thick sand layer drying tests of Ottawa sand in NREF L2-040, University of Alberta between December 19 and 25, 2012.

The typical plots of the air temperature and relative humidity of the ambient environment in the laboratory room are presented in Figures 5.27 and 5.28 for the drying experiments for Ottawa sand and Devon silt, respectively. A summary of the test results of the evaporation tests for thick soil layers of Ottawa sand and Devon silt conducted are provided in Tables 5.9 and 5.10, respectively.

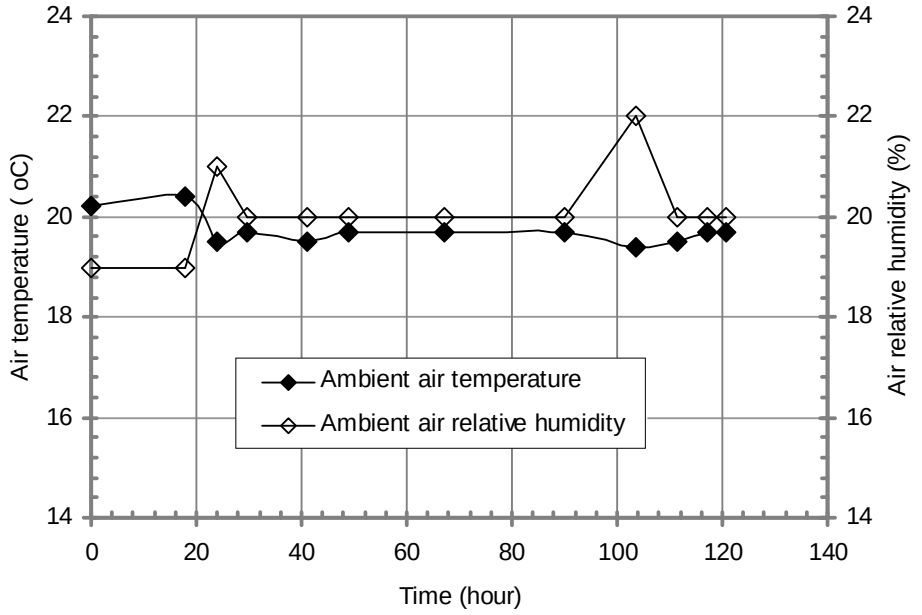

Figure 5.27 Measured ambient temperature and relative humidity of the air around the 30 mm thick sand layer drying tests of Ottawa sand.

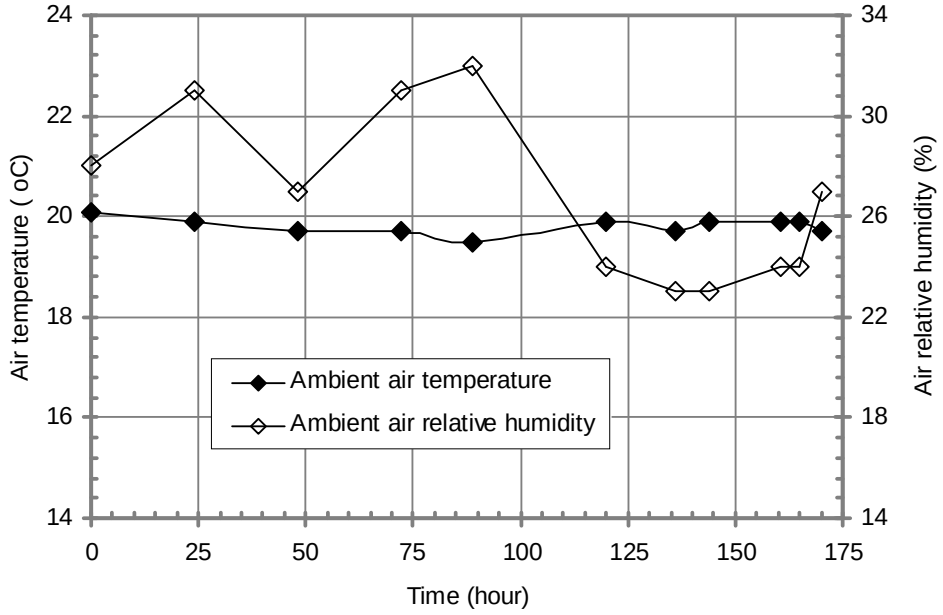

Figure 5.28 Measured ambient temperature and relative humidity of the air around the 30 mm thick sand layer drying tests of Devon silt.

Table 5.9 Summary of the test results of thick soil layer evaporation testing for Ottawa sand between December 19 and 25, 2012.

Time (hour)	PE (mm/day)	AE (mm/day)	R.H. Air	Temp. Air (^{o} C)	Temp. Water (^{o} C)	Temp. Soil (^{o} C)	Water content at 1 cm (%)
0	-	-	0.19	20.2	16.4	16.4	30.0
18	2.87	2.57	0.19	20.4	16.5	16.8	19.2
24	2.68	2.43	0.21	19.5	16.5	17.5	16.2
29.5	2.90	2.60	0.20	19.7	16.5	17.2	14.6
41	2.76	2.47	0.20	19.5	16.5	17.2	11.5
49	2.70	2.55	0.20	19.7	16.5	17.2	8.4
67	2.59	2.44	0.20	19.7	16.5	17.1	6.9
90	2.55	2.46	0.20	19.7	16.5	17.1	4.2
103.5	2.56	1.70	0.22	19.4	16.5	18.2	2.6
111.5	2.48	0.68	0.20	19.5	16.5	18.5	1.2
117	2.44	0.55	0.20	19.7	16.5	20.7	1.0

Table 5.10 Summary of the test results of thick soil layer evaporation testing for Devon silt between January 5 and 14, 2013.

Time (hour)	PE (mm/day)	AE (mm/day)	R.H. Air	Temp. Air (^{o} C)	Temp. Water (^{o} C)	Temp. Soil (^{o} C)	Water content at 1 cm (%)
0	-	-	0.28	20.1	17.1	17.1	51.0
24	2.65	2.47	0.31	19.9	17.1	17.1	43.0
48	2.68	2.43	0.27	19.7	17.1	17.1	35.5
72	2.62	2.32	0.31	19.7	17.1	17.1	28.6
89	2.48	2.22	0.32	19.5	17.1	17.4	25.3
120	2.21	1.95	0.24	19.9	17.1	17.4	16.3
136	2.62	1.99	0.23	19.7	17.1	17.6	11.9
144	2.65	1.83	0.23	19.9	17.1	17.8	9.3
160.5	2.53	1.37	0.24	19.9	17.1	17.8	9.3
165	2.54	1.09	0.24	19.9	17.1	17.9	6.9
170	2.47	0.98	0.27	19.7	17.1	18.0	7.6

5.2.6 Interpretation of Test Results from Thick Soil Layer Drying Tests

Figures 5.29 and 5.30 show the rate of evaporation versus time measured in the drying experiments of Ottawa sand and Devon silt in thick soil layers. The patterns of evaporation observed during these drying experiments agree with the classic pattern described in the research literature (i.e., three stages of soil evaporation, Hillel, 1980). The actual rate of soil evaporation is close to potential evaporation rate from the water-filled pan during the first 90 and 160.5 hours for the Ottawa sand and Devon silt, respectively. The evaporation rate declines rapidly between 90 hours and 111.5 hours of drying for the Ottawa sand as shown in Figure 5.29. The rapid decline in evaporation between approximately 160.5 and 165 hours represents the intermediate falling-rate stage for Devon silt drying experiment as shown in Figure 5.30. The prolonged intermediate period following 111.5 and 165 hours of evaporation may be considered as the residual slow-rate stage.

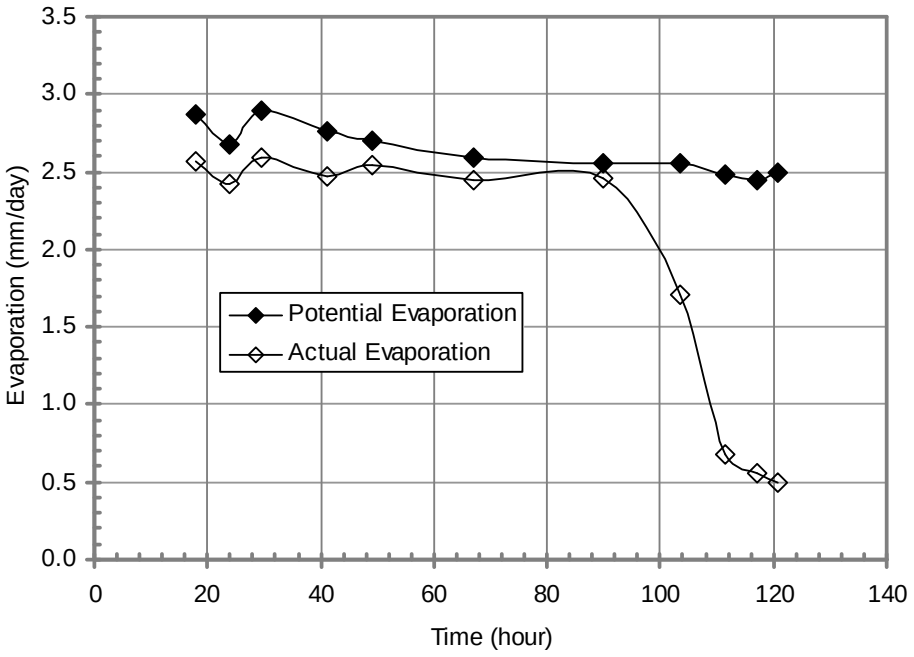

Figure 5.29 Measured Actual and Potential Evaporation rates versus drying time for Ottawa sand in the thick soil layer drying tests.

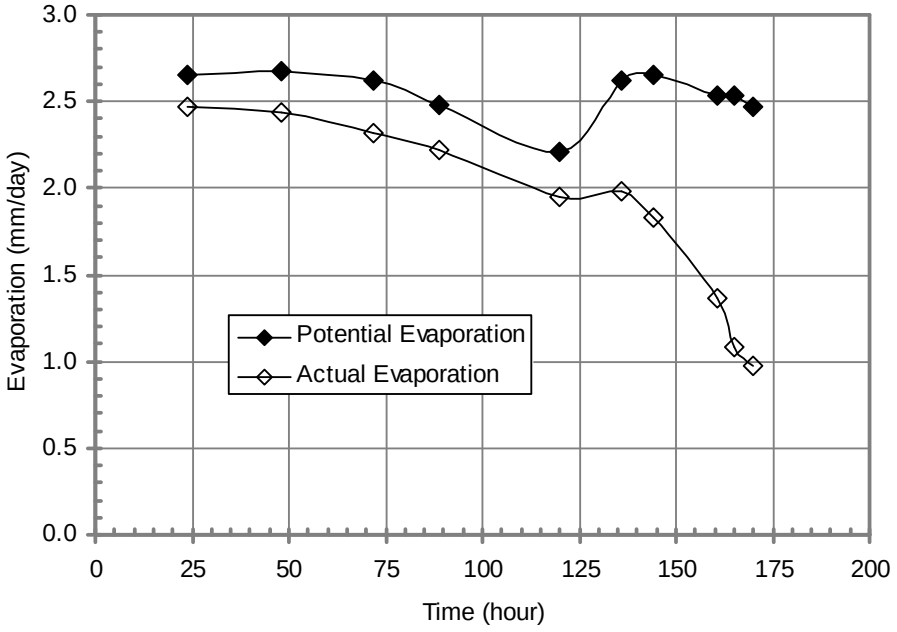

Figure 5.30 Measured Actual and Potential Evaporation rates versus drying time for Devon silt in the thick soil layer drying tests.

The measured actual and potential evaporation rates can be expressed as relative evaporation, *AE/PE*, for which a value of unity indicates equality. Figures 5.31 and 5.32 show the relative evaporation versus the measured gravimetric water content for the Ottawa sand and Devon silt, respectively. The gravimetric water contents at the breaking point in evaporation are different for each tested soil. For example, the gravimetric water contents at the breaking point in evaporation are found to be approximately 5 percent for Ottawa sand and 16 percent for the Devon silt. These water contents correspond to suctions of approximately 13 kPa and 4,300 kPa at evaporation-rate reduction points for Ottawa sand and Devon silt, respectively. These values of suction appear to be between air-entry value and residual soil suction (as shown in Figures 5.1 and 5.2). This finding appears to agree with the observation made for the drying experiments by Wilson (1990), Bruch (1993) and Yanful and Choo (1997) which are presented in Section 5.3 of this chapter.

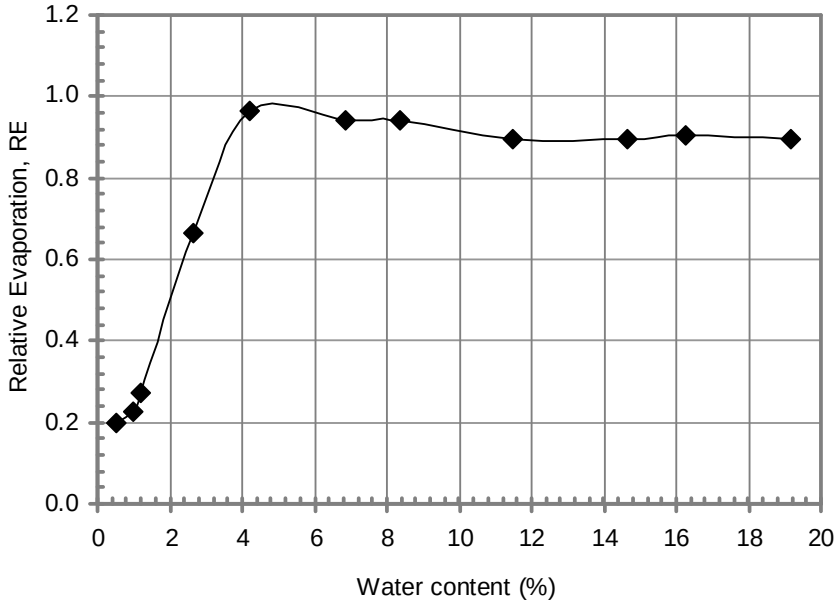

Figure 5.31 Plot of Relative Evaporation (*AE/PE*) versus gravimetric water content for Ottawa sand in the thick soil layer drying tests.

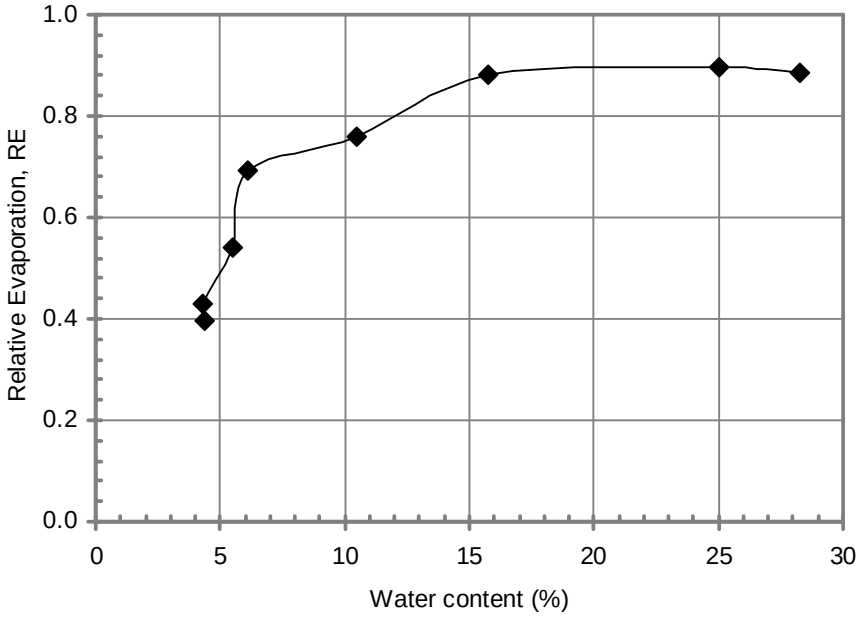

Figure 5.32 Plot of Relative Evaporation (*AE/PE*) versus gravimetric water content for Devon silt in the thick soil layer drying tests.

Figures 5.33 and 5.34 show that changes in water content occur below the surface of the sand and silt as drying progresses, respectively. For example, after 18 hours of drying, the surface water content in 3 cm thick layer of

Ottawa sand is 6.4 percent, as shown in Figure 5.33 while the water content increases to 19.2 percent at the depth of 10 mm. This observation shows that a distinct drying front forms as the sand desiccates. The drying front continues to advance deeper into the sand as drying continues. The drying front reaches to a depth of approximately 10 mm after 120.6 hours (5 days) of continuous drying. The similar behaviour of the drying front appears to be observed in 3 cm thick layer of Devon silt, as shown in Figure 5.34.

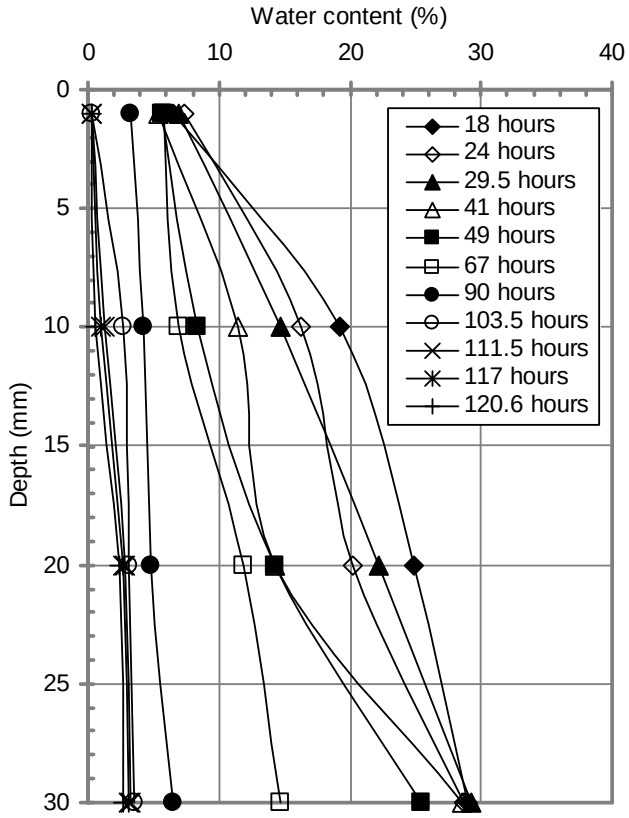

Figure 5.33 Gravimetric water content with depth during drying process for Ottawa sand in the thick soil layer drying tests.

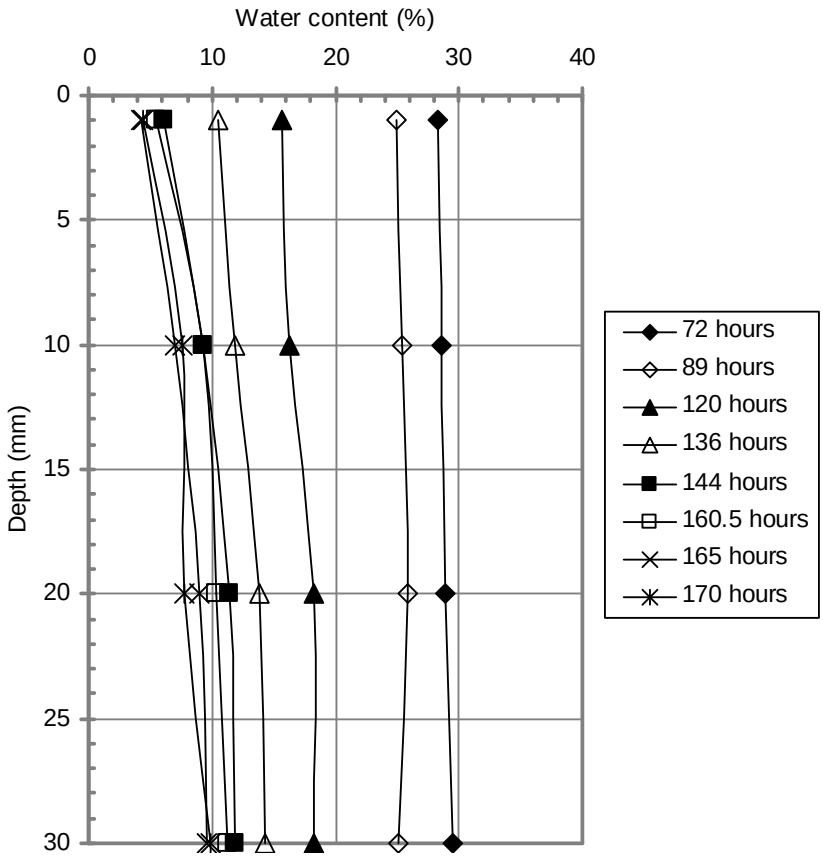

Figure 5.34 Gravimetric water content with depth during drying process for Devon silt in the thick soil layer drying tests.

5.3 INTERPRETATION OF DATABASE OF SOILS FROM THE RESEARCH LITERATURE

Datasets of evaporative fluxes from thin soil sections and soil columns from the research literature were also collected and are included in Appendices B, C, D and E for subsequent comparison with theoretical considerations. These datasets were collected from the research by Wilson (1990), Bruch (1993), Yanful and Choo (1997) and Dunmola (2012). The results include:

1. The thin soil section evaporation tests for the Beaver Creek sand, Custom silt and Regina clay by Wilson (1990); for non-saline silt by Dunmola (2012).

2. The soil columns drying tests on the Beaver Creek sand by Wilson (1990); Beaver Creek sand, Processed silt and Natural silt by Bruch (1993); Fine sand and Coarse sand by Yanful and Choo (1997); non-saline silt, salinizied silt and mine tailings by Dunmola (2012).

Some researchers tabulated soil datasets (Wilson, 1990; Bruch, 1993); the others provided soil datasets in graphs (Yanful and Choo, 1997; Dunmola, 2012). The soil datasets in graphs were collected with the assistance of the GetData Graph Digitizer software program version 2.24. The program allows the collection of data points from the graphs scanned from the research literature.

The following subsections focuses on the interpretation of evaporative patterns from thin soil layer and soil column drying. Besides, effect of salt content on evaporation rate is also interpreted.

5.3.1 Soil Database from Wilson (1990)

The drying tests were conducted on Beaver Creek sand in both thin soil layer and soil column by Wilson (1990). The representative test results of the relative evaporation are presented along with water content and the corresponding suction in order to discuss patterns of evaporation and re-evaluate at what suction the evaporation rate starts to reduce from potential evaporation rate. The test results of evaporation by Wilson (1990) are provided in Appendix B.

Figures 5.35 and 5.36 show the relative evaporation versus water content from the drying tests on Beaver Creek sand in thin soil layer and soil column, respectively. The patterns of relative evaporation are remarkably different for the thin soil layers and soil columns. Figure 5.35 shows that the relative evaporation from the thin soil layers is approximately equal to unity before it suddenly begins to decline at 2 percent in water content at the surface. The relative evaporation then begins to decline rapidly to zero.

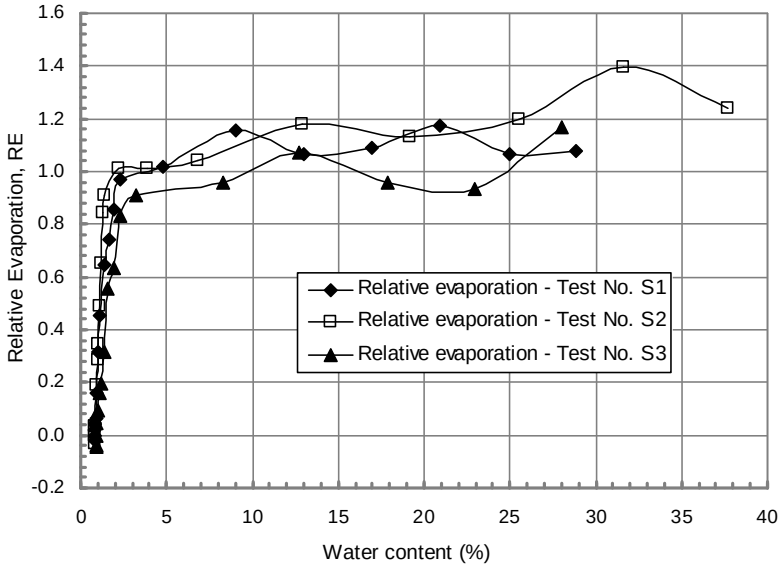

Figure 5.35 Plots of Relative Evaporation versus water content for Test No. S1, S2 and S3 on Beaver Creek sand (adapted after Wilson, 1990).

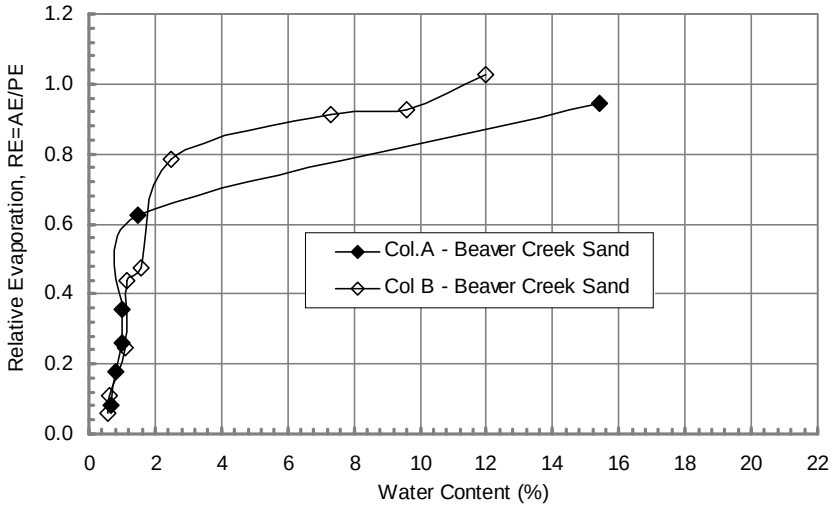

Figure 5.36 Plots of Relative Evaporation versus water content at the top surface for soil columns A and B on Beaver Creek sand (adapted after Wilson, 1990).

Meanwhile, the relative evaporation for the soil columns begins to decline gradually at approximately 12 and 16 percent in water content at the top surface for soil column A and B, respectively (see Figure 5.36). The sharper declination in the relative evaporation occurs at approximately 2 percent in water content. The known water content at the surface was converted into total suction using the SWCC of Beaver Creek sand. The plots of the relative

evaporation versus the total suction for the thin soil layers and soil columns are presented in Figures 5.37 and 5.38, respectively.

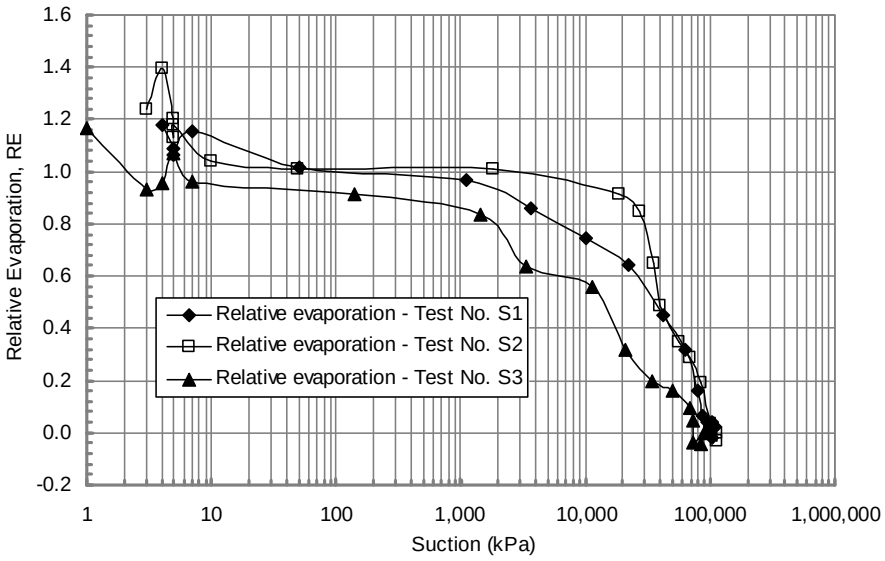

Figure 5.37 Plots of Relative Evaporation versus Total Suction for Test No. S1, S2 and S3 on Beaver Creek sand (adapted after Wilson, 1990).

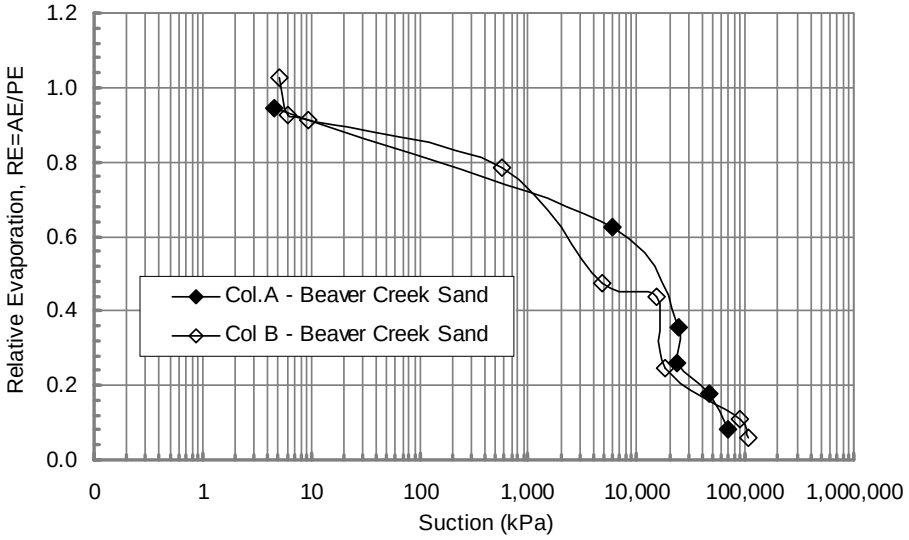

Figure 5.38 Plots of Relative Evaporation versus Total Suction at the top surface for soil columns A and B on Beaver Creek sand (adapted after Wilson, 1990).

Figure 5.37 shows the relative evaporation from the thin soil layers of the Beaver Creek sand begins to decline at the total suction of approximately 3,000 kPa (Wilson, 1990). The relative humidity at the surface estimated by

the Lord Kelvin's formula also starts to decline at the total suction of approximately 3,000 kPa. This indicates that the Lord Kelvin's formula is valid for the thin soil layers during drying process. However, the results appear to be different for the soil columns of the Beaver Creek sand. As seen in Figure 5.38, the relative evaporation from the soil columns gradually decline at the total suction of approximately 5 kPa. This value is between the air entry value and the residual suction of the SWCC of the Beaver Creek sand. The hydraulic conductivity of the Beaver Creek sand at the total suction of 5 kPa was found to be approximately 5×10^{-8} m/s or 4.32 mm/day (Gitirana, 2005 and Ebrahimi et al., 2005). This value of the hydraulic conductivity was realized to be less than the evaporation rate of 6.96 mm/day at the total suction of 5 kPa. It appears that the soil surface was not supplied enough water from the below for evaporation under the hydraulic gradient of unity. The evaporating surface appeared to move down during the drying process. It caused the soil surface to become unsaturated at the total suction of 5 kPa. This finding is different from the observation from thin soil layer drying. The Lord Kelvin's formula appears to be invalid for the soil column drying. The relative humidity at the surface of the soil column will be estimated using the proposed method described in the section 3.5.2.1 of Chapter 3.

5.3.2 Soil Database from Bruch (1993)

The soil column drying was also conducted on the Beaver Creek sand, Processed silt and Natural silt by Bruch (1993). The relative evaporation versus water content for the soil columns during drying process are re-plotted in Figure 5.39. The other figures and tables presenting the test results of evaporation by Bruch (1993) are provided in Appendix C.

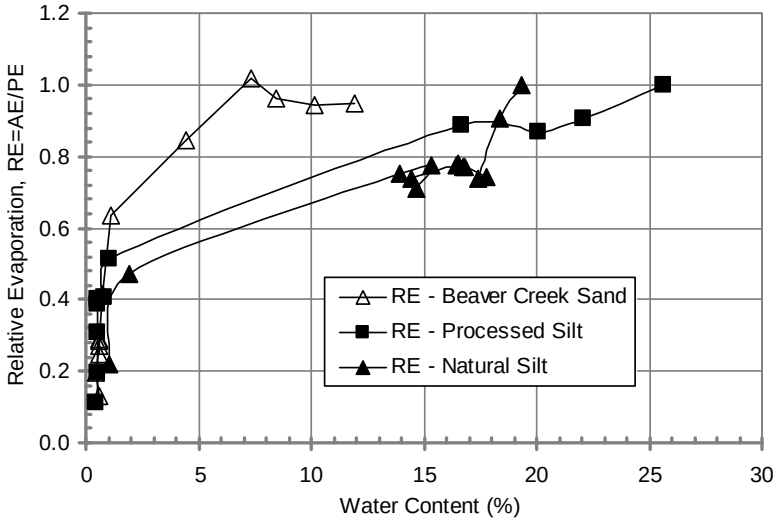

Figure 5.39 Plots of Relative Evaporation versus Water Content for the Beaver Creek sand, Processed silt and Natural silt (adapted after Bruch, 1993).

The relative evaporation for the soil columns begins to decline gradually at approximately 11, 10 and 9 percent in terms of water content at the top surface for the Beaver Creek sand, Processed silt and Natural silt, respectively. The corresponding total suctions at the evaporation-reduction point in Figure 5.40 are 7 kPa, 62 kPa and 116 kPa for the Beaver Creek sand, Processed silt and Natural silt, respectively. These values are realized to be sufficiently close to the residual suction for the respective soils of 8.5 kPa, 97 kPa and 167 kPa.

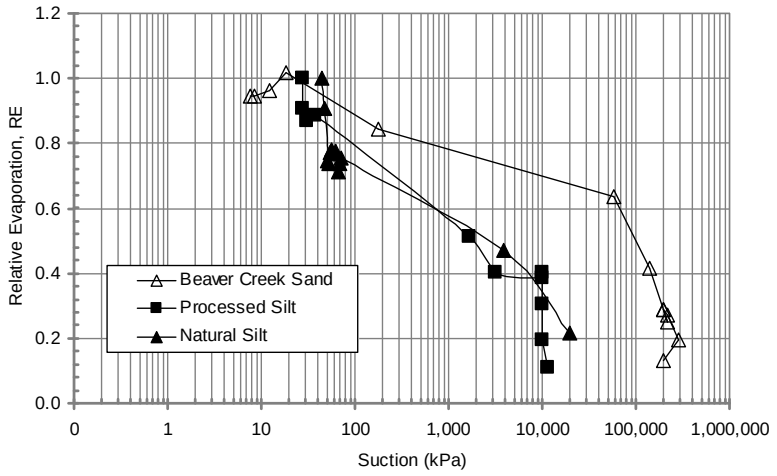

Figure 5.40 Plots of Relative Evaporation versus Total Suction at the top surface for the soil columns of the Beaver Creek sand, Processed silt and Natural silt (adapted after Bruch, 1993).

The hydraulic soil parameters for the Beaver Creek sand, Processed silt and Natural silt are summarized in Table 5.11 (after Bruch, 1993). The hydraulic conductivity function was obtained from the saturated hydraulic conductivity and using the Brooks and Corey (1964) equation. The hydraulic conductivity for the Beaver Creek sand, Processed silt and Natural silt were found to be as 2.7×10^{-9} m/s (or 0.23 mm/day), 6.8×10^{-11} m/s (or 0.006 mm/day) and 5.1×10^{-11} m/s (or 0.004 mm/day) at the total suction of 7 kPa, 62kPa and 116 kPa, respectively (see Figure 5.41). These values of the hydraulic conductivity are observed to be less than the evaporation rates of 5.54 mm/day, 4.27 mm/day and 3.79 mm/day at the evaporation-reduction points for the tested soils. Therefore, the soil surface may not be provided with enough water to satisfy the evaporation rate under a hydraulic gradient of unity. The evaporating surface will move downward during the drying process; hence, the soil surface became unsaturated at the total suction of 7 kPa, 62kPa and 116 kPa for the Beaver Creek sand, Processed silt and Natural silt, respectively.

Table 5.11 Summary of hydraulic soil parameters (after Bruch, 1993).

Parameters	**Beaver Creek sand**	**Processed silt**	**Natural silt**
Saturated Hydraulic Conductivity (m/s)	4.26×10^{-8}	8.36×10^{-9}	2.07×10^{-8}
Air Entry Value (kPa)	4.6	34	46
Pore Size Distribution Index, L	2.5	2.0	1.5

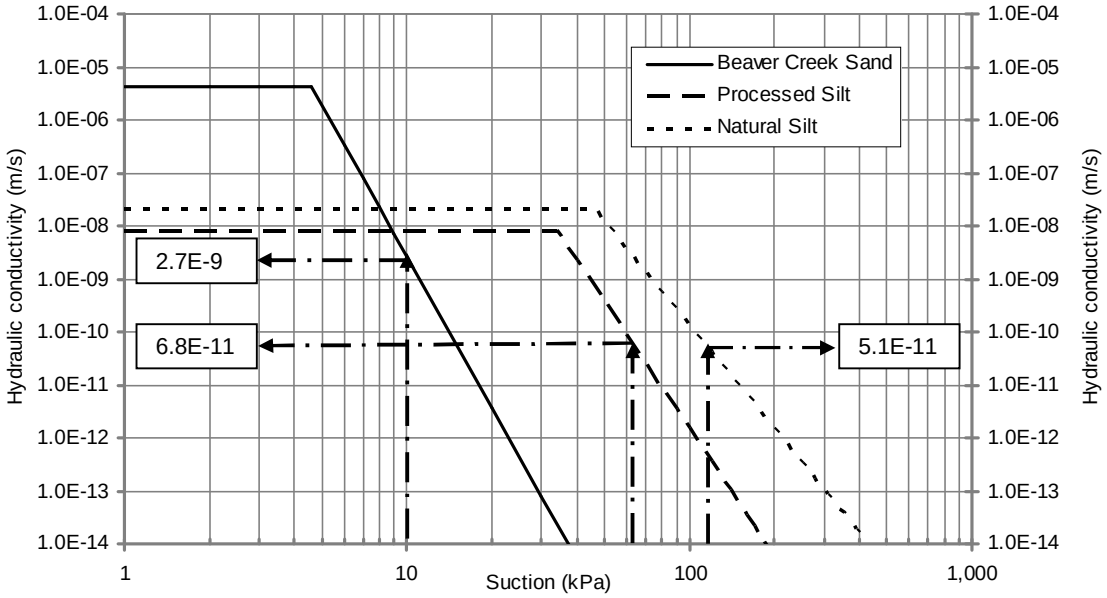

Figure 5.41 Hydraulic conductivity functions for the Beaver Creek sand, Processed silt and Natural silt (based on the parameters shown in Table 5.11).

5.3.3 Soil Database from Yanful and Choo (1997)

The test results obtained from the soil column drying of the Coarse sand and Fine sand by Yanful and Choo (1997) are somewhat similar to those by Wilson (1990) and Bruch (1993). The relative evaporation for the soil columns begins to decline gradually at approximately 15 and 14 percent in terms of volumetric water content at the top 0 – 1 cm for the Coarse sand and Fine sand, respectively (see Figure 5.42). These volumetric water contents corresponded to the total suctions of 1.3 kPa and 3.7 kPa, respectively (see Figure 5.43). These suctions at the evaporation-rate reduction point are observed to be in between the air-entry value and the residual suction for the Coarse sand and Fine sand, respectively (see Section 3.5.1.2 of Chapter 3). The other figures and tables presenting the test results of evaporation by Yanful and Choo (1997) are provided in Appendix D.

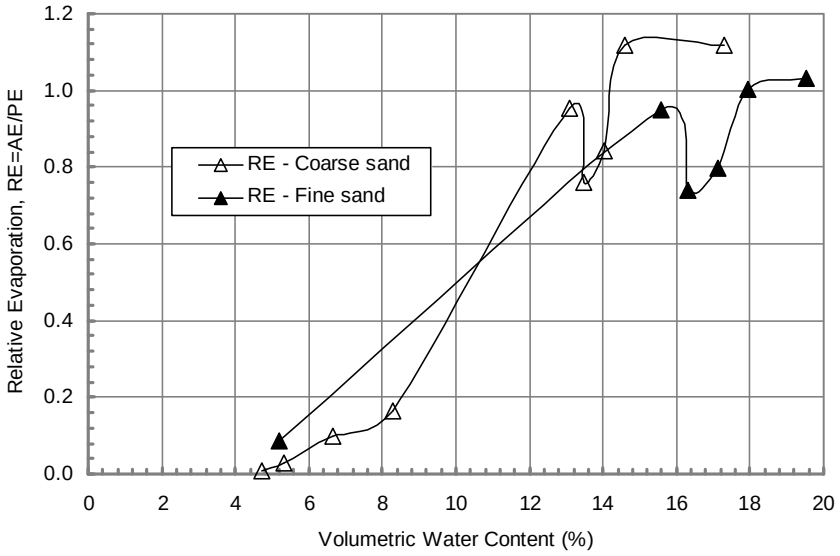

Figure 5.42 Plots of Relative Evaporation versus Volumetric Water Content at 0 – 1 cm for the Coarse sand and Fine sand (adapted after Yanful and Choo, 1997).

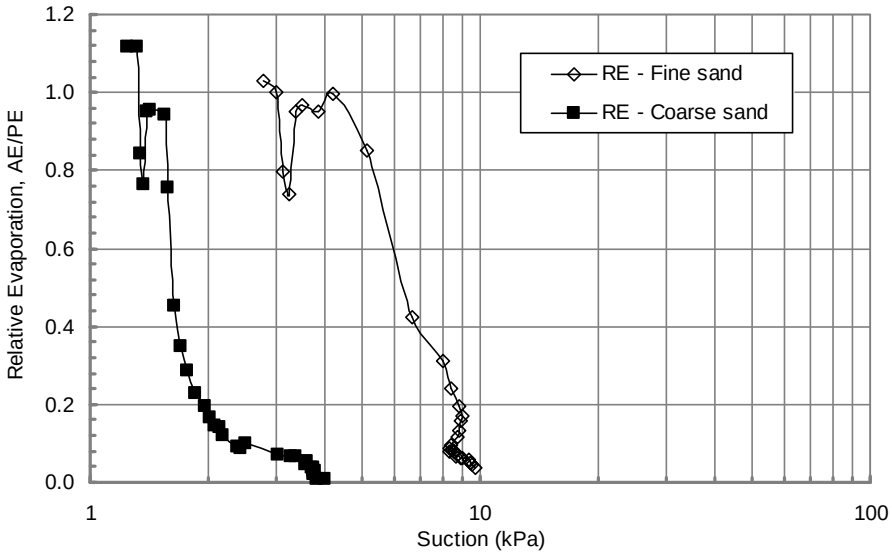

Figure 5.43 Plots of Relative Evaporation versus Total Suction at the top 0 – 1 cm for the soil columns of the Coarse sand and Fine sand (adapted after Yanful and Choo, 1997).

5.3.4 Soil Database from Dunmola (2012)

The drying tests were conducted on silt formed as thin soil layer (2 mm thick) and soil column (10 cm thick) by Dunmola (2012). The representative test results of the relative evaporation are presented along with the measured total suction in order to discuss patterns of evaporation. The evaporation-rate reduction points for the thin soil layer and the soil column are observed. The some figures and tables presenting the test results of evaporation by Dunmola (2012) are provided in Appendix E.

Figure 5.44 shows the relative evaporation versus total suction from the drying test on silt material in 2 mm thick soil layers. Similarly, the relative evaporation begins to decline at the total suction of approximately 3,000 kPa. This phenomenon was found on three replicates. This finding agrees with the test results of thin soil layer drying on Beaver Creek sand by Wilson (1990).

Figure 5.45 shows the relative evaporation versus total suction at top 0 – 1 cm from the drying test on silt material in 10 cm thick soil layers. The relative evaporation begins to decline at the total suction of approximately 300 kPa which appears to be lower than the value of 3,000 kPa. This phenomenon was found on three replicates. This finding appears to be slightly different from the test results from Wilson (1990), Bruch (1993) and Yanful & Choo (1997). This finding is also different from the observation from the 2 mm thick soil layer drying. The suction at the evaporation-reduction point was found to be closer the residual suction of 22 kPa than the total suction of 3,000 kPa.

After examination of all test results collected from the research literature, it was concluded that the evaporation from the soil columns begins to decline at a suction close to the residual suction. The Lord Kelvin's formula of the relative humidity appears to be invalid for the soil column drying. The relative humidity at the surface of the soil column will be estimated using the proposed method described in the section 3.5.2.1 of Chapter 3. Verification of the proposed method for estimating the relative humidity at the soil surface of the soil columns will be presented in Chapter 6.

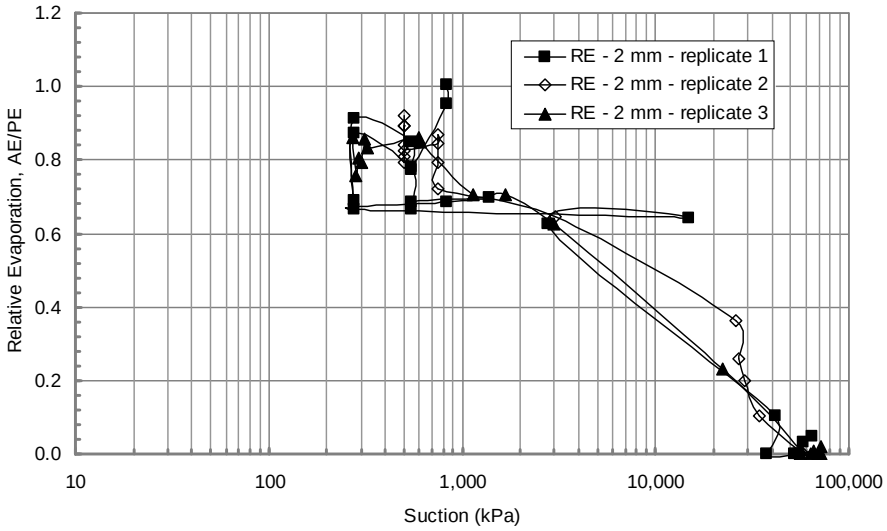

Figure 5.44 Plots of Relative Evaporation versus Total Suction for Replicates 1, 2, 3 of 2 mm thick silt (adapted after Dunmola, 2012).

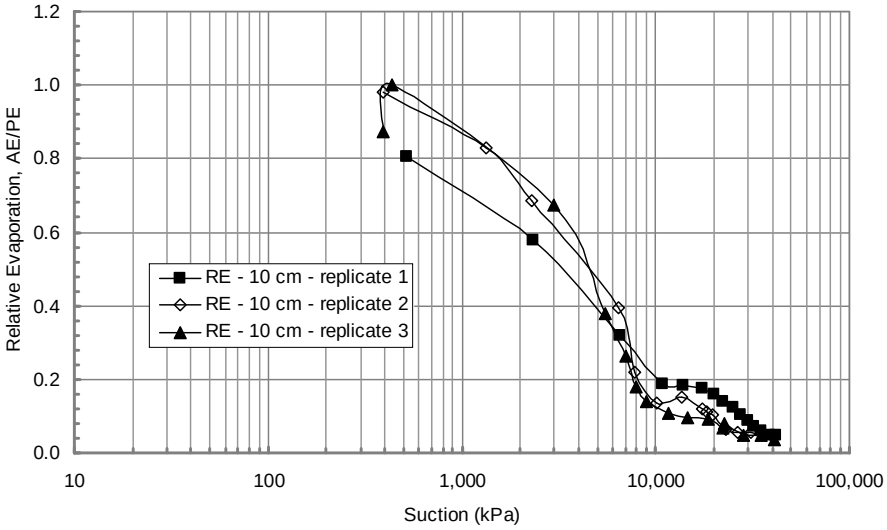

Figure 5.45 Plots of Relative Evaporation versus Total Suction for Replicates 1, 2, 3 of 10 cm thick silt (adapted after Dunmola, 2012).

5.4 CHAPTER SUMMARY

This chapter presented the test results from the current laboratory testing and the dataset of soils collected from the research literature.

Presentations along with interpretation of the test results from the current laboratory testing were presented in Section 5.2. The soil-water characteristic

curves for the Ottawa sand, sieved Devon silt and Kaolinite were obtained from the Golder cells and Vacuum Desiccators. The test results of osmotic suction were presented for the sieved Devon silt mixed with 50 g/l NaCl and the Kaolinite mixed with 50 g/l NaCl in the subsection 5.2.2. The test results of thin soil layer drying and 3 cm thick soil layer drying were presented in the subsections 5.2.3 and 5.2.5, respectively.

Section 5.3 presented the interpretation of the test results collected from the research literature. The results show that the relative evaporation from the thin soil layers begins to decline at the total suction of approximately 3,000 kPa. However, the relative evaporation from the soil columns begins to decline at a total suction close to the residual suction which is smaller than the suction of 3,000 kPa. This observation was found in the drying tests from two soil columns of the Beaver Creek sand (Wilson, 1990), the soil columns of the Beaver Creek sand, Processed silt, Natural silt (Bruch, 1993), the soil columns of the Coarse sand, Fine sand (Yanful and Choo, 1997) and the soil columns of the silt (Dunmola, 2012).

CHAPTER 6
VERIFICATION THE PROPOSED EQUATIONS

6.1 GENERAL

This chapter presents information on the verifications of the relative humidity and soil surface resistance using the new proposed equations for thin soil sections and soil columns. Comparisons are made between measured evaporative data and predicted results using the new proposed soil-atmosphere model presented in Chapter 3. The equations used for the verification are summarized in Table 6.1. The soil data used in the comparison includes data collected from the research literature as well as test results obtained from the laboratory testing program.

Section 6.2 presents a comparison between the various methods available for the determination of relative humidity for the thin soil layers which are collected from the research literature. This section also presents computations of soil suction under the situation that there is a point of evaporation-rate reduction, ψ_R for soil columns. The point of evaporation-rate reduction was described in Chapter 3 using Eq. (3.80). The corresponding volumetric water content under evaporation-rate reduction, θ_R, conditions is generated from soil-water characteristic curves using the Fredlund and Xing's equation (1994) implemented in the SVFlux software from SoilVision Company, (Saskatoon, SK). The values of θ_R are used as reference points when computing the relative humidity and soil surface resistance. These values are later used in verification of the new proposed soil-atmosphere model.

Chapter 5 has presented evidence to show effect of salt content on the evaporation rates. It is noted that the function of osmotic suction was proposed in Chapter 3. Section 6.3 presents the information on the verification of the proposed function of osmotic suction using data measured in the laboratory program (i.e., Devon silt and Kaolinite mixed with various salt contents of

Sodium Chloride). The effect of some factors related to the salt content is analyzed in this section using an Excel spreadsheet. This function of osmotic suction is used to predict the evaporation rate from thin soil sections (e.g., the salinized Ottawa sand and Devon silt in the current laboratory testing program) and from the salinized soil columns (e.g., Low-saline silt, Saline silt and Hyper-saline silt which are collected from the research literature).

Section 6.4 presents the verification of proposed soil-atmosphere flux equation presented in Chapter 3. The verification was undertaken using the software, ComSol Multiphysics for soil columns of bare soil. The accuracy of the proposed model is also discussed in this section.

Finally, section 6.5 presents a summary of the content of this chapter.

Table 6.1 Summary of key equations used for verification.

Terminology (1)	Equation (2)	Equation number (3)	Input parameters (4)
New soil-atmosphere model	$E_A = \dfrac{\Gamma Q + \eta \dfrac{f'(u)}{f(u)} E'_a}{\Gamma + \eta A \dfrac{f'(u)}{f(u)}}$	Eq. (3.69)	Q = net radiation (converted to mm/day); Γ = slope of the saturation vapour pressure versus temperature curve at the mean temperature of the air, (Pa/^{o}C); η = psychromatric constant, 66.8 (Pa/^{o}C); $f(u)$ and $f'(u)$ = transmission functions for water vapor and heat, respectively which depend on wind speed, roughness and turbulence conditions; E'_a = an aerodynamic evaporative term (mm/day/Pa);

			A = inverse of soil relative humidity.
Suction at evaporation-rate point	$\psi_R = \begin{cases} \psi_{aev} & if\ a=0 \\ \psi_{res} & if\ a=1 \\ \psi_{res}^{a} \times \psi_{aev}^{1-a} & if\ 0<a<1 \end{cases}$	Eq. (3.80)	ψ_R = suction at evaporation-rate reduction point, kPa; ψ_{aev} = air-entry value, to be determined from SWCC, kPa; ψ_{res} = residual soil suction, to be determined from SWCC, kPa; a = an empirical factor which varies between 0 and 1.
Soil moisture availability factor	$\beta = \begin{cases} \frac{1}{4}\left[1 - cos\left(\frac{\theta}{\theta_R}\pi\right)\right]^2 & \theta < \theta_R \\ 1 & \theta \geq \theta_R \end{cases}$	Eq. (3.82)	β = coefficient representing the surface moisture availability; θ_R = volumetric water content at evaporation-rate reduction point; θ = soil volumetric water content of the topsoil layer.
Actual water vapour pressure	$p_v = \beta \times p_v^{sat} + (1-\beta) \times p_v^{air}$	Eq. (3.83)	p_v = actual vapour pressure at soil surface, kPa; p_v^{sat} = saturated vapour pressure at soil surface, kPa; p_v^{air} = actual air pressure immediately above soil surface, kPa.
Relative humidity	$RH = \frac{p_v}{p_v^{sat}}$	Eq. (3.84)	p_v = actual vapour pressure at soil surface, kPa; p_v^{sat} = saturated vapour pressure at soil surface, kPa.
Soil surface resistance at top 0 – 1 cm	$r_s = 10 \times e^{0.3563(\theta_R - \theta_{top})}$	Eq. (3.86)	r_s = soil surface resistance at top 0 – 1 cm, s/m; θ_{top} = volumetric water content of the top 1 cm layer, (%); θ_R = volumetric water content value at the evaporation-rate reduction point, (%), which is

			generated from the total suction at the evaporation-rate reduction point, ψ_R (e.g., Eq. 3.80).
Osmotic suction	$\pi = 2 \times \left(\frac{\theta_{salt0} \times \theta_{sat} \times \rho_s}{\theta_{SWCC} \times M_{molar}} \right) RT$	Eq. (3.100)	ρ_s = density of salt, (g/cm^3) (e.g., 2.16 g/cm^3 for Sodium Chloride); M_{molar} = molar mass of salt, g/mol (e.g., 58.5 g/mol for Sodium Chloride); R = ideal gas constant, 8.314 J/mol/^{o}K; T = absolute temperature in Kelvin degree, ^{o}K; θ_{sat}, = saturated initial volumetric water content; θ_{salt0} = initial salt content; θ_{SWCC} = volumetric water content determined from SWCC.
Salt crust resistance	$r_{sc} = 0.69 ln(\Gamma_s) - 1.04$	Eq. (3.101)	r_{sc} = salt crust resistance (s/m); Γ_s= mass of salt accumulated at surface (mg/cm^2). It can be obtained from the salt concentration, θ_{salt} and the thickness of salt crust layer; $\Gamma_s = \theta_{salt} \times \rho_s \times t_s$ (mg/cm^2) t_s = thickness of the salt crust layer (assumed to be uniform over soil surface).

6.2 COMPARISON BETWEEN THE METHODS OF DETERMINATION OF THE RELATIVE HUMIDITY

Chapter 3 presented modifications to the theory for the calculation of relative humidity (i.e., Eqs. 3.82, 3.83 and 3.84) and soil surface resistance (i.e., Eq. 3.86). The desire was to formulate a methodology which could be more realistically applied in geotechnical engineering. The formulation showed that the relative humidity and soil surface resistance are different when studying evaporation from thin soil sections than when studying evaporation from soil columns. It is important to be able to compute actual evaporation rates using soil data collected from the research literature and the laboratory program. The results of both thin layer evaporation and column evaporation need to be simulated numerically.

The procedures used to compute the relative humidity and soil surface resistance are described in the following section. It should be noted that all procedures are applied to soil columns. Only steps (iii) to (v) are applied to thin soil sections in this chapter. The water content at the point of evaporation-rate reduction in thin soil sections are obtained at a total suction of approximately 3,000 kPa.

The proposed steps in the analysis of actual evaporation are as follows:

i. Generate a soil-water characteristic curve based on experimental data (i.e., water content versus suction);

ii. Obtain the air-entry value and residual soil suction from the soil-water characteristic curve. Determine the suction corresponding to the point of evaporation-rate reduction using equation (3.80), and generate the corresponding water content;

iii. Determine soil water content availability factor, β as a reference point for the calculation of relative humidity using (3.82);

iv. Compute actual vapour pressure, p_v and relative humidity, RH, at the soil surface using equations (3.83) and (3.84), respectively;

v. Finally, compute soil surface resistance, r_s using equation (3.86).

6.2.1 Verification Using the Data Collected from the Research Literature

Comparisons between predictions by the newly proposed equations for the relative humidity (i.e., Eqs. 3.82, 3.83 and 3.84) and the measured data for soils collected from the research literature are presented in this section. In order to verify the proposed equations, each collected soil dataset must have (or at least have it possible to estimate) the soil-water characteristic curve of the soil and soil water content (i.e., volumetric water content or gravimetric water content) with the ratio of *AE/PE*. The predictions are presented for twelve thin soil sections and eight soil columns collected from the research literature below:

- The thin soil sections of Beaver Creek sand, Custom silt and Regina clay and soil columns of Beaver Creek sand with properties measured by Wilson (1990);

- The soil columns of Beaver Creek sand, Processed silt and Natural silt with properties measured by Bruch (1993);

- The soil columns of coarse sand and fine sand with properties measured by Yanful and Choo (1997);

- The thin soil sections and soil columns of non-saline silt with properties measured by Dunmola (2012).

The soil datasets for the ten soils were collected from the research literature with the assistance of the GetData Graph Digitizer software program version

2.24. The program allows the collection of data points manually from the graphs scanned from the research literature. Considerable data collected for each soil can be used to verify the proposed equations of relative humidity. Only representative and important data collected for each soil are presented in this section. For each soil used in the verification of these equations, several graphs showing the measured data and predicted results are presented for comparison.

6.2.1.1 Verification Using the Soil Dataset by Wilson (1990)

As presented in Chapter 5, the soil datasets by Wilson (1990) include the thin soil sections for Beaver Creek sand, Custom silt and Regina clay; and the soil columns for the Beaver Creek sand.

a. For Thin Soil Section Drying

The suction at the point of evaporation-rate reduction for the thin soil sections was approximately 3,000 kPa (Wilson, 1990). The corresponding water content was 1.7, 4 and 22 percent generated from the soil-water characteristic curves for the sand, silt and clay, respectively. These values are close to the "breaking point" of water content observed by Wilson (1990) (i.e., 2, 5 and 20 percent for the sand, silt and clay, respectively). A summary of calculation of the relative humidity at the soil surface for Test No. S1 is provided in Table 6.2. Calculations of the relative humidity for the other thin soil section tests are presented in Appendix F. Comparisons of the relative humidity predicted using the Lord Kelvin's formula and the new proposed equation (i.e., Eq. 3.84) are shown in Figures 6.1, 6.2 and 6.3 for the sand, silt and clay, respectively. As expected, the results show that the predicted relative humilities agree well with the predicted data when using the Lord Kelvin's formula presented by Wilson (1990). Moreover, the maximum value of the soil surface resistance calculated for the thin soil sections using Eq. (3.86) is approximately 25 s/m at the drying soil surface. This result is attributed to the negligible distance for water vapour travel to the soil-atmosphere interface. In other words, the

evaporating front is located at the soil surface where the vapour pressure of air adjacent to the evaporating front is in equilibrium with liquid water in the soil pores during the drying process. Consequently, soil surface resistance can be ignored. It can be concluded that the proposed equation of the relative humidity (i.e., Eq. 3.84) is acceptable for the thin soil sections.

Table 6.2 Summary of calculations of the relative humidity for sand drying Test No. S1 using the Lord Kelvin's formula and the proposed equation (3.84).

MEASURED DATA					CALCULATED DATA				
Relative humidity of air	Temperature of air (^oC)	Temperature of water (^oC)	Temperature of soil surface (^oC)	Water content at soil surface	Total suction from SWCC (kPa)	Relative humidity using Lord Kelvin's formula	Soil moisture availability factor using Eq. (3.82)	Vapour pressure at soil surface using Eq. (3.83) (kPa)	Relative humidity using Eq. (3.84)
0.51	22.9	20.4	20.7	0.2888	0	1.00	1.0000	2.44	1.00
0.53	23.2	20.4	20.8	0.2498	0	1.00	1.0000	2.46	1.00
0.53	23.0	20.6	20.5	0.2092	4	1.00	1.0000	2.41	1.00
0.54	23.0	20.6	20.3	0.1695	5	1.00	1.0000	2.38	1.00
0.56	23.0	20.7	20.5	0.1303	5	1.00	1.0000	2.41	1.00
0.56	23.1	20.6	20.6	0.0904	7	1.00	1.0000	2.43	1.00
0.56	23.1	20.4	20.2	0.0483	51	1.00	1.0000	2.37	1.00
0.54	23.1	20.3	20.1	0.0234	1,100	0.99	1.0000	2.35	1.00
0.54	23.1	20.4	20.3	0.0196	3,600	0.97	0.9980	2.38	1.00
0.53	23.0	20.5	20.6	0.0162	10,000	0.93	0.8346	2.27	0.94
0.53	23.0	20.3	21.2	0.0135	22,000	0.85	0.5795	2.09	0.83
0.53	23.0	20.5	22.0	0.0114	42,000	0.73	0.3710	1.92	0.73
0.53	23.0	20.5	22.7	0.0100	64,000	0.63	0.2500	1.81	0.65
0.53	22.9	20.4	23.4	0.0092	80,000	0.56	0.1913	1.75	0.61
0.53	23.0	20.4	24.1	0.0089	88,000	0.53	0.1714	1.75	0.58
0.53	23.1	20.2	23.9	0.0087	94,000	0.50	0.1589	1.73	0.58
0.52	23.1	20.4	24.1	0.0084	104,000	0.47	0.1411	1.69	0.56
0.52	23.2	20.4	24.1	0.0082	110,000	0.45	0.1300	1.68	0.56
0.52	23.0	20.3	24.1	0.0084	104,000	0.47	0.1411	1.68	0.56
0.53	24.0	21.0	25.0	0.0085	98,000	0.49	0.1469	1.81	0.57

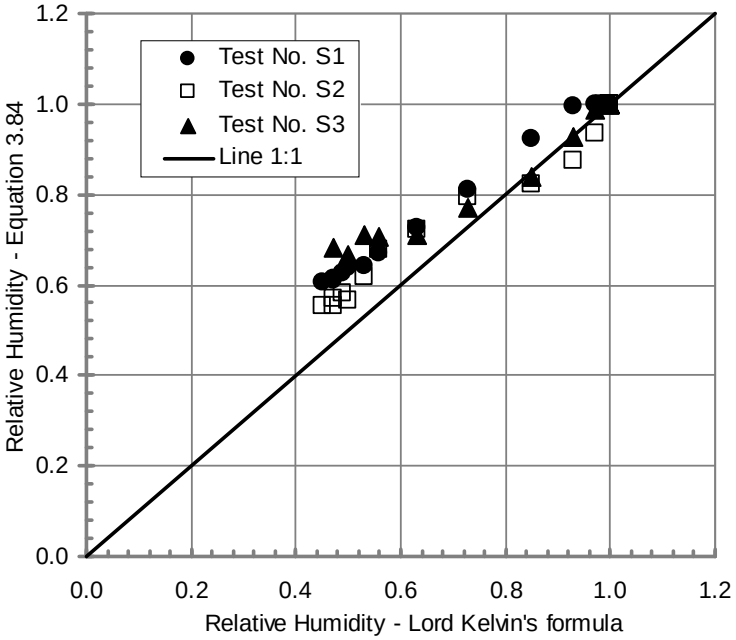

Figure 6.1 Relative humidity at the soil surface estimated using the Lord Kelvin's formula and the proposed equation (i.e., Eq. 3.84) for Test Nos. S1, S2 and S3 – Beaver Creek sand.

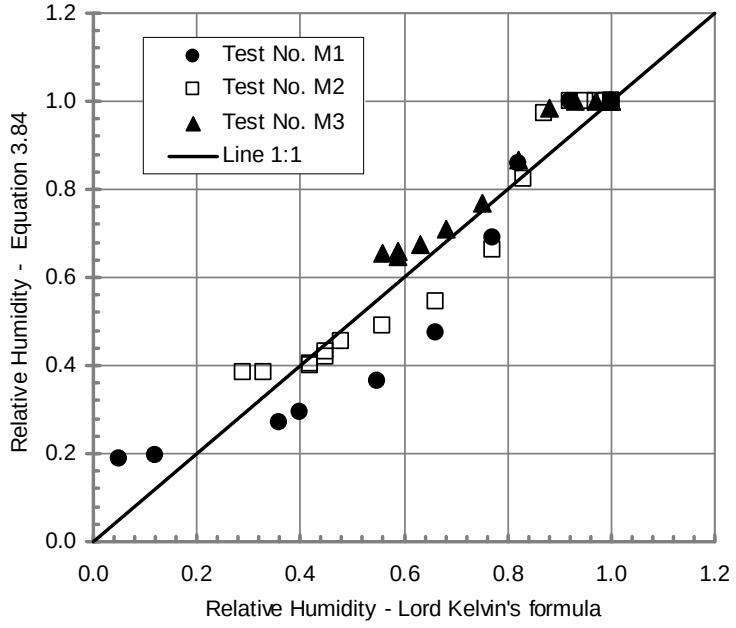

Figure 6.2 Relative humidity at the soil surface estimated using the Lord Kelvin's formula and the proposed equation (i.e., Eq. 3.84) for Test Nos. M1, M2 and M3 – Custom silt.

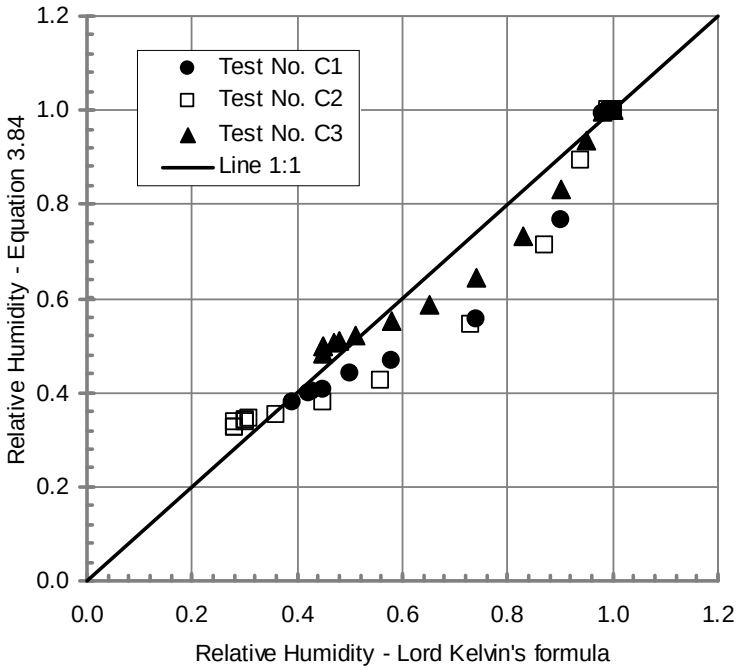

Figure 6.3 Relative humidity at the soil surface estimated using the Lord Kelvin's formula and the proposed equation (i.e., Eq. 3.84) for Test Nos. C1, C2 and C3 – Regina clay.

b. For Soil Colum Drying (Column A and B)

This section applies to the method of determining the suction at the point of evaporation-rate reduction for sand (i.e., Eq. 3.80 developed in Chapter 3). The value of "*a*" was assumed to be 0.6 for the sand, then the total suction at the point of evaporation-rate reduction was 5 kPa using Eq. (3.80). The corresponding water content of 11 percent (or 18 percent in terms of volumetric water content) from the SWCC of the Beaver Creek sand (see Figure 3.8). The relative humidity was predicted using the new set of the proposed equations (3.82), (3.83) and (3.84) at the measured water content at a depth of 0 – 1 cm. A summary of the calculation of the relative humidity at the soil surface in Columns A and B is provided in Table 6.3. The results of the predicted relative humidity for the sand column A and B are presented in Figures 6.4 and 6.5, respectively. The relative humidity obtained by the proposed equations appears to be consistent with the reduction of the relative evaporation as shown in Figure 5.34. As expected, the predicted results

showed decrease in the relative humidity with increase in the total suction which was converted from the measured water content at the depth of 0 – 1 cm using the SWCC of the Beaver Creek sand. In fact, the relative humidity begins to decline at the total suction of approximately 5 kPa which is different from the suction at the evaporation-reduction in the thin soil layer drying of the Beaver Creek sand (i.e., approximately 3,000 kPa). It is concluded that it is possible to use the new set of the equations (3.82), (3.83) and (3.84) to estimate the actual vapour pressure and relative humidity at the soil surface during the soil column drying.

Figures 6.6 and 6.7 shows that the vapour pressure of the soil calculated by Eq. (3.83) for the soil columns A and B is initially equal to that of the water at approximately 4.2 kPa. The vapour pressure of the soil gradually decreases with time. The calculated vapour pressures are consistent with decrease in the relative humidity at the soil surface as the total suction increases as shown in Figures 6.4 and 6.5. The lower vapour pressure of the ambient air at approximately 1.0 kPa provides the gradient for evaporation. The decrease in the vapour pressure in the sand continues until the water potential in the soil is in equilibrium with the water potential in the air. As a result, the gradient of the vapour pressure is close to zero which indicates the evaporation to be nearly ceased.

The value of the soil surface resistance calculated for the sand columns vary from a value close to zero at or near the saturated surface to several thousand second per meter as the soil dries out. The calculated values of the soil surface resistance are consistent with the soil surface resistance values measured in the research literature. This observed behaviour accounts the existence of the surface resistance to water vapour diffusion from the depth of 1 cm to the soil-atmosphere interface.

Table 6.3 Summary of calculations of the relative humidity for the soil columns A and B of Beaver Creek sand using the set of the proposed equations.

Soil column	MEASURED DATA					CALCULATED DATA			
	Relative humidity of air	Temp of air (^{o} C)	Temp of water (^{o} C)	Temp of soil surface (^{o} C)	Water content at 0 – 1 cm (%)	Total suction from SWCC (kPa)	Soil moisture availability factor using Eq. (3.82)	Vapour pressure using Eq. (3.83) (kPa)	Relative humidity using Eq. (3.84)
A	0.22	38.2	31.3	30.2	17.88	4	1.0000	4.29	1.00
	0.15	38.7	30.5	31.6	7.74	8	0.5305	2.95	0.63
	0.17	37.8	30.9	34.8	3.92	70	0.0601	1.38	0.25
	0.16	38.7	30.4	35.7	3.05	221	0.0236	1.21	0.21
	0.165	38.0	30.9	37.1	1.77	2,795	0.0029	1.11	0.18
	0.125	37.5	30.2	38.0	0.75	55,719	0.0001	0.81	0.12
B	0.23	38.6	29.0	30.0	16.20	4	1.0000	4.24	1.00
	0.22	38.2	31.3	30.0	11.54	5	0.9850	4.20	0.99
	0.20	38.1	31.0	29.8	9.55	6	0.7875	3.59	0.85
	0.18	38.0	30.5	30.0	6.59	12	0.3161	2.16	0.51
	0.15	38.1	30.8	33.2	5.71	17	0.2019	1.82	0.36
	0.16	39.0	30.7	34.2	3.13	195	0.0236	1.22	0.23
	0.13	39.1	30.7	36.6	1.71	3,246	0.0023	0.93	0.15
	0.12	37.5	30.4	37.4	0.69	68,630	0.0001	0.77	0.12
	0.14	38.3	30.2	38.0	0.84	41,056	0.0001	0.94	0.14

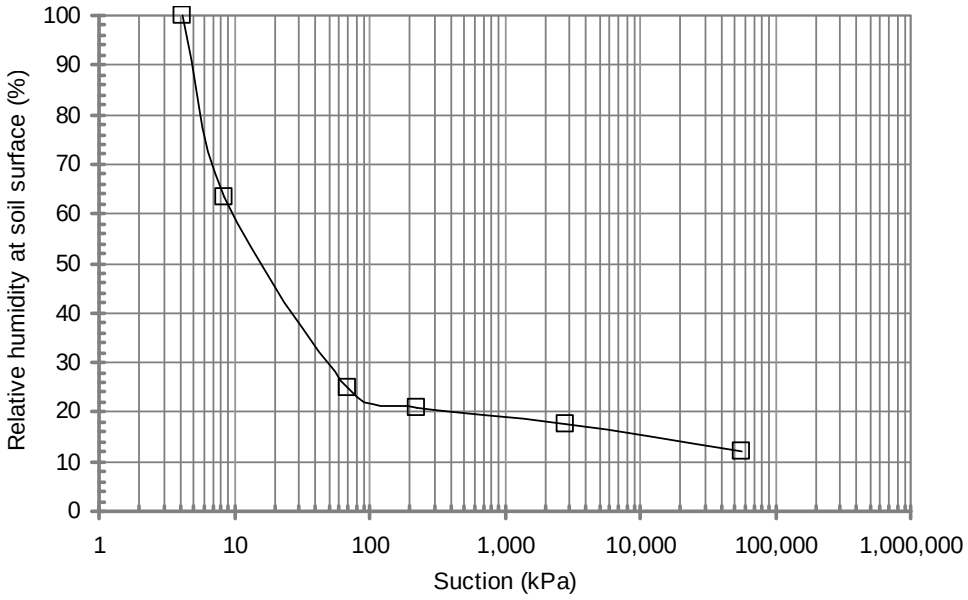

Figure 6.4 Relative humidity at a depth of 0 – 1 cm for Column A of Beaver Creek sand estimated using the new set of proposed equations (i.e., Eqs. 3.82, 3.83 and 3.84) and the measured water content.

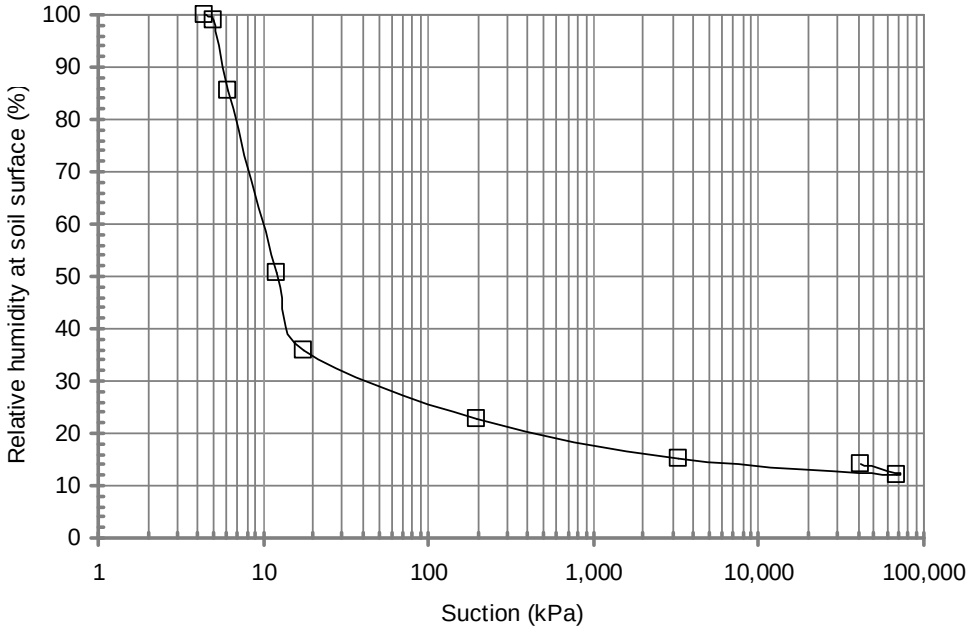

Figure 6.5 Relative humidity at a depth of 0 – 1 cm for Column B of Beaver Creek sand estimated using the new set of proposed equations (i.e., Eqs. 3.82, 3.83 and 3.84) and the measured water content.

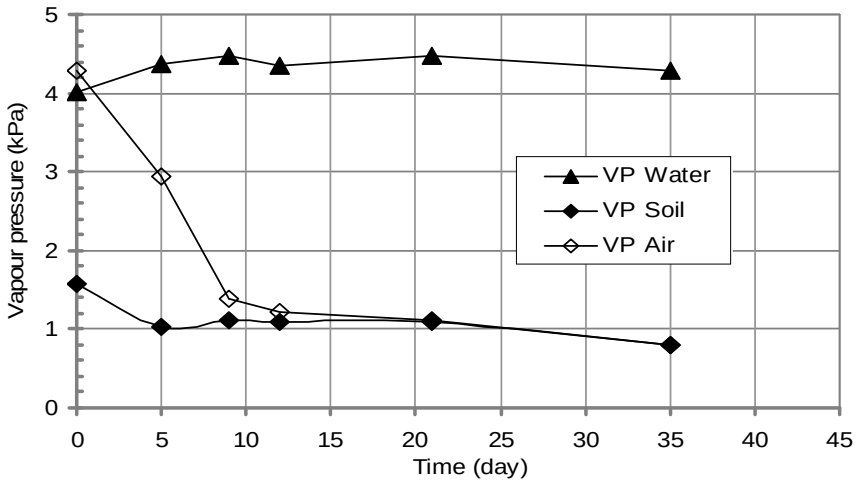

Figure 6.6 Vapor pressure versus time for Column A of Beaver Creek sand estimated using the new proposed equation (i.e., Eq. 3.83).

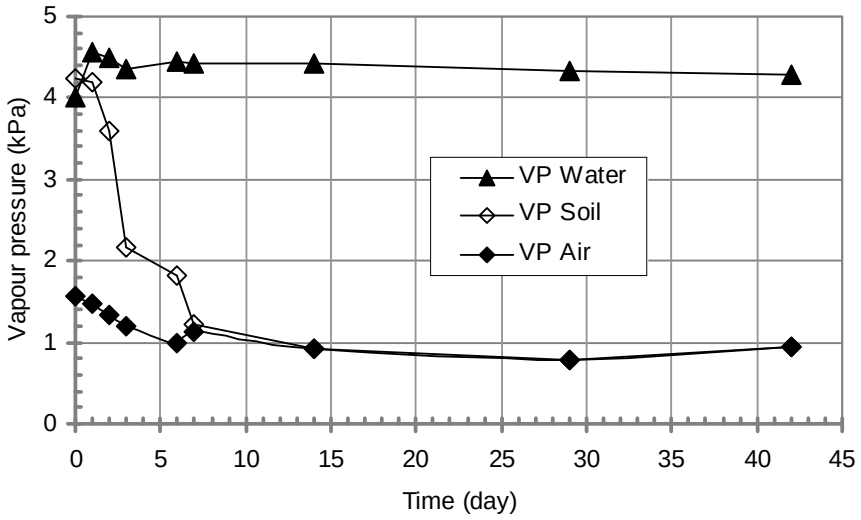

Figure 6.7 Vapor pressure versus time for Column B of Beaver Creek sand estimated using the new proposed equation (i.e., Eq. 3.83).

6.2.1.2 Verification Using the Soil Dataset by Bruch (1993)

The soil datasets measured by Bruch (1993) include the soil columns for the Beaver Creek sand, Processed silt and Natural silt. The measured data and the calculated results of the relative humidity are provided in Tables 6.4, 6.5 and 6.6. Similarly, equation (3.80) gave the total suction at the point of evaporation-rate reduction of 7 kPa, 62 kPa and 116 kPa for Beaver Creek sand, Processed silt and Natural silt, respectively. The corresponding water

contents of 11, 10 and 9 percent (or 18, 15 and 14 percent in volumetric water contents, respectively) were generated from the SWCCs, respectively. The relative humidity was predicted by the new set of the proposed equations (3.82), (3.83) and (3.84). The results of the predicted relative humidity for the soil columns of the Beaver Creek sand, Processed silt and Natural silt are presented in Figures 6.8, 6.9 and 6.10, respectively. The relative humidity obtained by the proposed equations appears to be consistent with the reduction of the relative evaporation as shown in Figure 5.36. As expected, the predicted results showed a decrease in the relative humidity with an increase in the total suction. These results were obtained from the measured water content at a depth of 0 – 1 cm using the SWCCs. The relative humidity begins to decline at a total suction of approximately 7 kPa, 62 kPa and 116 kPa for the Beaver Creek sand, Processed silt and Natural silt, respectively. These values are much lower than the total suction value of 3,000 kPa suggested by Wilson (1990).

Figures 6.11, 6.12 and 6.13 shows that the vapour pressure of the soil calculated by Eq. (3.83) for the soil columns of the Beaver Creek sand, Processed silt and Natural silt gradually changes with time. The calculated vapour pressures are consistent with the decrease in relative humidity at the soil surface as the total suction increases as shown in Figures 6.8, 6.9 and 6.10. The lower vapour pressure of the ambient air provides the gradient for evaporation. The decrease in the vapour pressure in the sand continues until the total suction (i.e., water potential), in the soil is in equilibrium with the water potential of the air. As a result, evaporation seemed to be ceased.

The calculated values of the soil surface resistance for the soil columns vary from a value close to zero at or near the saturated surface and go to values of approximately 994 s/m, 1,575 s/m and 634 s/m for the Beaver Creek sand, Processed silt and Natural silt, respectively as the soils dry. The calculated values of soil surface resistance are consistent with soil surface resistance values measured in the research literature. This observed behaviour once again accounts for the existence of the surface resistance to water vapour diffusion from the depth of 1 cm to the soil-atmosphere interface.

Table 6.4 Summary of calculations of the relative humidity for the soil column drying of the Beaver Creek sand using the set of the proposed equations.

MEASURED DATA					CALCULATED DATA			
Relative humidity of air	Temperature of air (^{o} C)	Temperature of water (^{o} C)	Temperature of soil surface (^{o} C)	Water content at 0 – 1 cm	Total suction from SWCC (kPa)	Soil moisture availability factor using Eq. (3.82)	Vapour pressure at soil surface using Eq. (3.83) (kPa)	Relative humidity using Eq. (3.84)
0.131	37.1	32.0	29.0	0.124	8	1.0000	4.01	1.00
0.136	35.5	31.6	29.2	0.010	9	0.9201	3.79	0.94
0.140	36.0	31.8	30.0	0.098	9	0.8952	3.89	0.92
0.118	35.8	31.8	28.6	0.083	13	0.6819	2.89	0.74
0.139	36.0	31.8	29.2	0.052	79	0.1820	1.41	0.35
0.116	36.5	31.8	30.6	0.039	328	0.0692	0.96	0.22
0.115	37.0	32.2	32.4	0.031	1,041	0.0301	0.85	0.17
0.113	36.8	31.8	33.6	0.019	10,291	0.0042	0.72	0.14
0.122	36.9	32.4	33.8	0.016	20,064	0.0020	0.77	0.15
0.122	36.8	32.2	34.2	0.020	8,309	0.0053	0.78	0.15
0.104	36.8	32.0	33.8	0.018	12,021	0.0036	0.66	0.13
0.108	36.8	32.5	34.6	0.016	19,632	0.0021	0.68	0.12
0.117	36.9	32.5	35.4	0.012	45,724	0.0007	0.73	0.13

Table 6.5 Summary of calculations of the relative humidity for the soil column drying of the Processed silt using the set of the proposed equations.

MEASURED DATA					CALCULATED DATA			
Relative humidity of air	Temperature of air (^{o} C)	Temperature of water (^{o} C)	Temperature of soil surface (^{o} C)	Water content at 0 – 1 cm	Total suction from SWCC (kPa)	Soil moisture availability factor using Eq. (3.82)	Vapour pressure at soil surface using Eq. (3.83) (kPa)	Relative humidity using Eq. (3.84)
0.131	36.3	32.6	30.9	0.235	26	1.0000	4.47	1.00
0.136	35.2	31.0	29.0	0.207	30	1.0000	4.01	1.00
0.118	35.5	31.0	29.8	0.161	39	1.0000	4.19	1.00
0.116	35.6	32.2	31.9	0.049	115	0.2909	1.85	0.39
0.113	36.0	32.3	32.7	0.031	195	0.0570	0.91	0.18
0.122	35.6	32.7	32.6	0.032	177	0.0669	0.99	0.20
0.122	36.3	32.5	33.4	0.026	249	0.0316	0.88	0.17
0.104	35.7	32.2	33.3	0.011	1,465	0.0010	0.61	0.12
0.108	36.2	32.5	34.3	0.009	1,935	0.0006	0.65	0.12
0.117	36.9	32.3	34.6	0.006	5,501	0.0001	0.73	0.13

Table 6.6 Summary of calculations of the relative humidity for the soil column drying of the Natural silt using the set of the proposed equations.

MEASURED DATA					CALCULATED DATA			
Relative humidity of air	Temperature of air (^{o} C)	Temperature of water (^{o} C)	Temperature of soil surface (^{o} C)	Water content at 0 – 1cm	Total suction from SWCC (kPa)	Soil moisture availability factor using Eq. (3.82)	Vapour pressure at soil surface using Eq. (3.83) (kPa)	Relative humidity using Eq. (3.84)
0.128	35.9	32.6	31.3	0.182	48	1.0000	4.57	1.00
0.116	36.1	32.5	30.7	0.180	49	1.0000	4.42	1.00
0.139	36.0	32.5	30.7	0.181	49	1.0000	4.42	1.00
0.118	36.2	32.9	30.7	0.182	49	1.0000	4.42	1.00
0.135	36.3	33.4	30.9	0.172	53	1.0000	4.47	1.00
0.113	36.2	33.1	30.7	0.170	54	1.0000	4.42	1.00
0.116	36.7	33.1	30.9	0.169	55	1.0000	4.47	1.00
0.131	36.2	33.3	31.2	0.155	62	1.0000	4.54	1.00
0.120	36.3	33.4	31.1	0.163	58	1.0000	4.52	1.00
0.104	36.3	33.1	31.0	0.160	59	1.0000	4.49	1.00
0.094	36.5	32.9	31.1	0.134	75	1.0000	4.52	1.00
0.082	36.8	33.0	33.6	0.025	1,749	0.0345	0.67	0.13
0.082	36.5	32.8	34.8	0.015	7,890	0.0046	0.52	0.09

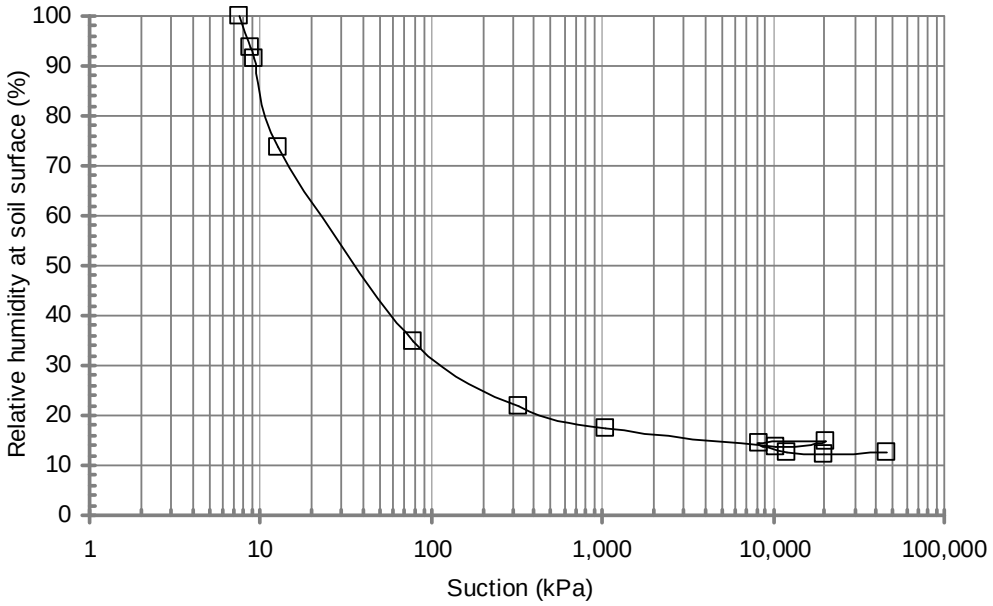

Figure 6.8 Relative humidity at a depth of 0 – 1 cm for the soil column of Beaver Creek sand estimated using the new set of the proposed equations (i.e., Eqs. 3.82, 3.83 and 3.84) and the measured water contents.

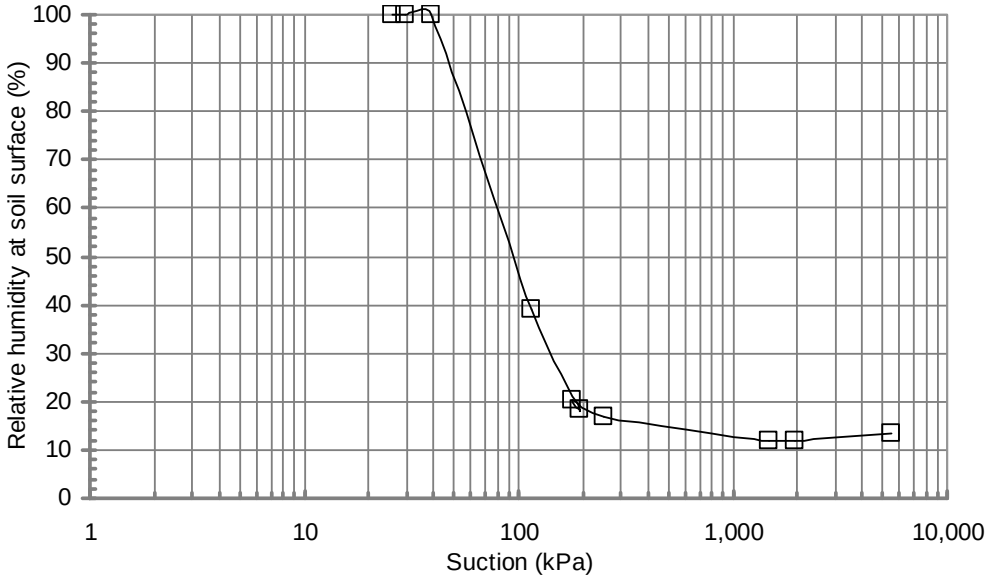

Figure 6.9 Relative humidity at a depth of 0 – 1 cm for the soil column of Processed silt estimated using the new set of the proposed equations (i.e., Eqs. 3.82, 3.83 and 3.84) and the measured water content.

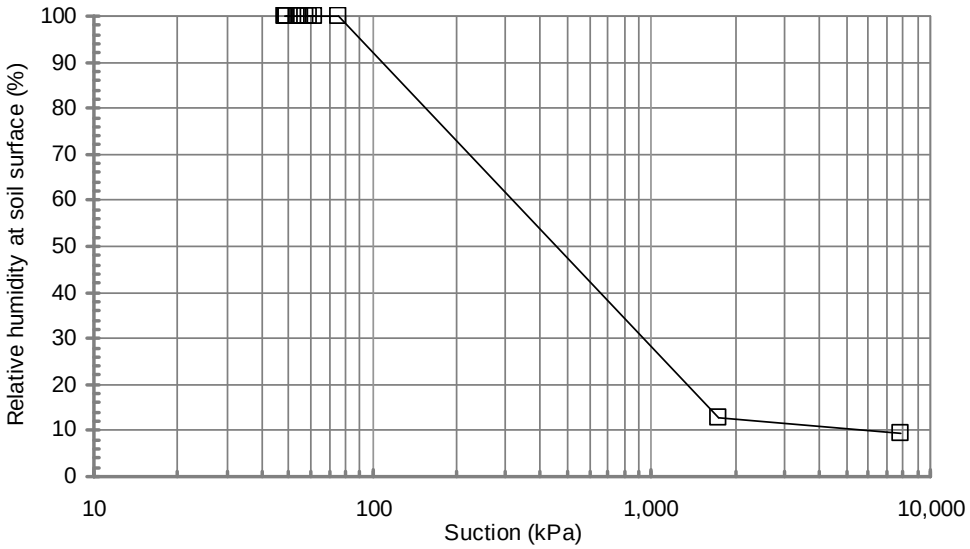

Figure 6.10 Relative humidity at a depth of 0 – 1 cm for the soil column of Natural silt estimated using the new set of the proposed equations (i.e., Eqs. 3.82, 3.83 and 3.84) and the measured water content.

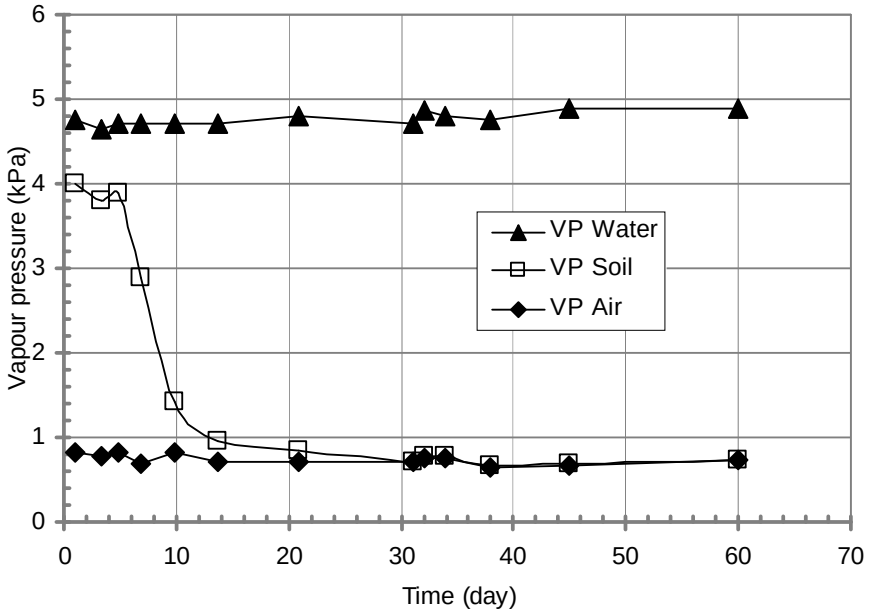

Figure 6.11 Vapor pressure versus time for the soil column of the Beaver Creek sand estimated using the new proposed equation (i.e., Eq. 3.83).

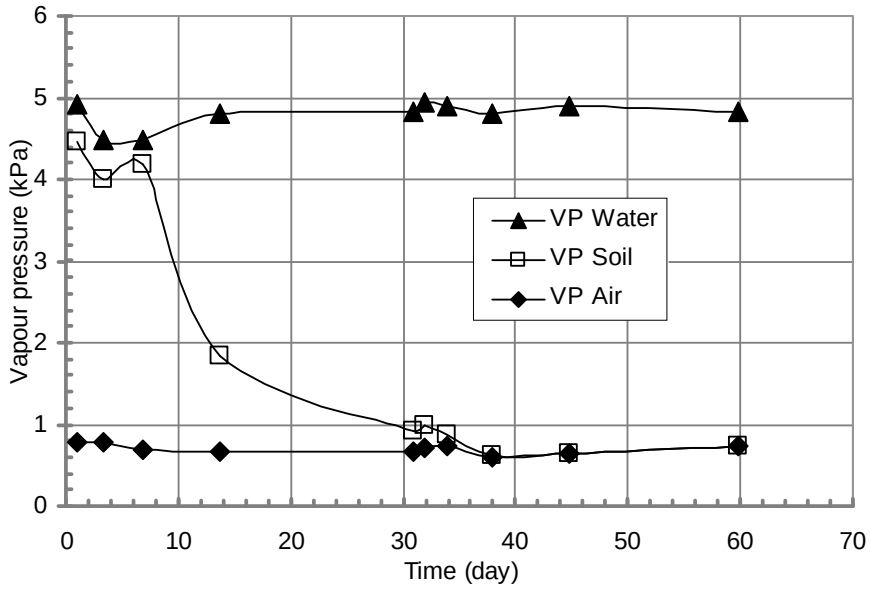

Figure 6.12 Vapor pressure versus time for the soil column of the Processed silt estimated using the new proposed equation (i.e., Eq. 3.83).

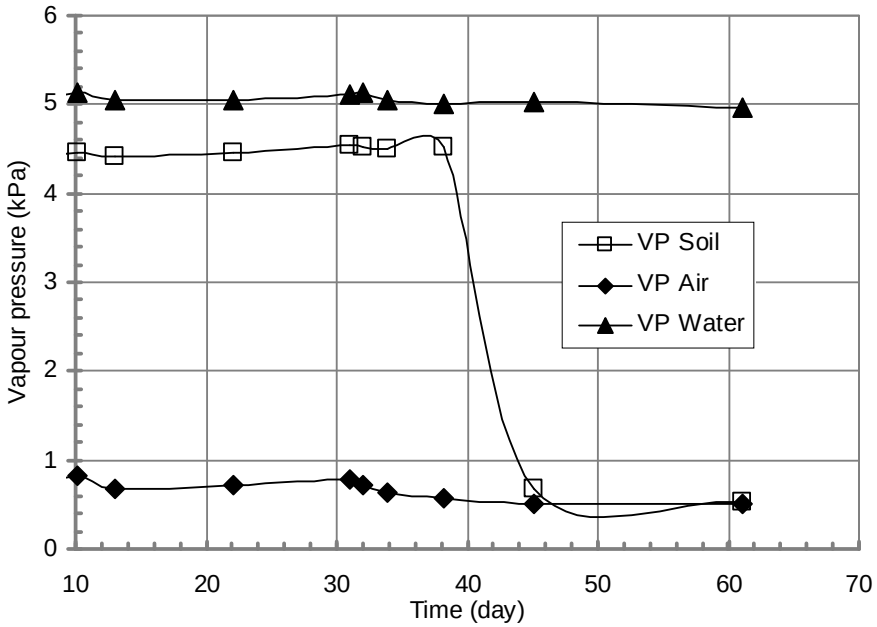

Figure 6.13 Vapor pressure versus time for the soil column of the Natural silt estimated using the new proposed equation (i.e., Eq. 3.83).

6.2.1.3 Verification Using the Soil Dataset by Yanful and Choo (1997)

The soil datasets measured by Yanful and Choo (1997) include the soil columns for the coarse sand, fine sand and topsoil. The measured data and the calculated results are provided in Tables 6.7 and 6.8.

Equation (3.80) yielded a total suction value at the point of evaporation-rate reduction of 1.5 kPa and 3.7 kPa for the coarse sand and fine sand, respectively. The corresponding volumetric water content of 15 and 14 percent was generated from the SWCCs, respectively. The relative humidity was predicted using the new set of the proposed equations (3.82), (3.83) and (3.84). The results of the predicted relative humidity for the soil columns of the coarse sand and fine sand are presented in Figures 6.14 and 6.15, respectively. The relative humidity obtained by the proposed equations appears to be consistent with the reduction of the relative evaporation as shown in Figure 5.39. As expected, the predicted results showed a decrease in the relative humidity with an increase in the total suction which was converted from the measured water content at a depth of 0 – 1 cm using the SWCCs. In fact, the relative humidity began to decline at a total suction of approximately 1.5 kPa and 3.7 kPa for the coarse sand and fine sand, respectively which is much lower than the value of 3,000 kPa.

Figures 6.16 and 6.17 shows that the vapour pressure of the soil calculated by Eq. (3.83) for the soil columns of the coarse sand and fine sand gradually changes with time. The calculated vapour pressures are consistent with decrease in the relative humidity at the soil surface as the total suction increases as shown in Figures 6.14 and 6.15. The lower vapour pressure of the ambient air provides the gradient for evaporation. The decrease in the vapour pressure in the sand continued until the water potential in the soil was in equilibrium with the water potential in the air. As a result, the evaporation appeared to be ceased.

The calculated values of soil surface resistance for sand columns vary from a value close to zero at or near the saturated surface to the values of approximately 390 s/m and 330 s/m for coarse sand and fine sand, respectively as the soils dry out. This observed behaviour is again attributable to the

surface resistance to water vapour diffusion from some depth to the soil-atmosphere interface.

Table 6.7 Summary of calculations of the relative humidity for the soil column drying of the Coarse sand using the set of the proposed equations.

MEASURED DATA					CALCULATED DATA			
Relative humidity of air	Temperature of air (^{o} C)	Temperature of water (^{o} C)	Temperature of soil surface (^{o} C)	Volumetric water content at 0 – 1cm	Total suction from SWCC (kPa)	Soil moisture availability factor using Eq. (3.82)	Vapour pressure at soil surface using Eq. (3.83) (kPa)	Relative humidity using Eq. (3.84)
0.37	23.5	24.2	22.56	0.173	1	1.0000	2.74	1.00
0.50	23.1	24.2	22.03	0.146	1	0.9961	2.64	1.00
0.52	23.4	24.2	22.12	0.135	1	0.9496	2.60	0.98
0.51	23.1	24.2	23.04	0.127	1	0.8919	2.67	0.95
0.70	24.4	24.2	23.98	0.112	2	0.7282	2.75	0.92
0.70	26.0	24.2	25.55	0.083	2	0.3388	2.67	0.82
0.54	24.2	24.2	26.01	0.067	3	0.1701	1.93	0.57
0.51	24.2	24.2	26.20	0.053	4	0.0786	1.70	0.50
0.72	24.6	24.2	26.26	0.047	4	0.0513	2.29	0.67

Table 6.8 Summary of calculations of the relative humidity for the soil column drying of the Fine sand using the set of the proposed equations.

MEASURED DATA					CALCULATED DATA			
Relative humidity of air	Temperature of air (^{o} C)	Temperature of water (^{o} C)	Temperature of soil surface (^{o} C)	Volumetric water content at 0 – 1cm	Total suction from SWCC (kPa)	Soil moisture availability factor using Eq. (3.82)	Vapour pressure at soil surface using Eq. (3.83) (kPa)	Relative humidity using Eq. (3.84)
0.37	23.5	24.2	24.86	0.195	3	1.0000	3.14	1.00
0.55	23.1	24.2	22.58	0.179	3	1.0000	2.74	1.00
0.53	23.4	24.2	22.41	0.163	3	1.0000	2.71	1.00
0.53	23.1	24.2	23.58	0.149	4	1.0000	2.91	1.00
0.71	24.4	24.2	24.23	0.134	4	0.9908	3.02	1.00
0.54	24.4	24.2	24.81	0.069	7	0.2350	2.00	0.64
0.68	24.3	24.2	25.27	0.048	9	0.0674	2.15	0.67
0.55	24.2	24.2	25.80	0.052	8	0.0917	1.82	0.55
0.52	24.2	24.2	25.85	0.044	9	0.0513	1.66	0.50
0.72	24.6	24.2	26.18	0.042	10	0.0417	2.27	0.67

Figure 6.14 Relative humidity at a depth of 0 – 1 cm for the soil column of the coarse sand estimated using the new set of the proposed equations (i.e., Eqs. 3.82, 3.83 and 3.84) and the measured volumetric water content.

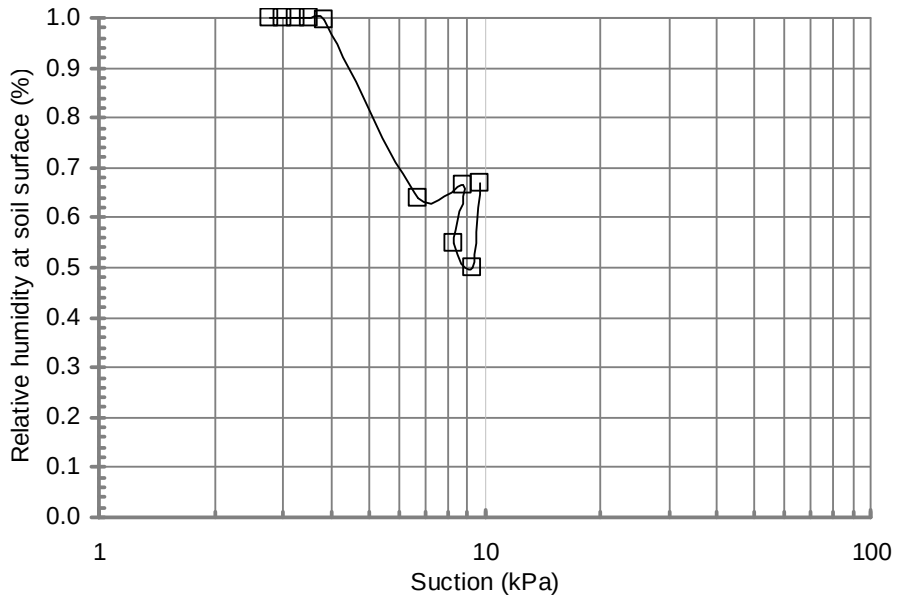

Figure 6.15 Relative humidity at a depth of 0 – 1 cm for the soil column of the fine sand estimated using the new set of the proposed equations (i.e., Eqs. 3.82, 3.83 and 3.84) and the measured volumetric water content.

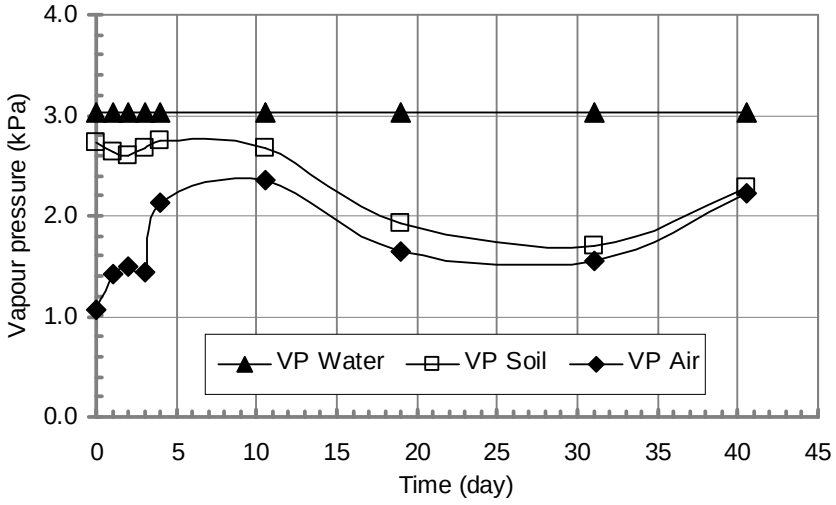

Figure 6.16 Vapor pressure versus time for the soil column of the coarse sand estimated using the new proposed equation (i.e., Eq. 3.83).

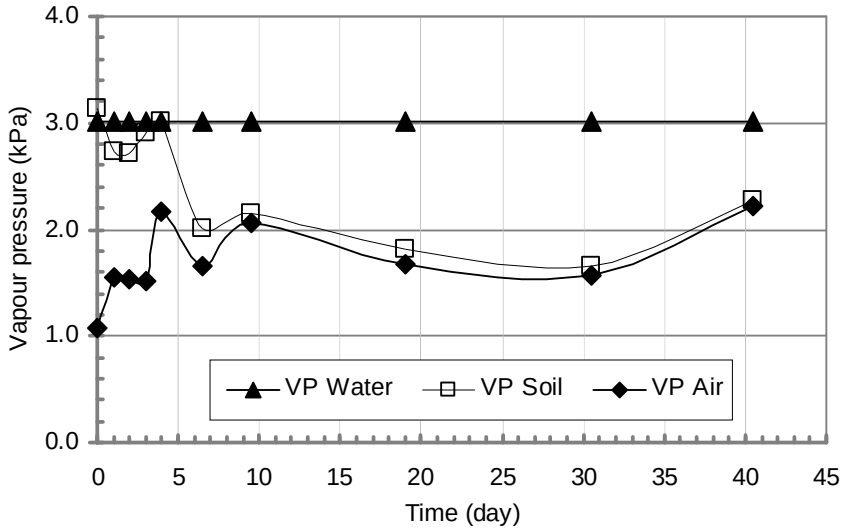

Figure 6.17 Vapor pressure versus time for the soil column of the fine sand estimated using the new proposed equation (i.e., Eq. 3.83).

6.2.1.4 Verification Using the Soil Dataset by Dunmola (2012)

The soil datasets by Dunmola (2012) include the thin soil sections and soil columns of non-saline silt. The drying tests for the soil columns of non-saline silt were conducted under simulated wind condition (e.g., high evaporative demand) and without wind simulation (e.g., low evaporative demand). Verification is presented for both ambient conditions.

a. For Thin Soil Sections of Non-Saline Silt

The air temperature, soil temperature and water temperature are assumed to be 22.5 ^{o}C and the average relative humidity of the ambient air to be 25 percent. Summary of the calculated results of the relative humidity at the soil surface are provided in Table 6.9.

The suction at the point of evaporation-rate reduction for the thin soil sections is approximately 3,000 kPa (Wilson, 1990). The corresponding water content was about 2 percent as calculated from the soil-water characteristic curve for the non-saline silt. A summary of calculations of the relative humidity at the soil surface for Replicate No. 3 is typically presented in Table 6.9. Calculations of the relative humidity for the other two replicates are presented in Appendix F. Comparisons of the relative humidity predicted using the Lord Kelvin's formula and the newly proposed equation (i.e., Eq. 3.84) are shown in Figure 6.18. As expected, the results show that the predicted relative humidity agrees well with the predicted data by the Lord Kelvin's formula. Moreover, the maximum value of the soil surface resistance for the thin soil sections calculated using Eq. (3.86) is approximately 16 s/m at the dry soil surface. This result is attributed to the negligible distance over which water vapour must travel to the soil-atmosphere interface. In other words, the evaporating front is located at the soil surface where the vapour pressure in the air adjacent to the evaporating front is in equilibrium with the liquid water in the soil pores during the drying process. The soil surface resistance should be ignored. It is concluded that the proposed equation for relative humidity (i.e., Eq. 3.84) is acceptable for the thin soil sections.

Table 6.9 Summary of calculations of the relative humidity for non-saline silt drying replicate No.3 using the Lord Kelvin's formula and the proposed equation (3.84).

Relative humidity using Lord Kelvin's formula	Total suction from the relative humidity (kPa)	Water content at soil surface from SWCC	Soil moisture availability factor using Eq. (3.82)	Vapour pressure at soil surface using Eq. (3.83) (kPa)	Relative humidity using Eq. (3.84)
1.00	461	0.029	1.0000	2.73	1.00
1.00	478	0.028	1.0000	2.73	1.00
1.00	498	0.028	1.0000	2.73	1.00
1.00	516	0.028	1.0000	2.73	1.00
1.00	535	0.028	1.0000	2.73	1.00
1.00	553	0.028	1.0000	2.73	1.00
0.99	1,016	0.026	1.0000	2.73	1.00
0.99	1,035	0.026	1.0000	2.73	1.00
0.99	1,946	0.023	1.0000	2.73	1.00
0.98	2,862	0.022	1.0000	2.73	1.00
0.96	5,155	0.020	0.9978	2.72	1.00
0.74	40,566	0.012	0.4157	1.53	0.56
0.42	117,552	0.008	0.1141	0.91	0.34
0.42	119,701	0.008	0.1107	0.91	0.33
0.36	137,871	0.007	0.0866	0.86	0.31
0.34	147,977	0.007	0.0759	0.84	0.31
0.34	146,737	0.007	0.0771	0.84	0.31
0.43	116,727	0.008	0.1154	0.92	0.34
0.34	145,558	0.007	0.0783	0.84	0.31
0.32	154,889	0.007	0.0695	0.82	0.30
0.30	164,915	0.007	0.0613	0.81	0.30
0.31	162,055	0.007	0.0635	0.81	0.30
0.30	165,038	0.007	0.0612	0.81	0.30
0.33	151,060	0.007	0.0730	0.83	0.30

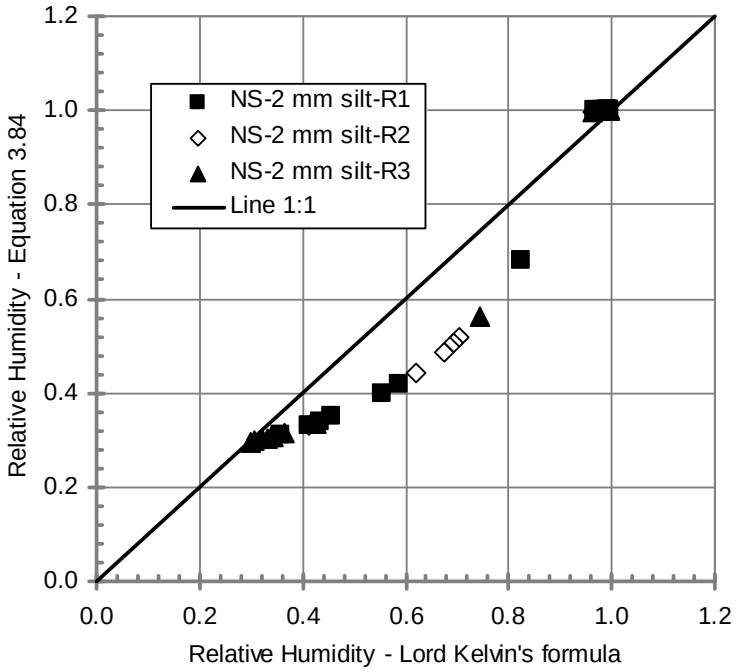

Figure 6.18 Relative humidity at soil surface estimated using the Lord Kelvin's formula and the proposed equation (i.e., Eq. 3.84) for three replicates of non-saline silt.

b. For Soil Columns of Non-Saline Silt

The actual evaporation rate from the soil columns in this case was calculated using three proposed values for the suction at the point of evaporation-rate reduction. These values of suction at evaporation-rate reduction point were 3,000 kPa, the residual suction of 22 kPa and a suction of 16 kPa which was obtained using Eq. (3.80). It is noted that a value for the "*a*" variable used in Eq. (3.80) is 0.75 for the silt soil. The water content at the point of evaporation-rate reduction generated from the SWCC of the non-saline silt (shown in Figure 6.19). Water content of 2, 4 and 9 percent correspond to suction values of 3,000 kPa, 22 kPa and 16 kPa, respectively. Calculations of the relative evaporation (*AE/PE*) using these values of the water content are hereafter referred to as RE–Cal. 1, RE–Cal. 2 and RE–Cal. 3 for the water content equal to 2, 4, and 9 percent, respectively. The vapour pressure at the soil surface was calculated using Eq. (3.83). The soil surface resistance was calculated using Eq. (3.86). The calculated results for the non-saline silt (i.e.,

Replicate No. 3) under simulated wind (e.g., high evaporative demand) are typically presented in Figure 6.20. The calculated results for the soil column of the non-saline silt without wind simulation (e.g., low evaporative demand) are presented in Figure 6.21. The other calculated results for Replicates No. 1 and No. 2 under simulated wind are presented in Appendix F.

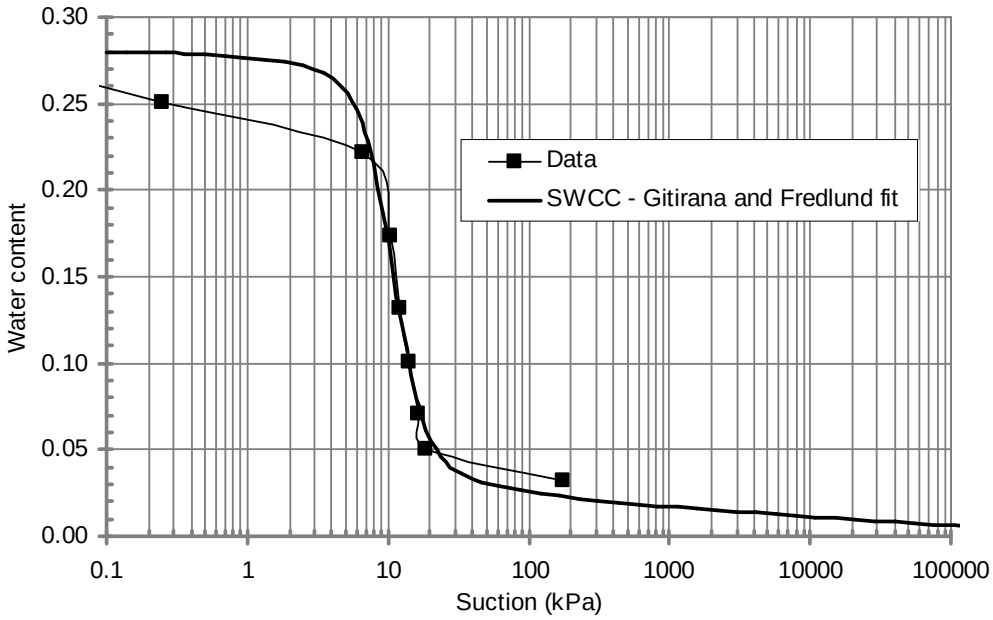

Figure 6.19 Data and soil-water characteristic curve of non-saline silt (after Dunmola, 2012).

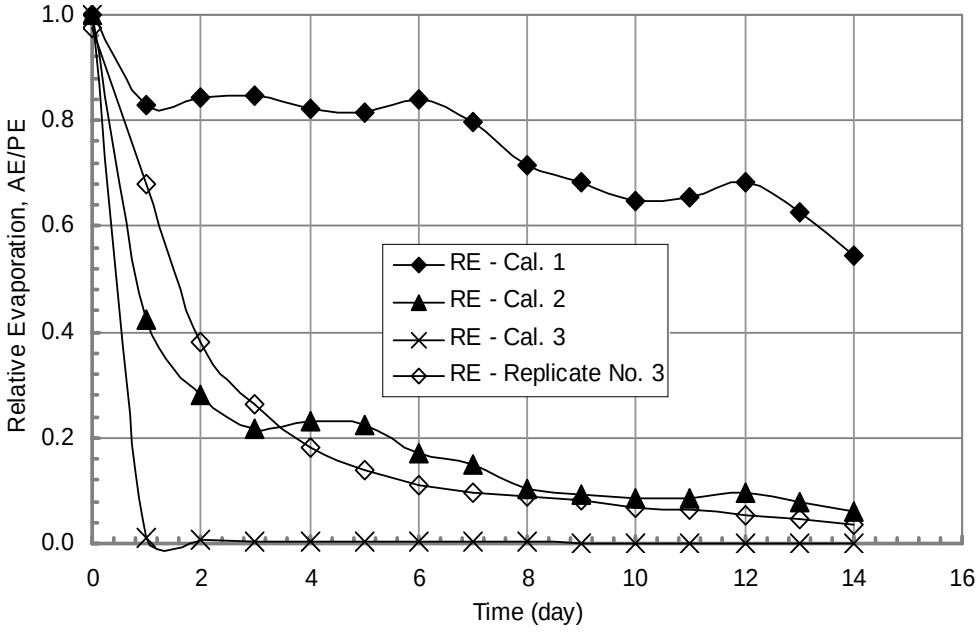

Figure 6.20 Typical calculation of the Relative Evaporation, *AE/PE* using the suction at evaporation-rate reduction point under simulated wind – Replicate No. 3.

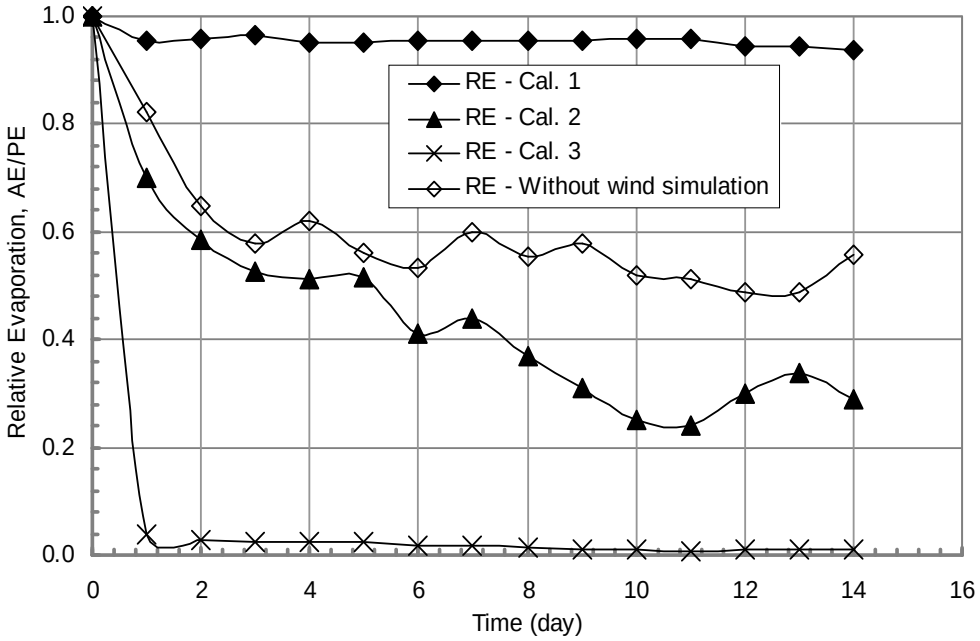

Figure 6.21 Typical calculation of the Relative Evaporation, *AE/PE* using the suction at evaporation-rate reduction point without wind simulation.

Both figures 6.20 and 6.21 show the calculated relative evaporation using the water content at 3,000 kPa and 16 kPa (i.e., in between air-entry value and residual suction) do not agree with the measured relative evaporation. In fact, RE– Cal. 1 gives much higher values than the measured evaporation data. In contrast, RE–Cal. 3 gives much lower values than the measured data. Meanwhile, these figures show reasonably good agreement between the calculated and measured relative evaporation when using a water content of 4 percent as a reference point which corresponds to the residual suction (i.e., RE–Cal. 2). The calculated results, RE–Cal. 2 indicate that the evaporation actually begins to decline at the point when residual suction in this case. There appears to be some difference between the residual suction and the suction value obtained using Eq. (3.80) (i.e., 22 kPa compared to 16 kPa). However, there is a large difference between the water contents corresponding to these suctions (i.e., 4 percent compared to 9 percent). It follows that the vapour pressure obtained using Eq. (3.83) with the water content of 9 percent is smaller than that corresponding to a water content of 4 percent (as summarized in Table 6.10) and hence there is a smaller relative evaporation. The reduced evaporation rate may be attributed to variations in water content at a depth of 0 – 2 mm applied in Eq. (3.83). The surface of the soil column may be drier than at the depth of 1 cm. This difference would be corrected if the variation in water content at a depth of 1 cm was known as defined for Eq. (3.83).

The results of the drying tests for 10 cm soil columns by Dunmola (2012) once again demonstrate that the evaporative fluxes from the soil columns begins to decline as total suction reaches the suction close to residual suction of material. This finding appears to be different from the conclusion arrived by Wilson (1990). The suction at the point of evaporation-rate reduction appears to be dependent on the soil type or soil texture through unsaturated soil properties (i.e., air-entry value and residual suction). The total suction of 3,000 kPa applies only for the case of a thin soil layer.

Table 6.10 Summary of calculation of evaporation rate for non-saline silt – replicate No. 3.

Time (days)	Measured RE = *AE/PE*	R.H. Air	Air Temp (^{o} C)	Soil moisture content at 0 – 2 mm (%)	Vapour pressure for RE–Cal. 1 (kPa)	Vapour pressure for RE– Cal. 2 (kPa)	Vapour pressure for RE–Cal. 3 (kPa)	RE–Cal. 1	RE–Cal. 2	RE–Cal. 3
0	0.974	0.63	23.3	27.1	2.86	2.86	2.86	1.00	1.00	1.00
1	0.681	0.67	22.5	2.7	2.72	2.36	1.87	0.83	0.42	0.01
2	0.379	0.56	21.8	2.3	2.61	1.90	1.49	0.84	0.28	0.01
3	0.263	0.52	22.1	2.1	2.66	1.77	1.42	0.85	0.22	0.00
4	0.181	0.62	22.3	2.1	2.70	2.01	1.69	0.82	0.23	0.00
5	0.138	0.63	22.2	2.1	2.67	2.00	1.69	0.82	0.22	0.00
6	0.112	0.50	22.7	1.9	2.74	1.70	1.40	0.84	0.17	0.00
7	0.095	0.58	21.7	1.9	2.56	1.74	1.51	0.80	0.15	0.00
8	0.091	0.50	22.1	1.7	2.48	1.53	1.35	0.72	0.10	0.00
9	0.082	0.52	22.4	1.6	2.48	1.57	1.41	0.68	0.09	0.00
10	0.069	0.41	22.2	1.5	2.30	1.27	1.09	0.65	0.08	0.00
11	0.065	0.36	22.5	1.5	2.30	1.17	0.99	0.66	0.09	0.00
12	0.052	0.57	23.6	1.6	2.69	1.82	1.66	0.68	0.09	0.00
13	0.047	0.61	22.8	1.6	2.54	1.82	1.69	0.63	0.08	0.00
14	0.034	0.62	22.6	1.5	2.42	1.80	1.70	0.55	0.06	0.00

6.2.2 Verification Using the Data from the Laboratory Program

The current laboratory program and testing results were presented in Chapter 4 and 5, respectively. This section presents the verification of the theory described in Chapter 3 on the thin soil layer drying (i.e., 1 mm thick) and thick soil drying (i.e., 30 mm thick) for the Ottawa sand and Devon silt.

The water content at the total suction of 3,000 kPa generated from the soil water characteristic curve for the non-saline Ottawa sand is approximately 0.35 percent (see Figure 5.1). The soil water moisture availability factor, vapour pressure and soil surface resistance at the soil surface are calculated using Eq. (3.82), Eq. (3.83) and Eq. (3.86), respectively. A summary of the calculated evaporation for the Ottawa sand in Set 1 is typically provided in Table 6.11.

Table 6.11 Summary of results for thin soil layer drying test of Ottawa sand in Set 1.

Time (hours)	PE (mm/day)	AE (mm/day)	R.H. Air	Air Temp (^{o} C)	Soil moisture content at surface (%)	Soil moisture availability factor .Eq. (3.82)	Vapour pressure. Eq. (3.83) (kPa)	R.H., Eq. (3.84)	Soil surface resistance, Eq. (3.86) (s/m)	AE– Calculated, (mm/day)
21.5	2.89	2.88	0.2	19.5	29.60	1.0000	2.27	1.00	0.0	2.89
43.3	2.54	2.42	0.2	19.5	27.13	1.0000	2.27	1.00	0.0	2.54
62.4	2.38	2.16	0.21	19.4	25.19	1.0000	2.25	1.00	0.0	2.38
82.1	2.34	2.22	0.21	19.4	23.14	1.0000	2.25	1.00	0.0	2.34
108.0	2.30	2.12	0.21	19.4	20.56	1.0000	2.25	1.00	0.0	2.30
130.8	2.42	2.31	0.21	19.6	18.08	1.0000	2.28	1.00	0.0	2.42
152.0	2.36	2.38	0.21	19.4	15.72	1.0000	2.25	1.00	0.0	2.36
174.8	2.51	2.31	0.2	19.6	13.24	1.0000	2.28	1.00	0.0	2.51
200.0	2.65	2.64	0.2	19.8	10.12	1.0000	2.31	1.00	0.0	2.65
219.9	2.53	2.65	0.2	19.6	7.64	1.0000	2.28	1.00	0.1	2.53
241.3	2.57	2.58	0.2	19.6	5.06	1.0000	2.28	1.00	0.6	2.57
268.9	2.66	2.33	0.2	19.4	2.05	1.0000	2.25	1.00	3.7	2.66
295.4	2.59	1.47	0.2	19.6	0.22	0.4582	1.29	0.57	10.8	1.19
316.1	2.78	0.11	0.2	19.6	0.11	0.0466	0.54	0.24	11.5	0.13
338.8	2.62	0.00	0.2	19.6	0.11	0.0466	0.54	0.24	11.5	0.12
359.6	2.65	0.00	0.2	19.6	0.11	0.0466	0.54	0.24	11.5	0.12
379.7	2.74	0.00	0.2	19.6	0.11	0.0466	0.54	0.24	11.5	0.13
401.7	2.61	0.00	0.2	19.6	0.11	0.0466	0.54	0.24	11.5	0.12

Figure 6.22 shows a plot of the potential evaporation rate (PE–Measured) from the water surface, the measured actual evaporation rate (AE–Measured) from the sand surface and the calculated evaporation rate (AE–Calculated) for thin non-saline Ottawa sand in Set 1. The calculated evaporation rate agrees well with the measured evaporation. In addition, the soil surface resistance for this thin soil layer has the maximum value approximately 11 s/m at the dry soil surface.

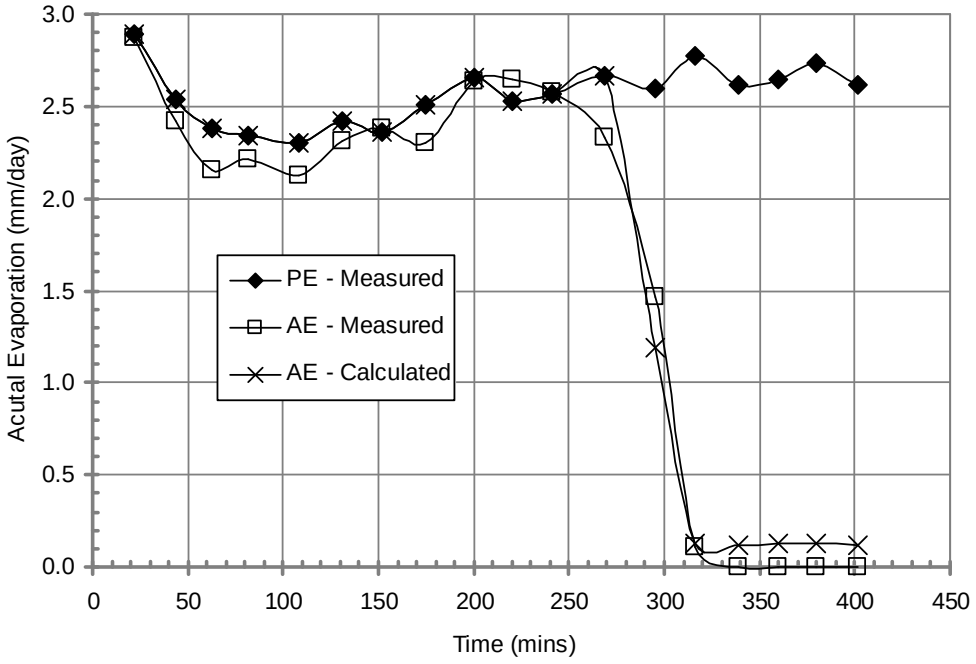

Figure 6.22 Calculated, Actual and Potential evaporation rates for thin non-saline Ottawa sand in Set 1.

Figure 6.23 shows the calculated, actual and potential evaporation rates for the Devon silt in Set 1. The figure shows that the calculated evaporation rate does not agree well with and measured actual evaporation rate. The agreement is not as close as that for the Ottawa sand. There appears to be a slightly offset for the calculated evaporation rate. For example, the calculated evaporation rate breaks or falls below the potential evaporation rate at an earlier time than does the actual evaporation rate of evaporation. It should be noted that the residual suction (i.e., 12,600 kPa) is larger than the value of 3,000 kPa in this particular case. This case is different from the other cases throughout this

chapter in which the residual suction is smaller than the value of 3,000 kPa. In fact, the water content at the evaporation-rate reduction point is assumed to be 19 percent (corresponding to 3,000 kPa) which is larger than the value of 5 percent observed during the drying test of the silt. This results in the computation of a lower vapour pressure at the soil surface and hence a lower rate of evaporation. Moreover, the maximum soil surface resistance of approximately 2,900 s/m computed at the end of the test is too large for the thin soil layer as the soil dries out.

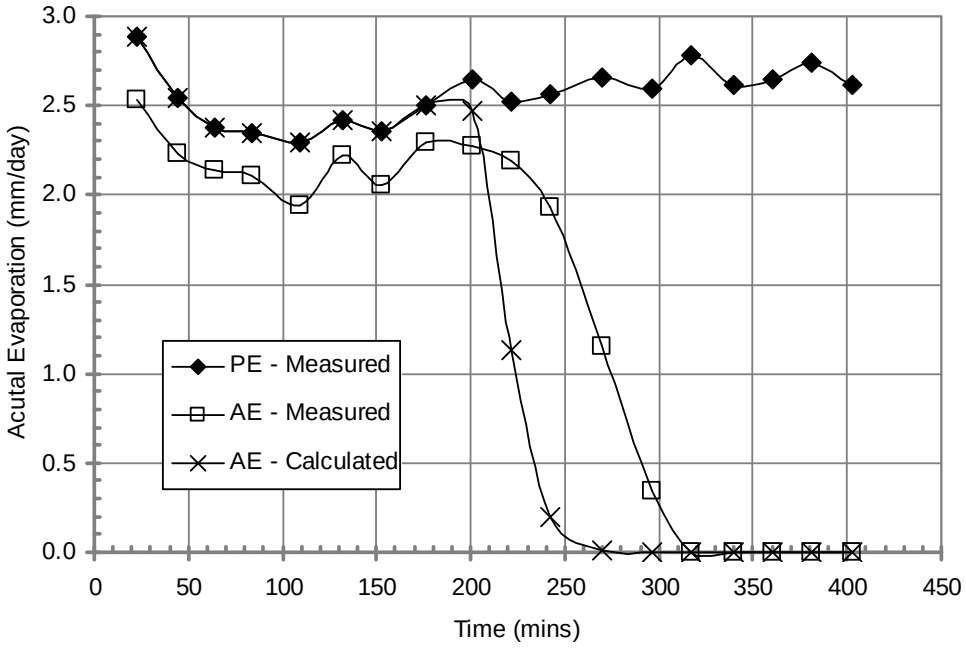

Figure 6.23 Calculated, Actual and Potential evaporation rates for thin non-saline Devon silt in Set 1 with water content at total suction of 3,000 kPa assumed to be a reference point for vapour pressure at the soil surface.

Figure 6.24 shows the calculated, actual and potential evaporation rates for the Devon silt in Set 1 with assumption of water content of 5 percent to be as reference point for soil moisture availability factor or vapour pressure at the soil surface. The figure shows reasonably good agreement between the calculated and measured actual evaporation rates. However, a discrepancy is noted at the end of the test where the soil evaporation goes to zero. For

example, the evaporative fluxes of 0.26 mm/day are computed when the actual evaporation is approximately zero. This discrepancy is attributed to experimental errors associated with the corrected measurement of water content, temperature of the soil, water and air, and relative humidity of the air. Besides, maximum soil surface resistance of approximately 20 s/m computed at the end of the test is reasonable for the thin soil layer as the soil dries out.

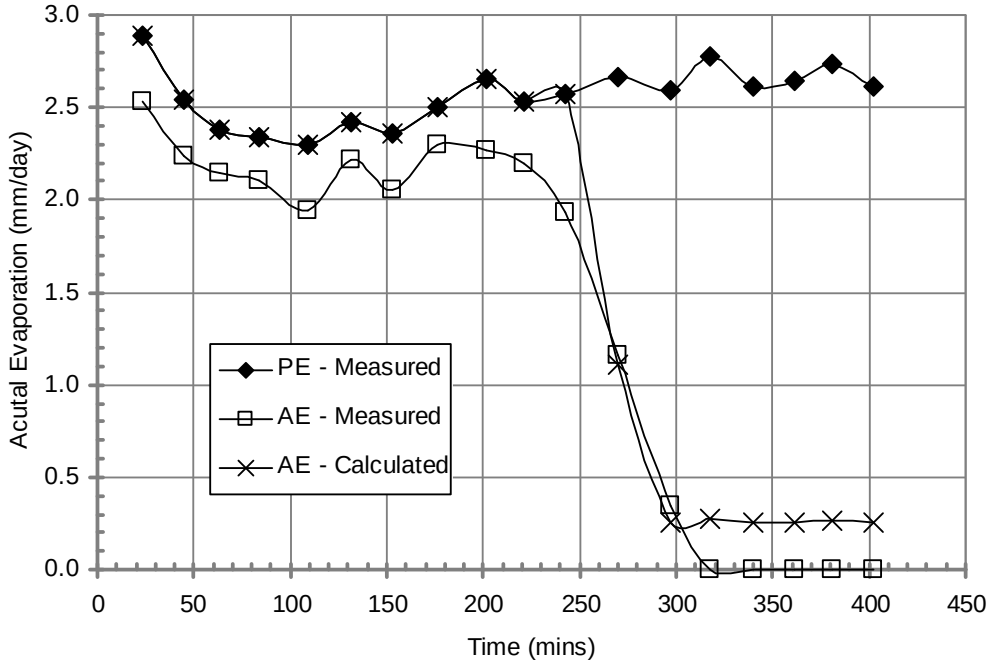

Figure 6.24 Calculated, Actual and Potential evaporation rates for thin non-saline Devon silt in Set 1 with water content at the point of evaporation-rate reduction observed during the drying test.

In addition, a comparison of the relative humidity predicted using the Lord Kelvin's formula and the proposed equation (i.e., Eq. 3.84) is shown in Figure 6.25. As expected, the results show that the predicted relative humidity agrees well with the predicted data by the Lord Kelvin's formula for the thin soil layer drying.

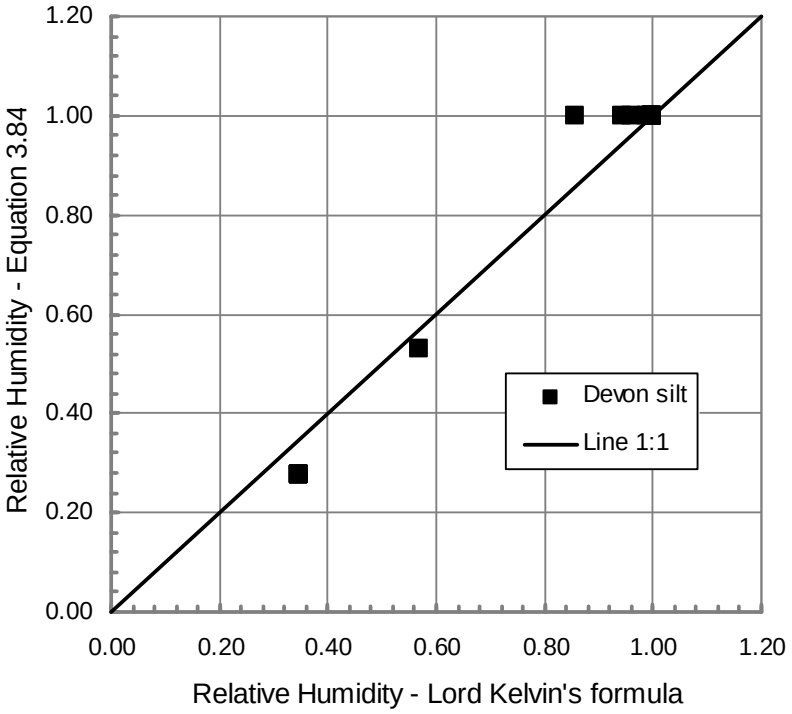

Figure 6.25 Relative humidity at soil surface estimated using the Lord Kelvin's formula and the proposed equation (i.e., Eq. 3.84) for the non-saline Devon silt in Set 1 with water content of 5 percent assumed to be the one at the point of evaporation-rate reduction.

Verification of the thick soil layer drying tests for the Ottawa sand and Devon silt is also presented in this section. The test results of evaporative fluxes along with the soil water content and climatic data were presented in Chapter 5. Theoretically, the suction at evaporation-rate reduction point obtained for both Ottawa sand and Devon silt using Eq. (3.80) is approximately 12 kPa and 4,380 kPa, respectively. The corresponding water content at evaporation-rate reduction point generated from the SWCCs of the Ottawa sand and Devon silt as shown in Figure 6.26 was 7 and 17 percent, respectively. The soil moisture availability factor, vapour pressure and soil surface resistance at the soil surface are calculated using Eq. (3.82), Eq. (3.83) and Eq. (3.86), respectively. The evaporative fluxes for the thick soil layers or soil columns are computed using Eq. (3.69). Since soil water content at the surface was recorded along with the evaporative fluxes, the calculated evaporation rate is conducted in Excel Spreadsheet. It is noted that soil water content used in Eq. (3.82) is

taken at the depth of 1 cm. A summary of the calculated evaporation for the Ottawa sand and Devon silt is provided in Tables 6.12 and 6.13, respectively.

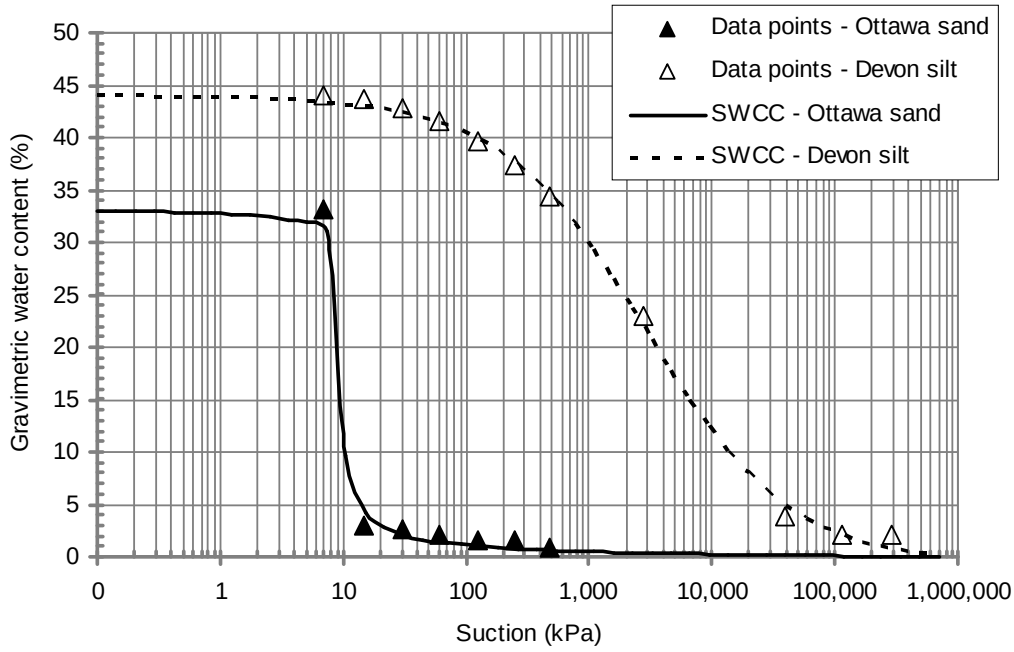

Figure 6.26 Soil-water characteristic curves of Ottawa sand and Devon silt using Fredlund and Xing (1994) method.

Figures 6.27 and 6.28 shows the calculated, actual and potential evaporation rates for the Ottawa sand and Devon silt, respectively. Both figures show reasonably good agreement between the calculated and measured actual evaporation rates. This indicates that the rate of evaporation from the soil columns likely begins to decline at total suction lower than residual suction. The soil surface resistance for the sand and silt varies from zero at high water content to few hundreds as the soil dries out. For example, it varies from zero to 331 s/m and 361 s/m for the Ottawa sand and Devon silt, respectively. It is consistent with the soil surface resistance measured in the research literature. This observed behaviour accounts for the existence of the surface resistance to water vapour diffusion from the depth of 1 cm to the soil-atmosphere interface.

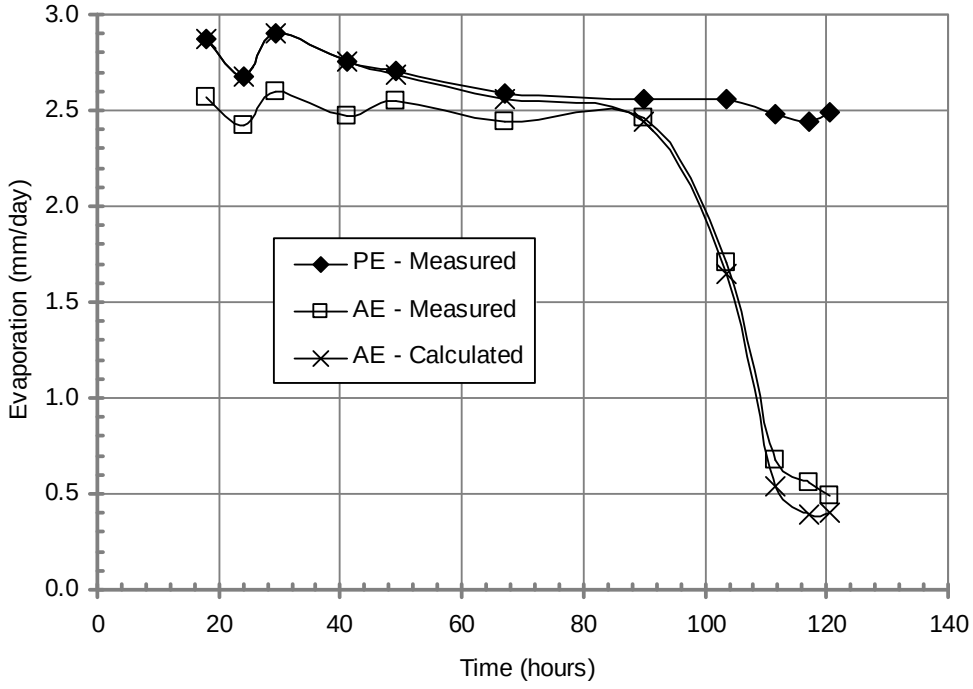

Figure 6.27 Calculated, Actual and Potential evaporation rates for thick non-saline Ottawa sand (i.e., 3 cm thick).

Table 6.12 Summary of results for the thick soil layer drying test for 3 cm-thick Ottawa sand.

Time (hours)	PE (mm/day)	AE (mm/day)	R.H. Air	Air Temp (^{o} C)	Water Temp (^{o} C)	Soil Temp (^{o} C)	Soil moisture content at 0 – 1 cm (%)	Soil moisture availability factor .Eq. (3.82)	Vapour pressure. Eq. (3.83) (kPa)	R.H., Eq. (3.84)	Soil surface resistance, Eq. (3.86) (s/m)	Ratio of f'(u)/f(u)	AE – Calculated, Eq. (3.69) (mm/day)
18	2.87	2.57	0.19	20.4	16.5	16.8	19.16	1.0000	1.91	1.00	0.0	1.00	2.87
24	2.68	2.43	0.21	19.5	16.5	17.5	16.24	1.0000	2.00	1.00	0.0	1.00	2.68
29.5	2.90	2.60	0.20	19.7	16.5	17.2	14.63	1.0000	1.96	1.00	0.1	1.00	2.90
41	2.76	2.47	0.20	19.5	16.5	17.2	11.47	1.0000	1.96	1.00	0.7	1.00	2.76
49	2.70	2.55	0.20	19.7	16.5	17.2	8.37	1.0000	1.96	1.00	4.5	1.01	2.69
67	2.59	2.44	0.20	19.7	16.5	17.1	6.88	1.0000	1.95	1.00	10.7	1.03	2.56
90	2.55	2.46	0.20	19.7	16.5	17.1	4.18	0.9978	1.95	1.00	51.8	1.15	2.44
103.5	2.56	1.70	0.22	19.4	16.5	18.2	2.64	0.4642	1.24	0.59	127.3	1.37	1.65
111.5	2.48	0.68	0.20	19.5	16.5	18.5	1.20	0.0337	0.51	0.24	294.4	1.80	0.54
117	2.44	0.55	0.20	19.7	16.5	20.7	1.00	0.0169	0.49	0.20	331.1	1.89	0.39
120.7	2.49	0.49	0.20	19.7	16.5	20.7	1.00	0.0169	0.49	0.20	331.1	1.91	0.40

Table 6.13 Summary of results for the thick soil layer drying test for 3 cm-thick Devon silt.

Time (hours)	PE (mm/day)	AE (mm/day)	R.H. Air	Air Temp (^{o} C)	Water Temp (^{o} C)	Soil Temp (^{o} C)	Soil moisture content at 0 – 1 cm (%)	Soil moisture availability factor .Eq. (3.82)	Vapour pressure. Eq. (3.83) (kPa)	R.H., Eq. (3.84)	Soil surface resistance, Eq. (3.86) (s/m)	Ratio of f'(u)/f(u)	AE – Calculated, Eq. (3.69) (mm/day)
24	2.65	2.47	0.31	19.9	17.1	17.1	43.00	1.0000	1.95	1.00	0.0	1.00	2.65
48	2.68	2.43	0.27	19.7	17.1	17.1	35.50	1.0000	1.95	1.00	0.0	1.00	2.68
72	2.62	2.32	0.31	19.7	17.1	17.1	28.57	1.0000	1.95	1.00	0.2	1.00	2.62
89	2.48	2.22	0.32	19.5	17.1	17.4	25.34	1.0000	1.99	1.00	0.5	1.00	2.48
120	2.21	1.95	0.24	19.9	17.1	17.4	16.34	0.9926	1.98	0.99	12.7	1.03	2.19
136	2.62	1.99	0.23	19.7	17.1	17.6	11.88	0.6273	1.46	0.73	62.1	1.18	2.09
144	2.65	1.83	0.23	19.9	17.1	17.8	9.28	0.3268	1.03	0.50	156.6	1.46	1.46
160.5	2.53	1.37	0.24	19.9	17.1	17.8	9.33	0.3326	1.05	0.52	153.6	1.44	1.42
165	2.54	1.09	0.24	19.9	17.1	17.9	6.94	0.1278	0.75	0.36	360.8	2.03	0.81
170	2.47	0.98	0.27	19.7	17.1	18.0	7.58	0.1728	0.87	0.42	286.5	1.83	0.95

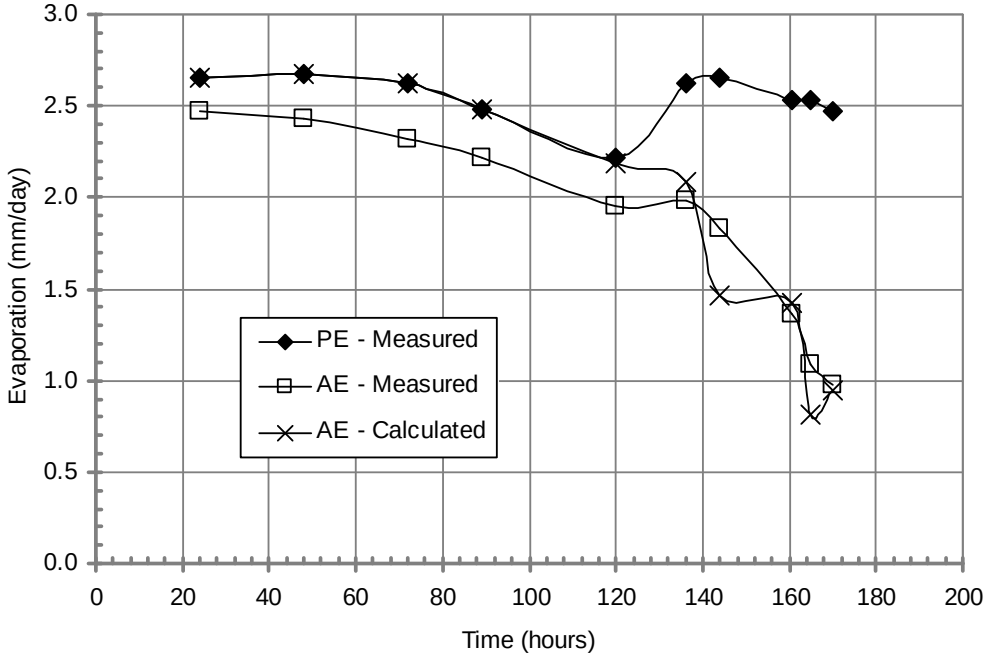

Figure 6.28 Calculated, Actual and Potential evaporation rates for thick non-saline Devon silt (i.e., 3 cm thick).

In summary, the calculated and laboratory results of the thick soil layer drying test demonstrate two basic principles for evaluating evaporation from soil columns. Evaporation begins to decline at the suction value in between air entry value and residual soil suction. Soil surface resistance to diffusion of water vapor is existed at the depth of 0 – 1 cm as soil dries out.

6.3 VERIFICATION OF EFFECT OF OSMOTIC SUCTION ON EVAPORATION

Comparisons between the measured and predicted evaporation rate using the new proposed function of osmotic suction (i.e., Eq. 3.100) described in Chapter 3 are presented in this section. The comparisons are presented in both soil datasets collected from the research literature and the laboratory program. In order to verify the proposed function, each soil dataset must have (or at least have it possible to estimate) the soil-water characteristic curve of the soil

and soil water content (volumetric water content or gravimetric water content) with the ratio of *AE/PE*.

However, the proposed function of osmotic suction which was presented in Chapter 3 is necessary to be verified before its application on calculating evaporation rate or relative evaporation.

6.3.1 Verification of Function of Osmotic Suction

Comparisons between the test results measured from the laboratory testing program and predicted results using the proposed function of osmotic suction (i.e., Eq. 3.100) are presented in this section. The comparisons are presented for osmotic suction measured using the pore-fluid squeezer for the Devon silt mixed with 50 g/l NaCl and Kaolinite mixed with 50 g/l NaCl. Discussions are also presented along with graphs plotting measured and predicted data.

6.3.1.1 Prediction Results for Devon silt mixed with 50 g/l NaCl

Comparisons between the measured and predicted osmotic suction for the Devon silt mixed with 50 g/l NaCl are presented. The initial salt content (i.e., ratio of volume of salt to volume of water) is assumed to be the same as the salt content of the mixture of the sieved Devon silt with 50 g/l NaCl at the beginning of the squeezing test which corresponds to 2.3 percent. The initial water content of the mixture was monitored to be 43 percent at the beginning. The salt content and osmotic suction at various water contents are calculated using Eq. (3.100).

Figure 6.29 shows the calculated and measured osmotic suction along with the soil-water characteristic curve for the mixture of Devon silt and salt. It is shown that the calculated osmotic suction agrees well with the measured osmotic suction.

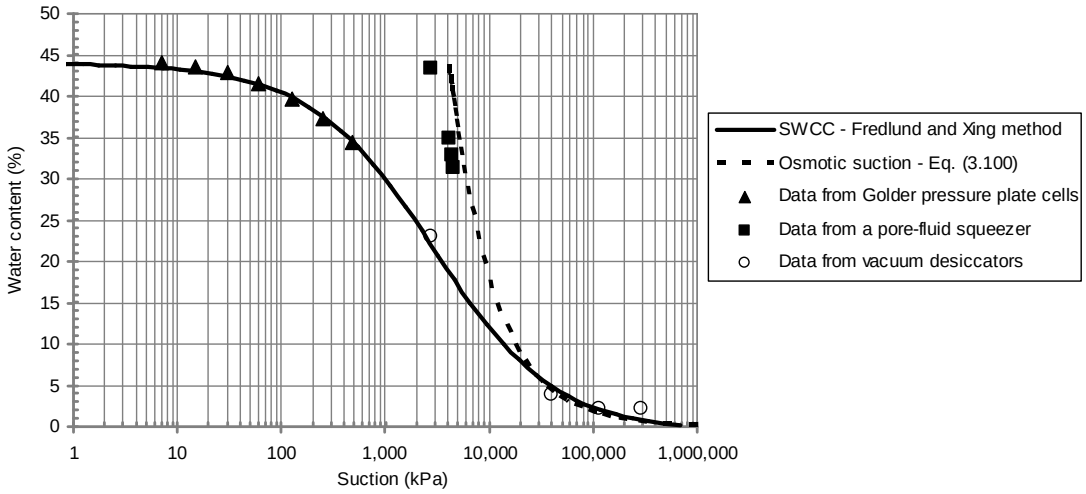

Figure 6.29 Measured and predicted osmotic suction along with the best-fitted soil-water characteristic curve for the Devon silt mixed with 50 g/l NaCl.

6.3.1.2 Prediction Results for Kaolinite mixed with 50 g/l NaCl

Similarly, comparisons between the measured and predicted osmotic suction for the Kaolinite mixed with 50 g/l NaCl are presented. The initial salt content (i.e., ratio of volume of salt to volume of water) is assumed to be the same as the salt content of the mixture of the Kaolinite Silt with 50 g/l NaCl at the beginning of the squeezing test which corresponds to 2.3 percent. The initial water content of the mixture was monitored to be 55 percent at the beginning. The salt content and osmotic suction at various water contents are calculated using Eq. (3.100).

Figure 6.30 shows the calculated and measured osmotic suction along with the soil-water characteristic curve for the mixture of Kaolinite and salt. The figure shows reasonably good agreement between the calculated and measured osmotic suction. As expected, it reflects that osmotic suction increases as water content of the soil specimen decreases during squeezing. However, slight decrease in osmotic suction is noted at the end of squeezing. This decrease is attributed to the experimental error associated with the corrected measurement of electrical conductivity of pore-water squeezed from the soil

specimen. For example, the electrical conductivity at water content of 45 and 38 percent was monitored to be 71 and 69 mS/cm.

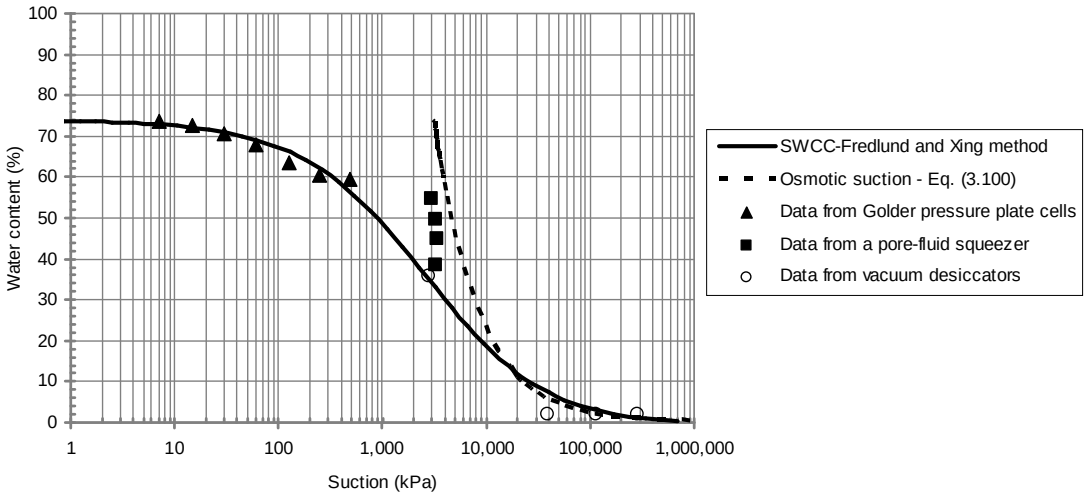

Figure 6.30 Measured and predicted osmotic suction along with the best-fitted soil-water characteristic curve for the Kaolinite mixed with 50 g/l NaCl.

6.3.2 Verification of Evaporation Data Collected from the Research Literature

The soil datasets were collected from the research literature with the assistance of the GetData Graph Digitizer software program version 2.24. The program allows the collection of data points manually from the graphs scanned from the research literature. Only representative and important data collected for each soil is presented in this section. For each soil used for verification, several graphs showing the measured data and predicted results are deliberately presented for comparison. Discussions and analysis are also presented along with these graphs.

Since influence of surface reflectivity (albedo) is out of scope of this thesis, two factors such as osmotic suction and salt crust resistance are evaluated in calculation of evaporation from salinized soil. Therefore, the rate of evaporation from the salinized soil is calculated using the Limiting Function equation for Actual Evaporation (Wilson et al., 1994). This equation calculates Actual Evaporation based on an assumption related to temperature conditions

above the soil surface and at the soil surface (i.e., Eq. 2.6). A flowchart of the three procedures that can be used calculate Actual Evaporation from salinized soil surfaces is presented in Figure 6.31. The osmotic suction can be calculated using Eq. (3.100).

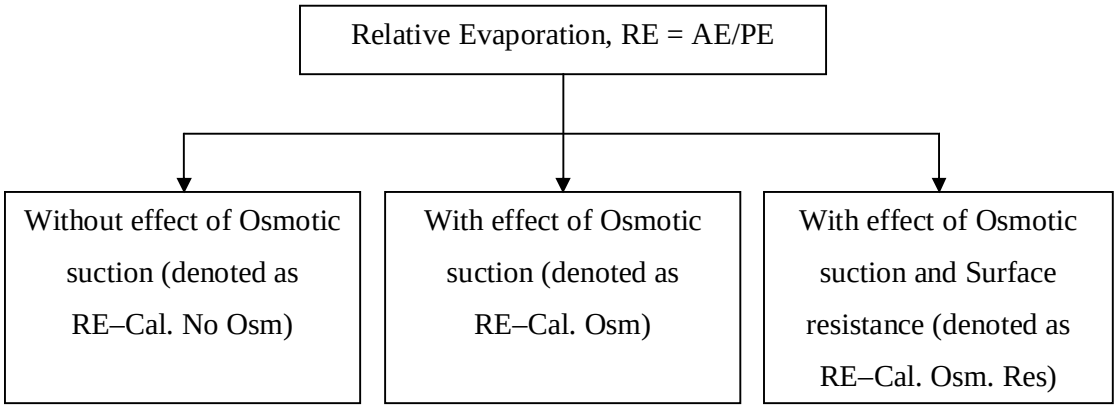

Figure 6.31 A flowchart of the three procedures used to calculated relative evaporation from salinized soil surfaces.

In case that salt crust resistance is taken into account, the Limiting Function equation is modified as follows:

$$\frac{AE}{PE} = \frac{f(u)}{f'(u)} \frac{u_v - u_v^{air}}{u_w - u_v^{air}} \tag{3.100a}$$

where:

AE = actual evaporation from soil surface, mm/day;

PE = potential evaporation from water surface, mm/day;

u_v = actual vapor pressure at soil surface, kPa;

u_w = vapor pressure at water surface, kPa;

u_v^{air} = vapor pressure at the air immediately above the soil surface, kPa.

As described in Chapter 3, the ratio of $\frac{f'(u)}{f(u)}$ was derived to be as a function of the surface resistance.

$$\frac{f'(u)}{f(u)} = 1 + \frac{r_s}{r_{av}} \tag{3.75}$$

$$\frac{AE}{PE} = \left(\frac{r_{av}}{r_{av} + r_s} \right) \frac{u_v - u_v^{air}}{u_w - u_v^{air}} \tag{3.100b}$$

where:

r_{av} = aerodynamic resistance (s/m) determined from the measurement of *PE* from water surface;

$$r_{av} = \frac{u_w - u_v^{air}}{PE}$$

r_s = surface resistance (s/m), as soil surface resistance and salt crust resistance determined using Eq. (3.86) and Eq. (3.101), respectively in this section.

Hereinafter, RE–Cal. No Osm, RE–Cal. Osm and RE–Cal. Osm. Res in the following figures denote the relative evaporation calculated using Eq. (3.100b) associated with each of three procedures shown in Figure 6.31. Description of each symbol is provided in Table 6.14.

Table 6.14 A summary of symbols denoting three procedures of the calculated relative evaporation.

Symbols	Description
RE–Cal. No Osm	Calculated relative evaporation (RE) without effect of osmotic suction (No Osm).
RE–Cal. Osm	Calculated relative evaporation (RE) with effect of osmotic suction (Osm).
RE–Cal. Osm. Res	Calculated relative evaporation (RE) with effect of osmotic suction (Osm) and surface resistance (Res).

6.3.2.1 Evaporation from Low-Saline, Saline and Hyper Saline Silt by Dunmola (2012)

Verification of evaporation rate for the Low-saline (LS), Saline (S) and Hyper-saline (HS) silt is also presented in this section. The test results of evaporative fluxes along with climatic data were provided in Appendix D. The soil water content and salt concentration at the depth of 0 – 1 cm were collected from the soil water content and NaCl concentration profiles for LS, S and HS, respectively as shown in Appendix D. A summary of the calculated relative evaporation for HS is typically provided in Table 6.15. Other calculations for LS and S are presented in Appendix E.

Figures 6.32, 6.33 and 6.34 shows the calculated and measure relative evaporation for LS, S and HS, respectively. The calculated results analyzed by Dunmola (2012) are also re-plotted for comparison in those figures. Three figures show the relative evaporation calculated without effect of osmotic suction (denoted as RE–Cal. No Osm) does not decline from unity during the drying process. These results contrast with the measured relative evaporation which is observed to reduce from 0.8 at the beginning to 0.3 for Low-saline silt and 0.04 for Saline and Hyper-saline silt at the end of the tests, respectively. This result indicates that actual evaporation from saline soil could not be explained if only suction generated by the SWCCs is used to calculate relative humidity and vapour pressure at the soil surface.

Effect of osmotic suction is taken into account to calculate the relative evaporation (denoted as RE–Cal. Osm). As expected, osmotic suction increases with increase in salt concentration at the depth of 0 – 1 cm (see Table 6.15). The more initial pore-water salinity has the surface, the larger osmotic suction develops. For example, osmotic suction for HS varies from about 19,000 kPa to about 61,000 kPa which is larger than that for S (i.e., from 9,300 kPa to 50,000 kPa) and LS (i.e., from 5,600 kPa to 32,000 kPa). As a result, total suction (i.e., sum of matric suction and osmotic suction) increases during the drying process; hence, relative humidity and vapor pressure at the soil surface decreases. It somewhat explains reduction in relative evaporation

as shown in Figures 6.32, 6.33 and 6.34. However, the calculated relative evaporation with effect of osmotic suction does not agree well with the measured relative evaporation for three soil columns (LS, S and HS).

Table 6.15 Summary of results of relative evaporation for Hyper-saline silt.

Time (day)	*AE/PE*	R.H. Air	Air Temp (^{o} C)	Soil moisture content at 0 – 1 cm (%)	Salt content at 0 – 1 cm (ppt)	r_{av} (s/m)	r_s (s/m)	Suction		Relative Humidity		Relative Evaporation		
								From SWCC (kPa)	Osmotic suction (kPa)	No osmotic suction	With Osmotic suction	RE–Cal. No Osm	RE–Cal. Osm	RE–Cal. Osm. Res
0	0.65	0.56	25.1	24.2	224.6	152.7	62.9	5	19,025	1.00	0.87	1.00	0.71	0.50
1	0.39	0.55	24.0	22.3	294.8	132.3	81.7	6	24,968	1.00	0.83	1.00	0.63	0.39
2	0.29	0.60	25.0	20.3	364.9	152.9	96.5	6	30,910	1.00	0.80	1.00	0.50	0.30
3	0.24	0.53	23.5	18.4	435.1	139.3	108.8	7	36,853	1.00	0.76	1.00	0.49	0.28
4	0.13	0.48	22.6	18.1	578.0	154.0	128.4	7	48,959	1.00	0.70	1.00	0.42	0.23
5	0.07	0.55	23.5	18.1	585.9	129.2	129.4	7	49,625	1.00	0.70	1.00	0.33	0.17
6	0.06	0.55	24.0	17.6	593.7	154.4	130.4	7	50,290	1.00	0.69	1.00	0.32	0.17
7	0.05	0.57	22.0	17.3	601.6	123.8	131.4	8	50,955	1.00	0.69	1.00	0.28	0.14
8	0.06	0.57	23.9	16.2	660.1	139.0	138.1	8	55,911	1.00	0.67	1.00	0.23	0.11
9	0.07	0.57	25.8	15.2	718.6	154.2	144.5	9	60,867	1.00	0.64	1.00	0.17	0.09
10	0.06	0.55	23.6	14.1	777.1	143.1	150.8	10	65,822	1.00	0.62	1.00	0.16	0.08
11	0.05	0.55	22.9	13.1	835.6	143.9	157.3	10	70,778	1.00	0.60	1.00	0.10	0.05
12	0.05	0.60	21.0	13.3	798.4	120.3	153.8	10	67,630	1.00	0.61	1.00	0.02	0.01
13	0.04	0.63	21.5	13.6	761.3	122.9	150.1	10	64,481	1.00	0.62	1.00	-0.01	-0.01
14	0.04	0.63	21.5	13.9	724.1	139.6	146.3	10	61,332	1.00	0.64	1.00	0.02	0.01

Note: The interpolated values are filled in the highlighted cells.

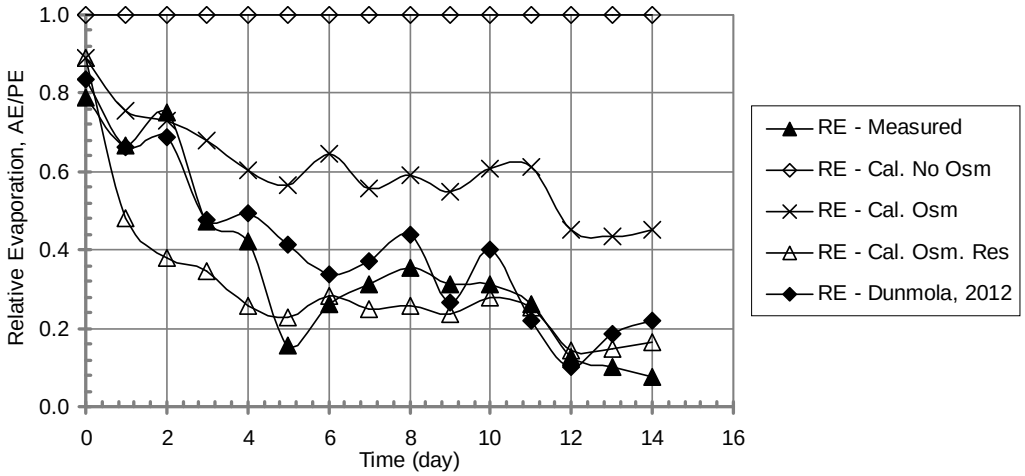

Figure 6.32 Calculated and measured relative evaporation for Low-saline silt. The calculated results using three procedures are in comparison with that by Dunmola (2012). Symbols are described in Table 6.14.

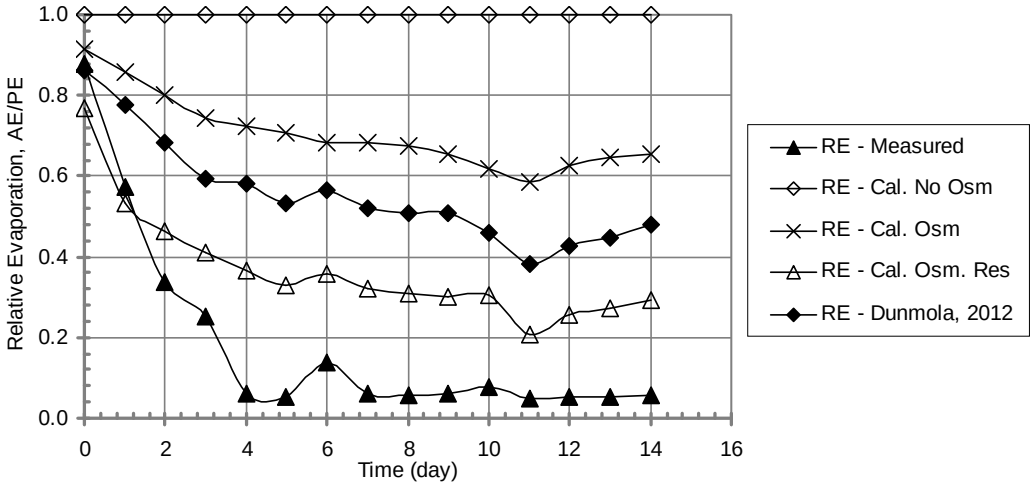

Figure 6.33 Calculated and measured relative evaporation for Saline silt. The calculated results using three procedures are in comparison with that by Dunmola (2012). Symbols are described in Table 6.14.

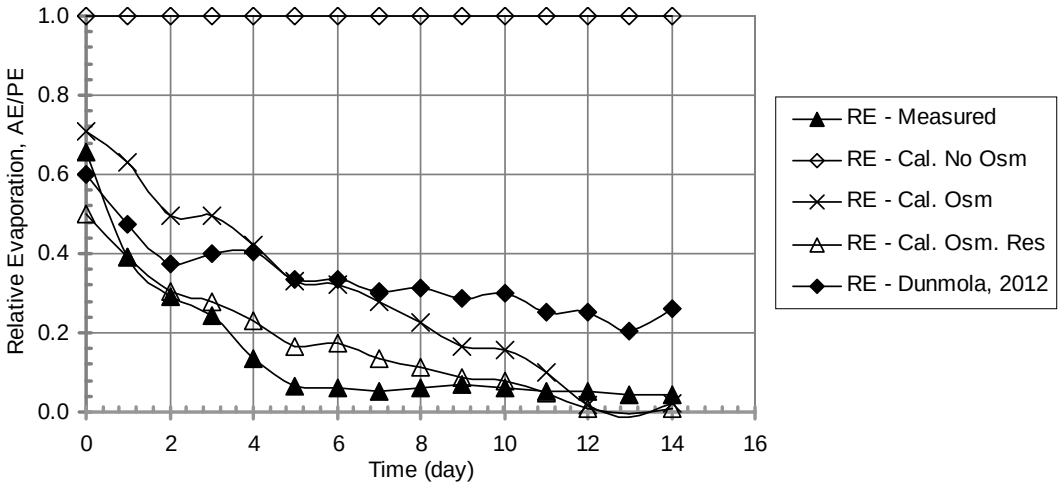

Figure 6.34 Calculated and measured relative evaporation for Hyper-saline silt. The calculated results using three procedures are in comparison with that by Dunmola (2012). Symbols are described in Table 6.14.

Along with development of osmotic suction due to increase in salt concentration at the soil surface, surface resistance also develops due to formulation of salt crust at the surface. As expected, salt crust resistance increases as salt concentration increases. Consequently, the surface resistance (i.e., sum of salt crust resistance and soil surface resistance) increases during the drying process. The third procedure of calculation of relative evaporation is considered by taking both osmotic suction and surface resistance at the soil surface into account (denoted as RE–Cal. Osm. Res). It appears that RE-Cal. Osm. Res gives the best result among the afore-mentioned procedures. This finding appears to be consistent for three soil columns (LS, S and HS).

6.3.2.2 Evaporation from Salinized Silt and Tailings under Various Wind Condition by Dunmola (2012)

Verification of evaporation rate for the salinized silt and tailings under ambient wind and simulated wind condition is also presented in this section. Similarly, the test results of evaporative fluxes along with climatic data were provided in Appendix D. The soil water content and salt concentration at the depth of 0 – 1 cm were collected from the soil water content and NaCl

concentration profiles for salinized silt and tailings, respectively as shown in Appendix D. A summary of the calculated relative evaporation for salinized silt under ambient wind condition (Salinized silt – AW) is typically provided in Table 6.16. Other calculations for salinized silt under simulated wind condition, tailings under ambient wind condition and tailings under simulated wind condition are presented in Appendix E.

Figures 6.35, 6.36, 6.37 and 6.38 show the calculated and measured relative evaporation for salinized silt under ambient wind condition, simulated wind condition, tailings under ambient wind condition and tailings under simulated wind condition, respectively. In consistent with explanation for the cases of Low-saline, Saline and Hyper-saline silt, the third procedure of calculation of relative evaporation (denoted as RE–Cal. Osm. Res) gives the best result among three procedures.

After examination of the results collected from the research literature, it is concluded that evaporation from the columns of salinized soil is effected not only osmotic suction, but also surface resistance developed at the surface. The next section examines effect of those factors in thin salinized soil layers.

Table 6.16 Summary of results of relative evaporation for Salinized silt – AW.

Time (day)	*AE/PE*	R.H. Air	Air Temp (^{o} C)	Soil moisture content at 0 – 1 cm (%)	Salt content at 0 – 1 cm (ppt)	r_{av} (s/m)	r_s (s/m)	Suction		Relative Humidity		Relative Evaporation		
								From SWCC (kPa)	Osmotic suction (kPa)	No osmotic suction	With Osmotic suction	RE–Cal. No Osm	RE–Cal. Osm	RE–Cal. Osm. Res
0	0.89	0.13	23.7	33.0	96.7	260.6	4.8	63	6,996	1.00	0.95	1.00	0.94	0.93
1	0.84	0.14	23.3	30.5	148.4	377.3	34.4	75	12,150	1.00	0.91	1.00	0.90	0.83
2	0.78	0.17	23.0	28.0	200.0	369.0	55.2	90	17,861	1.00	0.88	1.00	0.85	0.74
3	0.73	0.18	23.7	25.6	251.6	376.7	71.7	110	24,021	1.00	0.84	1.00	0.80	0.67
4	0.68	0.14	23.7	23.8	241.8	421.2	70.1	127	22,813	1.00	0.85	1.00	0.82	0.70
5	0.59	0.14	23.6	22.1	231.9	296.3	70.1	149	21,619	1.00	0.85	1.00	0.83	0.67
6	0.47	0.16	23.3	20.3	222.0	693.4	73.8	213	20,440	1.00	0.86	1.00	0.83	0.75
7	0.37	0.18	23.5	18.6	212.2	400.2	86.0	317	19,276	1.00	0.87	1.00	0.84	0.69
8	0.32	0.17	23.5	17.7	246.6	944.7	111.3	398	23,398	1.00	0.84	1.00	0.81	0.72
9	0.28	0.16	23.5	16.8	281.0	501.3	143.4	505	27,692	1.00	0.81	1.00	0.78	0.60
10	0.26	0.14	23.5	15.9	315.4	471.9	187.2	652	32,141	1.00	0.79	0.99	0.75	0.54
11	0.23	0.11	23.7	15.0	349.8	439.7	249.9	854	36,733	0.99	0.76	0.99	0.73	0.47
12	0.19	0.14	23.5	14.1	384.2	439.6	342.5	1,137	41,458	0.99	0.73	0.99	0.69	0.39
13	0.24	0.14	23.5	13.1	418.6	536.4	482.0	1,540	46,308	0.99	0.71	0.99	0.66	0.35
14	0.20	0.14	23.5	12.2	453.0	364.9	694.7	2,125	51,274	0.98	0.68	0.98	0.63	0.22

Note: The interpolated values are filled in the highlighted cells.

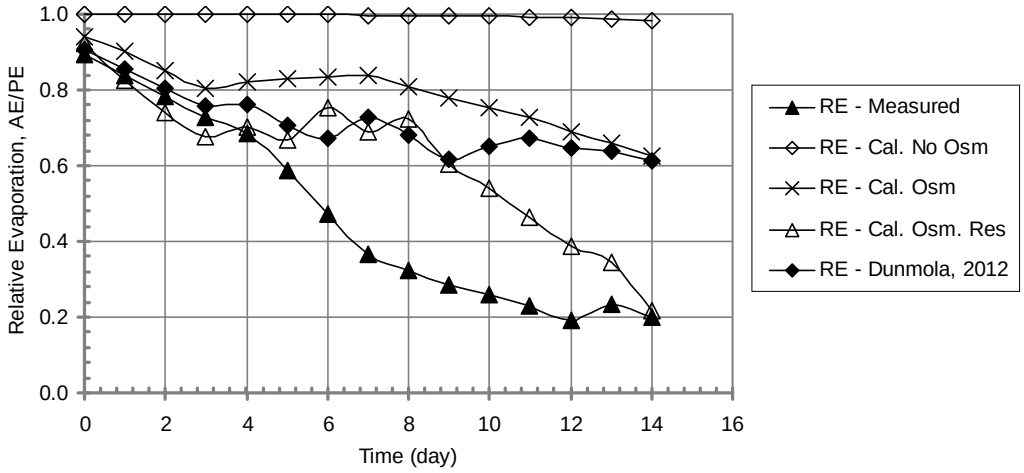

Figure 6.35 Calculated and measured relative evaporation for Salinized silt under ambient wind condition (Salinized silt – AW). The calculated results using three procedures are in comparison with that by Dunmola (2012). Symbols are described in Table 6.14.

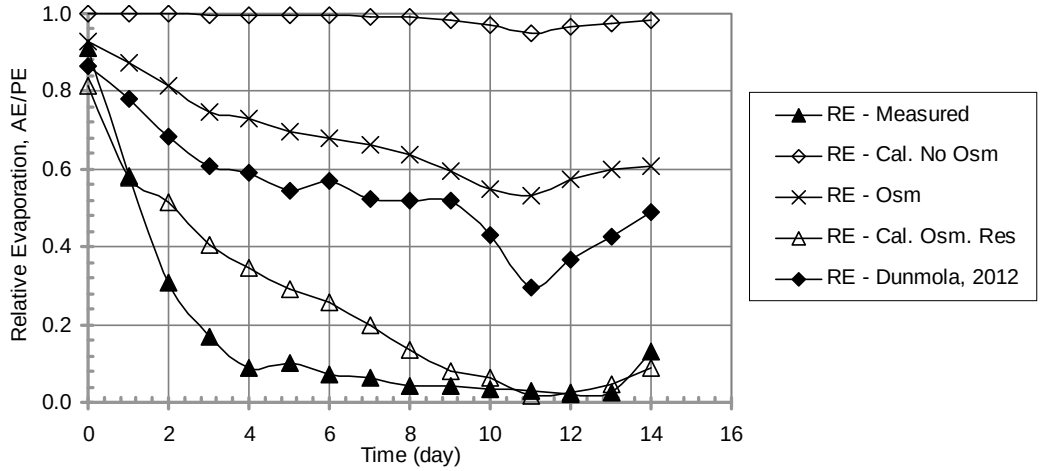

Figure 6.36 Calculated and measured relative evaporation for Salinized silt under simulated wind condition (Salinized silt – SW). The calculated results using three procedures are in comparison with that by Dunmola (2012). Symbols are described in Table 6.14.

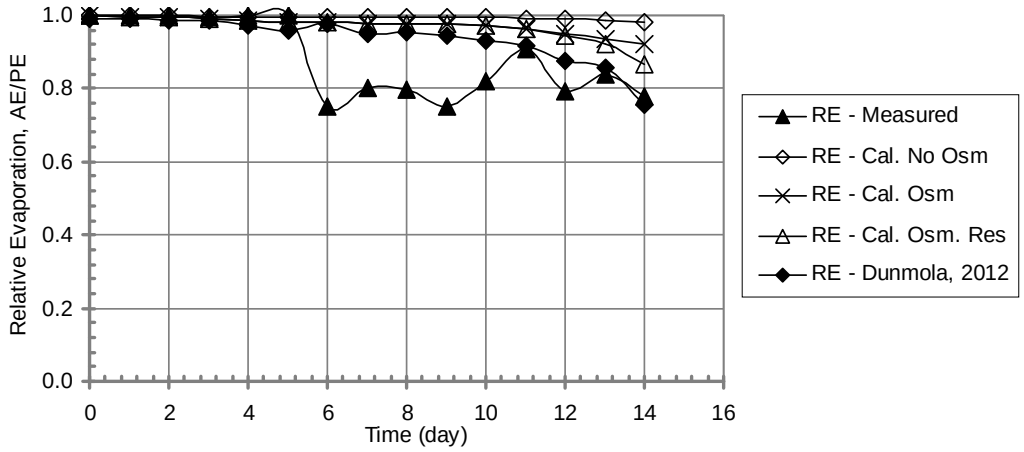

Figure 6.37 Calculated and measured relative evaporation for Tailings under ambient wind condition (Tailings – AW). The calculated results using three procedures are in comparison with that by Dunmola (2012). Symbols are described in Table 6.14.

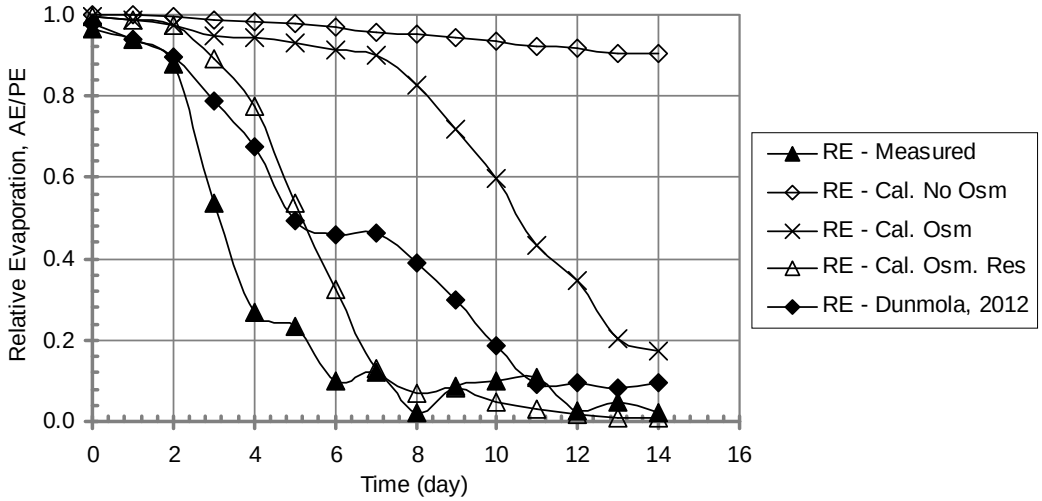

Figure 6.38 Calculated and measured relative evaporation for Tailings under ambient wind condition (Tailings – SW). The calculated results using three procedures are in comparison with that by Dunmola (2012). Symbols are described in Table 6.14.

6.3.3 Verification of Evaporation Data Measured from the Laboratory Program

Verification of the thin soil layer drying for the Ottawa sand and Devon silt mixed with four solutions of NaCl (i.e., 50 g/l, 100 g/l, 200 g/l and 250 g/l) is

presented in this section. The test results of evaporative fluxes along with the soil water content and climatic data were provided in Chapter 5.

Hereinafter, AE–Cal. No Osm, AE–Cal. Osm and AE–Cal. Osm. Res in the following figures denote the calculated rates of actual evaporation using Eq. (3.100b) associated with each of three procedures shown in Figure 6.31. Description of each symbol is provided in Table 6.17.

Table 6.17 A summary of symbols denoting three procedures of the calculated rate of actual evaporation.

Symbols	Description
AE–Cal. No Osm	Calculated rate of actual evaporation (AE) without effect of osmotic suction (No Osm).
AE–Cal. Osm	Calculated rate of actual evaporation (AE) with effect of osmotic suction (Osm).
AE–Cal. Osm. Res	Calculated rate of actual evaporation (AE) with effect of osmotic suction (Osm) and salt crust resistance (Res).

6.3.3.1 Thin Soil Layers for Salinized Ottawa sand

A summary of the calculated rate of actual evaporation for the Ottawa sand mixed with 100 g/l is typically provided in Table 6.18. Other calculations for the Ottawa sand mixed with 50 g/l, 200 g/l and 250 g/l are presented in Appendix E.

Figure 6.39 shows a typical calculated, actual and potential evaporation rates for the salinized Ottawa sand (i.e., the Ottawa sand mixed with 100 g/l NaCl). Similar to evaporation from salinized soil columns, the figure shows the evaporation rate calculated without effect of osmotic suction (denoted as AE–Cal. No Osm) does not decline from the potential evaporation rate during the drying process. This result contrasts with the measured rate of evaporation which is observed to be depressed from 2.77 mm/day (compared to the potential rate of 2.89 mm/day) at the beginning to approximately zero

(compared to the potential rate of 2.61 mm/day) at the end of the test. This result indicates that actual evaporation from the thin salinized soil could not be explained if only suction generated by the SWCCs is used to calculate relative humidity and vapour pressure at the soil surface.

Effect of osmotic suction is taken into account to calculate the evaporation rate (denoted as AE–Cal. Osm). As expected, osmotic suction increases with increase in salt concentration at the soil surface (see Table 6.18). The more salt concentration has the surface, the larger osmotic suction develops. For example, osmotic suction varies from approximately 8,470 kPa to approximately 273,168 kPa which corresponds to variation of salt concentration from 100 ppt to approximately 3,225 ppt, respectively. As a result, total suction increases during the drying process; hence, relative humidity and vapor pressure at the soil surface decreases. It somewhat explains reduction in the rate of evaporation. The calculated rate of evaporation with effect of osmotic suction agrees well with the measured rate of evaporation for the Ottawa sand mixed with 100 g/l NaCl as a typical case of sand material.

Surface resistance also develops due to formulation of salt crust at the surface. As expected, salt crust resistance increases as salt concentration increases. The third procedure of calculation of actual evaporation rate is considered by taking both osmotic suction and salt crust resistance at the soil surface into account (denoted as AE–Cal. Osm. Res). It appears that AE–Cal. Osm. Res and AE–Cal. Osm give the close results. This result indicates salt crust resistance does not significantly effect on evaporation from thin salinized soil. It is attributed that the evaporating front locates right at the surface. There is apparently no distance for water vapour travel to the soil-atmosphere interface. The surface resistance should be ignored.

It should be noted that the above finding and explanation appears to be consistent with the other calculations for the Ottawa sand mixed with 50 g/l, 200 g/l and 250 g/l NaCl.

Table 6.18 Summary of results of evaporation for Ottawa sand mixed with 100 g/l NaCl.

Time (hour)	PE (mm/ day)	AE (mm/ day)	R.H. Air	Air Temp (^{o} C)	Soil moisture content at surface (%)	Salt content at surface (ppt)	r_{av} (s/m)	r_s (s/m)	Suction		Relative Humidity		Actual Evaporation (mm/day)		
									From SWCC (kPa)	Osmotic suction (kPa)	No osmotic suction	With Osmotic suction	AE–Cal. No Osm	AE–Cal. Osm	AE–Cal. Osm. Res
21.5	2.89	2.77	0.20	19.5	30.79	100	401.1	7.1	7	8,470	1.00	0.94	2.89	2.67	2.62
43.3	2.54	2.33	0.20	19.5	28.16	109	456.7	13.2	9	9,260	1.00	0.93	2.54	2.33	2.26
62.4	2.38	2.03	0.21	19.4	26.13	118	478.7	18.4	9	9,979	1.00	0.93	2.38	2.16	2.08
82.1	2.34	1.99	0.21	19.4	24.11	128	485.7	23.9	10	10,819	1.00	0.92	2.34	2.11	2.01
108.0	2.30	1.86	0.21	19.4	21.60	143	494.9	31.5	10	12,074	1.00	0.91	2.30	2.05	1.93
130.8	2.42	1.92	0.21	19.6	19.33	159	475.5	39.2	10	13,490	1.00	0.90	2.42	2.13	1.97
152.0	2.36	1.94	0.21	19.4	17.18	179	482.2	47.3	10	15,176	1.00	0.89	2.36	2.04	1.86
174.8	2.51	1.80	0.20	19.6	15.04	205	465.6	56.5	10	17,344	1.00	0.88	2.51	2.13	1.90
200.0	2.65	1.91	0.20	19.8	12.53	246	445.5	69.1	10	20,813	1.00	0.86	2.65	2.18	1.89
219.9	2.53	1.73	0.20	19.6	10.74	287	461.6	79.7	11	24,282	1.00	0.84	2.53	2.01	1.71
241.3	2.57	1.71	0.20	19.6	8.83	349	454.3	93.2	11	29,532	1.00	0.80	2.57	1.94	1.61
268.9	2.66	1.66	0.20	19.4	6.44	478	432.8	115.0	11	40,469	1.00	0.74	2.66	1.80	1.42
295.4	2.59	1.73	0.20	19.6	4.06	759	449.9	146.9	14	64,275	1.00	0.62	2.59	1.37	1.03
316.1	2.78	1.21	0.20	19.6	2.27	1,358	420.1	187.0	26	115,018	1.00	0.43	2.78	0.79	0.55
338.8	2.62	0.51	0.20	19.6	1.19	2,580	445.7	231.3	89	218,534	1.00	0.20	2.62	0.00	0.00
359.6	2.65	0.22	0.20	19.6	0.95	3,225	440.8	246.7	153	273,168	1.00	0.13	2.64	-0.22	-0.14
379.7	2.74	0.00	0.20	19.6	0.95	3,225	426.0	246.7	153	273,168	1.00	0.13	2.73	-0.23	-0.15
401.7	2.61	0.00	0.20	19.6	0.95	3,225	446.6	246.7	153	273,168	1.00	0.13	2.61	-0.22	-0.14

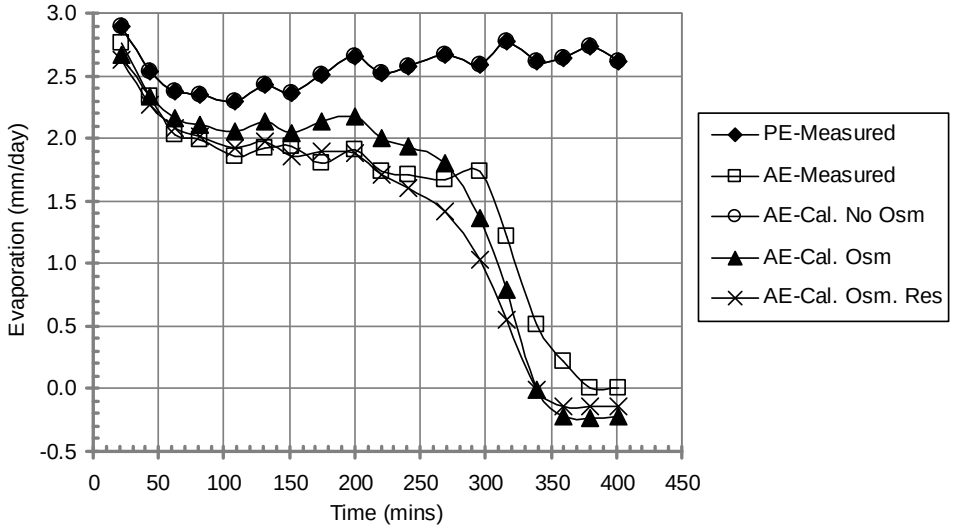

Figure 6.39 Typical calculated and measured rates of actual evaporation corresponding to three procedures for Ottawa sand mixed with 100 g/l NaCl. Symbols are described in Table 6.17.

6.3.3.2 Thin Soil Layers for Salinized Devon silt

A summary of the calculated rate of evaporation for the Devon silt mixed with 250 g/l is typically provided in Table 6.19. Other calculations for the Devon silt mixed with 50 g/l, 100 g/l and 200 g/l are presented in Appendix E.

Figure 6.40 shows a typical calculated, actual and potential evaporation rates for the salinized Devon silt (i.e., the Devon silt mixed with 250 g/l NaCl). The figure shows the evaporation rate calculated without effect of osmotic suction (denoted as AE–Cal. No Osm) does not decline from the potential evaporation rate during the drying process. This result contrasts with the measured rate of evaporation which is observed to be depressed from 2.08 mm/day (compared to the potential rate of 2.89 mm/day) at the beginning to approximately 0.32 mm/day (compared to the potential rate of 2.61 mm/day) at the end of the test. This indicates that actual evaporation from the thin salinized soil could not be explained if only suction generated by the SWCCs is used to calculate relative humidity and vapour pressure at the soil surface.

Effect of osmotic suction is taken into account to calculate the evaporation rate (denoted as AE–Cal. Osm). As expected, osmotic suction increases with

increase in salt concentration at the soil surface (see Table 6.19). The more salt concentration has the surface, the larger osmotic suction develops. For example, osmotic suction varies from approximately 21,176 kPa to approximately 172,432 kPa which corresponds to variation of salt concentration from 250 ppt to approximately 2,036 ppt, respectively. As a result, total suction increases during the drying process; hence, relative humidity and vapor pressure at the soil surface decreases. It somewhat explains reduction in the rate of evaporation. The calculated rate of evaporation with effect of osmotic suction only agrees well with the measured rate evaporation for the Devon silt mixed with 250 g/l NaCl as a typical case of silt material.

Surface resistance also develops due to formulation of salt crust at the surface. As expected, salt crust resistance increases as salt concentration increases. The third procedure of calculation of actual evaporation rate is considered by taking both osmotic suction and salt crust resistance at the soil surface into account (denoted as AE–Cal. Osm. Res). It appears that AE–Cal. Osm. Res and AE–Cal. Osm give the close results. This indicates salt crust resistance does not significantly effect on evaporation from the thin salinized soil. It is attributed that the evaporating front locates right at the surface. There is apparently no distance for water vapour travel to the soil-atmosphere interface. The surface resistance should be ignored. This finding is remarkably different from that from the columns of salinized soil.

It should be noted that the above finding and explanation appears to be consistent with the other calculations for the Devon silt mixed with 50 g/l and 100 g/l NaCl.

There was a big gap between the measured data and the calculated result for the case of Devon silt mixed with 200 g/l NaCl in the third stage of drying process (see Figure 6.41). It is believed that there were some errors in the measurement of the evaporation rate for Devon silt mixed with 200 g/l. It may be attributed to low accuracy of the electrical scale (e.g. accuracy of 0.05g).

Table 6.19 Summary of results of evaporation for Devon silt with mixed 250 g/l NaCl.

Time (hour)	PE (mm/ day)	AE (mm/ day)	R.H. Air	Air Temp (^{o} C)	Soil moisture content at surface (%)	Salt content at surface (ppt)	r_{av} (s/m)	r_s (s/m)	Suction		Relative Humidity		Actual Evaporation (mm/day)		
									From SWCC (kPa)	Osmotic suction (kPa)	No osmotic suction	With Osmotic suction	AE–Cal. No Osm	AE–Cal. Osm	AE–Cal. Osm. Res
21.5	2.89	2.08	0.20	19.5	53.4	250	401.1	70.3	0	21,176	1.00	0.85	2.88	2.36	2.01
43.3	2.54	1.92	0.20	19.5	49.2	271	456.7	75.9	0	22,991	1.00	0.84	2.53	2.04	1.75
62.4	2.38	1.66	0.21	19.4	45.9	291	478.7	80.7	0	24,633	1.00	0.83	2.37	1.87	1.60
82.1	2.34	1.51	0.21	19.4	42.9	311	485.7	85.4	49	26,383	1.00	0.82	2.34	1.82	1.54
108.0	2.30	1.50	0.21	19.4	38.9	343	494.9	92.2	167	29,085	1.00	0.81	2.30	1.73	1.46
130.8	2.42	1.72	0.21	19.6	34.9	383	475.5	99.6	275	32,403	1.00	0.79	2.42	1.76	1.46
152.0	2.36	1.63	0.21	19.4	31.4	425	482.2	106.9	419	36,030	1.00	0.76	2.35	1.65	1.35
174.8	2.51	1.60	0.20	19.6	27.6	483	465.6	115.7	676	40,916	1.00	0.74	2.49	1.68	1.34
200.0	2.65	1.82	0.20	19.8	23.0	582	445.5	128.5	1,344	49,266	0.99	0.69	2.62	1.62	1.26
219.9	2.53	1.61	0.20	19.6	19.7	679	461.6	139.2	2,355	57,477	0.98	0.64	2.47	1.40	1.07
241.3	2.57	1.40	0.20	19.6	16.6	803	454.3	150.8	4,286	68,001	0.97	0.59	2.47	1.24	0.93
268.9	2.66	0.99	0.20	19.4	13.8	966	432.8	163.6	5,170	81,832	0.96	0.53	2.54	1.08	0.79
295.4	2.59	0.78	0.20	19.6	11.7	1,140	449.9	175.0	7,171	96,562	0.95	0.46	2.43	0.86	0.62
316.1	2.78	0.55	0.20	19.6	10.5	1,267	420.1	182.2	8,783	107,291	0.94	0.42	2.56	0.78	0.54
338.8	2.62	0.61	0.20	19.6	9.1	1,462	445.7	192.1	11,496	123,797	0.92	0.37	2.35	0.55	0.38
359.6	2.65	0.44	0.20	19.6	8.2	1,629	440.8	199.6	14,028	137,945	0.90	0.33	2.32	0.41	0.28
379.7	2.74	0.45	0.20	19.6	7.3	1,839	426.0	208.0	17,464	155,745	0.88	0.28	2.32	0.27	0.18
401.7	2.61	0.32	0.20	19.6	6.6	2,036	446.6	215.0	20,919	172,432	0.86	0.24	2.14	0.13	0.09

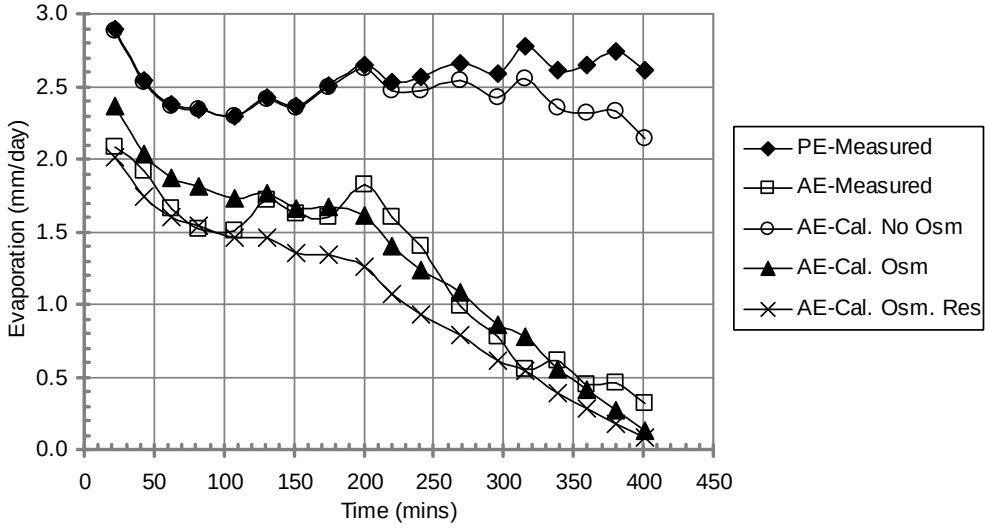

Figure 6.40 Typical calculated and measured rates of actual evaporation corresponding to three procedures for Devon silt mixed with 250 g/l NaCl. Symbols are described in Table 6.17.

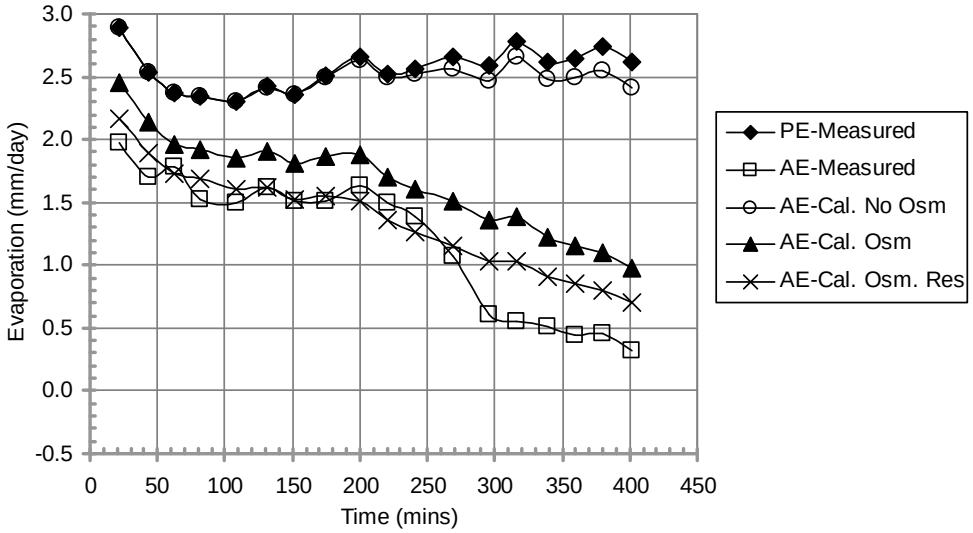

Figure 6.41 Typical calculated and measured evaporation rates corresponding to three procedures for Devon silt mixed with 200 g/l NaCl. Symbols are described in Table 6.17.

6.4 VERIFICATION OF THE SOIL-ATMOSPHERE FLUX EQUATION IN UNCOUPLING PROCEDURE (UNCOUPLED MOISTURE FLOW)

The objective of this section presents information on the verification of the soil-atmosphere flux equation (i.e., Eq.3.69) which was developed in Chapter 3. Two procedures of the verification are presented in Figure 6.42. The calculated results obtained from these procedures are observed and discussed in the following sections.

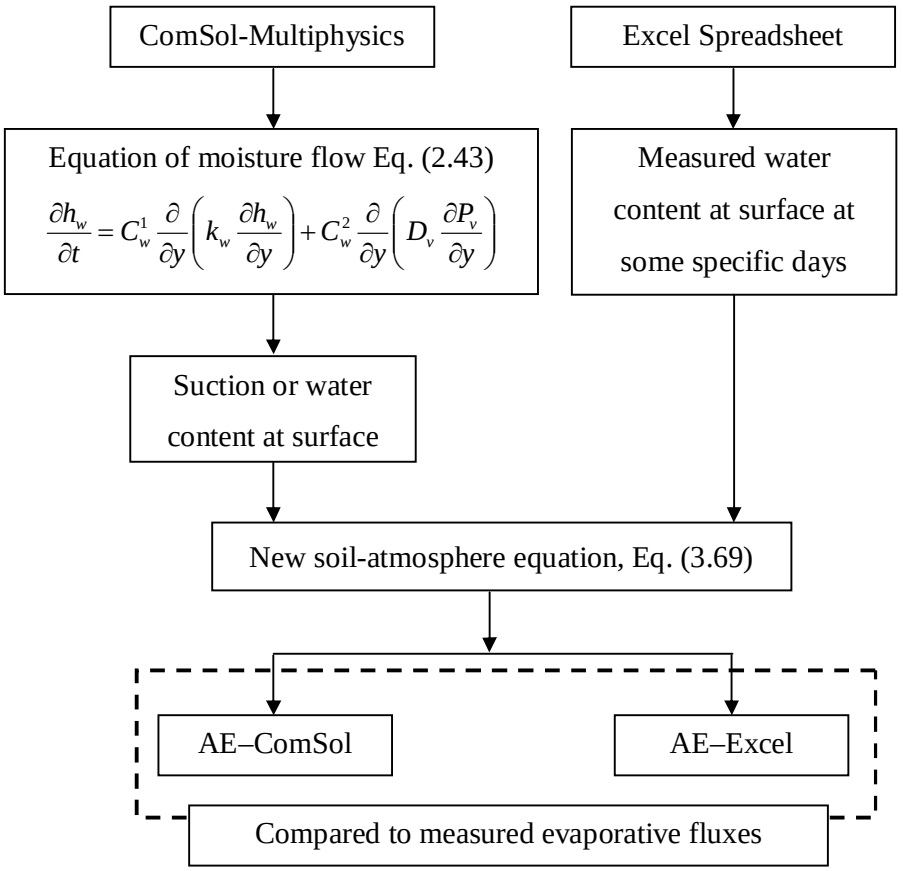

Figure 6.42 Illustration of two procedures of the verification of the new soil-atmosphere equation.

The evaporative fluxes from soil columns in the first procedure are numerically computed using the ComSol-Multiphysics software (finite element method basis). Only moisture flow equation may be solved for 1-D

domain of the soil profile with respect to space and time; so-called uncoupled moisture flow. The results of the evaporative fluxes from this simulation are hereinafter denoted as AE–ComSol in the following figures.

The input data for the equation of moisture flow consist of the observed microclimatic parameters and the soil properties. A summary of soil types and soil properties used to verify the new soil-atmosphere flux equation is provided in Table 6.20. Measured data of water content versus suction is used to estimate soil-water characteristic curve (SWCC) using SVFlux, a commercial product from SoilVision Systems Ltd. (Saskatoon, SK). The Fredlund and Xing method (1994) of the SWCC is used throughout this section. The coefficient of water storage is automatically estimated as a derivative of the soil-water characteristic curve with respect to suction. Depending on the soil properties available in each drying test, the unsaturated hydraulic conductivity is determined in different methods. The lower limit of the unsaturated hydraulic conductivity is set up at 10^{-14} m/s (Ebrahimi et al., 2005). For example, the unsaturated hydraulic conductivity curve for the soil columns A and B (Wilson, 1990) is determined using the input data of saturated hydraulic conductivity of $3x10^{-5}$ m/s (see Table 6.20) and the SWCC of Beaver Creek sand. The Brooks and Corey method (1964) is used for the other drying tests (Bruch, 1993; Yanful and Choo, 1997). The suction value at a break point in the unsaturated hydraulic conductivity function proposed by Brooks and Corey (1964) is determined using datasets plotted by Gitirana (2005). For example, the suction value at the break point is lower than the air-entry value obtained from the SWCC. The maximum value of suction at the break point has been observed to be as low as 10 kPa (Gitirana, 2005). Therefore, the suction value at the break point is chosen as 10 kPa for the silt soil in this section. The molecular diffusivity of water vapour in air and the tortuosity factor of the soil are determined using Kimball et al. (1976).

The partial vapour pressure for the equation of moisture flow is determined using the total suction in the soil domain and Eq. (2.44). However, the partial vapour pressure for the soil-atmosphere flux equation is determined using the new set of the proposed equations (3.80), (3.82) and (3.83) associated with the

water content at soil surface. Mean daily air temperature and relative humidity in the environmental chamber are used to determine the vapour pressure of the air. Potential rate of evaporation and water surface temperature are used to determine net radiation from free water surface using Penman's equation (1948) and mass transfer equation. Net radiation from the soil surface is assumed to be equal to that from the adjacent water surface in the same chamber. A zero flux boundary is specified for both liquid and vapour flow at the bottom of the column base. Finally, the flux of water vapour to the atmosphere is computed using the vapour transfer profile equation (3.69).

In addition, the evaporative fluxes in the second procedure are calculated using Excel Spreadsheet. The measured water content and temperature at or near the soil surface at specific days are input data into Eq. (3.69) for this procedure. The obtained results are hereinafter denoted as AE–Excel.

The calculated evaporative fluxes, AE–ComSol and AE–Excel are compared to the measured evaporative fluxes.

Table 6.20 Summary of soil types and properties used for verification using ComSol-Multiphysics.

No.	Soil type	Method estimating SWCC	Saturated hydraulic conductivity (m/s)	Method estimating unsaturated hydraulic conductivity	Suction at evaporation-reduction point (kPa)	Volumetric water content at evaporation-reduction point (%)	Source
1	Beaver Creek sand	Fredlund and Xing (1994)	$3.0x10^{-5}$	Fredlund and Xing (1994)	5.0	18	Wilson (1990)
2	Beaver Creek sand	Fredlund and Xing (1994)	$3.9x10^{-6}$	Brooks and Corey (1964)	7.0	18	Bruch (1993)
3	Processed silt	Fredlund and Xing (1994)	$8.39x10^{-9}$	Brooks and Corey (1964)	62	15	Bruch (1993)
4	Natural silt	Fredlund and Xing (1994)	$2.07x10^{-8}$	Brooks and Corey (1964)	116	14	Bruch (1993)
5	Fine sand	Fredlund and Xing (1994)	$1.0x10^{-5}$	Brooks and Corey (1964)	1.5	15	Yanful and Choo (1997)
6	Coarse sand	Fredlund and Xing (1994)	$2.0x10^{-4}$	Brooks and Corey (1964)	3.7	15	Yanful and Choo (1997)

6.4.1 Evaporation from soil columns A and B by Wilson (1990)

Soil-water characteristic curve of the Beaver Creek sand was presented in Chapter 3. The unsaturated hydraulic conductivity curve is determined using the saturated hydraulic conductivity and Fredlund and Xing (1994). Zero flux boundary condition is specified at the bottom of the soil columns. Figure 6.43 presents the actual evaporation rate obtained using numerical model (denoted as AE–ComSol); using the measured water content and temperature at the soil surface (denoted as AE–Excel); and the experimental results from Wilson (1990). Close agreement was observed between all the results.

A summary of the calculated rate of evaporation for the soil columns A and B using the measured water content and temperature at the soil surface is typically provided in Table 6.21.

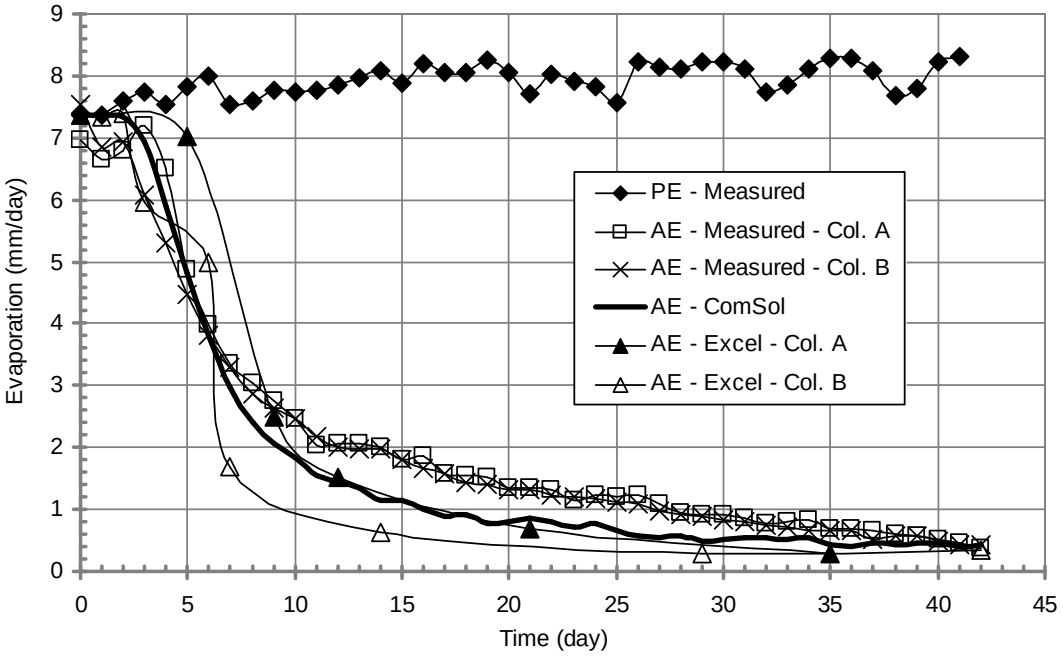

Figure 6.43 Typical calculated and measured evaporation rates for soil columns A and B of the Beaver Creek sand (Wilson, 1990). Symbols are presented in Figure 6.42.

Table 6.21 Summary of calculation of evaporative fluxes for soil columns A and B using the measured water content at soil surface.

Soil column	Time (day)	PE (mm/day)	AE (mm/day)	R.H.air	Temp. Air (^oC)	Temp. Water (^oC)	Temp. Soil (^oC)	Water content	Q_n (mm/day)	Γ (Pa/^oC)	r_{av} (s/m)	r_s (s/m)	f'(u)/f(u)	V.P. soil (kPa)	E'_a	A	AE–Excel (mm/day)
Column A	0	7.37	6.96	0.23	38.6	29.0	30.2	0.1788	5.81	368.38	210.96	0	1.0	4.29	16.0	1.00	7.37
	5	7.82	4.88	0.15	38.7	30.5	31.6	0.0774	6.76	370.10	272.60	59	1.2	3.48	10.6	1.34	7.02
	9	7.76	2.76	0.17	37.8	30.9	34.8	0.0392	6.85	354.86	276.25	582	3.1	1.50	1.8	3.70	2.50
	12	7.86	2.06	0.16	38.7	30.4	35.7	0.0305	6.75	370.10	263.59	980	4.7	1.27	0.9	4.61	1.53
	21	7.72	1.36	0.165	38.0	30.9	37.1	0.0177	6.80	358.20	279.42	2,112	8.6	1.12	0.1	5.65	0.70
	35	8.27	0.69	0.125	37.5	30.2	38.0	0.0075	7.29	349.90	269.49	3,891	15.4	0.81	0.0	8.21	0.29
Column B	0	7.37	7.55	0.23	38.6	29.0	30.0	0.1620	5.81	368.38	210.96	0	1.0	4.24	15.9	1.00	7.37
	1	7.38	6.84	0.22	38.2	31.3	30.0	0.1154	6.44	361.57	268.26	7	1.0	4.24	12.1	1.00	7.35
	2	7.60	6.94	0.20	38.1	31.0	29.8	0.0955	6.63	359.88	265.86	23	1.1	3.96	11.6	1.06	7.40
	3	7.74	6.08	0.18	38.0	30.5	30.0	0.0659	6.71	358.20	262.16	130	1.5	2.50	7.5	1.70	5.97
	6	8.01	3.80	0.15	38.1	30.8	33.2	0.0571	7.05	359.88	274.78	218	1.8	2.15	5.6	2.37	4.98
	7	7.53	3.31	0.16	39.0	30.7	34.2	0.0313	6.48	375.30	280.00	982	4.5	1.27	1.1	4.24	1.68
	14	8.08	1.98	0.13	39.1	30.7	36.6	0.0171	7.01	377.05	277.15	2,248	9.1	0.93	0.3	6.59	0.64
	29	8.23	0.90	0.12	37.5	30.4	37.4	0.0069	7.30	349.90	277.15	4,078	15.7	0.77	0.0	8.28	0.28
	42	7.26	0.44	0.14	38.3	30.2	38.0	0.0084	6.29	363.26	294.95	3,736	13.7	0.94	0.0	7.02	0.34

6.4.2 Evaporation from Soil Column of Beaver Creek Sand by Bruch (1993)

Soil-water characteristic curve of the Beaver Creek sand was presented in Chapter 3. The unsaturated hydraulic conductivity curve is determined using Brooks and Corey method (1964). Constant head boundary condition (CHBC) is set for the first 30 days, and then zero flux boundary condition (ZFBC) is turn on at the bottom of the soil column until the end of the drying test. Figure 6.44 presents the actual evaporation rate obtained using the numerical model, AE–ComSol; using the measured water content and temperature at the soil surface, AE–Excel; and the experimental results from Bruch (1993). In phase 1, the result of the numerical model does not agree with the measured data. In fact, it is close to the potential evaporation rate due to large hydraulic conductivity. In phase 2, the result shows more reasonable agreement since the unsaturated hydraulic conductivity is determined to reach the lower limit of 10^{-14} m/s. The result of AE–Excel shows reasonable agreement with the measured data for both phases.

A summary of the calculated rate of evaporation for the soil column of the Beaver Creek sand using the measured water content and temperature at the soil surface is typically provided in Table 6.22.

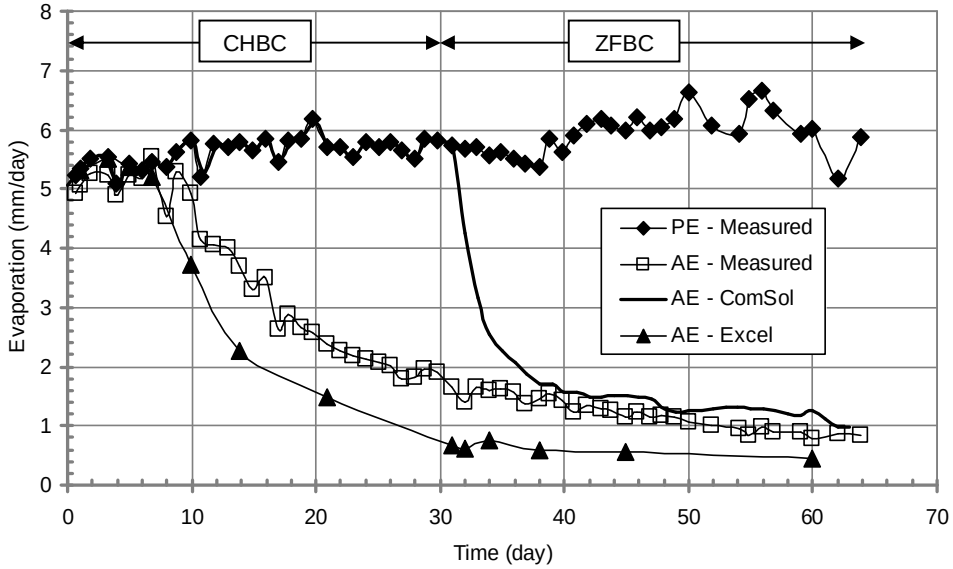

Figure 6.44 Typical calculated and measured evaporation rates for the soil column of the Beaver Creek sand (Bruch, 1993). Symbols are presented in Figure 6.42.

Table 6.22 Summary of calculation of evaporative fluxes for soil column of the Beaver Creek sand using the measured water content at soil surface.

Time (day)	PE (mm/day)	AE (mm/day)	R.H.air	Temp. Air (^oC)	Temp. Water (^oC)	Temp. Soil (^oC)	Water content	Q_n (mm/day)	Γ (Pa/^oC)	r_{av} (s/m)	r_s (s/m)	f'(u)/f(u)	V.P. soil (kPa)	E'_a	A	AE–Excel (mm/day)
1	5.33	5.05	0.131	37.1	32	29.0	0.124	4.92	343.38	471.19	3	1.01	4.01	7.40	1.00	5.32
3.28	5.55	5.24	0.136	35.5	31.6	29.2	0.100	5.21	318.28	444.91	12	1.03	4.03	6.98	1.00	5.52
4.91	5.42	5.22	0.14	36.0	31.8	30.0	0.098	5.06	325.95	456.44	14	1.03	4.19	6.93	1.01	5.38
6.83	5.45	5.54	0.118	35.8	31.8	28.6	0.083	5.12	322.86	470.16	35	1.07	3.36	6.42	1.16	5.20
9.92	5.83	4.93	0.139	36.0	31.8	29.2	0.052	5.45	325.95	424.99	242	1.57	1.65	3.75	2.46	3.72
13.78	5.79	3.69	0.116	36.5	31.8	30.6	0.039	5.38	333.78	440.91	530	2.20	1.08	2.12	4.07	2.26
20.96	5.72	2.37	0.115	37.0	32.2	32.4	0.031	5.32	341.76	456.83	868	2.90	0.91	1.16	5.37	1.48
31	5.74	1.66	0.113	36.8	31.8	33.6	0.019	5.31	338.55	445.52	1,898	5.26	0.73	0.33	7.13	0.67
32.06	5.67	1.41	0.122	36.9	32.4	33.8	0.016	5.30	340.15	462.52	2,308	5.99	0.78	0.25	6.79	0.62
33.96	5.58	1.60	0.122	36.8	32.2	34.2	0.020	5.20	338.55	464.21	1,761	4.79	0.79	0.31	6.77	0.74
37.94	5.37	1.46	0.104	36.8	32.0	33.8	0.018	5.00	338.55	489.23	1,989	5.06	0.67	0.29	7.85	0.60
44.94	5.98	1.16	0.108	36.8	32.5	34.6	0.016	5.61	338.55	451.21	2,294	6.08	0.69	0.19	8.02	0.55
59.9	6.01	0.78	0.117	36.9	32.5	35.4	0.012	5.63	340.15	442.60	2,895	7.54	0.74	0.10	7.81	0.46

6.4.3 Evaporation from soil column of Processed Silt by Bruch (1993)

Soil-water characteristic curve of the Processed silt was presented in Chapter 3. The unsaturated hydraulic conductivity curve is determined using Brooks and Corey method (1964). Constant head boundary condition (CHBC) is set for the first 30 days, and then zero flux boundary condition (ZFBC) is turn on at the bottom of the soil column until the end of the drying test. Figure 6.45 presents the actual evaporation rate obtained using the numerical model, AE–ComSol; using the measured water content and temperature at the soil surface, AE–Excel; and the experimental results from Bruch (1993). In phase 1, the result of the numerical model does not agree with the measured data. In fact, it is close to the potential evaporation rate due to large hydraulic conductivity. In phase 2, the result shows more reasonable agreement since the unsaturated hydraulic conductivity is determined to reach the lower limit of 10^{-14} m/s. The result of AE–Excel shows reasonable agreement with the measured data for both phases.

A summary of the calculated rate of evaporation for the soil column of the Processed silt using the measured water content and temperature at the soil surface is typically provided in Table 6.23.

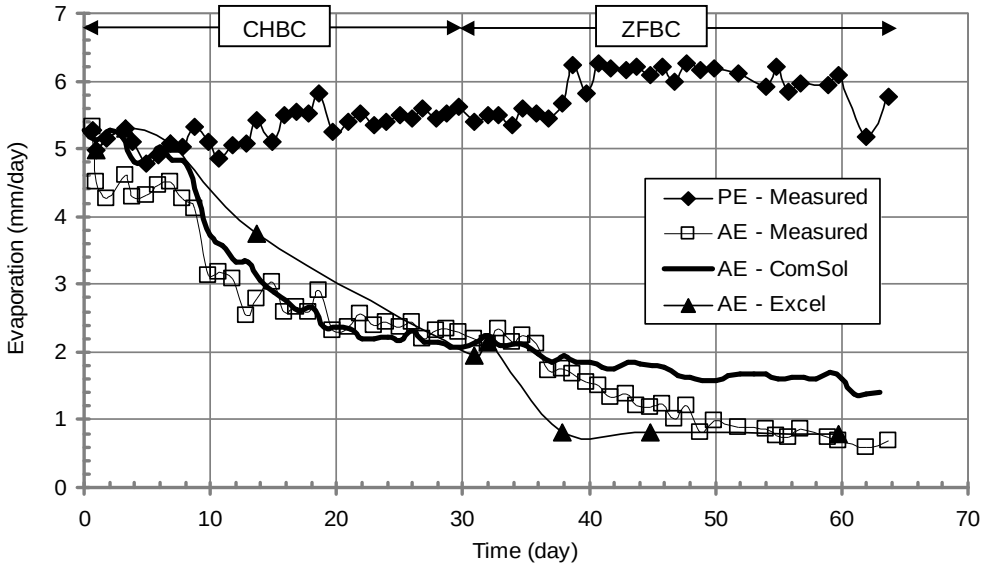

Figure 6.45 Typical calculated and measured evaporation rates for the soil column of the Processed silt (Bruch, 1993). Symbols are presented in Figure 6.42.

Table 6.23 Summary of calculation of evaporative fluxes for soil column of the Processed silt using the measured water content at soil surface.

Time (day)	PE (mm/day)	AE (mm/day)	R.H.air	Temp. Air (^oC)	Temp. Water (^oC)	Temp. Soil (^oC)	Water content	Q_n (mm/day)	Γ (Pa/^oC)	r_{av} (s/m)	r_s (s/m)	f'(u)/f(u)	V.P. soil (kPa)	E'_a	A	AE–Excel (mm/day)
1	5.33	5.05	0.131	37.1	32.0	29.0	0.124	4.92	343.38	471.19	3	1.01	4.01	7.40	1.00	5.32
3.28	5.55	5.24	0.136	35.5	31.6	29.2	0.100	5.21	318.28	444.91	12	1.03	4.03	6.98	1.00	5.52
4.91	5.42	5.22	0.14	36.0	31.8	30.0	0.098	5.06	325.95	456.44	14	1.03	4.19	6.93	1.01	5.38
6.83	5.45	5.54	0.118	35.8	31.8	28.6	0.083	5.12	322.86	470.16	35	1.07	3.36	6.42	1.16	5.20
9.92	5.83	4.93	0.139	36.0	31.8	29.2	0.052	5.45	325.95	424.99	242	1.57	1.65	3.75	2.46	3.72
13.78	5.79	3.69	0.116	36.5	31.8	30.6	0.039	5.38	333.78	440.91	530	2.20	1.08	2.12	4.07	2.26
20.96	5.72	2.37	0.115	37.0	32.2	32.4	0.031	5.32	341.76	456.83	868	2.90	0.91	1.16	5.37	1.48
31	5.74	1.66	0.113	36.8	31.8	33.6	0.019	5.31	338.55	445.52	1,898	5.26	0.73	0.33	7.13	0.67
32.06	5.67	1.41	0.122	36.9	32.4	33.8	0.016	5.30	340.15	462.52	2,308	5.99	0.78	0.25	6.79	0.62
33.96	5.58	1.60	0.122	36.8	32.2	34.2	0.020	5.20	338.55	464.21	1,761	4.79	0.79	0.31	6.77	0.74
37.94	5.37	1.46	0.104	36.8	32.0	33.8	0.018	5.00	338.55	489.23	1,989	5.06	0.67	0.29	7.85	0.60
44.94	5.98	1.16	0.108	36.8	32.5	34.6	0.016	5.61	338.55	451.21	2,294	6.08	0.69	0.19	8.02	0.55
59.9	6.01	0.78	0.117	36.9	32.5	35.4	0.012	5.63	340.15	442.60	2,895	7.54	0.74	0.10	7.81	0.46

6.4.4 Evaporation from soil column of Natural Silt by Bruch (1993)

Soil-water characteristic curve of the Natural silt was presented in Chapter 3. The unsaturated hydraulic conductivity curve is determined using Brooks and Corey method (1964). Constant head boundary condition (CHBC) is set for the first 30 days, and then zero flux boundary condition (ZFBC) is turn on at the bottom of the soil column until the end of the drying test. Figure 6.46 presents the actual evaporation rate obtained using the numerical model, AE–ComSol; using the measured water content and temperature at the soil surface, AE–Excel; and the experimental results from Bruch (1993). In phase 1, the result of the numerical model does not agree with the measured data. In fact, it is close to the potential evaporation rate due to large hydraulic conductivity. In phase 2, the result shows more reasonable agreement since the unsaturated hydraulic conductivity is determined to reach the lower limit of 10^{-14} m/s. The result of AE–Excel shows reasonable agreement with the measured data for both phases.

A summary of the calculated rate of evaporation for the soil column of the Natural silt using the measured water content and temperature at the soil surface is typically provided in Table 6.24.

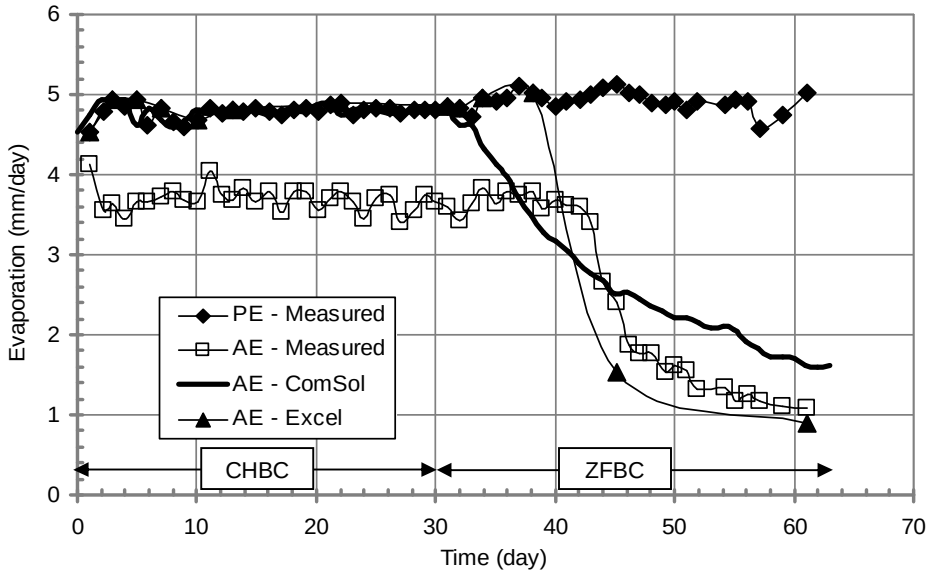

Figure 6.46 Typical calculated and measured evaporation rates for the soil column of the Natural silt (Bruch, 1993). Symbols are presented in Figure 6.42.

Table 6.24 Summary of calculation of evaporative fluxes for soil column of the Natural silt using the measured water content at soil surface.

Time (day)	PE (mm/day)	AE (mm/day)	R.H.air	Temp. Air (^oC)	Temp. Water (^oC)	Temp. Soil (^oC)	Water content	Q_n (mm/day)	Γ (Pa/^oC)	r_{av} (s/m)	r_s (s/m)	f'(u)/f(u)	V.P. soil (kPa)	E'_a	A	AE–Excel (mm/day)
0.96	4.54	4.12	0.128	35.9	32.6	31.3	0.1824	4.32	324.40	586.11	0.0	1.000	4.57	5.62	1.00	4.54
2.94	4.94	3.64	0.116	36.1	32.5	30.7	0.1805	4.68	327.50	543.28	0.0	1.000	4.42	6.21	1.00	4.94
5.02	4.93	3.67	0.139	36.0	32.5	30.7	0.1811	4.67	325.95	527.15	0.0	1.000	4.42	6.20	1.00	4.93
7.00	4.82	3.72	0.118	36.2	32.9	30.7	0.1816	4.59	329.06	569.46	0.0	1.000	4.42	5.95	1.00	4.82
10.08	4.69	3.65	0.135	36.3	33.4	30.9	0.1719	4.49	330.63	590.09	0.1	1.000	4.47	5.66	1.00	4.69
13.00	4.8	3.69	0.113	36.2	33.1	30.7	0.1700	4.59	329.06	583.35	0.1	1.000	4.42	5.84	1.00	4.80
22.08	4.89	3.79	0.116	36.7	33.1	30.9	0.1689	4.64	336.95	567.73	0.1	1.000	4.47	6.14	1.00	4.89
31.04	4.86	3.59	0.131	36.2	33.3	31.2	0.1552	4.66	329.06	569.42	0.2	1.000	4.54	5.86	1.00	4.86
31.97	4.82	3.43	0.12	36.3	33.4	31.1	0.1628	4.62	330.63	586.19	0.1	1.000	4.52	5.80	1.00	4.82
33.95	4.96	3.84	0.104	36.3	33.1	31.0	0.1595	4.74	330.63	571.06	0.2	1.000	4.49	6.06	1.00	4.96
38.19	5.03	3.79	0.094	36.5	32.9	31.1	0.1336	4.78	333.78	562.82	0.7	1.001	4.52	6.28	1.00	5.03
45.15	5.13	2.41	0.082	36.8	33.0	33.6	0.0248	4.87	338.55	563.46	356.2	1.632	0.67	1.57	7.75	1.54
61.15	5.02	1.09	0.082	36.5	32.8	34.8	0.0147	4.77	333.78	569.70	633.9	2.113	0.52	0.42	10.61	0.90

6.4.5 Evaporation from Soil Column of Coarse Sand by Yanful et al. (1997)

Soil-water characteristic curve of the coarse sand was presented in Chapter 3. The unsaturated hydraulic conductivity curve is determined using Brooks and Corey method (1964). Zero flux boundary condition is specified at the bottom of the soil column until the end of the drying test. Figure 6.47 presents the actual evaporation rate obtained using the numerical model, AE–ComSol; using the measured water content and temperature at the soil surface, AE–Excel; and the experimental results from Yanful and Choo (1997). Close agreement was observed between all the results.

A summary of the calculated rate of evaporation for the soil column of the coarse sand using the measured water content and temperature at the soil surface is typically provided in Table 6.25.

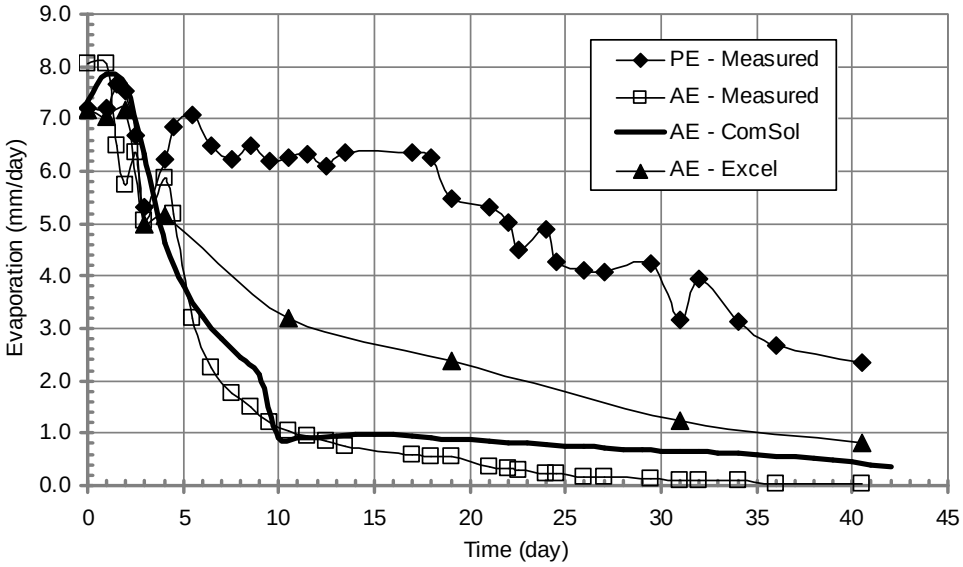

Figure 6.47 Typical calculated and measured evaporation rates for the soil column of the coarse sand (Yanful and Choo, 1997). Symbols are presented in Figure 6.42.

Table 6.25 Summary of calculation of evaporative fluxes for soil column of the Coarse sand using the measured water content at soil surface

Time (day)	PE (mm/day)	AE (mm/day)	R.H.air	Temp. Air (^oC)	Temp. Water (^oC)	Temp. Soil (^oC)	Water content	Q_n (mm/day)	Γ (Pa/^oC)	r_{av} (s/m)	r_s (s/m)	f'(u)/f(u)	V.P. soil (kPa)	E'_a	A	AE–Excel (mm/day)
0.00	7.21	8.05	0.37	23.5	24.2	22.56	0.1732	7.38	174.69	172.84	4.4	1.025	2.74	6.60	1.00	7.16
1.00	7.21	8.05	0.50	23.1	24.2	22.03	0.1458	7.56	170.61	142.31	11.6	1.082	2.64	5.84	1.00	7.04
2.00	7.53	5.74	0.52	23.4	24.2	22.12	0.1347	7.80	173.52	129.31	17.3	1.134	2.60	5.87	1.02	7.16
3.00	5.32	5.07	0.51	23.1	24.2	23.04	0.1273	5.56	171.19	189.12	22.5	1.119	2.67	3.95	1.06	4.99
4.00	6.23	5.88	0.70	24.4	24.2	23.98	0.1125	6.15	182.49	90.79	38.1	1.419	2.75	3.65	1.08	5.15
10.50	6.26	1.04	0.70	26.0	24.2	25.55	0.0829	5.16	198.96	67.57	109.3	2.618	2.67	1.71	1.23	3.21
19.00	5.49	0.55	0.54	24.2	24.2	26.01	0.0666	5.48	181.27	160.86	195.2	2.214	1.93	0.31	1.74	2.37
31.00	3.18	0.09	0.51	24.2	24.2	26.20	0.0533	3.17	181.27	295.67	313.8	2.061	1.70	-0.09	2.00	1.23
40.50	2.33	0.02	0.72	24.6	24.2	26.26	0.0474	2.27	184.33	217.77	387.5	2.779	2.29	-0.25	1.49	0.80

6.4.6 Evaporation from Soil Column of Fine Sand by Yanful et al. (1997)

Soil-water characteristic curve of the fine sand was presented in Chapter 3. The unsaturated hydraulic conductivity curve is determined using Brooks and Corey method (1964). Zero flux boundary condition is specified at the bottom of the soil column until the end of the drying test. Figure 6.48 presents the actual evaporation rate obtained using the numerical model, AE–ComSol; using the measured water content and temperature at the soil surface, AE–Excel; and the experimental results from Yanful and Choo (1997). Close agreement was observed between all the results.

A summary of the calculated rate of evaporation for the soil column of the fine sand using the measured water content and temperature at the soil surface is typically provided in Table 6.26.

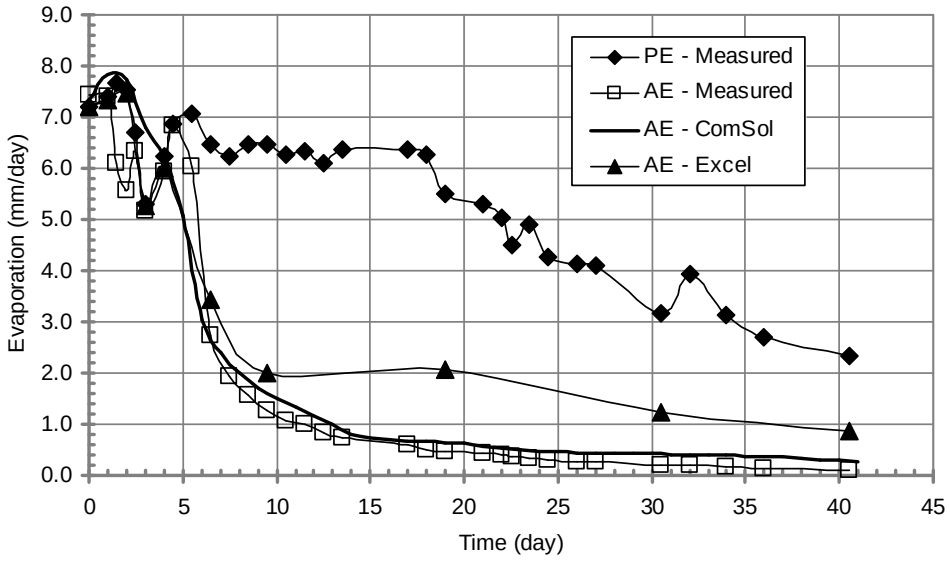

Figure 6.48 Typical calculated and measured evaporation rates for the soil column of the fine sand (Yanful and Choo, 1997). Symbols are presented in Figure 6.42.

Table 6.26 Summary of calculation of evaporative fluxes for soil column of the Fine sand using the measured water content at soil surface.

Time (day)	PE (mm/day)	AE (mm/day)	R.H.air	Temp. Air (^oC)	Temp. Water (^oC)	Temp. Soil (^oC)	Water content	Q_n (mm/day)	Γ (Pa/^oC)	r_{av} (s/m)	r_s (s/m)	f'(u)/f(u)	V.P. soil (kPa)	E'_a	A	AE–Excel (mm/day)
0.0	7.21	7.43	0.37	23.5	24.2	24.86	0.1954	7.38	174.69	172.84	1.4	1.008	3.14	6.71	1.00	7.19
1.0	7.39	7.39	0.55	23.1	24.2	22.58	0.1793	7.78	170.61	126.77	2.5	1.019	2.74	6.27	1.00	7.35
2.0	7.53	5.57	0.53	23.4	24.2	22.41	0.1632	7.80	173.52	126.97	4.4	1.034	2.71	6.58	1.00	7.45
3.0	5.32	5.15	0.53	23.1	24.2	23.58	0.1486	5.57	171.19	181.94	7.4	1.040	2.91	4.48	1.00	5.26
4.0	6.23	5.92	0.71	24.4	24.2	24.23	0.1339	6.15	182.49	87.20	12.4	1.142	3.02	5.60	1.00	5.98
6.5	6.47	2.74	0.54	24.4	24.2	24.81	0.0686	6.40	183.10	134.58	127.1	1.944	2.00	1.15	1.56	3.42
9.5	6.47	1.27	0.68	24.3	24.2	25.27	0.0477	6.43	181.88	93.90	268.5	3.859	2.15	-0.12	1.50	2.00
19.0	5.49	0.47	0.55	24.2	24.2	25.80	0.0519	5.48	181.27	157.49	230.6	2.464	1.82	-0.03	1.83	2.05
30.5	3.18	0.19	0.52	24.2	24.2	25.85	0.0442	3.17	181.27	291.01	303.5	2.043	1.66	-0.14	2.00	1.22
40.5	2.33	0.08	0.72	24.6	24.2	26.18	0.0418	2.27	184.33	217.77	330.9	2.520	2.27	-0.28	1.49	0.85

6.5 CHAPTER SUMMARY

This chapter presented information on the verification of osmotic suction and the new proposed soil-atmosphere flux equation (i.e., Eq. 3.69) using the dataset of soils collected from the research literature and the current laboratory testing program.

Comparison between the methods of determination of relative humidity for the thin soil layers was presented in Section 6.2. The comparisons of the relative humidity predicted using the Lord Kelvin's formula and the new proposed equation (i.e., Eq. 3.84) were presented for the thin soil layers of the sand, silt and clay collected from the research literature (Wilson, 1990; Dunmola, 2012). As expected, the predicted relative humidity using Eq. (3.84) agrees well with the predicted data by the Lord Kelvin's formula. This section also presents calculation of water vapour pressure and relative humidity for the soil columns. The data for these soil columns were collected from the research literature and measured from the laboratory testing program.

Section 6.3 presented the verification of the effect of the osmotic suction on evaporation. The verification was done for the columns of the salinized silt from the drying tests conducted by Dunmola (2012). The verification was also done for the thin soil layers of the Ottawa sand and Devon silt mixed with 50 g/l, 100 g/l, 200 g/l and 250 g/l NaCl. These results show the evaporation rate from the columns of salinized soil depends not only on osmotic suction, but also salt crust resistance developed at the surface. However, the salt crust resistance does not significantly effect on evaporation from the thin salinized soil.

Section 6.4 presented the verification of the new soil-atmosphere flux equation in uncoupling procedure. The verification was done for the soil columns collected from the research literature. Two procedures of the verification are carried out for the soil columns. The evaporative fluxes from soil columns in the first procedure are numerically computed using the ComSol-Multiphysics

software to solve the moisture flow equation with the new soil-atmosphere equation as a boundary condition. The computed results using this procedure were denoted as AE–ComSol. It appeared that the results of AE–ComSol depend much on the unsaturated hydraulic conductivity function implemented in ComSol-Multiphysics

In addition, the evaporative fluxes in the second procedure are calculated using Excel Spreadsheet with the measured water content as data input to the new soil-atmosphere equation. The calculated results for this procedure were denoted as AE–Excel. It was observed that the results of AE–Excel show reasonable agreement with the measured evaporative data for all investigated tests in Section 6.4.

CHAPTER 7
CONCLUSIONS AND RECOMMENDATIONS

7.1 STUDY OBJECTIVES

The objectives of this thesis as stated in Chapter 1 are summarized as follows:

1. To enhance and possibly modify a soil-atmosphere equation for prediction of the actual evaporation from soil surfaces.

2. To derive an enhanced formulation for estimating suction at evaporation-rate reduction point and generate water content at evaporation-rate reduction point.

3. To re-visit and possibly develop a new set of equations for estimating water vapour pressure, relative humidity and soil surface resistance at soil surface.

4. To develop a new formulation that incorporates osmotic suction in the soil and the effect of salt accumulation at soil surfaces.

5. To carry out the laboratory tests on the actual rate of evaporation from thin and thick soil layers of bare soil and saline soil.

6. To compare the test results collected from the research literature and the current laboratory testing program with the computed results using the new theoretical approach.

The primary objective was to re-visit and possibly modify the commonly used soil-atmosphere model and to propose a function for the effect of osmotic suction that could be used for estimating the actual rate of evaporation from salinized soil surfaces. In addition, the new set of evaporation equations would

be considered for estimating water content at the evaporation-rate reduction point, relative humidity and soil surface resistance at the soil surface.

A comprehensive laboratory testing program was carried out to measure important factors related to water evaporation from thin and thick soil layers. The test results measured in the current laboratory program, (as well as data collected from the literature), were used to verify the new proposed equations presented in Chapter 3.

The results of the theoretical approach and laboratory research program indicate the study objectives have been met. The research objectives were achieved in a progressive manner. Several conclusions can be derived from specific parts of the research program. The research study also revealed that there are other topics that need to be addressed in future research programs. Some recommendations for future research have been made.

7.2 CONCLUSIONS

The process of evaporation from a soil surface has been studied. Theoretical equations used for estimating evaporation were modified and applied to simulate laboratory results. The following conclusions can be drawn from the research program:

1. The soil-atmosphere flux equation describing evaporation from a soil surface on the basis of net radiation, wind speed, relative humidity of the air and the soil surface, and soil surface resistance was modified and takes the following form,

$$E_A = \frac{\Gamma Q + \eta \dfrac{f'(u)}{f(u)} E'_a}{\Gamma + \eta A \dfrac{f'(u)}{f(u)}} \qquad (3.69)$$

Equation (3.69) contains not only a component of the relative humidity at a soil surface, but also incorporates a soil surface resistance term. Equation (3.69) indicates that the evaporation rate will decrease during the drying process in which the relative humidity of the soil surface decreases and the soil surface resistance increases.

The ratio of $f'(u)/\ f(u)$ can be calculated as follows:

$$\frac{f'(u)}{f(u)} = 1 + \frac{C_{at}}{C_s} = 1 + \frac{r_s}{r_{av}} \tag{3.75}$$

Equation (3.75) can be substituted into Eq. (3.69) for actual evaporation to demonstrate the effect of soil surface resistance on the actual evaporation rate.

$$r_s = 10 \times e^{0.3563(\theta_R - \theta_{top})} \tag{3.86}$$

Equation (3.69) reduces to the conventional Penman (1948) equation when the *A* variable is equal to unity (i.e., relative humidity of 100 percent for a saturated surface) and surface resistance is assumed to be zero. Equation (3.69) also reduces to the Wilson (1990) equation when $\frac{f'(u)}{f(u)} = 1$ (i.e., the transmission functions for mass and heat are assumed to be the same or the soil surface resistance equals to zero).

2. The rate of evaporation begins to decline at total suction approximately 3,000 kPa for thin soil layers. However, the finding of the total suction at evaporation-rate reduction point appears to be different for thick soil layers or soil columns. The following formula can be used to determine the total suction at which the rate of evaporation begins to decline for the thick soil layers or soil columns.

$$\psi_R = \begin{cases} \psi_{aev} & if\ \ a = 0 \\ \psi_{res} & if\ \ a = 1 \\ \psi_{res}^{a} \times \psi_{aev}^{1-a} & if\ \ 0 < a < 1 \end{cases} \tag{3.80}$$

Equation (3.80) is a function of the unsaturated soil mechanics parameters that can be determined from the soil-water characteristic curve, SWCC; namely, the air-entry value and residual soil suction. These parameters need to be taken into consideration and applied when solving typical geotechnical engineering problems.

3. The Lord Kelvin's formula of relative humidity is only valid for thin soil layers, but it is not valid for thick soil layers or soil columns during drying process. The vapour pressure of air is not always in equilibrium with liquid water in the soil pores at soil surface of the thick soil layers or soil columns during drying process.

4. The distance for water vapour travel to the soil-atmosphere interface in thin soil layers is negligible. In this case, the soil surface resistance can be ignored. However, the soil surface resistance is significant for estimating evaporation from thick soil layers or soil columns. This behaviour is particularly of interest when considering evaporation from coarser soils (e.g., sand).

5. Field capacity (i.e., volumetric water content) is a term familiar to agricultural engineers and is sometimes used for estimating relative humidity and soil surface resistance at soil surfaces; however, it is not familiar to geotechnical engineers. Water content at evaporation-rate reduction point is better generated from the total suction at evaporation-reduction point using soil-water characteristic curves. Hence, water content at evaporation-rate reduction point depends on the soil properties of unsaturated-soil engineering (i.e., air-entry value and residual soil suction).

6. Water vapour pressure for thick soil layers or soil columns was found to be the following formula:

$$p_v = \beta \times p_v^{sat} + (1-\beta) \times p_v^{air} \tag{3.83}$$

where:

p_v = actual vapour pressure at soil surface, kPa;

p_v^{sat} = saturated vapour pressure at soil surface, kPa;

p_v^{air} = actual air pressure immediately above soil surface, kPa;

β = coefficient representing the surface moisture availability.

The relative humidity is determined as the definition of the ratio of actual vapor pressure to saturated vapor pressure under the same surface condition (i.e., the same surface temperature).

$$RH = \frac{p_v}{p_v^{sat}} \tag{3.84}$$

7. The magnitude of the difference between the actual evaporation rate from a non-saline soil surfaces and a salinized soil surface depends on the initial pore-water salinity. The evaporation rates from salinized surfaces are lower than that from non-saline surface during the first period of drying. The higher the initial pore-water salinity at the surface, the greater will be the depression of the actual evaporation rate from the surface. For example, the relative evaporation was 0.8, 0.75, 0.65 and 0.63 for the Ottawa sand mixed with 50 g/l, 100 g/l, 200 g/l and 250 g/l NaCl, respectively in the laboratory testing program. This pattern of relative evaporation is similar to the sieved Devon Silt mixed with 50 g/l, 100 g/l, 200 g/l and 250 g/l NaCl.

8. Osmotic suction for thin soil layers can be found as a function of initial salt content and the water content determined from the soil-water characteristic curves:

$$\pi = 2 \times \left(\frac{\theta_{salt0} \times \theta_{sat} \times \rho_s}{\theta_{SWCC} \times M_{molar}} \right) RT \tag{3.100}$$

Osmotic suction increases total suction and hence reduces the relative humidity at the soil-salinized surface. This behaviour reduces evaporation rate from the soil-salinized surface due to reduction of the pressure gradient between the soil surface and the atmosphere above.

9. Effects of factors related to salt content on evaporative rate were separately analyzed for thin soil layers and soil columns. The computed rate of evaporation from the thin soil layers was found to mainly depend on osmotic suction. However, the computed rate of evaporation from the soil columns of salinized soil was found to depend not only on osmotic suction, but also on the salt crust resistance developed at the surface.

7.3 RECOMMENDATION FOR FUTURE RESEARCH

The primary objective of this thesis was to modify a soil-atmosphere flux equation and to develop a function of osmotic suction which is a factor to control evaporation from a soil surface. Although this objective has been achieved, further theoretical studies are recommended for the proposed methodology before being applied to engineering practise.

1. Scale-up and field verification of the soil-atmosphere equation for evaluating fluxes should be undertaken. Currently, the net radiation at soil surface is assumed to be equal to that at water surface, which is conservative for dry soil surfaces due to ignorance of the effect of higher albedo.

2. The proposed model theory should be incorporated into a numerical software package (e.g., finite element method) and used to solve real-world problems.

3. The proposed equation of suction at the evaporation-rate reduction point should be checked. This equation is limited for sand and silt material throughout this thesis. More data sets of evaporation on various soil textures should be assessed to verify this equation. Further assessment is required to study effects of shrinkage and cracking on suction at which the rate of evaporation begins to decline from potential evaporation rate.

4. The squeezing test was conducted to measure osmotic suction for verifying the proposed function of osmotic suction. This function was also used to estimate evaporation rate from salinized soil measured in the

laboratory testing program. However, it should be checked before being applied to engineering practise.

5. An equation of solute transport should be coupled with the equations for the transient flow of water and heat so that the accumulation of salt on the soil surface can be simulated.

6. Limited data on soil surface resistance was used in this thesis. The data was collected from the research literature. It is recommended that measurement of soil surface resistance should be carried out in further research of evaporation from bare soil and salinized soil. The results are used to verify the proposed equation of soil surface resistance.

7. Further evaluation of the coefficient of permeability during evaporation process is necessary. A laboratory test of the coefficient of permeability should be carried out in columns of bare soil and salinized soil. In other words, evaluation of effect on salt content on movement of water the bottom of the soil columns to surface is also necessary.

REFERENCES

Aluwihare, S., and Watanabe, K. 2003. Measurement of evaporation on bare soil and estimating surface resistance. Journal of Environmental Engineering, Vol. 129, No. 12, pp. 1157–1168

Alvenas, G., and Jansson, P.E. 1997. Model for evaporation, moisture and temperature of bare soil: calibration and sensitivity analysis. Agricultural and Forest Meteorology, Elsevier Science, Vol. 88, pp. 47–56.

Arenson, L., Xia, D., Biggar, K., and Sego, D. 2005. Freezing process in Devon silt-Using time laps photography. Proceedings of the Fifty Eighth Canadian Geotechnical Conference, Saskatoon, SK., Canada.

Arifin, Y.F., and Schanz, T. 2009. Osmotic suction of highly plastic clays. Acta Geotechnica, Vol. 4, pp. 177–191.

Avissar, R., and Mahrer, Y. 1988. Mapping frost-sensitive areas with a three-dimensional local-scale numerical model. Part I: Physical and numerical aspects. Journal of Applied Meteorology, Vol. 27, pp. 400–413.

Bittelli, M., Ventura, F., Campbell., G., Snyder, R., Gallegati., F. and Pisa, P. 2008. Coupling of heat, water vapor and liquid water fluxes to compute evaporation in bare soils. Journal of Hydrology, Vol. 362, pp. 191–205.

Bouyoucos, G. J. 1915. Effect of temperature on the movement of water vapor and capillary moisture in soils. Journal of Agricultural Research, Vol. 5, pp. 141-172.

Brooks, R.H., and Corey, A.T. 1964. Hydraulic properties of porous media. Colorado State University Hydrology Paper, No.3. Fort Collins, CO.

Bruch, P.G. 1993. A laboratory study of evaporative fluxes in homogeneous and layered soils. Master of Science Thesis, University of Saskatchewan, Saskatoon, SK., Canada.

Brutsaert, W. 1982. Evaporation into the atmosphere: theory, history, and applications. Dordrecht, The Netherlands: Kluwer Academic Publishers. 299 pp.

Camillo, P.J., and Gurney, R.J. 1986. A resistance parameter for bare-soil evaporation models. Soil Science, Vol. 141, No. 2, pp. 95–105.

Camillo, P.J., Gurney, R.J., and Schmugge, T.J. 1983. A soil and atmospheric boundary layer model for evapotranspiration and soil moisture studies. Water Resources Research, Vol. 19, No. 2, pp. 371–380.

Campbell, G.S. 1985. Soil physics with basic-Transport models for soil-plant systems. Developments in Soil Science. Elsevier Science, Amsterdam, Netherlands.

Chen, X.Y. 1992. Evaporation from a salt-encrusted sediment surface: Field and laboratory studies. Australian. Journal of Soil Research, Vol. 30, pp. 429–442.

COMSOL ,Inc. 2008. COMSOL Multiphysics Modeling Guide. Los Angeles, CA, USA.

COMSOL ,Inc. 2008. COMSOL Multiphysics User's Guide. Los Angeles, CA, USA.

Couvillion, R. J. 1981. Heat and mass transfer in a semi-infinite moist soil with a drying front present. Ph.D. Thesis, Georgia Institute of Technology, U.S.A.

Covey, W. 1959. Testing a hypothesis concerning the quantative dependence of evapotranspiration on availability of moisture. Soil Physics, A. & M. College of Texas, College Station, Master of Science Thesis, 58 pp.

Daamen, C.C., and Simmonds, L.P. 1996. Measuring evaporation and its estimation using surface resistance. Water Resources Research, Vol. 32, No. 5, pp. 1393–1402.

Dempsey, B. J., and Elzeflawy, A. 1976. Mathematical model for predicting moisture movement in pavement systems. Transp. Res. Rec. 612, pp. 48-55, National Academy of Sciences, Washington, D. C.

Doornenbos, J., and W.O. Pruitt. 1977. Guidelines for predicting crop water requirements. FAO Irrig. Drain. Paper No. 24, 2nd ed., Food and Agric. Orgn. of the United Nations, Rome, Italy, 156 pp.

Dunmola, A. S. 2012. Predicting evaporative fluxes in saline soil and surface-deposited thickened mine tailings. Ph.D. Thesis, Department of Civil and Environmental Engineering, Carleton University, Ottawa, Ontario, Canada.

Ebrahimi-Birang, N., Gitirana Jr, G.F.N., Fredlund, D.G., Fredlund, M.D. and Samarasekera, L. 2004. A lower limit for the water permeability coefficient. Proceedings of the Fifty-Severnth Canadian Geotechnical Conference, Quebec City. October 24 -27. Vol. 1, pp. 12–19.

Edlefsen, N.E., and Anderson, A.B.C. 1943. Thermodynamics of soil moisture, Hilgardia, Vol. 15, No. 2, pp. 31–298.

Fahey, M., Fujiyasu, Y., 1994. The influence of evaporation on the consolidation behaviour of gold tailings. Proceedings of the First International Congress on Environmental and Geotechnics. Bitech Publishers, Edmonton, Alberta, Canada, pp. 481–486.

Fen Shu, S. 1982. Moisture and heat transport in a soil layer forced by atmospheric conditions. Master of Science Thesis, University of Connecticut, USA.

Fredlund, D.G. and Dakshanamurthy, V. 1982. Transient flow process in unsaturated soils under flux boundary conditions. Proceedings of the Fourth International Conference on Numerical Methods in Geomechanics, Edmonton.

Fredlund, D.G., Rahardjo, H., and Fredlund, M. D. 2012. Unsaturated soil mechanics in engineering practice. John Willey & Sons, Inc., Hoboken, New Jersey, USA.

Fredlund, D.G. and Xing, A. 1994. Equations for the soil-water characteristic curve. Canadian Geotechnical Journal, Vol. 31, pp. 521–532.

Fredlund, M.D. Zhang, J.M., Tran, D., and Fredlund, D.G. 2011. Coupling heat and moisture flow for the computation of actual evaporation. Paper No. 1058, Proceedings of the Canadian Geotechnical Conference and Fifth Pan-American Conference, Toronto, ON, Canada. October 2-6.

Fujimaki, H., Shimao, T., Inoue, M., and Nakane, K. 2006. Effects of salt crust on evaporation from a bare soil. Vadoze Zone Journal, Vol. 5, pp. 1246–1256.

Fujimaki, H., Shiozawa, S., and Inoue, M. 2003. Effect of salty crust on soil albedo. Agricultural and Forest Meteorology, Vol. 118, pp. 125–135.

Fujiyasu, Y. and Fahey, M. 2000. Experimental study of evaporation from saline tailings. Journal of Geotechnical and Geoenvironmental Engineering, Vol. 126, No. 10, pp. 18–27.

Fujiyasu, Y., Fahey, M., and Newson, T. 2000. Field investigation of evaporation from freshwater tailings. Journal of Geotechnical and Geoenvironmental Engineering, Vol. 126, No. 6, pp. 556–567.

Gitirana Jr., G.F.N. 2005. Weather-related geo-hazard assessment model for railway embankment stability. PhD Thesis, Department of Civil Engineering, University of Saskatchewan, Saskatoon, Canada, 411p.

Gran, M.,J. Carrera, J. Massana, S. Olivella, and M. W. Saaltink. 2011. Dynamics of water vapour flux and water separation processes during evaporation from a salty dry soil. Journal of Hydrology, Vol. 396, pp. 215–220.

Gran, M.,J. Carrera, S. Olivella, and M. W. Saaltink. 2011. Modeling evaporation processes in a saline soil from saturation to oven dry conditions. Hydrology and Earth System Sciences, Vol. 15, pp. 2077–2089.

Gray, D.M. 1970. Handbook on the principles of hydrology. Canadian National Committee for the International Hydrological Decade, National Research Council of Canada, Ottawa, Canada.

Hillel, D., 1980. Applications of Soil Physics. Academic Press, New York.

Howell, T. A., and Evett, S. R. 2004. The Penman-Monteith Method. USDA-Agricultural Research Service, Conservation & Production Research Laboratory, P.O. Drawer 10, Bushland, Texas 79012-0010.

Jame, Y.W., and Norum, D.I. 1980. Heat and Mass Transfer in a Freezing Unsaturated Porous Medium. Water Resources Research, Vol. 16, No. 4, pp. 811–819.

Jury, W. A. 1973. Simultaneous transport of heat and moisture through a medium sand. Ph.D. Thesis, University of Wisconsin.

Kimball, B.A., Jackson, R.D., Reginato, R.J., Nakayama, F.S., and Idso, S.B. 1976. Comparison of field-measured and calculated soil-heat fluxes. Soil Science Society of America Journal, Vol. 40, No. 1, pp. 18–25.

Kohsiek, W. 1981. Rapid circulation chamber for measuring bulk stomatal resistance. Journal of Applied Meteorology, American Meteorological Society, Vol. 20, pp. 42–52.

Kondo, J., and Saigusa, N. 1992. A model and experimental study of evaporation from bare-soil surfaces. Journal of Applied Meteorology, American Meteorological Society, Vol. 31, pp. 304–312.

Kondo, J., Saigusa, N., and Sato, T. 1990. A parameterization of evaporation from soil surfaces. Journal of Applied Meteorology, American Meteorological Society, Vol. 29, pp. 385–389.

Konukcu, F., Istanbulluoglu, A., Kocaman, I. 2004. Determination of water content in drying soils: incorporating transition from liquid phase to vapour phase. Australian Journal of Soil Research, Vol. 42, pp. 1–8.

Krahn, J., and Fredlund, D.G. 1972. On total, matric and osmotic suction. Journal of Soil Science, Vol. 114, No. 5, pp. 339–348.

La Mer, V.K., and Healy, T.W. 1965. Evaporation of water: its retardation by monolayers. Science, Vol. 148, pp. 36–41.

Lee, T.J., and Pielke, R. 1992. Estimating the soil surface specific humidity, Notes and Correspondence. Journal of Applied Meteorology, American Meteorological Society, Vol. 31, pp. 480–484.

Lowe, P.R. 1977. An approximating polynomial for the computation of saturation vapor pressure, Journal of Applied Meteorology, Vol. 16, pp. 100-103.

Machibroda, R.L., Wilson, G. W., and Barbour, S. L. 1993. Evaluation of the net infiltrative fluxes across the surface of exposed mine tailings. Proceedings of the Canadian Geotechnical Conference, pp. 167–174.

Mahfouf, J. F., and Noilhan, J. 1991. Comparative study of various formulations of evaporation from bare soil using in-situ data. Journal of Applied Meteorology, American Meteorological Society, Vol. 30, pp. 1354–1365.

McCumber, M.C., and Pielke, R.A. 1981. Simulation of the effects of surface fluxes of heat and moisture in a mesoscale numerical model. Part I: Soil layer. Journal of Geophysical Research, Vol. 86, pp. 9929–9938.

Mihalovi'c, D.T., Pielke, R. A., Rajkovi'c, B., Lee, T.J., Jefti'c, M. 1993. A resistance representation of schemes for evaporation from bare and partly plant-covered surfaces for use in atmospheric models. Journal of Applied Meteorology, Vol. 32, pp. 1038–1054.

Mohamed, A.A., Watanabe, K., and Kurokawa, U. 1997. Simple method for determining the bare soil resistance to evaporation. Journal of Groundwater Hydrology, Vol. 40, No. 2, pp. 185–202.

Monteith, J. L., and Unsworth, M. H. 2008. Principles of Environmental Physics (3rd Edition). Academic Press, Saint Louis, MO, USA.

Monteith, J.L. 1965. Evaporation and the environment. In the movement of water in living organisms. XIX Symposium Society for Experimental Biology, Swansea, Cambridge, University Press, Vol. 19, pp. 205–234.

Morton, F.I. 1969. Potential evaporation as a manifestation of regional evaporation. Water Resources Research, Vol. 5, No. 6, pp. 1244–1255.

Morton, F.I. 1971. Catchment evaporation and potential evaporation - further development of a climatologic relationship. Journal of Hydrology, Vol. 12, pp. 81–99.

Morton, F.I. 1975. Estimating evaporation and transpiration from climatological observations. Journal of Applied Meteorology, American Meteorological Society, Vol. 14, No. 4, pp. 488–497.

Morton, F.I. 1985. The complementary relationship areal evapotranspiration model: How it works. Proceedings of the National Conference on Advances in Evapotranspiration, ASAE, Chicago, IL, pp. 377–384.

Nappo, C.J. 1975. Parameterization of surface moisture and evaporation rate in a planetary boundary layer model. Journal of Applied Meteorology, Vol. 14, pp. 289–296.

Newson, T.A., and Fahey, M. 2003. Measurement of evaporation from saline tailings storages. Engineering Geology, Vol. 70, pp. 217–233.

Nixon, J.F. 1991. Discrete ice lens theory for frost heave in soils. Canadian Geotechnical Journal, Vol. 28, pp. 843–859.

Oke, T.R. 1993. Boundary layer climates. Cambridge University Press, Cambridge, 435 pages.

Passerat de Silans, A., Bruckler, L., Thony, J.L., and Vauclin, M. 1989. Numerical modeling of coupled heat and water flows during drying in a stratified bare soil-Comparison with field observation. Journal of Hydrology, Vol. 105, pp.109–138

Penman, H.L. 1948. Natural evapotranspiration from open water, bare soil and grass. Proceedings of the Royal Society of London, Series A193, pp. 120–145.

Penman, H.L. 1953. The physical basis of irrigation control. Rep. 13th Intl. Hort. Congr., Vol. 2, pp. 913-914.

Philip, J.R. 1957. The theory of infiltration: the infiltration equation and its solution. Journal of Soil Science, Vol. 83, pp. 345–357.

Philip, J.R., and de Vries, D.A. 1957. Moisture movement in porous materials under temperature gradient. Transactions, American Geophysical Union, Vol. 38, pp. 222–232.

Priestley, C.H.B., and Taylor, R.J. 1972. On the assessment of the surface heat flux and evaporation using large-scale parameters. Monthly Weather Review, Vol. 100, pp. 81–92.

Raupach, M.R., and J.J. Finnigan. 1988. Single-layer models of evaporation from plant canopies are incorrect but useful, whereas multilayer models are correct but useless: Discussion. Australian Journal of Plant Physiology, Vol. 15, pp. 706–716.

Richards, L.A. 1931. Capillary conduction of liquids through porous medium. Journal of Physics, Vol. 1, pp. 318–333.

Richards, B.G. 1965. Measurement of the free energy of soil moisture by the psychrometric technique using thermistors. Moisture Equilibria and Moisture Changes in Soils Beneath Covered Areas, A Symposium in Print, Butterworths, Sydney, pp. 39–46.

Rijtema, P.E. 1965. Analysis of actual evapotranspiration. Agric. Res. Rep. No. 69, Centre for Agric. Publ. and Doc., Wageningen, 111 p.

Ritchie, J.T. 1972. Model for predicting evapotranspiration from a row crop with incomplete cover. Water Resources Research, Vol. 8, pp. 1204–1213.

Robinson, R.A., and Stokes R. H. 1968. Electrolyte Solutions. 2nd ed., Butterworths, London.

Shimojima, E., Yoshioka, R., and Tamagawa, I. 1996. Salinization owing to evaporation from bare-soil surfaces and its influence on the evaporation. Journal of Hydrology, Vol. 178, pp. 109–136.

Simms, P., Grabinsky, M., and Zhan, G. 2007. Modeling evaporation of paste tailings from the Bulyanhulu mine. Canadian Geotechnical Journal, Vol. 44, pp. 1417–1432.

Smith, W.O. 1939. Thermal conductivities in moist soils. Soil Science Society of America Proceedings, Vol. 4, pp. 521-524.

Sophocleous, M.A. 1978. Analysis of heat and water transport in unsaturated-saturated porous media. Ph.D. Thesis, University of Alberta, Edmonton, Canada.

Sophocleous, M.A. 1979. Analysis of water and heat flow in unsaturated-saturated porous media. Water Resources Research, Vol. 15, No. 5, pp. 1195–1206.

Sreedeep, S., and Singh, N. 2006. Methodology for determination of osmotic suction of soils. Geotechnical and Geological Engineering, Vol. 24, pp. 1469–1479.

SVFlux Users Manual. 2009. SoilVision Systems Ltd., Saskatoon SK., Canada.

Toth, B.M. 1999. Evaporation from bare soil following rainfall. Master of Science, Department of Agricultural and Bioresource Engineering, University of Saskatchewan, Saskatoon, SK., Canada.

Van de Griend, A.A., and Owe, M. 1994. Bare soil surface resistance to evaporation by vapor diffusion under semiarid conditions. Water Resources Research, Vol. 30, No. 2, pp. 181–188.

Watanabe, K., and Tsutsui, Y. 1994. A new equipment used for measuring evaporation in a field. Proceedings of the Seventh International Congress, Portugal, IAEG, pp. 309–313.

Wetzel, P.J., and Chang, J. 1987. Concerning the relationship between evapotranspiration and soil moisture. Journal of Applied Meteorology and Climatology, Vol. 26, pp. 18–27.

Wilson, G.W. 1990. Soil evaporative fluxes for geotechnical engineering problems. Ph.D. Thesis, University of Saskatchewan, Saskatoon, SK., Canada.

Wilson, G.W., Barbour, S.L., and Fredlund, D.G. 1997. The effect of soil suction on evaporative fluxes from soil surfaces. Canadian Geotechnical Journal, Vol. 34, No. 1, pp. 145–155.

Wilson, G.W., Fredlund, D.G., and Barbour, S.L. 1991. The evaluation of evaporative fluxes from soil surfaces for problems in geotechnical engineering. Proceedings of the Canadian Geotechnical Conference, pp. 1–9.

Wilson, G.W., Fredlund, D.G., and Barbour, S.L. 1994. Coupled soil-atmosphere modeling for soil evaporation. Canadian Geotechnical Journal, Vol. 31, No. 2, pp. 151–161.

Yanful, E.K., and Choo, L.P. 1997. Measurement of evaporative fluxes from candidate cover soils. Canadian Geotechnical Journal, Vol. 34, pp. 447–459.

Yanful, E.K., Mousavi SM, Yang M. 2003. Modeling and measurement of evaporation in moisture-retaining soil covers. Advances in Environmental Research, Vol. 7, No. 4, pp. 783–801.

APPENDIX A

TEST RESULTS OF THIN LAYER DRYING FROM THE LABORATORY TESTING PROGRAM

Table A.1 Summary of measured rate of evaporation and gravimetric water contents for Ottawa sand in set 2 on December 1, 2012.

Time (mins)	PE (mm/day)	Actual Evaporation (mm/day)					Gravimetric water content (%)				
		S2	S2+50	S2+100	S2+200	S2+250	S2	S2+50	S2+100	S2+200	S2+250
20	2.64	2.86	2.52	2.52	2.06	1.83	34.47	29.53	28.59	25.52	24.77
40	2.41	2.41	2.06	1.95	1.60	1.38	31.31	26.85	25.96	23.43	22.91
60	2.29	2.18	1.83	1.83	1.49	1.38	28.66	24.67	23.92	21.81	21.51
80	2.41	2.18	1.95	1.72	1.49	1.38	26.26	22.72	22.01	20.30	20.12
100	2.52	2.41	2.06	1.95	1.60	1.38	23.86	20.66	20.22	18.79	18.72
120	2.41	2.06	1.83	1.72	1.26	1.26	21.21	18.47	18.18	17.17	17.33
140	2.29	2.06	1.72	1.60	1.26	1.26	18.94	16.52	16.39	15.89	16.05
160	2.29	1.95	1.83	1.49	1.26	1.38	16.67	14.70	14.71	14.62	14.77
180	2.29	2.06	1.72	1.49	1.26	1.26	14.52	12.76	13.16	13.34	13.37
200	2.29	2.06	1.60	1.49	1.26	1.26	12.25	10.94	11.60	12.06	12.09
220	2.29	2.06	1.60	1.15	1.26	1.26	9.97	9.23	10.05	10.79	10.81
240	2.29	2.06	1.49	1.38	1.38	1.26	7.70	7.53	8.85	9.51	9.53
260	2.29	1.95	1.26	1.26	1.26	1.26	5.43	5.95	7.42	8.12	8.26
280	2.18	1.83	1.15	1.15	1.26	1.26	3.28	4.62	6.10	6.84	6.98
300	2.29	0.92	1.26	1.38	1.38	1.26	1.26	3.40	4.90	5.57	5.70
320	2.29	0.11	0.92	1.15	1.15	1.15	0.25	2.07	3.47	4.18	4.42
340	2.18	0	0.46	1.03	1.26	1.26	0.13	1.09	2.27	3.02	3.26
360	2.29	0	0.11	0.46	1.03	0.92	0.13	0.61	1.20	1.74	1.98
380	2.29	0	0	0.11	0.23	0.34	0.13	0.49	0.72	0.70	1.05
400	2.18	0	0	0	0	0.11	0.13	0.49	0.60	0.46	0.70
420	2.18	0	0	0	0	0	0.13	0.49	0.60	0.46	0.58

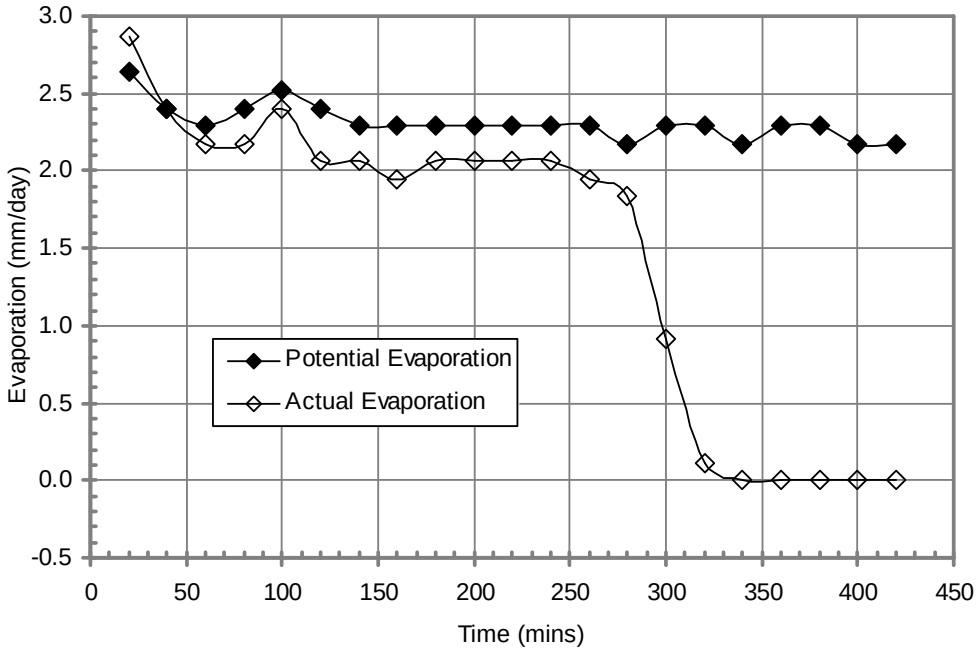

Figure A.1 Actual and Potential Evaporation rates versus drying time for Ottawa sand in Set 2.

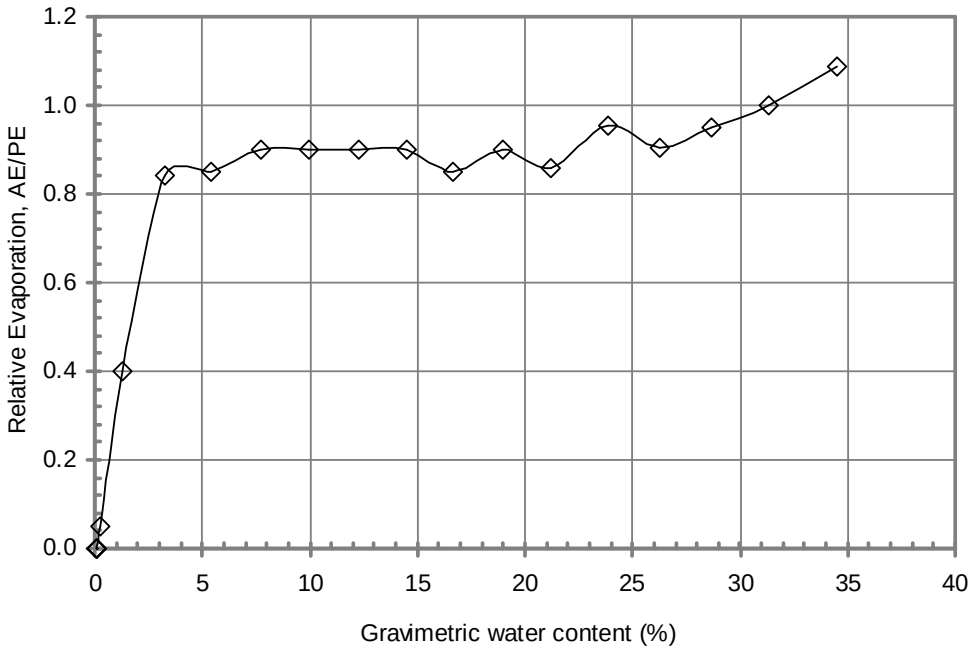

Figure A.2 Plot of Relative Evaporation (*AE/PE*) versus gravimetric water content for Ottawa sand in Set 2.

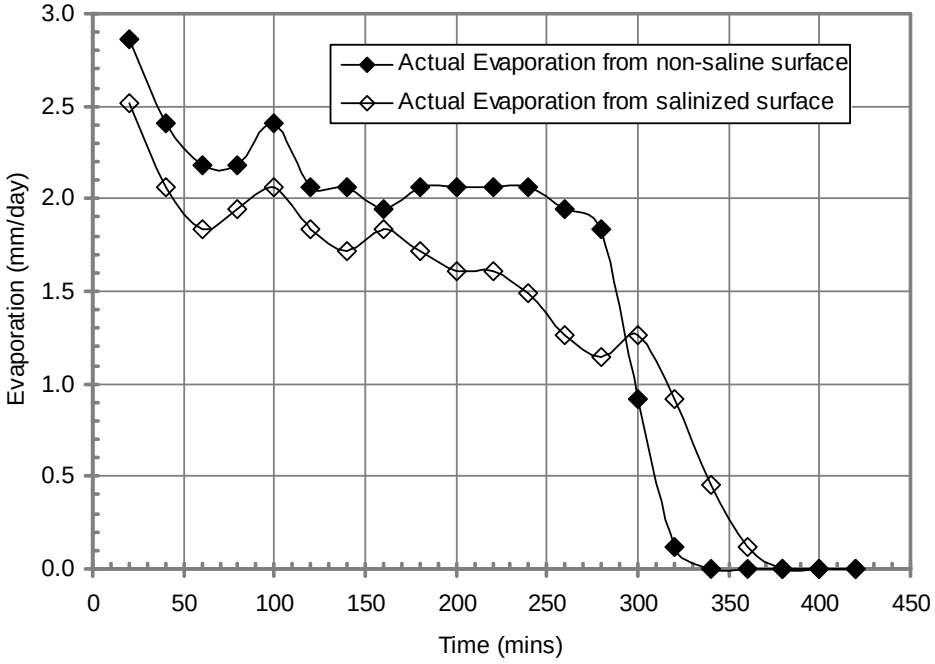

Figure A.3 Actual Evaporation rates versus drying time for Ottawa sand and Ottawa sand mixed with 50 g/l NaCl in Set 2.

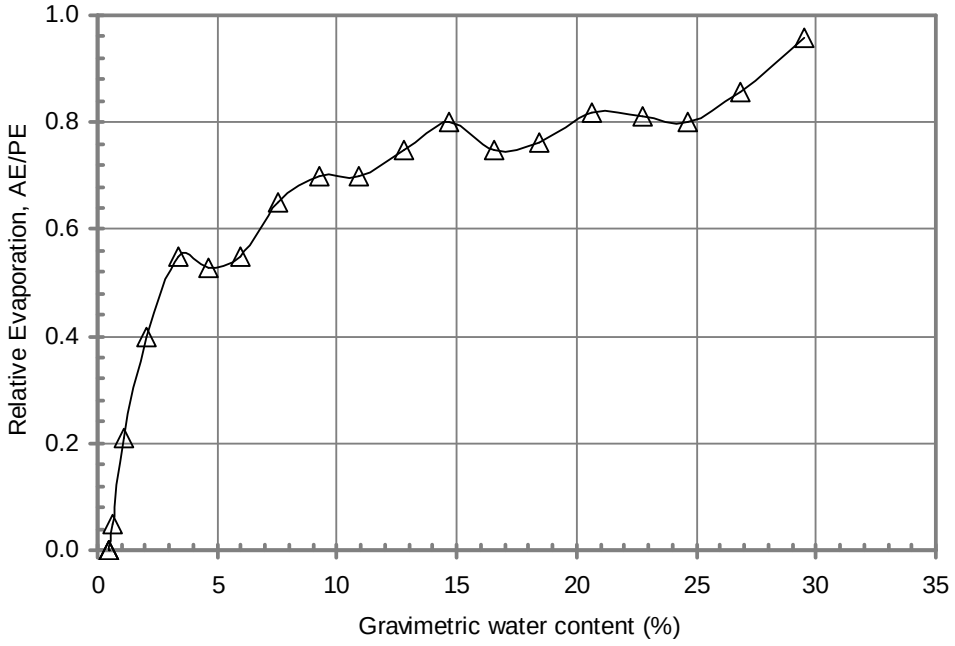

Figure A.4 Plot of Relative Evaporation (*AE/PE*) versus gravimetric water content for Ottawa sand mixed with 50 g/l NaCl in Set 2.

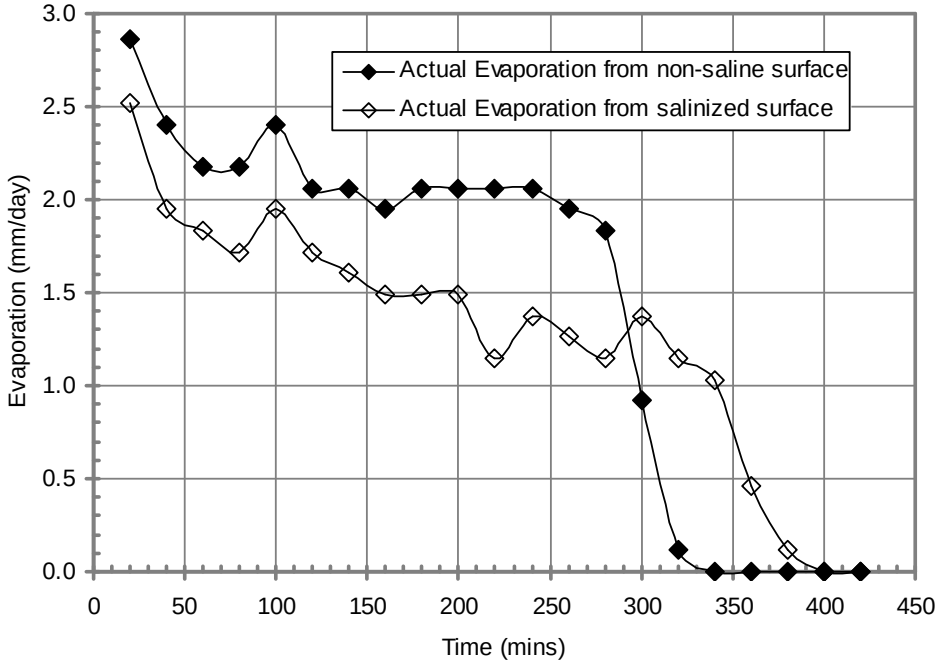

Figure A.5 Actual Evaporation rates versus drying time for Ottawa sand and Ottawa sand mixed with 100 g/l NaCl in Set 2.

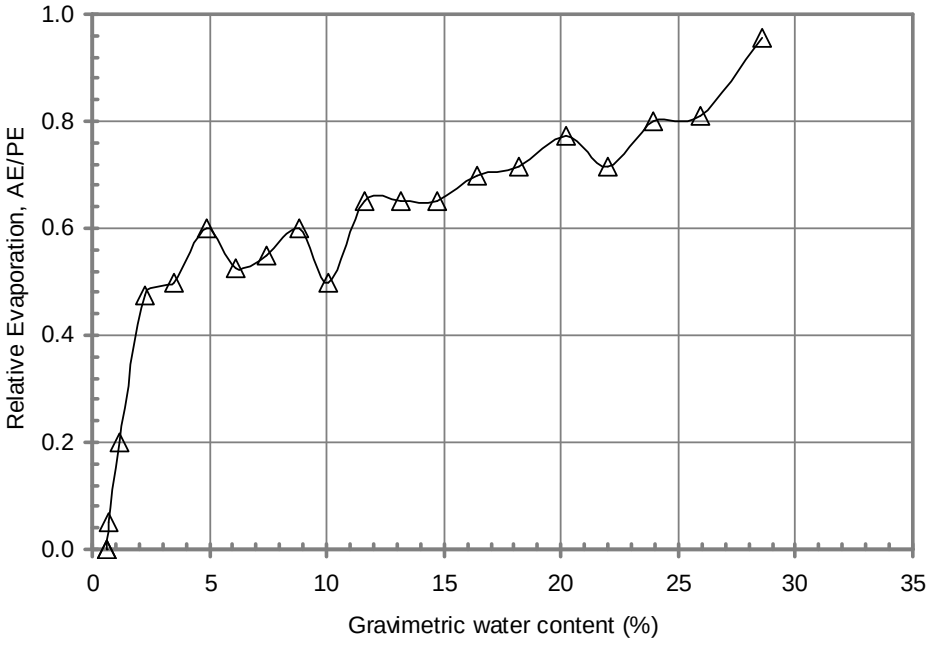

Figure A.6 Plot of Relative Evaporation (*AE/PE*) versus gravimetric water content for Ottawa sand mixed with 100 g/l NaCl in Set 2.

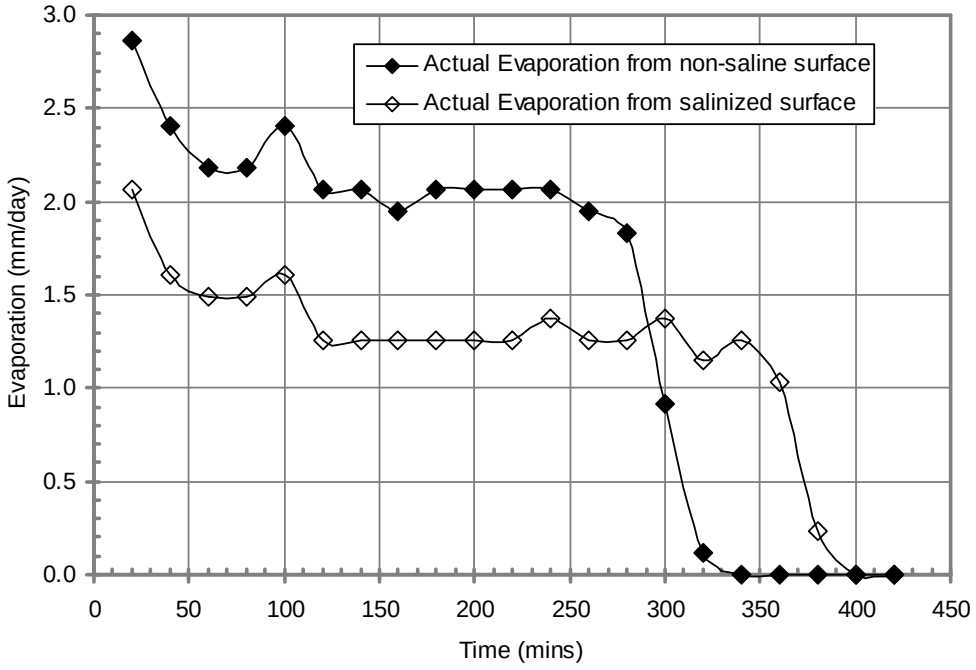

Figure A.7 Actual Evaporation rates versus drying time for Ottawa sand and Ottawa sand mixed with 200 g/l NaCl in Set 2.

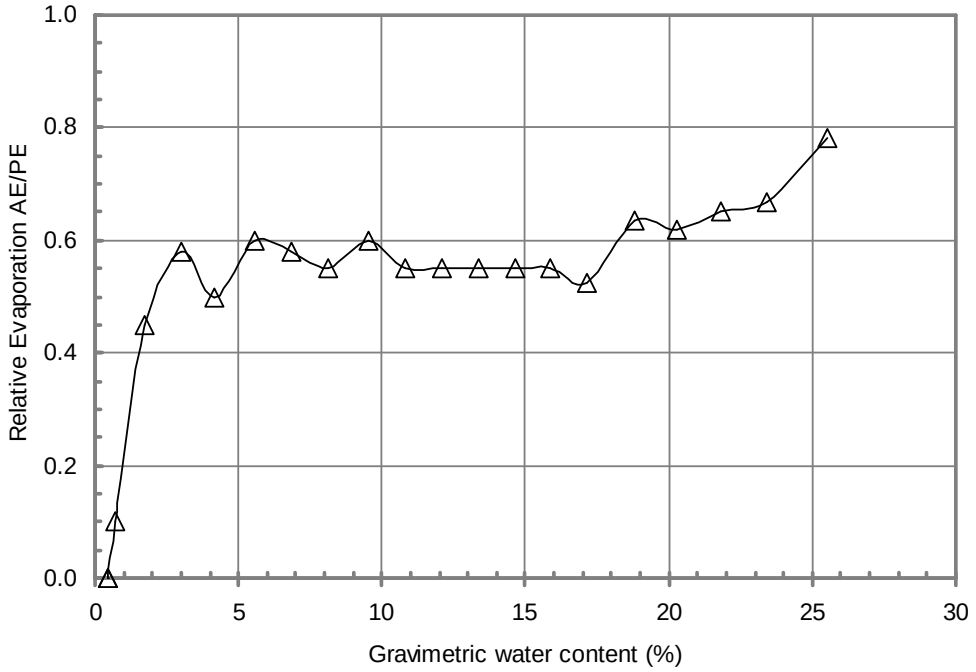

Figure A.8 Plot of Relative Evaporation (*AE/PE*) versus gravimetric water content for Ottawa sand mixed with 200 g/l NaCl in Set 2.

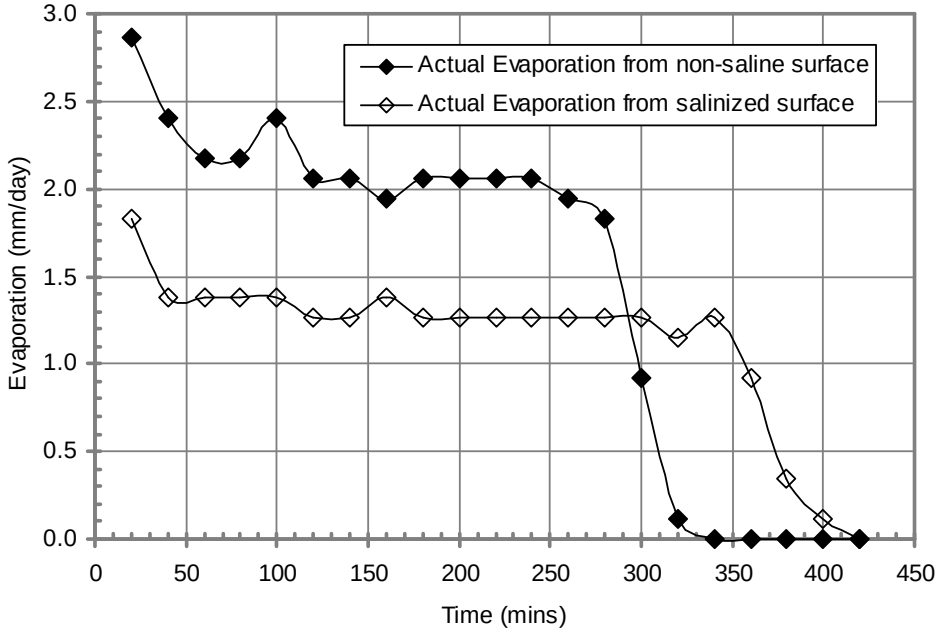

Figure A.9 Actual Evaporation rates versus drying time for Ottawa sand and Ottawa sand mixed with 250 g/l NaCl in Set 2.

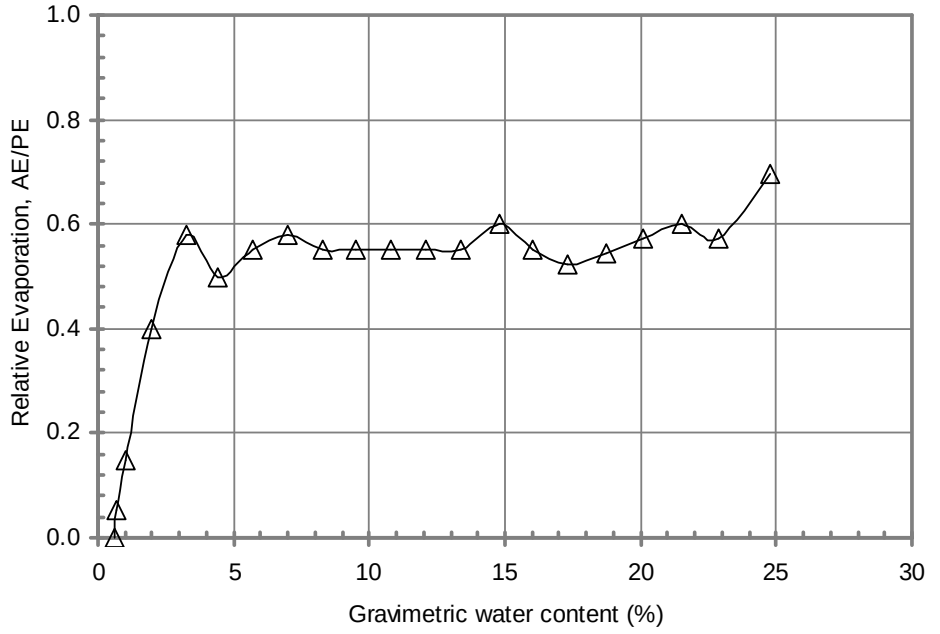

Figure A.10 Plot of Relative Evaporation (*AE/PE*) versus gravimetric water content for Ottawa sand mixed with 250 g/l NaCl in Set 2.

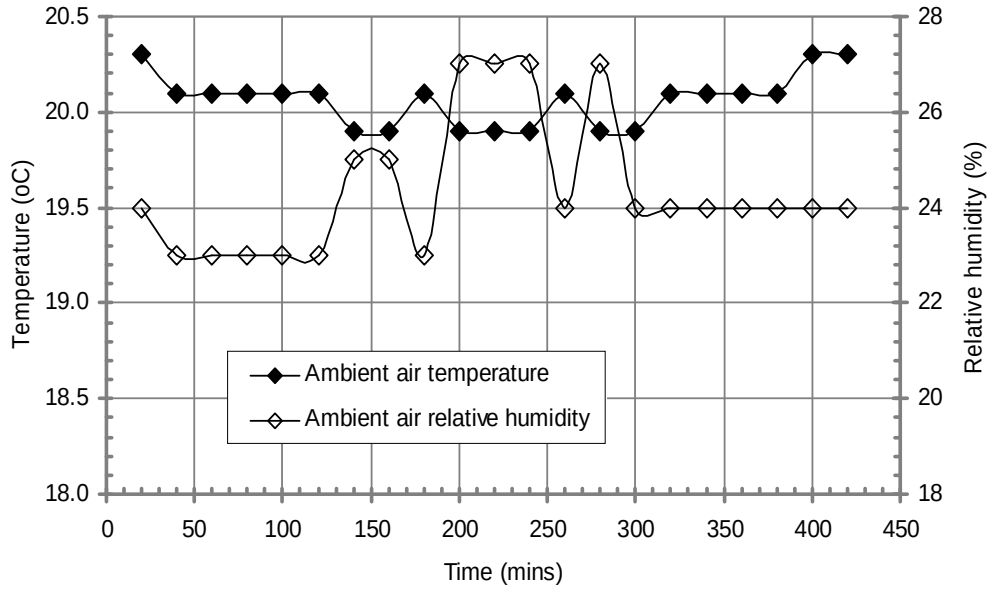

Figure A.11 Measured ambient temperature and relative humidity of the air around the thin sand layer drying tests of Ottawa sand in Set 2.

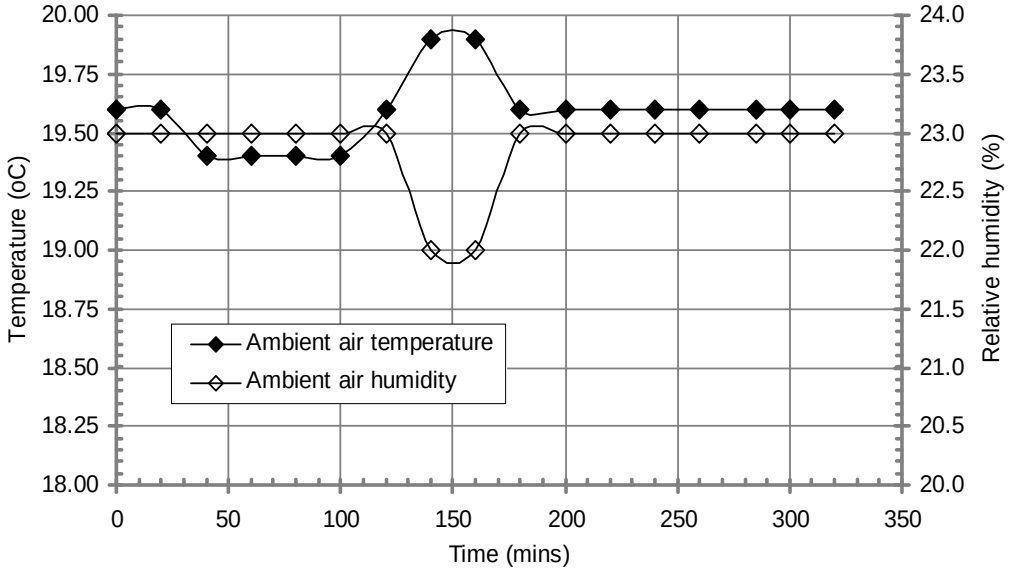

Figure A.12 Measured ambient temperature and relative humidity of the air around the thin sand layer drying tests of Devon silt in Set 2.

Table A.2 Summary of measured rate of evaporation and gravimetric water contents for the Devon silt in Set 2 on December 3, 2012

Time (mins)	PE (mm/day)	Actual Evaporation (mm/day)					Gravimetric water content (%)				
		M2	M2+50	M2+100	M2+200	M2+250	M2	M2+50	M2+100	M2+200	M2+250
20	2.59	2.64	2.41	2.29	1.83	1.49	58.30	55.10	60.36	54.84	53.29
40	2.59	2.06	1.95	1.72	1.49	1.83	51.35	48.16	55.00	50.18	47.75
60	2.48	1.95	1.60	1.60	1.26	1.26	44.79	42.45	50.00	46.24	43.94
80	2.36	2.06	1.83	1.72	1.38	1.26	37.84	35.92	44.64	41.94	40.14
100	2.25	1.95	1.60	1.60	1.26	1.38	31.27	30.20	39.64	37.99	35.99
120	2.25	1.95	1.60	1.72	1.15	1.38	24.71	24.49	34.29	34.41	31.83
140	2.48	1.95	1.49	1.15	1.03	1.26	18.15	19.18	30.71	31.18	28.03
160	2.25	1.95	1.49	1.72	1.26	1.38	11.58	13.88	25.36	27.24	23.88
180	2.25	1.49	1.03	1.26	1.15	1.26	6.56	10.20	21.43	23.66	20.07
200	2.36	1.03	1.26	1.49	1.15	1.49	3.09	5.71	16.79	20.07	15.57
220	2.36	0.46	0.69	1.15	1.26	1.26	1.54	3.27	13.21	16.13	11.76
240	2.36	0.11	0.46	1.38	1.15	1.26	1.16	1.63	8.93	12.54	7.96
260	2.36	0	0	1.03	1.15	0.80	1.16	1.63	5.71	8.96	5.54
280	2.43	0	0	0.73	0.92	0.37	1.16	1.63	2.86	5.38	4.15
300	2.56	0	0	0.31	0.61	0.15	1.16	1.63	2.14	3.94	3.81
320	2.25	0	0	0.11	0.46	0	1.16	1.63	1.79	2.51	3.81

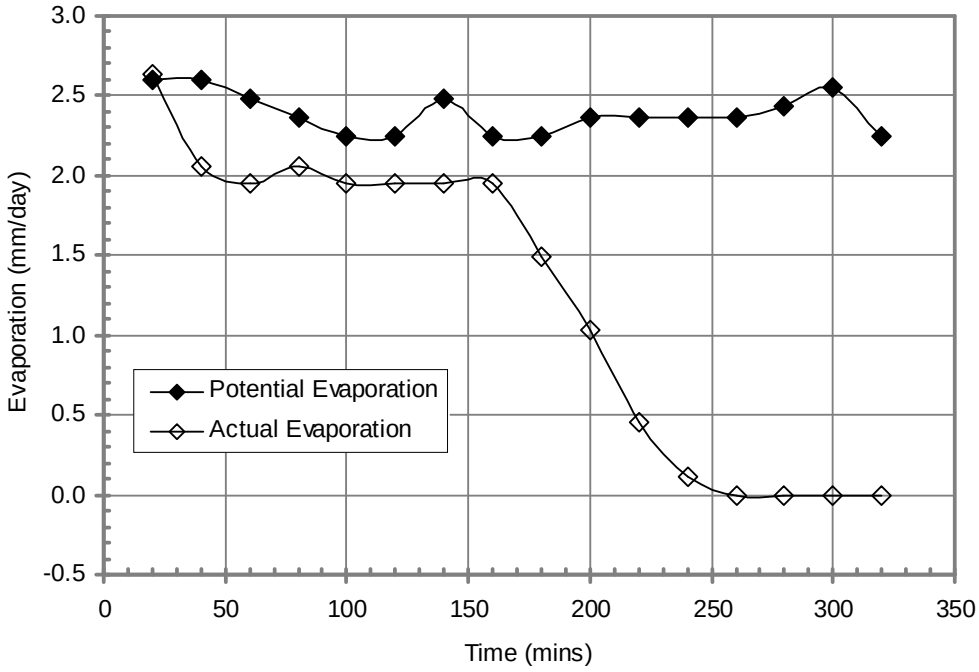

Figure A.13 Actual and Potential Evaporation rates versus drying time for Devon silt in Set 2.

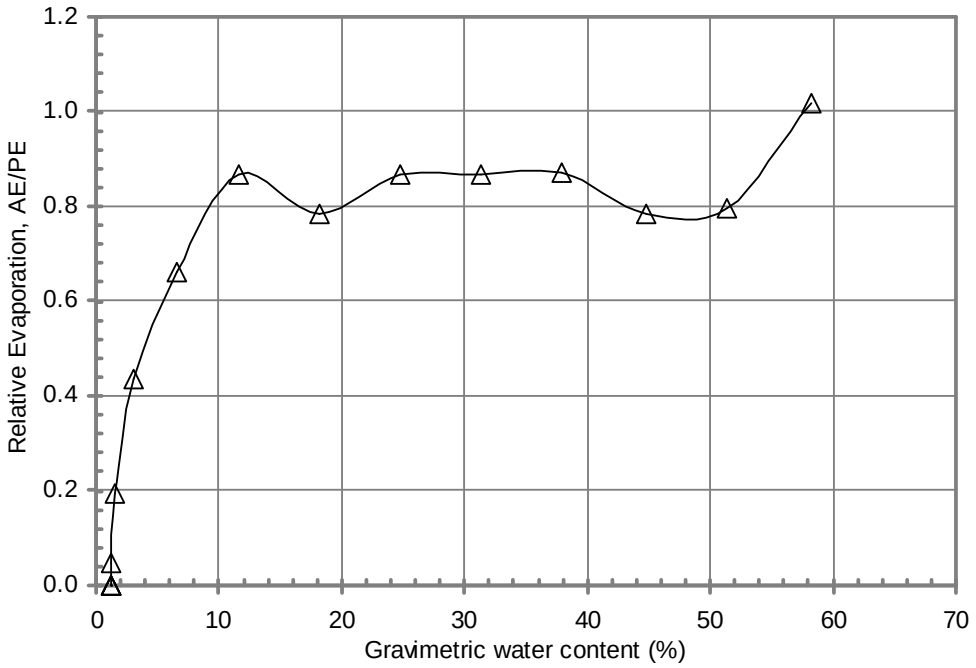

Figure A.14 Plot of Relative Evaporation (*AE/PE*) versus gravimetric water content for Devon silt in Set 2.

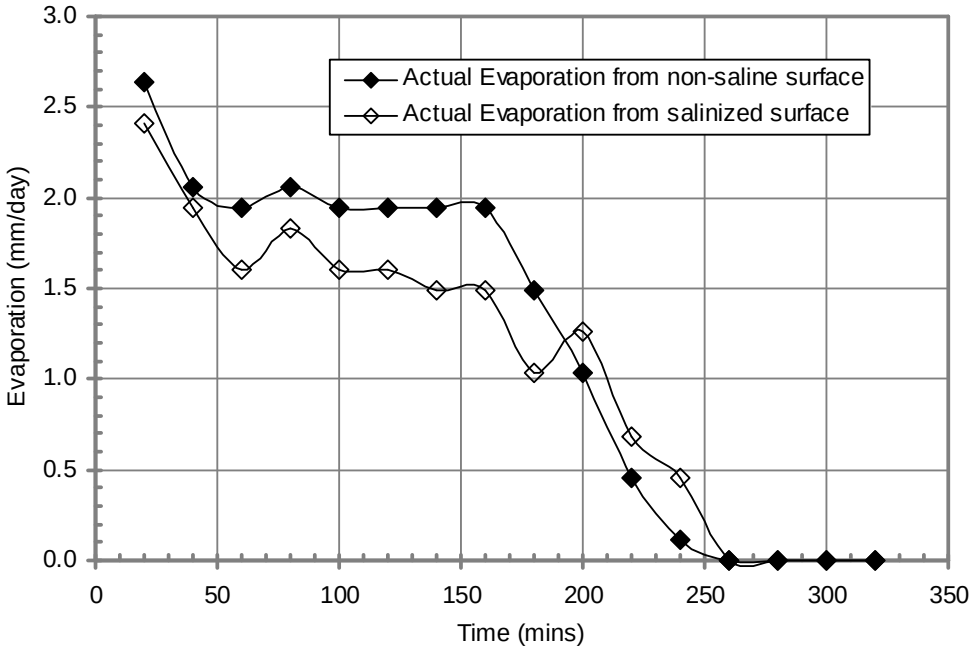

Figure A.15 Actual Evaporation rates versus drying time for Devon silt and Devon silt mixed with 50 g/l NaCl in Set 2.

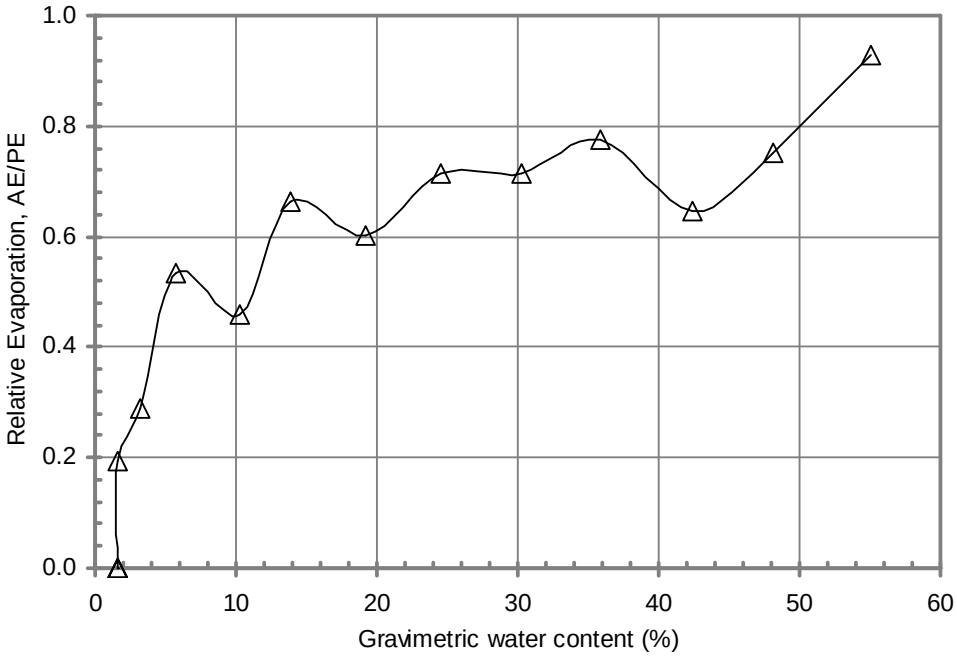

Figure A.16 Plot of Relative Evaporation (*AE/PE*) versus gravimetric water content for Devon silt mixed with 50 g/l NaCl in Set 2.

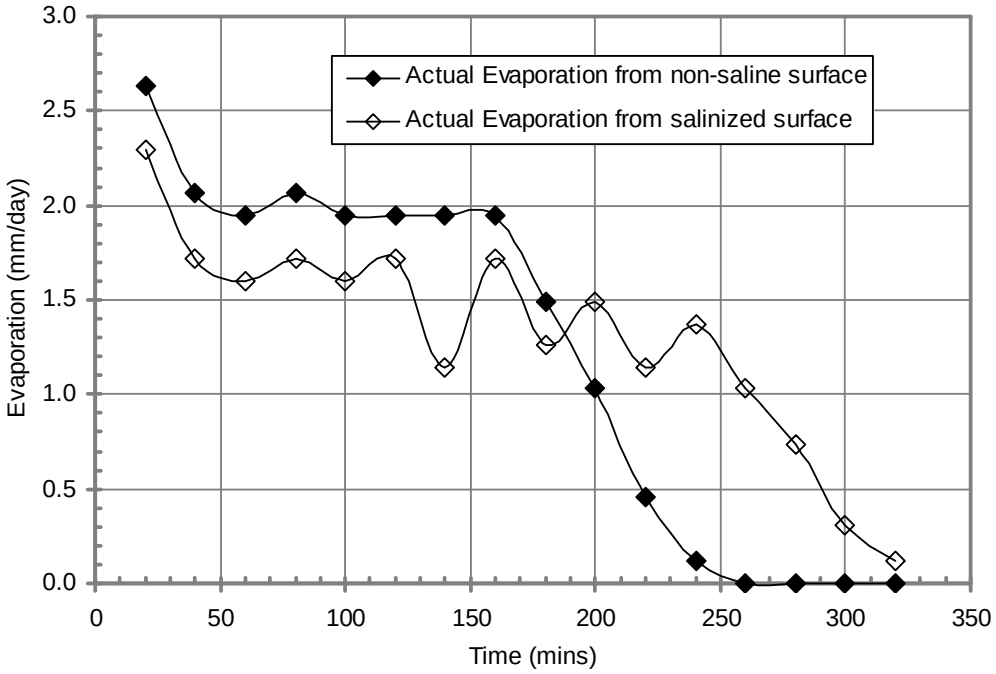

Figure A.17 Actual Evaporation rates versus drying time for Devon silt and Devon silt mixed with 100 g/l NaCl in Set 2.

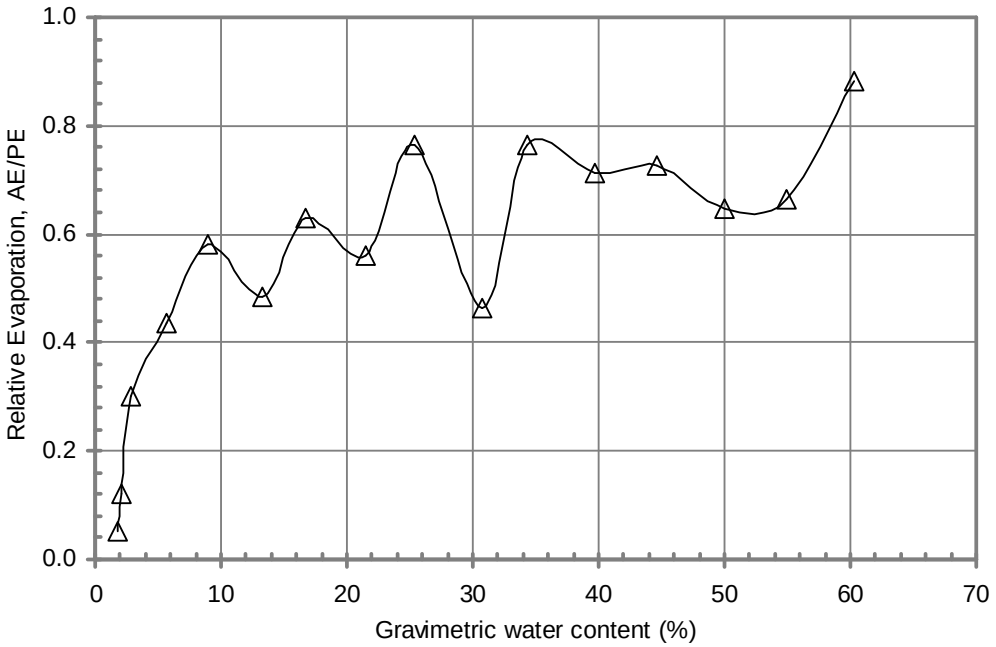

Figure A.18 Plot of Relative Evaporation (*AE/PE*) versus gravimetric water content for Devon silt mixed with 100 g/l NaCl in Set 2.

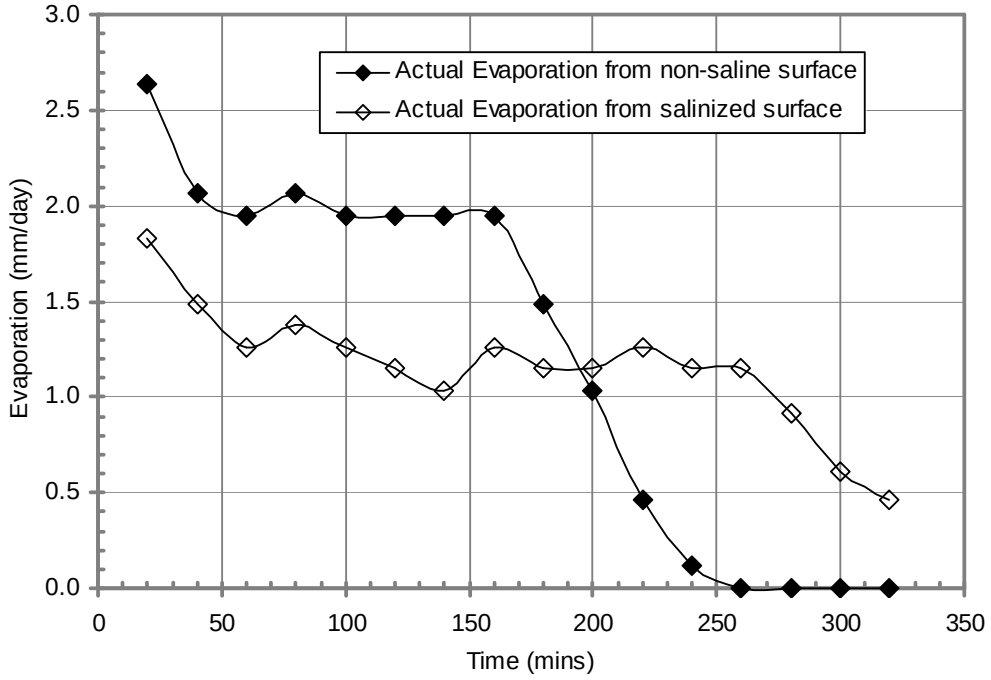

Figure A.19 Actual Evaporation rates versus drying time for Devon silt and Devon silt mixed with 200 g/l NaCl in Set 2.

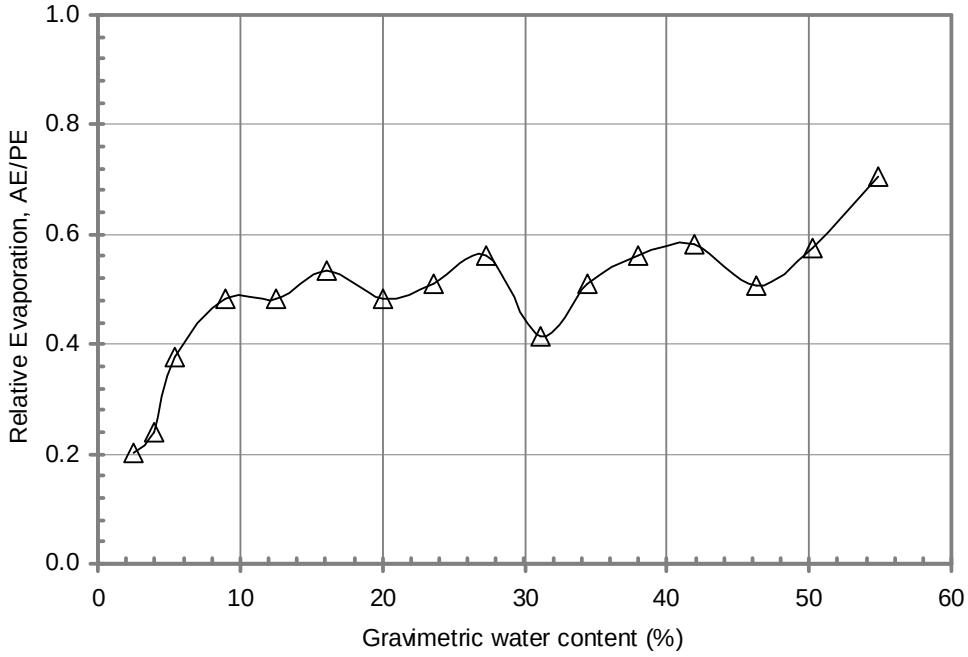

Figure A.20 Plot of Relative Evaporation (*AE/PE*) versus gravimetric water content for Devon silt mixed with 200 g/l NaCl in Set 2.

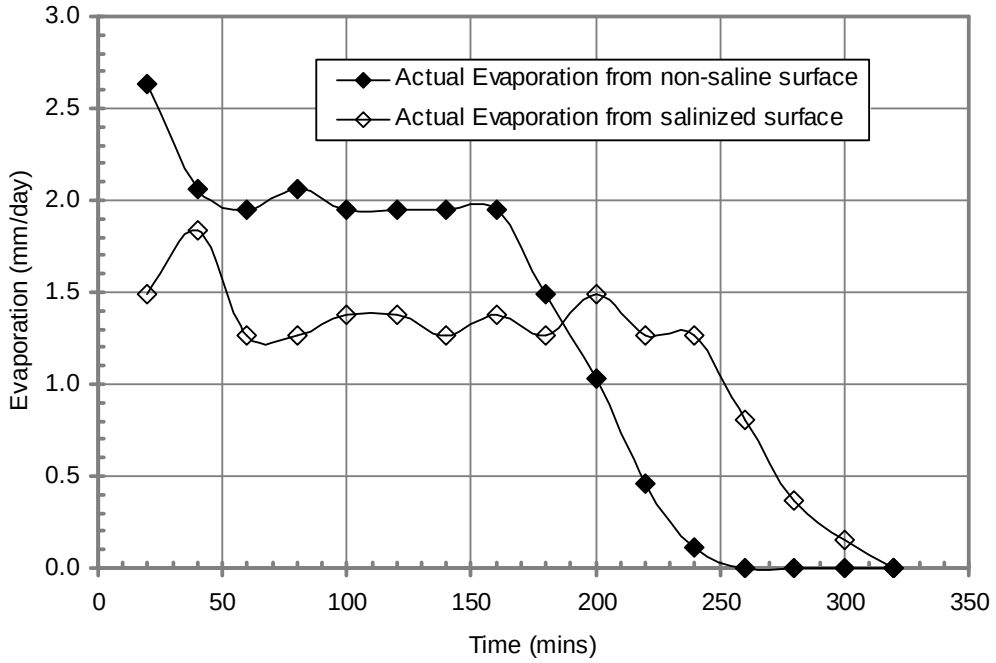

Figure A.21 Actual Evaporation rates versus drying time for Devon silt and Devon silt mixed with 250 g/l NaCl in Set 2.

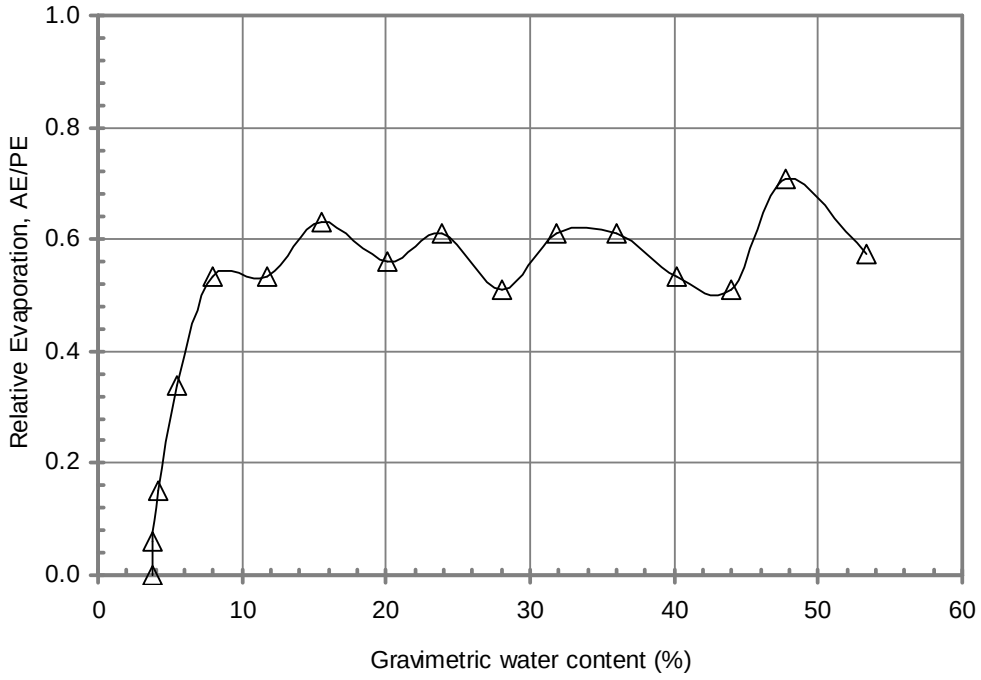

Figure A.22 Plot of Relative Evaporation (*AE/PE*) versus gravimetric water content for Devon silt mixed with 250 g/l NaCl in Set 2.

APPENDIX B

SOIL PROPERTIES AND SCHEMES OF DRYING EXPERIMENTS AND TEST RESULTS COLLECTED FROM WILSON'S THESIS (1990)

Table B.1 Summary of soil properties of used for each soil type in the drying experiments.

Item	Beaver Creek sand	Custom silt	Regina clay*
Description	fine uniform clean sand aoeline	coarse to medium clean silt laboratory produced	highly plastic clay lacustrine
Texture	98.0 % sand 2.0 % silt & clay	7.0 % sand 84.0 % silt 9.0 % clay	8.0 % sand 41.0 % silt 51.0 % clay
Atterberg Limits Liquid Limits Plastic Limit Plasticity Index	non-plastic	26.8 % 25.4 % 1.4 %	75.5 % 24.4 % 50.6 %
USCS[a]	SP	ML	CH
Specific Gravity	2.67	not measured 2.72 estimated	2.83
Void Ratio at 100 kPa Suction	0.63	0.85	1.34
Hydraulic Conductivity	Falling Head Permeameter 3.9×10^{-6} m/sec	not measured	1×10^{-9} m/sec estimated from constant volume Oedometer tests
Total Dissolved Solids	9 mg/gm	11 mg/gm	10 mg/gm

*Note: After Fredlund and Dakshanamurthy, 1982.

[a]Unified Soil Classification System.

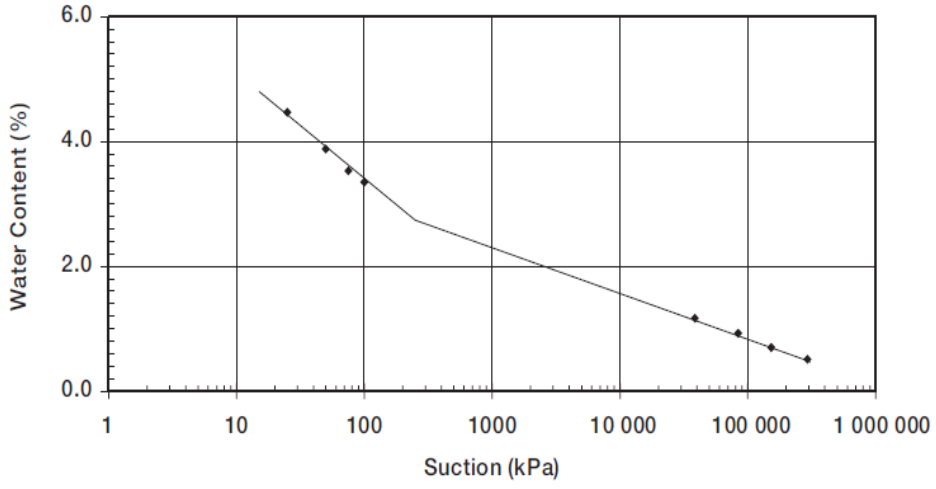

Figure B.1 Soil-water characteristic curve for Beaver Creek sand at 20 ^{o}C.

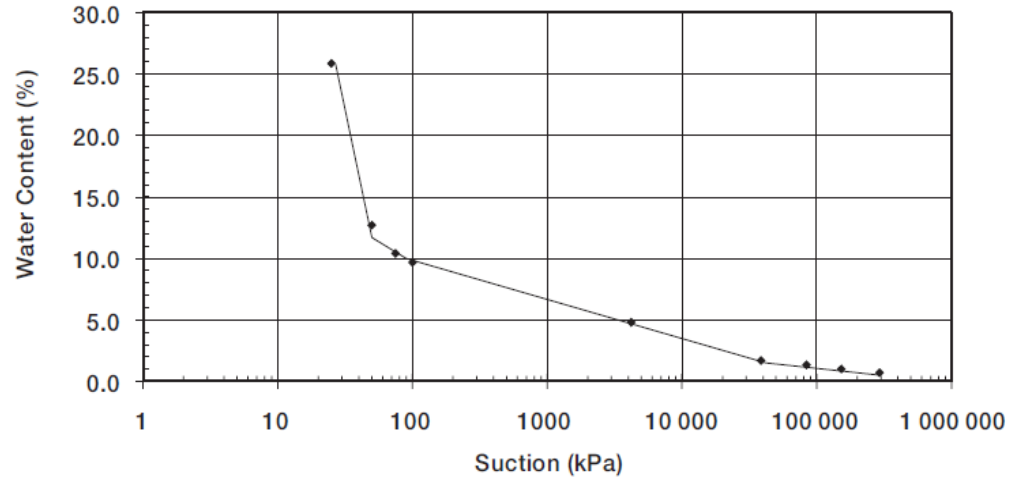

Figure B.2 Soil-water characteristic curve for Custom silt at 20 ^{o}C.

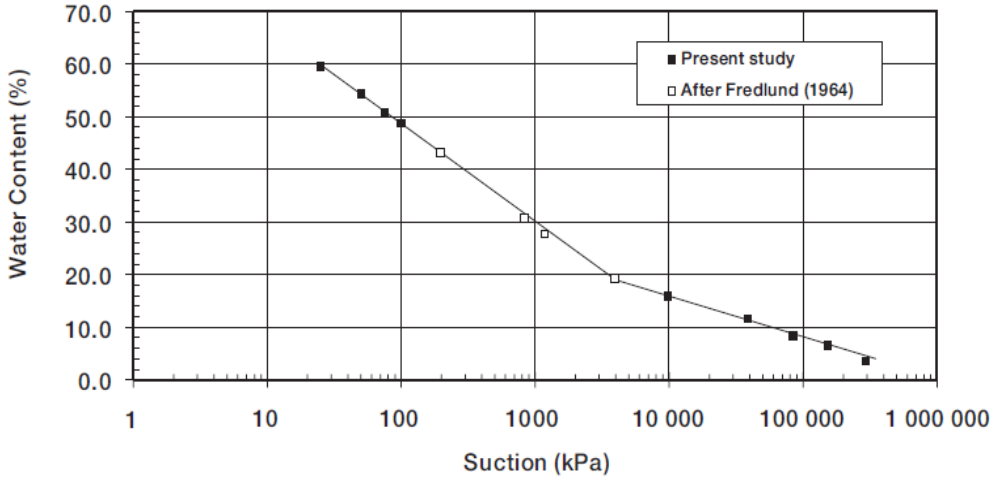

Figure B.3 Soil-water characteristic curve for Regina clay at 20 ^{o}C.

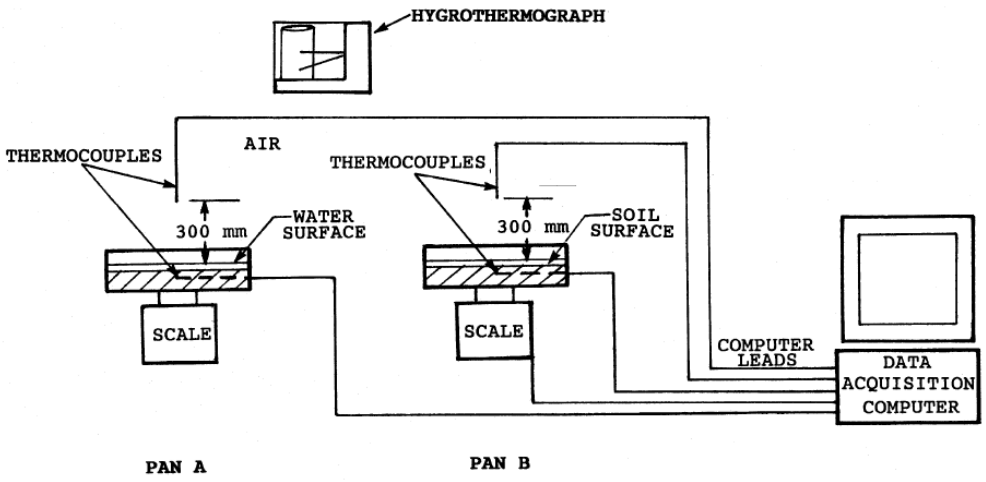

Figure B.4 Thin soil section drying test apparatus.

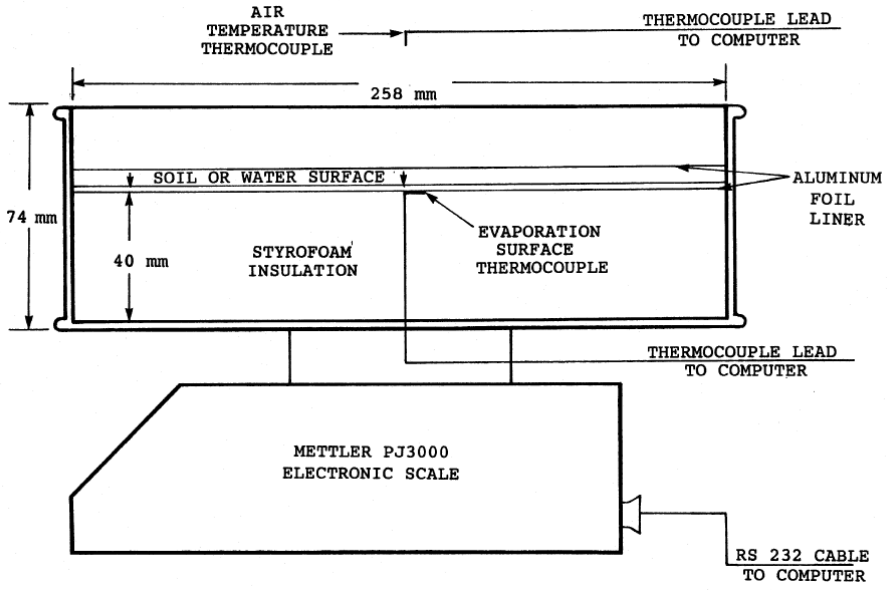

Figure B.5 Detailed section of the evaporation pan used for the thin soil section evaporation test.

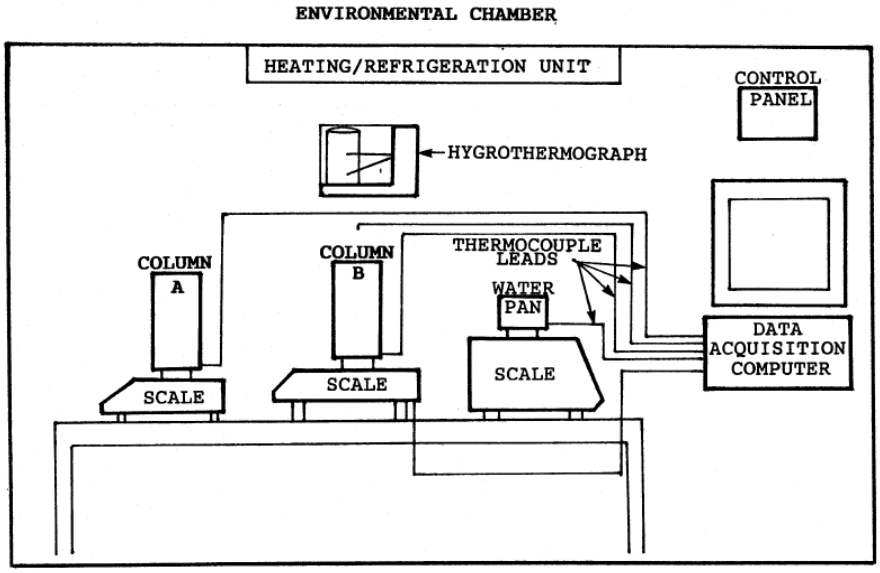

Figure B.6 Soil column drying test apparatus.

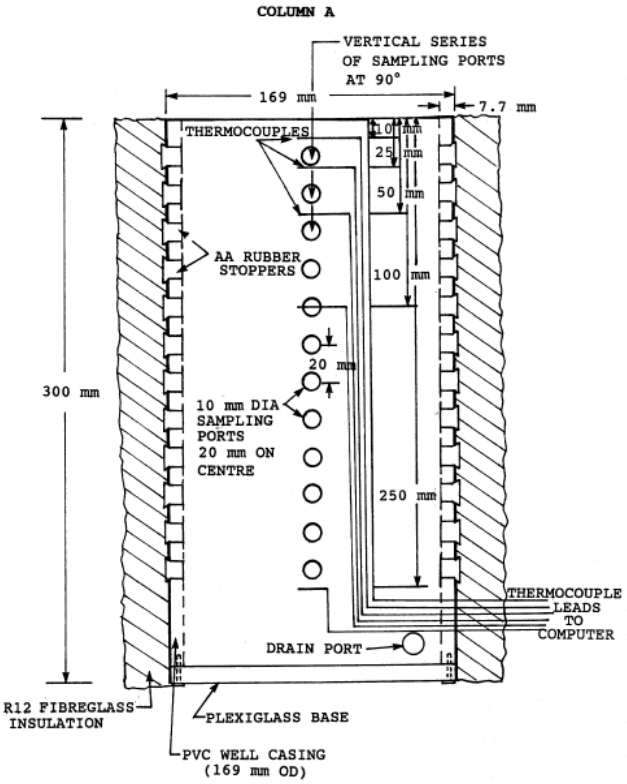

Figure B.7 Detailed section of drying column A.

Table B.2 Summary of measured results for the thin soil section drying test Test No. S1 Beaver Creek sand

Time (mins)	PE (gms/hr)	AE (gms/hr)	Total suction (kPa)	R.H. Soil	R.H. Air	Air Temp (^{o}C)	Water Temp (^{o}C)	Soil Temp (^{o}C)	Moisture Content (%)
0	2.63	2.83	-	1	0.51	22.9	20.4	20.7	28.88
50	2.61	2.78	-	1	0.53	23.2	20.4	20.8	24.98
100	2.49	2.93	4	1	0.53	23.0	20.6	20.5	20.92
150	2.52	2.74	5	1	0.54	23.0	20.6	20.3	16.95
200	2.61	2.78	5	1	0.56	23.0	20.7	20.5	13.03
250	2.61	3.02	7	1	0.56	23.1	20.6	20.6	9.04
300	2.97	3.02	51	1	0.56	23.1	20.4	20.2	4.83
330	2.97	2.88	1,100	0.99	0.54	23.1	20.3	20.1	2.34
335	2.97	2.55	3,600	0.97	0.54	23.1	20.4	20.3	1.96
340	2.97	2.21	10,000	0.93	0.53	23.0	20.5	20.6	1.62
345	2.97	1.91	22,000	0.85	0.53	23.0	20.3	21.2	1.35
350	2.97	1.34	42,000	0.73	0.53	23.0	20.5	22.0	1.14
355	2.97	0.94	64,000	0.63	0.53	23.0	20.5	22.7	1.00
360	2.97	0.48	80,000	0.56	0.53	22.9	20.4	23.4	0.92
365	2.97	0.19	88,000	0.53	0.53	23.0	20.4	24.1	0.89
370	2.97	0.13	94,000	0.50	0.53	23.1	20.2	23.9	0.87
375	2.97	0.12	104,000	0.47	0.52	23.1	20.4	24.1	0.84
380	2.97	0.07	110,000	0.45	0.52	23.2	20.4	24.1	0.82
390	2.97	-0.06	104,000	0.47	0.52	23.0	20.3	24.1	0.84
510	2.65	-0.01	98,000	0.49	0.53	24.0	21.0	25.0	0.85

Table B.3 Summary of measured results for the thin soil section drying test Test No. S2 Beaver Creek sand

Time (mins)	PE (gms/hr)	AE (gms/hr)	Total suction (kPa)	R.H. Soil	R.H. Air	Air Temp (^{o}C)	Water Temp (^{o}C)	Soil Temp (^{o}C)	Moisture Content (%)
0	2.58	3.2	3	1	0.40	22.6	19.5	20.4	37.66
50	2.58	3.6	4	1	0.40	22.7	19.6	20.0	31.63
100	2.75	3.3	5	1	0.40	22.5	19.7	20.0	25.50
150	2.83	3.2	5	1	0.42	22.8	19.8	20.2	19.17
200	2.88	3.4	5	1	0.43	22.8	20.5	20.0	12.86
250	3.07	3.2	10	1	0.44	22.8	20.4	20.3	6.85
275	3.07	3.1	49	1	0.44	22.7	20.3	19.9	3.83
289	3.07	3.1	1,800	0.99	0.44	22.7	20.3	20.0	2.18
297	3.07	2.8	18,500	0.97	0.44	22.7	20.0	20.1	1.41
298	3.07	2.6	27,000	0.93	0.44	22.6	20.1	20.1	1.29
299	3.07	2.0	35,000	0.85	0.44	22.7	20.1	20.4	1.20
300	3.07	1.5	40,000	0.73	0.44	22.7	20.1	20.5	1.15
302	3.16	1.1	56,000	0.63	0.44	22.8	20.0	20.9	1.04
304	3.16	0.9	69,000	0.56	0.45	22.7	20.0	21.4	0.97
308	3.16	0.6	84,000	0.53	0.45	22.6	20.3	22.4	0.90
312	3.16	0.1	100,000	0.50	0.45	22.6	20.2	23.1	0.83
320	3.16	-0.1	112,000	0.47	0.46	22.5	20.3	23.6	0.81
353	2.93	0.0	112,000	0.45	0.47	22.6	20.1	23.9	0.81
400	2.93	0.1	100,000	0.47	0.48	22.5	20.1	24.0	0.83
450	2.93	0.0	100,000	0.49	0.50	22.6	20.1	24.1	0.83

Table B.4 Summary of measured results for the thin soil section drying test Test No. S3 Beaver Creek sand

Time (mins)	PE (gms/hr)	AE (gms/hr)	Total suction (kPa)	R.H. Soil	R.H. Air	Air Temp (^{o}C)	Water Temp (^{o}C)	Soil Temp (^{o}C)	Moisture Content (%)
0	2.57	3.0	1	1	0.58	22.3	20.7	20.7	28.06
50	2.57	2.4	3	1	0.58	22.8	20.8	21.1	22.96
100	2.51	2.4	4	1	0.58	22.6	21.0	21.1	17.88
150	2.52	2.7	5	1	0.58	22.7	21.1	21.2	12.71
200	2.50	2.4	7	1	0.58	22.7	20.8	21.2	8.30
250	2.52	2.3	140	1	0.58	22.8	20.8	21.1	3.18
260	2.52	2.1	1,450	1	0.58	22.7	20.7	21.6	2.26
265	2.52	1.6	3,300	0.99	0.58	22.8	20.9	21.8	1.89
270	2.52	1.4	11,500	0.97	0.58	22.7	20.7	22.6	1.57
275	2.52	0.8	21,000	0.93	0.58	22.7	20.7	23.2	1.38
280	2.52	0.5	34,000	0.85	0.58	22.7	20.6	23.6	1.20
285	2.52	0.4	50,000	0.73	0.58	22.7	20.8	23.8	1.08
290	2.52	0.2	68,000	0.63	0.58	22.7	20.7	24.1	0.98
295	2.52	0.1	73,000	0.56	0.58	22.8	20.7	24.0	0.96
300	2.52	-0.1	73,000	0.53	0.59	22.7	20.7	24.0	0.96
325	2.62	0.0	90,000	0.50	0.59	22.7	20.6	24.2	0.88
350	2.62	-0.1	84,000	0.47	0.59	22.7	20.6	24.2	0.91

Table B.5 Summary of measured results for the thin soil section drying test Test No. M1 Custom silt

Time (mins)	PE (gms/hr)	AE (gms/hr)	Total suction (kPa)	R.H. Soil	R.H. Air	Air Temp (^{o}C)	Water Temp (^{o}C)	Soil Temp (^{o}C)	Moisture Content (%)
0	4.60	4.68	8	1	0.23	22.6	22.6	17.1	48.32
5	4.60	4.68	8	1	0.23	22.5	22.5	17.3	47.27
60	4.60	4.46	14	1	0.23	22.6	22.6	18.1	35.66
110	4.84	3.64	22	1	0.23	22.6	22.6	18.4	27.58
180	5.16	4.20	42	1	0.21	22.7	22.7	18.5	15.64
230	5.16	6.50	11,500	0.92	0.21	22.6	22.6	18.3	3.34
235	5.16	3.04	27,500	0.82	0.21	22.7	22.7	18.3	2.41
240	5.16	1.94	36,000	0.77	0.21	22.7	22.7	18.3	2.08
245	5.16	1.36	56,000	0.66	0.21	22.7	22.7	18.3	1.67
250	5.16	1.02	82,000	0.55	0.21	22.9	22.9	18.2	1.42
255	5.16	0.62	125,000	0.40	0.21	22.7	22.7	18.1	1.21
260.6	5.10	0.48	140,000	0.36	0.20	22.6	22.6	17.7	1.15
280.6	5.10	0.04	400,000	0.05	0.20	22.7	22.7	18.0	0.60
430	5.27	-0.50	290,000	0.12	0.20	22.6	22.6	17.9	0.71

Table B.6 Summary of measured results for the thin soil section drying test Test No. M2 Custom silt

Time (mins)	PE (gms/hr)	AE (gms/hr)	Total suction (kPa)	R.H. Soil	R.H. Air	Air Temp (^{o}C)	Water Temp (^{o}C)	Soil Temp (^{o}C)	Moisture Content (%)
0	3.91	2.70	2	1	0.38	23.6	19.7	19.7	59.3
25	3.91	3.90	5	1	0.36	22.6	19.2	19.2	49.39
50	3.91	3.72	10	1	0.35	22.5	19.1	19.5	39.61
75	3.56	3.54	20	1	0.36	22.5	19.1	19.7	29.96
100	3.56	3.56	32	1	0.39	22.6	19.3	19.5	20.24
125	3.74	3.54	60	1	0.40	22.4	19.2	19.5	11.29
140	3.74	3.36	1,600	0.99	0.39	22.4	19.3	19.7	5.99
144	3.74	3.24	4,700	0.97	0.39	22.5	19.2	19.8	4.54
146	3.74	3.10	7,600	0.95	0.39	22.6	19.2	19.9	3.91
148	3.74	2.80	12,000	0.92	0.39	22.6	19.2	20.4	3.27
150	3.74	2.50	18,300	0.87	0.39	22.5	19.4	21.1	2.71
152	3.74	1.86	26,000	0.83	0.39	22.5	19.3	21.5	2.20
154	3.74	1.38	36,000	0.77	0.39	22.3	19.2	22	1.82
156	3.74	1.02	56,000	0.66	0.39	22.4	19.3	22.4	1.51
158	3.74	0.53	79,000	0.56	0.39	22.6	19.2	22.7	1.32
160	3.74	0.24	100,000	0.48	0.39	22.6	19.2	22.9	1.19
162	3.74	0.06	110,000	0.45	0.38	22.7	19.2	23.2	1.13
167	3.74	0.00	110,000	0.45	0.38	22.5	19.2	23.5	1.13
175	3.74	0.08	120,000	0.42	0.38	22.5	19.1	23.7	1.07
200	3.74	0.00	120,000	0.42	0.37	22.7	19.1	23.8	1.07
225	3.74	-0.12	170,000	0.29	0.38	22.9	18.9	23.9	0.88
250	3.74	0.00	150,000	0.33	0.38	22.5	19.2	23.8	0.94

Table B.7 Summary of measured results for the thin soil section drying test Test No. M3 Custom silt

Time (mins)	PE (gms/hr)	AE (gms/hr)	Total suction (kPa)	R.H. Soil	R.H. Air	Air Temp (^{o}C)	Water Temp (^{o}C)	Soil Temp (^{o}C)	Moisture Content (%)
0	2.57	2.37	6	1	0.64	22.5	21.0	21.5	56.71
50	2.57	2.30	10	1	0.64	23.0	21.1	21.2	42.93
100	2.42	2.46	20	1	0.63	23.2	21.5	21.4	28.79
150	2.45	2.52	44	1	0.63	23.1	21.4	21.4	14.37
175	2.45	2.34	540	1	0.62	23.1	21.3	21.5	7.44
185	2.45	2.16	3,900	0.97	0.62	23.0	21.2	21.8	4.83
190	2.61	1.86	9,500	0.93	0.62	23.0	21.2	21.5	3.63
195	2.61	1.20	18,000	0.88	0.62	22.9	21.2	22.4	2.71
200	2.61	0.78	26,500	0.82	0.62	22.9	21.1	23.1	2.14
205	2.61	0.54	39,000	0.75	0.62	22.9	21.1	23.5	1.79
210	2.61	0.24	52,000	0.68	0.62	22.8	21.0	23.7	1.58
220	2.61	0.00	72,000	0.59	0.62	23.0	21.1	24.0	1.36
250	2.49	0.12	64,000	0.63	0.62	23.0	21.0	24.0	1.43
290	2.49	0.00	72,000	0.59	0.62	22.8	20.9	24.2	1.36
330	2.49	-0.12	80,000	0.56	0.61	23.9	21.2	24.4	1.29
360	2.49	0.10	72,000	0.59	0.61	24.1	21.5	24.9	1.36

Table B.8 Summary of measured results for the thin soil section drying test Test No. C1 Regina clay

Time (mins)	PE (gms/hr)	AE (gms/hr)	Total suction (kPa)	R.H. Soil	R.H. Air	Air Temp (^{o}C)	Water Temp (^{o}C)	Soil Temp (^{o}C)	Moisture Content (%)
0	3.45	3.00	-	1.00	0.41	24.0	20.2	21.1	102.00
125	3.38	3.53	-	1.00	0.39	23.9	20.8	20.3	91.89
250	2.82	3.31	2	1.00	0.39	23.9	20.8	20.5	81.86
375	2.82	3.17	5	1.00	0.46	23.7	21.0	20.9	72.58
500	2.65	3.18	17	1.00	0.48	23.4	20.9	20.6	63.27
625	2.65	2.70	47	1.00	0.46	25.2	21.8	22.3	54.88
750	3.19	2.71	130	1.00	0.43	25.3	22.3	22.7	46.75
875	3.19	2.53	340	1.00	0.41	25.8	22.2	22.7	38.92
1,000	3.19	2.16	800	0.99	0.39	25.8	22.0	23.6	31.98
1,125	3.19	1.75	1,600	0.99	0.39	26.0	22.2	24.4	26.17
1,255	3.19	2.10	3,300	0.98	0.39	24.1	21.0	22.8	20.94
1,375	3.78	1.67	14,500	0.90	0.39	23.4	20.1	23.5	15.30
1,500	3.47	1.10	42,000	0.74	0.41	23.3	20.0	23.7	11.15
1,625	3.47	0.44	74,000	0.58	0.41	23.2	19.9	24.1	8.99
1,750	3.47	0.30	95,000	0.50	0.41	23.0	20.2	23.9	7.96
1,875	3.70	0.14	110,000	0.45	0.39	22.6	19.6	23.7	7.34
1,925	3.70	0.07	115,000	0.43	0.39	22.7	19.4	23.7	7.16
1,975	3.70	0.08	120,000	0.42	0.39	22.5	19.5	23.7	7.10
2,050	3.70	0.06	128,000	0.39	0.39	22.5	20.8	24.5	6.89

Table B.9 Summary of measured results for the thin soil section drying test Test No. C2 Regina clay

Time (mins)	PE (gms/hr)	AE (gms/hr)	Total suction (kPa)	R.H. Soil	R.H. Air	Air Temp (^{o}C)	Water Temp (^{o}C)	Soil Temp (^{o}C)	Moisture Content (%)
0	3.39	3.30	-	1.00	0.37	22.5	18.9	19.5	127.10
30	3.39	3.78	-	1.00	0.37	22.5	19.4	19.8	112.03
60	3.39	3.60	3	1.00	0.37	22.5	19.3	19.7	97.39
90	3.34	3.72	10	1.00	0.37	22.5	19.2	19.8	82.14
125	3.39	3.48	15	1.00	0.37	22.7	19.2	19.7	63.54
150	3.39	3.36	84	1.00	0.36	22.7	19.2	19.9	51.19
181	3.59	3.54	490	1.00	0.36	22.9	19.2	19.7	35.77
200	3.59	3.42	1,560	0.99	0.36	22.8	19.2	20.0	26.42
220	3.59	2.76	8,000	0.94	0.36	22.6	19.1	20.2	17.61
230	3.59	2.40	19,000	0.87	0.36	22.7	19.2	20.6	14.17
240	3.59	1.98	43,000	0.73	0.36	23.0	19.3	21.7	11.08
250	3.59	1.26	80,000	0.56	0.35	22.9	19.3	22.7	8.61
260	3.59	0.96	110,000	0.45	0.35	22.9	19.1	23.4	7.29
270	3.59	0.24	140,000	0.36	0.35	22.7	19.2	23.8	6.50
280	3.59	0.00	160,000	0.31	0.35	22.8	19.1	24.0	5.97
290	3.71	0.12	165,000	0.30	0.35	22.7	19.0	24.3	5.88
300	3.71	0.06	165,000	0.30	0.35	22.9	19.3	24.2	5.88
330	3.71	0.06	165,000	0.30	0.35	22.8	19.2	24.1	5.88
360	3.71	0.12	175,000	0.28	0.35	22.6	19.0	24.1	5.62
390	3.71	-0.12	175,000	0.28	0.34	22.8	18.9	24.3	5.62
420	3.71	-0.12	175,000	0.28	0.34	22.8	18.8	24.3	5.62

Table B.10 Summary of measured results for the thin soil section drying test Test No. C3 Regina clay

Time (mins)	PE (gms/hr)	AE (gms/hr)	Total suction (kPa)	R.H. Soil	R.H. Air	Air Temp (^{o}C)	Water Temp (^{o}C)	Soil Temp (^{o}C)	Moisture Content (%)
225	2.85	3.00	22	1.00	0.52	25.5	22.6	22.9	61.17
250	2.60	2.64	70	1.00	0.51	25.4	22.7	22.9	50.55
275	2.60	2.52	255	1.00	0.51	25.4	22.6	23.1	41.14
300	2.76	2.94	810	0.99	0.51	25.4	22.9	23.2	31.82
320	2.76	2.46	2,000	0.99	0.50	25.5	22.7	23.2	24.40
330	2.76	2.52	3,250	0.98	0.50	25.4	22.8	22.9	20.94
340	2.76	1.80	7,000	0.95	0.50	25.5	22.9	23.7	18.09
350	2.76	1.68	14,000	0.90	0.50	25.5	22.5	24.0	15.42
360	2.90	1.50	25,000	0.83	0.50	25.5	22.6	24.3	13.17
370	2.90	1.20	41,000	0.74	0.50	25.4	22.4	25.0	11.27
380	2.90	0.90	60,000	0.65	0.50	25.6	22.6	25.6	9.81
390	2.90	0.48	76,000	0.58	0.50	25.5	22.5	25.8	8.86
400	2.90	0.30	92,000	0.51	0.50	25.4	22.5	26.4	8.17
410	2.90	0.18	100,000	0.48	0.50	25.5	22.7	26.5	7.73
420	2.90	0.06	105,000	0.47	0.50	25.6	22.7	26.7	7.56
450	2.90	-0.06	110,000	0.45	0.50	25.6	22.7	26.8	7.30
475	2.90	0.12	110,000	0.45	0.49	25.7	23.0	26.6	7.30
500	2.90	-0.12	110,000	0.45	0.48	25.6	23.1	26.7	7.30
525	2.90	0.00	110,000	0.45	0.48	25.6	23.0	26.7	7.30

Table B.11 Summary of measured results for the soil column A-Beaver Creek sand.

Time (days)	PE (mm/day)	AE (mm/day)	R.H. Air	Air Temp (°C)	Water Temp (°C)	Soil Temp (°C)	Moisture Content (%)		
							Depth of 0 mm	Depth of 10 mm	Depth of 20 mm
0	7.37	6.96	0.230	38.6	29.0	30.2	15.41	-	20.35
1	7.38	6.65	0.220	38.2	31.3	30.2	-	-	-
2	7.60	6.78	0.200	38.1	31.0	30.1	-	-	-
3	7.74	7.18	0.180	38.0	30.5	29.7	-	-	-
4	7.53	6.52	0.155	38.4	30.7	29.6	-	-	-
5	7.82	4.88	0.150	38.7	30.5	31.6	1.48	7.74	7.43
6	8.01	3.97	0.150	38.1	30.8	32.7	-	-	-
7	7.53	3.35	0.160	39.0	30.7	33.8	-	-	-
8	7.59	3.04	0.180	37.7	30.6	34.4	-	-	-
9	7.76	2.76	0.170	37.8	30.9	34.8	1.00	3.92	6.77
10	7.74	2.47	0.165	38.8	30.7	35.2	-	-	-
11	7.76	2.04	0.165	37.7	30.8	35.4	-	-	-
12	7.86	2.06	0.160	38.7	30.4	35.7	1.01	3.05	4.67
13	7.96	2.05	0.170	38.2	30.9	35.9	-	-	-
14	8.08	2.02	0.130	39.1	30.7	36.3	-	-	-
15	7.87	1.81	0.160	38.7	30.7	36.4	-	-	-
16	8.21	1.85	0.140	38.2	30.6	36.4	-	-	-
17	8.05	1.59	0.130	38.2	30.4	36.8	-	-	-
18	8.04	1.56	0.135	38.4	30.7	36.7	-	-	-
19	8.25	1.52	0.125	37.6	30.3	36.8	-	-	-
20	8.05	1.36	0.125	38.6	30.4	36.8	-	-	-
21	7.72	1.36	0.165	38.0	30.9	37.1	0.80	1.77	3.43
22	8.03	1.31	0.150	38.5	30.6	37.2	-	-	-
23	7.92	1.15	0.145	38.3	30.4	37.2	-	-	-
24	7.83	1.22	0.165	38.3	30.7	37.0	-	-	-
25	7.57	1.19	0.140	38.0	30.8	37.2	-	-	-
26	8.24	1.23	0.125	38.0	30.4	37.4	-	-	-
27	8.13	1.08	0.125	37.6	30.4	37.5	-	-	-
28	8.12	0.94	0.125	38.6	30.4	37.7	-	-	-
29	8.23	0.93	0.120	37.5	30.4	37.6	-	-	-
30	8.24	0.91	0.125	38.0	30.3	37.8	-	-	-
31	8.12	0.87	0.125	38.0	30.7	37.4	-	-	-
32	7.74	0.78	0.140	38.2	30.7	38.0	-	-	-
33	7.86	0.81	0.125	38.9	30.6	37.7	-	-	-
34	8.11	0.82	0.140	38.8	30.4	37.8	-	-	-
35	8.27	0.69	0.125	37.5	30.2	38.0	0.69	0.75	1.45
36	8.29	0.70	0.115	38.0	30.3	38.0	-	-	-
37	8.09	0.67	0.125	38.9	30.4	38.2	-	-	-
38	7.68	0.61	0.130	37.7	30.6	38.0	-	-	-
39	7.79	0.58	0.130	38.5	30.7	37.9	-	-	-
40	8.24	0.53	0.145	38.5	30.3	38.3	-	-	-
41	8.32	0.46	0.125	37.7	30.4	38.1	-	-	-
42	7.26	0.36	0.140	38.3	30.2	38.1	-	-	-

Table B.12 Summary of measured results for the soil column B-Beaver Creek sand

Time (days)	PE (mm/day)	AE (mm/day)	R.H. Air	Air Temp (^{o}C)	Water Temp (^{o}C)	Soil Temp (^{o}C)	Moisture Content (%)		
							Depth of 0 mm	Depth of 10 mm	Depth of 20 mm
0	7.37	7.55	0.230	38.6	29.0	30.0	11.98	-	20.42
1	7.38	6.84	0.220	38.2	31.3	30.0	9.58	-	13.49
2	7.60	6.94	0.200	38.1	31.0	29.8	7.30	-	-
3	7.74	6.08	0.180	38.0	30.5	30.0	2.50	6.59	9.63
4	7.53	5.29	0.155	38.4	30.7	31.2	-	-	-
5	7.82	4.47	0.150	38.7	30.5	32.4	-	-	-
6	8.01	3.80	0.150	38.1	30.8	33.2	1.56	5.71	8.26
7	7.53	3.31	0.160	39.0	30.7	34.2	1.15	3.13	-
8	7.59	2.87	0.180	37.7	30.6	34.5	-	-	-
9	7.76	2.65	0.170	37.8	30.9	35.1	-	-	-
10	7.74	2.46	0.165	38.8	30.7	35.6	-	-	-
11	7.76	2.17	0.165	37.7	30.8	35.6	-	-	-
12	7.86	2.02	0.160	38.7	30.4	35.8	-	-	-
13	7.96	1.98	0.170	38.2	30.9	36.2	-	-	-
14	8.08	1.98	0.130	39.1	30.7	36.6	1.09	1.71	4.63
15	7.87	1.81	0.160	38.7	30.7	36.6	-	-	-
16	8.21	1.65	0.140	38.2	30.6	36.6	-	-	-
17	8.05	1.59	0.130	38.2	30.4	36.6	-	-	-
18	8.04	1.44	0.135	38.4	30.7	36.6	-	-	-
19	8.25	1.40	0.125	37.6	30.3	36.6	-	-	-
20	8.05	1.32	0.125	38.6	30.4	36.8	-	-	-
21	7.72	1.32	0.165	38.0	30.9	36.9	-	-	-
22	8.03	1.22	0.150	38.5	30.6	36.9	-	-	-
23	7.92	1.19	0.145	38.3	30.4	37.0	-	-	-
24	7.83	1.18	0.165	38.3	30.7	37.0	-	-	-
25	7.57	1.12	0.140	38.0	30.8	37.1	-	-	-
26	8.24	1.10	0.125	38.0	30.4	37.2	-	-	-
27	8.13	0.98	0.125	37.6	30.4	37.3	-	-	-
28	8.12	0.91	0.125	38.6	30.4	37.5	-	-	-
29	8.23	0.90	0.120	37.5	30.4	37.4	0.62	0.69	0.89
30	8.24	0.83	0.125	38.0	30.3	37.6	-	-	-
31	8.12	0.81	0.125	38.0	30.7	37.5	-	-	-
32	7.74	0.75	0.140	38.2	30.7	37.7	-	-	-
33	7.86	0.73	0.125	38.9	30.6	37.9	-	-	-
34	8.11	0.66	0.140	38.8	30.4	37.7	-	-	-
35	8.27	0.66	0.125	37.5	30.2	37.7	-	-	-
36	8.29	0.66	0.115	38.0	30.3	37.9	-	-	-
37	8.09	0.52	0.125	38.9	30.4	38.1	-	-	-
38	7.68	0.57	0.130	37.7	30.6	37.8	-	-	-
39	7.79	0.56	0.130	38.5	30.7	38.1	-	-	-
40	8.24	0.50	0.145	38.5	30.3	38.1	-	-	-
41	8.32	0.44	0.125	37.7	30.4	38.1	-	-	-
42	7.26	0.44	0.140	38.3	30.2	38.0	0.57	0.84	1.01

APPENDIX C

SOIL PROPERTIES AND SCHEMES OF DRYING EXPERIMENTS AND TEST RESULTS COLLECTED FROM BRUCH'S THESIS (1993)

Table C.1 Summary of soil properties of used for each soil type in the drying experiments (adapted after Bruch, 1993).

Soil Properties	**Beaver Creek sand**	**Natural silt**	**Processed silt**
% Sand	96.5	6.1	0.1
% Silt	3.5 % silt and clay	82.09	92.9
% Clay		11.0	7.0
D_{60} (mm)	0.24	0.03	0.028
D_{10} (mm)	0.093	0.0013	0.0075
C_u	2.58	23.1	3.73
Atterberg Limits			
Liquid Limit	–	20.1	24.0
Plastic Limit	–	20.1	24.0
Plasticity Index	NON-PLASTIC	NON-PLASTIC	NON-PLASTIC
Specific Gravity	2.67	2.71	2.67
Void Ratio (at 10 kPa Load)[4]	0.532[1]	0.692[2]	0.690[3]
Porosity (at 10 kPa Load)[4]	0.347[1]	0.409[2]	0.408[3]
K_{SAT} (m/sec) (at 10 kPa Load)[4]	4.26×10^{-6}	2.07×10^{-8}	8.36×10^{-9}

Note: 1. Consolidated from slurry with approximate initial water content of 24 percent.
2. Consolidated from slurry with approximate initial water content of 27 percent.
3. Consolidated from slurry with approximate initial water content of 26 percent.
4. Values obtained from consolidation tests.

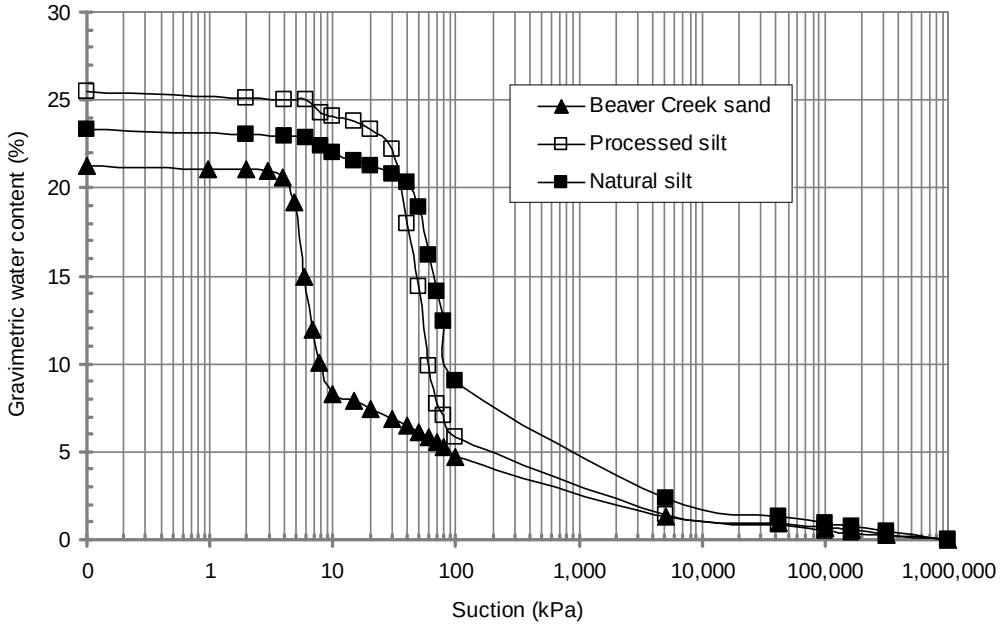

Figure C.1 Soil-water characteristic curves for Beaver Creek sand, Natural silt and Processed silt (adapted after Bruch, 1993).

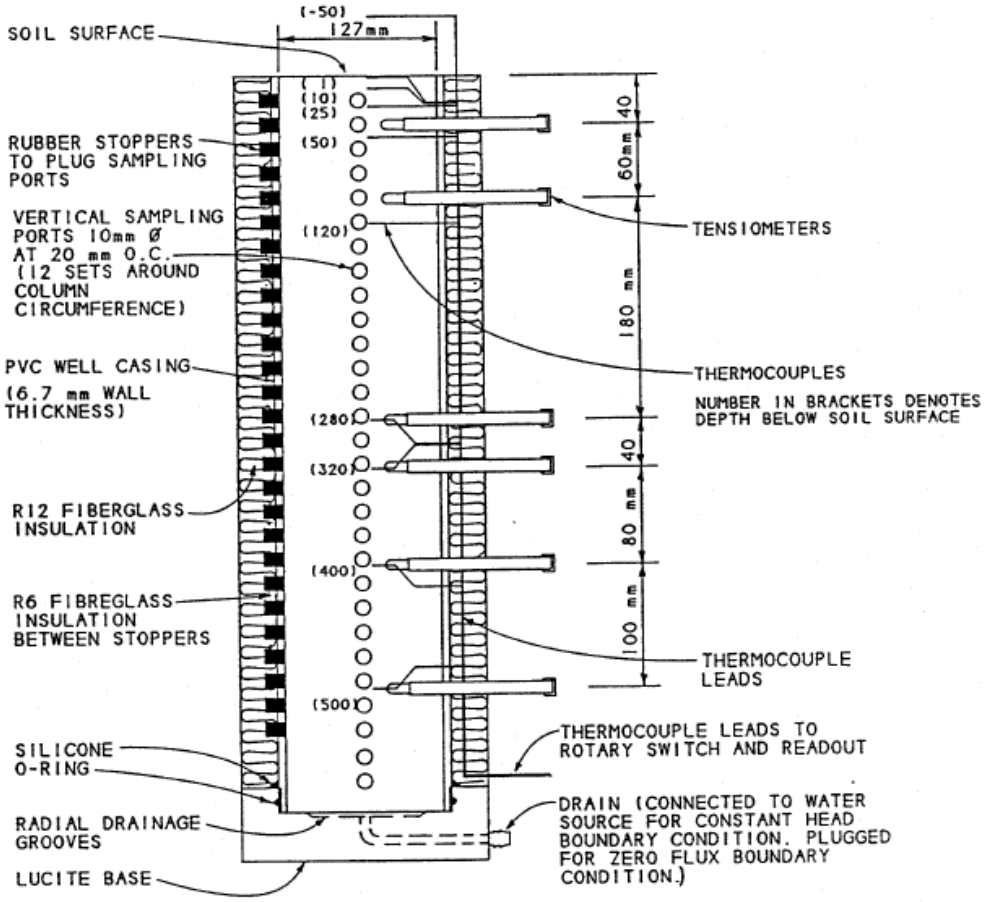

Figure C.2 Schematic Diagram of a Typical Evaporation Column Used in the Column Evaporation Tests (adapted after Bruch, 1993).

Table C.2 Summary of measured results for the soil column of Beaver Creek sand.

Time (days)	PE (mm/day)	AE (mm/day)	R.H.Air	Air Temp (^{o}C)	Water Temp (^{o}C)	Soil Temp (^{o}C)	Moisture Content (%)	
							Depth of 0 mm	Depth of 20 mm
0					30.8		14.00	14.38
0.67	5.24	4.93	0.131	37.1	31.8	28.4	-	-
1.00	5.33	5.05	0.131	37.1	32.0	29.0	11.90	12.88
1.89	5.52	5.25	0.123	36.5	32.4	29.5	-	-
3.28	5.55	5.24	0.136	35.5	31.6	29.2	10.13	9.85
3.90	5.09	4.89	0.130	35.7	31.9	29.6	-	-
4.91	5.42	5.22	0.140	36.0	31.8	30.0	8.47	11.06
6.00	5.32	5.18	0.128	35.9	32.1	30.5	-	-
6.83	5.45	5.54	0.118	35.8	31.8	28.6	7.37	9.29
7.94	5.37	4.53	0.116	36.2	32.7	28.5	-	-
8.81	5.62	5.30	0.115	36.0	32.0	28.5	-	-
9.92	5.83	4.93	0.139	36.0	31.8	29.2	4.44	5.96
10.73	5.20	4.15	0.121	36.1	31.8	29.6	-	-
11.81	5.75	4.05	0.118	36.2	31.6	30.0	-	-
12.92	5.70	4.01	0.117	36.5	31.7	30.0	-	-
13.78	5.79	3.69	0.116	36.5	31.8	30.6	1.10	6.77
14.94	5.65	3.31	0.135	36.6	33.0	31.9	-	-
15.99	5.84	3.49	0.114	36.8	32.3	31.9	-	-
16.96	5.45	2.64	0.106	36.7	32.4	31.9	-	-
17.81	5.81	2.88	0.113	36.8	32.2	32.4	-	-
18.76	5.84	2.67	0.115	36.8	31.9	32.4	-	-
19.76	6.17	2.58	0.115	40.0	32.0	32.4	-	-
20.96	5.72	2.37	0.115	37.0	32.2	32.4	0.74	5.54
21.94	5.70	2.26	0.116	36.8	32.0	33.1	-	-
23.01	5.55	2.18	0.111	36.8	32.0	33.1	-	-
24.00	5.79	2.12	0.107	36.8	32.0	33.4	-	-
25.05	5.70	2.07	0.105	36.7	32.0	33.4	-	-
26.03	5.79	2.02	0.103	36.7	32.0	33.4	-	-
26.92	5.66	1.80	0.116	36.7	31.9	33.4	-	-
27.92	5.51	1.83	0.113	36.3	32.1	33.4	-	-
28.77	5.84	1.96	0.105	36.6	32.0	33.4	-	-
29.79	5.81	1.89	0.104	36.6	31.8	33.6	-	-
31.00	5.74	1.66	0.113	36.8	31.8	33.6	0.61	3.15
32.06	5.67	1.41	0.122	36.9	32.4	33.8	0.57	2.56
32.96	5.72	1.64	0.140	36.8	32.2	34.2	-	-
33.96	5.58	1.60	0.122	36.8	32.2	34.2	0.61	3.36
34.86	5.62	1.62	0.128	36.6	32.2	34.1	-	-
35.88	5.51	1.56	0.131	36.5	32.2	34.3	-	-
36.80	5.44	1.38	0.120	36.5	32.2	34.2	-	-
37.94	5.37	1.46	0.104	36.8	32.0	33.8	0.57	3.04
38.78	5.85	1.54	0.104	36.7	32.0	34.2	-	-
39.89	5.61	1.43	0.105	36.1	32.1	34.3	-	-
40.78	5.90	1.23	0.092	36.9	32.1	34.3	-	-
41.74	6.10	1.33	0.087	36.7	31.9	34.3	-	-
43.02	6.19	1.30	0.094	36.5	32.0	34.3	-	-
43.77	6.06	1.26	0.105	36.7	32.0	34.3	-	-

44.94	5.98	1.16	0.108	36.8	32.5	34.6	0.46	2.69
45.82	6.21	1.23	0.112	36.8	32.0	34.6	-	-
46.86	5.99	1.15	0.113	36.8	32.4	34.8	-	-
47.82	6.03	1.17	0.093	36.6	32.1	34.8	-	-
48.85	6.19	1.16	0.086	36.6	31.8	35.1	-	-
49.98	6.62	1.06	0.082	36.8	31.8	35.0	-	-
51.86	6.06	1.01	0.104	36.6	32.1	35.0	-	-
54.04	5.92	0.95	0.111	36.8	32.3	34.9	-	-
54.89	6.52	0.85	0.109	36.6	32.0	34.9	-	-
55.86	6.67	0.98	0.108	36.8	31.9	35.0	-	-
56.78	6.33	0.89	0.110	36.7	32.0	35.0	-	-
59.07	5.93	0.90	0.105	36.7	32.0	35.4	-	-
59.90	6.01	0.78	0.117	36.9	32.5	35.4	0.61	1.79
62.00	5.17	0.87	0.124	36.0	29.8	35.4	-	-
63.80	5.87	0.83	0.080	36.8	31.9	35.4	-	-

Table C.3 Summary of measured results for the soil column of Processed silt.

Time (days)	PE (mm/day)	AE (mm/day)	R.H.Air	Air Temp (^{o}C)	Water Temp (^{o}C)	Soil Temp (^{o}C)	Moisture Content (%)	
							Depth of 0 mm	Depth of 20 mm
0				35.2	31.1	34.2	25.65	29.52
0.67	5.27	5.33	0.131	36.3	32.0	30.6	-	-
1.00	4.97	4.50	0.131	36.3	32.6	30.9	22.08	24.93
1.81	5.16	4.27	0.123	36.7	32.4	30.9	-	-
3.27	5.30	4.60	0.136	35.2	31.0	29.0	20.11	21.37
3.81	5.11	4.28	0.130	35.4	31.9	29.7	-	-
4.90	4.79	4.31	0.140	36.5	31.5	30.9	-	-
5.92	4.91	4.45	0.128	35.3	32.2	29.8	-	-
6.82	5.08	4.51	0.118	35.5	31.0	29.8	16.70	15.51
7.85	5.04	4.27	0.116	35.2	32.0	29.7	-	-
8.73	5.32	4.11	0.115	35.0	32.2	30.0	-	-
9.83	5.10	3.12	0.139	35.2	32.5	30.7	-	-
10.65	4.85	3.19	0.121	35.4	31.9	31.3	-	-
11.73	5.06	3.09	0.118	35.8	32.3	31.7	-	-
12.83	5.07	2.55	0.117	36.5	32.0	31.7	-	-
13.70	5.43	2.78	0.116	35.6	32.2	31.9	1.03	8.94
14.86	5.10	3.02	0.135	36.3	33.0	32.6	-	-
15.91	5.49	2.59	0.114	36.8	32.2	32.6	-	-
16.88	5.55	2.66	0.106	36.7	32.4	32.6	-	-
17.73	5.53	2.59	0.113	36.1	32.4	32.4	-	-
18.64	5.82	2.92	0.115	36.8	32.2	32.4	-	-
19.68	5.26	2.32	0.115	36.7	32.3	32.4	-	-
20.88	5.41	2.37	0.115	37.0	32.3	32.4	-	-
21.85	5.52	2.56	0.116	36.2	32.5	32.6	-	-
22.93	5.36	2.40	0.111	36.8	32.3	32.6	-	-
23.92	5.39	2.44	0.107	36.3	32.4	33.0	-	-
24.97	5.49	2.37	0.105	36.7	32.3	33.0	-	-
25.95	5.45	2.44	0.103	36.7	32.2	33.0	-	-
26.83	5.60	2.19	0.116	36.7	32.2	33.0	-	-

27.83	5.45	2.31	0.113	36.3	32.3	33.0	-	-
28.69	5.52	2.34	0.105	36.6	32.2	33.0	-	-
29.71	5.61	2.29	0.104	36.0	32.1	32.7	-	-
30.92	5.41	2.19	0.113	36.0	32.3	32.7	0.79	5.38
31.98	5.49	2.12	0.122	35.6	32.7	32.6	0.50	5.95
32.88	5.50	2.34	0.140	35.6	32.0	32.5	-	-
33.88	5.34	2.15	0.122	36.3	32.5	33.4	0.50	4.76
34.78	5.60	2.25	0.128	36.2	32.4	32.7	-	-
35.79	5.51	2.11	0.131	35.5	32.4	32.6	-	-
36.72	5.44	1.72	0.120	35.9	32.2	33.3	-	-
37.85	5.67	1.74	0.104	35.7	32.2	33.3	0.50	1.66
38.69	6.24	1.67	0.104	35.6	32.1	33.4	-	-
39.80	5.81	1.56	0.105	35.2	32.1	33.4	-	-
40.70	6.25	1.50	0.092	36.9	32.2	33.4	-	-
41.66	6.18	1.33	0.087	36.7	31.9	33.4	-	-
42.94	6.16	1.37	0.094	35.8	32.2	34.1	-	-
43.69	6.22	1.21	0.105	36.7	32.0	34.1	-	-
44.85	6.10	1.19	0.108	36.2	32.5	34.3	0.50	1.43
45.74	6.21	1.23	0.112	36.8	32.0	34.3	-	-
46.78	6.00	1.00	0.113	35.8	32.4	34.4	-	-
47.74	6.25	1.21	0.093	36.6	32.0	34.4	-	-
48.77	6.17	0.81	0.086	35.8	32.1	34.3	-	-
49.90	6.18	0.99	0.082	35.8	31.8	34.6	-	-
51.78	6.12	0.88	0.104	36.6	32.3	34.6	-	-
53.96	5.91	0.87	0.111	35.7	32.4	34.9	-	-
54.80	6.20	0.76	0.109	36.6	32.0	34.9	-	-
55.78	5.84	0.73	0.108	35.8	31.9	34.8	-	-
56.70	5.96	0.87	0.110	36.7	32.0	34.8	-	-
58.99	5.93	0.73	0.105	36.0	32.1	35.0	-	-
59.81	6.10	0.68	0.117	36.9	32.3	34.6	0.48	0.79
61.92	5.17	0.59	0.124	36.0	29.8	34.6	-	-
63.72	5.77	0.70	0.080	36.8	32.0	34.6	-	-

Table C.4 Summary of measured results for the soil column of Natural silt.

Time (days)	PE (mm/day)	AE (mm/day)	R.H.Air	Air Temp (^oC)	Water Temp (^oC)	Soil Temp (^oC)	Moisture Content (%)	
							Depth of 0 mm	Depth of 20 mm
0.00			0.140	36.6	29.9	34.9	19.30	21.74
0.96	4.54	4.12	0.128	35.9	32.6	31.3	18.14	18.34
2.15	4.79	3.55	0.118	36.2	32.5	30.8	-	-
2.94	4.94	3.64	0.116	36.1	32.5	30.7	17.38	18.71
4.01	4.86	3.44	0.115	35.6	32.5	30.6	-	-
5.02	4.93	3.67	0.139	36.0	32.5	30.7	17.77	18.44
5.91	4.61	3.65	0.121	36.2	32.8	30.7	-	-
7.00	4.82	3.72	0.118	36.2	32.9	30.7	16.80	19.52
8.08	4.67	3.79	0.117	36.5	32.8	30.7	-	-
8.97	4.60	3.68	0.116	36.0	33.3	30.7	-	-
10.08	4.69	3.65	0.135	36.3	33.4	30.9	16.50	17.87
11.17	4.82	4.05	0.114	36.8	33.3	30.9	-	-
12.13	4.77	3.75	0.106	36.7	33.2	30.9	-	-
13.00	4.80	3.69	0.113	36.2	33.1	30.7	16.72	17.27

13.93	4.78	3.84	0.115	36.8	33.3	30.7	-	-
14.93	4.82	3.67	0.115	36.7	33.2	30.7	-	-
16.13	4.79	3.79	0.115	37.0	33.3	30.7	-	-
17.10	4.74	3.54	0.116	36.8	33.4	31.0	-	-
18.18	4.80	3.79	0.111	36.8	33.2	31.0	-	-
19.17	4.83	3.79	0.107	36.8	33.3	30.9	-	-
20.22	4.79	3.56	0.105	36.7	33.3	30.9	-	-
21.20	4.88	3.70	0.103	36.7	33.2	30.9	-	-
22.08	4.89	3.79	0.116	36.7	33.1	30.9	16.48	17.29
23.08	4.74	3.66	0.113	36.3	33.2	30.9	-	-
23.94	4.80	3.45	0.105	36.6	33.3	30.9	-	-
24.96	4.83	3.71	0.104	36.6	33.2	30.9	-	-
26.14	4.82	3.75	0.113	36.8	33.4	30.9	-	-
27.08	4.77	3.41	0.122	36.1	33.5	31.0	-	-
28.14	4.80	3.56	0.140	36.2	33.5	31.2	-	-
29.08	4.80	3.75	0.122	36.6	33.5	31.4	-	-
30.02	4.80	3.66	0.128	36.4	33.5	31.2	-	-
31.04	4.86	3.59	0.131	36.2	33.3	31.2	14.48	16.56
31.97	4.82	3.43	0.120	36.3	33.4	31.1	14.68	17.87
33.10	4.72	3.64	0.104	36.4	33.3	31.1	-	-
33.95	4.96	3.84	0.104	36.3	33.1	31.0	15.34	16.56
35.05	4.92	3.64	0.105	36.3	33.1	31.2	-	-
35.95	4.96	3.79	0.092	36.9	33.3	31.2	-	-
36.91	5.10	3.75	0.087	36.7	33.1	31.2	-	-
38.19	5.03	3.79	0.094	36.5	32.9	31.1	13.89	12.83
38.94	4.96	3.57	0.105	36.7	33.4	31.1	-	-
40.10	4.86	3.69	0.108	36.8	33.2	31.1	-	-
40.99	4.92	3.61	0.112	36.8	33.2	31.1	-	-
42.03	4.94	3.60	0.113	36.7	33.3	31.6	-	-
42.99	5.00	3.41	0.093	36.6	33.4	31.6	-	-
44.02	5.08	2.66	0.086	36.8	33.1	32.9	-	-
45.15	5.13	2.41	0.082	36.8	33.0	33.6	1.89	3.07
46.13	5.03	1.87	0.076	36.8	33.3	33.6	-	-
47.03	5.00	1.76	0.104	36.6	33.3	34.1	-	-
48.07	4.89	1.76	0.114	36.7	33.2	34.1	-	-
49.21	4.87	1.53	0.111	36.6	32.8	34.7	-	-
50.05	4.92	1.61	0.109	36.6	33.0	34.7	-	-
51.04	4.81	1.55	0.108	36.8	33.4	34.7	-	-
51.95	4.91	1.32	0.110	36.7	33.4	34.7	-	-
54.24	4.88	1.35	0.105	36.7	33.1	34.7	-	-
55.06	4.93	1.18	0.117	36.9	33.4	34.7	-	-
56.08	4.91	1.25	0.123	36.2	33.1	34.8	-	-
57.17	4.57	1.17	0.124	36.0	31.5	34.8	-	-
58.97	4.75	1.10	0.080	36.8	33.0	34.8	-	-
61.15	5.02	1.09	0.082	36.5	32.8	34.8	1.06	1.88

APPENDIX D

SOIL PROPERTIES AND SCHEMES OF DRYING EXPERIMENTS AND TEST RESULTS FROM YANFUL AND CHOO (1997)

Table D.1 Summary of soil properties of used for each soil type in the drying experiments (adapted after Yanful and Choo, 1997).

Soil Properties	Coarse sand	Fine sand
Volumetric water content	0.295	0.310
Degree of saturation	0.91	0.74
Suction (kPa)	1	1
Estimated unsaturated hydraulic conductivity (m/sec)	3×10^{-5}	1×10^{-5}
Saturated hydraulic conductivity (m/sec)	2×10^{-4}	1×10^{-5}

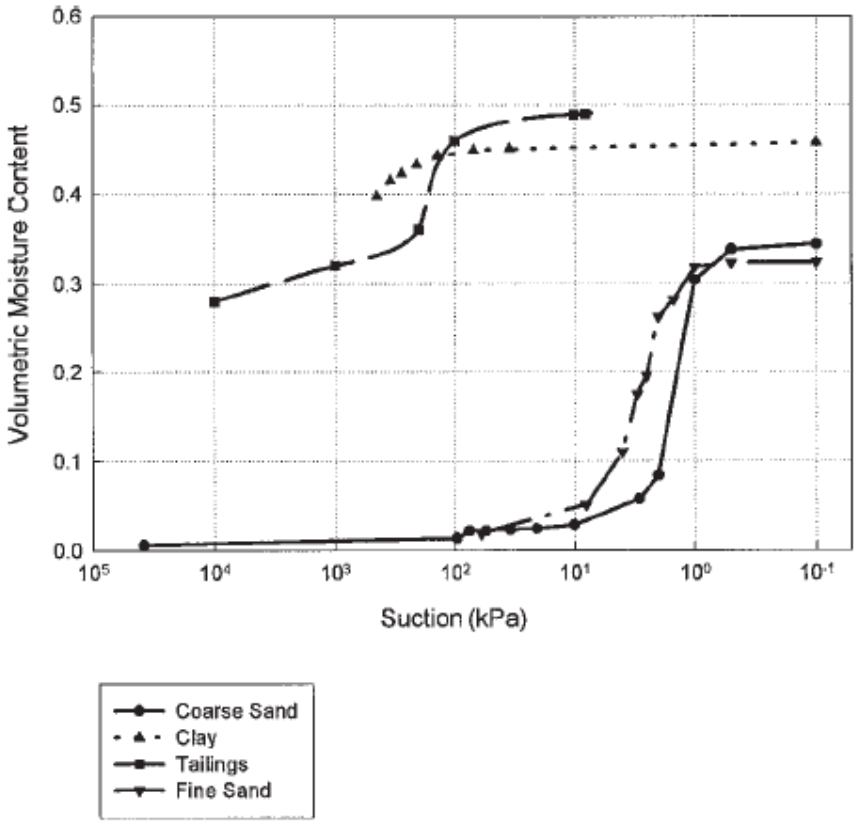

Fgiure D.1 Soil-water characteristic curves for test soils and tailings (adapted after Yanful and Choo, 1997).

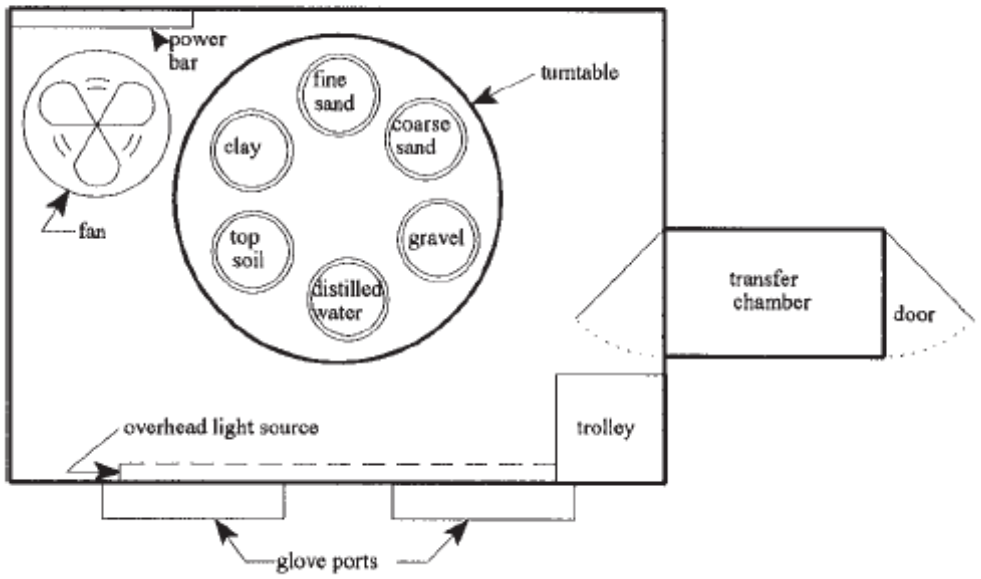

Fgiure D.2 Plan view of environmental chamber showing location of soil columns (adapted after Yanful and Choo, 1997).

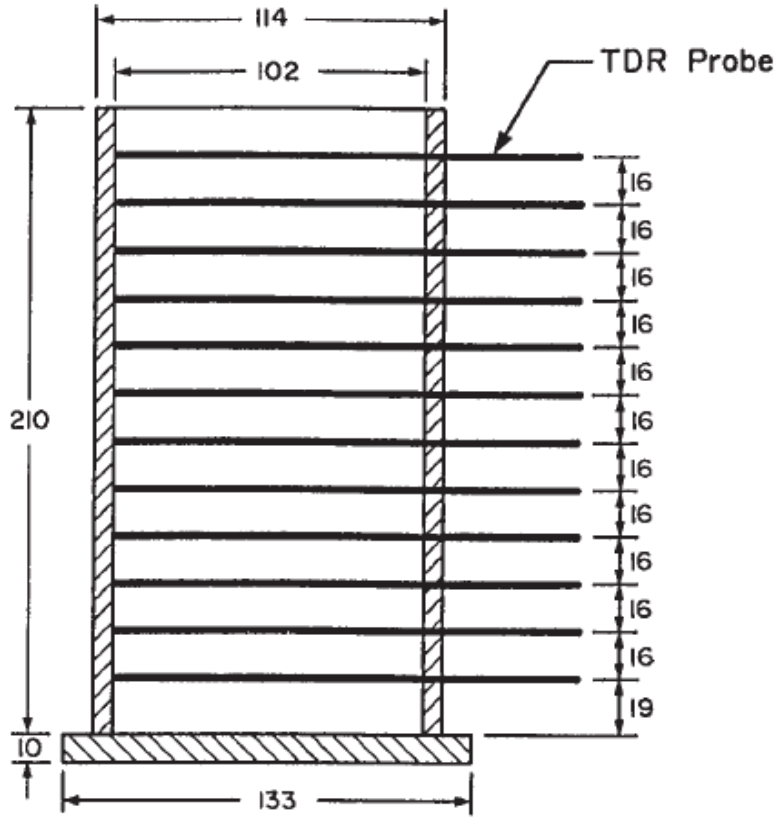

Fgiure D.3 Evaporation column showing location of TDR (time-domain reflectometry) probes. All dimensions in millimetres (adapted after Yanful and Choo, 1997).

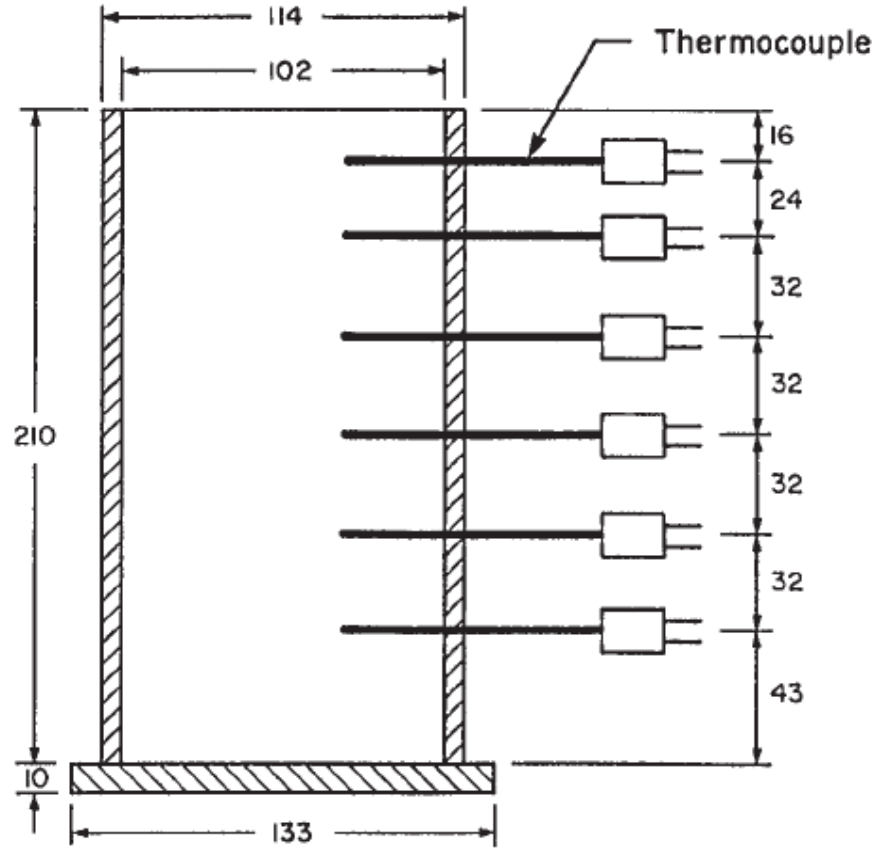

Fgiure D.4 Evaporation column showing location of thermocouples. All dimensions in millimetres (adapted after Yanful and Choo, 1997).

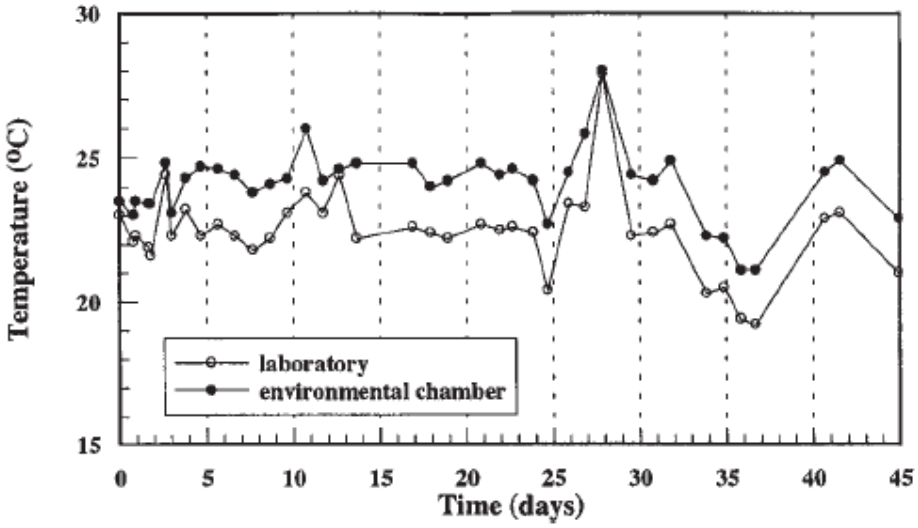

Fgiure D.5 Temperature in environmental chamber and laboratory (after Yanful and Choo, 1997).

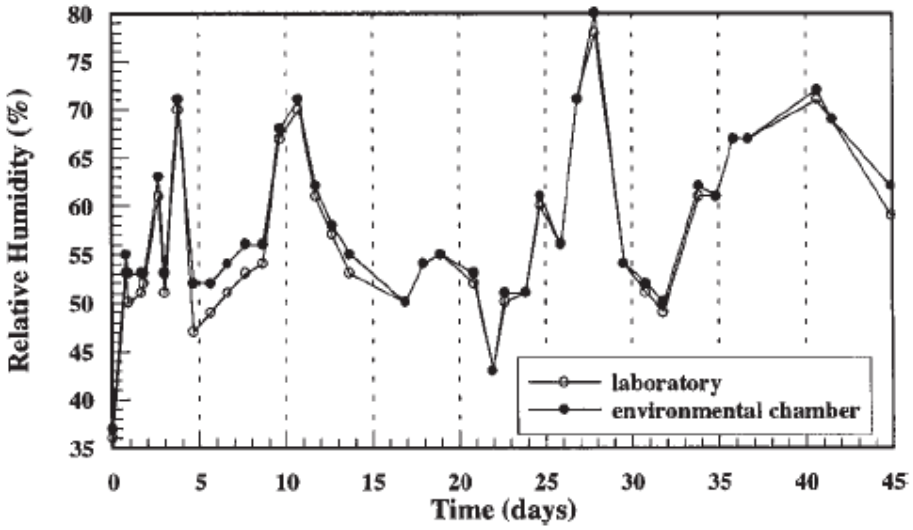

Fgiure D.6 Relative humidity in environmental chamber and laboratory (after Yanful and Choo, 1997).

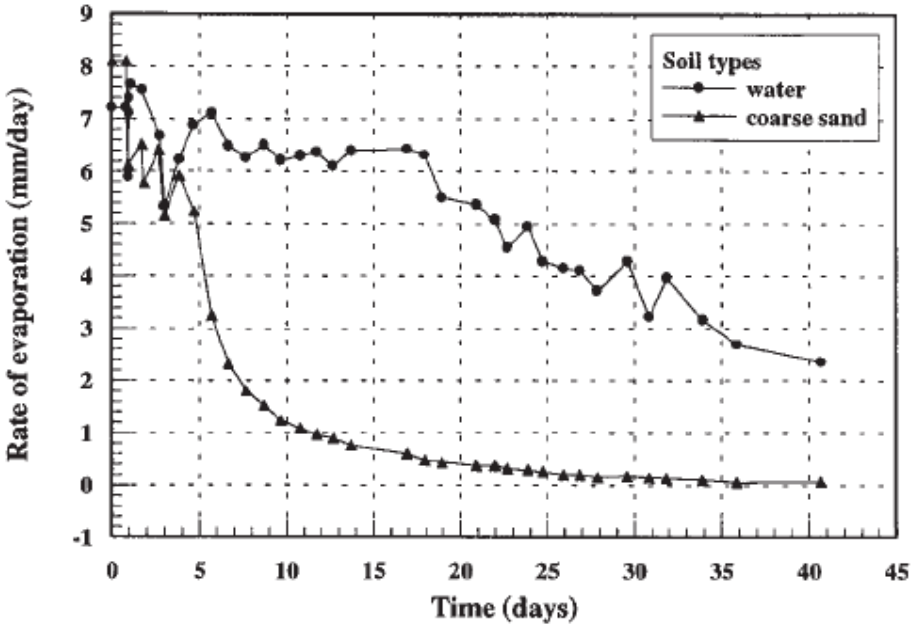

Fgiure D.7 Rate of evaporation for Coarse sand (after Yanful and Choo, 1997).

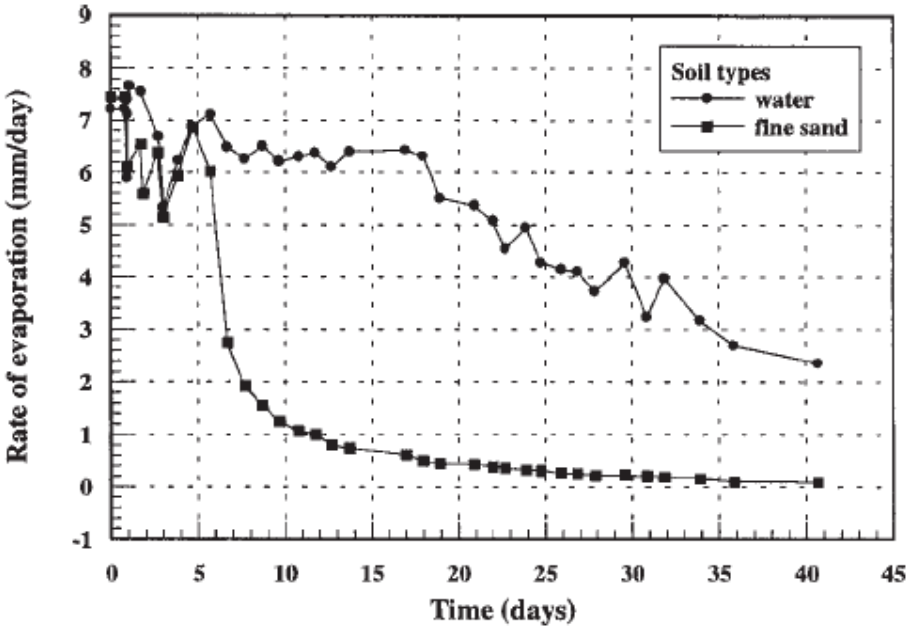

Fgiure D.8 Rate of evaporation for Fine sand (after Yanful and Choo, 1997).

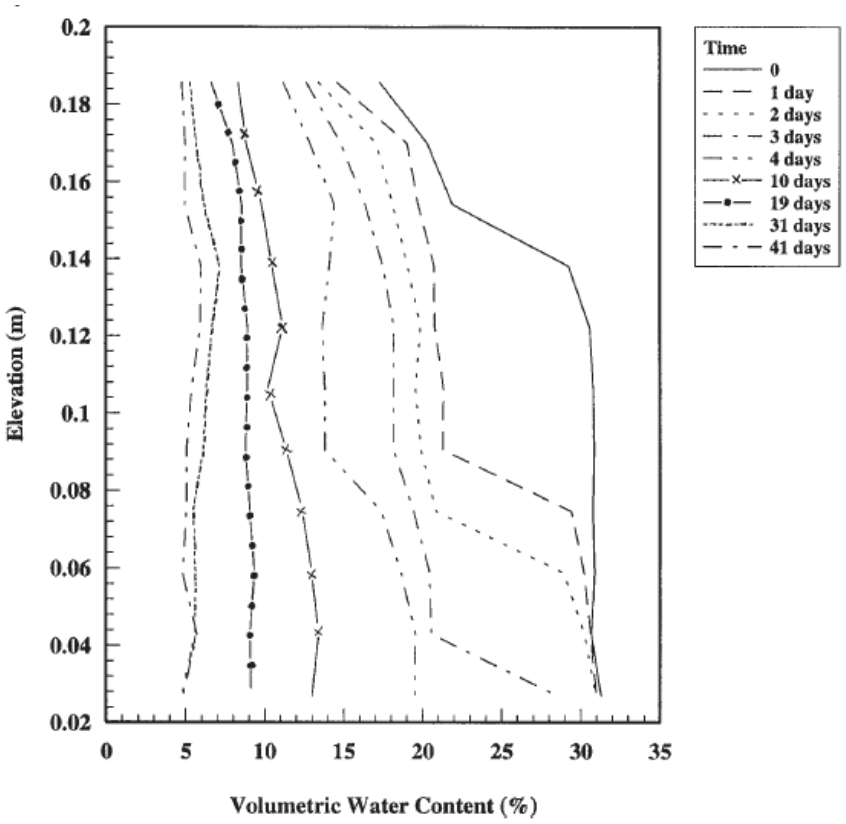

Fgiure D.9 Water content profile for Coarse sand (after Yanful and Choo, 1997).

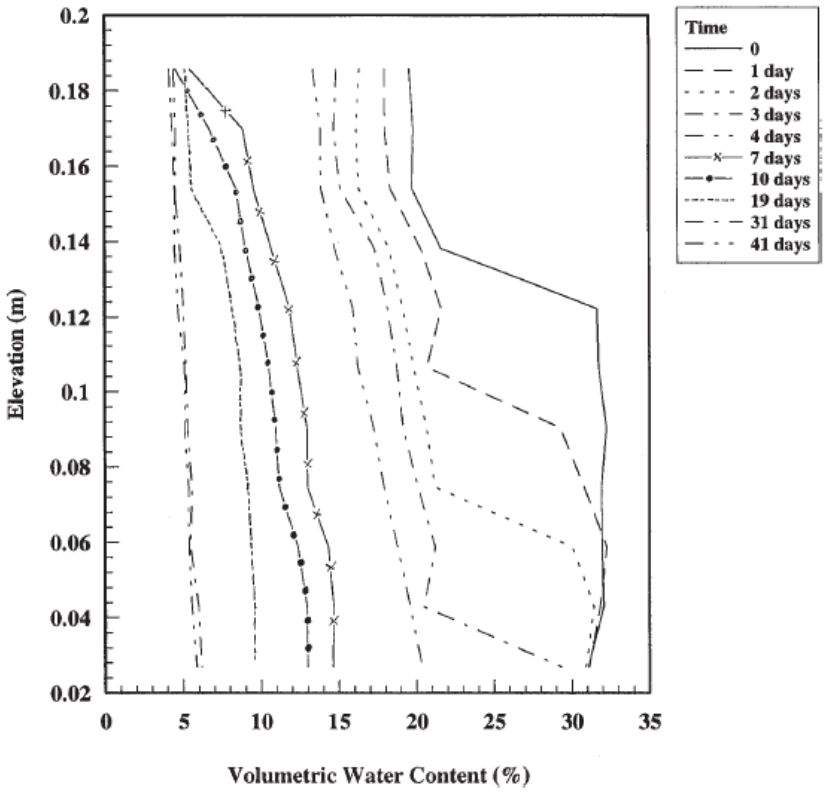

Fgiure D.10 Water content profile for Fine sand (after Yanful and Choo, 1997).

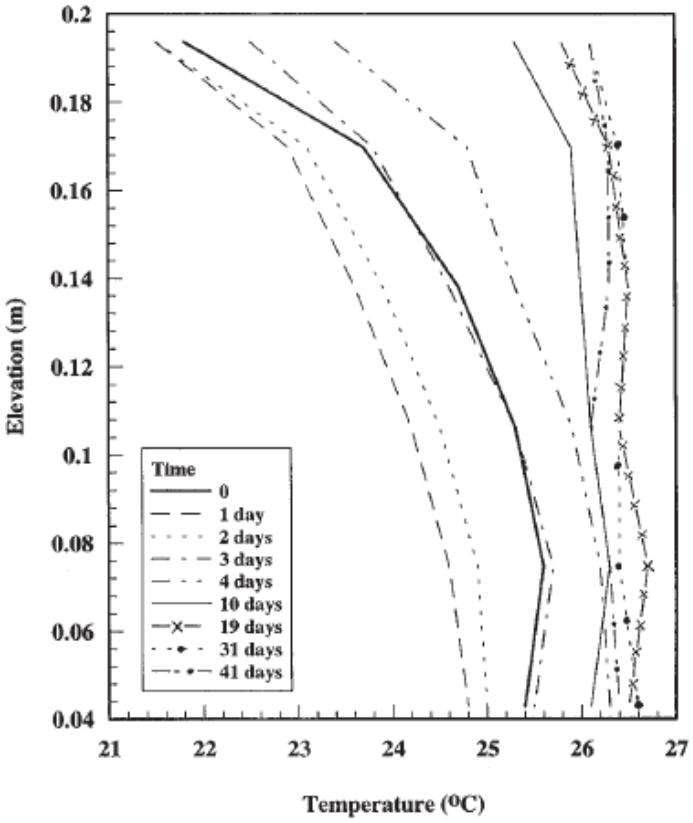

Fgiure D.11 Temperature profile for Coarse sand (after Yanful and Choo, 1997).

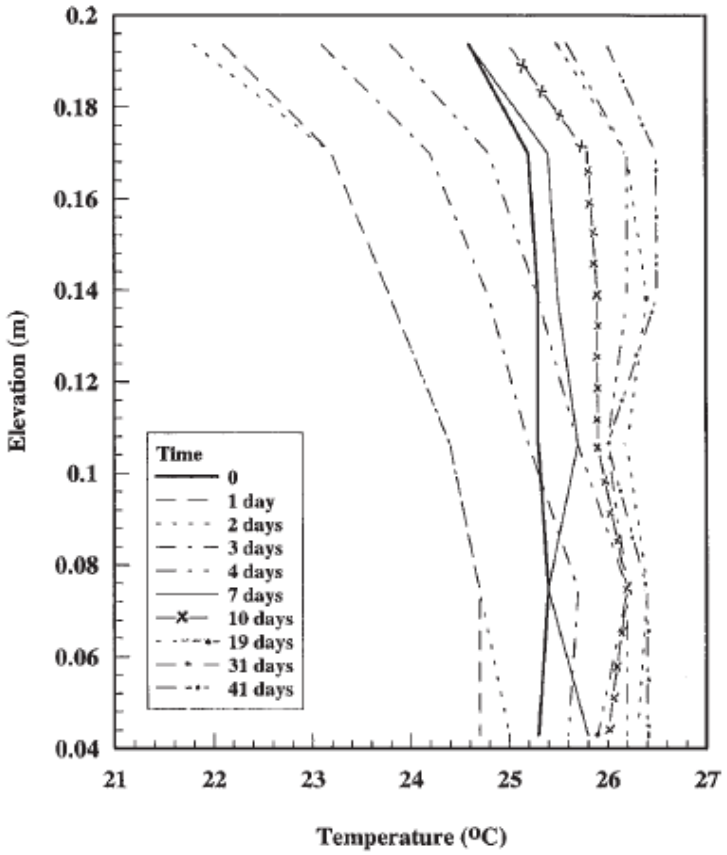

Fgiure D.12 Temperature profile for Fine sand (after Yanful and Choo, 1997).

APPENDIX E

SOIL PROPERTIES, SCHEMES OF DRYING EXPERIMENTS AND TEST RESULTS COLLECTED FROM DUNMOLA'S THESIS (2012)

Table E.1 Geotechnical properties of the tested mine tailings and silt.

Parameter	Mine Tailings	Silt
Specific Gravity	2.9	2.48
D_{10}, D_{50}, D_{60} (microns)	2, 35, 55	1, 31, 41
Cu (D_{60}/D_{10})	27.5	41
Liquid limit (%)	20	19
Plastic limit (%)	19	13
Saturated hydraulic conductivity (m/s)*	2.0E-7	1.7E-6

*Saturated hydraulic conductivity values were determined by falling head tests at void ratio of 0.8 as per Fisseha et al. (2007) and Fisseha et al. (2010).

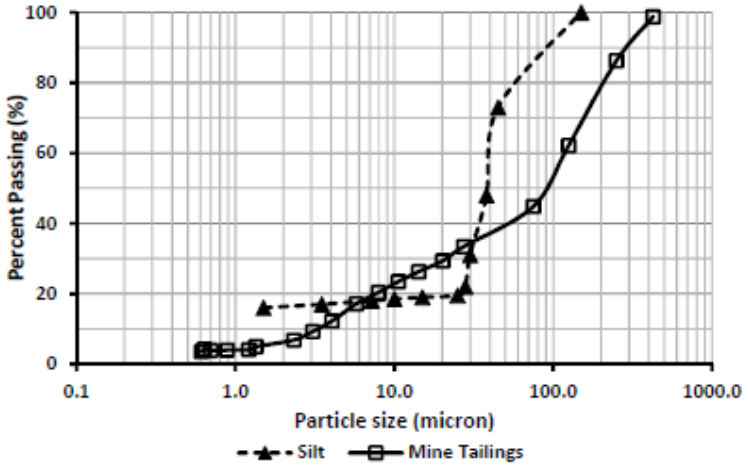

Figure E.1 Particle size distributions of silt and mine tailings.

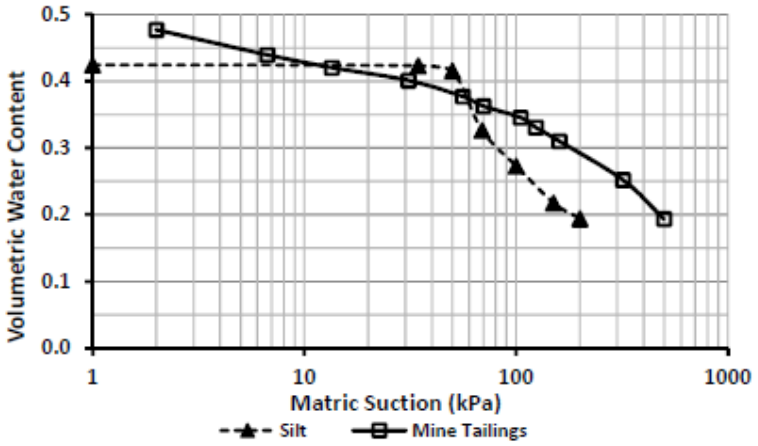

Figure E.2 Soil-water characteristic curves for silt and mine tailings obtained using axis-translation technique in a pressure plate apparatus (after Dunmola, 2012).

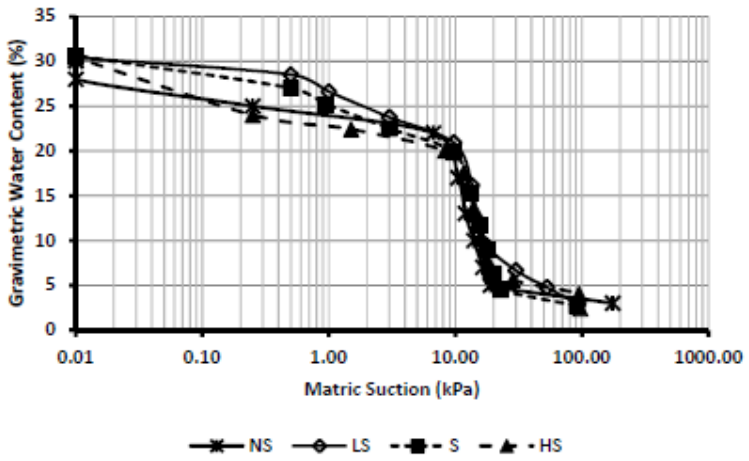

Figure E.3 Soil-water characteristic curves for remoulded Low-saline (LS), Saline (S), Hyper-saline (HS) and Non-saline (NS) soils.

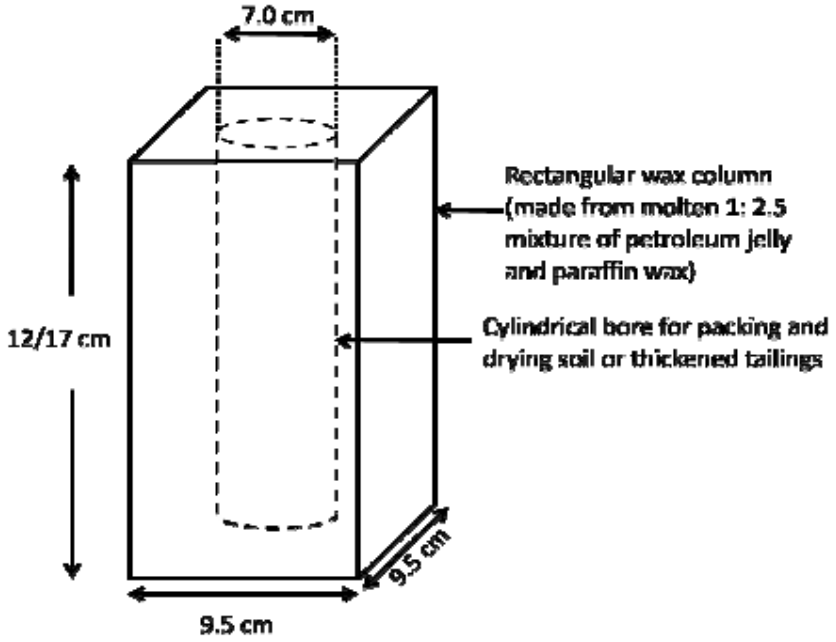

Figure E.4 Schematic of petroleum jelly-wax column for packing, drying and sampling soil and thickened tailings.

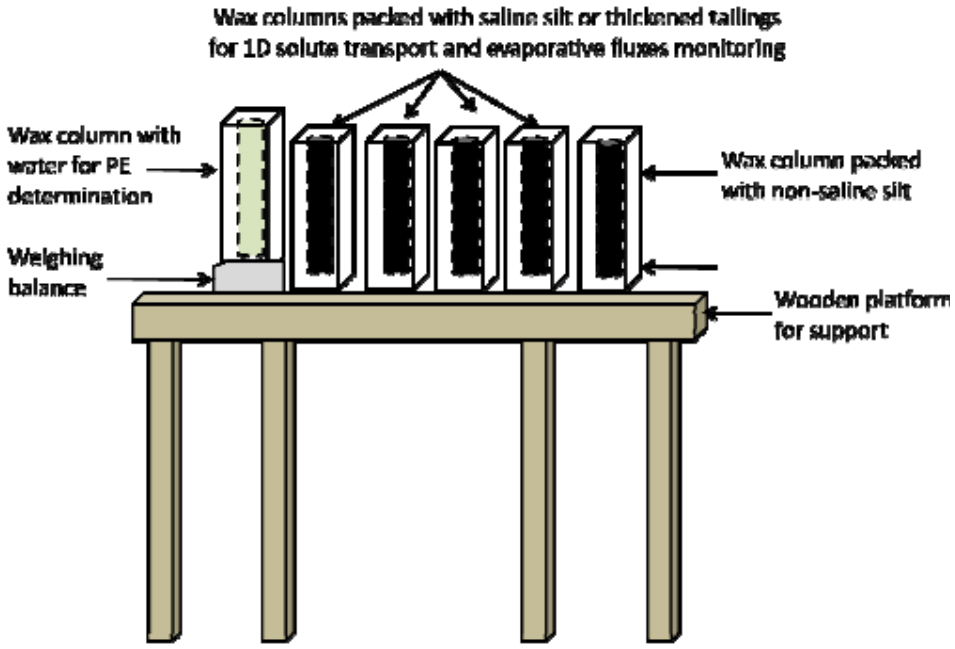

Figure E.5 Generalized experimental set-up for drying and sampling silt and thickened tailings columns.

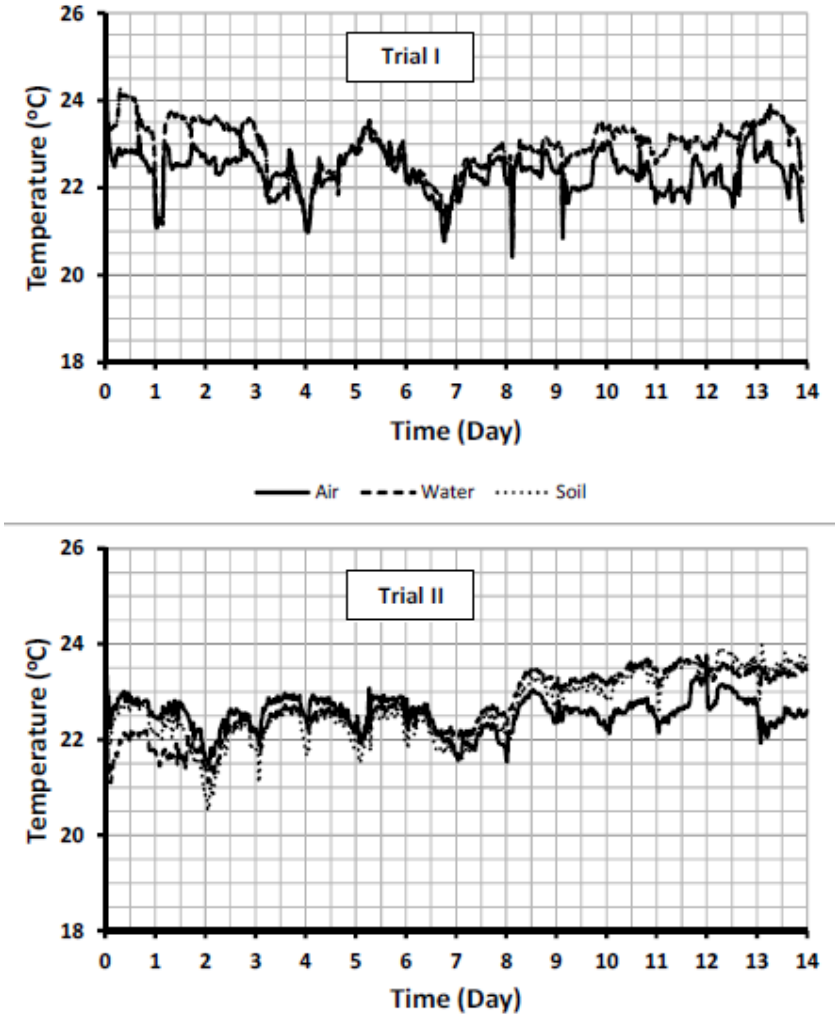

Figure E.6 Temperature at the surface of water and soil packed and drying inside was columns under ambient laboratory condition with wind simulated with fan. The air temperature at 2 cm height above the water and silt columns is also shown. Results presented are for 2 independent trials.

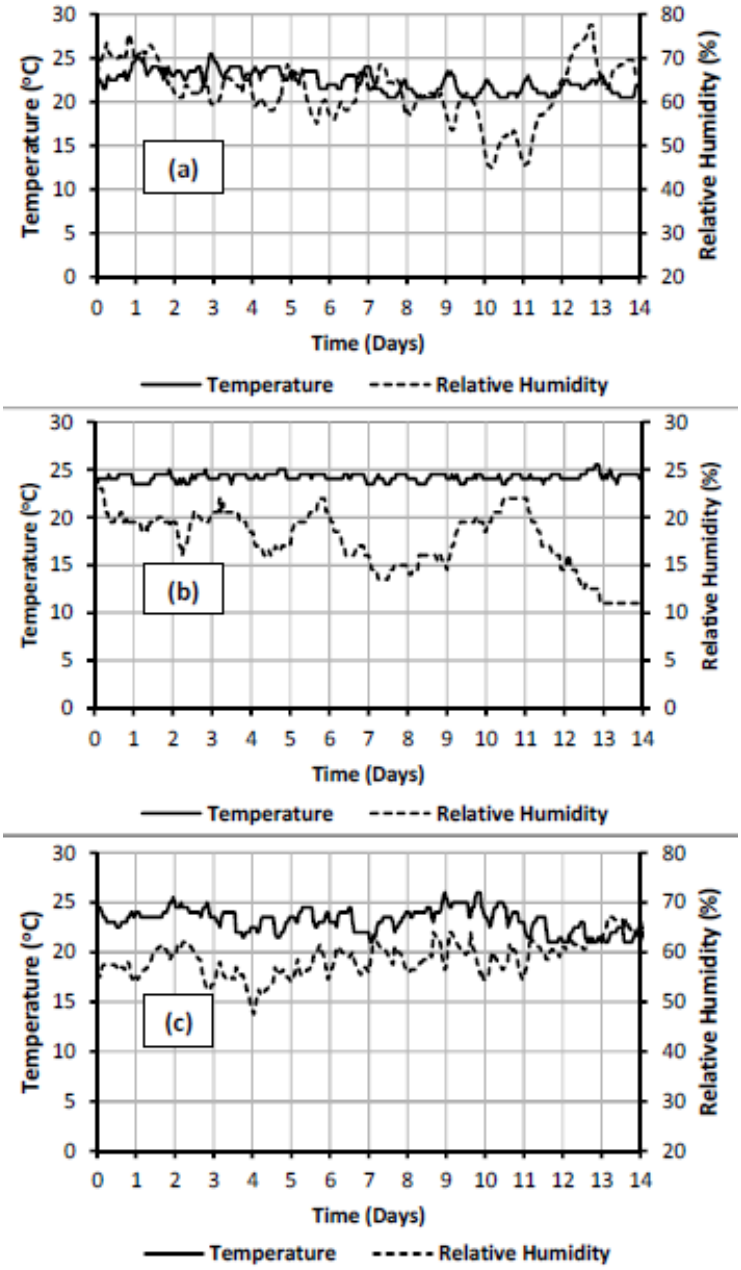

Figure E.7 Ambient relative humidity and temperature during the drying experiment for Low-saline (a), Saline (b) and Hyper-saline (c) treatment soil columns.

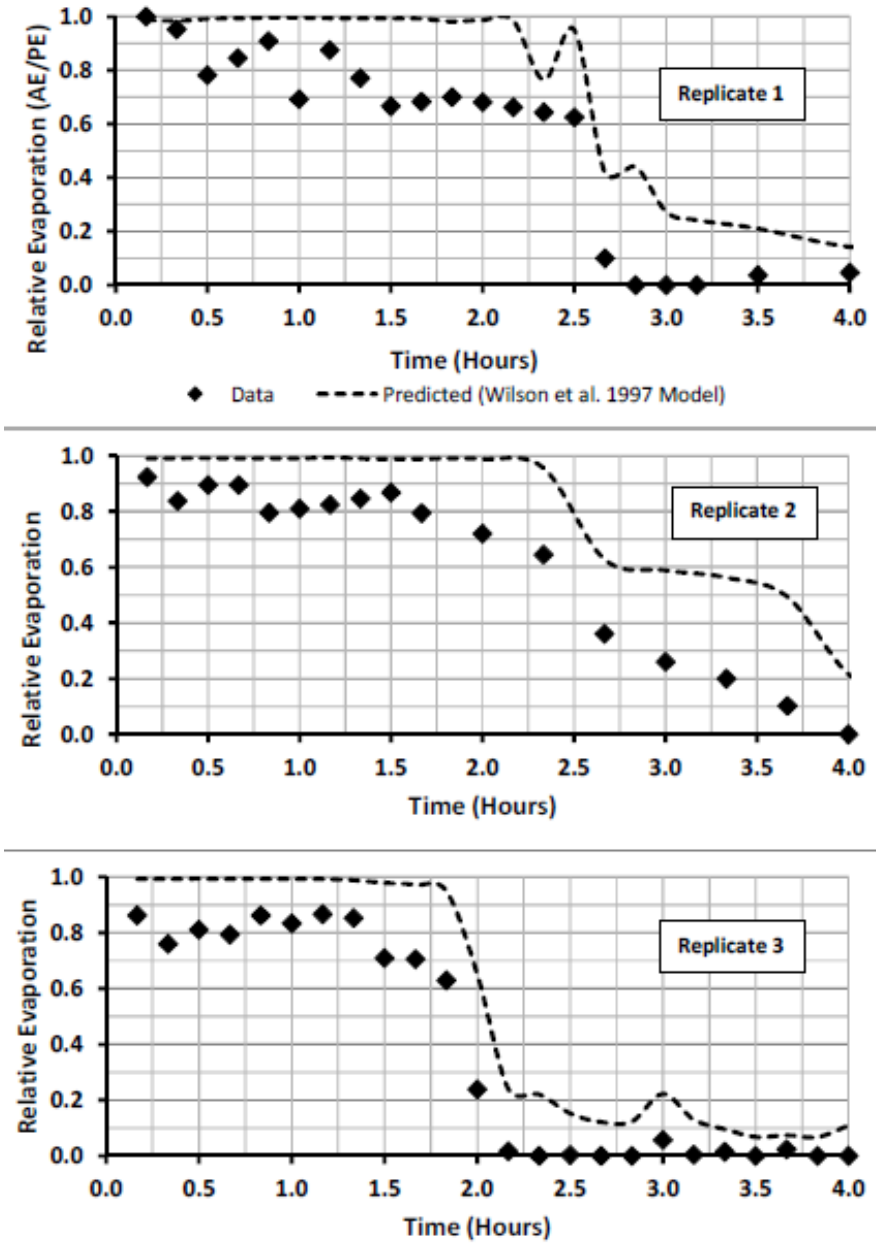

Figure E.8 Relative Evaporation measured from three independent replicate drying experiments of 2 mm-thick soil samples.

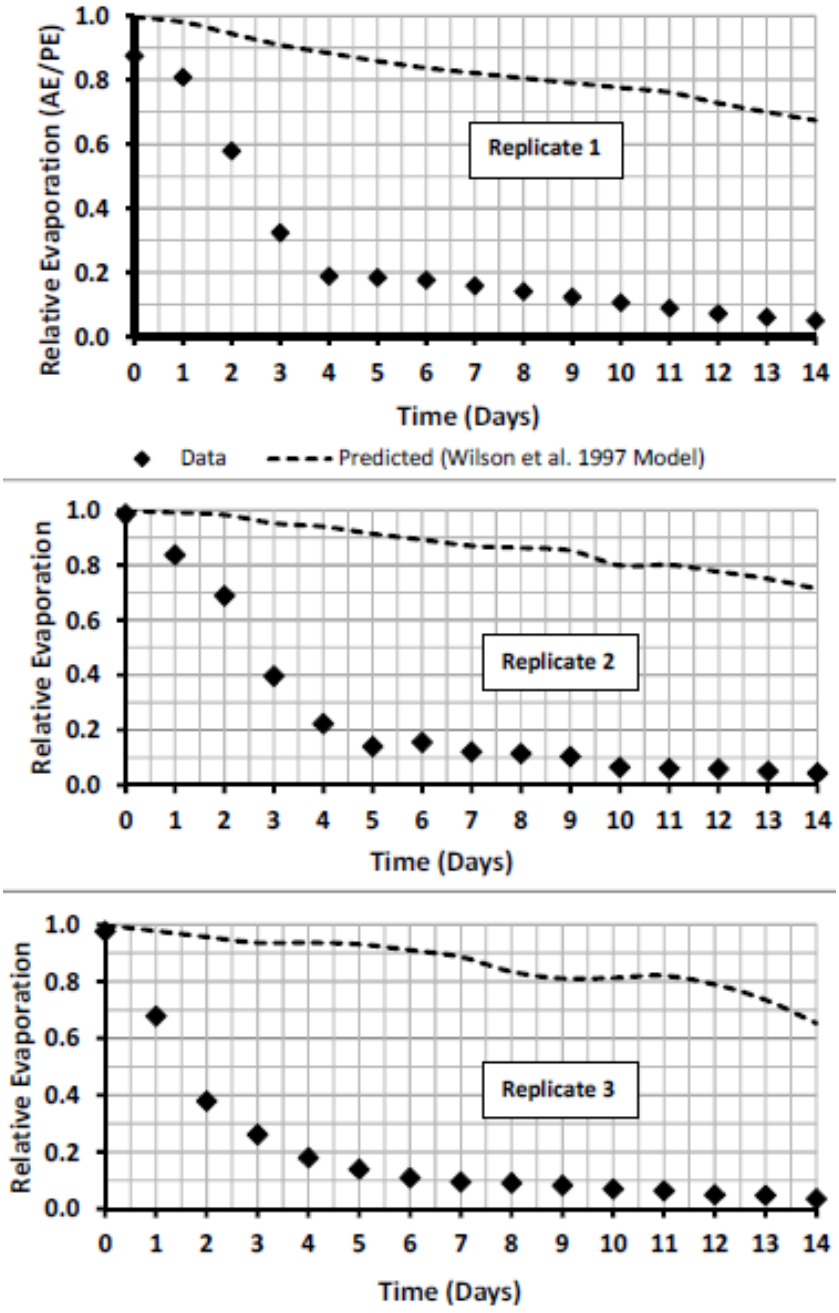

Figure E.9 Relative Evaporation measured from three independent replicate drying experiments of 10cm-thick soil samples. The predicted results were obtained from total suction in the top 1 cm of desiccating columns.

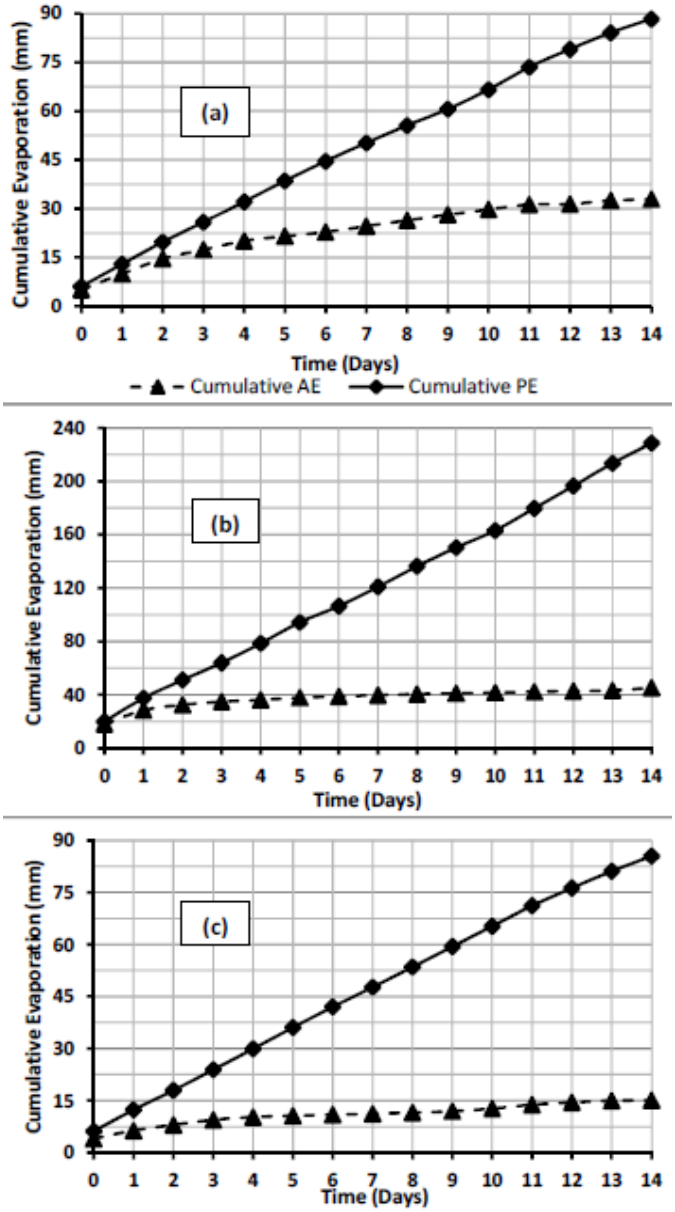

Figure E.10 Cumulative Actual and Potential Evaporation from Low-saline (a), Saline (b) and Hyper-saline (c) soil columns.

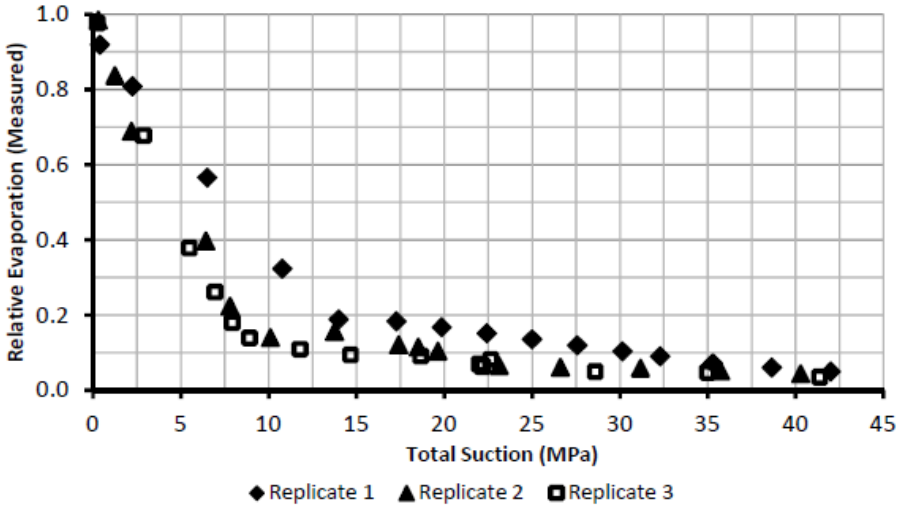

Figure E.11 Relative Evaporation measured for the 10 cm-thick NS soil columns as a function of total suctions measured for bulk samples obtained in the top 1 cm.

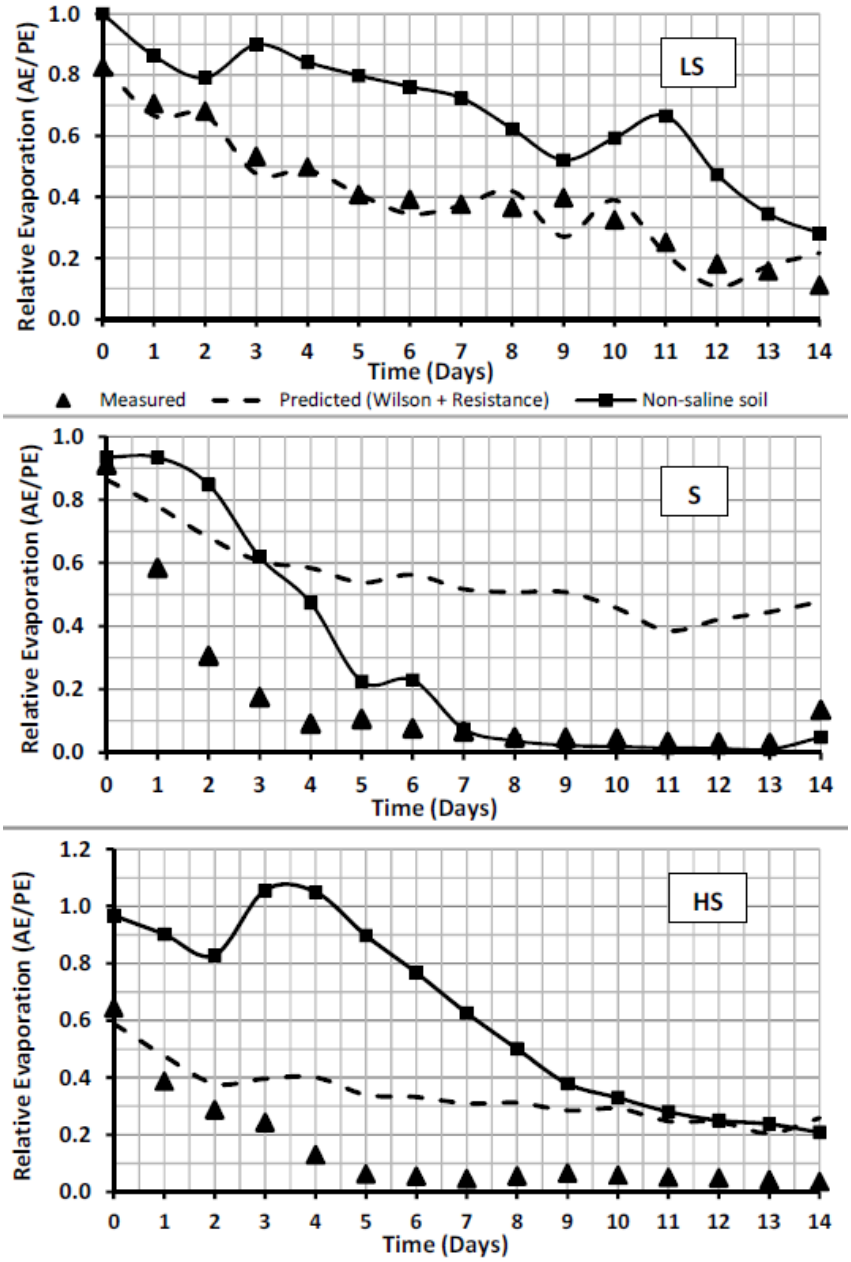

Figure E.12 Relative Evaporation measured and predicted for Low-saline (LS), Saline (S) and Hyper-saline (HS) soil columns and measured for corresponding Non-saline soil columns.

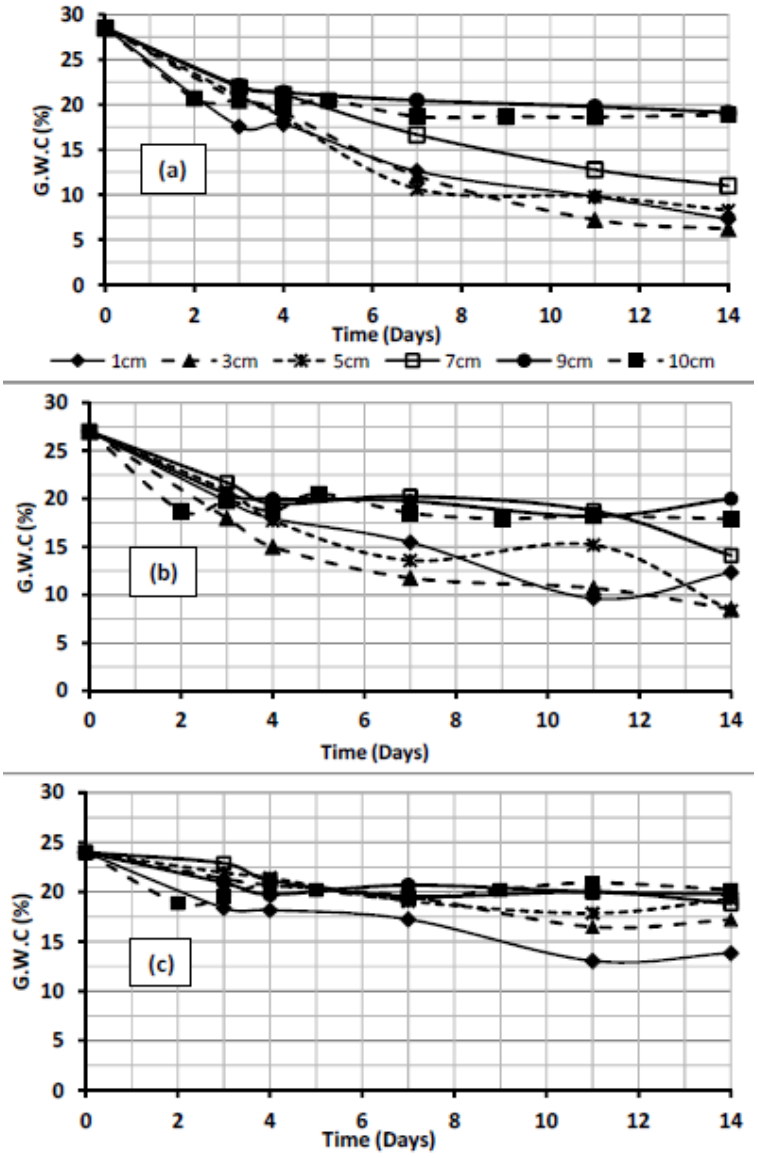

Figure E.13 Gravimetric water contents over time at different depths of the Low-saline (a), Saline (b) and Hyper-saline (c) soil columns.

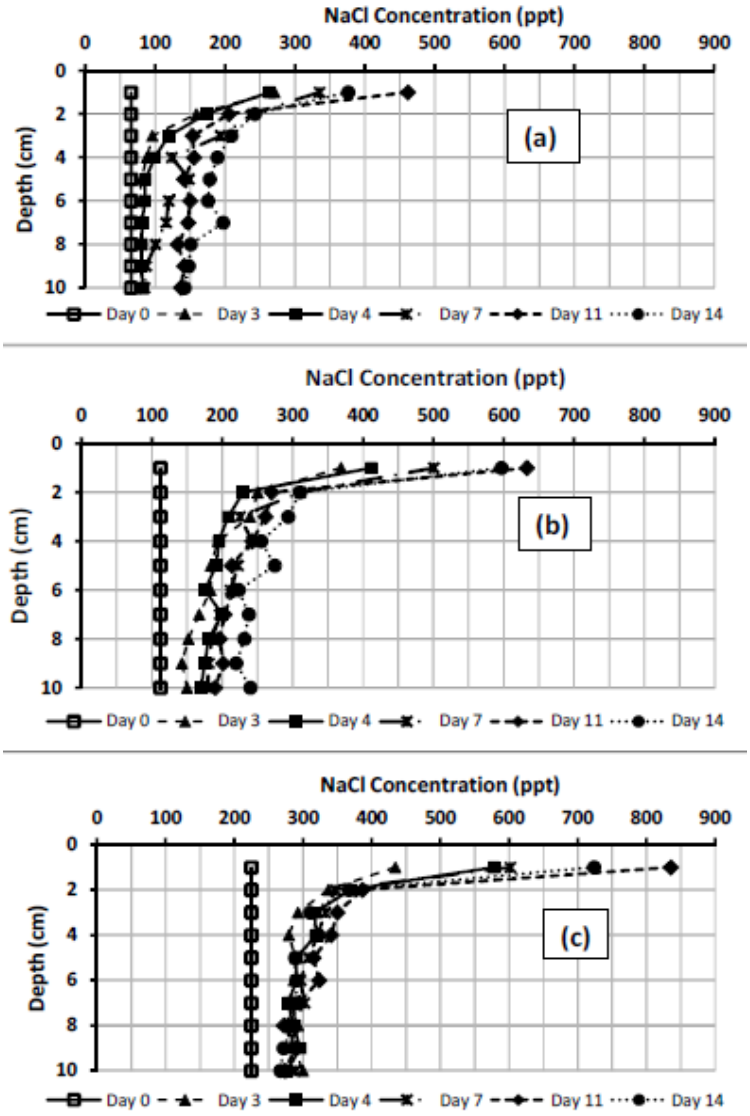

Figure E.14 Profile NaCl concentration over time at different depths of the Low-saline (a), Saline (b) and Hyper-saline (c) soil columns.

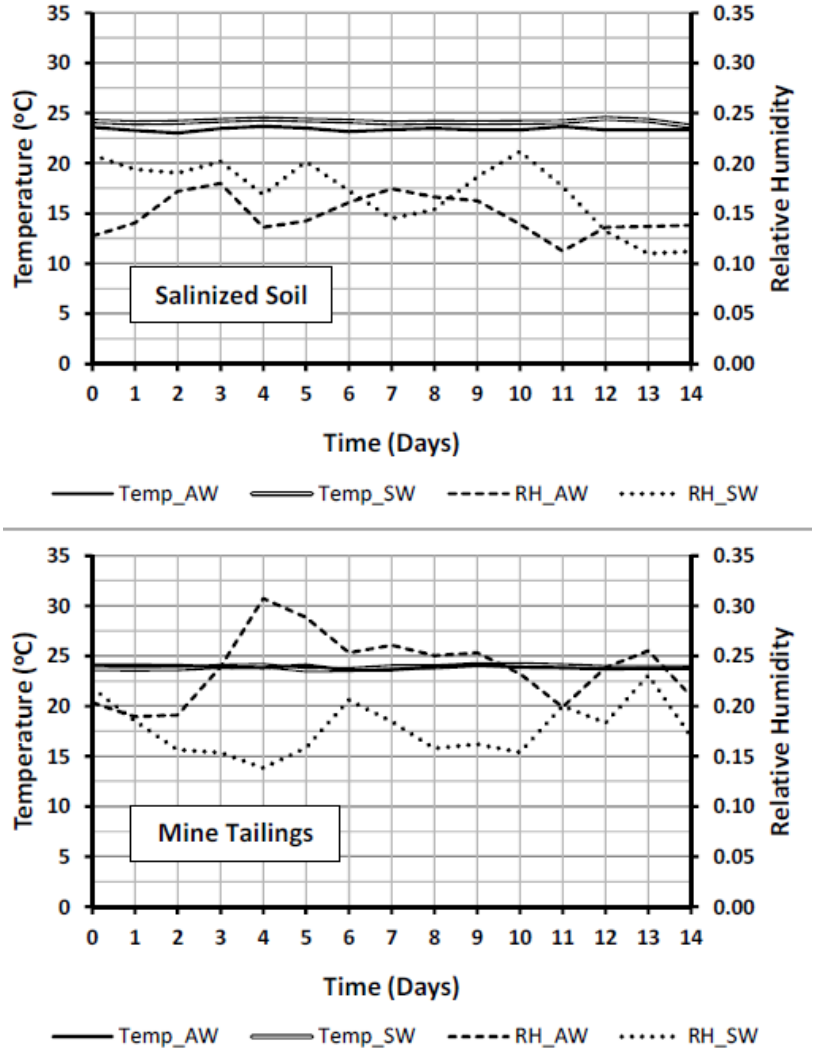

Figure E.15 Ambient temperature and relative humidity during desiccation of salinized soil and acid-generating thickened mine tailings under ambient (AW) and simulated (SW) wind boundary conditions.

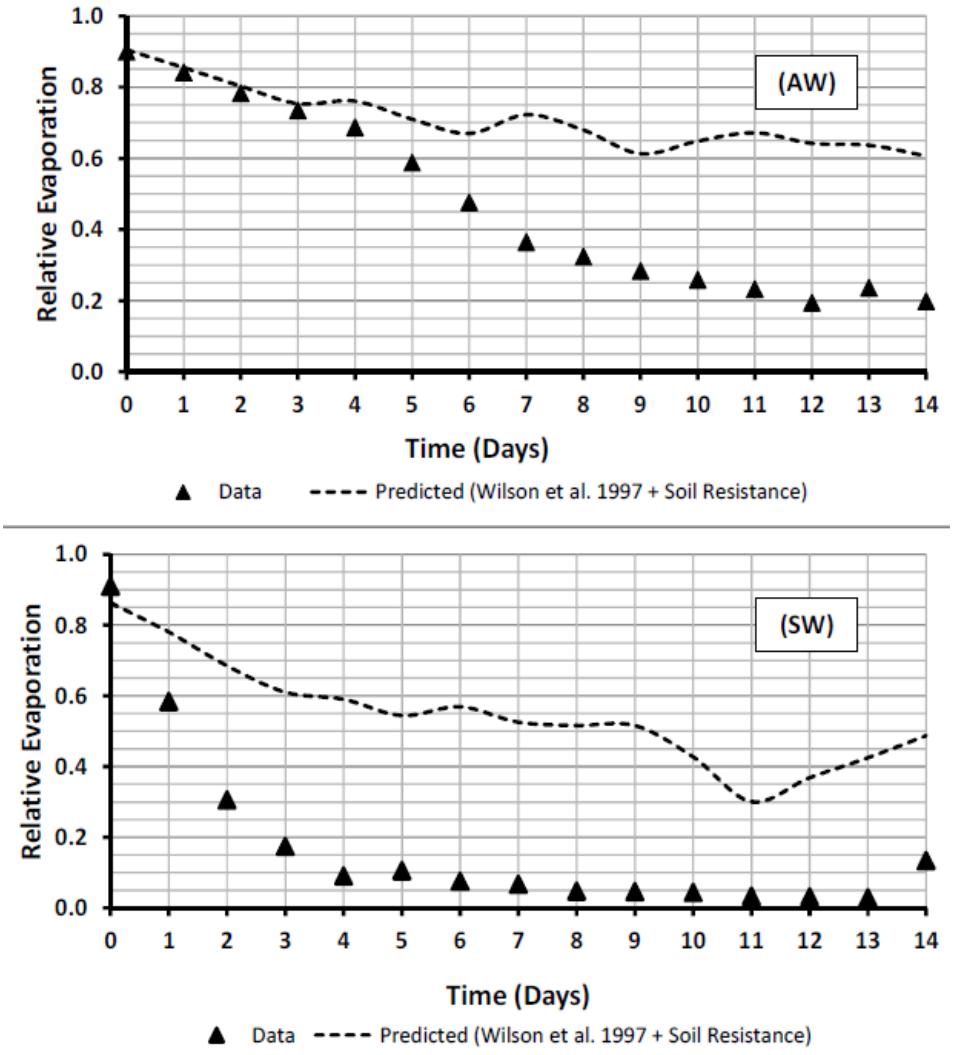

Figure E.16 Relative Evaporation measured from desiccating salinized soil columns and predicted results from total suction in the top 1 cm by Dunmola (2012) under ambient (AW) and simulated wind (SW) boundary conditions.

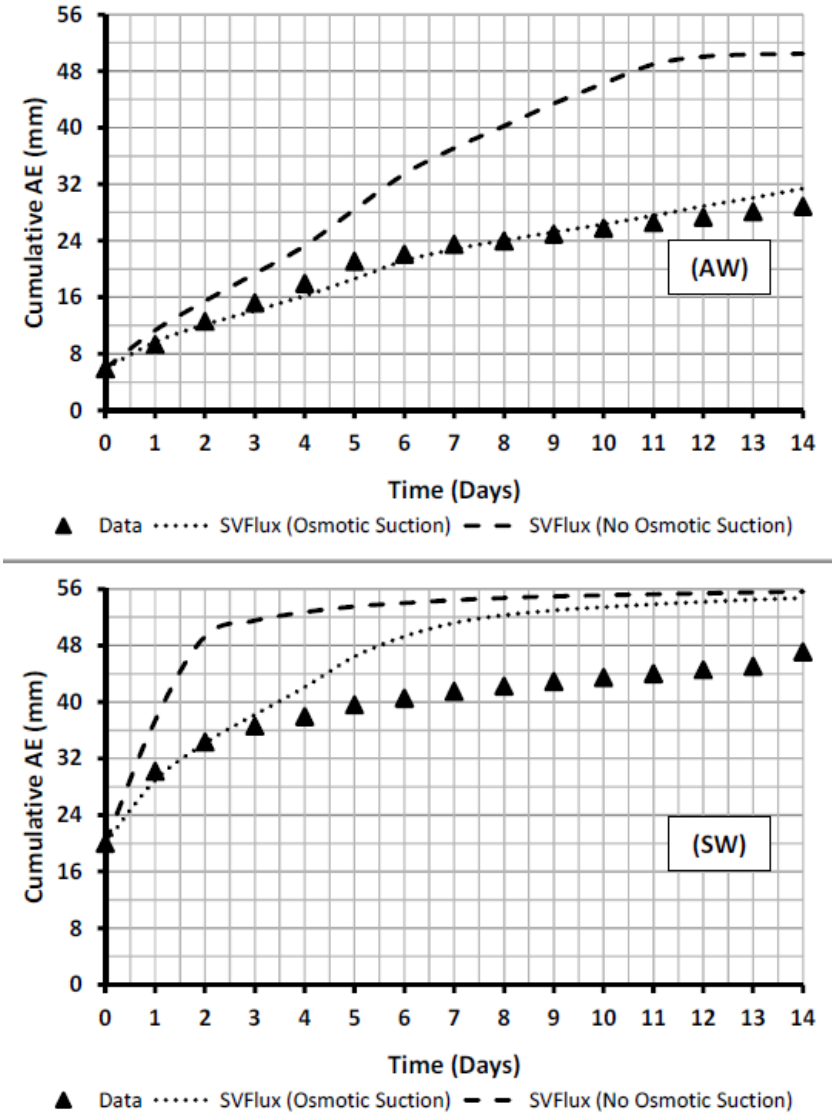

Figure E.17 Cumulative actual evaporation measured and predicted for salinized soil columns desiccating under ambient (AW) and simulated wind (SW) boundary conditions. Predictions with and without accouting for temporal evolution of osmotic suction are shown in the dot lines.

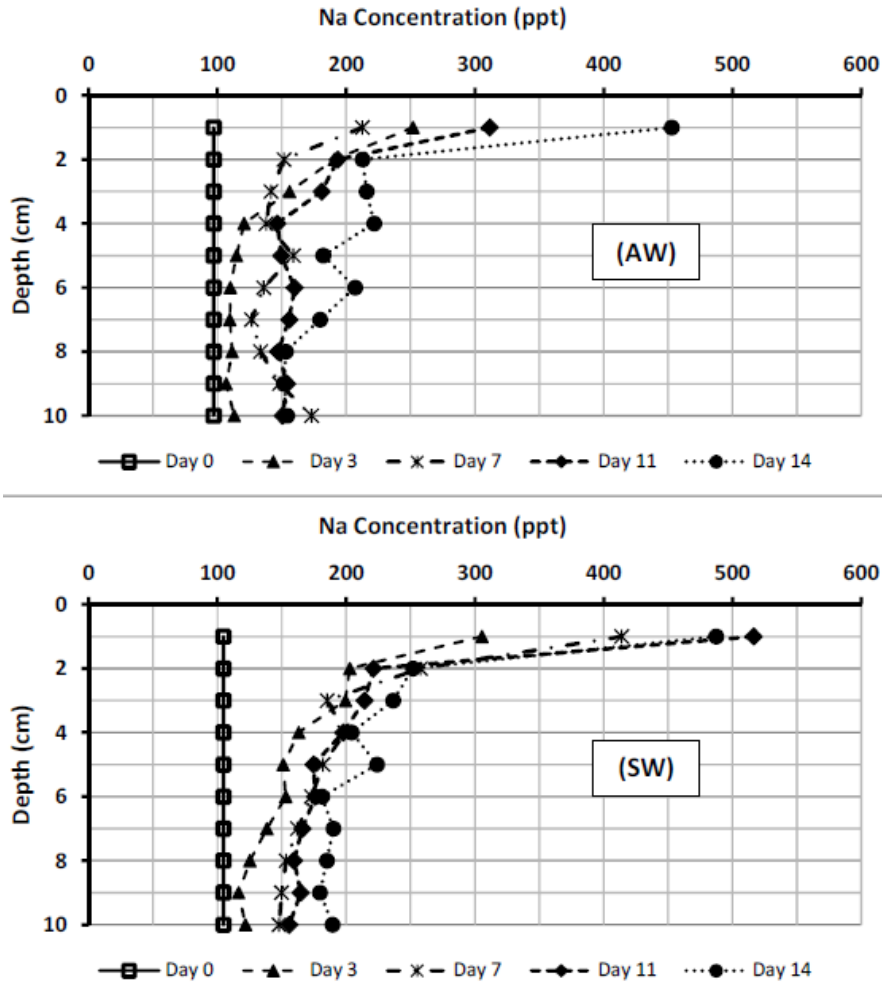

Figure E.18 NaCl concentrations over time at different depths of salinized soil columns of drying under ambient (AW) and simulated wind (SW) boundary conditions.

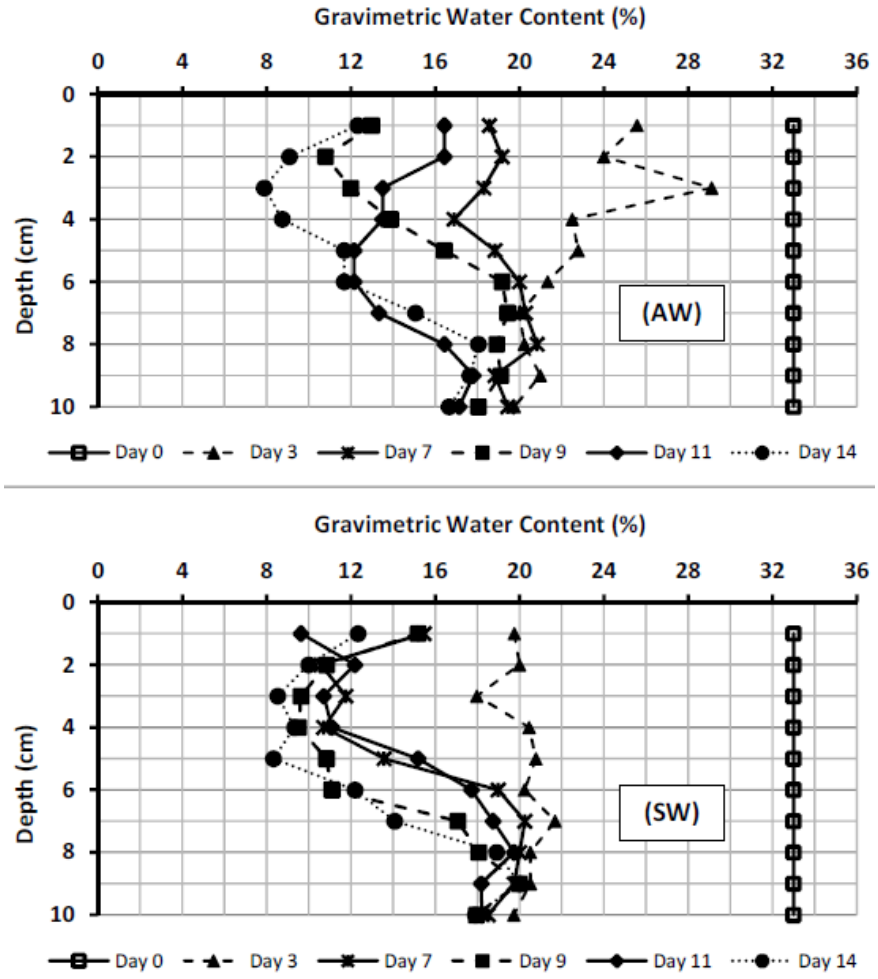

Figure E.19 Gravimetric water contents over time at different depths of salinized soil columns of drying under ambient (AW) and simulated wind (SW) boundary conditions.

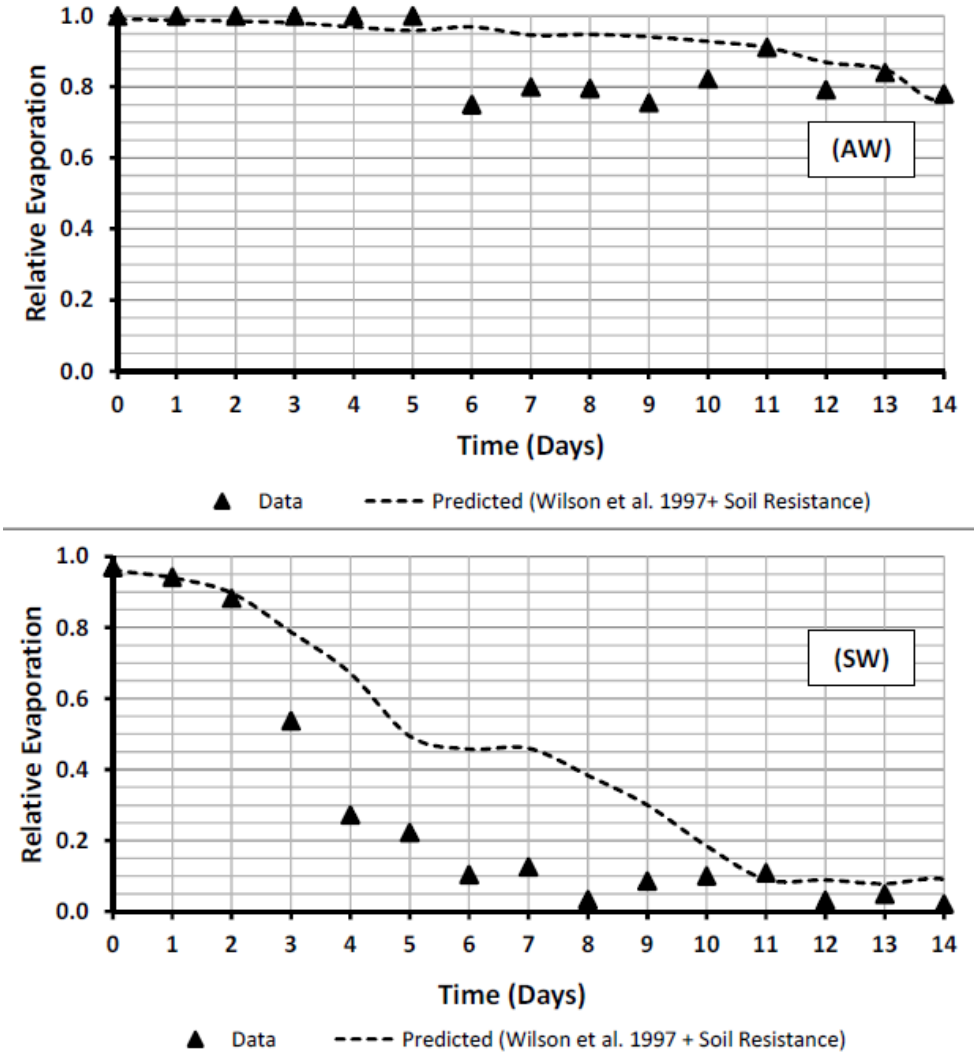

Figure E.20 Relative Evaporation measured from desiccating tailings columns and predicted results from total suction in the top 1 cm by Dunmola (2012) under ambient (AW) and simulated wind (SW) boundary conditions.

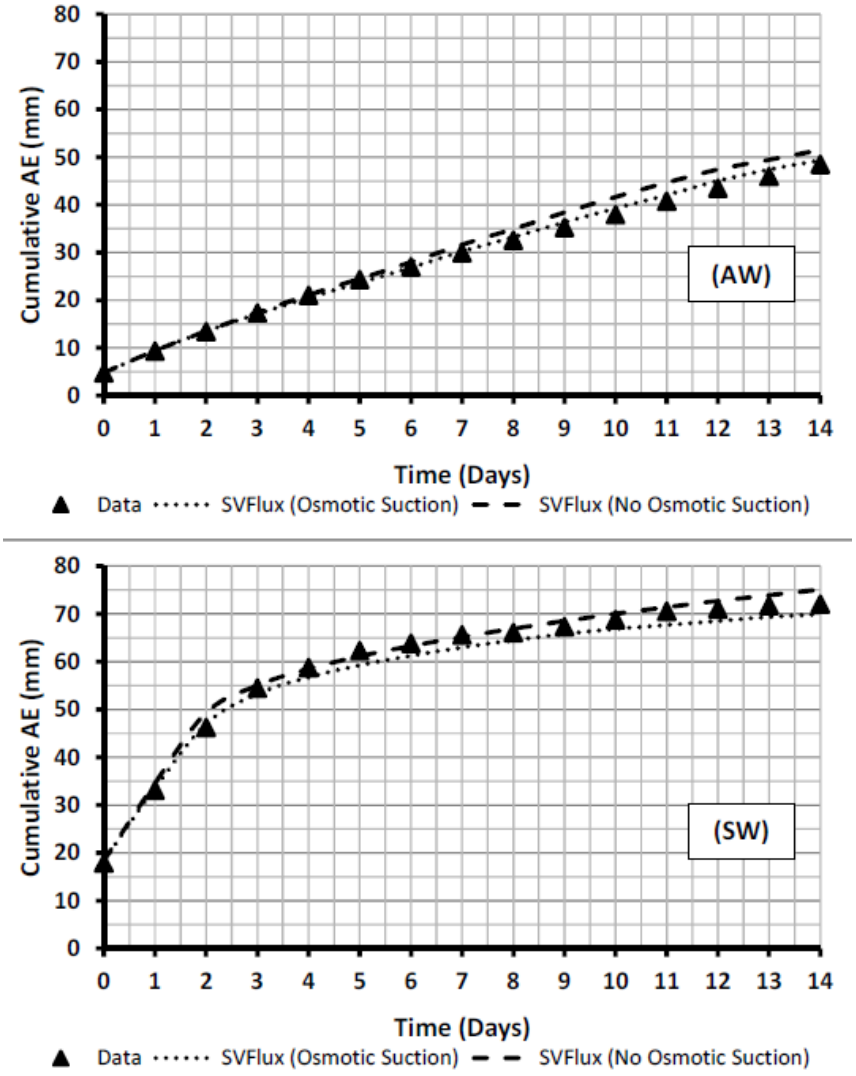

Figure E.21 Cumulative actual evaporation measured and predicted for tailings columns desiccating under ambient (AW) and simulated wind (SW) boundary conditions. Predictions with and without accouting for temporal evolution of osmotic suction are shown in the dot lines.

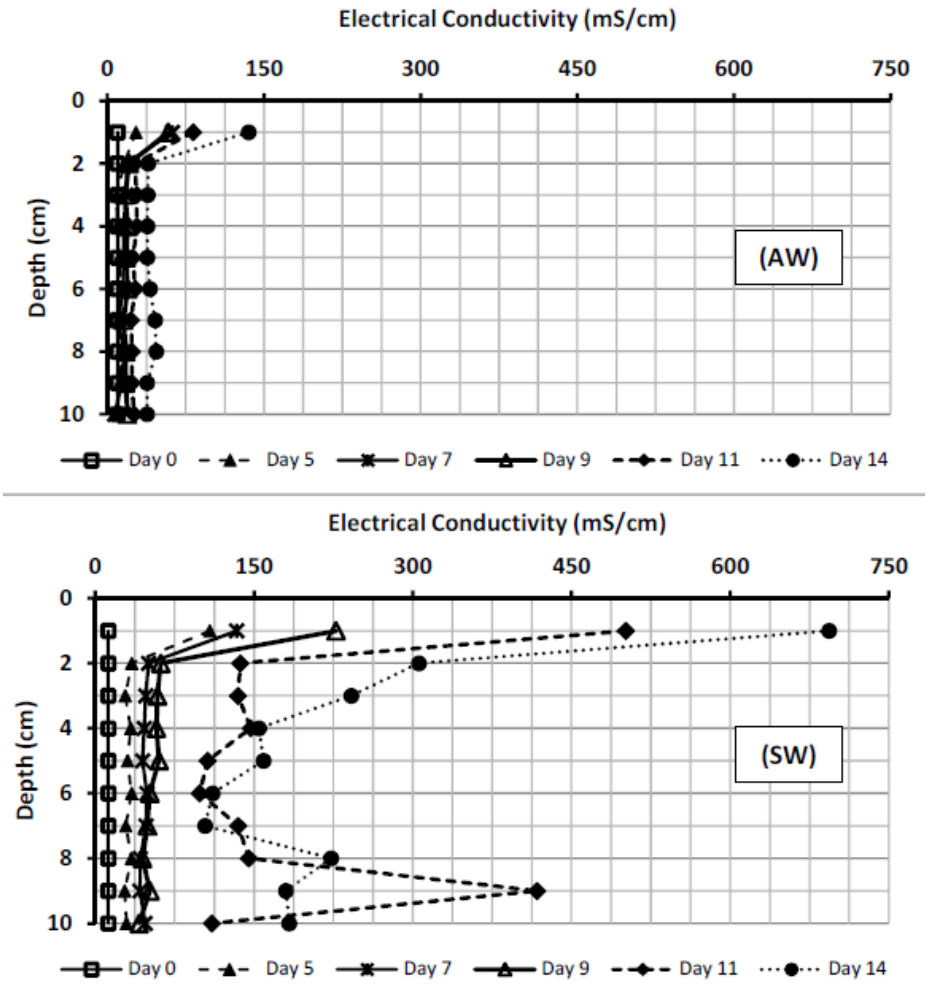

Figure E.22 Electrical conductivity (EC) of pore extracts over time at different depths of tailings columns drying under ambient (AW) and simulated wind (SW) boundary conditions.

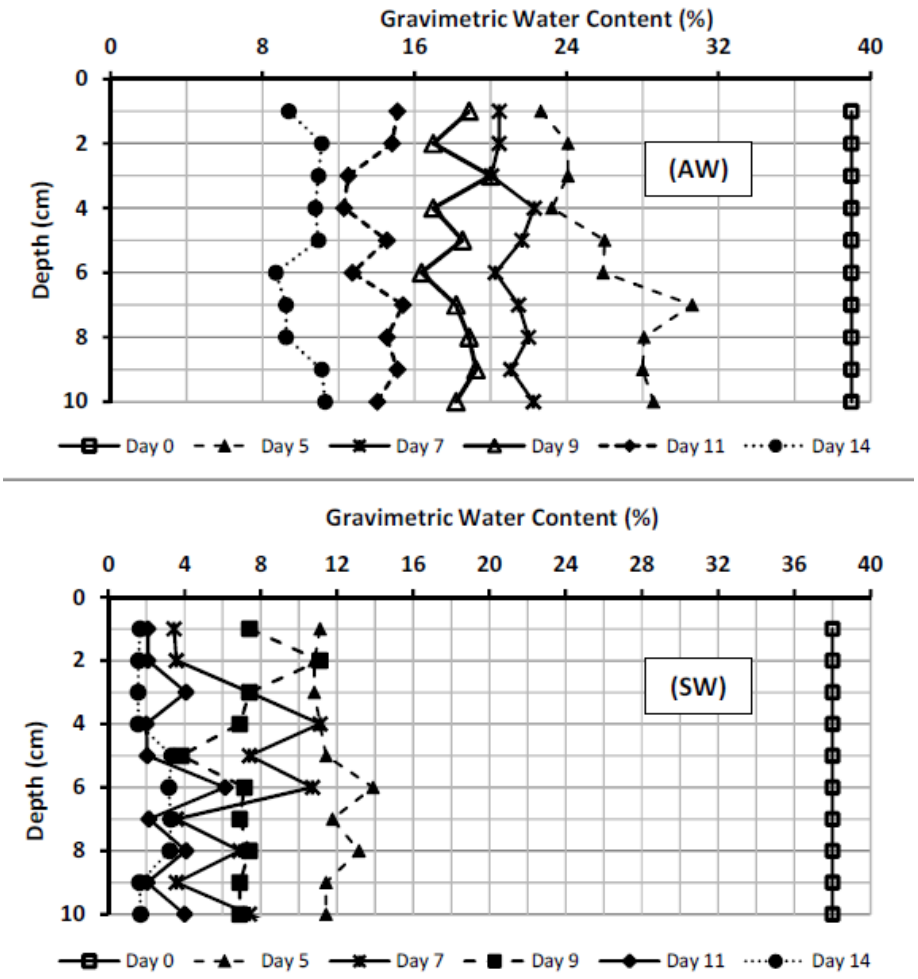

Figure E.23 Gravimetric water contents over time at different depths of tailings columns drying under ambient (AW) and simulated wind (SW) boundary conditions.

APPENDIX F

CALCULATIONS

Table F.1 Summary of results of evaporation for Ottawa sand mixed with 50 g/l NaCl in Set 1.

Time (hour)	PE (mm/ day)	AE (mm/ day)	R.H. Air	Air Temp (^{o} C)	Soil moisture content at surface (%)	Salt content at surface (ppt)	r_{av} (s/m)	r_s (s/m)	Suction		Relative Humidity		Actual Evaporation (mm/day)		
									From SWCC (kPa)	Osmotic suction (kPa)	No osmotic suction	With Osmotic suction	AE–Cal. No Osm	AE–Cal. Osm	AE–Cal. Osm. Res
20	2.52	2.41	0.2	19.4	27.38	50	457.1	0.0	9	4,235	1.00	0.97	2.52	2.42	2.42
40	2.98	2.41	0.2	19.4	25.06	55	386.7	0.0	9	4,629	1.00	0.97	2.98	2.85	2.85
60	2.98	2.41	0.2	19.4	22.73	60	386.7	0.0	10	5,103	1.00	0.96	2.98	2.84	2.84
80	2.98	2.29	0.2	19.4	20.51	67	386.7	0.0	10	5,655	1.00	0.96	2.98	2.83	2.83
100	2.86	2.52	0.2	19.1	18.07	76	394.8	0.0	10	6,418	1.00	0.95	2.86	2.70	2.70
120	2.98	2.18	0.2	19.6	15.96	86	391.6	0.0	10	7,264	1.00	0.95	2.98	2.78	2.78
140	2.64	2.18	0.21	19.1	13.86	99	423.7	6.2	10	8,369	1.00	0.94	2.64	2.44	2.40
160	2.98	2.18	0.2	19.6	11.75	117	391.6	17.6	10	9,869	1.00	0.93	2.98	2.72	2.60
180	2.86	2.06	0.2	19.6	9.76	140	407.2	30.4	11	11,887	1.00	0.92	2.86	2.56	2.39
200	2.52	1.83	0.22	18.9	7.98	172	432.0	44.3	10	14,529	1.00	0.90	2.52	2.19	1.99
220	2.75	1.83	0.2	19.4	6.21	221	419.0	61.6	11	18,680	1.00	0.87	2.75	2.31	2.01
240	2.86	1.83	0.2	19.4	4.43	309	402.2	84.8	13	26,152	1.00	0.82	2.86	2.23	1.85
260	2.98	1.72	0.2	19.4	2.77	494	386.7	117.3	20	41,843	1.00	0.73	2.98	1.99	1.53
280	2.64	1.38	0.2	19.1	1.44	950	429.1	162.4	59	80,468	1.00	0.55	2.63	1.16	0.84
300	2.75	0.92	0.2	19.6	0.55	2,470	424.2	228.3	715	209,217	0.99	0.21	2.73	0.04	0.03
320	2.98	0.23	0.2	19.6	0.33	4,117	391.6	263.6	3,525	348,695	0.97	0.07	2.88	-0.47	-0.28
340	3.09	0.11	0.2	19.6	0.22	6,175	377.1	291.5	12,081	523,043	0.91	0.02	2.76	-0.70	-0.39
360	2.75	0.00	0.2	19.6	0.22	6,175	424.2	291.5	12,081	523,043	0.91	0.02	2.46	-0.62	-0.37

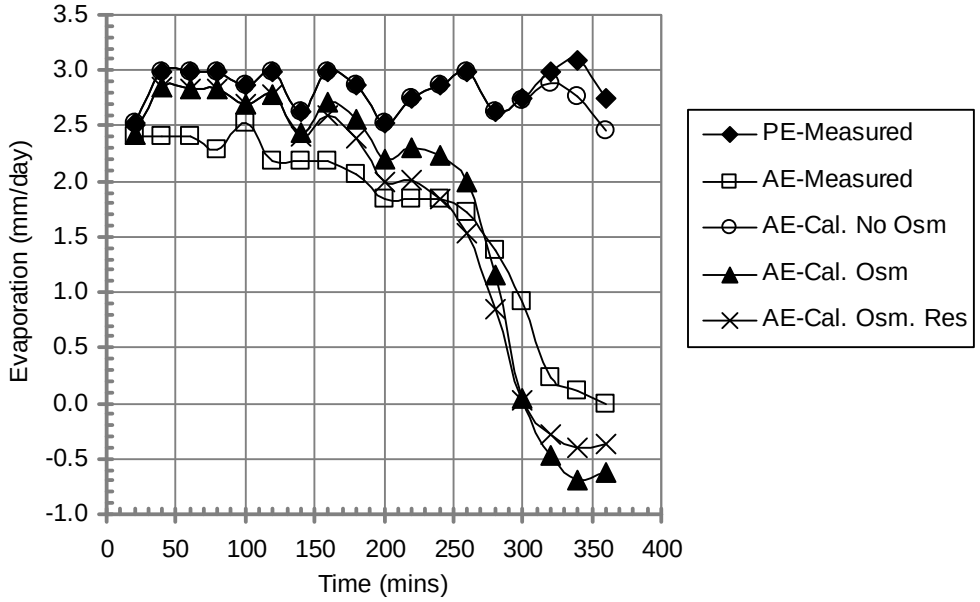

Figure F.1 Calculated and measured rates of actual evaporation corresponding to three procedures for Ottawa sand mixed with 50 g/l NaCl in Set 1. Symbols are described in Table 6.17.

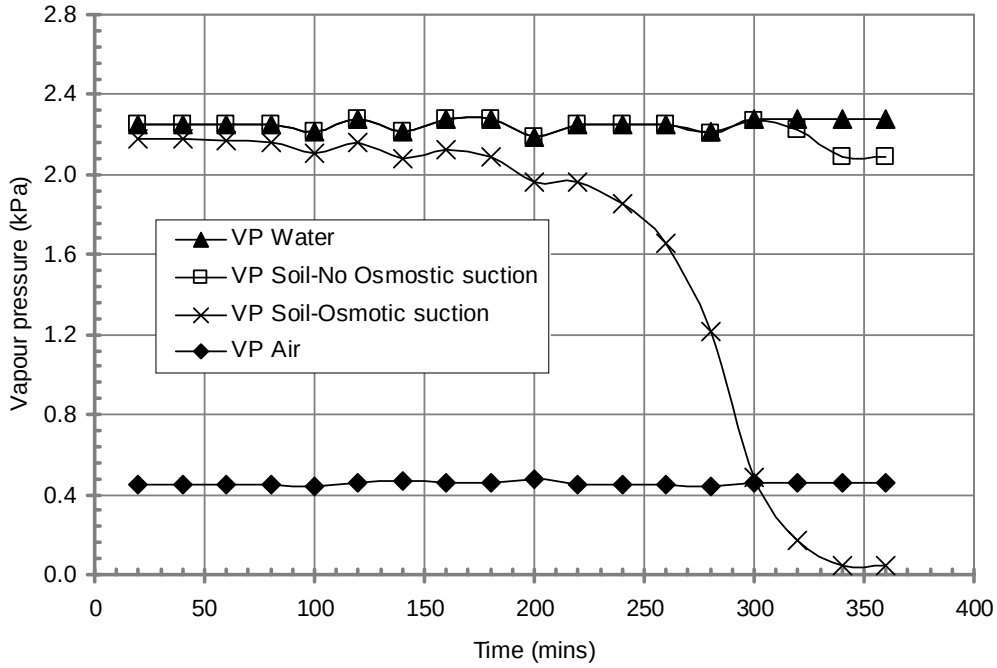

Figure F.2 Vapor pressure versus time for Ottawa sand mixed with 50 g/l NaCl in Set 1.

Table F.2 Summary of results of evaporation for Ottawa sand mixed with 200 g/l NaCl in Set 1.

Time (hour)	PE (mm/ day)	AE (mm/ day)	R.H. Air	Air Temp (^{o} C)	Soil moisture content at surface (%)	Salt content at surface (ppt)	r_{av} (s/m)	r_s (s/m)	Suction		Relative Humidity		Actual Evaporation (mm/day)		
									From SWCC (kPa)	Osmotic suction (kPa)	No osmotic suction	With Osmotic suction	AE–Cal. No Osm	AE–Cal. Osm	AE–Cal. Osm. Res
21.5	2.89	2.21	0.2	19.5	26.42	200	401.1	54.9	9	16,941	1.00	0.88	2.89	2.46	2.17
43.3	2.54	2.02	0.2	19.5	24.31	217	456.7	60.6	10	18,410	1.00	0.87	2.54	2.13	1.88
62.4	2.38	1.55	0.21	19.4	22.86	231	478.7	64.8	10	19,572	1.00	0.87	2.38	1.97	1.74
82.1	2.34	1.64	0.21	19.4	21.31	248	485.7	69.7	10	20,999	1.00	0.86	2.34	1.92	1.68
108.0	2.30	1.50	0.21	19.4	19.42	272	494.9	76.1	10	23,039	1.00	0.84	2.30	1.84	1.60
130.8	2.42	1.51	0.21	19.6	17.76	298	475.5	82.3	10	25,199	1.00	0.83	2.42	1.90	1.62
152.0	2.36	1.52	0.21	19.4	16.20	326	482.2	88.6	10	27,616	1.00	0.82	2.36	1.81	1.53
174.8	2.51	1.60	0.2	19.6	14.43	366	465.6	96.6	10	31,014	1.00	0.79	2.51	1.86	1.54
200.0	2.65	1.82	0.2	19.8	12.21	433	445.5	108.1	10	36,653	1.00	0.76	2.65	1.86	1.50
219.9	2.53	1.73	0.2	19.6	10.54	501	461.6	118.2	11	42,441	1.00	0.73	2.53	1.68	1.33
241.3	2.57	1.72	0.2	19.6	8.77	603	454.3	131.0	11	51,036	1.00	0.69	2.57	1.56	1.21
268.9	2.66	1.65	0.2	19.4	6.55	807	432.8	151.1	11	68,337	1.00	0.60	2.66	1.34	0.99
295.4	2.59	1.74	0.2	19.6	4.33	1,221	449.9	179.7	13	103,381	1.00	0.47	2.59	0.86	0.61
316.1	2.78	1.54	0.2	19.6	2.77	1,904	420.1	210.4	20	161,275	1.00	0.30	2.78	0.36	0.24
338.8	2.62	0.51	0.2	19.6	1.66	3,173	445.7	245.6	44	268,792	1.00	0.14	2.62	-0.21	-0.13
359.6	2.65	0.22	0.2	19.6	1.33	3,967	440.8	261.0	70	335,990	1.00	0.08	2.64	-0.39	-0.24
379.7	2.74	0.00	0.2	19.6	1.33	3,967	426.0	261.0	70	335,990	1.00	0.08	2.74	-0.40	-0.25
401.7	2.61	0.00	0.2	19.6	1.33	3,967	446.6	261.0	70	335,990	1.00	0.08	2.61	-0.38	-0.24

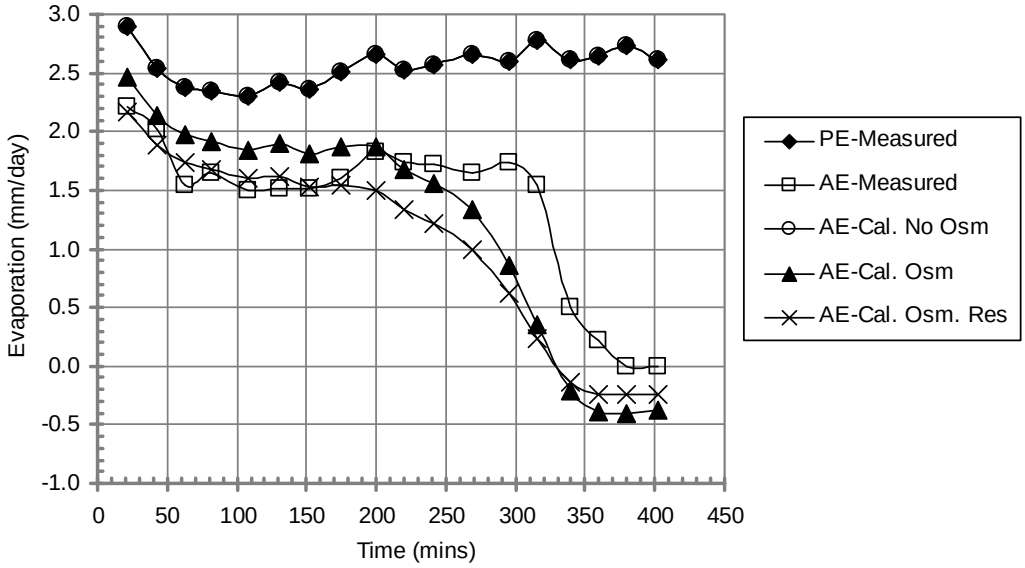

Figure F.3 Calculated and measured rates of actual evaporation corresponding to three procedures for Ottawa sand mixed with 200 g/l NaCl in Set 1. Symbols are described in Table 6.17.

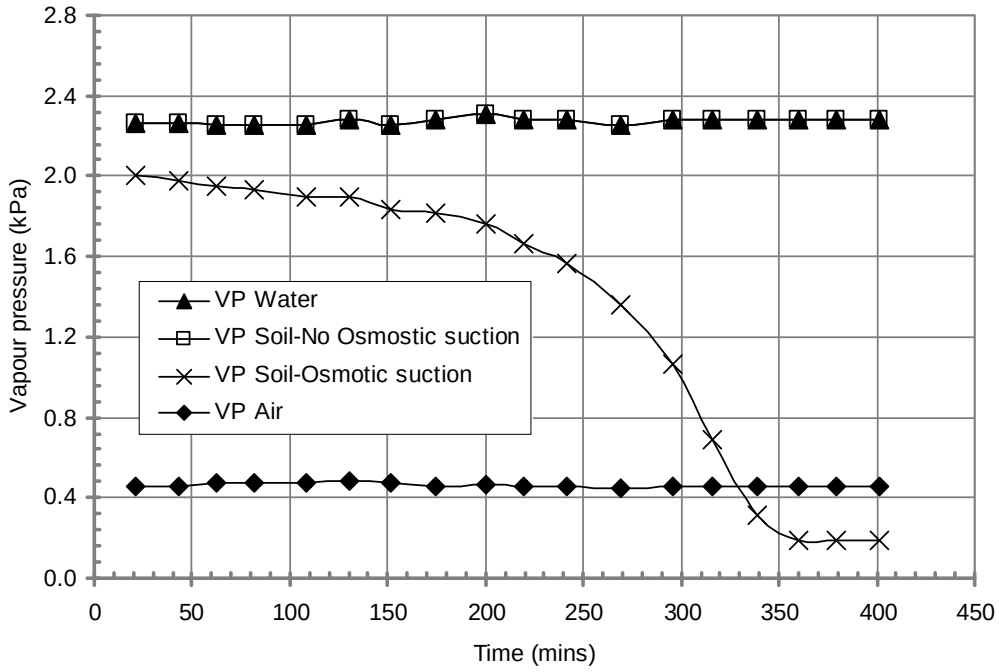

Figure F.4 Vapor pressure versus time for Ottawa sand mixed with 200 g/l NaCl in Set 1.

Table F.3 Summary of results of evaporation for Ottawa sand mixed with 250 g/l NaCl in Set 1.

Time (hour)	PE (mm/ day)	AE (mm/ day)	R.H. Air	Air Temp (^{o} C)	Soil moisture content at surface (%)	Salt content at surface (ppt)	r_{av} (s/m)	r_s (s/m)	Suction		Relative Humidity		Actual Evaporation (mm/day)		
									From SWCC (kPa)	Osmotic suction (kPa)	No osmotic suction	With Osmotic suction	AE–Cal. No Osm	AE–Cal. Osm	AE–Cal. Osm. Res
21.5	2.89	2.20	0.2	19.5	26.32	250	401.1	70.3	9	21,176	1.00	0.85	2.89	2.37	2.01
43.3	2.54	1.92	0.2	19.5	24.30	271	456.7	75.8	10	22,932	1.00	0.84	2.54	2.04	1.75
62.4	2.38	2.03	0.21	19.4	22.40	294	478.7	81.4	10	24,882	1.00	0.83	2.38	1.87	1.60
82.1	2.34	1.64	0.21	19.4	20.83	316	485.7	86.4	10	26,754	1.00	0.82	2.34	1.81	1.54
108.0	2.30	1.68	0.21	19.4	18.70	352	494.9	93.8	10	29,798	1.00	0.80	2.30	1.72	1.45
130.8	2.42	1.82	0.21	19.6	16.69	394	475.5	101.7	10	33,398	1.00	0.78	2.42	1.75	1.44
152.0	2.36	1.73	0.21	19.4	14.89	442	482.2	109.6	10	37,416	1.00	0.76	2.36	1.64	1.33
174.8	2.51	1.80	0.2	19.6	12.88	511	465.6	119.6	10	43,272	1.00	0.73	2.51	1.65	1.31
200.0	2.65	1.73	0.2	19.8	10.75	612	445.5	132.0	11	51,837	1.00	0.68	2.65	1.60	1.23
219.9	2.53	1.73	0.2	19.6	9.07	725	461.6	143.8	11	61,436	1.00	0.63	2.53	1.37	1.05
241.3	2.57	1.72	0.2	19.6	7.28	904	454.3	159.0	10	76,559	1.00	0.57	2.57	1.18	0.87
268.9	2.66	1.65	0.2	19.4	5.04	1,306	432.8	184.3	12	110,585	1.00	0.44	2.66	0.80	0.56
295.4	2.59	0.87	0.2	19.6	3.14	2,098	449.9	217.1	17	177,726	1.00	0.27	2.59	0.22	0.15
316.1	2.78	0.55	0.2	19.6	2.35	2,798	420.1	236.9	25	236,967	1.00	0.17	2.78	-0.09	-0.06
338.8	2.62	0.31	0.2	19.6	2.13	3,092	445.7	243.8	29	261,911	1.00	0.14	2.62	-0.18	-0.12
359.6	2.65	0.11	0.2	19.6	2.13	3,092	440.8	243.8	29	261,911	1.00	0.14	2.65	-0.18	-0.12
379.7	2.74	0.00	0.2	19.6	2.13	3,092	426.0	243.8	29	261,911	1.00	0.14	2.74	-0.19	-0.12
401.7	2.61	0.00	0.2	19.6	2.13	3,092	446.6	243.8	29	261,911	1.00	0.14	2.61	-0.18	-0.12

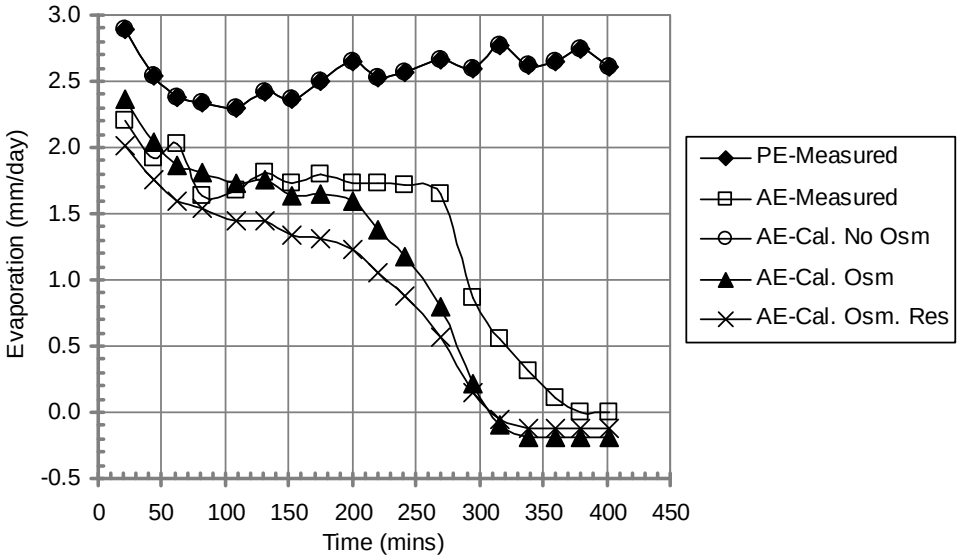

Figure F.5 Calculated and measured rates of actual evaporation corresponding to three procedures for Ottawa sand mixed with 250 g/l NaCl in Set 1. Symbols are described in Table 6.17.

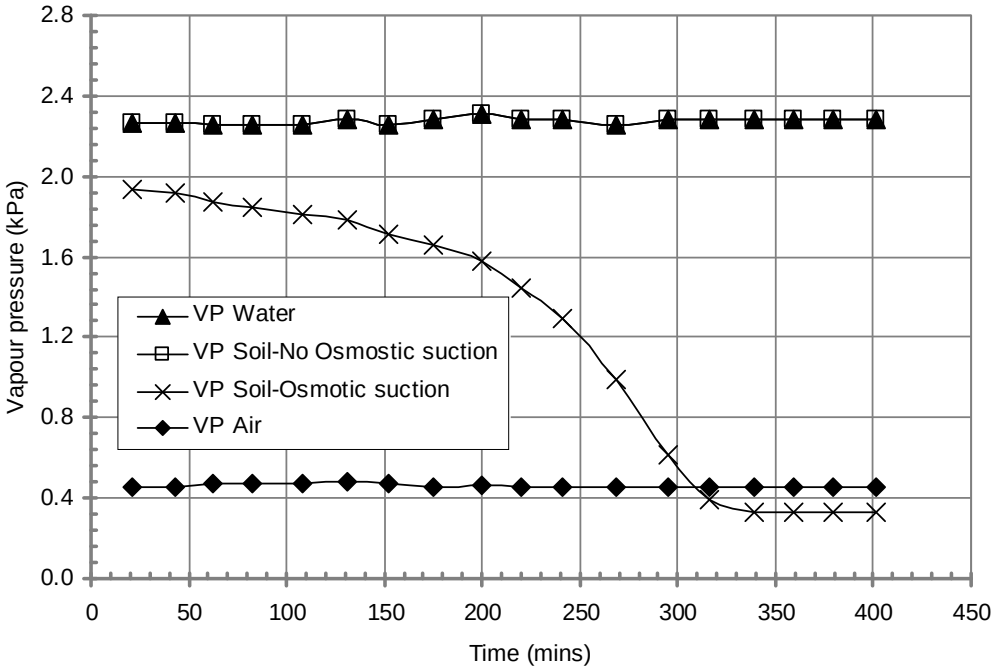

Figure F.6 Vapor pressure versus time for Ottawa sand mixed with 250 g/l NaCl in Set 1.

Table F.4 Summary of results of evaporation for Devon silt mixed with 50 g/l NaCl in Set 1.

Time (hour)	PE (mm/ day)	AE (mm/ day)	R.H. Air	Air Temp (^{o} C)	Soil moisture content at surface (%)	Salt content at surface (ppt)	r_{av} (s/m)	r_s (s/m)	Suction		Relative Humidity		Actual Evaporation (mm/day)		
									From SWCC (kPa)	Osmotic suction (kPa)	No osmotic suction	With Osmotic suction	AE–Cal. No Osm	AE–Cal. Osm	AE–Cal. Osm. Res
20	2.52	2.18	0.2	19.4	69.60	50	457.1	0.0	0	4,235	1.00	0.97	2.52	2.42	2.42
40	2.98	2.29	0.2	19.4	60.79	57	386.7	0.0	0	4,849	1.00	0.96	2.97	2.84	2.84
60	2.98	2.41	0.2	19.4	51.54	68	386.7	0.0	0	5,719	1.00	0.96	2.97	2.82	2.82
80	2.98	2.29	0.2	19.4	42.73	81	386.7	0.0	55	6,899	1.00	0.95	2.98	2.79	2.79
100	2.86	2.29	0.2	19.1	33.92	103	394.8	8.8	309	8,690	1.00	0.94	2.86	2.63	2.58
120	2.98	2.29	0.2	19.6	25.11	139	391.6	29.6	965	11,740	0.99	0.91	2.95	2.65	2.46
140	2.64	1.83	0.21	19.1	18.06	193	423.7	52.3	3,198	16,321	0.98	0.87	2.56	2.19	1.95
160	2.98	1.83	0.2	19.6	11.01	316	391.6	86.4	8,073	26,766	0.94	0.77	2.76	2.13	1.75
180	2.86	1.15	0.2	19.6	6.61	527	407.2	121.7	20,638	44,610	0.86	0.62	2.36	1.49	1.15
200	2.52	0.69	0.22	18.9	3.96	878	432.0	156.9	48,918	74,351	0.70	0.40	1.54	0.59	0.43
220	2.75	0.34	0.2	19.4	2.64	1,317	419.0	184.9	91,361	111,526	0.51	0.22	1.06	0.08	0.05
240	2.86	0.11	0.2	19.4	2.20	1,580	402.2	197.5	118,351	133,831	0.42	0.15	0.78	-0.16	-0.11
260	2.98	0.00	0.2	19.4	2.20	1,580	386.7	197.5	118,351	133,831	0.42	0.15	0.81	-0.17	-0.11
280	2.64	0.00	0.2	19.1	2.20	1,580	429.1	197.5	118,351	133,831	0.42	0.15	0.71	-0.15	-0.10
300	2.75	0.00	0.2	19.6	2.20	1,580	424.2	197.5	118,351	133,831	0.42	0.15	0.75	-0.16	-0.11
320	2.98	0.00	0.2	19.6	2.20	1,580	391.6	197.5	118,351	133,831	0.42	0.15	0.81	-0.17	-0.11
340	3.09	0.00	0.2	19.6	2.20	1,580	377.1	197.5	118,351	133,831	0.42	0.15	0.84	-0.17	-0.11
360	2.75	0.00	0.2	19.6	2.20	1,580	424.2	197.5	118,351	133,831	0.42	0.15	0.75	-0.16	-0.11

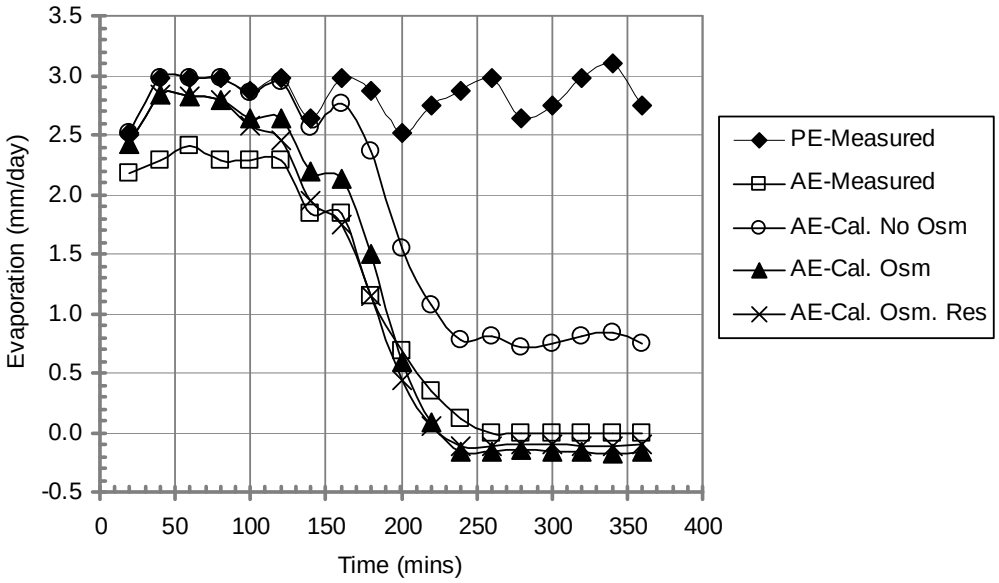

Figure F.7 Calculated and measured rates of actual evaporation corresponding to three procedures for Devon silt mixed with 50 g/l NaCl in Set 1. Symbols are described in Table 6.17.

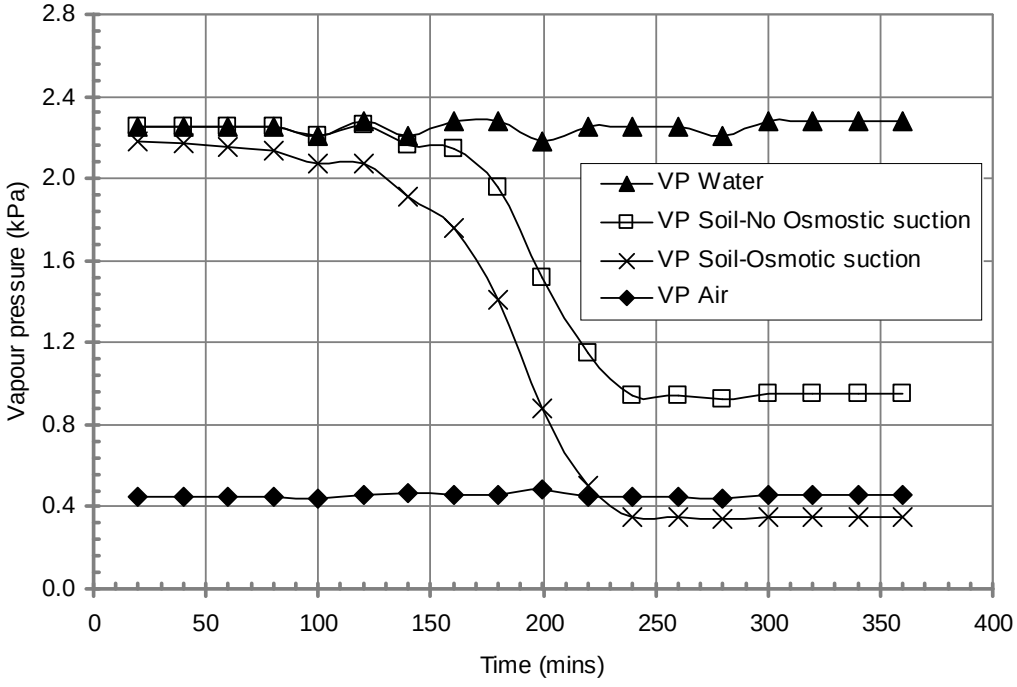

Figure F.8 Vapor pressure versus time for Devon silt mixed with 50 g/l NaCl in Set 1.

Table F.5 Summary of results of evaporation for Devon silt mixed with 100 g/l NaCl in Set 1.

Time (hour)	PE (mm/ day)	AE (mm/ day)	R.H. Air	Air Temp (^{o} C)	Soil moisture content at surface (%)	Salt content at surface (ppt)	r_{av} (s/m)	r_s (s/m)	Suction		Relative Humidity		Actual Evaporation (mm/day)		
									From SWCC (kPa)	Osmotic suction (kPa)	No osmotic suction	With Osmotic suction	AE–Cal. No Osm	AE–Cal. Osm	AE–Cal. Osm. Res
21.5	2.89	2.31	0.2	19.5	59.30	100	401.1	7.1	0	8,470	1.00	0.94	2.89	2.67	2.62
43.3	2.54	2.02	0.2	19.5	54.52	109	456.7	12.8	0	9,212	1.00	0.93	2.53	2.32	2.26
62.4	2.38	1.91	0.21	19.4	50.50	117	478.7	18.1	0	9,945	1.00	0.93	2.37	2.16	2.08
82.1	2.34	1.75	0.21	19.4	46.73	127	485.7	23.5	0	10,747	1.00	0.92	2.34	2.11	2.01
108.0	2.30	1.77	0.21	19.4	41.71	142	494.9	31.3	93	12,042	1.00	0.91	2.30	2.05	1.93
130.8	2.42	1.81	0.21	19.6	37.19	159	475.5	39.2	209	13,507	1.00	0.90	2.42	2.13	1.97
152.0	2.36	1.73	0.21	19.4	33.17	179	482.2	47.1	338	15,144	1.00	0.89	2.35	2.04	1.86
174.8	2.51	1.70	0.2	19.6	28.89	205	465.6	56.7	572	17,383	1.00	0.88	2.49	2.12	1.89
200.0	2.65	1.82	0.2	19.8	23.87	248	445.5	69.8	1,163	21,042	0.99	0.85	2.62	2.15	1.86
219.9	2.53	1.50	0.2	19.6	20.60	288	461.6	80.0	1,992	24,378	0.99	0.82	2.48	1.97	1.68
241.3	2.57	1.71	0.2	19.6	16.58	358	454.3	95.0	4,326	30,288	0.97	0.77	2.47	1.84	1.52
268.9	2.66	1.57	0.2	19.4	11.81	502	432.8	118.4	7,054	42,532	0.95	0.69	2.49	1.64	1.29
295.4	2.59	1.47	0.2	19.6	7.54	787	449.9	149.4	16,327	66,633	0.89	0.54	2.22	1.11	0.83
316.1	2.78	1.10	0.2	19.6	5.03	1,180	420.1	177.4	33,085	99,950	0.78	0.37	2.02	0.60	0.42
338.8	2.62	0.71	0.2	19.6	3.27	1,815	445.7	207.1	66,446	153,769	0.61	0.20	1.35	-0.01	-0.01
359.6	2.65	0.22	0.2	19.6	2.76	2,145	440.8	218.6	85,559	181,727	0.53	0.14	1.10	-0.20	-0.14
379.7	2.74	0.11	0.2	19.6	2.51	2,360	426.0	225.2	98,325	199,900	0.48	0.11	0.97	-0.31	-0.20
401.7	2.61	0.00	0.2	19.6	2.51	2,360	446.6	225.2	98,325	199,900	0.48	0.11	0.93	-0.29	-0.19

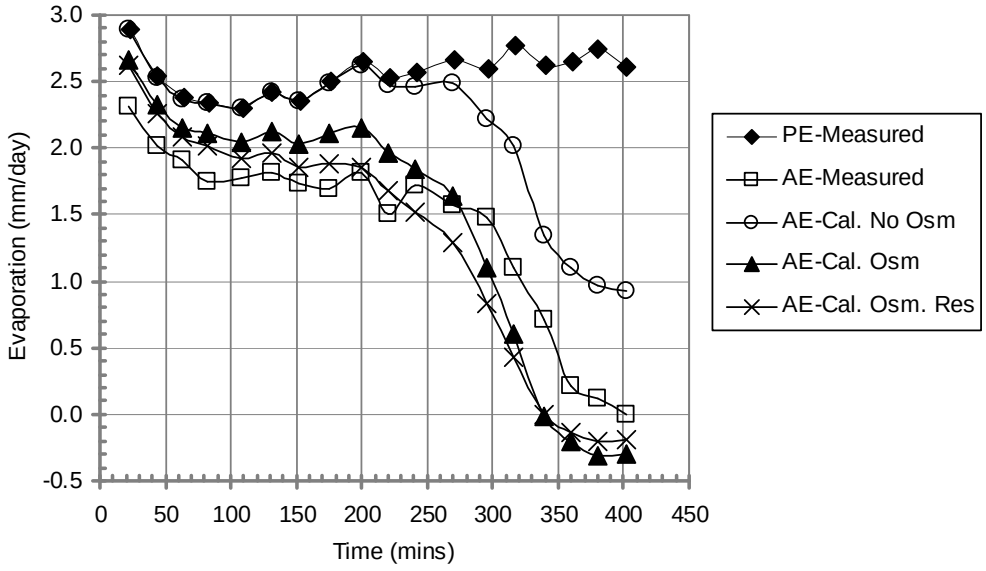

Figure F.9 Calculated and measured rates of actual evaporation corresponding to three procedures for Devon silt mixed with 100 g/l NaCl in Set 1. Symbols are described in Table 6.17.

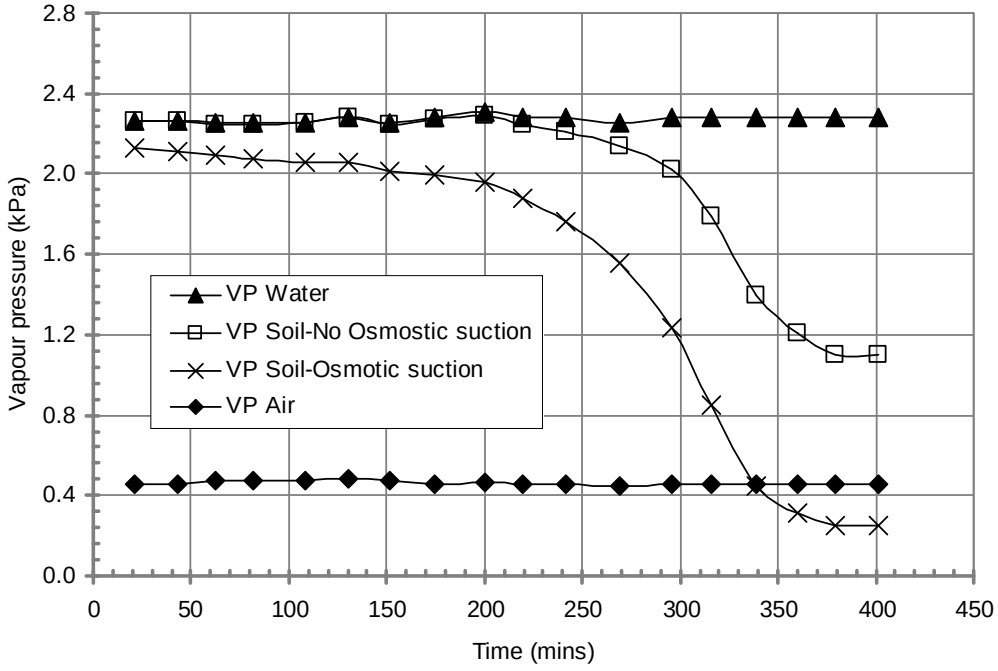

Figure F.10 Vapor pressure versus time for Devon silt mixed with 100 g/l NaCl in Set 1.

Table F.6 Summary of results of evaporation for Devon silt mixed with 200 g/l NaCl in Set 1.

Time (hour)	PE (mm/ day)	AE (mm/ day)	R.H. Air	Air Temp (^{o} C)	Soil moisture content at surface (%)	Salt content at surface (ppt)	r_{av} (s/m)	r_s (s/m)	Suction		Relative Humidity		Actual Evaporation (mm/day)		
									From SWCC (kPa)	Osmotic suction (kPa)	No osmotic suction	With Osmotic suction	AE–Cal. No Osm	AE–Cal. Osm	AE–Cal. Osm. Res
21.5	2.89	1.98	0.2	19.5	53.97	200	401.1	0.0	0	16,941	1.00	0.88	2.88	2.46	2.46
43.3	2.54	1.71	0.2	19.5	50.34	214	456.7	59.7	0	18,162	1.00	0.87	2.53	2.13	1.89
62.4	2.38	1.79	0.21	19.4	46.94	230	478.7	64.5	0	19,478	1.00	0.86	2.37	1.97	1.73
82.1	2.34	1.52	0.21	19.4	43.99	245	485.7	69.0	0	20,783	1.00	0.86	2.34	1.92	1.68
108.0	2.30	1.50	0.21	19.4	40.14	269	494.9	75.3	136	22,779	1.00	0.84	2.30	1.85	1.60
130.8	2.42	1.62	0.21	19.6	36.51	296	475.5	81.8	227	25,043	1.00	0.83	2.42	1.90	1.62
152.0	2.36	1.51	0.21	19.4	33.33	324	482.2	88.1	331	27,428	1.00	0.81	2.35	1.81	1.53
174.8	2.51	1.51	0.2	19.6	29.93	361	465.6	95.6	501	30,545	1.00	0.79	2.49	1.86	1.55
200.0	2.65	1.63	0.2	19.8	25.85	418	445.5	105.7	867	35,367	0.99	0.77	2.63	1.87	1.51
219.9	2.53	1.50	0.2	19.6	22.90	471	461.6	114.0	1,354	39,920	0.99	0.74	2.50	1.70	1.36
241.3	2.57	1.39	0.2	19.6	19.95	541	454.3	123.5	2,237	45,817	0.98	0.70	2.52	1.61	1.26
268.9	2.66	1.08	0.2	19.4	17.01	635	432.8	134.6	3,959	53,758	0.97	0.65	2.57	1.51	1.15
295.4	2.59	0.61	0.2	19.6	15.42	700	449.9	141.3	5,573	59,292	0.96	0.62	2.46	1.36	1.03
316.1	2.78	0.55	0.2	19.6	14.29	756	420.1	146.6	4,834	63,998	0.96	0.60	2.65	1.39	1.03
338.8	2.62	0.51	0.2	19.6	13.15	821	445.7	152.3	5,707	69,515	0.96	0.57	2.48	1.22	0.91
359.6	2.65	0.44	0.2	19.6	12.24	881	440.8	157.2	6,572	74,664	0.95	0.55	2.49	1.15	0.85
379.7	2.74	0.45	0.2	19.6	11.34	952	426.0	162.5	7,634	80,637	0.95	0.52	2.55	1.10	0.79
401.7	2.61	0.32	0.2	19.6	10.66	1,013	446.6	166.8	8,597	85,785	0.94	0.50	2.41	0.97	0.71

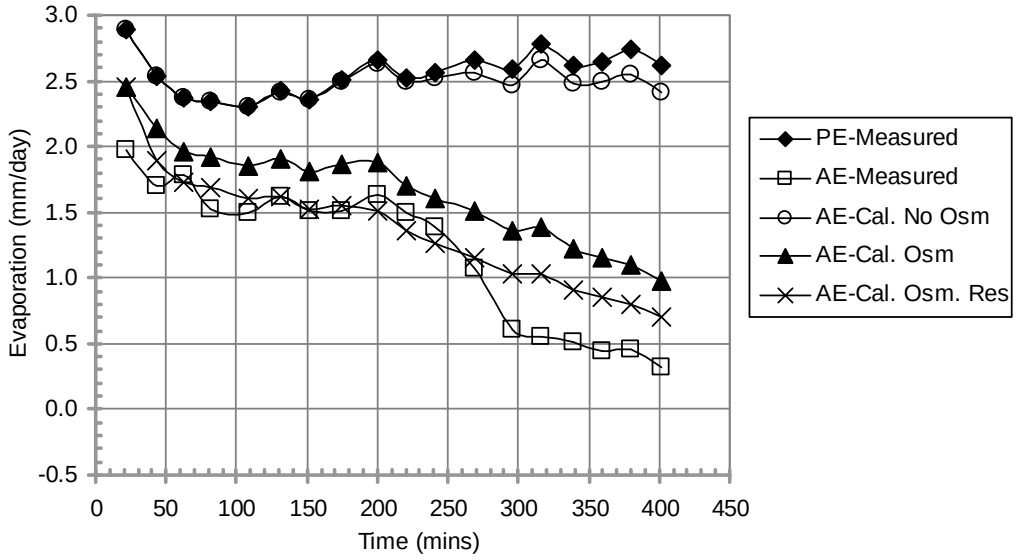

Figure F.11 Calculated and measured rates of actual evaporation corresponding to three procedures for Devon silt mixed with 200 g/l NaCl in Set 1. Symbols are described in Table 6.17.

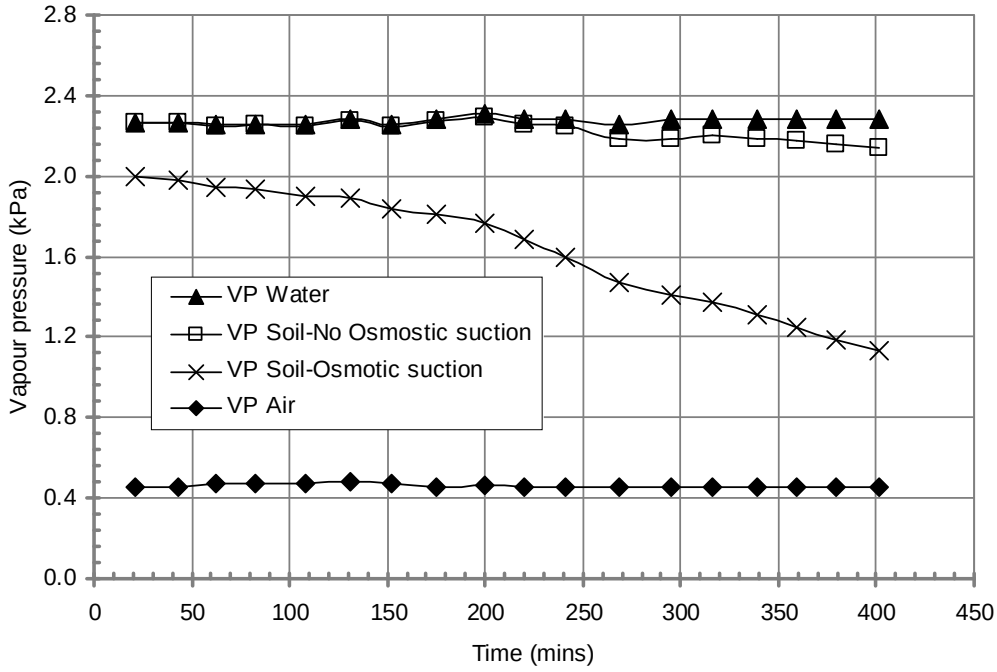

Figure F.12 Vapor pressure versus time for Devon silt mixed with 200 g/l NaCl in Set 1.

Table F.7 Summary of results for thin soil layer drying test of Non-saline Ottawa sand in Set 2.

Time (hours)	PE (mm/day)	AE (mm/day)	R.H. Air	Air Temp (^{o} C)	Soil moisture content at surface (%)	Soil moisture availability factor .Eq. (3.82)	Vapour pressure. Eq. (3.83) (kPa)	R.H., Eq. (3.84)	Soil surface resistance, Eq. (3.86) (s/m)	AE– Calculated, (mm/day)
20	2.64	2.86	0.24	20.3	34.47	1.0000	2.38	1.00	0.0	2.64
40	2.41	2.41	0.23	20.1	31.31	1.0000	2.35	1.00	0.0	2.41
60	2.29	2.18	0.23	20.1	28.66	1.0000	2.35	1.00	0.0	2.29
80	2.41	2.18	0.23	20.1	26.26	1.0000	2.35	1.00	0.0	2.41
100	2.52	2.41	0.23	20.1	23.86	1.0000	2.35	1.00	0.0	2.52
120	2.41	2.06	0.23	20.1	21.21	1.0000	2.35	1.00	0.0	2.41
140	2.29	2.06	0.25	19.9	18.94	1.0000	2.32	1.00	0.0	2.29
160	2.29	1.95	0.25	19.9	16.67	1.0000	2.32	1.00	0.0	2.29
180	2.29	2.06	0.23	20.1	14.52	1.0000	2.35	1.00	0.0	2.29
200	2.29	2.06	0.27	19.9	12.25	1.0000	2.32	1.00	0.0	2.29
220	2.29	2.06	0.27	19.9	9.97	1.0000	2.32	1.00	0.0	2.29
240	2.29	2.06	0.27	19.9	7.70	1.0000	2.32	1.00	0.1	2.29
260	2.29	1.95	0.24	20.1	5.43	1.0000	2.35	1.00	0.5	2.29
280	2.18	1.83	0.27	19.9	3.28	1.0000	2.32	1.00	1.8	2.18
300	2.29	0.92	0.24	19.9	1.26	1.0000	2.32	1.00	5.9	2.29
320	2.29	0.11	0.24	20.1	0.25	0.6733	1.77	0.75	10.6	1.54
340	2.18	0.00	0.24	20.1	0.13	0.0830	0.71	0.30	11.4	0.18
360	2.29	0.00	0.24	20.1	0.13	0.0830	0.71	0.30	11.4	0.19
380	2.29	0.00	0.24	20.1	0.13	0.0830	0.71	0.30	11.4	0.19
400	2.18	0.00	0.24	20.3	0.13	0.0830	0.72	0.30	11.4	0.18
420	2.18	0.00	0.24	20.3	0.13	0.0830	0.72	0.30	11.4	0.18

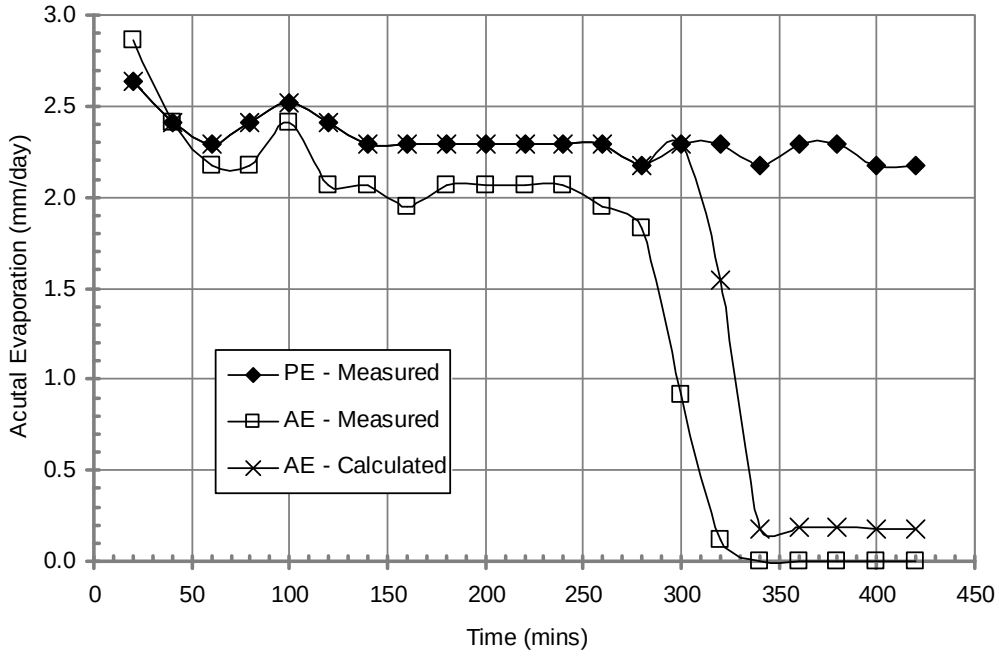

Figure F.13 Calculated, Actual and Potential evaporation rates for thin non-saline Ottawa sand in Set 2 with water content at the point of evaporation-rate reduction observed during the drying test.

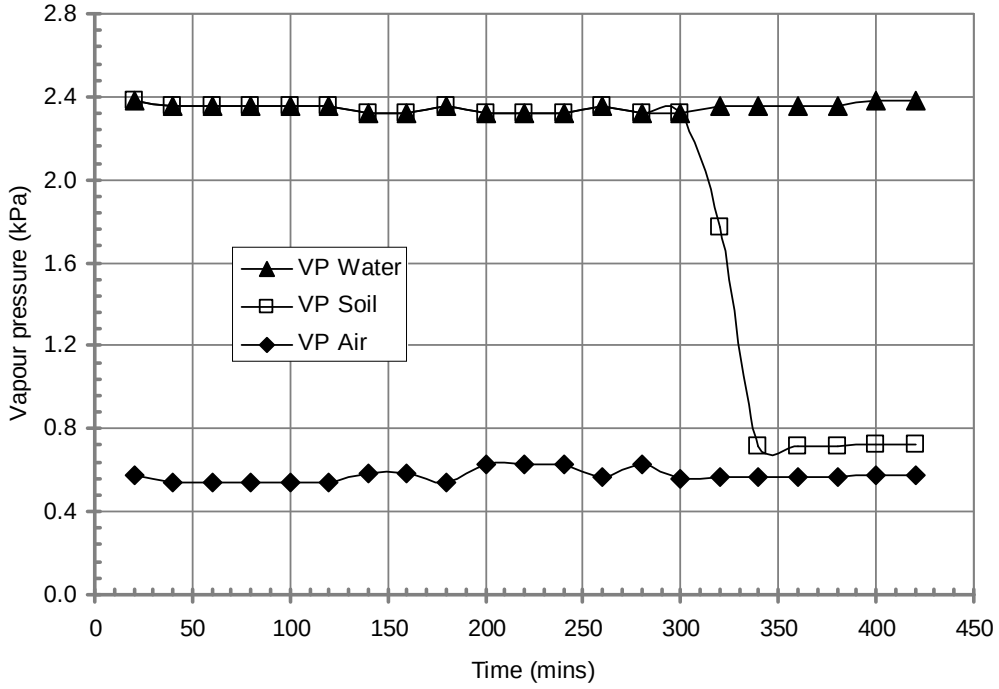

Figure F.14 Vapor pressure versus time for non-saline Ottawa sand in Set 2.

Table F.8 Summary of results of evaporation for Ottawa sand mixed with 50 g/l NaCl in Set 2.

Time (hour)	PE (mm/ day)	AE (mm/ day)	R.H. Air	Air Temp (^{o} C)	Soil moisture content at surface (%)	Salt content at surface (ppt)	r_{av} (s/m)	r_s (s/m)	Suction		Relative Humidity		Actual Evaporation (mm/day)		
									From SWCC (kPa)	Osmotic suction (kPa)	No osmotic suction	With Osmotic suction	AE–Cal. No Osm	AE–Cal. Osm	AE–Cal. Osm. Res
20	2.64	2.52	0.24	20.3	29.53	50	439.1	0.0	8	4,235	1.00	0.97	2.64	2.53	2.53
40	2.41	2.06	0.23	20.1	26.85	55	481.3	0.0	9	4,657	1.00	0.97	2.41	2.30	2.30
60	2.29	1.83	0.23	20.1	24.67	60	505.4	0.0	10	5,070	1.00	0.96	2.29	2.18	2.18
80	2.41	1.95	0.23	20.1	22.72	65	481.3	0.0	10	5,503	1.00	0.96	2.41	2.28	2.28
100	2.52	2.06	0.23	20.1	20.66	71	459.4	0.0	10	6,054	1.00	0.96	2.52	2.38	2.38
120	2.41	1.83	0.23	20.1	18.47	80	481.3	0.0	10	6,771	1.00	0.95	2.41	2.25	2.25
140	2.29	1.72	0.25	19.9	16.52	89	486.2	0.0	10	7,567	1.00	0.95	2.29	2.13	2.13
160	2.29	1.83	0.25	19.9	14.70	100	486.2	7.3	10	8,505	1.00	0.94	2.29	2.11	2.07
180	2.29	1.72	0.23	20.1	12.76	116	505.4	17.1	10	9,801	1.00	0.93	2.29	2.08	2.02
200	2.29	1.60	0.27	19.9	10.94	135	473.2	27.8	11	11,435	1.00	0.92	2.29	2.04	1.92
220	2.29	1.60	0.27	19.9	9.23	160	473.2	39.4	11	13,541	1.00	0.90	2.29	1.99	1.84
240	2.29	1.49	0.27	19.9	7.53	196	473.2	53.5	10	16,599	1.00	0.88	2.29	1.93	1.73
260	2.29	1.26	0.24	20.1	5.95	248	498.8	69.7	11	21,003	1.00	0.86	2.29	1.86	1.63
280	2.18	1.15	0.27	19.9	4.62	320	498.1	87.3	12	27,083	1.00	0.82	2.18	1.64	1.39
300	2.29	1.26	0.24	19.9	3.40	434	492.7	108.3	16	36,755	1.00	0.76	2.29	1.57	1.29
320	2.29	0.92	0.24	20.1	2.07	715	498.8	142.8	30	60,538	1.00	0.64	2.29	1.20	0.94
340	2.18	0.46	0.24	20.1	1.09	1,350	525.1	186.6	109	114,349	1.00	0.43	2.17	0.54	0.40
360	2.29	0.11	0.24	20.1	0.61	2,430	498.8	227.2	542	205,829	1.00	0.22	2.28	-0.07	-0.05
380	2.29	0	0.24	20.1	0.49	3,038	498.8	242.6	1,072	257,286	0.99	0.15	2.27	-0.28	-0.19
400	2.18	0	0.24	20.3	0.49	3,038	531.6	242.6	1,072	257,286	0.99	0.15	2.15	-0.26	-0.18
420	2.18	0	0.24	20.3	0.49	3,038	531.6	242.6	1,072	257,286	0.99	0.15	2.15	-0.26	-0.18

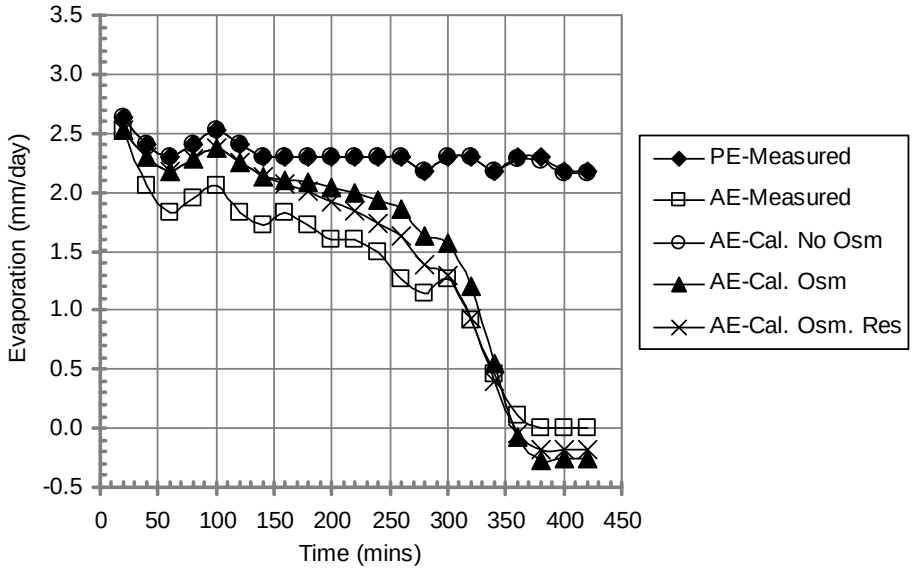

Figure F.15 Calculated and measured rates of actual evaporation corresponding to three procedures for Ottawa sand mixed with 50 g/l NaCl in Set 2. Symbols are described in Table 6.17.

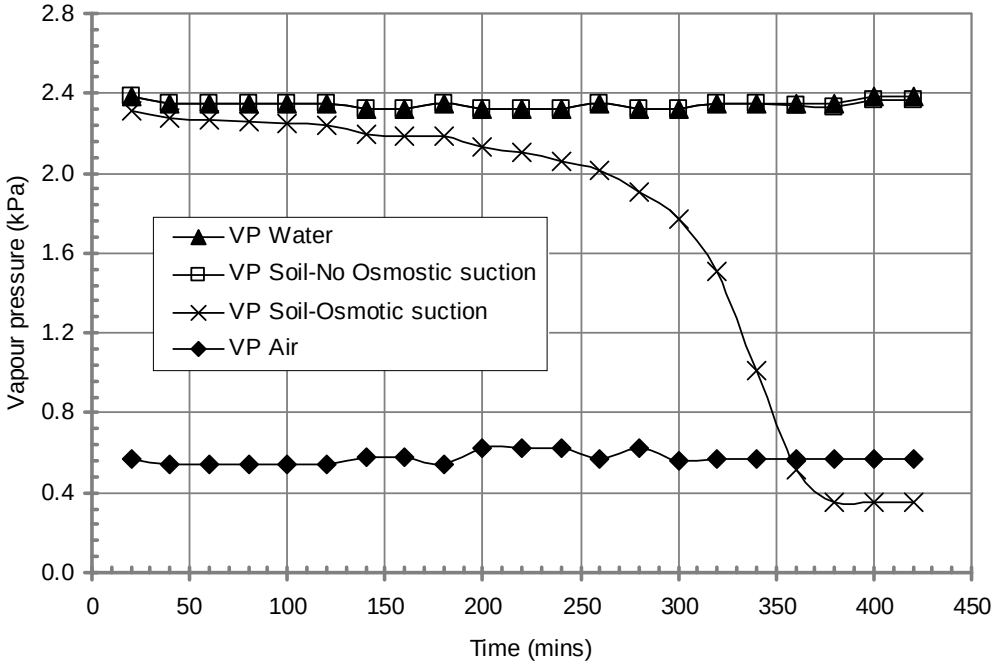

Figure F.16 Vapor pressure versus time for Ottawa sand mixed with 50 g/l NaCl in Set 2.

Table F.9 Summary of results of evaporation for Ottawa sand mixed with 100 g/l NaCl in Set 2.

Time (hour)	PE (mm/ day)	AE (mm/ day)	R.H. Air	Air Temp (^{o}C)	Soil moisture content at surface (%)	Salt content at surface (ppt)	r_{av} (s/m)	r_s (s/m)	Suction		Relative Humidity		Actual Evaporation (mm/day)		
									From SWCC (kPa)	Osmotic suction (kPa)	No osmotic suction	With Osmotic suction	AE–Cal. No Osm	AE–Cal. Osm	AE–Cal. Osm. Res
20	2.64	2.52	0.24	20.3	28.59	100	439.1	7.1	8	8,470	1.00	0.94	2.64	2.43	2.39
40	2.41	1.95	0.23	20.1	25.96	110	481.3	13.7	9	9,329	1.00	0.93	2.41	2.20	2.14
60	2.29	1.83	0.23	20.1	23.92	120	505.4	19.3	10	10,122	1.00	0.93	2.29	2.08	2.00
80	2.41	1.72	0.23	20.1	22.01	130	481.3	25.1	10	11,002	1.00	0.92	2.41	2.16	2.06
100	2.52	1.95	0.23	20.1	20.22	141	459.4	31.0	10	11,979	1.00	0.92	2.52	2.24	2.10
120	2.41	1.72	0.23	20.1	18.18	157	481.3	38.3	10	13,318	1.00	0.91	2.41	2.11	1.96
140	2.29	1.60	0.25	19.9	16.39	174	486.2	45.4	10	14,777	1.00	0.90	2.29	1.98	1.81
160	2.29	1.49	0.25	19.9	14.71	194	486.2	52.9	10	16,459	1.00	0.89	2.29	1.94	1.75
180	2.29	1.49	0.23	20.1	13.16	217	505.4	60.6	10	18,404	1.00	0.87	2.29	1.91	1.71
200	2.29	1.49	0.27	19.9	11.60	246	473.2	69.3	10	20,870	1.00	0.86	2.29	1.84	1.61
220	2.29	1.15	0.27	19.9	10.05	285	473.2	79.2	11	24,100	1.00	0.84	2.29	1.78	1.52
240	2.29	1.38	0.27	19.9	8.85	323	473.2	87.9	11	27,357	1.00	0.82	2.29	1.72	1.45
260	2.29	1.26	0.24	20.1	7.42	385	498.8	100.2	10	32,652	1.00	0.79	2.29	1.65	1.37
280	2.18	1.15	0.27	19.9	6.10	469	498.1	113.6	11	39,694	1.00	0.75	2.18	1.42	1.16
300	2.29	1.38	0.24	19.9	4.90	583	492.7	128.7	12	49,376	1.00	0.69	2.29	1.37	1.09
320	2.29	1.15	0.24	20.1	3.47	824	498.8	152.6	16	69,807	1.00	0.60	2.29	1.08	0.82
340	2.18	1.03	0.24	20.1	2.27	1,258	525.1	181.8	26	106,548	1.00	0.46	2.18	0.62	0.46
360	2.29	0.46	0.24	20.1	1.20	2,390	498.8	226.0	88	202,441	1.00	0.22	2.29	-0.05	-0.03
380	2.29	0.11	0.24	20.1	0.72	3,983	498.8	261.3	333	337,401	1.00	0.08	2.28	-0.47	-0.31
400	2.18	0	0.24	20.3	0.60	4,780	531.6	273.9	568	404,882	1.00	0.05	2.17	-0.54	-0.36
420	2.18	0	0.24	20.3	0.60	4,780	531.6	273.9	568	404,882	1.00	0.05	2.17	-0.54	-0.36

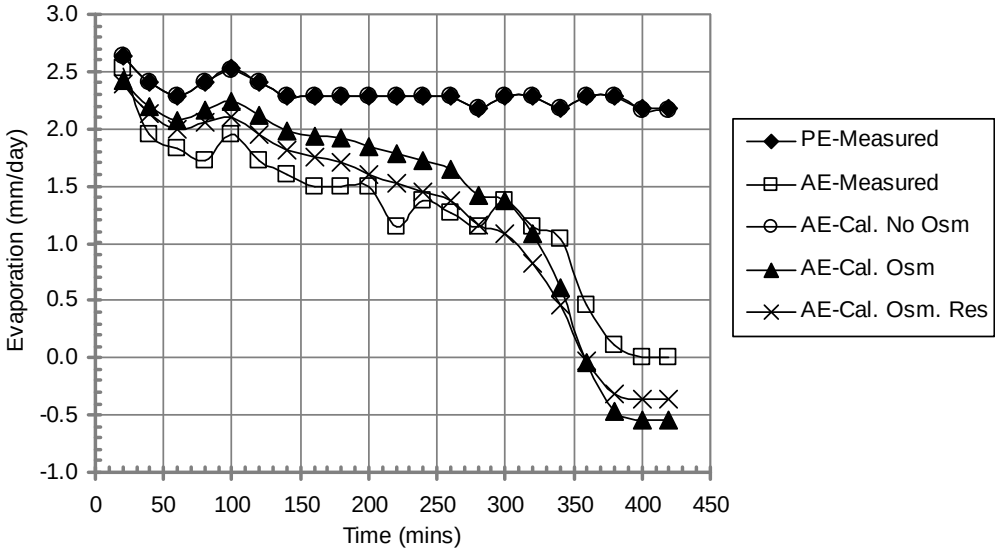

Figure F.17 Calculated and measured rates of actual evaporation corresponding to three procedures for Ottawa sand mixed with 100 g/l NaCl in Set 2. Symbols are described in Table 6.17.

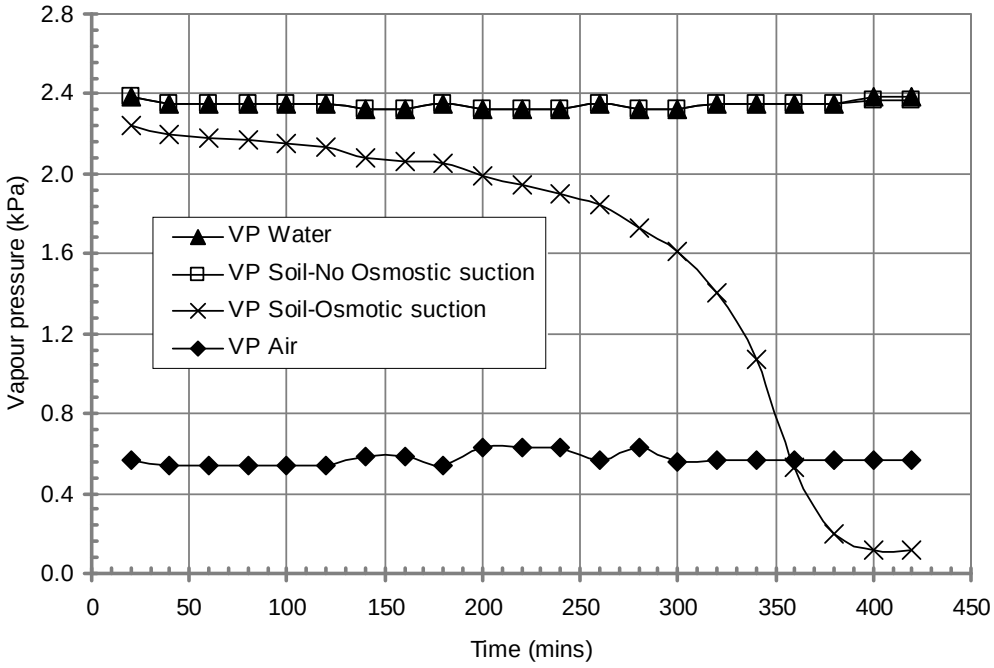

Figure F.18 Vapor pressure versus time for Ottawa sand mixed with 100 g/l NaCl in Set 2.

Table F.10 Summary of results of evaporation for Ottawa sand mixed with 200 g/l NaCl in Set 2.

Time (hour)	PE (mm/ day)	AE (mm/ day)	R.H. Air	Air Temp (^{o} C)	Soil moisture content at surface (%)	Salt content at surface (ppt)	r_{av} (s/m)	r_s (s/m)	Suction		Relative Humidity		Actual Evaporation (mm/day)		
									From SWCC (kPa)	Osmotic suction (kPa)	No osmotic suction	With Osmotic suction	AE–Cal. No Osm	AE–Cal. Osm	AE–Cal. Osm. Res
20	2.64	2.06	0.24	20.3	25.52	200	439.1	54.9	9	16,941	1.00	0.88	2.64	2.23	1.98
40	2.41	1.60	0.23	20.1	23.43	218	481.3	60.8	10	18,450	1.00	0.87	2.41	2.01	1.78
60	2.29	1.49	0.23	20.1	21.81	234	505.4	65.7	10	19,824	1.00	0.86	2.29	1.89	1.67
80	2.41	1.49	0.23	20.1	20.30	251	481.3	70.7	10	21,297	1.00	0.85	2.41	1.95	1.70
100	2.52	1.60	0.23	20.1	18.79	272	459.4	76.0	10	23,006	1.00	0.84	2.52	2.01	1.72
120	2.41	1.26	0.23	20.1	17.17	297	481.3	82.2	10	25,182	1.00	0.83	2.41	1.88	1.60
140	2.29	1.26	0.25	19.9	15.89	321	486.2	87.6	10	27,204	1.00	0.82	2.29	1.74	1.47
160	2.29	1.26	0.25	19.9	14.62	349	486.2	93.3	10	29,579	1.00	0.80	2.29	1.69	1.42
180	2.29	1.26	0.23	20.1	13.34	383	505.4	99.6	10	32,408	1.00	0.79	2.29	1.66	1.39
200	2.29	1.26	0.27	19.9	12.06	423	473.2	106.6	10	35,836	1.00	0.77	2.29	1.56	1.27
220	2.29	1.26	0.27	19.9	10.79	473	473.2	114.3	11	40,075	1.00	0.74	2.29	1.49	1.20
240	2.29	1.38	0.27	19.9	9.51	537	473.2	123.0	11	45,451	1.00	0.71	2.29	1.40	1.11
260	2.29	1.26	0.24	20.1	8.12	629	498.8	133.9	10	53,242	1.00	0.67	2.29	1.31	1.03
280	2.18	1.26	0.27	19.9	6.84	746	498.1	145.7	11	63,169	1.00	0.63	2.18	1.06	0.82
300	2.29	1.38	0.24	19.9	5.57	917	492.7	159.9	11	77,645	1.00	0.56	2.29	0.98	0.74
320	2.29	1.15	0.24	20.1	4.18	1,222	498.8	179.8	13	103,526	1.00	0.47	2.29	0.68	0.50
340	2.18	1.26	0.24	20.1	3.02	1,692	525.1	202.2	18	143,344	1.00	0.35	2.18	0.31	0.22
360	2.29	1.03	0.24	20.1	1.74	2,933	498.8	240.2	41	248,463	1.00	0.16	2.29	-0.24	-0.16
380	2.29	0.23	0.24	20.1	0.70	7,333	498.8	303.4	363	621,157	1.00	0.01	2.28	-0.69	-0.43
400	2.18	0	0.24	20.3	0.46	11,000	531.6	331.4	1,239	931,736	0.99	0.00	2.15	-0.68	-0.42
420	2.18	0	0.24	20.3	0.46	11,000	531.6	331.4	1,239	931,736	0.99	0.00	2.15	-0.68	-0.42

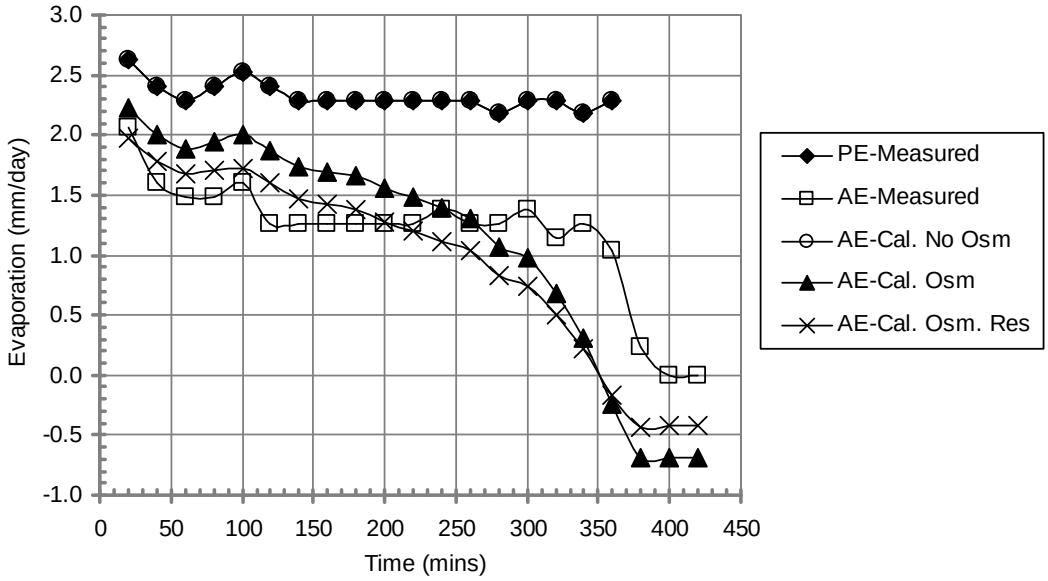

Figure F.19 Calculated and measured rates of actual evaporation corresponding to three procedures for Ottawa sand mixed with 200 g/l NaCl in Set 2. Symbols are described in Table 6.17.

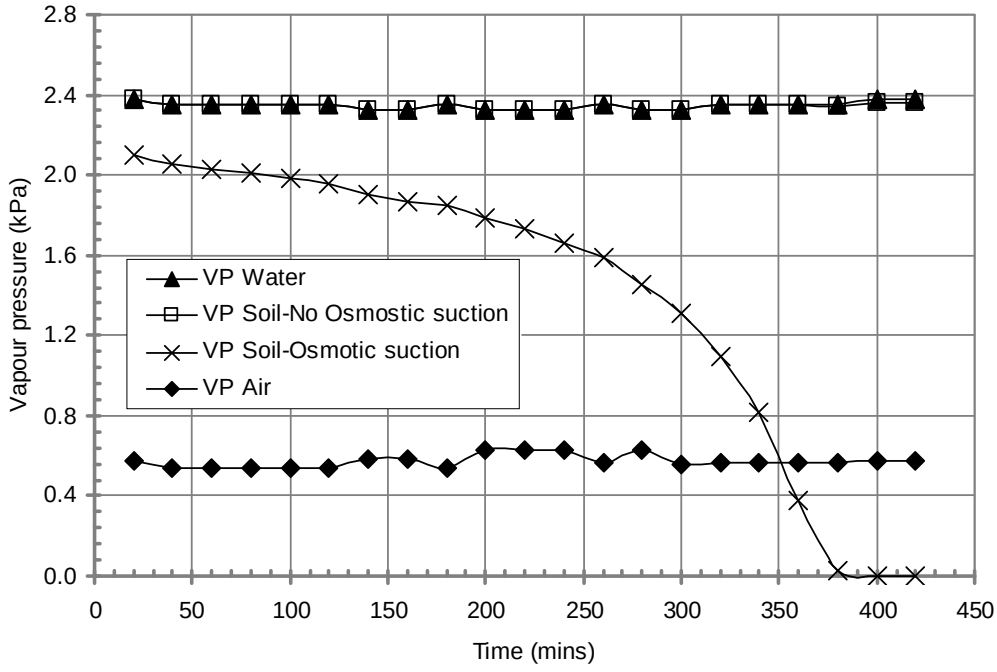

Figure F.20 Vapor pressure versus time for Ottawa sand mixed with 200 g/l NaCl in Set 2.

Table F.11 Summary of results of evaporation for Ottawa sand mixed with 250 g/l NaCl in Set 2.

Time (hour)	PE (mm/ day)	AE (mm/ day)	R.H. Air	Air Temp (^{o} C)	Soil moisture content at surface (%)	Salt content at surface (ppt)	r_{av} (s/m)	r_s (s/m)	Suction		Relative Humidity		Actual Evaporation (mm/day)		
									From SWCC (kPa)	Osmotic suction (kPa)	No osmotic suction	With Osmotic suction	AE–Cal. No Osm	AE–Cal. Osm	AE–Cal. Osm. Res
20	2.64	1.83	0.24	20.3	24.77	250	439.1	70.3	10	21,176	1.00	0.86	2.64	2.13	1.84
40	2.41	1.38	0.23	20.1	22.91	270	481.3	75.7	10	22,896	1.00	0.84	2.41	1.92	1.66
60	2.29	1.38	0.23	20.1	21.51	288	505.4	80.0	10	24,381	1.00	0.84	2.29	1.80	1.56
80	2.41	1.38	0.23	20.1	20.12	308	481.3	84.6	10	26,072	1.00	0.82	2.41	1.86	1.58
100	2.52	1.38	0.23	20.1	18.72	331	459.4	89.6	10	28,015	1.00	0.81	2.52	1.91	1.60
120	2.41	1.26	0.23	20.1	17.33	357	481.3	94.9	10	30,271	1.00	0.80	2.41	1.78	1.49
140	2.29	1.26	0.25	19.9	16.05	386	486.2	100.2	10	32,684	1.00	0.79	2.29	1.64	1.36
160	2.29	1.38	0.25	19.9	14.77	419	486.2	106.0	10	35,515	1.00	0.77	2.29	1.59	1.30
180	2.29	1.26	0.23	20.1	13.37	463	505.4	112.8	10	39,221	1.00	0.75	2.29	1.54	1.26
200	2.29	1.26	0.27	19.9	12.09	512	473.2	119.7	10	43,370	1.00	0.73	2.29	1.43	1.14
220	2.29	1.26	0.27	19.9	10.81	573	473.2	127.5	11	48,499	1.00	0.70	2.29	1.35	1.06
240	2.29	1.26	0.27	19.9	9.53	649	473.2	136.1	11	55,005	1.00	0.67	2.29	1.24	0.97
260	2.29	1.26	0.24	20.1	8.26	750	498.8	146.1	11	63,527	1.00	0.63	2.29	1.16	0.90
280	2.18	1.26	0.27	19.9	6.98	888	498.1	157.7	11	75,174	1.00	0.57	2.18	0.91	0.69
300	2.29	1.26	0.24	19.9	5.70	1,087	492.7	171.7	11	92,050	1.00	0.51	2.29	0.80	0.60
320	2.29	1.15	0.24	20.1	4.42	1,401	498.8	189.2	13	118,696	1.00	0.42	2.29	0.53	0.39
340	2.18	1.26	0.24	20.1	3.26	1,902	525.1	210.3	17	161,087	1.00	0.30	2.18	0.18	0.13
360	2.29	0.92	0.24	20.1	1.98	3,132	498.8	244.7	33	265,320	1.00	0.14	2.29	-0.30	-0.20
380	2.29	0.34	0.24	20.1	1.05	5,917	498.8	288.6	121	501,161	1.00	0.02	2.29	-0.65	-0.41
400	2.18	0.11	0.24	20.3	0.70	8,875	531.6	316.6	361	751,741	1.00	0.00	2.17	-0.68	-0.42
420	2.18	0.00	0.24	20.3	0.58	10,650	531.6	329.2	619	902,090	1.00	0.00	2.16	-0.68	-0.42

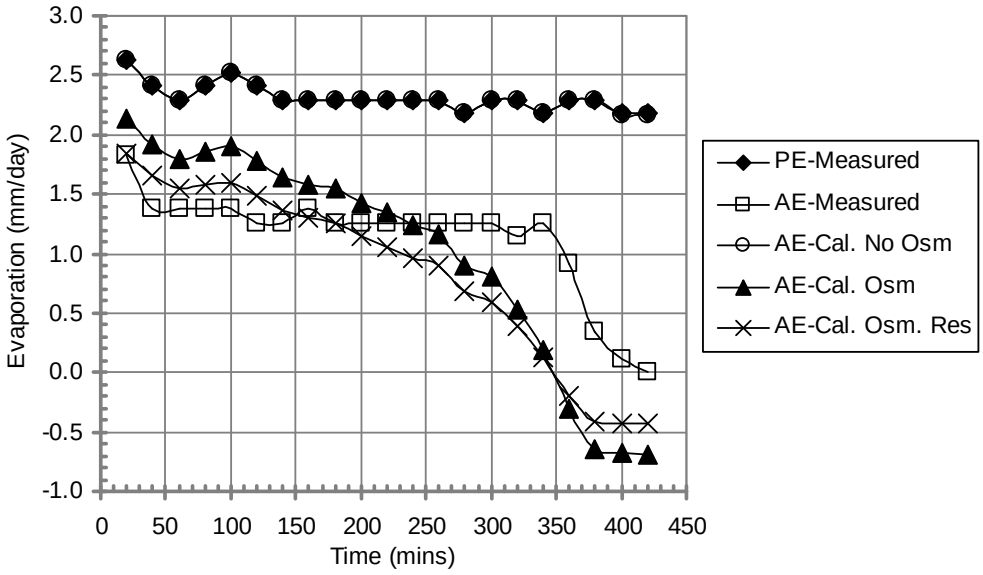

Figure F.21 Calculated and measured rates of actual evaporation corresponding to three procedures for Ottawa sand mixed with 250 g/l NaCl in Set 2. Symbols are described in Table 6.17.

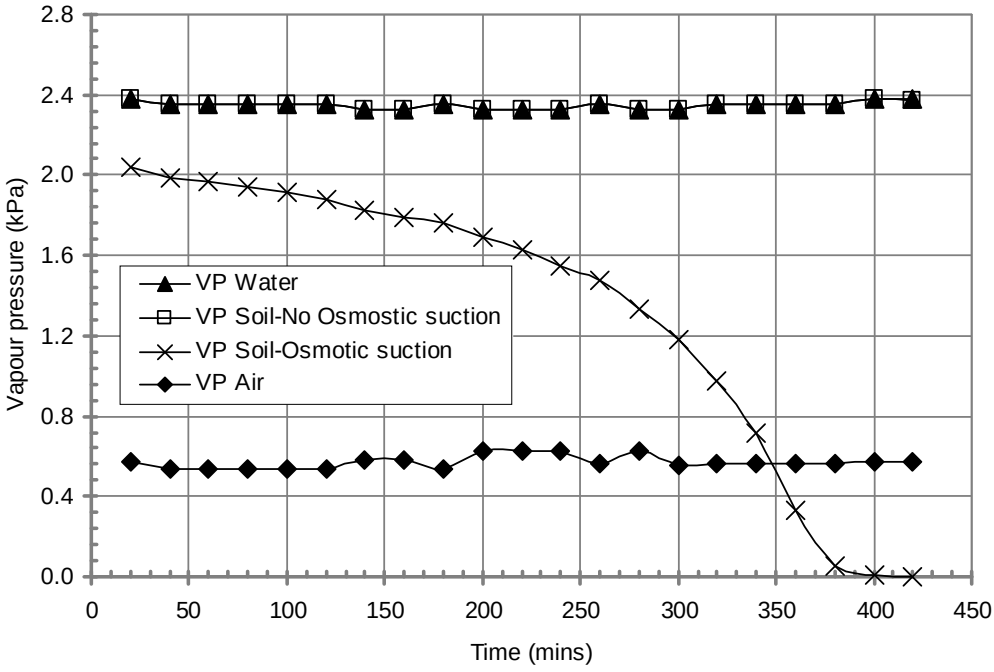

Figure F.22 Vapor pressure versus time for Ottawa sand mixed with 250 g/l NaCl in Set 2.

Table F.12 Summary of results for thin soil layer drying test of Non-saline Devon silt in Set 2.

Time (hours)	PE (mm/day)	AE (mm/day)	R.H. Air	Air Temp (^{o} C)	Soil moisture content at surface (%)	Soil moisture availability factor .Eq. (3.82)	Vapour pressure. Eq. (3.83) (kPa)	R.H., Eq. (3.84)	Soil surface resistance, Eq. (3.86) (s/m)	AE– Calculated, (mm/day)
20	2.59	2.64	0.23	19.60	58.30	1.0000	2.28	1.00	0.0	2.59
40	2.59	2.06	0.23	19.40	51.35	1.0000	2.25	1.00	0.0	2.59
60	2.48	1.95	0.23	19.40	44.79	1.0000	2.25	1.00	0.0	2.48
80	2.36	2.06	0.23	19.40	37.84	1.0000	2.25	1.00	0.0	2.36
100	2.25	1.95	0.23	19.40	31.27	1.0000	2.25	1.00	0.0	2.25
120	2.25	1.95	0.23	19.60	24.71	1.0000	2.28	1.00	0.0	2.25
140	2.48	1.95	0.22	19.90	18.15	1.0000	2.32	1.00	0.0	2.48
160	2.25	1.95	0.22	19.90	11.58	1.0000	2.32	1.00	0.1	2.25
180	2.25	1.49	0.23	19.60	6.56	1.0000	2.28	1.00	1.3	2.25
200	2.36	1.03	0.23	19.60	3.09	0.4635	1.34	0.59	9.8	1.10
220	2.36	0.46	0.23	19.60	1.54	0.0473	0.61	0.27	24.1	0.11
240	2.36	0.11	0.23	19.60	1.16	0.0160	0.55	0.24	30.2	0.04
260	2.36	0.00	0.23	19.60	1.16	0.0160	0.55	0.24	30.2	0.04
280	2.43	0.00	0.23	19.60	1.16	0.0160	0.55	0.24	30.2	0.04
300	2.56	0.00	0.23	19.60	1.16	0.0160	0.55	0.24	30.2	0.04
320	2.25	0.00	0.23	19.60	1.16	0.0160	0.55	0.24	30.2	0.04

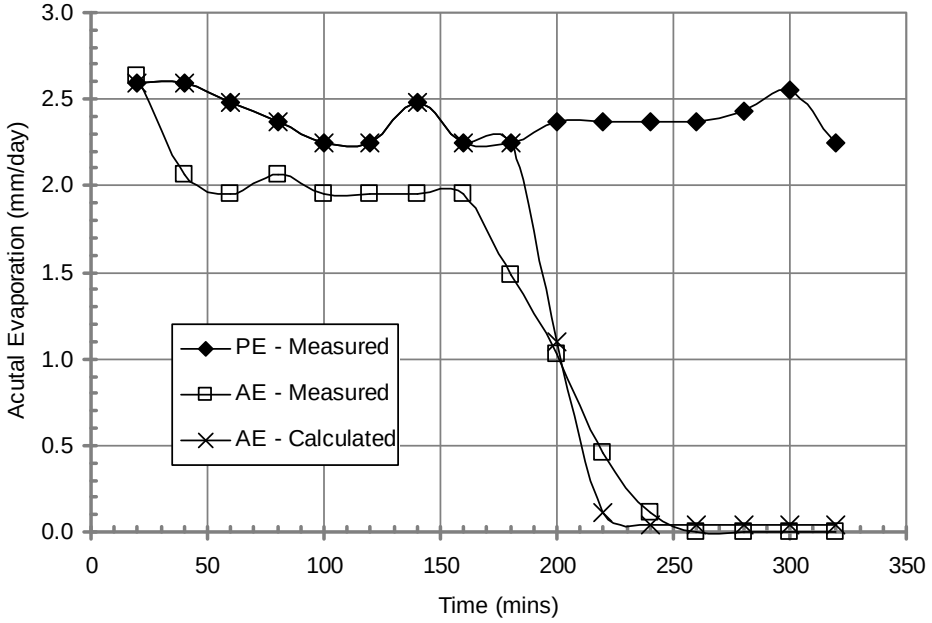

Figure F.23 Calculated, Actual and Potential evaporation rates for thin non-saline Devon silt in Set 2 with water content at the point of evaporation-rate reduction observed during the drying test.

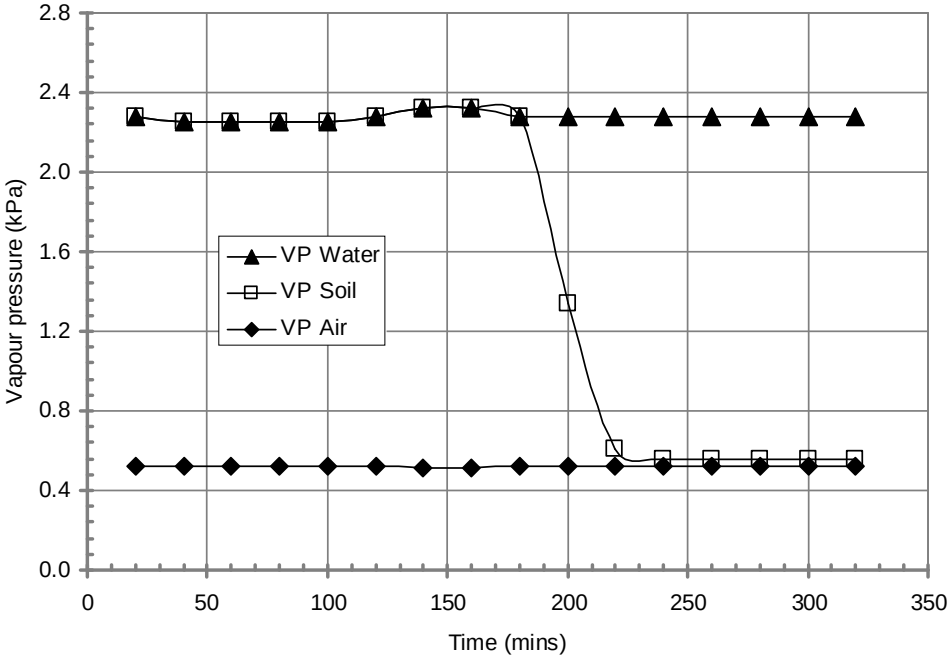

Figure F.24 Vapor pressure versus time for non-saline Devon silt in Set 2.

Table F.13 Summary of results of evaporation for Devon silt mixed with 50 g/l NaCl in Set 2.

Time (hour)	PE (mm/ day)	AE (mm/ day)	R.H. Air	Air Temp (^{o} C)	Soil moisture content at surface (%)	Salt content at surface (ppt)	r_{av} (s/m)	r_s (s/m)	Suction		Relative Humidity		Actual Evaporation (mm/day)		
									From SWCC (kPa)	Osmotic suction (kPa)	No osmotic suction	With Osmotic suction	AE–Cal. No Osm	AE–Cal. Osm	AE–Cal. Osm. Res
20	2.59	2.41	0.23	19.60	55.10	50	432.9	0.0	0	4,235	1.00	0.97	2.59	2.49	2.49
40	2.59	1.95	0.23	19.40	48.16	57	427.5	0.0	0	4,845	1.00	0.96	2.59	2.47	2.47
60	2.48	1.60	0.23	19.40	42.45	65	447.3	0.0	67	5,498	1.00	0.96	2.48	2.35	2.35
80	2.36	1.83	0.23	19.40	35.92	77	469.0	0.0	244	6,497	1.00	0.95	2.36	2.22	2.22
100	2.25	1.60	0.23	19.40	30.20	91	492.9	0.7	484	7,726	1.00	0.94	2.24	2.08	2.07
120	2.25	1.60	0.23	19.60	24.49	113	499.0	15.2	1,058	9,529	0.99	0.92	2.23	2.03	1.97
140	2.48	1.49	0.22	19.90	19.18	144	467.4	32.0	2,578	12,165	0.98	0.90	2.42	2.15	2.01
160	2.25	1.49	0.22	19.90	13.88	199	515.0	54.4	5,125	16,816	0.96	0.85	2.14	1.82	1.64
180	2.25	1.03	0.23	19.60	10.20	270	499.0	75.6	9,338	22,870	0.93	0.79	2.06	1.63	1.42
200	2.36	1.26	0.23	19.60	5.71	482	474.8	115.6	26,580	40,839	0.82	0.61	1.82	1.16	0.93
220	2.36	0.69	0.23	19.60	3.27	844	474.8	154.2	66,478	71,468	0.61	0.36	1.17	0.40	0.30
240	2.36	0.46	0.23	19.60	1.63	1,688	474.8	202.0	174,768	142,937	0.27	0.10	0.14	-0.41	-0.29
260	2.36	0.00	0.23	19.60	1.63	1,688	474.8	202.0	174,768	142,937	0.27	0.10	0.14	-0.41	-0.29
280	2.43	0.00	0.23	19.60	1.63	1,688	461.4	202.0	174,768	142,937	0.27	0.10	0.14	-0.43	-0.30
300	2.56	0.00	0.23	19.60	1.63	1,688	439.4	202.0	174,768	142,937	0.27	0.10	0.15	-0.45	-0.31
320	2.25	0.00	0.23	19.60	1.63	1,688	499.0	202.0	174,768	142,937	0.27	0.10	0.13	-0.39	-0.28

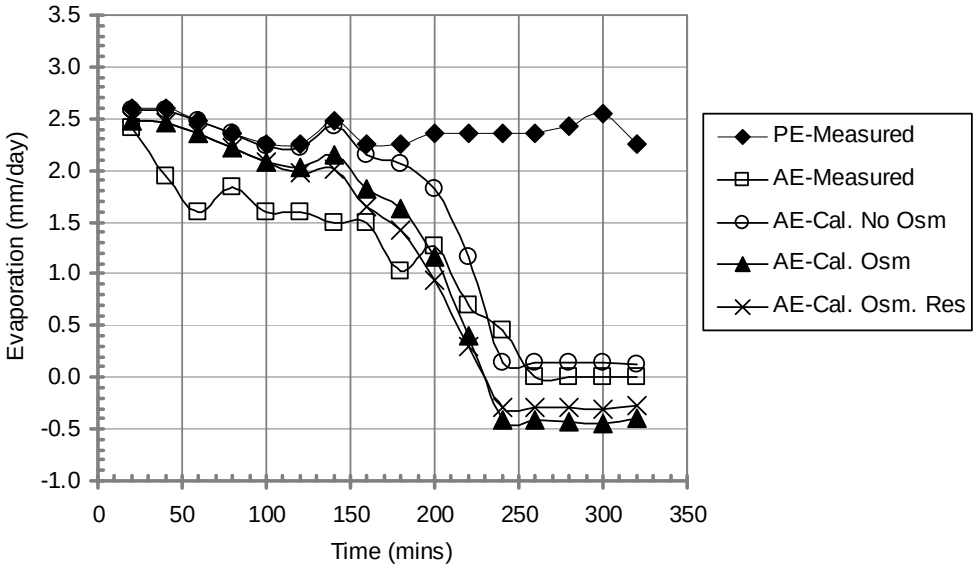

Figure F.25 Calculated and measured rates of actual evaporation corresponding to three procedures for Devon silt mixed with 50 g/l NaCl in Set 2. Symbols are described in Table 6.17.

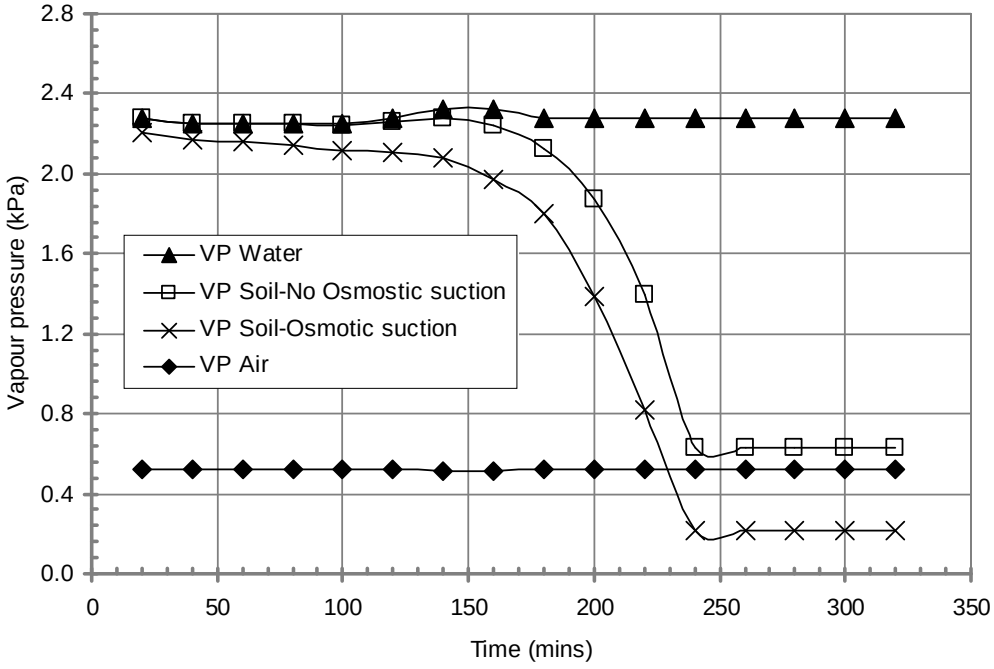

Figure F.26 Vapor pressure versus time for Devon silt mixed with 50 g/l NaCl in Set 2.

Table F.14 Summary of results of evaporation for Devon silt mixed with 100 g/l NaCl in Set 2.

Time (hour)	PE (mm/ day)	AE (mm/ day)	R.H. Air	Air Temp (^{o} C)	Soil moisture content at surface (%)	Salt content at surface (ppt)	r_{av} (s/m)	r_s (s/m)	Suction		Relative Humidity		Actual Evaporation (mm/day)		
									From SWCC (kPa)	Osmotic suction (kPa)	No osmotic suction	With Osmotic suction	AE–Cal. No Osm	AE–Cal. Osm	AE–Cal. Osm. Res
20	2.59	2.29	0.23	19.60	60.36	100	432.9	7.1	0	8,470	1.00	0.94	2.59	2.39	2.35
40	2.59	1.72	0.23	19.40	55.00	110	427.5	13.5	0	9,295	1.00	0.93	2.59	2.37	2.29
60	2.48	1.60	0.23	19.40	50.00	121	447.3	20.0	0	10,225	1.00	0.93	2.47	2.24	2.14
80	2.36	1.72	0.23	19.40	44.64	135	469.0	27.9	0	11,452	1.00	0.92	2.36	2.11	1.99
100	2.25	1.60	0.23	19.40	39.64	152	492.9	36.1	148	12,896	1.00	0.91	2.25	1.98	1.85
120	2.25	1.72	0.23	19.60	34.29	176	499.0	46.1	296	14,911	1.00	0.89	2.24	1.94	1.78
140	2.48	1.15	0.22	19.90	30.71	197	467.4	53.7	454	16,645	1.00	0.88	2.47	2.10	1.89
160	2.25	1.72	0.22	19.90	25.36	238	515.0	66.9	931	20,162	0.99	0.86	2.23	1.83	1.62
180	2.25	1.26	0.23	19.60	21.43	282	499.0	78.5	1,727	23,858	0.99	0.83	2.21	1.75	1.51
200	2.36	1.49	0.23	19.60	16.79	360	474.8	95.4	4,145	30,457	0.97	0.77	2.27	1.67	1.39
220	2.36	1.15	0.23	19.60	13.21	457	474.8	111.9	5,653	38,689	0.96	0.72	2.24	1.51	1.22
240	2.36	1.38	0.23	19.60	8.93	676	474.8	138.9	11,989	57,259	0.92	0.60	2.10	1.13	0.88
260	2.36	1.03	0.23	19.60	5.71	1,056	474.8	169.7	26,580	89,468	0.82	0.42	1.82	0.60	0.44
280	2.43	0.73	0.23	19.60	2.86	2,112	461.4	217.5	81,437	178,936	0.55	0.15	1.00	-0.27	-0.18
300	2.56	0.31	0.23	19.60	2.14	2,817	439.4	237.4	122,900	238,581	0.40	0.07	0.57	-0.53	-0.35
320	2.25	0.11	0.23	19.60	1.79	3,380	499.0	250.0	156,287	286,297	0.31	0.04	0.25	-0.56	-0.37

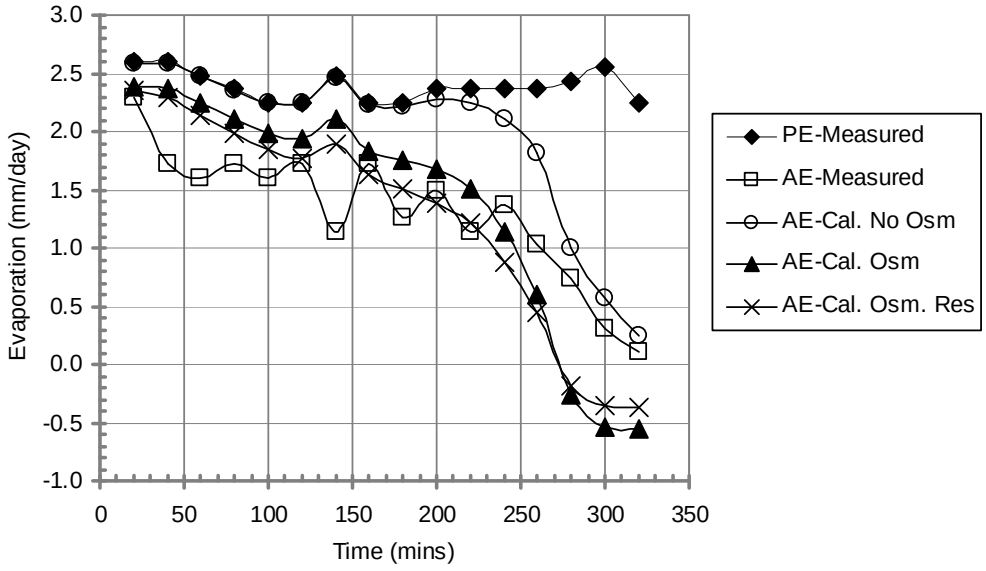

Figure F.27 Calculated and measured rates of actual evaporation corresponding to three procedures for Devon silt mixed with 100 g/l NaCl in Set 2. Symbols are described in Table 6.17.

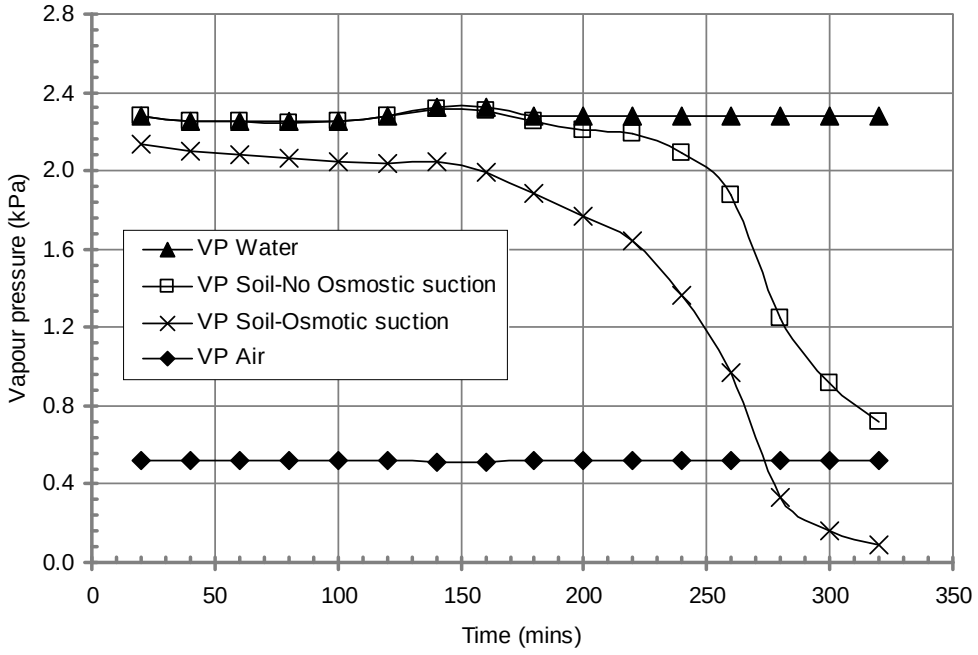

Figure F.28 Vapor pressure versus time for Devon silt mixed with 100 g/l NaCl in Set 2.

Table F.15 Summary of results of evaporation for Devon silt mixed with 200 g/l NaCl in Set 2.

Time (hour)	PE (mm/ day)	AE (mm/ day)	R.H. Air	Air Temp (^{o} C)	Soil moisture content at surface (%)	Salt content at surface (ppt)	r_{av} (s/m)	r_s (s/m)	Suction		Relative Humidity		Actual Evaporation (mm/day)		
									From SWCC (kPa)	Osmotic suction (kPa)	No osmotic suction	With Osmotic suction	AE–Cal. No Osm	AE–Cal. Osm	AE–Cal. Osm. Res
20	2.59	1.83	0.23	19.60	54.84	200	432.9	0.0	0	16,941	1.00	0.88	2.59	2.19	2.19
40	2.59	1.49	0.23	19.40	50.18	219	427.5	61.0	0	18,514	1.00	0.87	2.59	2.16	1.89
60	2.48	1.26	0.23	19.40	46.24	237	447.3	66.7	0	20,092	1.00	0.86	2.47	2.03	1.76
80	2.36	1.38	0.23	19.40	41.94	262	469.0	73.4	85	22,153	1.00	0.85	2.36	1.90	1.64
100	2.25	1.26	0.23	19.40	37.99	289	492.9	80.2	188	24,452	1.00	0.83	2.25	1.76	1.52
120	2.25	1.15	0.23	19.60	34.41	319	499.0	87.0	292	26,999	1.00	0.82	2.24	1.72	1.46
140	2.48	1.03	0.22	19.90	31.18	352	467.4	93.8	429	29,792	1.00	0.80	2.47	1.84	1.54
160	2.25	1.26	0.22	19.90	27.24	403	515.0	103.2	713	34,104	0.99	0.77	2.24	1.60	1.33
180	2.25	1.15	0.23	19.60	23.66	464	499.0	112.9	1,202	39,272	0.99	0.74	2.22	1.49	1.22
200	2.36	1.15	0.23	19.60	20.07	546	474.8	124.2	2,190	46,284	0.98	0.70	2.32	1.44	1.14
220	2.36	1.26	0.23	19.60	16.13	680	474.8	139.3	4,767	57,598	0.97	0.63	2.26	1.23	0.95
240	2.36	1.15	0.23	19.60	12.54	874	474.8	156.7	6,267	74,055	0.95	0.55	2.23	0.99	0.74
260	2.36	1.15	0.23	19.60	8.96	1,224	474.8	179.9	11,910	103,677	0.92	0.43	2.11	0.60	0.44
280	2.43	0.92	0.23	19.60	5.38	2,040	461.4	215.1	29,506	172,795	0.80	0.22	1.81	-0.02	-0.01
300	2.56	0.61	0.23	19.60	3.94	2,782	439.4	236.5	49,361	235,629	0.69	0.12	1.54	-0.36	-0.23
320	2.25	0.46	0.23	19.60	2.51	4,371	499.0	267.7	98,528	370,274	0.48	0.03	0.74	-0.58	-0.38

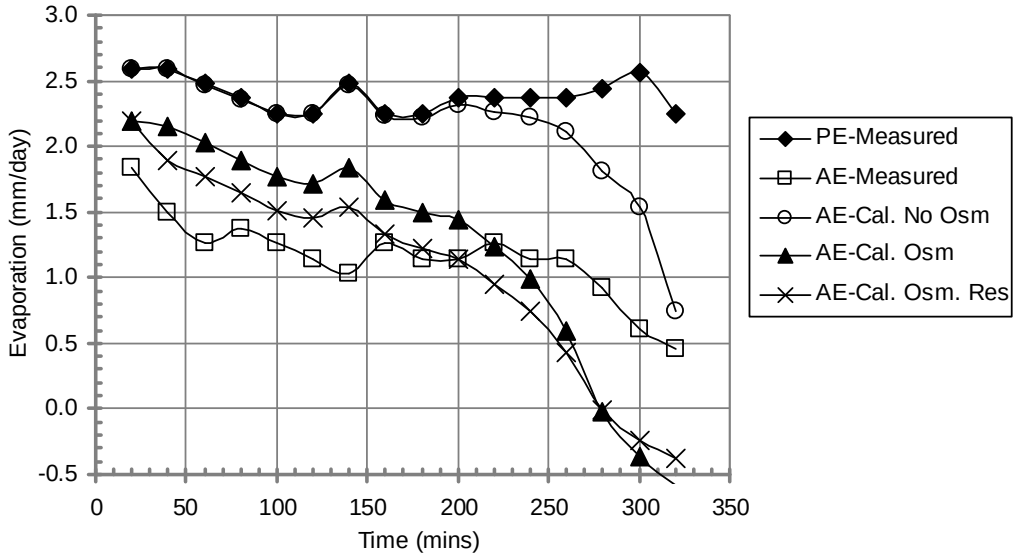

Figure F.29 Calculated and measured rates of actual evaporation corresponding to three procedures for Devon silt mixed with 200 g/l NaCl in Set 2. Symbols are described in Table 6.17.

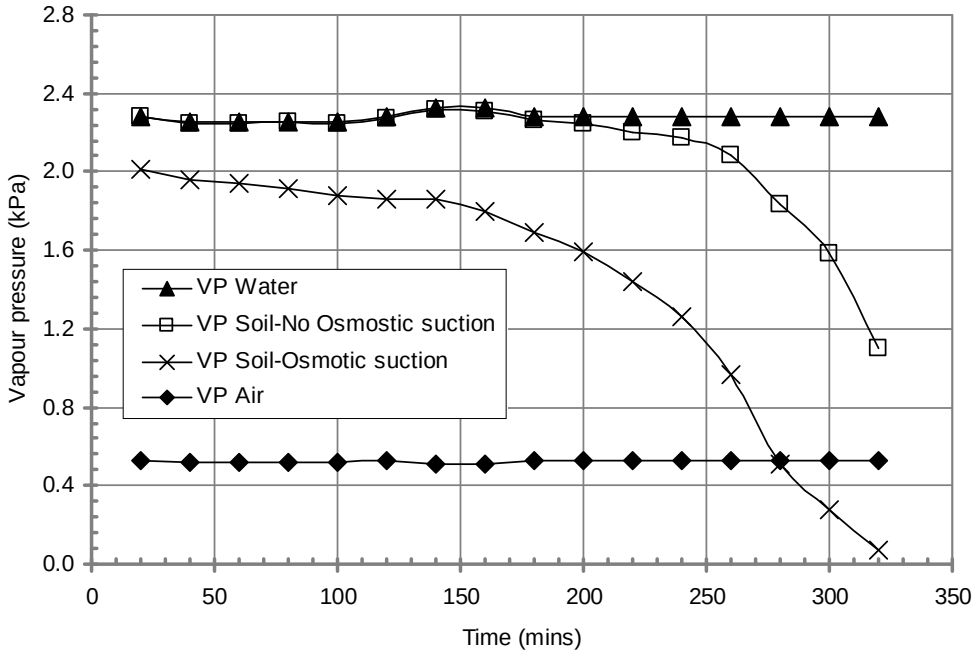

Figure F.30 Vapor pressure versus time for Devon silt mixed with 200 g/l NaCl in Set 2.

Table F.16 Summary of results of evaporation for Devon silt mixed with 250 g/l NaCl in Set 2.

Time (hour)	PE (mm/ day)	AE (mm/ day)	R.H. Air	Air Temp (^{o} C)	Soil moisture content at surface (%)	Salt content at surface (ppt)	r_{av} (s/m)	r_s (s/m)	Suction		Relative Humidity		Actual Evaporation (mm/day)		
									From SWCC (kPa)	Osmotic suction (kPa)	No osmotic suction	With Osmotic suction	AE–Cal. No Osm	AE–Cal. Osm	AE–Cal. Osm. Res
20	2.6	1.49	0.23	19.60	53.29	250	432.9	70.3	0	21,176	1.00	0.86	2.59	2.11	1.81
40	2.6	1.83	0.23	19.40	47.75	279	427.5	77.8	0	23,631	1.00	0.84	2.59	2.05	1.74
60	2.5	1.26	0.23	19.40	43.94	303	447.3	83.6	1	25,678	1.00	0.83	2.48	1.92	1.62
80	2.4	1.26	0.23	19.40	40.14	332	469.0	89.8	136	28,113	1.00	0.81	2.36	1.79	1.50
100	2.3	1.38	0.23	19.40	35.99	370	492.9	97.4	242	31,356	1.00	0.79	2.24	1.64	1.37
120	2.3	1.38	0.23	19.60	31.83	418	499.0	105.8	396	35,446	1.00	0.77	2.24	1.57	1.30
140	2.5	1.26	0.22	19.90	28.03	475	467.4	114.6	641	40,260	1.00	0.74	2.46	1.65	1.33
160	2.3	1.38	0.22	19.90	23.88	558	515.0	125.7	1,162	47,262	0.99	0.70	2.23	1.38	1.11
180	2.3	1.26	0.23	19.60	20.07	664	499.0	137.7	2,191	56,225	0.98	0.65	2.20	1.23	0.96
200	2.4	1.49	0.23	19.60	15.57	856	474.8	155.2	5,388	72,468	0.96	0.56	2.24	1.02	0.77
220	2.4	1.26	0.23	19.60	11.76	1,132	474.8	174.5	7,106	95,914	0.95	0.47	2.21	0.73	0.53
240	2.4	1.26	0.23	19.60	7.96	1,674	474.8	201.5	14,801	141,786	0.90	0.31	2.05	0.26	0.18
260	2.4	0.80	0.23	19.60	5.54	2,406	474.8	226.5	28,064	203,817	0.81	0.18	1.79	-0.15	-0.10
280	2.4	0.37	0.23	19.60	4.15	3,208	461.4	246.4	45,389	271,756	0.71	0.10	1.53	-0.42	-0.28
300	2.6	0.15	0.23	19.60	3.81	3,500	439.4	252.4	52,233	296,461	0.68	0.08	1.49	-0.51	-0.32
320	2.3	0.00	0.23	19.60	3.81	3,500	499.0	252.4	52,233	296,461	0.68	0.08	1.31	-0.45	-0.30

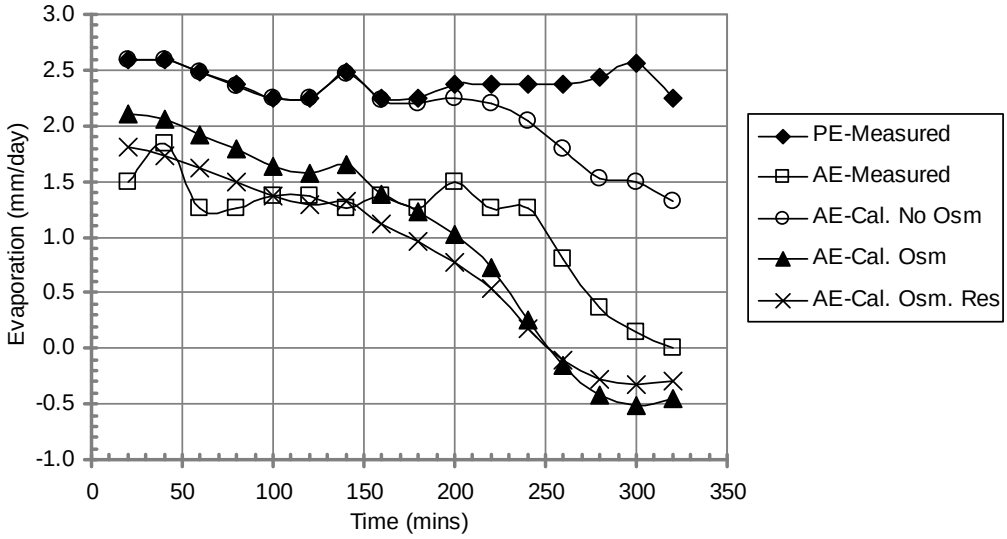

Figure F.31 Calculated and measured rates of actual evaporation corresponding to three procedures for Devon silt mixed with 250 g/l NaCl in Set 2. Symbols are described in Table 6.17.

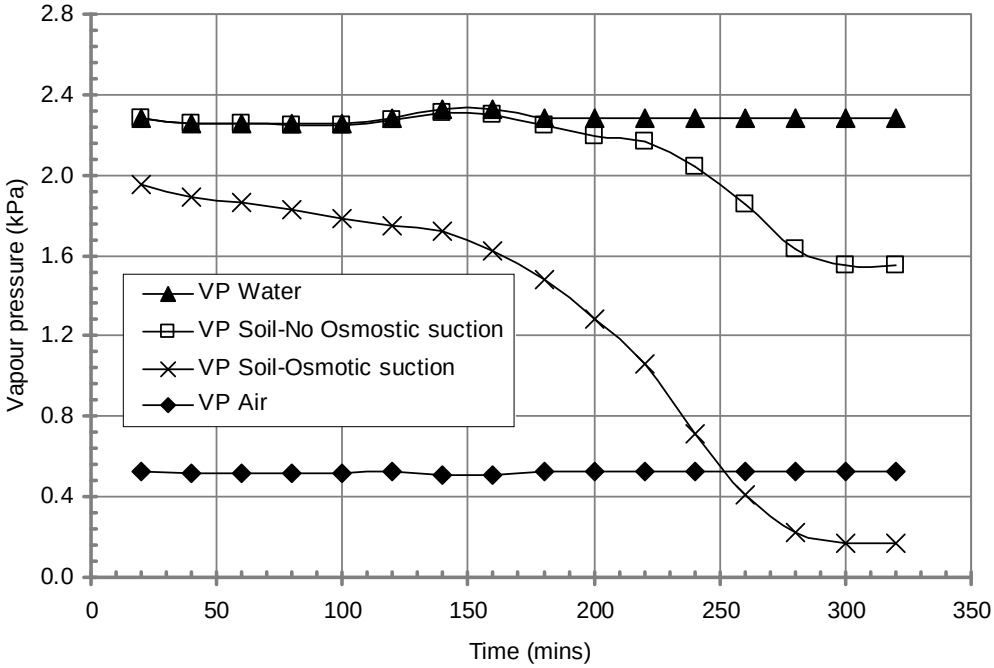

Figure F.32 Vapor pressure versus time for Devon silt mixed with 250 g/l NaCl in Set 2.

Table F.17 Summary of calculation of evaporation rate for non-saline silt – replicate No. 1.

Time (days)	Measured RE = *AE/PE*	R.H. Air	Air Temp (^{o} C)	Soil moisture content at 0 – 2 mm (%)	Vapour pressure for RE–Cal. 1 (kPa)	Vapour pressure for RE– Cal. 2 (kPa)	Vapour pressure for RE–Cal. 3 (kPa)	RE–Cal. 1	RE–Cal. 2	RE–Cal. 3
0	0.8735	0.63	23.3	27.1	2.86	2.86	2.86	1.00	1.00	1.00
1	0.8063	0.67	22.5	2.6	2.72	2.34	1.87	0.83	0.40	0.01
2	0.5771	0.56	21.8	2.1	2.61	1.83	1.48	0.84	0.23	0.01
3	0.3202	0.52	22.1	1.9	2.64	1.68	1.41	0.82	0.16	0.00
4	0.1858	0.62	22.3	1.9	2.68	1.90	1.68	0.79	0.15	0.00
5	0.1818	0.63	22.2	1.8	2.64	1.88	1.68	0.77	0.13	0.00
6	0.1739	0.50	22.7	1.7	2.57	1.59	1.40	0.72	0.11	0.00
7	0.1581	0.58	21.7	1.7	2.45	1.66	1.51	0.70	0.10	0.00
8	0.1383	0.50	22.1	1.6	2.40	1.51	1.35	0.67	0.09	0.00
9	0.1225	0.52	22.4	1.6	2.43	1.56	1.41	0.65	0.08	0.00
10	0.1028	0.41	22.2	1.5	2.17	1.23	1.09	0.58	0.07	0.00
11	0.0870	0.36	22.5	1.4	2.08	1.12	0.98	0.54	0.06	0.00
12	0.0711	0.57	23.6	1.5	2.57	1.78	1.66	0.60	0.07	0.00
13	0.0593	0.61	22.8	1.5	2.48	1.80	1.69	0.58	0.07	0.00
14	0.0474	0.62	22.6	1.5	2.44	1.80	1.70	0.56	0.07	0.00

Table F.18 Summary of calculation of evaporation rate for non-saline silt – replicate No. 2.

Time (days)	Measured RE = *AE/PE*	R.H. Air	Air Temp (^{o} C)	Soil moisture content at 0 – 2 mm (%)	Vapour pressure for RE–Cal. 1 (kPa)	Vapour pressure for RE– Cal. 2 (kPa)	Vapour pressure for RE–Cal. 3 (kPa)	RE–Cal. 1	RE–Cal. 2	RE–Cal. 3
0	0.9868	0.63	23.3	27.1	2.86	2.86	2.86	1.00	1.00	1.00
1	0.8370	0.67	22.5	3.1	2.72	2.57	1.90	0.85	0.62	0.02
2	0.6916	0.56	21.8	2.5	2.61	2.07	1.50	0.86	0.40	0.01
3	0.4009	0.52	22.1	2.2	2.66	1.83	1.42	0.85	0.26	0.01
4	0.2247	0.62	22.3	2.1	2.70	2.01	1.69	0.82	0.24	0.00
5	0.1410	0.63	22.2	2.0	2.67	1.95	1.69	0.81	0.19	0.00
6	0.1586	0.50	22.7	1.8	2.70	1.66	1.40	0.81	0.15	0.00
7	0.1233	0.58	21.7	1.8	2.54	1.71	1.51	0.78	0.13	0.00
8	0.1189	0.50	22.1	1.7	2.54	1.56	1.35	0.76	0.12	0.00
9	0.1057	0.52	22.4	1.7	2.58	1.62	1.41	0.75	0.12	0.00
10	0.0661	0.41	22.2	1.5	2.25	1.25	1.09	0.62	0.08	0.00
11	0.0617	0.36	22.5	1.5	2.20	1.15	0.98	0.60	0.07	0.00
12	0.0617	0.57	23.6	1.6	2.66	1.81	1.66	0.66	0.09	0.00
13	0.0529	0.61	22.8	1.6	2.56	1.82	1.69	0.64	0.08	0.00
14	0.0485	0.62	22.6	1.5	2.49	1.82	1.70	0.60	0.07	0.00

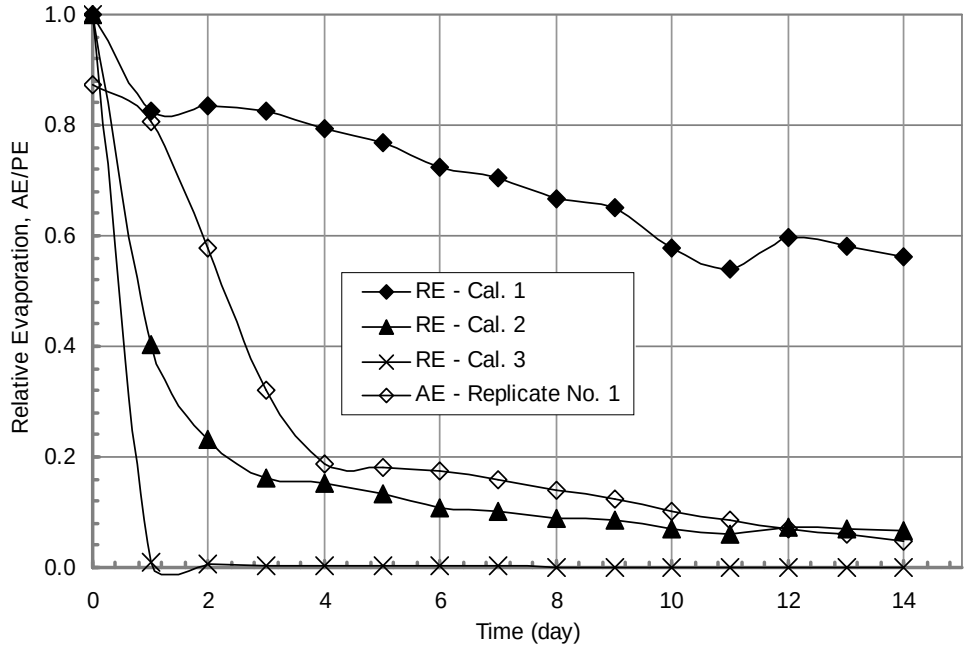

Figure F.33 Typical calculation of the Relative Evaporation, *AE/PE* using the suction at evaporation-rate reduction point under simulated wind – Replicate No. 1.

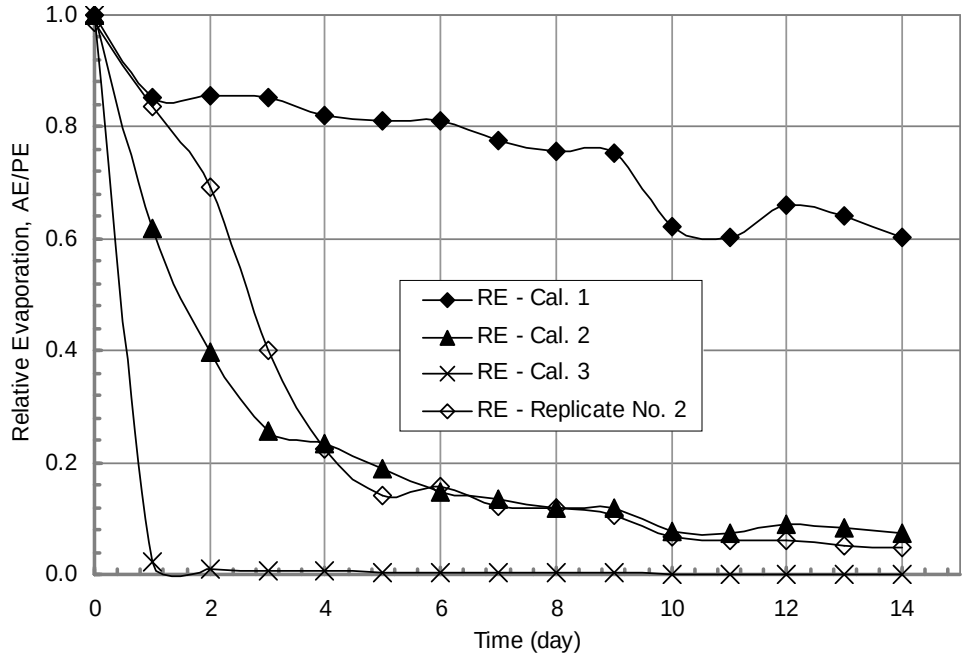

Figure F.34 Typical calculation of the Relative Evaporation, *AE/PE* using the suction at evaporation-rate reduction point under simulated wind – Replicate No. 2.

Table F.19 Summary of results of relative evaporation for Low-saline silt.

Time (day)	*AE/PE*	R.H. Air	Air Temp (^{o} C)	Soil moisture content at 0 – 1 cm (%)	Salt content at 0 – 1 cm (ppt)	r_{av} (s/m)	r_s (s/m)	Suction		Relative Humidity		Relative Evaporation		
								From SWCC (kPa)	Osmotic suction (kPa)	No osmotic suction	With Osmotic suction	RE–Cal. No Osm	RE–Cal. Osm	RE–Cal. Osm. Res
0	0.79	0.63	22.5	28.6	66.4	103.2	0.0	1	5,623	1.00	0.96	1.00	0.89	0.89
1	0.67	0.67	24.8	24.9	134.3	94.7	54.8	5	11,376	1.00	0.92	1.00	0.76	0.48
2	0.75	0.56	22.9	21.2	202.2	119.1	111.4	6	17,130	1.00	0.88	1.00	0.73	0.38
3	0.47	0.52	25.4	17.5	270.2	157.2	151.7	7	22,883	1.00	0.85	1.00	0.68	0.35
4	0.42	0.62	22.9	17.8	264.0	108.9	148.4	7	22,360	1.00	0.85	1.00	0.60	0.26
5	0.16	0.63	23.3	16.1	287.1	109.5	160.6	8	24,321	1.00	0.84	1.00	0.56	0.23
6	0.26	0.50	22.0	14.3	310.3	134.0	172.5	9	26,283	1.00	0.82	1.00	0.65	0.28
7	0.31	0.58	23.9	12.5	333.4	151.2	185.2	11	28,244	1.00	0.81	1.00	0.56	0.25
8	0.35	0.50	22.4	11.8	365.5	153.5	199.9	12	30,957	1.00	0.80	1.00	0.59	0.26
9	0.31	0.52	23.1	11.1	397.5	165.0	214.3	13	33,671	1.00	0.78	1.00	0.55	0.24
10	0.31	0.41	22.4	10.4	429.5	195.2	229.1	14	36,384	1.00	0.77	1.00	0.61	0.28
11	0.26	0.36	21.9	9.7	461.6	171.9	244.7	15	39,097	1.00	0.75	1.00	0.61	0.25
12	0.12	0.57	21.6	8.9	433.3	113.4	245.1	16	36,700	1.00	0.76	1.00	0.45	0.14
13	0.10	0.61	22.5	8.1	405.0	129.7	249.3	18	34,303	1.00	0.78	1.00	0.43	0.15
14	0.08	0.62	21.9	7.3	376.7	148.9	259.1	20	31,905	1.00	0.79	1.00	0.45	0.16

Note: The interpolated values are filled in the highlighted cells.

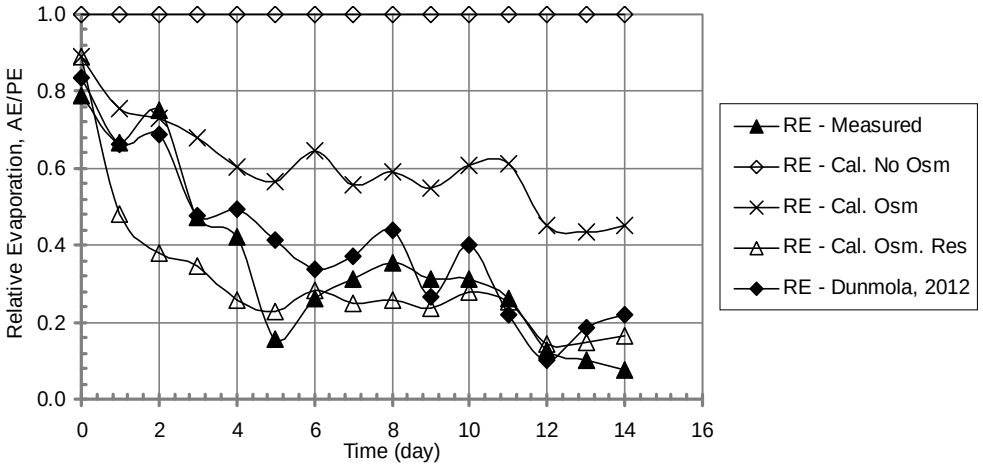

Figure F.35 Calculated and measured relative evaporation for Low-saline silt. The calculated results using three procedures are in comparison with that by Dunmola (2012). Symbols are described in Table 6.14.

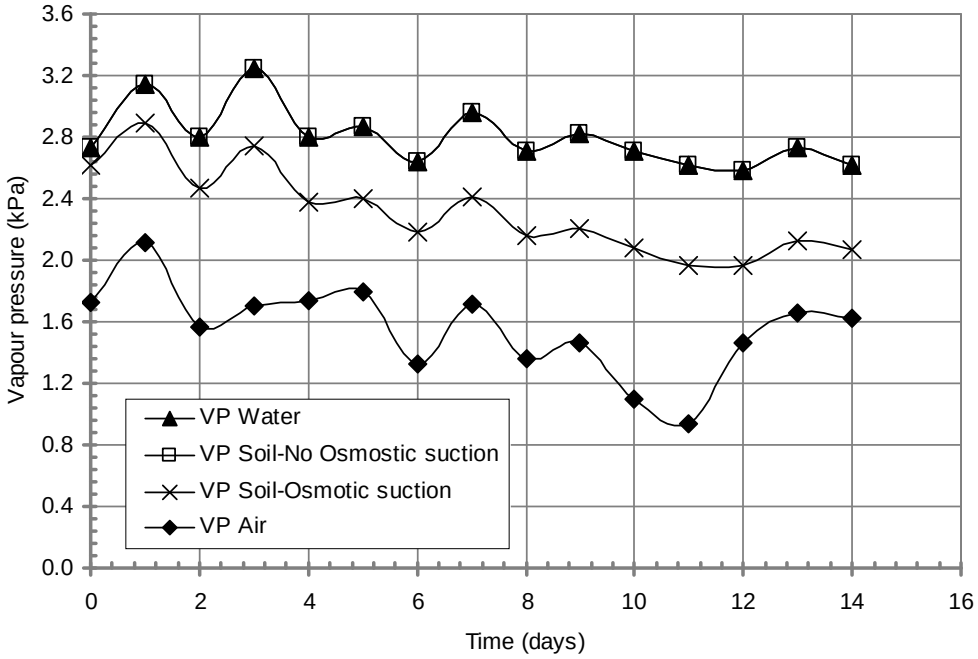

Figure F.36 Vapor pressure versus time for Low-saline silt.

Table F.20 Summary of results of relative evaporation for Saline silt.

Time (day)	*AE/PE*	R.H. Air	Air Temp (^{o} C)	Soil moisture content at 0 – 1 cm (%)	Salt content at 0 – 1 cm (ppt)	r_{av} (s/m)	r_s (s/m)	Suction		Relative Humidity		Relative Evaporation		
								From SWCC (kPa)	Osmotic suction (kPa)	No osmotic suction	With Osmotic suction	RE–Cal. No Osm	RE–Cal. Osm	RE–Cal. Osm. Res
0	0.88	0.24	24.0	27.0	110.4	72.1	13.9	4	9,351	1.00	0.93	1.00	0.91	0.77
1	0.57	0.20	23.6	24.6	196.3	88.2	53.6	5	16,623	1.00	0.89	1.00	0.86	0.53
2	0.34	0.19	24.4	22.2	282.1	107.7	78.7	6	23,896	1.00	0.84	1.00	0.80	0.46
3	0.25	0.20	24.1	19.8	368.0	118.2	97.1	6	31,168	1.00	0.80	1.00	0.75	0.41
4	0.06	0.19	24.1	18.1	410.9	107.3	104.9	7	34,805	1.00	0.78	1.00	0.73	0.37
5	0.05	0.19	24.1	17.2	440.5	96.3	109.9	8	37,316	1.00	0.76	1.00	0.71	0.33
6	0.14	0.20	24.1	16.3	470.2	125.8	114.6	8	39,826	1.00	0.75	1.00	0.68	0.36
7	0.06	0.16	23.5	15.4	499.8	106.3	119.3	9	42,337	1.00	0.73	1.00	0.68	0.32
8	0.06	0.14	24.1	14.0	532.8	106.8	124.9	10	45,129	1.00	0.72	1.00	0.67	0.31
9	0.06	0.15	24.1	12.6	565.8	112.0	131.4	11	47,922	1.00	0.71	1.00	0.65	0.30
10	0.08	0.19	24.1	11.2	598.7	136.3	140.1	12	50,714	1.00	0.69	1.00	0.62	0.30
11	0.05	0.22	24.1	9.7	631.7	84.1	153.2	15	53,506	1.00	0.68	1.00	0.59	0.21
12	0.05	0.15	24.1	10.6	619.9	100.7	145.3	13	52,510	1.00	0.68	1.00	0.63	0.26
13	0.05	0.11	24.1	11.5	608.2	100.3	139.6	12	51,515	1.00	0.69	1.00	0.65	0.27
14	0.06	0.11	24.1	12.4	596.4	110.8	135.5	11	50,519	1.00	0.69	1.00	0.65	0.29

Note: The interpolated values are filled in the highlighted cells.

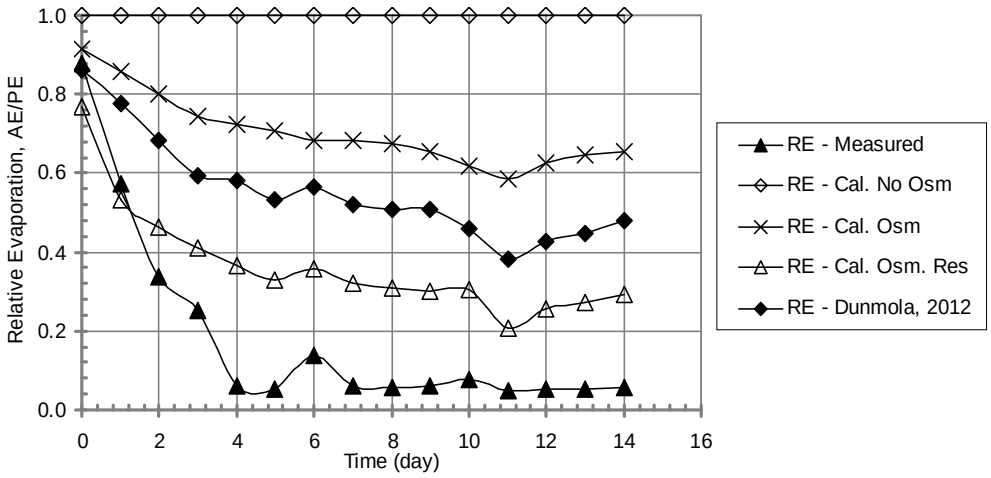

Figure F.37 Calculated and measured relative evaporation for Saline silt. The calculated results using three procedures are in comparison with that by Dunmola (2012). Symbols are described in Table 6.14.

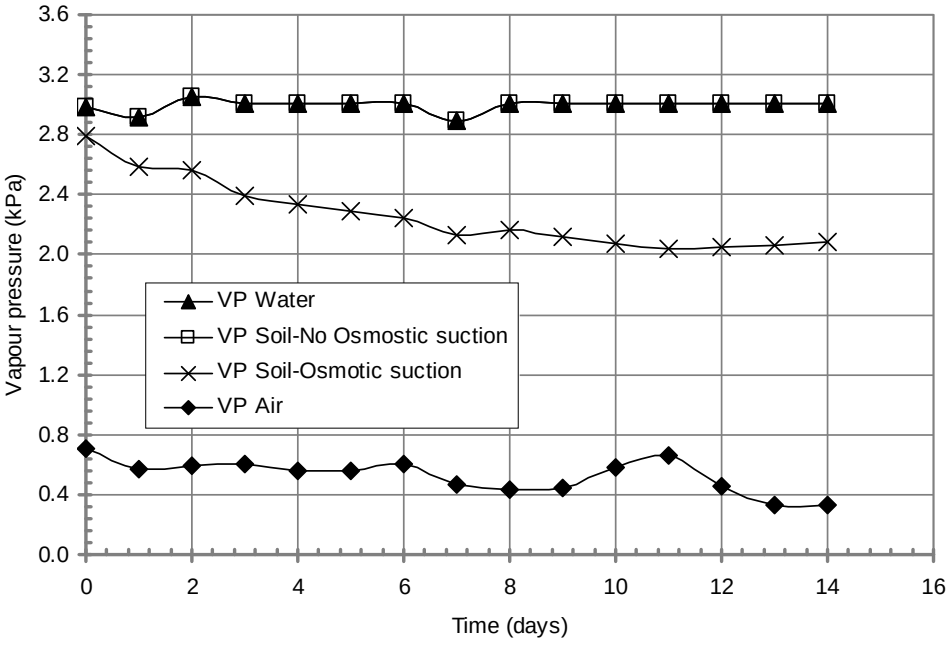

Figure F.38 Vapor pressure versus time for Saline silt.

Table F.21 Summary of results of relative evaporation for Salinized silt-SW.

Time (day)	*AE/PE*	R.H. Air	Air Temp (^{o} C)	Soil moisture content at 0 – 1 cm (%)	Salt content at 0 – 1 cm (ppt)	r_{av} (s/m)	r_s (s/m)	Suction		Relative Humidity		Relative Evaporation		
								From SWCC (kPa)	Osmotic suction (kPa)	No osmotic suction	With Osmotic suction	RE–Cal. No Osm	RE–Cal. Osm	RE–Cal. Osm. Res
0	0.91	0.21	24.3	33.0	104.8	71	10	63	7,758	1.00	0.94	1.00	0.93	0.81
1	0.58	0.19	24.2	28.6	171.3	86	44	87	14,630	1.00	0.90	1.00	0.87	0.58
2	0.31	0.19	24.2	24.2	237.9	119	69	124	22,341	1.00	0.85	1.00	0.81	0.52
3	0.17	0.20	24.4	19.7	304.4	117	99	243	30,712	1.00	0.80	1.00	0.75	0.40
4	0.09	0.17	24.6	18.7	332.1	104	116	313	34,361	1.00	0.78	1.00	0.73	0.35
5	0.10	0.20	24.4	17.6	359.8	102	140	409	38,098	1.00	0.76	1.00	0.69	0.29
6	0.07	0.17	24.3	16.5	387.5	108	175	546	41,920	1.00	0.73	1.00	0.68	0.26
7	0.06	0.15	24.0	15.4	415.2	99	231	745	45,822	0.99	0.71	0.99	0.66	0.20
8	0.04	0.15	24.2	14.0	440.6	98	361	1,166	49,478	0.99	0.69	0.99	0.64	0.14
9	0.04	0.18	24.2	12.5	466.1	94	618	1,907	53,195	0.99	0.67	0.98	0.59	0.08
10	0.04	0.21	24.2	11.1	491.5	150	1,129	3,271	56,972	0.98	0.64	0.97	0.55	0.06
11	0.03	0.18	24.2	9.7	517.0	64	2,148	5,901	60,807	0.96	0.62	0.95	0.53	0.02
12	0.02	0.13	24.5	10.5	507.1	68	1,445	4,089	59,311	0.97	0.63	0.97	0.57	0.03
13	0.02	0.11	24.4	11.4	497.2	81	984	2,889	57,824	0.98	0.64	0.98	0.60	0.05
14	0.13	0.11	23.8	12.3	487.3	114	683	2,079	56,345	0.98	0.65	0.98	0.61	0.09

Note: The interpolated values are filled in the highlighted cells.

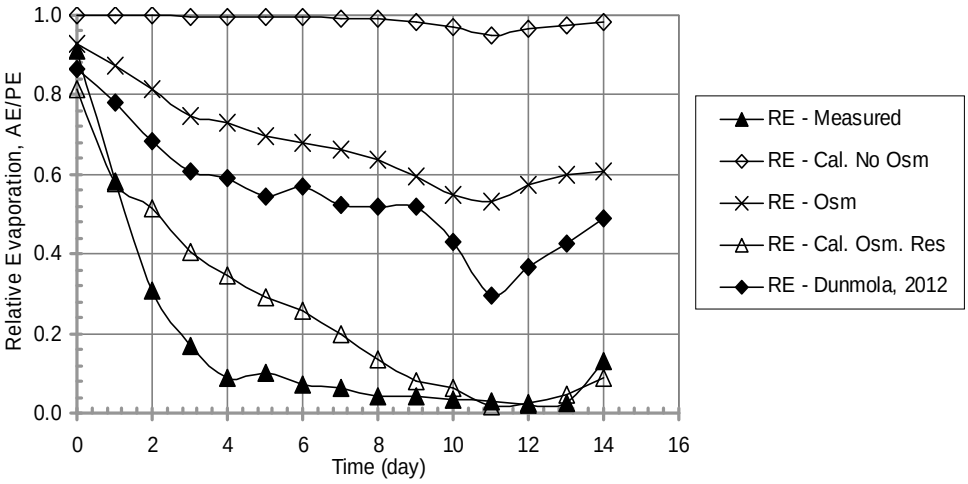

Figure F.39 Calculated and measured relative evaporation for Salinized silt under simulated wind condition (Salinized silt – SW). The calculated results using three procedures are in comparison with that by Dunmola (2012). Symbols are described in Table 6.14.

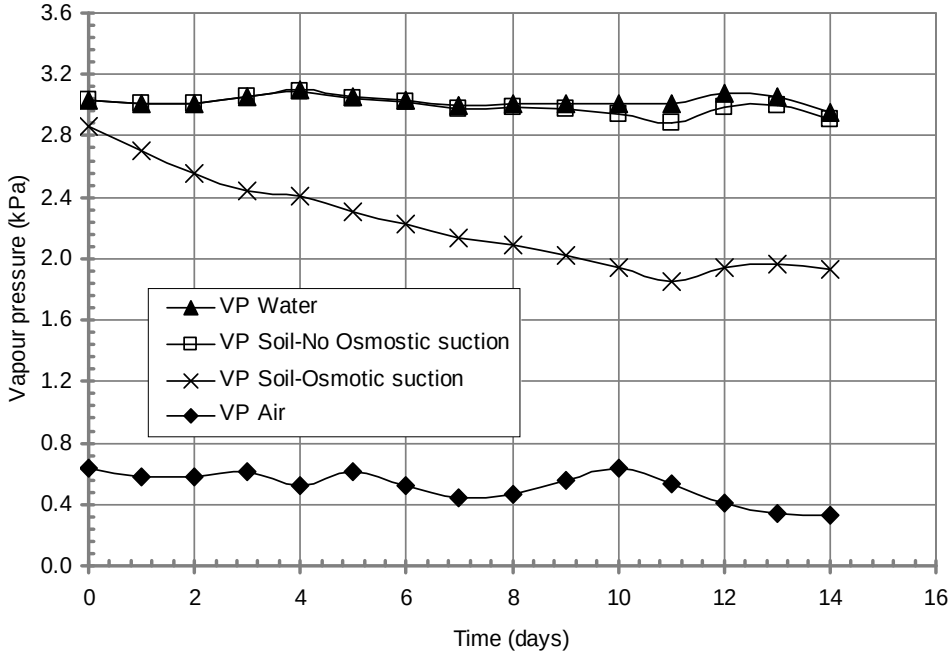

Figure F.40 Vapor pressure versus time for Salinized silt-SW.

Table F.22 Summary of results of relative evaporation for Tailings-AW.

Time (day)	*AE/PE*	R.H. Air	Air Temp (^{o} C)	Soil moisture content at 0 – 1 cm (%)	Salt content at 0 – 1 cm (ppt)	r_{av} (s/m)	r_s (s/m)	Suction		Relative Humidity		Relative Evaporation		
								From SWCC (kPa)	Osmotic suction (kPa)	No osmotic suction	With Osmotic suction	RE–Cal. No Osm	RE–Cal. Osm	RE–Cal. Osm. Res
0	1.00	0.21	24.2	39.0	5.6	322.9	0.0	48	177	1.00	1.00	1.00	1.00	1.00
1	1.00	0.19	24.1	33.5	8.7	367.5	0.0	102	312	1.00	1.00	1.00	1.00	1.00
2	1.00	0.19	24.1	28.1	11.8	366.2	0.0	187	466	1.00	1.00	1.00	0.99	0.99
3	1.00	0.24	24.1	22.6	15.1	342.7	0.0	337	637	1.00	0.99	1.00	0.99	0.99
4	1.00	0.31	23.8	22.1	20.1	379.9	0.0	358	925	1.00	0.99	1.00	0.99	0.99
5	1.00	0.29	24.0	21.5	25.4	396.3	0.0	381	1,247	1.00	0.99	1.00	0.98	0.98
6	0.75	0.25	23.6	21.0	30.9	437.2	0.0	405	1,603	1.00	0.99	1.00	0.98	0.98
7	0.80	0.26	23.7	20.4	36.5	380.8	0.0	432	1,992	1.00	0.98	1.00	0.98	0.98
8	0.80	0.25	24.0	19.6	35.3	393.8	0.1	473	1,906	1.00	0.98	1.00	0.98	0.98
9	0.75	0.25	24.1	18.8	34.1	407.5	0.1	520	1,822	1.00	0.98	0.99	0.98	0.98
10	0.82	0.23	24.0	16.9	42.9	413.9	0.3	652	2,449	1.00	0.98	0.99	0.97	0.97
11	0.91	0.20	23.8	15.1	52.1	517.8	0.8	825	3,152	0.99	0.97	0.99	0.96	0.96
12	0.79	0.24	23.7	13.1	65.4	428.7	2.3	1,063	4,224	0.99	0.96	0.99	0.95	0.95
13	0.84	0.25	23.7	11.2	79.5	495.6	6.8	1,389	5,435	0.99	0.95	0.99	0.93	0.92
14	0.78	0.21	24.0	9.3	94.5	400.4	26.8	1,846	6,790	0.99	0.94	0.98	0.92	0.86

Note: The interpolated values are filled in the highlighted cells.

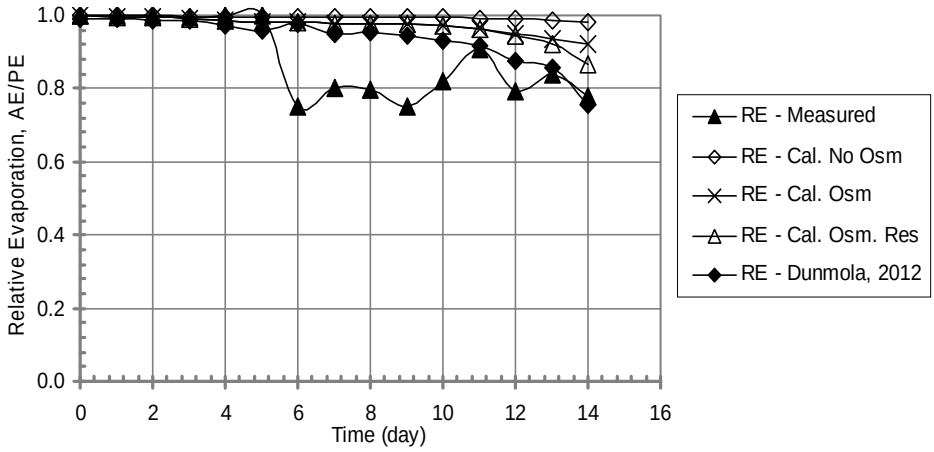

Figure F.41 Calculated and measured relative evaporation for Tailings under ambient wind condition (Tailings – AW). The calculated results using three procedures are in comparison with that by Dunmola (2012). Symbols are described in Table 6.14.

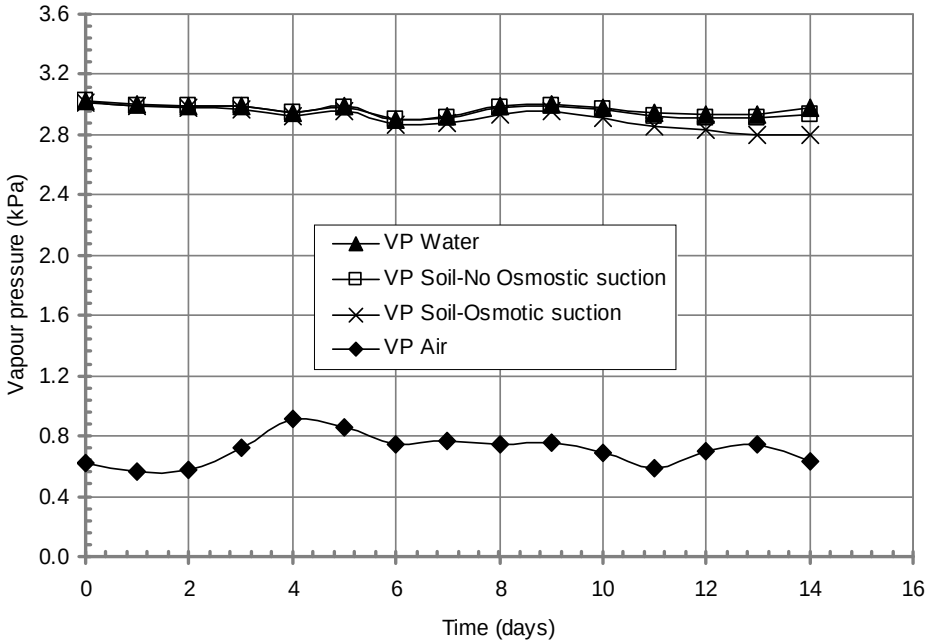

Figure F.42 Vapor pressure versus time for Tailings-AW.

Table F.23 Summary of results of relative evaporation for Tailings-SW.

Time (day)	*AE/PE*	R.H. Air	Air Temp (^{o} C)	Soil moisture content at 0 – 1 cm (%)	Salt content at 0 – 1 cm (ppt)	r_{av} (s/m)	r_s (s/m)	Suction		Relative Humidity		Relative Evaporation		
								From SWCC (kPa)	Osmotic suction (kPa)	No osmotic suction	With Osmotic suction	RE–Cal. No Osm	RE–Cal. Osm	RE–Cal. Osm. Res
0	0.97	0.22	23.8	38.1	6.9	82	0	56	232	1.00	1.00	1.00	1.00	1.00
1	0.94	0.19	23.8	29.1	25.4	91	0	168	1,248	1.00	0.99	1.00	0.99	0.99
2	0.88	0.16	23.8	20.1	46.8	106	0	448	2,740	1.00	0.98	1.00	0.97	0.97
3	0.54	0.15	24.2	11.1	70.9	113	7	1,417	4,690	0.99	0.96	0.99	0.95	0.89
4	0.27	0.14	24.2	9.2	76.1	104	22	1,885	5,134	0.99	0.95	0.98	0.94	0.78
5	0.23	0.16	23.6	7.2	81.3	91	67	2,556	5,596	0.98	0.94	0.98	0.93	0.54
6	0.10	0.21	23.8	5.3	86.7	110	201	3,537	6,078	0.97	0.93	0.97	0.91	0.32
7	0.12	0.18	24.0	3.4	92.2	102	606	4,937	6,578	0.96	0.92	0.96	0.90	0.13
8	0.02	0.16	24.0	3.1	184.9	71	782	5,673	16,137	0.96	0.85	0.95	0.83	0.07
9	0.08	0.16	24.2	2.7	301.3	128	970	6,559	30,300	0.95	0.76	0.94	0.72	0.08
10	0.10	0.15	24.2	2.4	441.4	100	1,184	7,636	49,597	0.95	0.66	0.94	0.60	0.05
11	0.11	0.20	24.0	2.1	605.3	103	1,433	8,964	74,534	0.94	0.54	0.92	0.43	0.03
12	0.03	0.18	24.0	1.9	733.7	79	1,550	9,584	95,514	0.93	0.46	0.92	0.34	0.02
13	0.05	0.23	24.0	1.8	873.5	87	1,674	10,267	119,626	0.93	0.39	0.91	0.21	0.01
14	0.02	0.17	23.8	1.7	1,024.9	119	1,806	11,023	147,020	0.92	0.32	0.91	0.17	0.01

Note: The interpolated values are filled in the highlighted cells.

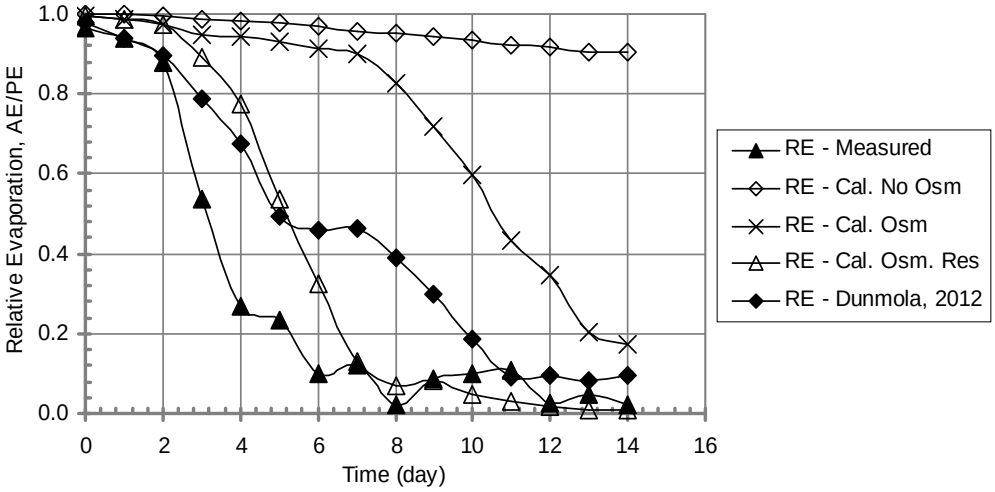

Figure F.43 Calculated and measured relative evaporation for Tailings under simulated wind condition (Tailings – SW). The calculated results using three procedures are in comparison with that by Dunmola (2012). Symbols are described in Table 6.14.

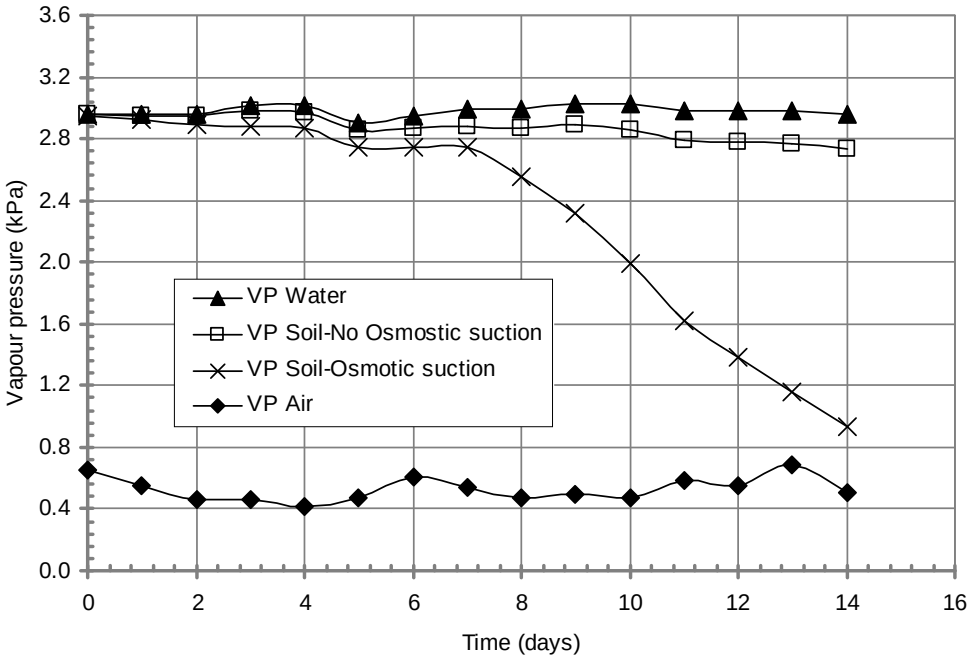

Figure F.44 Vapor pressure versus time for Tailings-SW.